Adaptive Detailing

Design and Fabrication Methods for In Place Wire and
Arc Additive Manufacturing Connection Details

A thesis submitted to attain the degree of
DOCTOR OF SCIENCES of ETH ZURICH
(Dr. sc. ETH Zurich)

presented by

Inés Ariza

M. Sc., Massachusetts Institute of Technology
Architect, Universidad de Buenos Aires

born on 05.02.1986
citizen of Argentina

accepted on the recommendation of

Prof. Matthias Kohler
Prof. Fabio Gramazio
Prof. Dr. Caitlin T. Mueller

2022

Abstract

This thesis presents an *additive joining* technique and an *adaptive detailing* pipeline for robotic assembly of spatial structures. The thesis starts by identifying how designing for and building with robots brings new challenges for the designer who –now in explicit control of both design and production– needs to be knowledgeable in the possibilities of robotic joining tools and processes. The context of inquiry is a case study of spatial structures in steel with non-planar interfaces between elements. The three-dimensional nature of the interfaces presents an unprecedented building challenge in robotic fabrication, requiring an investigation of appropriate materials, processes, and fitting techniques to fix the parts in space. These challenges, dependent on diverse expertise and knowledge, funnel back to the current lack of consolidated detailing concepts and methods for robotic fabrication. The investigation is, therefore, twofold:

First, an *additive joining* technique to join metal parts is developed. The technique applies the known Wire and Arc Additive Manufacturing (WAAM) process *in place* directly on the parts to be joined during assembly, in contrast with typical approaches where connections are prefabricated in an exclusive 3D printing environment. The resulting *in place WAAM* (IPWAAM) technique is developed alongside tolerance handling procedures to measure and adapt to the actual location of parts, as well as collision control methods to move safely between obstacles during the 3D printing process.

Second, a computational detailing pipeline is developed to coordinate the different challenges of designing and building IPWAAM connection details. The pipeline integrates robotic, material, and functional requirements and, by linking the digital and physical models of the IPWAAM connections, it allows the design to adapt as needed based on the building data gathered during production, resulting in a novel *adaptive detailing* approach.

The thesis develops through physical experiments to test the joining and detailing approaches and virtual experiments to anticipate the challenges of their application in the context of spatial structures. As a result, the physical outcomes demonstrate an unprecedented method for joining non-planar metal parts. Finally, the adaptive detailing approach provides a basis for detailing computationally in the context of robotic fabrication, aiming to support the current efforts of building a rich and transparent digital building culture.

Zusammenfassung

In dieser Dissertation wird eine *additive Fügetechnik* sowie eine Pipeline *adaptiver Baudetails* für die robotische Konstruktionräumlicher Strukturen vorgestellt. Zu Beginn identifiziert die Arbeit, dass das Entwerfen und Bauen mit Robotern neue Herausforderungen für EntwerferInnen mit sich bringt. Da sie nun in der expliziten Kontrolle sowohl für die Gestaltung, als auch für die Fabrikation sind, müssen sie sich fachkundiges Wissen robotischer Fügewerkzeuge und -prozesse aneignen. Der Untersuchungskontext ist eine Fallstudie über räumliche Strukturen, bestehend aus nicht-planaren Schnittstellen zwischen Stahlelementen. Die dreidimensionale Beschaffenheit der Schnittstellen stellt neuartige Herausforderungen für die robotische Fabrikation dar und erfordert die Untersuchung geeigneter Materialien, Verfahren und Verbindungstechniken zur räumlichen Fixierung der Teile. Diese Herausforderungen, welche von unterschiedlichem Fachwissen und Kenntnissen abhängen, lassen sich auf den derzeitigen Mangel an konsolidierten Konzepten und Methoden der Roboterfertigung zurückführen. Die Untersuchung ist daher zweigliedrig:

Zuerst wird eine *additive Fügetechnik* zur Verbindung von Metallteilen entwickelt. Bei dieser Technik wird das bekannte WAAM-Verfahren (Wire and Arc Additive Manufacturing) lokal auf die Teile angewendet, welche während der Montage zusammengefügt werden sollen, im Gegensatz zu üblichen Ansätzen, bei denen die Verbindungen in einer exklusiven 3D-Druckumgebung vorab gefertigt werden. Das daraus resultierende *In-Place-WAAM-Verfahren* (IPWAAM) wird zusammen mit Prozessen zur Handhabung von Toleranzen entwickelt, um die tatsächliche Lage der Teile zu messen und anzupassen – sowie mit Methoden zur Kollisionskontrolle, um eine sichere Bewegung während des 3D-Druckprozesses zwischen Hindernissen zu gewährleisten.

Zweitens wird eine computergestützte Pipeline für Baudetails entwickelt, um die verschiedenen Herausforderungen beim Entwurf und der Herstellung von IPWAAM-Verbindungsdetails zu koordinieren. Diese Pipeline integriert Roboter-, Material- und Funktionsanforderungen und ermöglicht durch die Verknüpfung der digitalen und physischen Modelle der IPWAAM-Verbindungen eine individuelle Anpassung des Designs auf der Grundlage der während der Produktion gesammelten Konstruktionsdaten, was zu einer neuartigen Herangehensweise für *adaptive Baudetails* führt.

Die Arbeit beinhaltet physikalische Experimente, um die Herstellungs- und Detaillierungskonzepte zu testen, und virtuelle Experimente, um die Herausforderungen ihrer Anwendung im Zusammenhang mit räumlichen Strukturen zu simulieren. Im Ergebnis zeigen die physikalischen Ergebnisse eine neuartige Methode für das Fügen von berührungslosen

Metallteilen. Letztlich bietet der adaptive Detaillierungsansatz eine Grundlage für computergestützte Detaillierungsaufgaben im Zusammenhang mit der Roboterfertigung, um die aktuellen Entwicklungen hin zu einer reichhaltigen und transparenten digitalen Baukultur zu unterstützen.

Acknowledgements

,

Contents

1 Introduction

This dissertation presents new joining and detailing strategies for the robotic assembly of spatial structures.[1] This chapter opens with the motivation and background of this research (Sections 1.1 and 1.2), followed by a summary of the challenges concerning robotic joining for spatial structures to date and the need of tailored detailing methods to address them (Section 1.3). The case study, research objectives and the proposed methods are outlined next (Sections 1.4 and 1.5). Finally, the thesis structure provides a roadmap with the content of each chapter (Section 1.6).

1.1 Motivation

This thesis exists in the context of the rise of a new digital building culture that is in the process of transforming how architecture is designed and built. At the core of this transformation lies a myriad of experiments in computational thinking, designing, and building with digital machines.[2] While the early exploration phase of computationally designed and manufactured architecture is crystallizing into consolidated efforts to transition from the laboratory to the industry, fundamental concepts core to architectural practice are still in transit from conventional disciplinary approaches. The work presented here aims to support this digital cultural transformation focusing on one unavoidable challenge in architectural production: the joining of distinct parts in space.

---

[1] A review of the key terms *joining*, *detailing*, and *spatial structure* used in this thesis is presented in Section 2.1.

[2] These experiments can be revisited in consolidated form in the proceedings of the most prominent computational research conferences held in the last three decades such as *ACADIA* (since 1981), *Advances in Architectural Geometry* (since 2008), *Design Modelling Symposium* (since 2011), *FABRICATE* (since 2011), and *Robotic Fabrication in Architecture, Art and Design* (since 2012), to name a few.

The way architecture has historically dealt with joining has cultural, economic, technological and material-based logics[3]. For the vast majority of the built environment, architecture presents patterns of joining organized by material domains, each of these presenting well-established techniques, tools, expertise, and trades.[4] Yet, the re-introduction of robots in architecture of the last seventeen years has shown different prospects for joining.[5] Instead of giving specification documents to a bricklayer, carpenter, or welder, scripted instructions are now sent to a robot to perform a variety of operations, including joining tasks. This specification aspect has a profound consequence for the designer who, now in explicit control of the construction process, requires a precise understanding of the constraints of diverse joining tools and materials (Figure 1.1).

<div align="center">(a)   (b)   (c)</div>
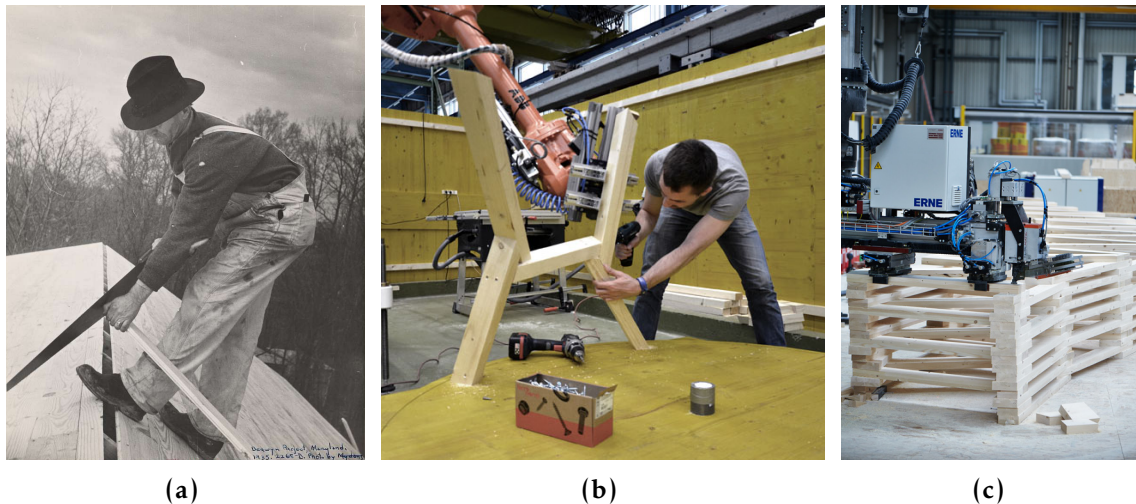
Figure 1.1: *Manual and robotic joining in timber: (a) A carpenter working on a roof, United States, 1936. Photo: Carl Mydans (Farm Security Administration Photographs), (b) Complex Timber Assemblies, Gramazio Kohler Research (2014), Photo: Gramazio Kohler Research, and (c) The Sequential Roof, Gramazio Kohler Research (2015), Photo: Andrea Diglas.*

---

[3]See *Studies in Tectonic Culture* for examples and *Style* for an interpretation of the origins of construction types (Frampton, 1995; Semper, Mallgrave, and Robinson, 2004).

[4]See examples organized by construction methods in *Constructing Architecture* (Deplazes, 2005).

[5]The first wave of robotic construction spans the decades of the 1980s and 1990s in Japan (Bock and Linner, 2015). A second endeavor with a focus on architectural applications was initiated at ETH Zurich in 2005 and followed by many research institutions in the late 2000s and the following decade and a half (Bechthold, 2010; Gramazio, Kohler, and Willmann, 2014).

These new challenges are illustrated by the diversity of the joining solutions explored in projects concerning architectural robotic assembly of the last decade (Gramazio, Kohler, and Willmann, 2014).[6] Within this context, exemplary projects have interpreted this new production context as a design opportunity for incorporating robotic constraints and detailing workflows as part of the computational design of the whole.[7] In alignment with this exemplary design and production approaches, this thesis argues that the lack of conceptualization of detailing methods required to tackle the numerous technical, logistical, and design challenges posed by joining for robotic assembly can result, in the long run, in a simplification of joining techniques to the trivial and intuitively feasible automation of manual production logics, leaving the inherent potential of digital design and fabrication underexploited.

The interest in scaling up algorithmic material logics from the component to the assembly goes hand in hand with maturing methods for designing and simulating non-standard performative structures. However, the robotic assembly of these structures is in its early development, and many of the problems concerning its joining are just starting to be studied and organized. In this context, this thesis takes the opportunity to focus on how to build the interfaces between robotically assembled parts. A case study in robotic additive joining in steel serves as a fruitful context for understanding the challenges and design opportunities of detailing for robotic assembly in alignment with the additive and algorithmic material logic of the whole.

1.2   Background

In the last decades, the research interest and development of digital technologies for the construction industry have experienced significant growth (Chan, 2020). A subgroup of digital fabrication (DFAB) technologies under the broad category of additive construction have taken the lead in this transformation as they build on principles particularly relevant in the AEC industry: (1) ability to produce on-demand

---

[6]A brief review of joining approaches in robotic assembly is discussed in Section 2.2.1.

[7]The most prominent example is the project *The Sequential Roof* by Gramazio Kohler Research which is reviewed in sections 2.2.1 and 2.2.2.

quantities, (2) of highly customized components, (3) with increased geometric freedom compared to standard manufacturing technologies, (4) reducing labor and improving productivity by replacing blueprints with digital instructions (Labonnote et al., 2016; Leary, 2020b; Tofail et al., 2018). Until recently, additive manufacturing principles were only applied to small scale parts and, therefore, relatively unsuitable for architecture besides model-scale prototyping. In the last decade, however, the development of robotic infrastructure has provided new ground for applying additive principles at a 1:1 scale.

(a)   (b)
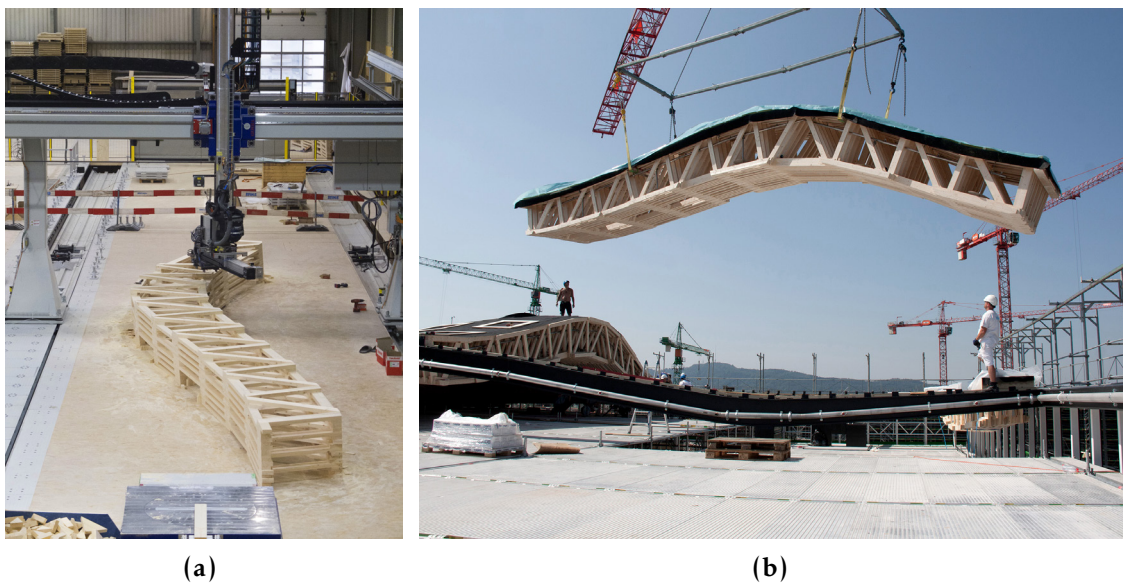
Figure 1.2: *Additive fabrication with robots: (a): Robotic assembly of a discrete-element prefabricated truss of The Sequential Roof, Gramazio Kohler Research (2014). Photo: A. Apolinarska, and (b) Assembly on site of trusses of The Sequential Roof, Gramazio Kohler Research (2015). Photo: A. Apolinarska.*

This is the case of mobile, cooperative, and large-scale robotic setups that provide an enlarged build space compared to enclosed additive manufacturing equipment (Ghaffar, Corker, and Mullett, 2020). Only very recently, breakthrough projects have demonstrated the suitability of robotic arms to assemble architectural-scale structures consisting of discrete elements (Figure 1.2). These results consolidate the first ten years of consistent developments in the field of robotic assembly in architecture following additive principles (Gramazio, Kohler, and

Willmann, 2014).[8]

This context counts to date with only a few full-size examples beyond the laboratory; however, the prospects of a robotic assembly approach are supported by numerous efforts across engineering disciplines that aim to radically optimize the use of resources and processes. As a result of these numerous efforts, spatial, non-orthogonal, and geometrically differentiated structures have been put forward as performance-driven structural solutions for small to long-span architectural structures (Figure 1.3). In this context, robotic arms provide the ideal materialization counterpart by being able to position parts in space without the need for additional scaffolding or bracing (Gramazio, Kohler, and Willmann, 2014, K. Wu, 2019, Bruun et al., 2021).
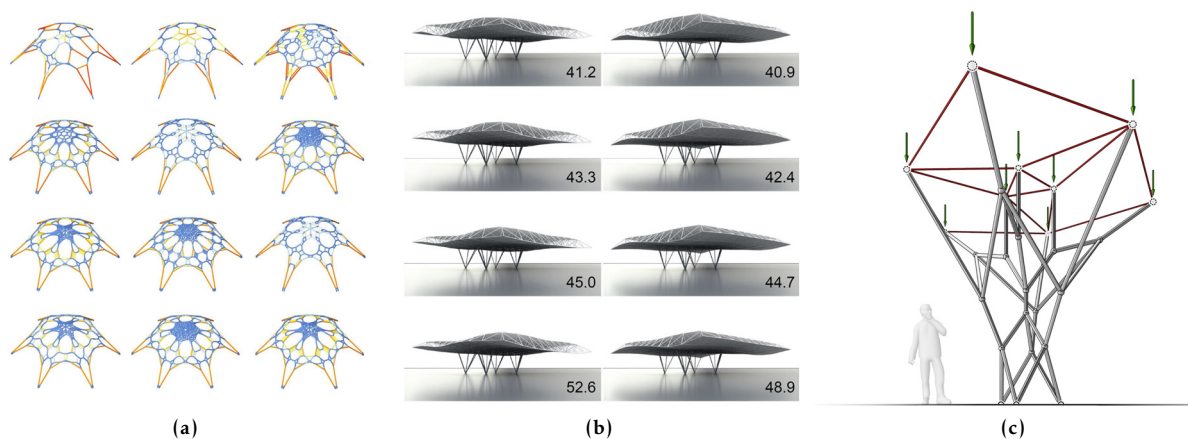
Figure 1.3: *Studies of performative spatial structures: (a) form-finding with machine learning (Zheng, Moosavi, and Akbarzadeh, 2020), (b) design subspace learning (Danhaive and Caitlin T. Mueller, 2021), and (c) form-finding using 3D graphic statics (Lee, Mele, and Block, 2018).*

Although promising, there are still numerous open challenges to realizing spatial structures robotically. In terms of assembly, extensive efforts have been made recently to deliver methods for designing, planning and building with robots (Willmann et al., 2016; K. Wu and Kilian, 2019; Parascho et al., 2017; Adel et al., 2018; Thoma, Jenny, et al., 2019; Y. Huang, Leung, et al., 2021; Y. Huang, C. R. Garrett, et al., 2021a). However, projects concerning the robotic assembly of spatial structures

---

[8]Previous keystone steps in the field of robotic assembly in architecture have been previously documented in Bock and Linner, 2015; Doerfler, 2018; Bonwetsch, 2015. Most notably, the work of John Bollinger, Xavier Mendoza and K. Wachsmann on the Location Orientation Manipulator illustrates the shifted focus from a mass-production to a mass-customization design paradigm (Bock and Lauer, 2010)

to date have predominantly focused on planning the robotic positioning and processing of elements, relying, in most cases, on manual procedures to join them (Figure 1.4). This context leaves the problem of robotic joining for spatial structures open for investigation.

<div align="center">(a)   (b)</div>

Figure 1.4: *Manual joining for robotic assembly: (a) Gradual Assemblies: insertion of wooden dowels (2018), Photo: Andreas Thoma, and (b) Lightweight Metal Structures: welding (2018), Photo: Martin Rusenov.*

1.3   Problem statement

As presented in Section 1.1, designing for and building with robots brings new requirements for the designer who, now in explicit control of production, needs to be knowledgeable in the possibilities of the joining tools and processes. In the context of joining spatial structures robotically, the new challenges for designers can be summarized in the following categories:

- Preparing the ground: understanding the possibilities and constraints of the robotic assembly setup and the reachable workspace between elements

- Joining: finding suitable materials and techniques compatible with spatial robotic assembly processes that provide ease of assembly and structural support

- Detailing: understanding the dependencies of fabrication, material, and functional constraints that are present at the interfaces between elements

The following sections discuss each category and its relevance to the thesis.

Preparing the ground

Setting up the scene: the robotic assembly setup

The first challenge of joining spatial assemblies with robots is the requirement of a multipurpose setup. Typically, at least one manipulator is required to support parts in space, and a second actuator -a multipurpose end-effector, a human, or an auxiliary machine or robotic manipulator- is needed to tighten, fix or dispense bonding material at the interface between parts. Only recently, tools for task and motion planning have been made accessible in the context of robotic construction (Y. Huang, 2022), opening the floor for advanced robotic manufacturing in the field of architecture. This work profits from these scientific and engineering advances to investigate the use of well-known robotic joining setups in the context of the robotic assembly of architecture scale.

Understanding the joining space: the spatial interface

Operating between objects is intuitively easy for dexterous humans. However, robotically manipulating tools and materials around objects requires an explicit understanding of the collision-free workspace. Moreover, the connection space becomes easily constrained in spatial assemblies, making the design space for joining less obvious. To solve the task of designing connections in such constrained spaces, the designer needs to understand early on where tools can access these spaces. This thesis presents planning methods for understanding the constrained connection space and maps it into a readable representation, so it can be used as a design canvas.

Joining

Joining spatially and additively: the need for new techniques and materials

The unprecedented challenge of robotically joining spatial structures of architectural scale requires selecting and testing suitable techniques and materials. To date, only a few robotic joining techniques are used in three dimensions, most notably robotic welding and filament winding. However, no project has investigated spatial additive joining during the robotic assembly process. This thesis investigates this additive joining scenario with a flexible and performative joining technique to allow the deposition of high-strength material in a wide range of geometric conditions.

Joining to fit: handling tolerances

Joining spatial structures presents the challenge of handling material tolerances in three dimensions. Manual assembly provides well-known correcting strategies such as working with malleable materials that can be sequentially accommodated to needs. Robotic assembly introduces the extra challenge of surveying and interpreting deviations at each stage of the construction process. This requires the integration of sensing technologies and design-and-production systems that can process and adapt to dynamic building data. This thesis puts these concepts into practice in a design-and-production adaptive pipeline.

Joining to support: integrating structural considerations

Joining has a first function to fix parts in place and transfer loads across elements to the supports. Therefore, a suitable location, mass, and distribution of the joining material at the interface must be found. However, very little is known to date about the material performance of these novel materials and printing techniques and their rigorous structural modeling approaches. This thesis proposes an early integration of structural considerations with robotic manufacturing constraints to support answering these questions and pave the way for further investigations in this direction.

Detailing

Integrating dependencies and constraints

The previously exposed challenges funnel back to the need to integrate often conflicting constraints. To date, different computational approaches investigate integrative methods for informing design with reachability, printability, structural and production performance (Bermano, Funkhouser, and Rusinkiewicz, 2017; Rolvink, C. Mueller, and Coenders, 2014). In this respect, spatial connections are a particularly telling place where the need for different expertise becomes evident.

Detailing, the core architectural task in the design, documentation, and control of how parts are joined together[9], is used here to pack the diverse problematics of design and fabrication of joining for spatial structures assembled robotically. This thesis argues that current detailing concepts and practices fall short of providing useful methods when using robots in the loop and presents the basis for an alternative approach: *adaptive detailing*.

1.4 Case study

> *You can't think seriously about thinking without thinking about thinking about something —Seymour Papert in* Mindstorms, *1980, p.10.*

Paraphrasing Papert, *we cannot think about joining without thinking about joining something*. This thesis practically explores the challenges mentioned earlier regarding preparation, joining, and detailing through an exemplary case study in additive joining tailored for the robotic assembly of lightweight steel structures.

The targeted building system comprises standard steel elements assembled in space in non-regular configurations without external support or scaffolding. The elements meet at varying conditions (cross, tee, or corners), and their degree of proximity can vary due to the potential accumulation of build-up tolerances. The spatial complexity of these

---

[9]See Key terms section for an expanded definition.

interfaces depends significantly on the symmetry of the cross-section
of the building members (e.g., I-shaped, circular, or rectangular) and
their relative orientation. The robotic assembly setup consists of two
robots: one robot is used to position parts, and a second robot is used
to join the parts together.

<div align="center">(a)   (b)</div>
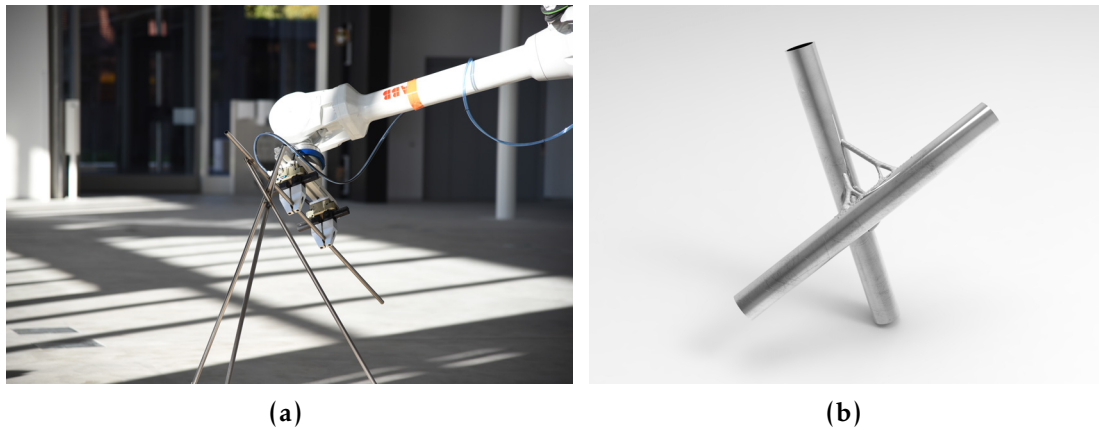
Figure 1.5: *Case study: additive joining for robotic assembly of spatial structures
in steel: (a) Precedent: Design and Robotic Assembly of Complex Lightweight
Structures, Gramazio Kohler Research (2014-2018). Photo: Stefana Parascho, and
 (b) Render of an additive joining prototype, Gramazio Kohler Research (2018).*

The selected joining method is a variant of the GMAW (Gas Metal
Arc Welding) process called WAAM (Wire and Arc Additive Manu-
facturing). GMAW joins elements by heating them to a molten state
and fusing them while adding additional joining material in between.
WAAM is a metal 3D printing technique based on the same melting, fus-
ing, and adding principle. It uses the same power source and deposition
tool and is coupled with a robotic system extending the conventional
process in three dimensions to precisely position material in space.

For the following reasons, joining steel elements with WAAM serves
as a case study for studying the new challenges and opportunities of
joining and detailing for robotic assembly of spatial structures:

In terms of the availability of tooling, industrial robotic welding is
one of the most widespread robotic processes found in industry (Hong,
Ghobakhloo, and Khaksar, 2014). This aspect allows for an integration
of off-the-shelf welding equipment with relative ease. Furthermore,

WAAM is currently under development as a novel additive manufacturing technique in many research centers around the world (B. Wu et al., 2018), which translates into interest from the industry to finance research and development in WAAM.[10]

Regarding the type of robotic infrastructure, the case study requires a multipurpose setup for cooperative assembly and welding. A cooperative setup of this type builds on precedents that have already demonstrated the versatility of multi-robotic assembly setups for lightweight metal structures (Figure 1.5a, Parascho, 2019). These precedents, however, have been joined by welding the elements manually. The integration of robotic joining within the robotic assembly of steel elements in non-regular configurations has not been investigated yet.

Regarding the joining technology and possible functionality for spatial assemblies, WAAM allows depositing material spatially with great versatility, i.e., in the tool orientation relative to gravity and relative to seam to print, as well as a broad material palette. The relatively high resolution of the WAAM deposition unit (as little as 3 mm of wall thickness) allows precise control of the connection geometry, potentially following optimal material distributions (Figure 1.5b). Moreover, the digital actuation of WAAM allows the deposition of joining material only *where* and *when* required, which in turn permits an adaptive control of the connection as needed during the buildup process. This last characteristic is suitable for accommodating the varying sizes and geometries of the interfaces, a convenient approach for handling a potential buildup of material tolerances.

Finally, in terms of the relevance of the results, steel structures are ubiquitous in architecture due to their structural performance (high strength relative to their weight). Due to its high carbon footprint, alternative building strategies for steel, such as reusing reclaimed components, is a critical field of research to support the rational use of limited resources. To this end, the versatility of joining with WAAM could be explored to provide a second life for reclaimed steel elements that often present varying dimensioning or surface conditions that impose uncertainties at the assembly stage.

---

[10]In this case, the Cold Metal Transfer setup was provided by Fronius Switzerland.

1.5   Objectives and methods

This thesis aims to explore the challenges and opportunities of joining and detailing for robotic assembly through the presented case study in making use of the WAAM technology to additively build up steel (Section 1.4). The objectives of the research consist of the concurrent development of an exemplary additive robotic joining technique (Objective 1), a detailing pipeline for the computational design and robotic production of connections (Objective 2), and the validation of both the joining technique and detailing pipeline through physical demonstrators (Objective 3).

Objective 1: Development of an exemplary additive robotic joining technique

The first objective is the practical development, testing, and validation of a robotic joining technique using additive manufacturing tailored for the robotic assembly of lightweight metal spatial structures. The joining technique is referenced in this thesis as in place WAAM, or IPWAAM in short. This objective first comprises the engineering of a suitable experimental setup for robotic welding, including sensors for the localization of base elements and surveying of printed material. Second, the objective entails the testing and development of execution procedures for robotic metal deposition, testing of suitable process parameters, and evaluation of material results. Third, suitable communication protocols for the online control, recording, evaluation, and updating of physical parts and deposited material are required. These objectives are developed empirically in an interdisciplinary setting and validated through physical experiments. The iterations of the robotic setup, IPWAAM procedures, and experiments are presented in Chapter 3.

Objective 2: Development of an adaptive detailing pipeline

The second objective is the development of a detailing pipeline to design and build IPWAAM connection details of discrete elements assembled by robotic means. This point focuses on the development of computational methods to integrate fabricability constraints imposed

by the robotic setup and to respond to the functional requirements during production, such as adaptive fitting, and after production, such as load transfer of structural members. The objective is achieved by a combination of design and engineering software development with physical and virtual testing. The design and fabrication components of the proposed pipeline are presented in Chapter 4.

Objective 3: Demonstrate the proposed approach to joining and detailing

Finally, the third objective is to explore and understand the versatility and design opportunities of additive joining and adaptive detailing. This is achieved through two sets of demonstrators. The first set, the IPWAAM connections demonstrators, builds cumulative knowledge on the joining technique (Objective 1) and enables the software development of the detailing pipeline (Objective 2) through the integration of the fabrication and computational design workflows. The second set of demonstrators, the structures with IPWAAM connections, are design opportunities to speculate on how to deploy the joining technique and the detailing pipeline in larger assemblies and (virtual) robotic assembly scenarios. The sets of demonstrators are presented and discussed in Chapter 5.

In sum, the thesis explores the in place WAAM *joining*, a robotic fabrication technique for joining metal lightweight components suitable for robotic assembly of spatial structures, and its computational design counterpart, the adaptive *detailing* pipeline. Finally, the thesis tests the integration of both fabrication technique and computational design in cumulative demonstrators.

1.6   Thesis structure

Chapter 1 The *Introduction* chapter has dealt with the motivation and context of production of this thesis, the challenges presented by robotic joining for robotic assembly of spatial structures, the case study subject of this thesis, and finally, the thesis' objectives and methodological steps to achieve them.

Chapter 2 The *Literature review* chapter presents conceptual tools, such as key terminology and the context of inquiry, in more detail.

Chapter 3 The *In place WAAM* chapter describes the joining technique presenting its parts in terms of the experimental setup, software, materials, procedures, and experiments.

Chapter 4 The *Adaptive detailing* chapter presents the components of the detailing pipeline for the design and fabrication of IPWAAM connections.

Chapter 5 The *Demonstrators* chapter presents physical and digital demonstrators and discusses learnings and approaches found in the application of IPWAAM for adaptive detailing with robots.

Chapter 6 The *Conclusion* summarizes the thesis results, identifies the contributions and discusses their implications along the directions for future work.

Appendix A The *Experimental data* includes the process parameters and results of experimental tests presented in Chapter 3.

Appendix B The *Virtual experiments* contains additional connection results of the virtual demonstrators presented in Chapter 5.

Appendix C The *Project credits* acknowledges contributors to the thesis.

2 Literature Review

This chapter first provides a guide of key terms and their definitions in the scope of this thesis. Then, it broadens the problem statement by presenting state-of-the-art examples of the current challenges regarding setting up, joining, and detailing presented in the introduction. Finally, based on the points discussed in this chapter, the research aims are presented.

2.1 Key terms

Spatial structure is a term to indicate a structure consisting of discrete elements organized in a three-dimensional configuration. The term overlaps with space frame, space structure, and space grid, which are regular, rigid, lightweight, truss-like, versions of spatial structures (See examples in Chilton, 1999). Elements of spatial structures are usually homogeneous in one or more properties (material, cross-section, or mass). In this thesis, the term *spatial structure* is used as a synonym for a three-dimensional structure of a non-repetitive and non-orthogonal configuration of linear elements.

Joining is a broad term to describe the process of combining distinct parts to form a continuous whole (Messler, 2004). The similar term *jointing* is used in architecture to describe the same process introduced above (see examples in Deplazes, 2005); however, also used in other trades to describe unrelated processes such as straightening or sharpening ("Edge jointing" 2022; "Jointing (sharpening)" 2022). The term *joining* is preferred in our context as it connects the present work to the literature on mechanical engineering (Roth, 1994a) and material sciences (Messler, 2004). For example, Messler's classification of joining by physical, chemical, and mechanical forces that are present at the interface helps us to differentiate the respective robotic joining processes

based on fusion, adhesives, and mechanical attachments mentioned in this chapter (see 2.2). Beyond these background examples, in this thesis, the term joining will be used to describe the fusion-based WAAM process conducted robotically, spatially, and additively (see 2.3).

Detailing in architecture is a task that encompasses the *design*, *documentation*, *and control* of the dependencies of the different systems of construction. In this thesis, the term detailing is used to denote a computational system that includes: (1) the *design task* of integration of robotic fabrication, functional, material constraints, and formal aspirations to resolve the joining of discrete spatial assemblies, (2) the *communication* of production data between the digital model and the robot controller, and (3) the *surveying*, *evaluation and (if required) adaptation* of the digital model of a connection detail to match the physical results built robotically.

Detail is a multivalent term (Ford, 2011; Kumpusch, 2016; Schor, 2007; Shelden, 2014). The term comes from the old French *détail* to refer to "a small piece or quantity", lit. "a cutting in pieces", where *de-* denotes separation and *-tail* refers to a "cut" or "piece" ("Detail" 2022). In architecture and engineering, "detail" most prominently refers to (1) the place or part where different elements of construction come together; and (2) the description or blueprint of such part of the construction. While there is consensus on (1) and (2), designers have different approaches to the concept of detail and what it refers to in the scope of each work (Schittich, 2000). In this thesis, the term detail refers to a connection detail.

Connection detail is a term that refers to the interfaces, or set of components, that keeps the elements of a structure together. The term also refers to the description or blueprint of such interface or part. Depending on the building system, connection detail can be replaced by a more specific term: e.g., node, joint, fixture, union, attachment, junction, juncture, link, bond, knot, or tie. An additional distinction can be made for standard connection details in steel: *connection* is used when referring to the discrete connecting components, and *joint* is used when the zone of interaction among the members of the structure is

considered ([Jaspart, 2016](#)). Regarding the case study in steel focus of this thesis, the term can be extended with these categories:

Planar, spatial A distinction between planar and spatial connection details can be made according to the predominant spatial dimensions needed to describe their interfaces. A *planar* interface can be fully described in two-dimensional space (x, y), while a *spatial* interface can only be described in three dimensions (x, y, z). The increase in complexity from planar to spatial connection details is discussed in Section [2.2.2](#).

Prefabricated, in-place, in situ The production location makes a second distinction. *Prefabricated* connection details are produced in a separate and prior process to the assembly. In steel and timber, this type of connection detail is called 'node' (See examples in [Meyer Boake, 2020](#)). *In-place* connection details are produced during the assembly process, in the workshop, or pre-assembly facility. *In situ* connection details are produced in the final location during the final assembly process on-site.

Standardized, bespoke, adaptive The last distinction relates to the flexibility of the design approach and manufacturing technique. *Standardized* connection details are mass-produced in large quantities with a limited number of types. *Bespoke* connection details are mass-customized according to pre-defined needs *before* production starts. *Adaptive* connection details are mass-customized before and *during* the production process.

This thesis is concerned with the spatial in-place adaptive connection details of spatial structures in steel.

2.2 Preparing the ground

This section organizes the unprecedented challenges the designer of spatial structures confronts concerning the robotic infrastructure and planning of joining tasks. *The robotic assembly setup* presents projects using computational design, advanced engineering, and robotic planning methods to illustrate the close relationship between the capabilities of the assembly setup, the material system, and the choice of joining

techniques. *The spatial interface* discusses the increased workspace constraints found in the interfaces of spatial assemblies through prototypical architectural material systems built by robots.

2.2.1   The robotic assembly setup

As presented in Section 1.3, the first challenge of robotic joining for spatial assemblies concerns the capabilities of the assembly setup. Beyond the specifics of the material system, the challenge resides in adding a bonding material or a locking mechanism at the interface at the right time while counteracting the joining forces applied to the assembly. This section discusses three different setup approaches and associated methods to solve these problems. *Multi-functional end-effectors* discusses the use of robotic manipulators with enhanced actuation capabilities for joining. *Human-machine collaborations* presents examples using robotic manipulators to position parts and collaborate with dexterous humans to join them. *Divide and conquer* discusses hybrid approaches using cooperative robots and machines to extend the robotic setup's capability space.[1]

Joining with multi-functional end-effectors

A common approach to robotic joining is to combine manipulation and joining tasks in a multi-functional end-effector. This approach has been particularly reliable when stacking parts with planar interfaces. In the project *Voxels* (Figure 2.1a), an end-effector is used for placing foam bricks and dispensing glue at the interface to join them (Gramazio Kohler Research, 2009). In the assembly of *The Sequential Roof* (Figure 2.1b), a nailing gun is attached to the robot manipulator to swiftly fix parts during the pick-and-place operation (Apolinarska et al., 2016). Both examples benefit from co-planar interfaces and the contribution of the force of gravity to fix parts in position without affecting the stability of the already assembled elements.

Fewer examples of this approach are found in the context of spatial discrete element assemblies. An exceptional case is the placing and joining of steel rods of the *Mesh Mould Metal* wall (Figure 2.1c), where

---

[1]Useful terminology of robot workspaces can be found in Zacharias, Borst, and Hirzinger, 2007.

a higher degree of functionality was needed to fix parts in space. Here, steel rods are fed, bent, cut, and welded -through resistance welding- on demand at the interface. The tool head is an engineering achievement that requires the iterative development and testing of custom solutions and integration of a referencing system using camera-based sensing (Kumar et al., 2017; Lussi et al., 2018; Buchli et al., 2018).

These exemplary cases show a range of complexity in engineering development, from relatively accessible tools and control methods to highly-sophisticated fully-automated solutions. In the context of industrial- or business-based applications, adjacent automated industries show that a *compound fabrication approach*[2] can provide large benefits increasing the manufacturing speed and part accuracy and reducing part costs and *"shop burden"*, i.e., reduced number of machines and space (Bi, 2011). However, while the efficiency of the process through an early investment in the proper tooling and development can approach the two orders of magnitude (Buchli et al., 2018), the high degree of expertise of the development team and starting costs could likely deter research projects not substantially funded from exploiting this approach.

| (a) | (b) | (c) |
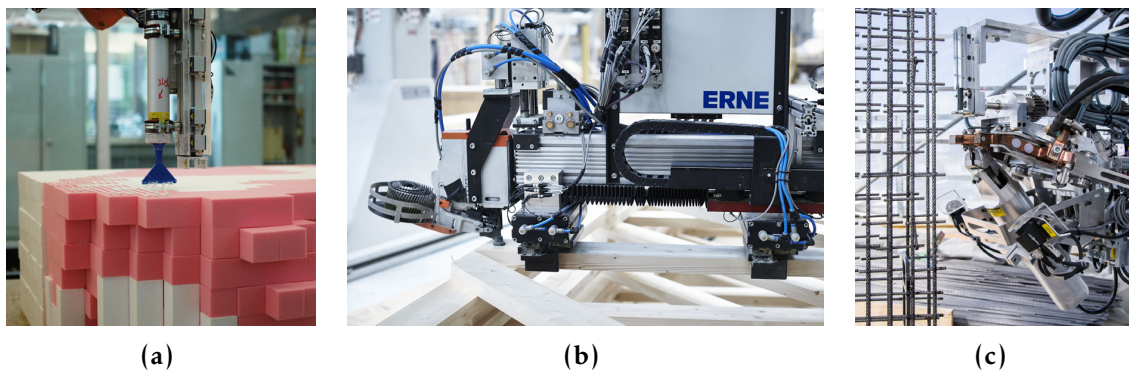
Figure 2.1: *Multi-functional end-effectors in previous Gramazio Kohler Research projects: (a) Voxels: manipulation and glueing (2009). Photo: Gramazio Kohler Research, (b) The Sequential Roof: manipulation and nailing (2015). Photo: Andrea Diglas, and (c) Mesh Mould Metal: feeding, bending, cutting, and resistance welding (2017). Photo: Roman Keller.*

---

[2]Compound approach refers to a fabrication setup that *"supports multi-functional and multi-material processes"*. See Keating and Oxman (2013) for terminology and outlook (Keating and Oxman, 2013).

Human-machine collaborations for joining

Extending robot capabilities (i.e., accuracy, precision, geometric versatility, robustness) with human capabilities (i.e., dexterity, autonomy) has been frequently exploited in the context of robotic assembly in architecture. Across different material systems, from single to multi-robotic setups, human collaborators have been key to solving the new challenges of joining spatial assemblies.

The stream of research on spatial timber assembly developed at Gramazio Kohler Research in the last decade can illustrate the challenge of handling joining forces in collaboration with humans. For example, in *Shifted Frames* (Figure 2.2a), low-grade timber elements are positioned spatially, leaving tight spaces for joining operations. Here, the low accessibility of the interface was not a design constraint, as an abundance of manpower was able to tackle this challenge efficiently. In *Complex Timber Structures* (Figure 2.2b), a single robotic arm is used to cut and position parts, while humans insert mechanical attachments at the interface. The amount of force needed in the drill can easily be controlled manually while the robot arm supports the exerted force on the structure during the drilling operation[3]. The much less dense frame of the spatial timber components for the *DFAB House* (Figure 2.2e) also benefits from a similar collaborative strategy, in this case between two robots and a human, to preserve the skeleton's integrity during the forces imposed by the insertion of screws (Thoma, Adel, et al., 2019; Adel et al., 2018). In *Gradual Assemblies* (Figure 2.2c), a robot supports timber slats while a human inserts and hammers in tight timber dowels (Thoma, Jenny, et al., 2019).

---

[3]A review of the reasoning behind the use of T-butt joints in robotic assembly can be found in A. Apolinarska's thesis, "Complex Timber Structures from Simple Elements" (Apolinarska, 2018)
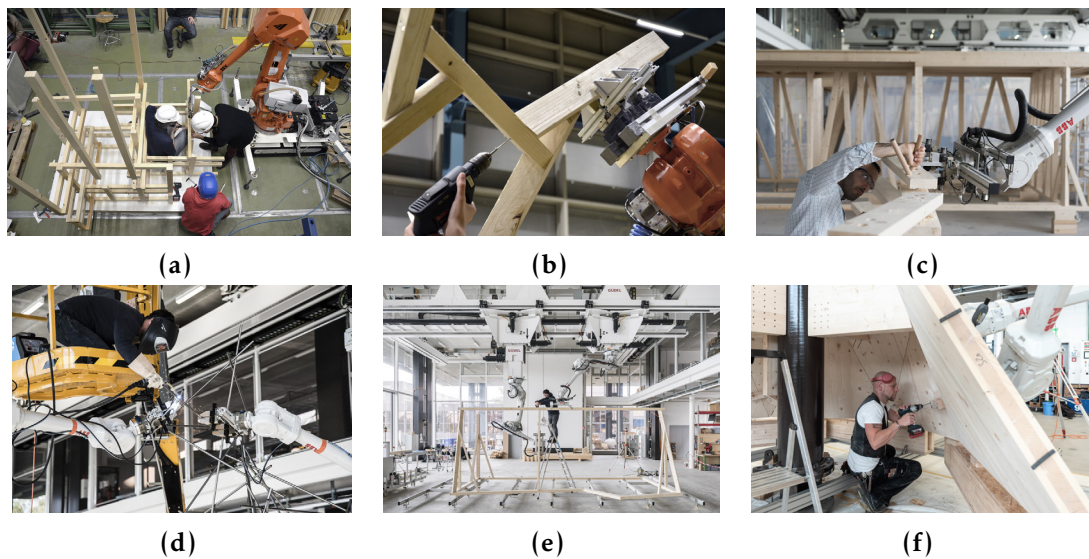
Figure 2.2: *Human collaborators in previous Gramazio Kohler Research projects: (a) The Sequential Structure: drilling and inserting screws (2013). Photo: Gramazio Kohler Research, (b) Complex Timber Structures: drilling and inserting screws (2013), (c) Gradual Assemblies: insertion of wooden dowels (2018), Photo: Andreas Thoma, (d) Lightweight Metal Structures: welding (2018), Photo: Martin Rusenov, (e) Spatial Timber Assemblies: (2018) Photo: Roman Keller, and (f) Semiramis (2021), Photo: Paschal Bach.*

The later examples using multi-robotic setups have in common the need for computational design and planning methods to enable feasible and stable assembly sequences (Y. Huang, C. R. Garrett, et al., 2021b). This is as well the case of the cooperative robotic assembly of *Metal Lightweight Structures* (Figure 2.2d), where two robots are used to support parts in place while a human operator manually welds them. Here, the reachability of the node decreases over time while more bars are added, a constraint that is efficiently resolved by manual welding operations and planning sequences (Parascho, 2019; Gandia, 2020). An extreme case of computational design and planning development is the *Semiramis* project (Figure 2.2f), where four robots synchronously assemble components of a folded timber shell while humans insert temporary locking elements before filling the interfaces with the bonding agent (Gramazio Kohler Research, 2022).

The benefits of robot-human collaborations are manifold. First, the examples show that manually executed tasks can reduce the imposed force on the structure during assembly (Thoma, Adel, et al., 2019), which is particularly relevant in spatial assemblies where moment

forces are often present at the interfaces. Second, these collaborations show efficiency in the continuity of the fabrication workload. In *Semiramis*, for example, while robots position groups of four timber plates spatially, humans can work simultaneously fixing the plates in their relative position and injecting the bonding adhesive. Third, manual operations are usually able to deal with imperfections and tolerances. In the case of fusion-based processes such as welding, it allows dealing with the build-up of tolerances ad-hoc during construction. However, a series of challenges are present when manually joining in the context of multi-robotic setups. First, providing robust safety plans for human operators and quality control of the manual joining operations can be a limiting factor for the scalability of the approach. Second, accessibility to the joining workspace needs to be considered early on, as interfaces can get easily overpopulated with manipulators and their additional surveying devices. Finally, although highly dexterous and flexible, humans present limited accuracy, precision, and payload handling, which limits the type of joining tooling and techniques that can be employed.[4]

Divide and conquer: cooperative and distributed joining approaches

Synchronized assembly and joining operations in multi-robotic setups are state of the art in adjacent industries (Sawik, 1999). Different strategies are used to increase the reachability of the joining interfaces, such as including additional degrees of freedom for the re-orientation of the workpiece. In the context of a spatial assembly, that is often not possible due to the size of the building volume. In *Timber Assembly with Distributed Architectural Robotics* (Figure 2.3a), the reachable workspace of a robotic arm is extended with synchronized robotic clamps to locally handle assembly forces imposed on the structure and possible build-up tolerances (Leung et al., 2021).

Other future-looking directions to enlarge the reachable robot workspace consider cooperative distributed approaches such as extensible, climbing, or flying robots. For example, in the project *SpiderFab* a joiner spinneret is used for bonding on-orbit extruded assemblies (Hoyt et al., 2016, Figure 2.3c). At a more tangible scale, a modular robot with an integrated drill and screw feeder is used for assembly

---

[4]See Matheson et al., 2019 for additional context and terminology.

and joining layer-based timber structures (Leder et al., 2019, Figure 2.3b). These visions present an encouraging outlook for the assembly of large-scale structures.

This thesis targets a building scenario where cooperative machines are used for assembly and joining, in this case, using an off-the-shelf robotic setup. In this domain, key areas of research include the development of tools for planning stable and reachable assemblies (Y. Huang, C. R. Garrett, et al., 2021b; Y. Huang, Leung, et al., 2021), hardware and software for design, communication, and manipulation of collective robotic construction (Petersen et al., 2019), and integration of capability maps for designing within the robotic constraints of the assembly setup (Porges et al., 2015).

| (a) | (b) | (c) |
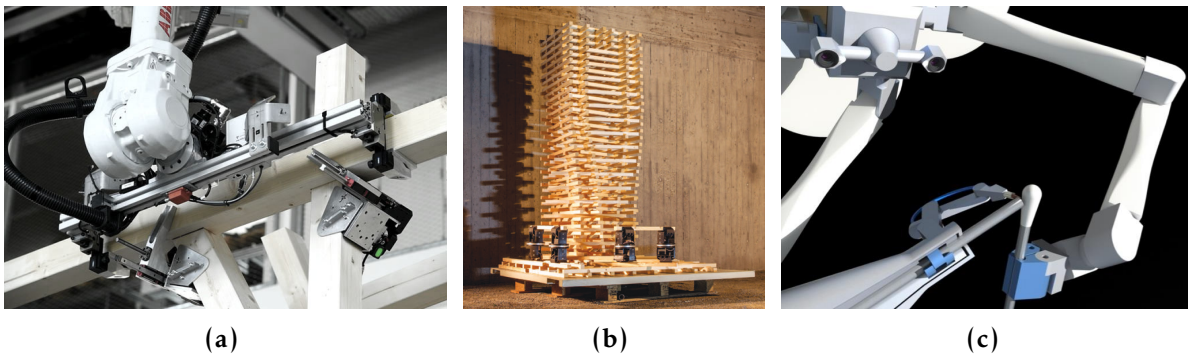
Figure 2.3: *Cooperative and distributed: (a) Timber Assembly with Distributed Architectural Robotics, Gramazio Kohler Research (2021). Photo: Victor Leung, (b) Distributed Robotic Timber Construction, Institute for Computational Design and Construction, Samuel Leder, Ramon Weber (2018-2019), and (c) SpiderFab (2013-2016) Photo: Innovative Advanced Concepts (NIAC), NASA.*

Conclusion

In short, the integration of joining in robotic assembly processes is a complex task that can be solved in many ways. A few remarks can be made based on existing approaches. First, it can be noted that increasing the number of robots in the assembly setup does not ensure that robotic joining provides a benefit in terms of time, material efficiency, or quality over manual joining. Second, project patterns suggest that a multi-robotic setup, a multi-functional end-effector, or the integration of auxiliary machines is a prerequisite for integrating robotic joining in

the robotic assembly setup.[5] Third, it is observable that the complexity of development and design for multipurpose setups increases quickly. However, current research proposes that when building approaches are backed by computational methods, the specifics of the setup should not significantly change the design and production pipeline (Y. Huang, Leung, et al., 2021). This thesis builds on these principles, aiming to provide concepts and methods for detailing that encourage an early understanding of the robotic setup capabilities and constraints to support the design of novel material systems.

2.2.2   The spatial interface

The second challenge of robotic joining concerns moving and operating in the space between elements to be joined. Humans count on spatial awareness and perception systems that allow them to easily move around obstacles. However, the robotic manipulation of tools and materials in constrained spaces is not as straightforward. Designing interfaces to be built by robots requires the designers' understanding and description methods of the collision-free space where tools and materials can be placed.

This constraint at the interface becomes more relevant in the context of spatial assemblies. As Dennis Shelden puts it, *the connection details are telling places where to assess the complexity of a structure, as is in the connection where the structure exposes its formal complexities* (Shelden,

---

[5]This complexity in the setup can partially explain why, to date, there are so few examples of full integration of robotic joining in robotic assembly.

2014).[6] Shelden's observation follows William J. Mitchell's design complexity definition as a ratio between design and construction content. In "Constructing Complexity", Mitchell explains how shapes with more input parameters are more "costly" to manipulate, yet they provide more adaptation opportunities to external needs (Mitchell, 2005).[7] From this perspective, it follows that a range in complexity exists in the interfaces between parts and that the amount of control/expense can be calibrated towards the project needs. In the context of robotic assembly, this range of complexity can be traced from layer-by-layer to spatial assemblies (Figure 2.4). This section revises four additive robotic joining projects presenting planar to spatial interfaces to illustrate this point.

(a)   **(b)**   **(c)**
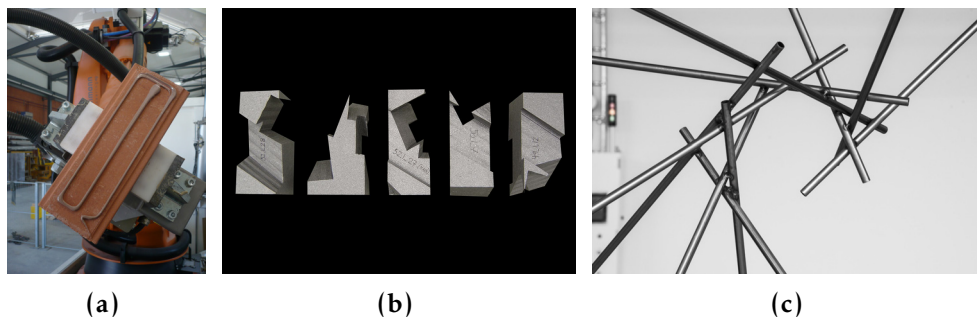
Figure 2.4: *From planar to spatial interfaces: (a) Flexbrick: a planar interface with orthogonal bonding pattern (2010). Photo: Chang Zhang, (b) The Catenary Pavilion: interlocking interfaces fabricated with a planar wire cutting (2010). Photo: Andrea Kondziela, and (c) Robotic Lightweight Structures: spatial interfaces defined by the bars double-tangents (2014-2018). Photo: Stefana Parascho.*

---

[6]In "Information, Complexity and the Detail", Shelden elaborates on this point backed by illustrative examples. He claims: "It would seem self-evident that today's non-Euclidean geometries are more complex than the orthogonal constructs of the past, and that the widespread availability of computing at vast scales and low cost has afforded architecture unprecedented capabilities to tractably manage and manipulate this complexity. An arc is more complex than a line, a sphere than a plane, and a curve or curved surface is considerably more complex still. A system for fabricating planar or space curve joints requires more complexity - more degrees of freedom, more gears, more memory and information processing - than one that produces a linear break edge. (...) From a computational perspective, we can see the increasing complexity of these richer shapes through the lens of their geometric descriptions: increasingly complex functions requiring higher-order factors, more nodes, and more data. We can simply say that the complexity of a project is proportional to the number of parameters necessary to describe it - a number that increases exponentially as form expands from planar to complex geometry, concept to detailing, and digital to physical space" (Shelden, 2014).

[7]See Mitchell, 2005 for an eloquent example on this point.

The planar interface of the brick adhesive bond

The brick components of the *Gantenbein Winery* present a stereotypical planar interface (Figures 2.5a-2.5b). In this case, the need for a reliable and automated bricklaying strategy resulted in replacing mortar with adhesive (Bonwetsch, 2015). This robotic constraint simplified the bonding interface from a three-dimensional manual laying of bricks to a two-dimensional control of the bond.[8] The planar interface results from the intersection of the faces of two stacked bricks. Within this planar region, the line segments that describe glue paths can be placed parallel to the axis of the wall to resist frontal loads (Bonwetsch, 2012; Gramazio, Kohler, and Willmann, 2014).

The planar interface of the timber-nail connection

A more complex planar interface can be found in the multi-layered nailed connections of *The Sequential Roof* (Gramazio, Kohler, and Willmann, 2014, Figures 2.5c-2.5d). Here, a feasibility bonding area is filled by a nail-fitting algorithm according to fabrication, structural, and building code requirements (Apolinarska et al., 2016). Although laid out in two dimensions, the algorithm needs to satisfy ten other neighboring interfaces, which, eventually, if no solution is found, affects the size of the slats across the entire truss section (Apolinarska, 2018). The chain of dependencies in three dimensions makes the order of complexity of this interface several degrees higher from the previous example. The complexity is such that the detailing workflow required significant efforts and integration of experts, becoming a milestone in computational design and fabrication. Inversely, complexity is significantly reduced at the fabrication stage. The nailing pattern is translated into x, y coordinates for the actuation of the nail gun, a simple and reliable task for the multipurpose end-effector (Figure 2.1b). Ultimately, the gains are enormous: the algorithmic control at the interface allows the reduction of material consumption by 59% compared to a non-optimal worst-case design scenario (Apolinarska, 2018).

---

[8]This simplification, however, created the challenge of controlling material tolerances, which can be handled by the flexible mortar interface.

(a) **(b)** **(c)** **(d)**

(e) **(f)** **(g)** **(h)**
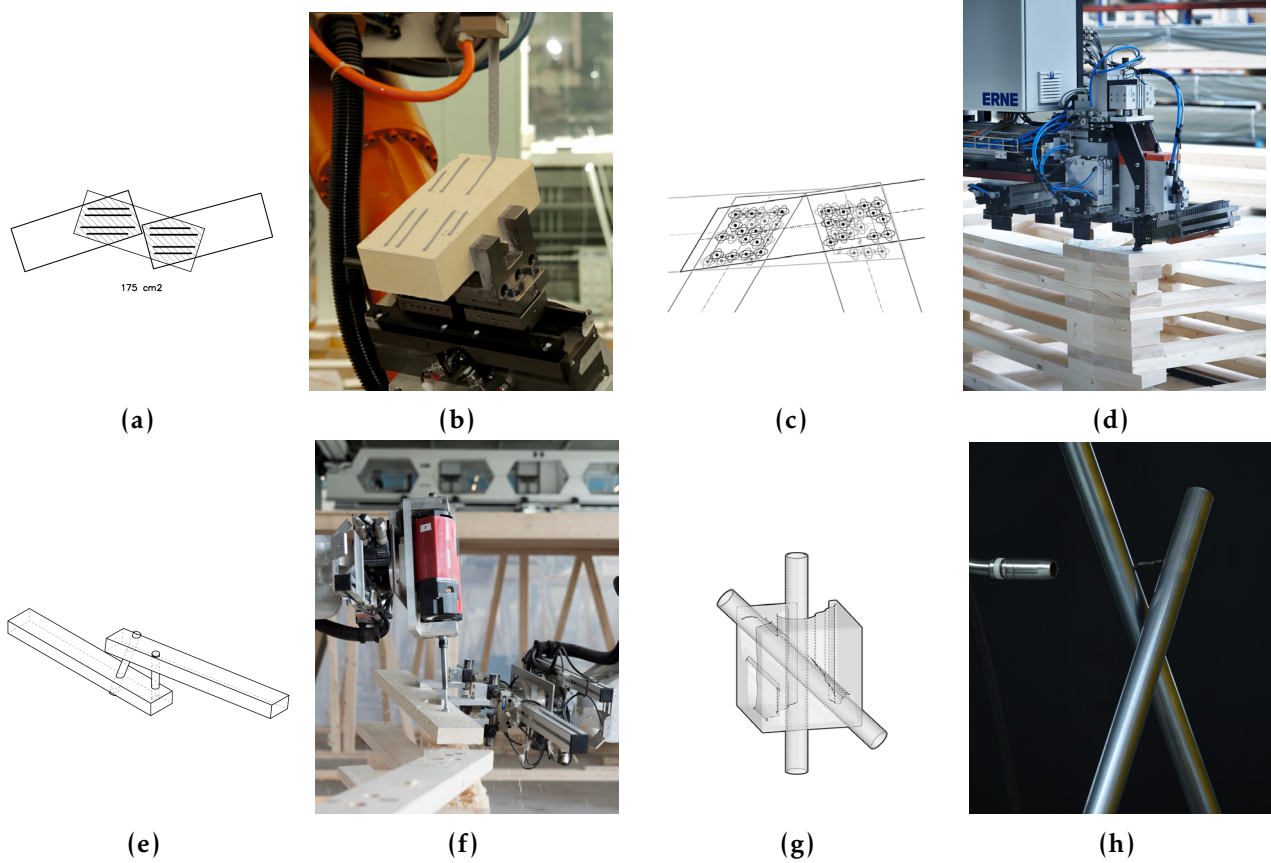
Figure 2.5: *Additive joining in robotic assembly by Gramazio Kohler Research: (a-b) Gantenbein Winery: planar glue paths (2006) Photo: Michael Lyrenmann, (c-d) The Sequential Roof (2016), Photo: Andrea Diglas (e-f) Gradual Assemblies (2018) Photo: Andreas Thoma, and (g-h) In place Detailing (2018).*

The spatial interface of the timber-dowel connection

The project *Gradual Assemblies* proposes a variation of the layer-based construction system of *The Sequential Roof* replacing the nailed connection with a pair of timber dowels (Figures 2.5e-2.5f). The dowel acts as a spatial connection that can transfer forces in different orientations. The production of the spatial connection utilizes a cooperative robotic setup where one robot holds a part in space while a second robot drills a hole at the correct angle through two consecutive slats.[9] The drilling angle is constrained by the eventual collision between the two robotic arms and the previously assembled slats; therefore, rules to generate drilling vectors were introduced. The angle of the dowels can be informed by successive structural requirements and design considerations, provided that a different angle between dowels is used to assure a mechanical lock between slats (Thoma, Jenny, et al., 2019). The final step consists in manually hammering in the dry dowel to lock the slats in place. In this case, the design space of the location of the timber dowels is loosely constrained. The dowel position needs to satisfy the drilling trajectory performed in a 6+3 axis robotic setup, which is positioned in the non-blocked area above the slat.[10] The result is a spatial interface composed of four divergent geometric objects: the two noncoplanar faces of the timber slats and two unaligned timber dowels (Thoma, Jenny, et al., 2019).

The spatial interface of in-place WAAM connections

The final example, main subject of this thesis, is a spatial interface entirely built robotically with the in place WAAM joining technique (Figures 2.5g-2.5h). The interface consists in a variation of the previously investigated material system proposed in Parascho, 2019 (Figure 2.4c). Here, a pair of non-touching tubular elements positioned at custom orientations are joined with an in-place additively manufactured connector. This strategy targets a cooperative setup where an assembly robot supports the element to join in space, while a second robot operates *in between* as opposed to *on top* of the elements to join

---

[9]The drilling is manufactured in-place as a type of "sequential processing" tolerance handling method, see categories in Section 2.3.2

[10]See Wan, Harada, and Nagata, 2016 for terminology and examples of assemblability constraints.

them. This building scenario creates a highly constrained design space and a subsequent need for relevant methods for finding collision-free printing trajectories.

Conclusion

In sum, the transition from manual to robotic operations and planar to spatial interfaces present new challenges, such as satisfying force transfer in three dimensions and the lack of intuitive solutions for finding feasible manufacturing trajectories. The higher the geometric complexity and fabrication constraints at the interface, the higher the complexity in describing and intuitively understanding the connection design space (Shelden, 2014). This complexity "cost," however, can be traded off by the inherent flexibility of the part positioning and, in the case of non-touching parts, by removing the need for part pre-processing and designed-in connection features.[11]

2.3 Joining

In the previous sections, examples have been reviewed showing how a robotic setup enables more degrees of freedom in the placement of elements in space. This freedom in movement creates a new type of connection point at the element-element scale called here *spatial interface*.

This section elaborates on three open challenges of joining spatial interfaces robotically. *Joining spatially and additively* revises the need to find suitable techniques and materials and discusses spatial joining examples to date, including welding and WAAM, the subject of this research. *Joining to fit* describes the need for tolerance handling methods in the context of robotic assembly and categorizes known strategies that are relevant to this context. Finally, *Joining to support* contextualizes the need for integrative structural analysis at an early stage of the design process.

---

[11] Part *pre-processing* refers to any processing technique required in advance of joining, such as machining a miter or notch to fit two elements or drilling and tapping a face to fit a screw. Designed-in features refer to any pre-machining work required to interlock, fit or fix parts, typically present in elements with integral-mechanical attachments (Messler, 2006).

2.3.1   Joining spatially and additively

As per our definition (see Section 2.1), joining is not always performed additively -by *add*ing material in-between parts-. The counter-example of additive joining is joining by integral mechanical attachments, where features embedded in the interfaces of the parts transfer forces through friction. Examples of integral mechanical attachment in robotic assembly can be found for both naturally occurring (Johns, Wermelinger, et al., 2020) and designed-in features (Robeller, Weinand, et al., 2017; Leung et al., 2021). On the opposite side of the joining spectrum, additive joining consists of *added* mechanical attachments, adhesives, or filler materials.

This thesis focuses on the additive joining scenario, as considerably less research has been done in this domain. This section first presents precedents in additive spatial joining in the context of digital fabrication featuring *Fibers and adhesives* (2.3.1.1) and then introduces in more detail the joining technique focus of this thesis in *Welding and WAAM* (2.3.1.2).

2.3.1.1   Fibers and adhesives

Fibers and adhesives are two malleable materials that have been identified for additive and spatial joining on different occasions.
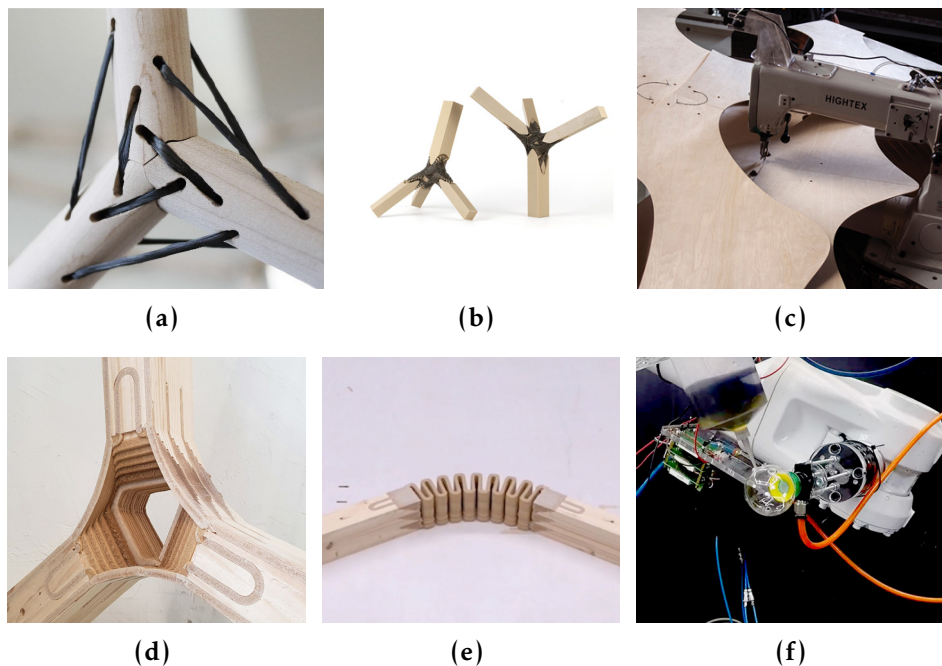
Figure 2.6: *Spatial additive joining with fibers and adhesives: (a) Fibrous Timber Joints (H. Wagner et al., 2021), (b) Controlled Anisotropy, Institute for Computational Design and Construction (2021), (c) Fiber sewing in veneer (Alvarez et al., 2019), (d,e) DualAdditive Manufacturing (Menges, H. J. Wagner, et al., 2020), and (f) Spatial Glass Bond (Sheng et al., 2019).*

Fibers Robotic placement, winding, and sewing of fiber are currently studied as alternatives to steel-wood and steel-steel connections. These techniques require continuity and proper tension on the fiber. To this end, recent projects have tackled cooperative fiber placement using mobile and flying machines (Yablonina and Menges, 2018; Menges and Knippers, 2020). However, using fibers for joining discrete elements has only been explored manually (Figures 2.6a-2.6b, and Dackweiler et al., 2019), or performed in surface-based motions where workspace considerations are considerably reduced (Figure 2.6c).

Adhesives Adhesive bonding shares many characteristics with additive manufacturing. An example of additive joining in timber is the form-fitting *DualAdditive* process which combines assembly and joining tasks (Figure 2.6e). The assembly of non-touching elements is performed on a surface, then a subtractive operation carves out grooves on the elements, and finally, a 3-axis 3D printing operation fills in

the grooves of the planar interface.[12] Although all the operations are carried out flat, the inclusion of flexible features in the printed joints allow to reposition the elements spatially (Figure 2.6e, Menges, H. J. Wagner, et al., 2020). Through cooperative robotic processes, the design space for spatial additive joints could be further explored. An example is shown in *Spatial Glass Bond*, where the curing time window of the adhesive allows for joining and assembly operations to happen sequentially in different locations (See, for example, Sheng et al., 2019, Figure 2.6f).

2.3.1.2   Welding and WAAM

Welding   In the most general term, welding concerns bringing compatible materials close enough so that they can be joined through a physical transformation of their atoms or molecules under heat or pressure (Messler, 1999). Therefore, welding operations are always performed *in between* all interfaces to be joined at the same time, as opposed to, e.g., some types of adhesive bonding that can be produced in different stages such as dispensing of bonding material on one interface and later joining of the interfaces together (See example in Figure 2.6f). The *in-place* nature of welding, therefore, imposes manipulation challenges for the tool and parts to avoid collisions in both manual and automated setups.

Only considering metallurgical processes, there exist around 50 different procedures to join metals together. This vast collection of welding processes can be classified into many subgroups (Messler, 2004). Two relevant classifications in our context are: *pressure* or *non-pressure*, and *fusion* or *non-fusion* processes (Messler, 2004). The one category that this thesis is concerned for joining spatial lightweight metal structures is the group of *non-pressure fusion-based homogeneous material bonding using filler metal in the form of a consumable electrode with protection from the atmosphere by gas shielding and energy sourced by an electric arc* (Figure 2.7)

---

[12]Alternatively, this process could be carried out spatially by combining 6-axis printing techniques such as spatial extrusion (Hack et al., 2017; L. Yu et al., 2016) or non-planar printing (Nisja, Cao, and C. Gao, 2021; Mitropoulou, Bernhard, and Dillenburger, 2020)
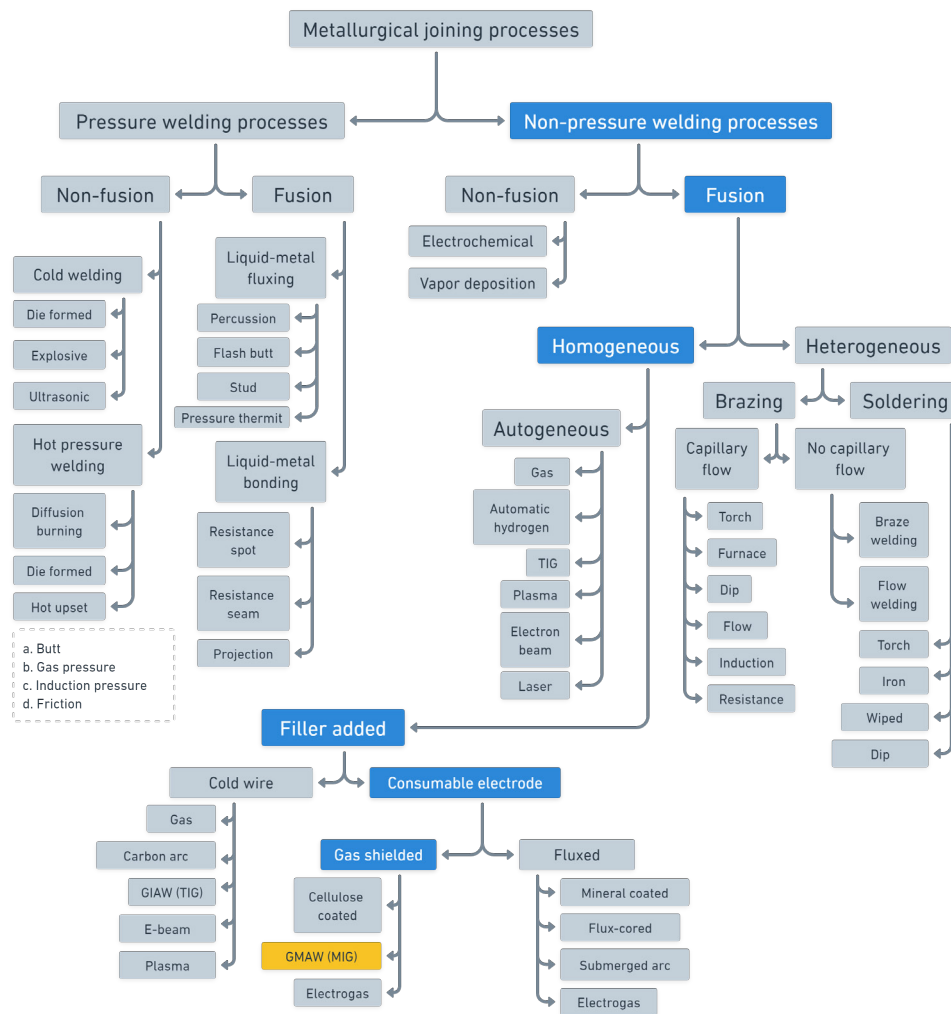
Figure 2.7: *Metallurgical joining processes after Messler (1993).*

Under this category, gas metal arc welding (GMAW) is particularly relevant in the construction industry due to its versatility. The GMAW process consists in bringing two differently charged electrodes (the wire electrode and the workpiece electrode) close enough in a gas atmosphere to produce an electric arc. The collisions between electrons and positive ions in the arc produce heat that locally melts the continuously fed wire electrode. The molten metal is then transferred to the substrate with the desired motion resulting in a fused *seam* while the arc is active. Shielding gas is supplied during the fusion process around the weld seam to protect the molten metal from creating residues inside the seam due to oxidation.

This technique can be applied to points, lines, or curved seams (Figure

2.8a). The quality of the fusion in the seam can vary to a great extent depending on the path, motion, energy, materials, and other process parameters. The orientation of the welded seam relative to gravity and the orientation of the welding tool relative to the welded seam have a significant impact on the result of the operation, causing strong constraints for the manipulation of the tools and parts. These challenges are most often tackled with complex robotic setups to manipulate parts and tools in ideal conditions, such as the one shown in Figure 2.8b. Therefore, considering manipulation constraints of parts relative to gravity and tools relative to parts is an important factor in the design of welded joints (Pashkevich, Dolgui, and Semkin, 2003).

(a)

(b)

Figure 2.8: *Welding: (a) Different welding methods used in car assembly: spot welding and a curved seam performed with the GMAW-based Cold Metal Transfer (CMT) process by Fronius, Photo: Fronius, Audi Robotics, and (b) Welding of a K-node of an offshore oil jacket structure. Photo: PEMA Welding.*

Because of its outstanding structural performance compared to other joining methods[13] and very good compatibility with automation, robotic arc welding processes have been actively developed since the 1960s.[14] Technological advances, most notably regarding sensing techniques, material processing, modeling and simulation, and performance of welded products, have been previously presented in several forms in the literature (See Pires, Loureiro, and Bolmsjö, 2006 or Tarn, S.-B. Chen, and C. Zhou, 2007) and are continually revisited and extended (See, for example, Zhang et al., 2020).

---

[13]Only possible through the transformation of the material structure itself as opposed to superficial interlocking forces happening in other joining methods (Messler, 2004).

[14]Indeed, robotic welding has been one of the first fully automated robotic processes (Pires, Loureiro, and Bölmsjo, 2006a).

WAAM One of these extensions proposes an alternative deposition technique where the electrode wire is fused on top of a previously fused seam instead of on top of the workpiece. In a sequential addition of accumulated seams or *layers*, a three-dimensional object can be created. This approach to additive welding is called wire and arc additive manufacturing (WAAM), and its concept was already filed as a patent a century ago by Ralph Baker (Baker, 1925). However, the process has only been a subject of systematic investigation in the last decade and a half (Treutler and Wesling, 2021; B. Wu et al., 2018) and is now officially categorized as a Directed Energy Deposition additive manufacturing process (*Standard Guide for Directed Energy Deposition of Metals* n.d.). The WAAM setup remains the same as in a conventional GMAW process, but the technique takes full advantage of the freedom of an additive manufacturing process.

The interest in WAAM resides in its substantially high deposition rate (1-4kg/h) compared to other powder-based metal additive manufacturing processes (0.1-0.2 kg/h) and the possibility of producing large and/or complex components with a low Buy-To-Fly (BTF) ratio.[15] Additionally, WAAM presents opportunities for locally designed strength and performance, and compatibility with post-processing processes such as milling to perfect the part accuracy (Figures 2.9a-2.9c, Williams et al., 2016; Rodrigues et al., 2019).

In the Architecture, Engineering, and Construction (AEC) industry, diverse applications of WAAM have been explored in the last decade. Most notably, in furniture (Figure 2.9d), small vehicles (Figure 2.9e), building components (Figure 2.9f-2.9h), and the largest 3D printed bridge to date (Figure 2.9i, Gardner et al., 2020). Other applications under study include reinforcement for concrete (Classen, Ungermann, and Sharma, 2020), and repairing or reinforcement of metal structures (Y. Li et al., 2019).

WAAM nodes The versatility of welding additively with WAAM has been recognized on many occasions as a good fit for replacing complex, and often expensive and problematic, bolted, cast, or welded

---

[15]The Buy-To-Fly ratio, a term borrowed from the aerospace industry, is the relation between the mass of the purchased raw material to the mass of the final, *ready-to-fly*, part.
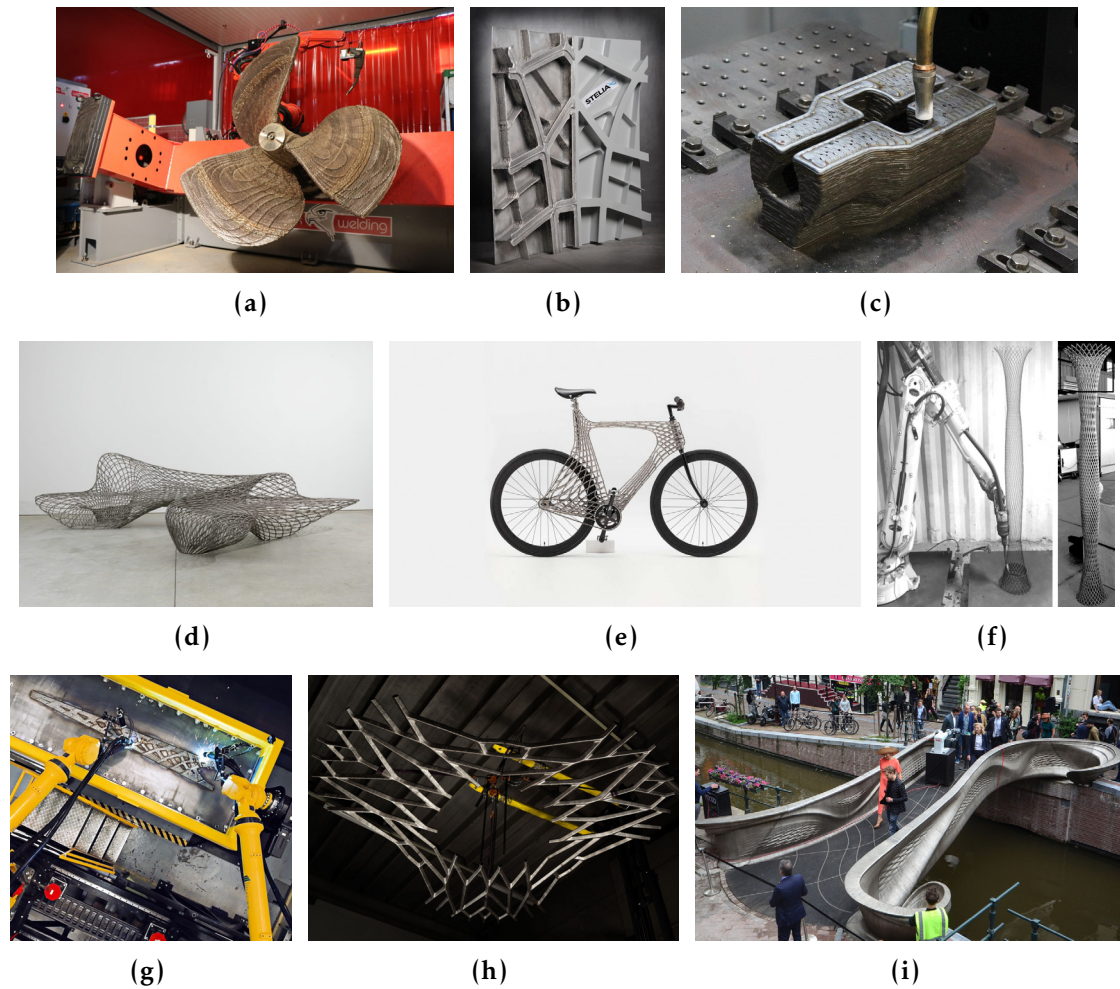
Figure 2.9: *WAAM in shipbuilding, aerospace, tool and die, and AEC industries: (a) WAAMpeller, RAMLAB (2017), (b) Fuselage panel, Stelia Aerospace (n.d.), (c) Tooling, Photo: Lincoln Electric (n.d.), (d) Dragons, Joris Laarman Lab/MX3D (2014), (e) Arc Bike I, MX3D (2017), (f) Diagrid Column, Vittoria Laghi and MX3D (2020), (g) Large-scale Additive and Subtractive Integrated Modular Machine, LASIMM (2020), (h) Ceiling structure, ESA (2020), and (i) MX3D Bridge, MX3D (2021).*

connections with custom nodes (Figure 2.10).[16] These studies showcase different concepts for interfacing and assembling nodes and elements, and prioritize the prefabrication of the node for later assembly on site. Aims and methods of using WAAM for building stand-alone nodes include reducing weight by optimizing the material distribution of the node (Erven, Lange, and Feucht, 2021; *Connector for Takenaka* 2019), producing geometric variations with parametric modeling (Reimann, Hildebrand, and Bergmann, 2020), and reducing the part deformation with spatial slicing and printing techniques (Heerdegen, 2021). Although prefabrication facilitates the planning and production of components, the approach remains inconclusive regarding the logistical and tolerance handling challenges present during the assembly stage (see Section 2.3.2).

In-place WAAM   A feasibility study for joining spatially was conducted by Samuel Cros in a three-month MAS thesis in the summer of 2017 (Cros, 2017).[17] The proposed "Spatial Robotic Welding" process consisted in locating spatial elements in place with two different scanning strategies and then welding them with an additive welding approach. The proposed design-production workflow allowed to create a short and straight connection between scanned bars oriented at different angles (Figure 2.11). These prototypes proved the potential of the technique for assembling steel components with an additive welding technique.

However, the connection design approach was limited to straight and symmetric lines positioned as an offset from the elements' axes, and a trial and error reorientation of the torch was used to avoid collisions. In addition, the robotic setup did not provide reliable printed results when printing in varying conditions against gravity. These challenges suggested that to develop a versatile joining approach for spatial structures more considerations of the robotic setup, and a comprehensive

---

[16] A comprehensive review of projects using complex node designs for steel structures can be found in the series *Understanding Steel Design*; *Diagrid Structures*; *Architecturally Exposed Structural Steel*; *Complex Steel Structures* by Terri Meyer Boake (Boake, 2013; Boake, 2014; Boake, 2015; Meyer Boake, 2020)

[17] The project was originated by Gramazio Kohler Research's researcher Ammar Mirjan and counted with the supervision and technical support of Augusto Gandia, Gonzalo Casas, Michael Lyrenmann and Philippe Fleischmann.
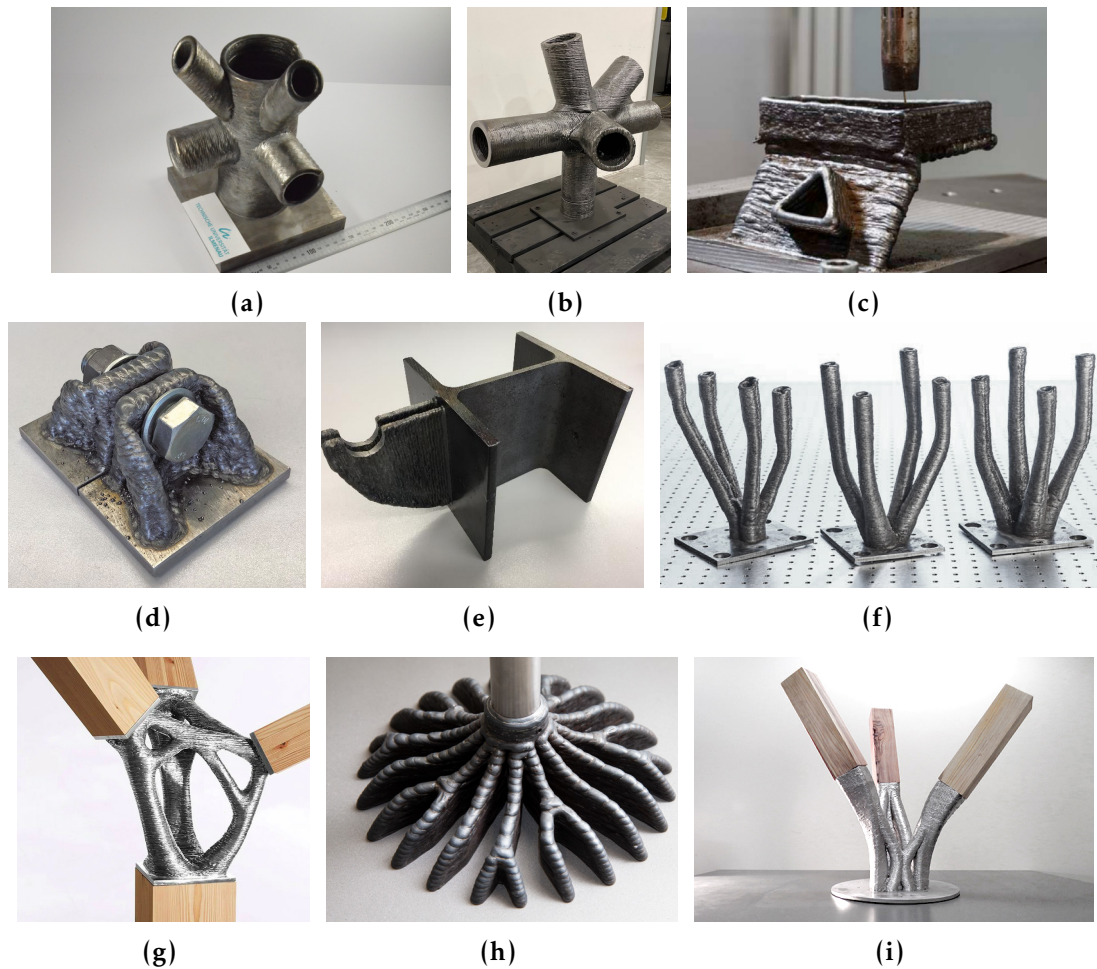
Figure 2.10: *WAAM nodes: (a) Reimann, Hildebrand, and Bergmann, 2020 (2019), (b) Lincoln Electric (n.d.), (c) PZH IFW TEWISS, Photo: Nico Niemeyer (n.d.), (d) Lange, Feucht, and Erven, 2020 (2018), (e) Feucht, Lange, Erven, et al., 2020 (2018), (f) Feucht, Lange, Erven, et al., 2020 (2018), (g) Takenaka Connector, MX3D (2020), (h) AdditiveTectonics Gmbh (n.d.), and (i) Heerdegen, 2021 Photo: TiDa (2020).*

computational design approach would be required.

(a)   (b)   (c)
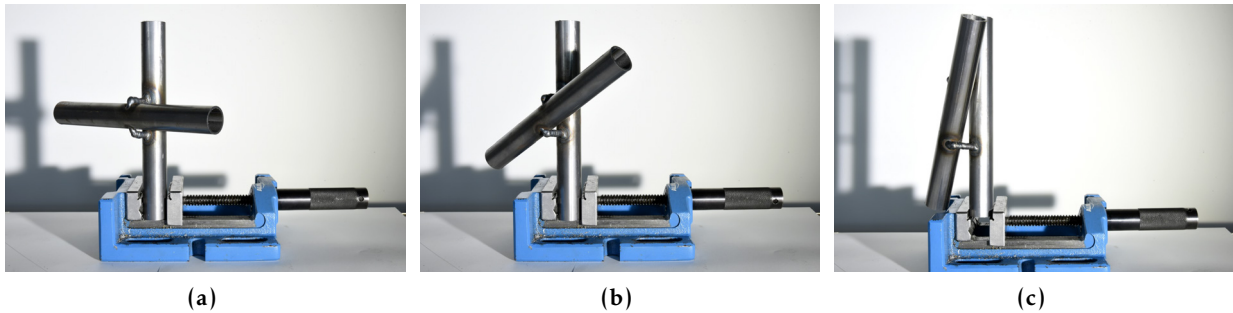
Figure 2.11: *Feasibility study of spatial robotic welding, Gramazio Kohler Research (2017), Photos: Samuel Cros (Cros, 2017).*

Conclusion

It is reasonable to expect that future developments in the robotic assembly of discrete spatial structures depend on finding suitable joining techniques and materials that can outperform standardized approaches at critical stages of the assembly process -such as securing its connections-. Good candidates should be chosen based on their performance metrics considering their strength-to-weight ratios and mechanical properties under a variety of loading conditions. Additionally, the flexibility in deposition, manipulation, and automation potential should be prioritized.

With this challenge in mind, this section has reviewed relevant materials and processes that show significant potential for this novel building scenario. In particular, the rich state-of-the-art of fusion-based welding shows that well-known techniques can radically extend their capabilities when applied with additive principles. GMAW welding, originally a joining technique to fuse seemingly touching parts, can now be used to join spatial interfaces where parts do not need to be in contact or machined.

However, the examples also present challenges on many fronts. Projects show that a high degree of control over the placement of the material is needed. This entails the development of planning and surveying methods for collision control between tools, assembled parts, and joining materials. In addition, projects using malleable and phase-change materials require higher control of material modeling and monitoring

during deposition. Finally, the spatial deposition of the material requires the development of suitable path generation approaches, such as the underway efforts for custom non-planar slicing (e.g., Mitropoulou, Burger, et al., 2020).

2.3.2   Joining to fit

The next challenge of joining spatial robotic assembly is fitting parts together according to a design plan.[18] To assure fitting, construction in architecture devises different strategies to control the tolerances of materials and parts. In our discourse, however, the term tolerance is often misused.

Tolerance is the measure of accepted variation of a construction element (Ballast, 2007). Each element of construction presents its own tolerance based on its manufacturing process, material characteristics, transport conditions, installation techniques, etc. (Allen and Rand, 2007). The distinction between *dimensional and geometrical tolerance* is used in engineering to distinguish the dimensional variation of parts from the geometric variation (e.g., shape and orientation) of parts (Polini, 2011). In architecture, the term *construction tolerance* is used to refer to the engineering term dimensional tolerance. *Material tolerance* is a loose term often used to refer to both dimensional and geometrical tolerances.

Another distinction can be made between *assembly tolerances* and *functional tolerances* required during the life cycle of a building, e.g., tolerances to allow for thermal expansion and contraction of materials (Allen and Rand, 2007; Mandil, Desrochers, and Rivière, 2009). Both types of tolerances may be handled at the same locations and specified in the same drawing. In this thesis, the term tolerance always refers to the assembly tolerance required for a successful assembly process.

Most joining operations depend on compliance with specified tolerances (Swift and Booker, 2003). For example, successful gluing can

---

[18]This statement can be challenged by other modes of practice. In "Design with Material Uncertainty", F. Raspall makes a distinction between what he calls "professional" (architecture, engineering, etc.) and "informal" practices (artistic production or informal building) which respectively use or disregard anticipatory measures to control the product's outcome (Felix Raspall, 2015).

only be achieved if the elements are within a certain dimensional or geometrical tolerance. In other words, if parts vary too much, for example leaving larger gaps or having too smooth or too wavy surface finishes, they should be rejected, as joining operations will not be correctly performed. Joining operations are more or less *tolerant* to variation.

Understanding tolerances is fundamental for the successful materialization of buildings, and a key component of architectural details where the coordination of different materials and processes is described (Allen and Rand, 2007). The *accumulation of tolerances*, i.e., the accumulation of variation, is an increasingly interesting topic in digital construction where methods for explicit handling of tolerances are now required for what was previously handled ad-hoc manually.

Engineering fields encapsulate standards and protocols under the topic of Geometric Dimensioning and Tolerancing or GD&T. Architecture does not have such a structured nomenclature, perhaps because different strategies can be used to handle tolerances during construction. A useful classification of methods to control the deviation from the planned model that are relevant for digital construction is proposed by Vasey, Maxwell and Pigram in *Adaptive Part Variation, A Near Real-Time Approach to Construction Tolerances* (Vasey, Maxwell, and Pigram, 2014) and extended here:

High accuracy A first approach consists in providing high control of the dimensional and geometric tolerance of materials and parts, in other words, reducing unplanned variation as much as possible in the first place. This approach is increasingly popular within digital design and fabrication, as digital technologies allow drawing and fabricating sub-millimeter parts. However, today this paradigm is still more theoretical than practical. Building with high accuracy has only been applied to small-scale assemblies, predominantly spatially isolated or mono-material, such as pavilions and furniture where variation and deformation of parts before and during assembly can be drastically minimized or ignored (Figure 2.12a).

(a)

(b)

(c)

(d)
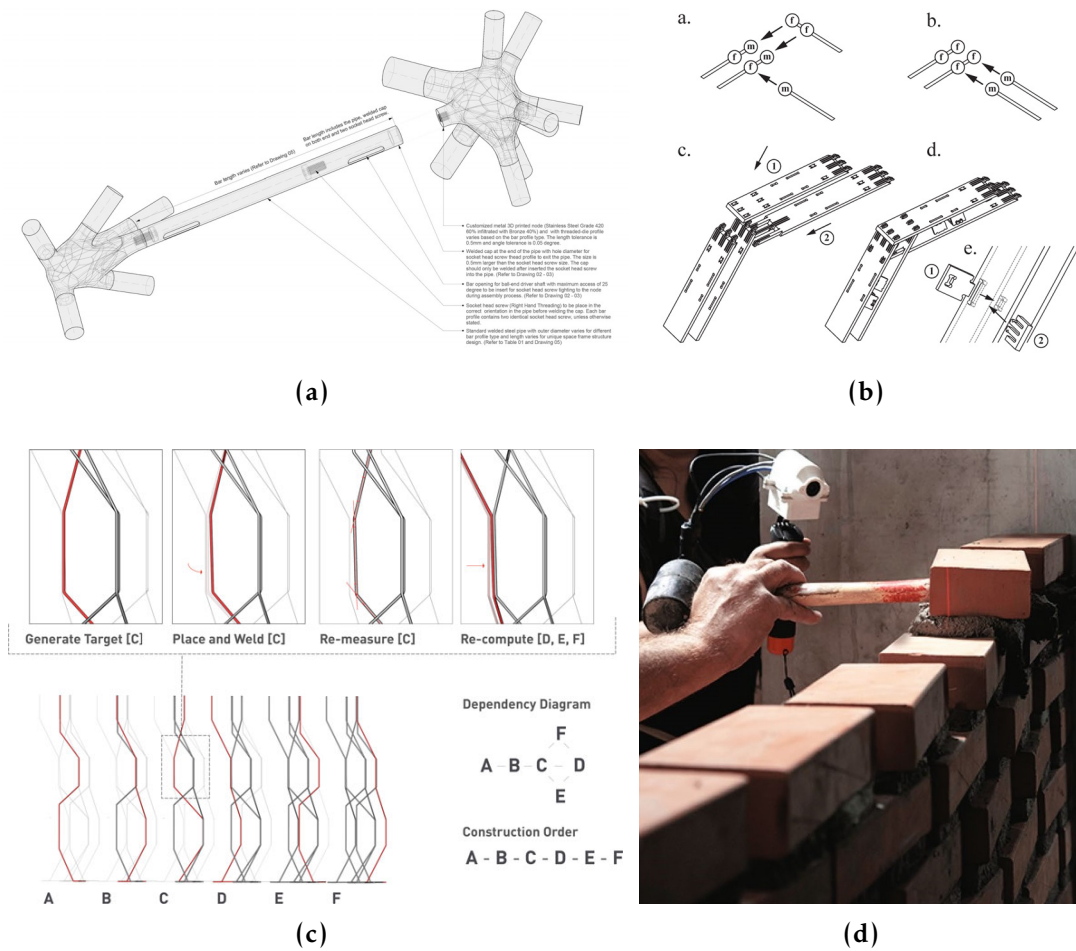
Figure 2.12: *Handling tolerance methods in digital fabrication: (a) Airmesh pavilion node, AIRLAB (Bañón and Félix Raspall, 2021), (b) Snap-fit joints (Robeller, Mayencourt, and Weinand, 2014, (c) Adaptive Part Variation (Vasey, Maxwell, and Pigram, 2014), and (d) Augmented bricklaying, Gramazio Kohler Research (Mitterberger et al., 2020).*

Adjustable features   A second approach for handling unplanned differences is using adjustable features, i.e., sliding, incremental or deformable fits. For example, a sliding fit minimizes tolerance by geometric means such as a guiding geometry or chamfers. An example of incremental fit is the inclusion of slotted or oversized holes, screws, bolts, washers, wedges, shims, etc. that provide extra space for alignment and progressive control during adjustment. Deformable features are elastic or plastic fits such as snap-fits that allow for local deformation of materials during fitting. These strategies have proven highly reliable for standardized and custom connections (Messler, 2006); however, can be of limited use in spatial assemblies where the degrees of freedom of

the interfaces do not benefit from a pre-defined directionality of the adjustment feature (Figure 2.12b).

Sequential processing   A third approach is to delay the final processing of parts until they are needed. This strategy can be used at different scales. At a building scale, it can be used between primary structure and secondary systems such as facade elements, where different trades work with higher or smaller tolerances. The approach can also be applied with an artisanal mindset where each part is processed sequentially in a cut-to-fit or shape-to-fit manner. In this case, unplanned variation is handled at each iteration of the construction process. This approach fits well with a digital fabrication scenario where sensing mechanisms can be used to handle the processing of parts continuously (Vasey, Maxwell, and Pigram, 2014). In this case, efficiency is tied to the speed of the measuring and processing system and the scale and number of parts (e.g., components made of small parts can accommodate variation more often than components made of larger parts (Allen and Rand, 2007; Gandia, 2020), (Figure 2.12c).

Accommodating materials   Finally, the fourth approach to fitting consists in using accommodating malleable materials. The ubiquitous formula of this type is found in the joining of bricks with mortar (adhesives, instead, are not as forgiving, see 2.2.2). In this case, the adjustment or leveling is achieved through the motor and visual skills of the bricklayer (Figure 2.12d). As explained in Bonwetsch (2015), the translation of these complex operations to an automated system requires the integration of several sensors (Bonwetsch, 2015). Yet, sensing strategies without a feedback-based design system become limited in accommodating possible dimensional or geometric variations.

Conclusion

The possible divergence between the planned and the built form is particularly relevant in discrete assemblies, where these divergences can easily accumulate. To this end, the presented fitting strategies range from predefined features to dynamic design-construction processes. Within this range, a final distinction can be made: passive and active tolerance handling approaches. Whereas passive methods such

as high-accuracy and adjustable features pre-determine how to handle uncertainty at the design stage, active systems such as sequential processing or accommodating materials handle uncertainty as needed, based on the actual variation found at the time of assembly. The anticipatory strategy of passive systems relies on consistency, modeling, and understanding of materials in advance of production. In contrast, the reactive strategy of the active systems relegates part of this control to the design-production pipeline itself, which can be beneficial when working with new materials and processes that present material uncertainties such as the ones investigated in this thesis.

2.3.3   Joining to support

For assemblies serving primary or secondary structure purposes, the main function of their joining is to transfer forces between parts. A fundamental challenge, therefore, is to define the location, mass, and distribution of the joining material to safely transfer loads to the supports of the structure. In practice, these challenges are most often answered by typological solutions based on building codes and standards. However, the additive constructive logic of robotic assembly of spatial assemblies might re-open these problematics in a new light, as typical solutions might not be enough for several reasons:

First, spatial assemblies present structural behaviors that deviate from well-known structural typologies (Apolinarska, 2018; Parascho, 2019). Respectively, spatial nodes[19] present complex behaviors that are dependent on the geometric variability of the structure's elements, which as well escape typical solutions.[20] Moreover, in steel structures, the task of accurately modeling and structural checking for standard orthogonal connections has been reported as an open and unsolved problem (Rugarli, 2018), let alone their spatial counterparts.

Second, as discussed in Section 2.3.1, spatial assemblies presenting spatial interfaces require the adaptation of known or the development of

---

[19]*Node* is used here in the structural modeling sense: "In systems of bar structures, the connection of elements can be described by nodes. Here, a node is defined as a topological entity that represents the connections of elements at or nearby one point within the system." from Kohlhammer et al., 2017.

[20]Examples of typical solutions in steel can be found in connection design handbooks such as Tamboli, 2017; Jaspart, 2016; Rugarli, 2018.

new materials and joining techniques. When known building materials are exposed to new loading conditions, simulation of structural behavior is common practice. However, when working with new materials, extensive groundwork experimentation is required. These steps take time and niche expertise, making the structural design, modeling, calculation, and evaluation of spatial structures, particularly challenging.

Third, good design always presents a negotiation between concurrent constraints (e.g., structural behavior, manufacturing possibilities, labor, and material availability, to name a few). However, current connection design approaches are grounded in production paradigms that are fundamentally challenged by digital design and construction chains (Graser et al., 2021). In this respect, the design of connections in steel presents a shocking picture. Jaspart and Weynand classify steel design approaches as "traditional", "consistent", and "intermediate" offering a snapshot into practice where expertise and roles are divided into consecutive phases of the design of the structure. In the "traditional" approach, engineers assume the performance and fabrication of joints focusing on the design of the steel members, and the fabricator designs the joints at a later stage based on the members' requirements. In the "consistent" approach, joints and members are designed by the engineer. Finally, the "intermediate" approach consists of fabricators designing both joints and members of the structure (Jaspart, 2016). These scenarios suggest that an idealization of constructability requirements or/and structural behavior would be done in advance by one part of the design team.[21] However, this separation is only possible due to the existence of standardization of building materials and assembly procedures, which fundamentally differ from additive fabrication principles.[22]

---

[21]This last point is particularly problematic not only from a structural performance point of view but also in terms of material consumption and costs (Horn, 2015; Paulson, 1976)

[22]In this respect, a particular challenge for conceptual design of spatial structures built robotically is to find relevant constructability measurements and rationalization principles. To date, constructability studies leave a large gap for entirely digital design-construction chains, as they address manual construction processes where high value is given to, for example, standardization of member length or cross-sections that are less critical in digital fabrication scenarios where parts are mass-customized—i.e., members are cut-to-fit during the assembly process—(See examples in Willmann et al., 2016).

These points suggest that known connection design approaches, specifically in the context of steel components, could only provide partial answers on location, mass, and distribution of joining material to ensure structural integrity.

Structural considerations for additive joining

In need of alternatives that consider additive fabrication principles (Section 1.2), the field of design for additive manufacturing (DfAM) provides relevant strategies (Leary, 2020a). Formulated as a shape design or layout design problem (Bendsøe, 2009), methods such as topology, shape, or sizing optimization use structural analysis to iteratively modify a base geometry until one or multiple performance criteria are met. The result is the prediction of the material distribution in space (Tam et al., 2018). Within this approach, relevant fabrication constraints can be incorporated during the optimization procedure to achieve results that comply with the possibilities of the tooling, material properties or deposition process parameters (Bermano, Funkhouser, and Rusinkiewicz, 2017, see example in Y. Huang, Carstensen, and Caitlin T Mueller, 2018).

Although topology optimization (TO) principles and methods have been under development since the beginning of the 20th century (Lógó and Ismail, 2020), the interest rapidly increased since the 1980s due to the digitalization of production processes in a wide range of applications (Rozvany, Bendsøℓ, and Kirsch, 1995; Sigmund and Maute, 2013; Zargham et al., 2016; J. Zhu et al., 2021). Jiang and Chirehdast first tackled the approach for designing spot-weld and adhesive bonding connections finding that significant material saving can be achieved by optimizing their layout (Jiang and Chirehdast, 1997). From then on, numerous methods have been developed in the scope of connection design to optimize material distribution based on additive fabrication principles (Ribeiro, Bernardo, and Andrade, 2021). Target applications include prefabricated nodes for modular (Z. Li, Tsavdaridis, and Gardner, 2021) and free-form construction (Galjaard, Hofman, and S. Ren, 2015; van der Linden, 2015; Prayudhi, 2016; Crolla et al., 2017; Hamed Seifi et al., 2018; Abdelwahab and Tsavdaridis, 2019; Novillo, 2019; Bergmann et al., 2020; Reimann, Henckell, et al., 2021; Holst et al.,
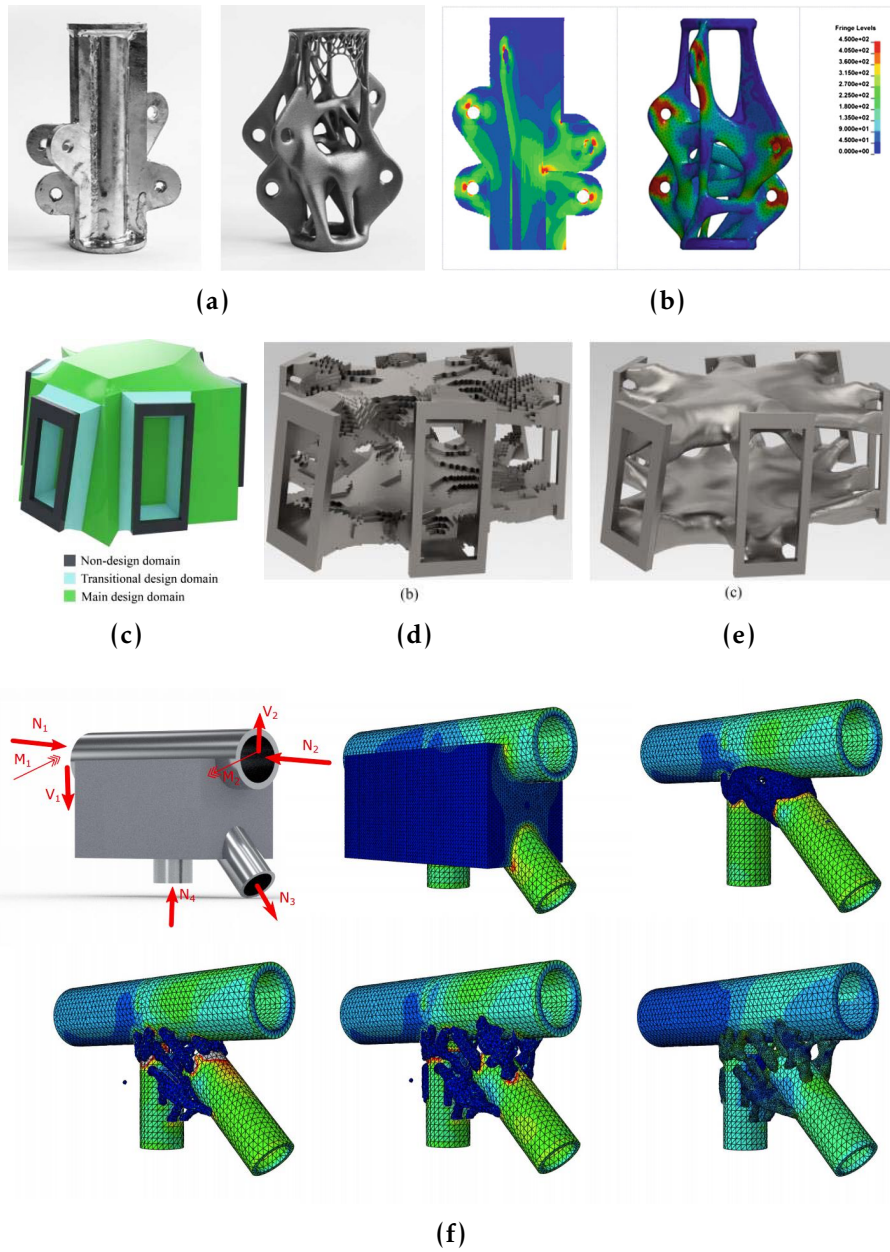
(a)

(b)

(c)

(d)

(e)

(f)

Figure 2.13: *Topology optimization in node design: (a-b) Galjaard, Hofman, and S. Ren, 2015, (c-e) H. Seifi, 2019, and (f) Holst et al., 2021.*

2021, Figure 2.13). To date, additive manufacturing is employed primarily as a separate prefabrication process, and therefore the boundary conditions are conceived based on print beds. However, the in-place joining approach tailored for robotic assembly requires a material distribution layout that is free of collisions and reachable by the robot. This characteristic can be used as a design constraint in the topology optimization task, an approach that has not been studied to date.

Conclusion

In short, spatial assemblies present many uncertainties regarding their structural integrity. This context, in turn, requires specific expertise and tailored solutions for the design of their connections. Joining robotically, additively and in place presents a fruitful context to investigate integrative material distribution methods that consider structural and fabrication constraints at once, as opposed to disciplinary fragmented approaches.

2.4   Detailing

The final challenge concerns the integration of fabrication, functional and material constraints previously presented regarding joining for spatial structures. This integrative task, generally called *design*[23], is here packed into the term *detailing* as it concerns not only the *planning* stage but also the *documentation* and *communication* of fabrication instructions, its execution, and *control* of the materialized outcome (see definition in Section 2.1).

At the core of the detailing lies a conflict between function, constructability, and aesthetics. According to Allen and Rand, good detailing solutions satisfy all these three aspects (Allen and Rand, 2007). However, in real practice, solutions lie in the area of expertise of the

---

[23]In *Design Q&A*, Charles Eames discusses this point: "Q: Does the creation of Design admit constraint? A: Design depends largely on constraints. Q: What constraints? A: The sum of all constraints. Here is one of the few effective keys to the design problem: the ability of the designer to recognize as many of the constraints as possible; his willingness and enthusiasm for working within these constraints. Constraints of price, of size, of strength, of balance, of surface, of time, and so forth. Each problem has its own peculiar list." (Eames Office, 1972).

designer or detailer. In the hands of an engineer, functional requirements often precede and are afterward checked for constructability, literally "setting up the scene" (Rugarli, 2018). Architects, conversely, will start with a materiality concept and then refine it by providing functional requirements with the input of different experts. In current practice, how synthetic the detail solution ends becomes a matter of how efficient the communication between the architect, the engineer, the constructor, and any other specialist, is during the detailing phases.

How could these collaborative modes of practice change with robotic joining and assembly? This section reviews existing detailing approaches and discusses how they manage to negotiate function, constructability, and expression.

Detailing through craftsmanship   A ubiquitous approach for integrating function and constructability is the craftsman approach. Through trial-and-error, repetition, and iteration within a certain domain, the craftsman builds construction knowledge tacitly (Sennett, 2008). Over time, an understanding of material behavior helps to anticipate the results of using particular tools and processes. Equipped with this implicit knowledge, the craftsman can influence materials to perform within a variety of functions and, conversely, can find synthetic material solutions to solve different functional requirements.

Examples of this approach can be found in designers such as Jean Prouvé, whose extensive background in metalworking led him to see the potential of novel metalworking techniques.[24] However, although fascinating, the creative process of synthesizing acquired expertise is hard to transfer and reproduce (Figure 2.14a, Prouvé, 1990).

Detailing with recipes   For the aspiring designer without a background in construction, detail recipes become handy. Documented in catalogs, handbooks, and compilations, standard details contain

---

[24]Prouvé's design process materialized in innovative products, expressive of the new manufacturing possibilities of metal forming to increase the resistance of lightweight metallic components.

(a)   (b)

(c)   (d)
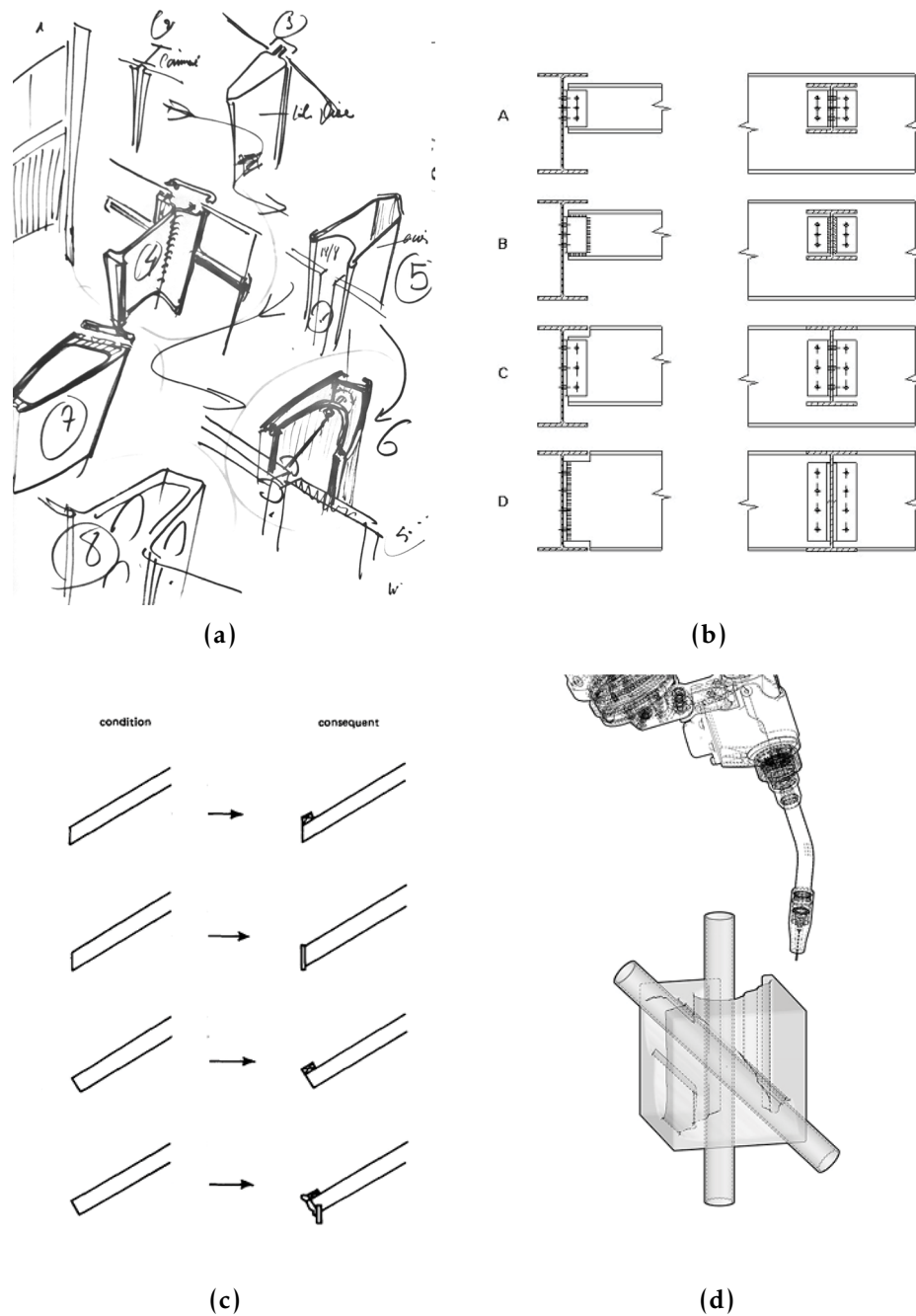
Figure 2.14: *Detailing approaches: (a) Detailing through craftsmanship (Prouvé, 1990), (b) Detailing with recipes, Beam to beam connection design in steel (Connection Design Static Loading: Simple Connections for Buildings. 2000), (c) Expert detailing systems (A. Radford and Gero, 1985), and (d) Detailing with robotic constraints, Gramazio Kohler Research (2018).*

proven functional and buildable solutions (Figure 2.14b).[25] An updated version of these catalogs is found in existing software libraries (e.g., Network, 2020). These easy-access repositories, however, in isolation fail to encourage reasoning through realistic material and assembly processes inherent to construction (Emmitt, 2003).

Essentially a data management system, Building Information modeling (BIM) promotes a collaborative approach to building that facilitates communication and control of design data. However, even with the main aim of providing standards for communication, numerous interoperability obstacles -i.e., data discrepancy and vendor-specific interfaces- still exist, hindering a truly synchronous and creative project development between specialists (Chong et al., 2020).

Expert detailing systems   Ultimately, detail recipes consist of a series of detailing patterns that can be organized in a knowledge-based system. Generally, expert systems consist of programs that reconstruct domain-specific decision-making capabilities in a problem-solving scenario (Puppe, 1993). Detailing can be as well seen as domain-specific problem-solving with or without human intervention. Radford and Gero suggested that constructability and functional detailing patterns could be encapsulated in shape grammars. With this, they proposed detailing as a generative tool and as an educational method, as detail solutions can be traced back to each constituent rule (Figure 2.14c, A. D. Radford, 1985). The author of this thesis previously presented a detail grammar as a generative method for solving structural joints (Ariza, 2016). In this detailing system, assembly and functional constraints need to be specified in advance, so they can be solved by the iterative matching and application of detail rules. Alternatively, the knowledge base can be implemented as a checking system to verify that the user inputs comply with quantitative or geometric constructability or functional constraints, providing relevant feedback to the designer or builder (Leung, 2023).

However, these approaches can hardly deal with unclassified, new, or

---

[25]An uncountable number of these are available since the 17th Century organized by trades -bricklaying, wood construction, metalworking, masonry-.

ambiguous problems, for which design is particularly known. Ultimately, without the constant input and steering, the functional logic prevails, eventually preventing the synthesis of novel solutions (Kilian, 2006; Caitlin T. Mueller, 2014).

Detailing with constraints   An alternative to looking for answers to a problem within indexed knowledge, is to reformulate the problem in terms of design constraints. Designers always use constraints to find possible solutions; however, they do not always use constraints as explicit design drivers of form (Kilian, 2006). This approach can be valuable for systems with numerous interdependencies, in particular when constraints are known but precedent solutions or knowledge bases are not available.

In "Design Exploration through Bidirectional Modeling of Constraints", Kilian describes the need of finding relevant representations and design environments for each type of constraint (Kilian, 2006). This requirement, he continues, produces domain-specific design explorers, which can be used in uni-directional or, preferably, bidirectional manners. The translations required between representations and domains -e.g., fabrication or structural domains-, Kilian proposes, are opportunities for *design innovation*.[26]

This brings us back to the motivation of this work: the need to explicitly understand the robotic and joining material's constraints can be as well a design innovation opportunity. In the scope of this thesis, examples of constraints are the robot arm's reachability (Figure 2.14d) and the dead load of the element to be supported. Each constraint influences the design process yet in distinct domains (i.e., fabricability and distribution of material). This thesis proposes an approach to detailing where the explicit integration of construction and functional constraints creates opportunities for design innovation. And, by doing so, there is a surplus. Explicitly understanding the constraints through relevant data representations, i.e., valid inverse kinematic solutions materialized in a combination of robot joint descriptions, creates the needed data for communication and execution of the design at the production stage.

---

[26]An implementation of this approach for robotic assembly can be found in K. Wu and Kilian, 2016.

Towards adaptive detailing   There is a unique opportunity when linking design and fabrication in a dynamic system: a two-way communication platform between physical and digital domains can inform one another on physical aspects that are challenging, or unlikely, to foresee. Within this approach, the task of detailing transforms from a primarily anticipatory to an explicitly active endeavor during the construction process. Instead of predicting reality, adaptive details can react and adapt to it as needed. This thesis is an inquiry into the design and production implications of detailing with machines.

2.5   Summary and research aims

This section presented approaches and practices regarding the current challenges that joining for robotic assembly of spatial structures faces concerning the setup, workspace, techniques and materials, and integration of functional requirements of its design and production.

Regarding the robotic setup, projects present diverse strategies for tackling the combination of assembly and joining tasks. Multipurpose setups increase the complexity of planning and reachability and require the development of computational workflows for the design of feasible assemblies.

The partially inaccessible quality of the connection interface in spatial assemblies brings challenges for visualization and design within a collision-free reachable robot workspace. This new need in architectural design asks for suitable reachability analysis and visualization methods that remain circumscribed to robotics research to date.

The spatial quality of the connection interface challenges standard joining materials and techniques to perform in three dimensions. The possibility of applying additive principles to both assembly and joining becomes an exciting area of research that is to this date, surprisingly, unexplored.

The challenge of handling tolerances during assembly is a common-place problem in construction and has been solved with multiple well-known approaches. Spatial assemblies, however, bring the specific challenge of handling divergences in three dimensions. The need for versatile joining approaches for adapting the design as needed remains open for further investigation.

The problem of finding an optimal location, mass and distribution of materials is currently actively studied across fields and disciplines. The early integration of robotic reachability as a design domain, however, has not been studied to date.

The unprecedented confluence of design potential presented by the spatial interface, the robotic additive spatial joining technique, and the adaptive design-and-production pipeline calls for a timely reexamination of known detailing approaches. An unpaved design territory lies at the interface of these diverse domains, which this thesis aims to integrate and explore.

Based on this research context and gaps, this thesis aims to:

   i) Build on the rich state-of-art of current developments of robotic motion and task planning by proposing a multi-functional cooperative assembly approach for assembly and joining.

  ii) Map and utilize the robot's workspace constraints as a design driver to find feasible connection locations.

 iii) Develop a suitable technology for joining spatially and additively partially inaccessible, geometrically complex varying interfaces.

  iv) Develop a design-and-production approach to survey the actual location of elements and adapt the deposition of joining material during the assembly process.

   v) Propose an integration of material distribution methods based on reachability constraints at an early phase of connection detailing.

  vi) Identify and integrate the exposed novel fabrication, functional, and material constraints in a readable, explorative, and adaptive detailing pipeline.

With these aims as a compass, this thesis presents fabrication techniques (Chapter 3) and computational design methods (Chapter 4) for adaptive in-place spatial connections tailored for robotic assembly of lightweight metal structures. The approach is then demonstrated and discussed in Chapter 5 and Chapter 6.

3 In place WAAM

This chapter introduces the in place wire and arc additive manufacturing (IPWAAM) technique, a joining application of WAAM technology tailored for the robotic assembly of spatial structures. The chapter opens with the definition of IPWAAM (Section 3.1), then introduces its associated equipment (Section 3.2), software (Section 3.3), materials (Section 3.4) and procedures (Section 3.5). Finally, the chapter presents a series of material experiments carried out to calibrate and understand the technique's variables and constraints (Section 3.6).

3.1 Definition

Conventionally, fusion-based welding operations consist of filling a gap or groove or reinforcing a corner or fillet with one or more welded seams (*AWS D1.1: Structural Welding Code–Steel* 1999). However, as introduced in Section 2.2.2, non-regular spatial structures present an increased geometric complexity at the interfaces between components that do not follow standard specifications. In this context, this work investigates an additive spatial welding strategy as a flexible method for joining varying geometric conditions. The approach builds on additive manufacturing (AM) or 3D printing principles where a layer-by-layer material deposition is used to form custom shapes. The employed AM technique to join steel components is wire and arc additive manufacturing or WAAM (see Section 2.3.1.2).

Performing WAAM *in place*, in the location where the printed part belongs, is referred to as IPWAAM. In IPWAAM, *in place* means *on the spot* or *in the location*, which in manufacturing terms means *in the*

location where parts are.[1] Fusion-based welding operations are always performed *in place*, as parts to be joined are required to perform the joining process. While AM and WAAM are most often employed as a stand-alone process in a separate prefabrication step, here it is used as a joining strategy and, therefore *in place*, in-between parts to be joined. This additive joining approach combines the performative nature of fusion-based welding operations with the geometric versatility of additive manufacturing.

IPWAAM requires a combination of manipulation, welding and sensing tasks and infrastructure. Manipulation consists of the positioning of parts and tools. Welding is the process of feeding, heating, melting, and cooling the feedstock to join elements. Finally, Sensing comprises localizing and monitoring tasks to handle uncertainties during the manipulation and welding tasks.

3.2   Experimental setup

During the development of this project, two experimental setups were used. The first setup, Experimental setup A, served as a testing ground to develop the IPWAAM concepts and processes through preliminary experiments. The need for higher control of the deposition process, which became evident from the experiments with setup A, led to a second setup Experimental setup B used in the experiments presented in Section 3.6. The following sections describe the key manipulation, welding, and sensing requirements and their associated equipment.

3.2.1   Manipulation

In robotic welding, and particularly Gas Metal Arc Welding (Section 2.3.1), a high degree of freedom of manipulation is required to orient the welding tools, materials and objects to achieve a functional welded seam (Pashkevich, Dolgui, and Semkin, 2003). In both experimental setups used in this work, two manipulators are employed. First, the

---

[1]The term *in place* should not be confused with *in situ*, or its English translation *on site*, which means the location where parts are finally positioned, usually at the construction site. Manual welding can be done in the prefabrication facility or *in situ* however robotic welding, to this date, is mostly never performed *in situ* except for a few research projects (Bock, 2008).

robot manipulates the welding tool and acts as a support for the welding equipment required to feed the wire (3.4.1) and the shielding gas (3.4.3). Second, the robot is mounted on a linear axis that serves as the manipulator of the robot base increasing the robot's reach. In practice, these two manipulators work as one. In state-of-the-art robotic welding it is standard practice to include a third manipulator, the part positioner, with two extra degrees of freedom so that the weld seam can be optimally oriented as horizontal as possible relative to the gravity vector (Joni and Dobra, 2010).[2] In this project, however, the objects are statically supported.[3].

Industrial robots are usually used in welding processes due to their sturdiness, durability, precision and compatibility with additional available welding components and software packages. Both experimental setups used in this research use an ABB industrial robot model IRB 4600 with a 40 kg payload and 2.55 meters reach (*IRB 4600 Data* 2022) mounted on a custom external linear axis.

3.2.2 Welding

As presented in Section 2.3.1, robotic arc welding is a very well-established technology spanning numerous industries. Therefore, the welding equipment options vary to a great extent. WAAM and IP-WAAM use off-the-shelf welding equipment consisting of **1.** a power source or welding machine, **2.** an end-effector or welding torch, **3.** the tooling for the feeding and transport of the wire, shielding gas and ground, and **4.** the gas supply (Figures 3.4a-3.4b).[4] Additionally, many communication and control platforms are available in the market at the time of writing. The two experimental setups used in this research illustrate the impact of the hardware and software configuration:

---

[2]As introduced in Section 2.2.1, the reachable workspace of the manipulation system is a critical characteristic to consider when designing a robotic task. Reachability measures for design and production with IPWAAM are further discussed in Chapter 4 (see 4.3.1.2).

[3]Three different fixed supports are used through the different demonstrators: a welding table, an articulated third arm, or a second robot static at the time of welding (this last option is only explored virtually, see Section 5.2)

[4]These are the same functionalities of a typical robotic welding system. However, WAAM differs in terms of the scale of the setup (Martina and Williams, 2015) and automation needs (Xia et al., 2020).

Experimental setup A combines off-the-shelf welding equipment usually used in manual operations on site. The power source consists of a portable MIG/MAG single-phase inverter for general GMAW jobs[5]. The end-effector is a MIG/MAG manual welding torch. Process parameters such as material thickness, voltage and current are set manually on the power source through the control panel.

In the first iteration of the setup, the welding process is controlled via a microcontroller board, triggered in a separate thread from the robotic motion. A lack of synchronization between the welding actuation and robotic motion led to an integration of the welding switch into the robot controller later on. However, robotic motion and welding are still independent, as there is no digital input to track the actual start and end of the welding task. The time between depositions is handled with waiting instructions, based on the pre-calculated operation times. Another aspect of the manual setup is that the gas valve control is coupled to the electric arc trigger, which results in a dependent and fixed shielding time (See procedure for details of the shielding operation 3.5). The least beneficial feature of the setup is the absence of control of the process parameters beyond the manual dial on the power source hardware. This lack of synchronization between motion and welding, and programmability options of the welding equipment led to the development of Setup B.

Experimental setup B is a robotic welding setup where the power source and its dependent components are integrated via the robot controller. The welding system is provided by Fronius with add-on components from ABB: the power source is a TPS/i 500 Pulse (Fronius, 2022b) and the end-effector a 60i Robacta Drive (Fronius, 2022a), with Cold Metal Transfer (CMT) technology (Figure 3.1, Selvi, Vishvaksenan, and Rajasekar, 2018; Fronius, 2004). The transport of the wire and gas is composed of modular tooling designed for easy attachment to an industrial robot. The setup additionally comprises an ABB Bulls Eye station for calibration and maintenance of the torch (*BullsEye* 2022),

---

[5]Two brands and options of inverters were tested, Oerlikon (*MIG MAG Inverter CITOMIG 200MP Brochure* 2013) and Sechy (*MIG/MAG 180 EASY* 2022), yielding similar controls and outputs.

and a smoke filter unit (*Welding Smoke Extractor* 2022).[6]

The key characteristic of the welding equipment is the CMT technology. CMT consists of a mechanically assisted transfer of molten metal droplets by an oscillating forward and backward feeding motion of the electrode (Kah, Suoranta, and Martikainen, 2013). Figure 3.1 illustrates the steps of the process. The term "cold" refers to the low heat present in the process compared to other "hotter" higher current welding transfer modes. This approach enables a controlled deposition suitable for thin materials and precision joining.
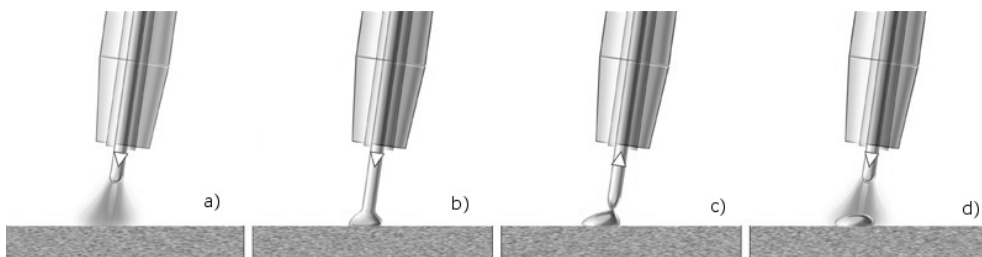
Figure 3.1: *Cold Metal Transfer process step-by-step: (a) An electrical arc is started, heating the substrate and the tip of the electrode until a molten globule is formed, (b) Once the tip of the electrode touches the substrate, a short-circuit occurs, followed by a substantial reduction of the arc voltage, (c) The electrode is pulled backward, supporting the detachment of the droplet by retraction and electromagnetic forces, and (d) The wire feeding is reversed, and the process is re-initiated. Image source: Fronius, 2004.*

The benefits of a CMT-based WAAM process have been recognized on many occasions and consists of a stable, low heat, and spatter-free deposition (Sequeira Almeida and Williams, 2010, Martina and Williams, 2015, Williams et al., 2016, Martina, 2014, Xizhang Chen et al., 2018, Müller et al., 2019). Müller et al. (2019) noted that the low heat input is particularly beneficial for the discrete WAAM deposition process (see Section 3.5.1) by providing consistency in the surface topography. Martina (2014) observed that the surface tension acting on the droplet during the deposition results in a round and smooth layer profile. These characteristic enable very fine structures compared with traditional GMAW (see Müller et al., 2019 and Yuan et al., 2021 for comparative examples). Additionally, it is expected that the low

---

[6]The welding system was provided by Fronius AG Switzerland with particular support from consultant Daniel Felix. The setup was planned, developed and integrated by the Robotic Fabrication Laboratory's robotics technician Philippe Fleischmann.

thermal input presents a particular advantage for IPWAAM structures by reducing potential residual stresses and distortions of the substrate.

Finally, both setups are completed by a stationary table and an articulated third arm, a commonly used flexible support, suitable for welding. An important aspect is to find a proper position in the table or the substrate for connecting the grounding clamp and cable which returns the current to the welding power source (*The Fronius Welding Dictionary* *2021*).[7]

3.2.3   Sensing

The need for sensing strategies for automated welding processes was identified early on, as large, heavy or complex parts present deformations or large tolerances that require continuous surveying (Agapakis, 1984). Generally, sensing is required at three stages: **1.** before welding: for localization of parts to be welded, where complete repeatability of the positioning and characteristics of parts cannot be achieved; **2.** during welding: tracking of the welded seam to ensure that the welding torch stays aligned with the target and monitoring welding parameters so that they stay in sync to geometric variations, and **3.** after welding: for inspection of the welded result in terms of quality control in conformity to the design requirements (Agapakis, 1984; Cook, 1983). Development of technologies for each of these tasks present more than 50 years of literature, and therefore numerous solutions (Cook, 1983; Ushio, 1991; Naidu, Ozcelik, and Moore, 2003; Pires, Loureiro, and Bölmsjo, 2006b; Wang et al., 2020).

WAAM sensing equipment is essentially the same as in GMAW or laser welding processes (Jienan Liu et al., 2020); however, WAAM monitoring methods are in an early stage of development, with most of the research efforts directed at gathering experimental data to create models of the WAAM process (Pan et al., 2018; Xia et al., 2020).

---

[7]The GMAW and CMT technologies require a continuous closed circuit to perform a clean weld. Both the distance between the weld seam and the grounding clamp, and the quality of the conductive surface where the clamping occurs affect the arc stability. With these constraints, finding a good clamp position can become challenging for complex structures, particularly if the ground needs to be re-clamped manually during the assembly process.

Using WAAM as an in place joining technique requires the integration of at least two sensing strategies. First, the localization of elements to be joined before printing, to consequently adapt the design to the actual location of parts. Second, the monitoring of the printing results in order to accommodate the design to the actual material buildup and possible deviations from the idealized CAD geometry. Each of these tasks required the integration of state-of-the-art sensors (3.2.3 and 3.2.3) and development of their respective procedures (3.5.3 and 3.5.4):

Localization

Profile laser sensor   This device measures profiles, edges or custom features using laser triangulation. In this study, the profile sensor in use is a dedicated round object profile sensor from Baumer (*PosCon CM 2017*, Figure 3.2a). This sensor can measure the center of a circle by analyzing its edges (Figure 3.2b). A similar device can be used for other profiles (Gandia, 2020). The sensor is mounted on the end-effector next to the welding torch and is enabled through the Localization procedure (see Section 3.5.3).

(a)   (b)
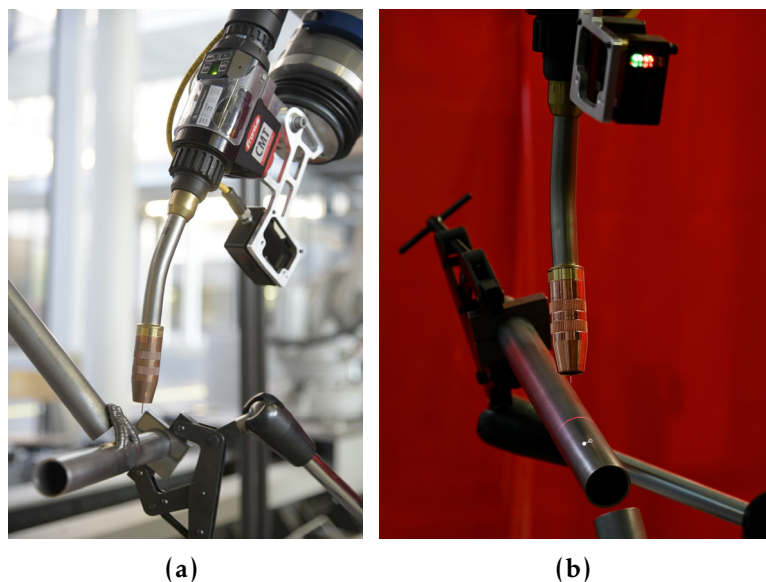
Figure 3.2: *Localization: (a) PosCon CM Baumer profile sensor with custom mount on the welding torch, and (b) Localization process: circle center measurement and comparison with target center location.*

Monitoring

Touch-sensor   This sensor consists of a converter unit that can trigger a stop signal to the robot if a closed circuit is found. The sensing technique consists in electrically charging the welding wire or electrode to use it as a probe in a programmed searching motion. If the electrode touches the workpiece, the closed circuit is recognized and the position of the electrode's tip and workpiece are stored. The technique is implemented with an off-the-shelf solution from ABB which includes the converter unit and search functions (*SmarTac, Application Manual* 2021, Figure 3.3b).

TCP calibration unit   As part of the automation of the touch-sensing process a TCP calibration station unit is used. This unit verifies the dimensional characteristics of the nozzle and electrode and is used in combination with the touch-sensing procedure as well as offering other useful functions such as measurement of the torch neck, cleaning of the interior of the welding nozzle and cutting of the electrode at the TCP stored length (*BullsEye* 2022, Figure 3.3a).

<div align="center">(a)   (b)</div>
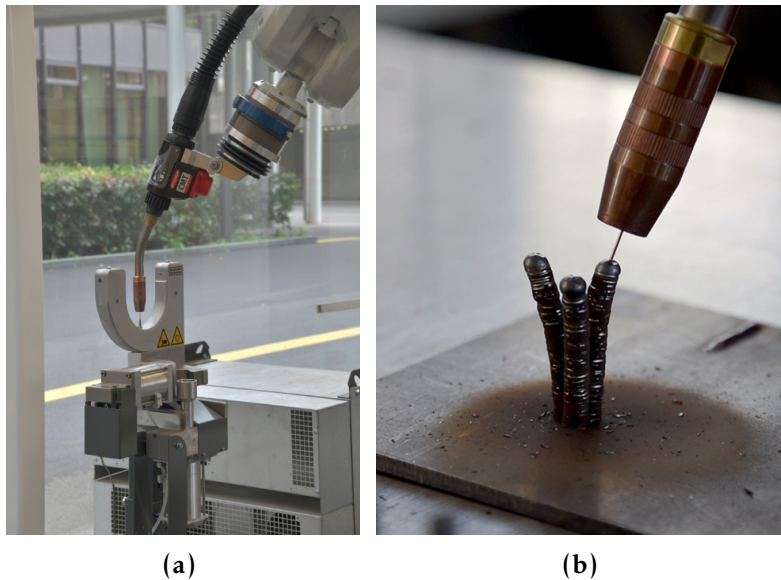
Figure 3.3: *Touch-sensing: (a) Bullseye station for torch calibration and cleaning, and (b) Touch-sensing on a freestanding WAAM part.*

3.2.4 Comparison of experimental setups

The setup specifications are illustrated in Figure 3.4 and Table 3.1. While Setup A provides an entry-level and accessible power source and low technical requirements, the lack of programmability of the process parameters and lack of integration with the robot controller makes it unsuitable for the aimed application. Setup B provides a wide range of process controls, sensing capabilities and a fully-integrated solution that perfectly matches the requirements of an IPWAAM application.

(a) Setup A

(b) Setup B

(c) Results Setup A
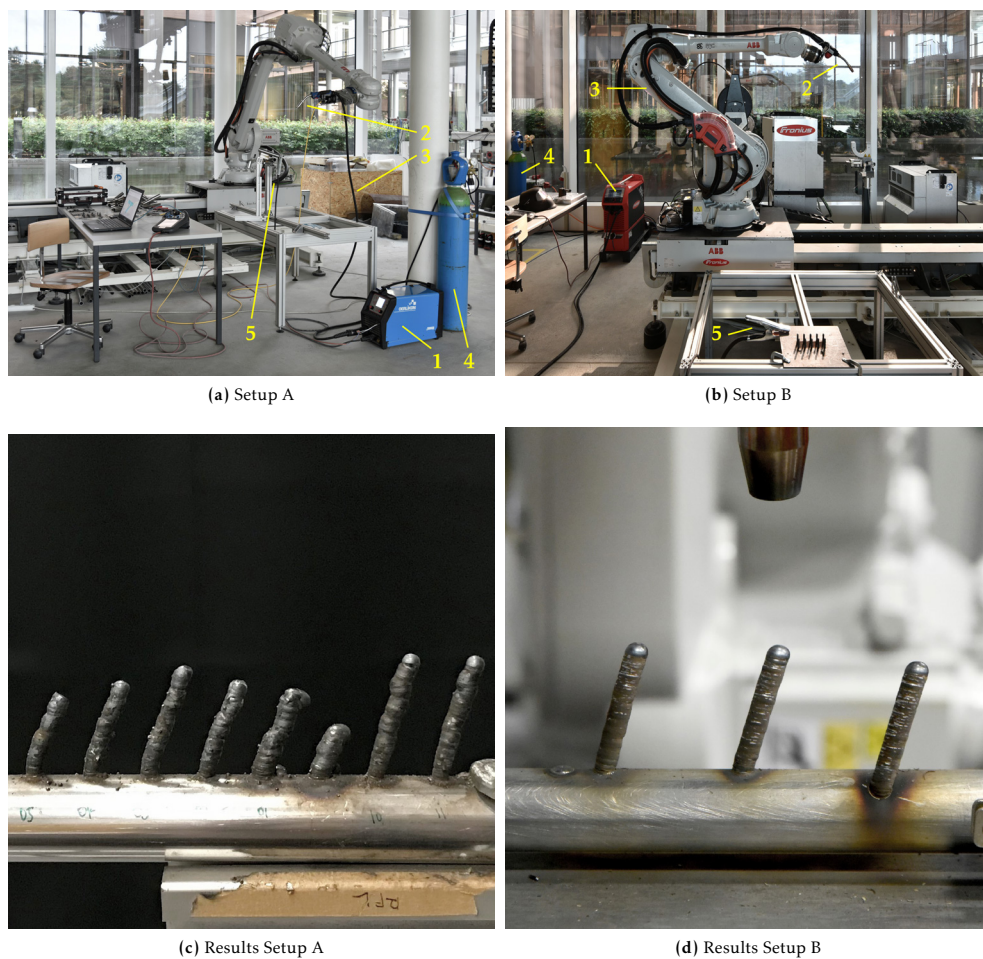
(d) Results Setup B

Figure 3.4: *Comparison of WAAM setups: (a-b) 1. Power source, 2. Welding torch, 3. Tooling for the feeding and transport of the wire, shielding gas and ground, 4. Gas supply, and 5. Ground clamp, and (c-d) Discrete deposition results.*

	Setup A	Setup B
Torch	GMAW	CMT
Wire (mm)	0.8	1.2
Heat input	High	Low-High
Welding sensors	N/A	SmarTac
Localization	PosConCM	PosConCM
Robot integration	No	Yes
Auxiliary	N/A	Torch cleaning station
Cost range	Low	Medium

Table 3.1: *Comparison of welding equipment setups*

3.3   Software

IPWAAM requires software for Geometry generation and visualization, Planning and execution, and Sensing tasks, and Data structures for organization and storage. The Workflow that connects these tasks relies on bidirectional communication between the design environment and the physical world: first, from design to execution, and then through monitoring of the manufactured results, back to the design. As introduced in Section 2.4, the feeding forward and feeding back of information is essential to ensure that design intent is carried out throughout the construction process and vice-versa, that the design can be constantly informed by the physical reality.

A key piece of the software development of this research is the intent to make use of different functionality made available by the COMPAS framework. COMPAS is an application-agnostic Python-based framework developed collaboratively at the Institute of Technology in Architecture at ETH Zurich since 2016 (van Mele and many others, 2017). The framework contains a core general-purpose library with flexible data structures, geometry processing functionality and numerical solvers, to name a few, and a series of extensions aligned with the fields of research developed at the Institute.

3.3.1 Workflow

The pipeline to design and fabricate IPWAAM connections is described in detail in Chapter 4. A primitive IPWAAM connection such as the one presented in Section 3.6.5 serves to illustrate a simplified workflow for IPWAAM objects:

i) To relate virtual and physical worlds, a user-defined `work object`, *a coordinate system used to describe the position of a work piece* (*Robotstudio* 2010), is measured and created in the robot controller and a parallel is constructed in the CAD interface. The two in place elements to connect, e.g., two tubes, are placed in the physical `work object` and then measured by teaching, touch-sensing, or localization procedures (Section 3.5) to bring that precise location back to the virtual environment (Figure 3.5i.).

ii) A simple connection between elements, such as a straight line, is drawn in the CAD interface and subdivided or *sliced* with a desired `layer height` resulting in subdivision points (Figure 3.5ii.)

iii) An algorithm is run to find collision-free torch orientations. This algorithm requires the actual geometry of the tool and an additional extra tolerance. The algorithm runs through each subdivision point and orients the tool normal to the path. Then, it checks if a boolean intersection between the mesh of the tool and the mesh of the in place elements exists. If no collision is found, the algorithm moves to the next subdivision point. If a collision is found, the tool is rotated away from the elements, iteratively increasing the `tool angle` until no collision is found (Figure 3.5iii.). If a maximum user-specified `tool angle` is reached, e.g., 45 degrees, a warning is raised for the user to manually change the geometry and run the algorithm again[8].

iv) When all the collision-free tool orientations along the path are found, the resulting `robot targets` are stored in a `WAAMPath` data

---

[8]These steps are superseded by the adaptive detailing workflow where only collision-free paths are created. However, the latest method can be considered an overhead for geometry involved in experiments such as the primitive connection, where the cost of the manual corrective operation is quite small.

structure and exported as a `.json` file. Execution tasks start by running a script that initializes the communication with the robot controller. The script then calls the requested printing procedure, e.g. `print_waam_column` passing the data stored in the previous step and the user-defined welding parameters. After an OK from the user on the robot teach-pendant, the robot procedure starts (Figure 3.5iv.).

v) At a user-defined length of the procedure, e.g. end of the column, a touch-sensing procedure is executed to measure the location of the last deposited layer (Section 3.5.4). The recorded data is sent back and visualized in the CAD interface (Figure 3.5v.).

vi) Based on the measured data, the remaining geometry to print is adapted to fit in between the in place elements and the as-built path, and continue with step ii) (Figure 3.5vi.).

The communication between the different software and hardware parts of the system explained above builds on different environments, libraries, and protocols (Figure 3.6). Usually, each software task from generation to monitoring shares more than one software platform, i.e., different software ecosystems with associated libraries and functionalities. In the following sections, an overview of the data structures, environments, APIs, and libraries required to accomplish the primitive connection example is described.

3.3.2 Data structures

The IPWAAM library or `ipwaamlib`, which has been developed to run the experiments, provides data structures for the fabrication and visualization of IPWAAM components. The library inherits serialization methods, design patterns and documentation style from the COMPAS framework. The `ipwaamlib` provides three custom data structures:

WAAMPath Wraps the design data structure `Path` (Section 4.2) with fabrication parameters. It contains:

- Description: I.D., type (e.g. column, line, curve).
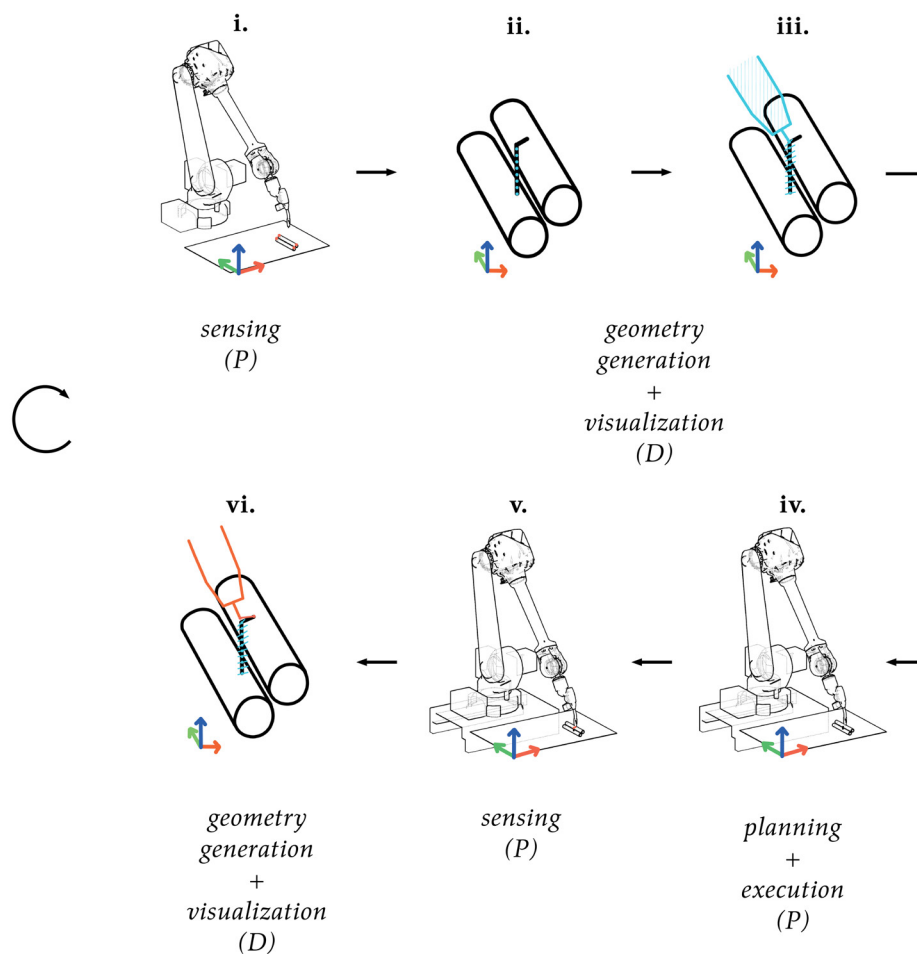
Figure 3.5: *Workflow for a primitive connection, physical (P) and digital (D) steps: i. Surveying the scene (P), ii. Generation and visualization of geometry and robot targets (D), iii. Preparation of fabrication data (D), iv. Execution of IPWAAM (P), v. Monitoring the printed result (P), vi. Adaptation of the remaining printed path (D), and repeat.*

- Fabrication data: robot target `Frames`, robot `Trajectory`, `cooling time` per layer, `seam length`.

- Process description: `build angle` relative to gravity, `layer height`, number of layers.

- Geometry: inherited attributes from `Path` (Section 4.2).

WAAMConnection   Wraps the design data structure `Connection` for describing and operating with multiple `WAAMPaths`. It includes:

- Description: I.D., type (e.g. columns).

Environments   Software and core libraries

CAD

Conda

Docker

Machines
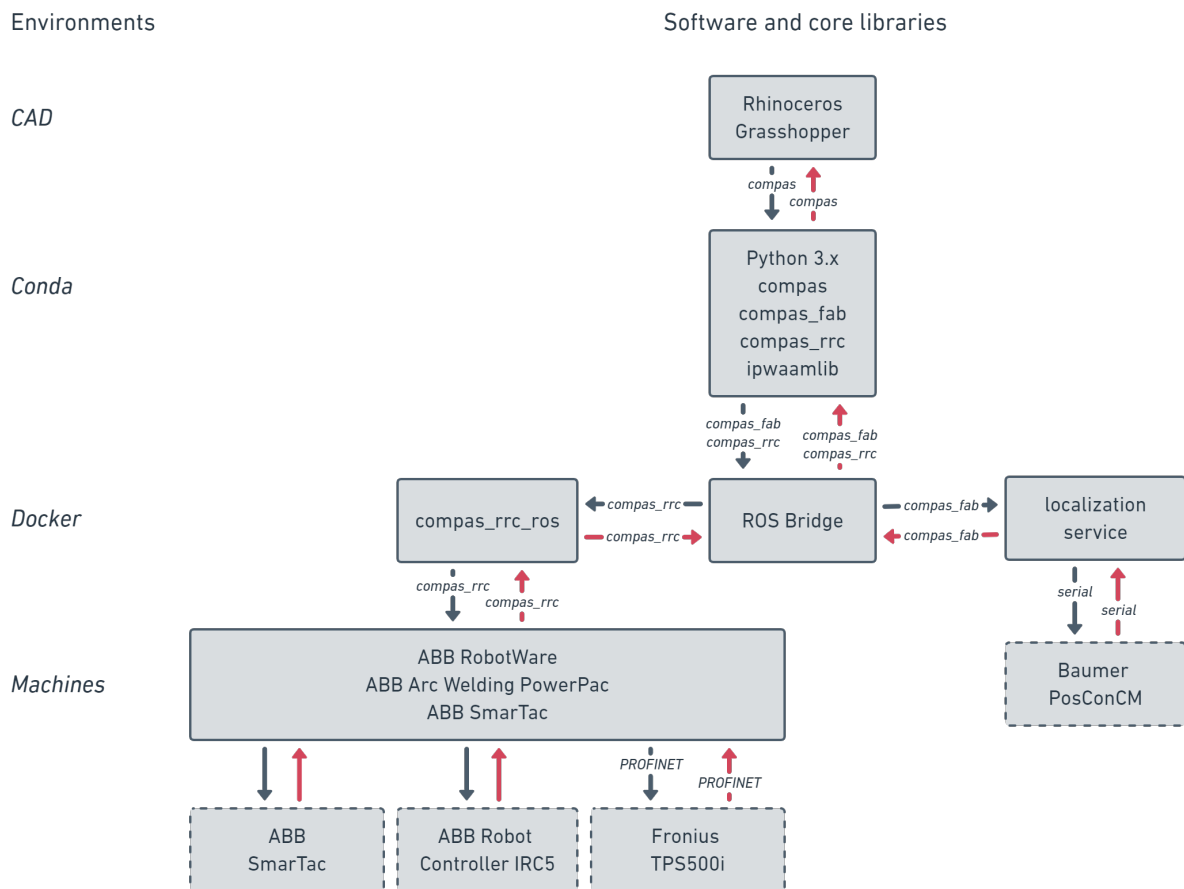
Figure 3.6: *IPWAAM communication diagram. Adapted for IPWAAM after* Robotic Assembly with COMPAS *2019* and *Fleischmann, Casas, and Lyrenmann, 2020.*

- Fabrication data: WAAMPaths.

- Geometry: inherited attributes from `Connection` (Section 4.2).

SensePath   The data structure consisting of fabrication data needed to execute a sensing procedure. It contains:

- Description: I.D., sensor, sensing procedure.

- Fabrication data for localization procedures: robot target `Frames` to scan. Fabrication data for touch-sensing procedures: robot target `Frames` to search.

- Recorded data for localization procedures: radius, coordinates in x, and z of the laser beam. Recorded data for touch-sensing procedures: found robot target `Frame`.

3.3.3 Geometry generation and visualization

In IPWAAM, geometry-related tasks consist of creating, manipulating and visualizing in place elements and printing paths. These tasks rely on a CAD interface with scripting functionality and an integrated development environment (IDE) that support Python programming.[9] The main libraries and APIs in use for this group of tasks are:

> `Rhino.Geometry` The geometry namespace of `RhinoCommon` used for description, processing and visualization of geometric objects (McNeel, 2010). In IPWAAM, `Rhino.Geometry` is the main library used for the manipulation and generation of printable paths.

> `compas` The core library of the COMPAS framework provides data structures and methods extending geometry processing available in `RhinoCommon` with Python libraries such as `NumPy`. Furthermore, `compas` provides design patterns to serialize and de-serialize geometric data (van Mele and many others, 2017).

> `compas_rhino` **and** `compas_ghpython` Are the CAD packages from `compas` that work as translators between `Rhino.Geometry` and `compas` as well as artists for visualization in Rhinoceros and Grasshopper of `compas` geometry (van Mele and many others, 2017).

In addition to its geometry library, Rhinoceros 3D (McNeel, 2010) is used as a CAD visual interface or canvas for plotting and manually interacting with geometry. The Rhinoceros plugin Grasshopper 3D (Rutten, 2007) is used for programmatically interacting and visualizing objects, organizing scripts, and annotating steps of the workflow.

3.3.4 Planning and execution

In the field of robotics, *planning* refers to solving the sequence of tasks and motions performed by a robot to achieve a certain goal. Motion planning is also generally referred to *path planning*. Although beneficial, path planning is not required for IPWAAM objects when the scale

---

[9]The communication between the CAD platform and the IDE is supported by the `utilities` module of the `compas` library and by the `conda` package manager. `conda` allows creating virtual environments to consolidate the required versions of the project libraries and make them available across software platforms.

of parts or the complexity of motion between robot targets is limited. This is the case of the material experiments presented in this chapter including a primitive connection (see Section 3.6).[10] Here, *planning* tasks include finding possible robot targets and preparing the fabrication instructions to be executed by the robot controller. *Execution* consists in calling robot procedures (see Section 3.5). The libraries involved in planning and execution tasks are:

`compas` provides data structures such as `Frame` and `Transformation` with useful constructors for robotic fabrication. (van Mele and many others, 2017).

`COMPAS FAB` is the COMPAS framework package for robotic fabrication initiated by Gramazio Kohler Research in 2017. In addition to motion planning tools through different backends, the package provides the interface for the Robot Operating System (ROS), an open-source framework for writing robot software, and is used here as a communication platform between the user's computer and the robot controller.

`roslibpy` is the Python wrapper to communicate with ROS via WebSockets (Casas, Lytle, Lüdtke, et al., 2018).

`compas_rrc` facilitates online control for robots as a Python wrapper for RAPID functions. This library is used to send and receive fabrication data for all procedures described in 3.5 sent to the robot controller (Fleischmann, Casas, and Lyrenmann, 2020).

`compas_rrc_ros` is the ROS package to connect to the vendor-specific RRC driver (Fleischmann, Casas, and Lyrenmann, 2020).

`RRC` is the RRC driver for ABB robots (Fleischmann, Casas, and Lyrenmann, 2020).

`ipwaamlib` is the WAAM-specific library providing data structures (3.3.2), printing procedures and process settings.

---

[10]In these cases, the robot trajectory is solved by the robot controller based on the user-defined robot targets. However, when more complex tasks are involved, motion planning becomes essential for finding suitable trajectories. This approach is further tackled by the adaptive detailing pipeline integrating planning strategies to create collision-free and WAAM-suitable trajectories with the Robot reachability and Path slicing components presented in Chapter 4.

Finally, a `Docker` container is implemented to bundle all the components together and facilitate a stable reproduction of the system's versions (Figure 3.6).

3.3.5 Sensing

Sensing tasks requires software to prepare and execute surveying and monitoring tasks, and communicate, store and retrieve recorded data. The software and libraries involved in these tasks are:

> `SmarTac` is a RAPID system module that provides the functions to search and detect contact with metallic components (*SmarTac, Application Manual* 2021).

> `COMPAS FAB` provides the interface between ROS Bridge and the serial protocol used by the localization sensor (Casas, Lytle, Gandia, et al., 2021).

> `compas_rrc` provides the interface to feed back and retrieve the result of the search operation during touch-sensing (Fleischmann, Casas, and Lyrenmann, 2020).

> `ipwaamlib` provides data structures (3.3.2), procedures, and visualization of the recorded data.

3.4 Materials

IPWAAM requires three consumables: an electrode to melt; a shielding gas to protect the fusion process from oxidation; and a substrate to melt the electrode onto. In this thesis, the material selection for the three consumables is based on availability and potential use in architectural-scale applications, and, in the case of the electrode, on its suitability for the CMT WAAM process.

3.4.1 Wire

The selected electrode is a mild steel welding wire type AWS ER70S-6. This category of wire includes silicon and manganese as deoxidizing elements to decrease the sensitivity to rust and impurities normally found on the substrate surface while at the same time increasing the

yield and tensile strength of the weld (Tyagi, 2002). Two wires of this type with similar chemical compositions presented in Table 3.2 were used and mechanically characterized in experiments 3.6.6.2 and 3.6.6.3:

Solid wire	Experiments	$\varnothing$ [mm]	C	Si	Mn
CARBOFIL 1	Setup A	0.8	0.08	0.90	1.50
UNION SG 2-H	Setup B	1.2	0.08	0.80	1.40

Table 3.2: *Chemical composition of solid wires of type ER70S-6*

Specific 3D printing wire alternatives (e.g. 3DPrint AM 35) were tested with less successful results, suggesting that a higher percentage of alloying elements in the wire composition could have a detrimental effect on the ignition phase of the discrete WAAM deposition (3.5).

3.4.2 Substrate

The substrate is the base material where the bar or connection is printed onto. The selection of substrates includes circular and square cross-sections of mild steel S235 of 2 mm thickness. The cross-section minimum size (30mm) was selected based on the recording range of available sensors for circular and rectangular profiles. The material experiments presented in 3.6, were carried out onto plates with similar surface characteristics, and different thicknesses (details are provided on each experiment's and prototype's description).

3.4.3 Gas

Both GMAW and CMT processes require a shielding gas to avoid air from the atmosphere getting in contact with the electrode during the melting and solidification process. The gas mixture has a great influence on the penetration form of the resulting properties of the products (*The Fronius Welding Dictionary* 2021), therefore a selection was made based on existing literature. In this research, a mixture of 82% Argon and 18% CO_2 commercialized as ARCAL 5 was used in all experiments.

3.5 Processes

`IPWAAM` comprises printing and sensing production processes. Figure 3.7 illustrates a typical IPWAAM flowchart. This section first describes the WAAM depositions known to date, followed by the specific IP-WAAM challenges that inform the variations in the printing procedures known from the literature. Then, each subtype process is described: Discrete printing, Continuous and hybrid printing, Localization, and Touch-sensing.

Depositions

There are at least two distinct deposition techniques in WAAM: discrete and continuous. WAAM *discrete*, also referred as *point-by-point* or *dot-by-dot*, enables the production of 3D objects formed by single drops or point depositions. When these depositions are extended from points to lines, they are called here *continuous deposition*, or in the literature simply, WAAM. Many other combinations between these are possible (Figure 3.8).

Regardless of which deposition technique is used, the in place constraint determines two spatial conditions for IPWAAM printing:

> **Spatial paths** As a result of an optimal material distribution given the limited accessible and reachable space constraints, IP-WAAM paths often present three-dimensional curved shapes. Slicing a three-dimensional curve while maintaining the tool aligned to the path curve results in non-planar layers. Furthermore, the varying orientation of the tool relative to the gravity vector has an effect on the shape of the deposited seam (Figure 3.10).

> **Spatial layers** In addition, as a result of printing in between collision objects, an accessible and reachable tool orientation must be found for each layer. This constraint results in an additional re-orientation of the tool relative to the path curve, with an additional effect on the shape of the deposited seam (Figure 3.10).
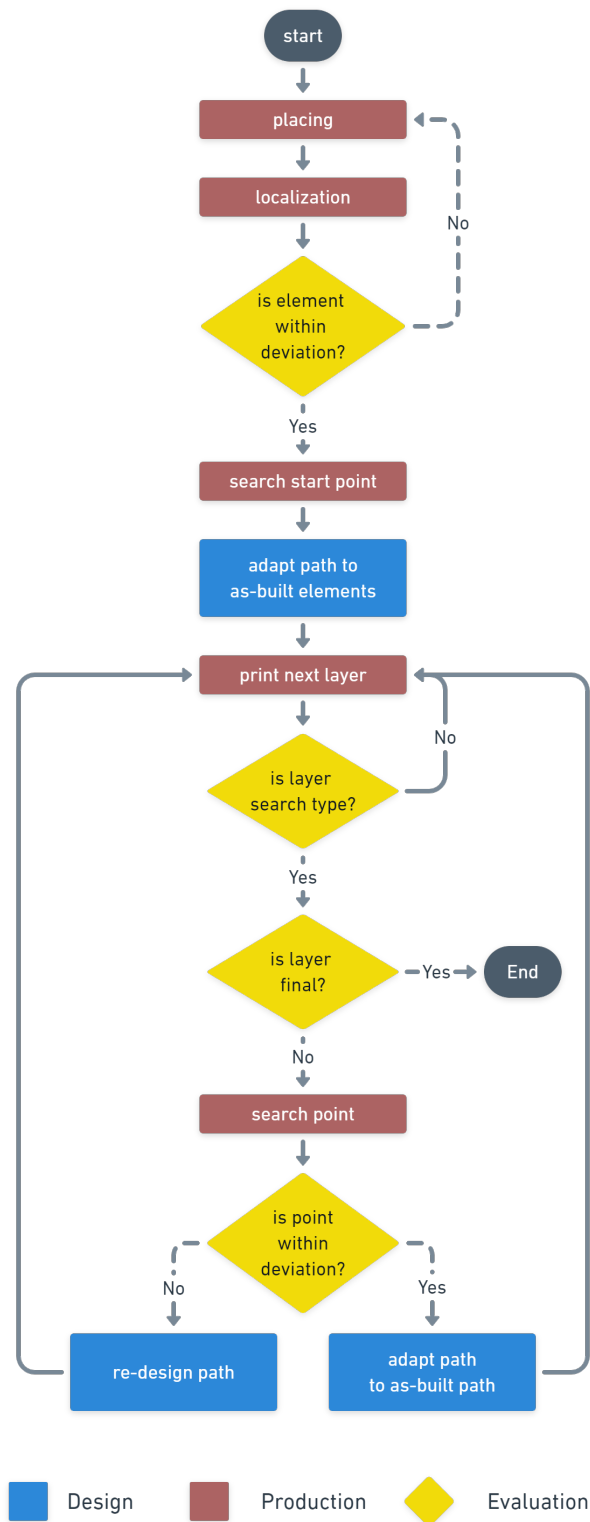
Figure 3.7: *Production flowchart*
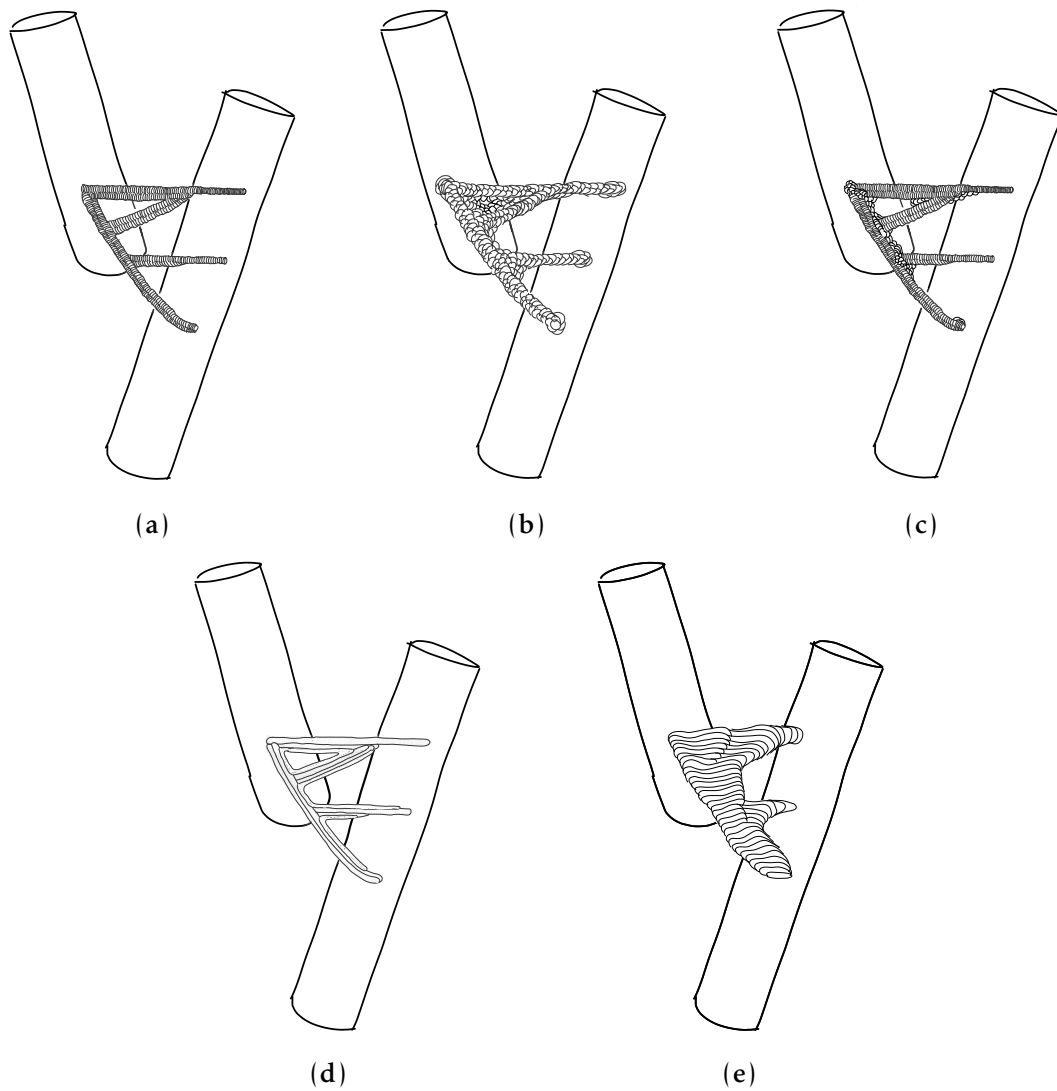
Figure 3.8: *Deposition strategies: (a) Point-by-point linear paths (main deposition explored in this thesis), (b) Point-by-point volumetric paths or "grape-like" as in Figure 5.2f, (c) Combination of point-by-point linear + "grape-like" depositions used as reinforcements, (d) Hybrid deposition, point-by-point linear paths + continuous depositions on top as reinforcements, and (e) Only continuous deposition.*

A comparison between a freestanding discrete WAAM deposition and a constrained IPWAAM deposition between collision objects is provided in Figure 3.9.

(a)   (b)

Figure 3.9: *WAAM vs. IPWAAM: (a) freestanding, and (b) collision constrained.*
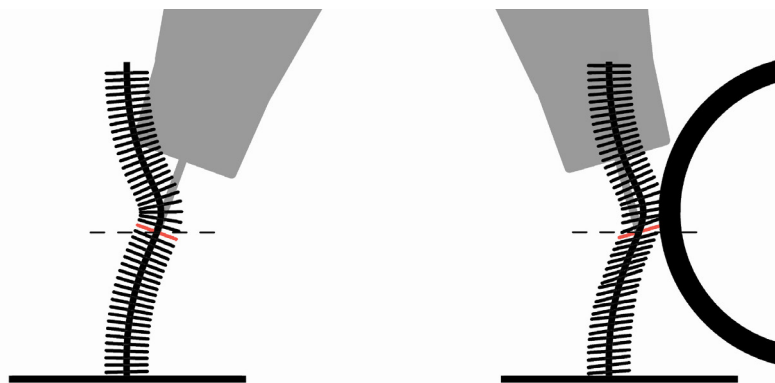
Figure 3.10: *Slicing comparison WAAM vs. IPWAAM of the same curve: (a) Freestanding WAAM slicing with a tool orientation normal to the path's tangent results in non-planar layers, and (b) Constrained IPWAAM slicing with non-planar layers and additional rotation of the tool to avoid collisions. The dashed line indicates the same layer number where two different tool orientations are found.*

3.5.1   Discrete printing

The discrete deposition is the transfer of material by single points, dots, or very short seams with a cooling time in between (Figure 3.11). To date, most applications using discrete printing have targeted linear or curvilinear elements (Figures 2.9d, 2.9e, 2.9f), however, a surface element could also be printed with discrete deposition. Applications of discrete printing to date include reinforcement for concrete structures (Mechtcherine et al., 2018; Müller et al., 2019; Classen, Ungermann,

and Sharma, 2020), complex network and lattice structures (Laghi et al., 2020; Z. Yu, Yuan, et al., 2019; Radel et al., 2019; Abe and Sasahara, 2019), and non-standard connectors (*Wire and Arc Additive Manufacturing (WAAM) of Complex Individualized Steel Components* 2022).
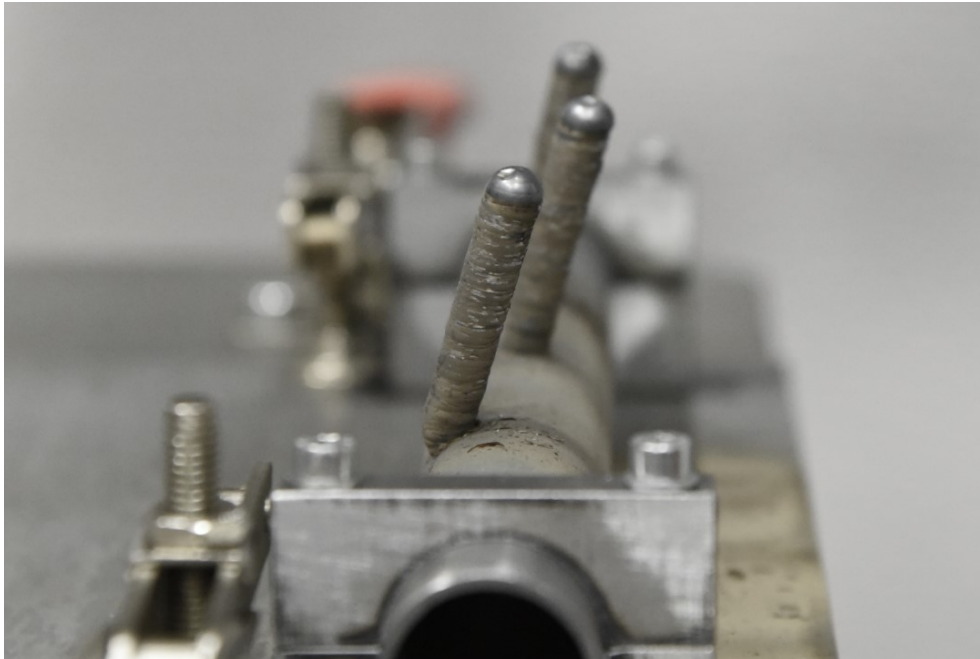
Figure 3.11: *Discrete printing*

Procedures

Each iteration of the discrete printing process consists of the following steps:

i. The robot moves to the first layer, positioning the tool center point (TCP), i.e., the tip of the wire electrode, at the center of the target frame and leaving a `stick-out length` between the tip and the torch nozzle

ii. The gas valve is started with a `gas pre-flow time`, shielding the target location from the atmosphere

iii. The arc process is enabled: the wire is fed and pulled at a certain `wire feed speed` with the CMT process (3.2.2)

iv.   The robot moves outwards of the target at a certain `welding speed` following the `build direction` vector for a certain distance or `seam height`. The arc process is disabled

v.   A gas `post-flow time` protects the seam as it solidifies

vi.   An idle time or `cooling time` lets the layer solidify

vii.   The process is repeated a certain number of iterations or layers with a custom `layer height`

Process parameters

The process parameters are here structured in the following three groups:

Geometric parameters   Each layer has the following associated geometric parameters (Figure 3.12):

(a)   **(b)**
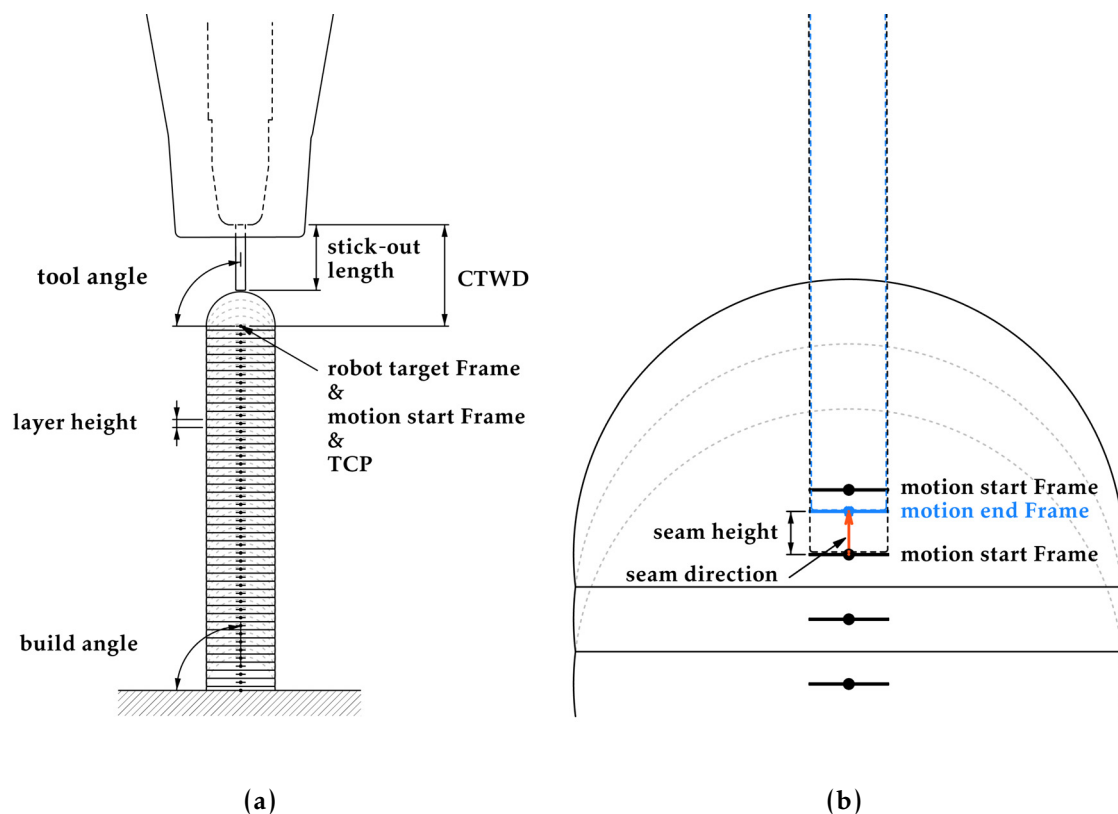
Figure 3.12: *Discrete printing, geometric parameters: (a) Layer height, build angle, tool angle, CTWD, stick-out length and robot target Frame (also motion start Frame and TCP) and (b) Seam height, seam direction, motion start and end Frames.*

Layer height is the euclidean distance between two consecutive points and is expressed in metric units, e.g. millimeters. The layer height is determined empirically in experiments 3.6.1 and 3.6.4 and is used as an input in the slicing process. The layer height is a dependent variable of the volume and shape of the previously deposited material.

Seam direction is the vector describing the motion between the point motion start and the point motion end during the arc process. This vector typically follows the `build orientation`.

Seam height is the euclidean distance between the `motion start Frame` and a `motion end Frame` during the arc process and is as well expressed in metric units, i.e., millimeters. The seam height is equivalent to the magnitude of the `seam direction` vector. This distance can be altered independently of the layer height, which in combination with the `welding speed`, will affect the volume of the deposited material.

Build orientation is the rotation of the tangent of the path curve relative to the gravity vector at a specific layer point measured in angle degrees as a `build angle`.

Tool orientation is the rotation of the tool frame normal at the print point relative to the path tangent measured in angle degrees as a `tool angle`. For the symmetry of the printed seam and consistency of the printing process, the ideal tool orientation is when the tool is tangent to the path curve, i.e., with a tool angle of 0 degrees.

Contact tip to workpiece distance or *CTWD* is the euclidean distance between the internal contact tip and the robot target or center of the ideal sphere of the workpiece expressed in metric units.

Stick-out length is the euclidean distance between the end of the electrode and the internal contact tip expressed in metric units.

Execution parameters

The following parameters are assigned to each layer. This set of parameters is defined in the fabrication process execution scripts.

Welding speed   The motion speed during welding in mm/s.

Motion speed   The motion speed during travel in mm/s.

Cooling time   The time in between one deposition and the following directly in contact, in seconds.

Welding parameters

The welding process can be controlled with a wide range of parameters, usually documented in the specific power source documentation. The key welding parameters presented next are assigned to each seam or layer and directly set in the power source in the "Job" settings. For reference, an example discrete WAAM job with its full list of process parameters can be accessed in A.1:

Wire feed speed   or *WFS* is the speed at which the wire is fed during the arc welding process, measured in mm/s.

Welding current   or *I* is the measure of the flow of electrons moving through the electric arc. The current is measured in amperes (A) and its value has a direct influence on the seam profile depth (*The Fronius Welding Dictionary* 2021; Pires, Loureiro, and Bölmsjo, 2006c).

Welding voltage   or *U* is the arc length or potential difference between the electrode and the workpiece. The voltage is measured in volts (V) and has a direct influence on the seam profile width (*The Fronius Welding Dictionary* 2021; Pires, Loureiro, and Bölmsjo, 2006c).

Gas pre-flow and post-flow   A fixed time during which the gas valve is open before and after the arc welding process to protect the seam from the surrounding atmosphere. The pre-flow assures

that the shielding has started before the deposition process. The post-flow shielding prevents oxidation and impurities from entering the seam during solidification (*The Fronius Welding Dictionary* 2021).

Arc characteristic   The curve that describes the relationship between the voltage and current for a specific material and shielding gas (*The Fronius Welding Dictionary* 2021).

The key discrete printing parameters are studied in the Experiments presented in this Chapter and demonstrated through the Adaptive Detailing pipeline in Chapter 5.

3.5.2   Continuous and hybrid printing

Continuous printing is the most widespread additive manufacturing deposition technique consisting of linear instead of point layers. Most of WAAM research has focused on developing this technique, as presented in Chapter 2. Continuous printing is of particular interest for its high-deposition rate for producing complex or large parts. For spatial connections, the technique could be used with at least four building strategies: **i.** prefabrication of nodes (see examples in Figure 2.10), **ii.** in place continuous build-up (Cros, 2017; Feucht, Lange, and Erven, 2019), **iii.** in place entry and exit sections for connections built with a discrete deposition (Figure 3.13), or **iv.** as in place reinforcement of previously printed discrete bridges (Figure 3.14, Ariza et al., 2018; Mitropoulou, Ariza, et al., 2019). The combination of a discrete bridge with a continuous print is what is referred to as *hybrid printing*.
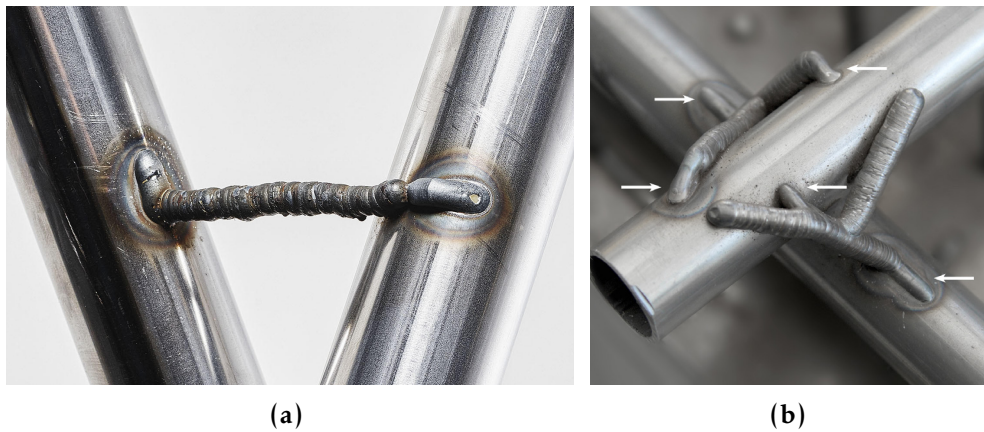
Figure 3.13: *Application of continuous printing type **iii.** at entry and exits in point-by-point connections: (a) A primitive connection printed in Setup A with one continuous entry and one continuous exit, and (b) Tree-like connection printed in Setup B with two continuous entries and three continuous exits.*

(a)   (b)
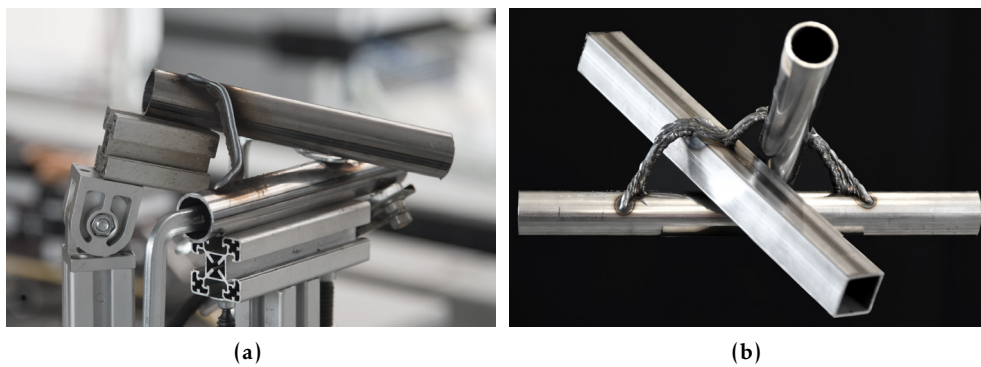
Figure 3.14: *Hybrid printing: (a) Ariza et al., 2018, (b) Mitropoulou, Ariza, et al., 2019.*

Procedures and key process parameters

Procedures for *continuous entries and exits* and *hybrid printing* were tested during the development of the IPWAAM technique. Figure 3.15 show a diagram and results of the two procedures on the same connection type:
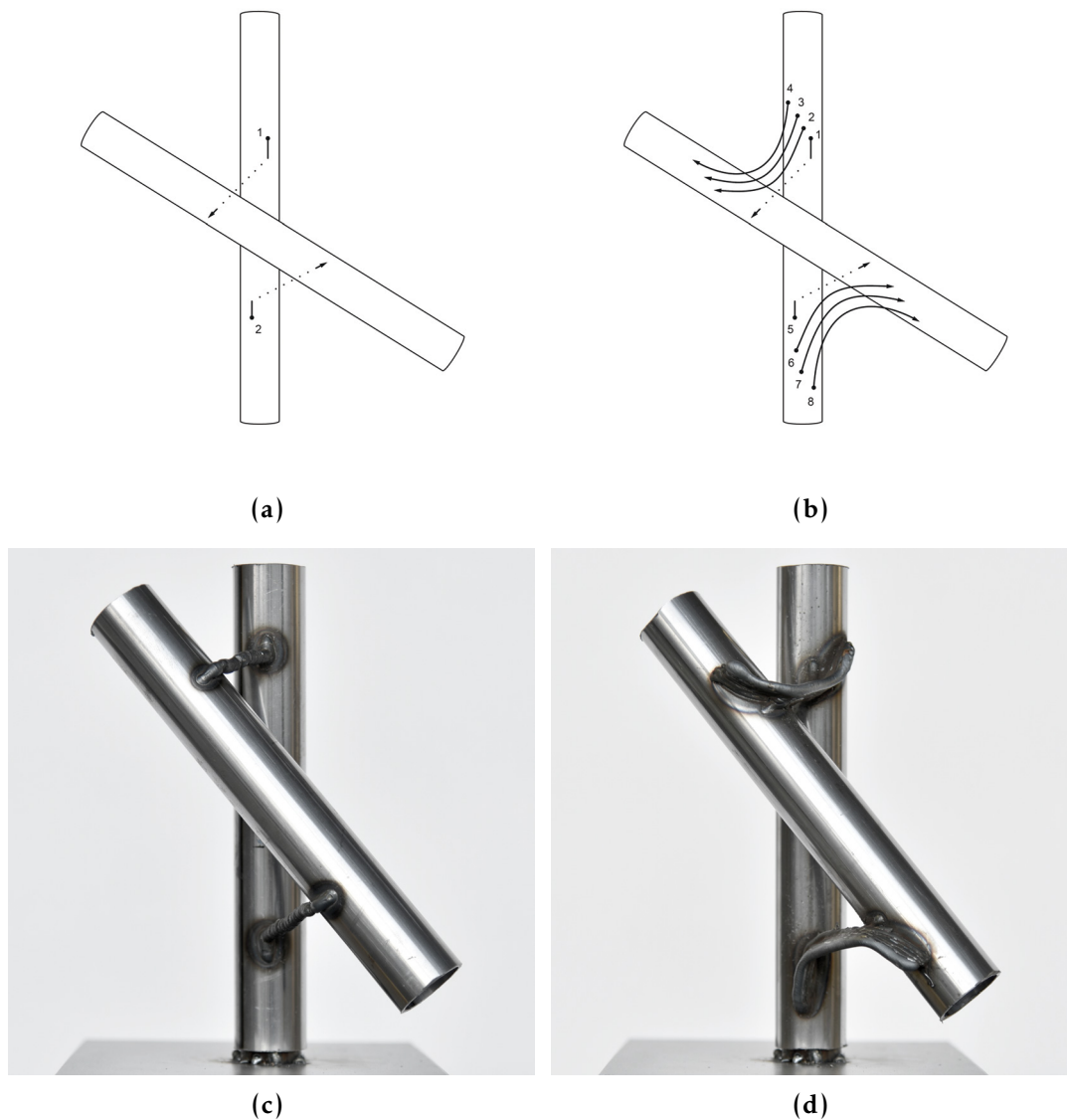
Figure 3.15: *Sequence of printing procedures and results for continuous printing: (a, c) Continuous entries and exits of a point-by-point connection (type **iii.**), and (b, d) Hybrid printing (type **iv.**).*

Continuous entry and exits of a point-by-point connection To increase the attachment area at the entries and exits of a connection built with a discrete deposition, continuous segments can be built at the start and end of the path directly on the base and target substrates (Figure 3.16). Additional parameters to the ones described in 3.5.1 need to be considered:
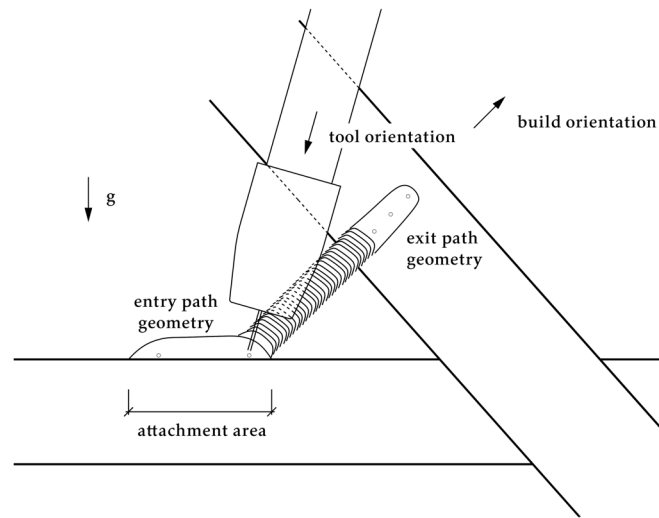
Figure 3.16: *Continuous entries and exits parameters*

Path geometry   The number and position of the target robot frames.

Attachment area   The size of the path, a variable of the functional requirements and the welding process parameters (see examples in 3.6.5).

Tool orientation   The orientation of the tool relative to the substrate. An ideal orientation maintains the tool normal to the target substrate (see example in Figure 3.17).

Welding speed   The motion speed during welding in mm/s, directly linked with the WFS and welding process parameters.

(a)   (b)   (c)   (d)
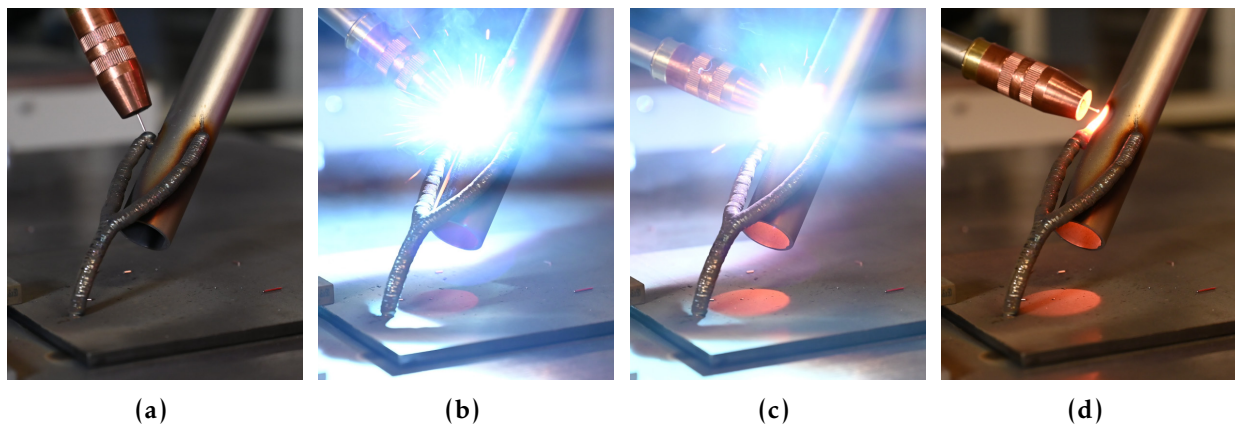
Figure 3.17: *Sweep motion trajectory in a continuous exit*

Hybrid printing   A high-deposition alternative to discrete printing is the combination of discrete and continuous depositions (Figure 3.15b). This strategy can be used as a planned or *a posteriori* reinforcement of a discrete path. The key process parameters of this approach are illustrated in Figures 3.18 and 3.19:
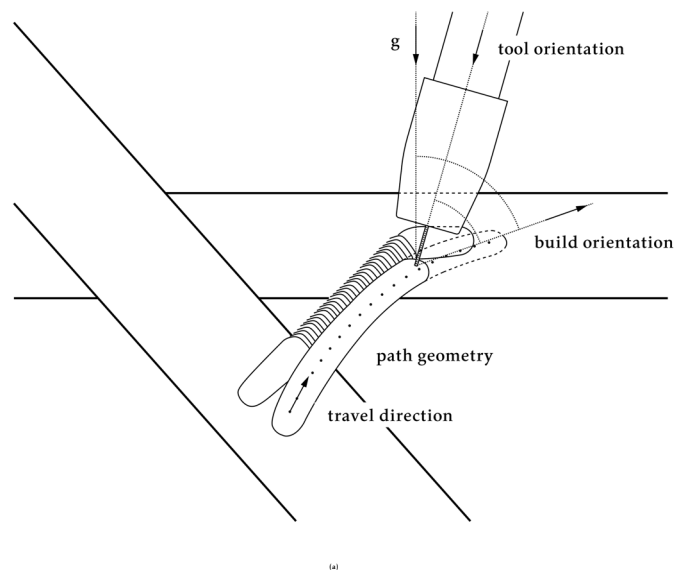
Figure 3.18: *Hybrid printing parameters*

Path geometry   Provided that a substrate exists, the continuous path can fully or partially follow the shape of the previously printed material (see examples in Figure 3.14).

Tool orientation   The orientation of the tool relative to the substrate. Increased flexibility of the torch orientation is observed for continuous depositions compared to discrete deposition. For continuous welding, the orientation of the tool relative to the direction of travel is formalized as pull or push welding, i.e., with the tool aligned to the direction of travel or with the tool opposing the direction of travel (Y. Liu, L. Ren, and Tian, 2019).

Travel direction   The required welding parameters depend to a great extent on the direction of travel relative to the gravity vector. This is formalized as uphill or downhill welding, i.e., against gravity or aligned with gravity (see for example Y. Liu, L. Ren, and Tian, 2019).

Welding speed   The motion speed during welding in mm/s, directly linked with the WFS and welding process parameters.

(a)   (b)
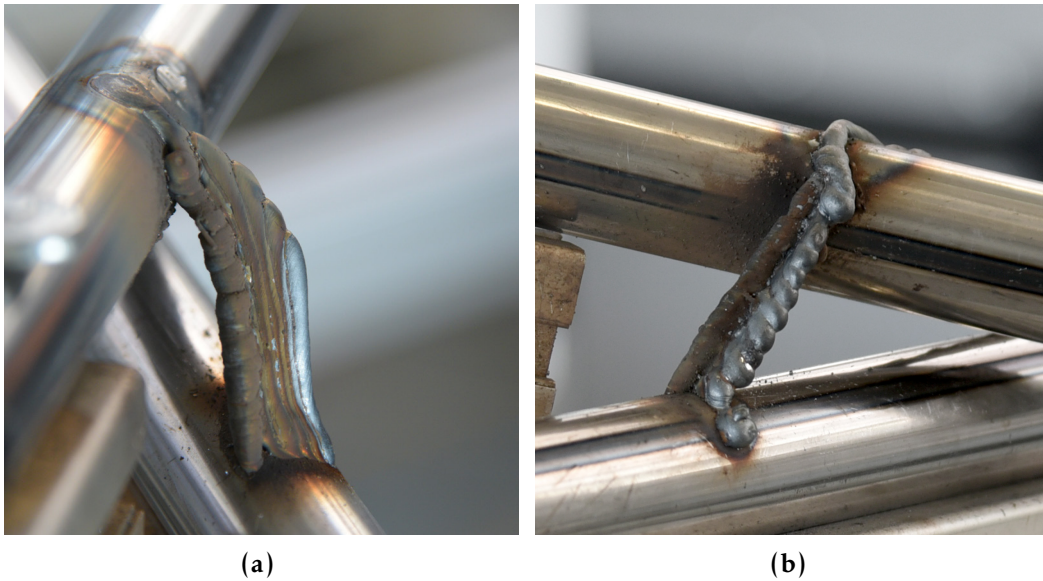
Figure 3.19: *Hybrid printing: (a) Continuous deposition on top of a previously built discrete bridge, and (b) Continuous deposition with a very slow welding speed.*

3.5.3   Localization

The goal of this process is to get the *as-built* position of in place elements. The process is structured in three procedures: **1.** pre-processing of data to be measured, **2.** execution of the localization sensor procedure, and

3. reconstruction of the as-built element position in the digital model. The procedures are targeted to the sensing setup described in Section 3.2.3. With this setup, the strategy consists of scanning independent sections of the element to find its axis.

Procedures

1. Pre-processing   The number of section measurements depends on the symmetry of the cross-section and the characteristics of the material of the elements. For circular stiff cross-sections, two measurements are enough to reconstruct the element's axis. The position of the sections to measure depends on space availability, i.e. if the element is supported by a robotic arm, then the gripping locations should be avoided.

To get a valid orientation of the sensor tool, a tentative location is defined and checked for collisions.[11] The target `Frames` to measure are then wrapped in the `SensePath` data structure, with additional fabrication data such as safe positions and approach offsets. Finally, speed motion parameters and type of measurement requested to the sensor are set (Figure 3.20).
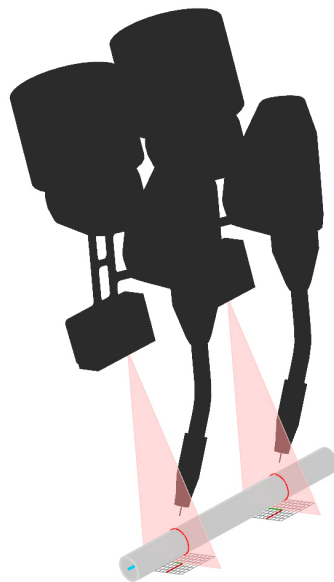
Figure 3.20: *Pre-processing: data for localization procedure*

---

[11] The collision-free orientation can be set or searched with the information provided in the Planning Scene (4.3.5.1).

2. Localization   This procedure executes the program prepared in
1.. The sensor is initialized by calling a ROS service via serial; then,
the localization procedure is executed. Once the robot reaches the
localization frame, the sensor is triggered by a topic request, and the
measured data (response) is then published and stored back in the
`SensePath`. These steps are repeated for each section (Figure 3.21).
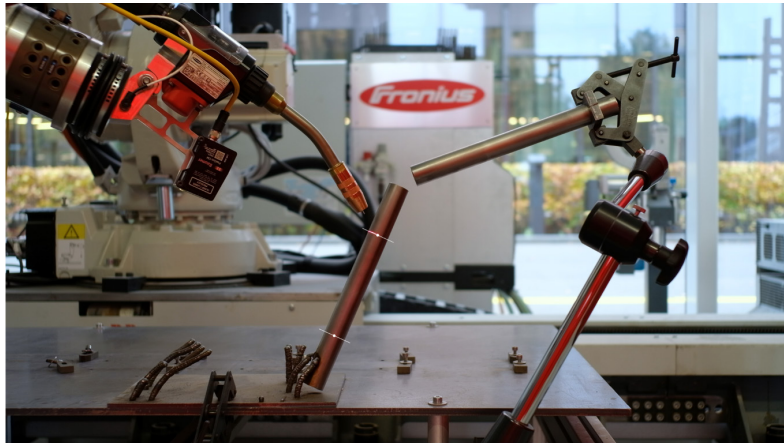
Figure 3.21: *Localization: the procedure is executed for each element of the
assembly.*

3. Reconstruction   The last step consists in reconstructing the re-
trieved data. This requires integrating the original `Frame` information
with the values stored in the sensing procedure, as the sensor only
stores numerical values with no cartesian space information. Three
reconstruction methods can be used with the sensor data. In all three,
the goal is to reconstruct the center point of the scanned circle section.
This center can be reconstructed **a.** as a center between the edges of the
scanned cross-section, **b.** as an offset from the X-center and Z-center of
the localization `Frame`, or **c.** as a three-point circle with the edges and Z-
Top offset values (Figure 3.22). At this point, the user can choose which
reconstruction method to use. Usually, method **c.** is preferred as it uses
three measured values compared to the other two methods.[12] Finally,
the results are visualized in the CAD environment, and deviations from
the original position are shown to the user.

---

[12] During the development of this procedure, experiments have shown only a sub-
millimeter difference between the different reconstruction methods, therefore, only
one method is used in practice.
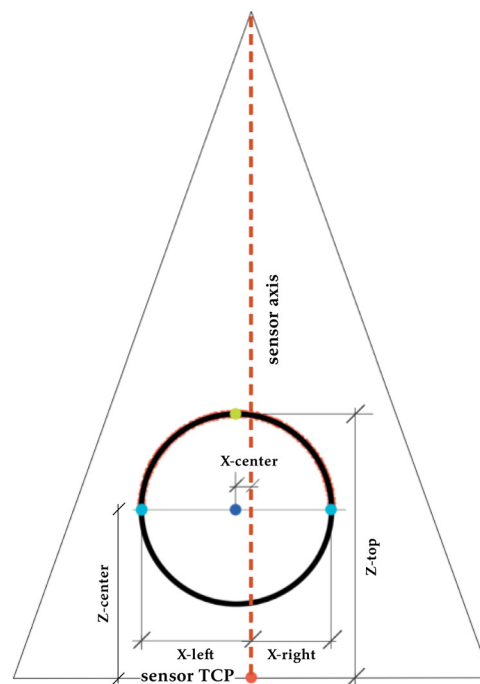
Figure 3.22: *Reconstruction of recorded PosCon CM data: reference point, sensor TCP and center of the localization Frame (in red), point at the top of the scanned cross-section, Z-top offset (in yellow), points at the edges of the scanned cross-section, X-left and X-right offsets (in cyan), center, X-center and Z-center offsets (in blue). With this data, any of the methods a.-c. can be used.*

Discussion on localization

Validity   The implementations of the process procedures are targeted to a specific laser sensor and, therefore, only applicable for round profiles that fit in the light range, in this case, of a diameter between 30 and 130 mm.

Known limitations   The accuracy of the results depends to a great extent on the sensor and robot arm calibrations, and therefore it is required to further test the accuracy and precision limits of both systems.

Depending on the scale of the assembly and the placing method in use, a certain redundancy can be noted within the localization approach. This sensing strategy builds on the assumption that some inaccuracy in the placing procedure, the manipulator and/or from the elements is plausible. For very small-scale parts, however, deviations can be negligible. When the number of parts increases, on the contrary, a re-measurement of the elements that are not supported by the robot

manipulator is required, as these elements will likely settle in a slightly different position once the gripper has been released.

Alternative methods   Sensing strategies with broader recognition capabilities should be considered in the presence of components with varying geometric or surface qualities (see examples in Johns and Anderson, 2018).

3.5.4   Touch-sensing

The goal of this process is to get precise *as-built* positions of the elements as well as the last printed layer (Figure 3.24). In the same fashion as in Localization, the process is structured in three procedures: **1.**pre-processing of data to be measured, **2.** execution of the search procedure, **3.** reconstruction of the as-built last layer position. The procedures are tailored for the touch-sensing setup described in 3.2.3. The sensing strategy consists of a robotic probing of the built parts through a programmed search path. The procedure is used in two conditions: on top of building elements, i.e., the circular profiles, before the printing starts, and at any time of the production process on the last printed layer.[13]

Procedures

1. Pre-processing   The search path consists of a linear motion *from* and *to* predefined positions. The start and end positions result from linear transformations of a print `Frame` along its Z axis (Figure 3.23). The search range is defined by the user (e.g., 20 mm). In addition to this data, a search motion speed needs to be predefined. This speed is an important parameter, as it affects the accuracy of the result (e.g., 2 mm/s). This data is then packed in a `SensePath` data structure to be called by the search procedure.

---

[13]See Chapter 4 (4.3.5.3) for different geometric conditions where this procedure becomes relevant in the design process.
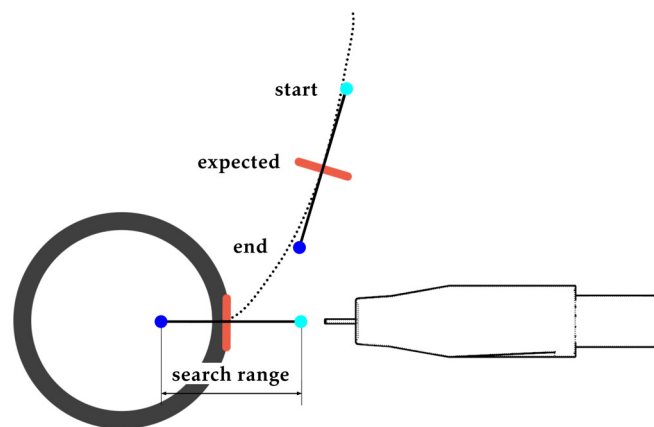
Figure 3.23: *Touch-sensing pre-processing: search range (in black), search start point (in cyan), search endpoint (in blue), expected search point (in red).*

2. Search   The search procedure wraps the RAPID function `Search_1D` which takes two `robtargets` (start and end search points). The program automatically stops once a close circuit is detected, storing the pose of the robot at that exact time. It is mandatory that at this point, the TCP calibration is very accurate, as the TCP, i.e., the tip of the electrode, is used as the recording position. To ensure that the TCP is correctly calibrated, a manual cut of the electrode and automatic feeding of the correct length is done before the procedure. Alternatively, the torch calibration station is used[14]. Finally, the robot pose is stored in the `SensePath` for later access.

---

[14]However, this procedure takes twice the time as the manual process

(a)   **(b)**
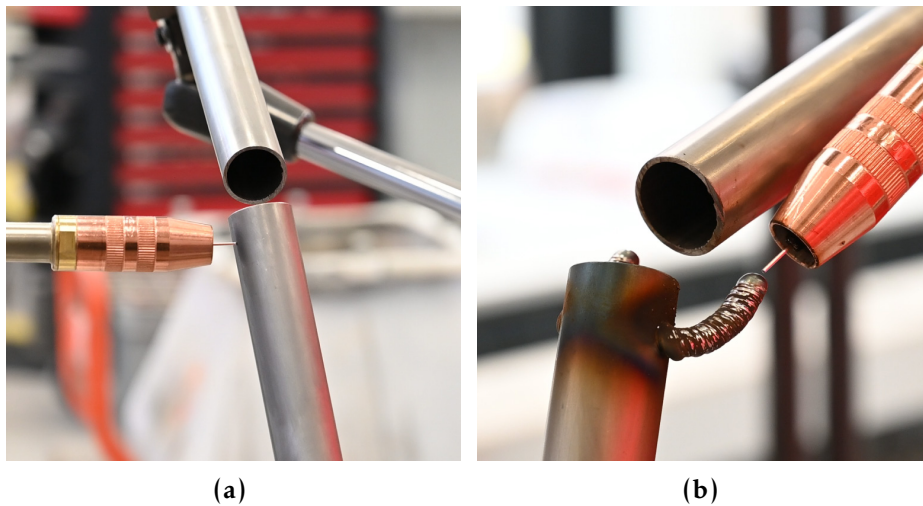
Figure 3.24: *Touch-sensing: (a) Search procedure on element, and (b) Search procedure on path.*

3. Reconstruction   The recorded data is reconstructed in the CAD environment for an immediate visual check of the result. The point coordinates can be seen immediately after the search procedure is finalized (Figure 3.25). This information is then interpreted by the `Path adaptation` component to resume printing with an adapted path.
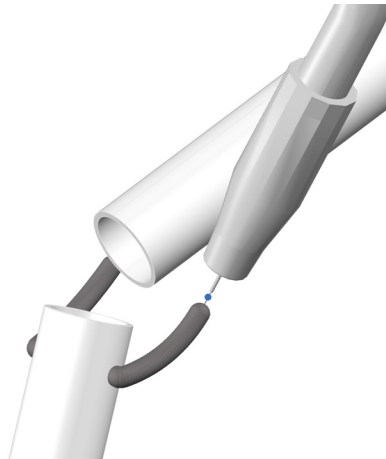
Figure 3.25: *Touch-sensing reconstruction: measured coordinates (in blue)*

Discussion on touch-sensing

Validity   The touch-sensing procedure as presented here is a standard procedure with wide acceptance in the industry. It presents large

flexibility, as it can be used for any type of workpiece as long as it is conductive. However, surface conditions presenting rust or dirt might require preprocessing (which is in any case necessary for proper fusion).

Known limitations In the context of WAAM, the main limitation is the measurement of only 1 point at a time. For simple cross-sections such as the ones explored in this work, it is perfectly viable; however, more complex cross-sections or surface conditions may require a combination of multiple searching paths or more complex searching strategies. The interpretation of the last layer proposed in Touch-sensing is a simplification that could also be extended with more probing points. During the development of the Adaptive connection demonstrator, a range from 1 to 5 points was needed to reconstruct complex path intersections. How many points should be recorded for an accurate reconstruction depends on the expected deformation of the seam, i.e., on the build and tool orientations, and should be further investigated.

Alternative methods An alternative to single-point probing is to use vision-based sensing strategies that are well-known in the industry. This can as well be a good fit for more complex surface geometries or hybrid printing. However, the precision of these methods is expected to be less accurate than touch-sensing measurements.

3.6 Experiments

The control of process parameters in WAAM is, to this date, an open challenge. As opposed to other additive manufacturing techniques where the translation between the digital model and the physical result has become relatively seamless, currently, no WAAM modeling approach describes the characteristics of input parameters to match a desirable outcome. Within this state of development of the WAAM technology as background, this section describes a series of material experiments in discrete printing carried out to collect data that could inform an intuitive understanding of the relevant process variables for IPWAAM.

The experiments pay particular attention to variables that provide geo-
metric flexibility in IPWAAM: the build and tool orientations and the
path curvature. To this end, the first series of experiments (Sections
3.6.1 to 3.6.5) focus on geometric parameters to prioritize geometric
variation and adaptability over repeatability. Once an acceptable under-
standing of the geometric variables was achieved, questions regarding
the performance of the printed products motivated the rest of the
performance-driven experiments (Sections 3.6.6.1 to 3.6.6.5) carried
out collaboratively with experts in each domain. Table 3.3 presents an
overview of the experiments' subjects and characteristics:

Section	Subject	Object	Substrate	Variables	Specimens
3.6.1	Build orientation	bar	tube	build angle	10
3.6.2	Tool orientation	bar	tube	tool angle	10
3.6.3	Curvature	bar	tube	relative angle change	10
3.6.4	Layer height	bar	tube	layer height	8
3.6.5	Primitive connection	entry, bar, exit	tube, plate	entry, exit	4
3.6.6.1	Surface quality	bar	plate	build angle, tool angle	21
3.6.6.2	Structural behavior under tensile loading	bar	plate	build angle, tool angle	36
3.6.6.2	Structural behavior under tensile loading	bar	plate	touch sensing	6
3.6.6.3	Structural behavior under compressive loading	bar	plate	build angle, tool angle	39
3.6.6.4	Corrosion behavior	bar	plate	build angle, tool angle	29
3.6.6.4	Corrosion behavior	bar	plate	touch sensing	5
3.6.6.5	Heat transfer	bar	plate	cooling time	10

Table 3.3: *Overview of IPWAAM experiments*

Experimental Setup

The experiments were carried out in Setup B (see Experimental setup
B) with the Fronius Characteristic-ID 3542, electrode Union SG-2 (see
3.2) and shielding gas ARCAL 5 (see 3.4.3).

Data storage

The experiments' data, i.e., WAAM and geometric process parameters,
is stored for documentation and later reproduction. The experiment's
storage has two parts, one that stores the process data, i.e., numerical
data of experiments, and one that records the qualitative results, i.e.,
visually inspecting the results once the experiment is concluded.

The data storage is based on an exemplary workflow for handling large
amounts of experiment data developed for the Data-Driven Acoustic

Design project developed at Gramazio Kohler Research with the Swiss Data Science Center (Gramazio Kohler Research, 2021). For all experiments, a data file in `.json` format containing the description and geometric parameters is first exported from the design environment. The `.json` file is then picked up by the robotic procedure call, updated with fabrication data, and then sent to the robot controller. During the experiment, if the process includes a feedback procedure, the data file is updated during production with the requested data to record. Once the experiment is concluded, the file is updated including a timestamp and completion status. This data storage approach is also used to retrieve physical data during the production process (e.g., Execution and survey). Finally, experiments are visually inspected and manually measured once finished and described for later comparison and further development.

3.6.1 Build orientation

Objective To join elements in non-standard configurations flexibility in the build direction of the paths is required. In this experiment, the working range for the `build angle`, or the angle between the WAAM bar axis and the gravity vector, also referred as `path orientation to gravity` or `build direction` is tested (Ariza et al., 2018; Silvestru, Ariza, Vienne, et al., 2021). Previous studies have shown that a build angle between 0º and 60º is achievable without drastic material failure (Z. Yu, Pan, et al., 2021). These previously obtained results need to be verified for the intended materials and experimental setup and process parameters.

Relevant parameters For each specimen, the `build angle` is modified, and all other parameters are kept constant. The final height of each specimen, the `overall height`, is measured and compared. Additionally, diameters along the height of the column are recorded and the `average diameter` is compared.

Description This experiment consists of 10 WAAM bars of input length 35 mm and 28 layers, each with an increase of 10º of the `build angle` (Figures 3.26 and 3.27). The measured range is between 0º and 90º. The experiment was sent in two batches between 0º and 40º

(C#305_01-05) and 50º and 90º (C#305_06-10). The `layer height` and
`seam length` remain constant for all specimens at 1.3 mm.
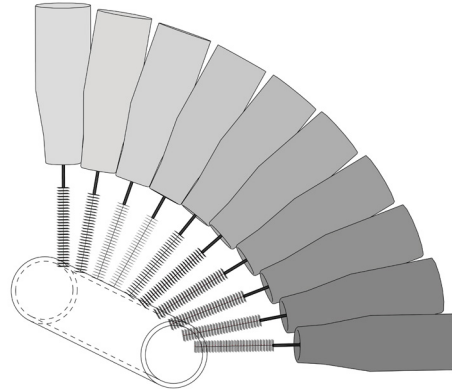
Figure 3.26: *Build direction experiment setup*

| (a) | (b) |
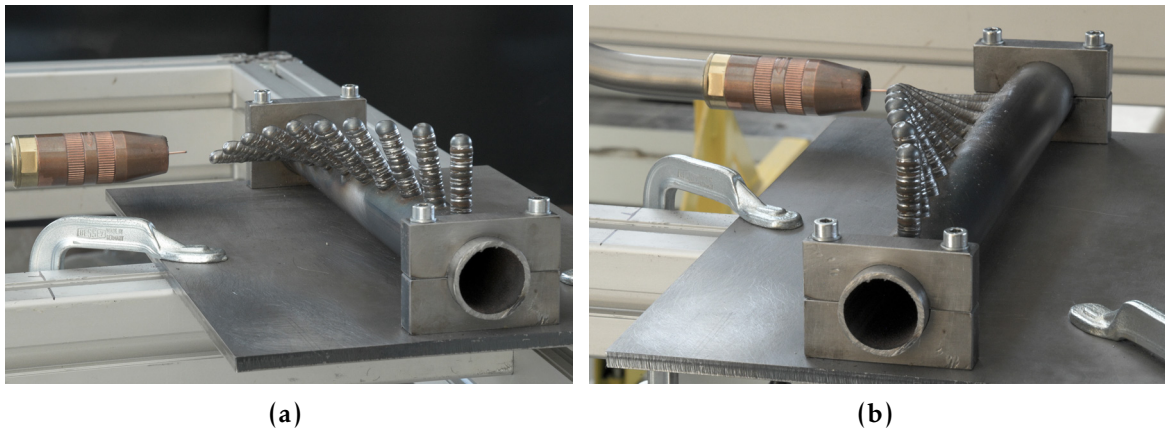
Figure 3.27: *Build orientation setup*

Results   The shape of the path follows the original straight geometry
in all cases. The cross-section geometry of the columns increasingly
tends to an ellipsis for larger build angles. The `overall height` in-
creases with the build angle linearly. It is visible that with an increase
of the `build angle`, the interface between consecutive layers starts ro-
tating from its original normal direction to the path (Figure 3.28b). The
elongation and cross-section change is summarized in Figure 3.29a and
Figures 3.29b (measured values are available in the Appendix A.3).

(a) 0º　　　　　　　　　　　　　　　　**(b)** 90º
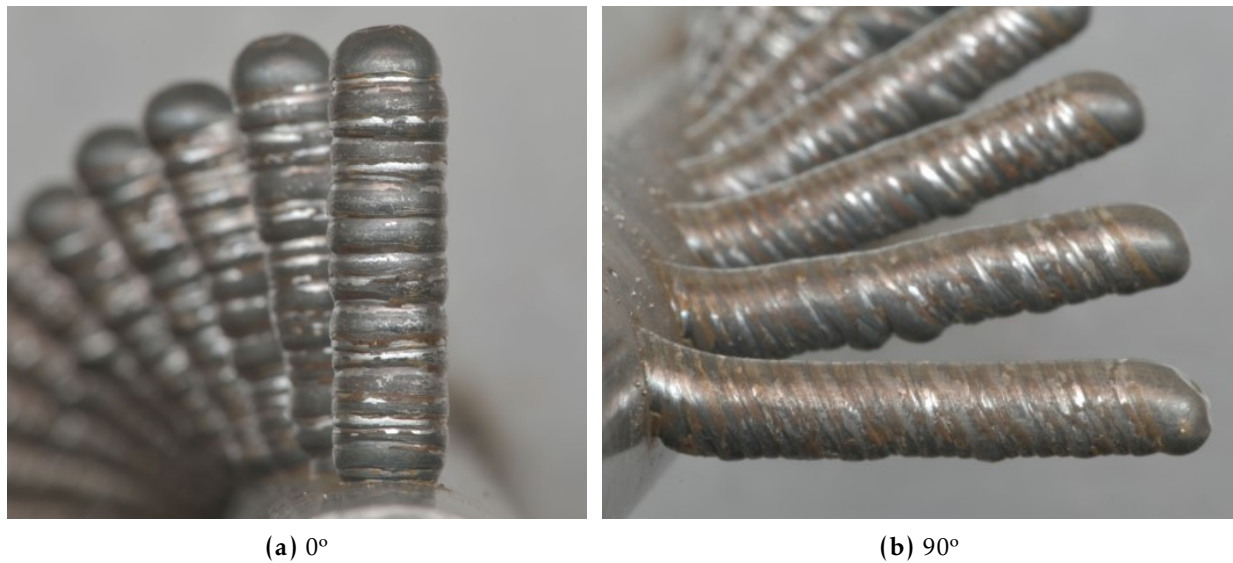
Figure 3.28: *Build orientation results*

(a)　　　　　　　　　　　　　　　　**(b)**
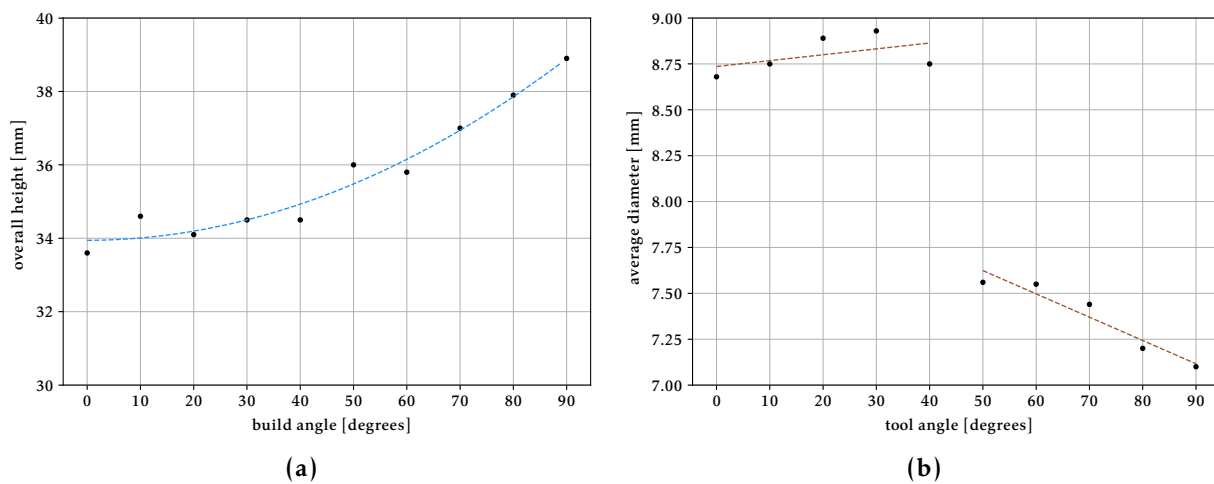
Figure 3.29: *Build orientation results: (a) Effect of build orientation on the overall height of the bar, and (b) Effect of build orientation on the diameter of the bar. The sudden drop at 50 degrees could be associated with a difference between batches 1 and 2. However, the only changed variable between batches is the robot arm configuration, independent of the build and tool orientations that remained constant. According to further experimental work, it can be assumed that the robot arm configuration should not affect the results, as the tool profile is radially symmetric. The reason for the sudden drop is then not confirmed.*

3.6.2　Tool orientation

Objective　To avoid collisions, flexibility in the orientation of the tool along the path is of particular interest for IPWAAM. In this experiment,

the effect of modifying the tool orientation while the build direction remains constant is studied through the geometric parameter `tool angle`, also known as `tool orientation to path` or `nozzle angle` (Ariza et al., 2018; Silvestru, Ariza, Vienne, et al., 2021).

Relevant parameters   The independent variable is `tool angle`. All other parameters are kept constant. The measured parameters are the `overall height`, the final height of the printed bar, and the `average diameter` of each column.

Description   This experiment consists of 10 WAAM straight bars of input length 35 mm and 28 layers, each with an increase of 5º of the `tool angle`. The measured range is between 0º (tool aligned with path) and 45º (Figure 3.30). The experiment was sent in one batch (C#306_01-10). The `layer height` and `seam length` remain constant for all specimens at 1.3 mm.
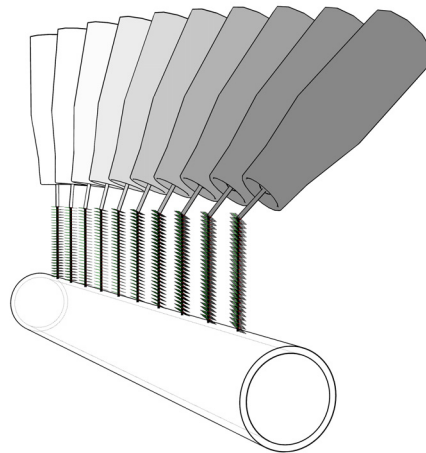
Figure 3.30: *Tool orientation setup*

Results   The `overall height` presents a ±2 mm deviation, but no patterns in visible respect to the `tool angle` (Figure 3.31a). The diameter of the bar increases with `tool angle` (Figure 3.31b, full measured values are available in the Appendix A.4).
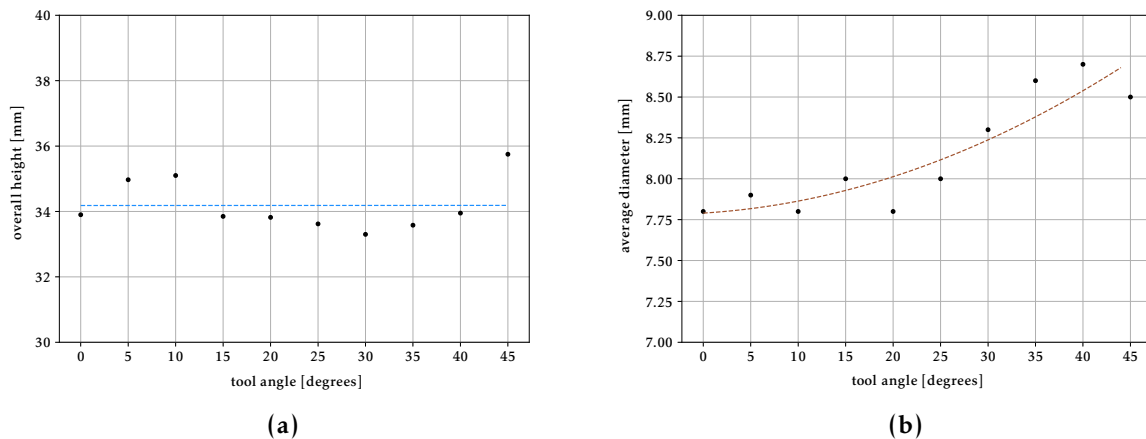
Figure 3.31: *Tool orientation results: (a) Effect of tool orientation on the overall height of the bar, and (b) Effect of tool orientation on the diameter of bar.*

3.6.3 Curvature

Objective   For practical purposes in the design process, one could decide to only work with straight paths as these are comparatively easier to describe, manipulate, evaluate and compare with standardized construction components than curved paths. However, there are at least two reasons why one would like to include curvature as possible design freedom for WAAM paths. First, straight paths are more difficult to achieve with IPWAAM than curved paths, as the latter allows for smaller collision-free tool angles (see graphic explanation in Figure 3.32). The shortest paths between the base and target found on the edge of the inaccessible space further illustrate this point (5.2d). Second, the structural efficiency of elements depends on the distribution of their mass relative to the intervening forces. Even for standard orthogonal beam-column configurations, the force flow does not follow rectilinear patterns (Allen and Zalewski, 2012). It is expected, therefore, that the force transfer between non-standard configurations of elements results in non-rectilinear patterns. To understand how to print curvilinear paths, the starting point is to test the accuracy of the printing method for the simplest curved shape: the arc.

(a)   **(b)**
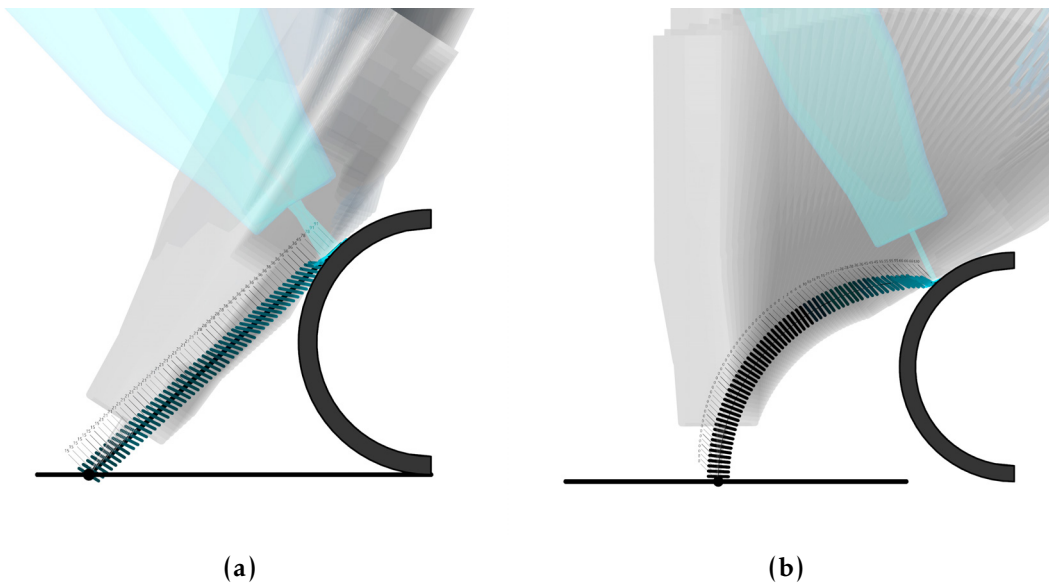
Figure 3.32: *Explanation of preference of curvilinear paths for IPWAAM. Comparison of collision-free frames for linear versus curvilinear paths connecting the same start and endpoints. The compared frames use the minimum tool rotation possible to avoid colliding with the circular pipe. The tool angle is indicated with colors from black (no deviation from an ideal tool position normal to the path curve) to cyan (maximum deviation from an ideal tool position): (a) a linear path with an initial tool angle of 15 degrees at start and a total tool deviation –sum of tool angles for all frames– of 1766 degrees, versus (b) a curvilinear path with an initial tool angle of 0 degrees and total tool deviation of 979 degrees. The total tool deviation in a curvilinear path is roughly half of the tool deviation of a linear path.*

Relevant parameters   The input variable is the `arc radius` with dependent `relative angle change`. The metric is `overall height` and `middle ordinate`.

Description   The experiment consists of 10 specimens `C#307_01-10` with increasing `arc radius` or curvature.   In all cases, the `tool orientation` relative to the `build direction` remains constant, with the robot `Frame` oriented with the tangent of the arc at the subdivision point (Figures 3.33 and 3.34). The `layer height` and `seam length` remain constant at 1.3 mm, resulting in a different number of frames per column.
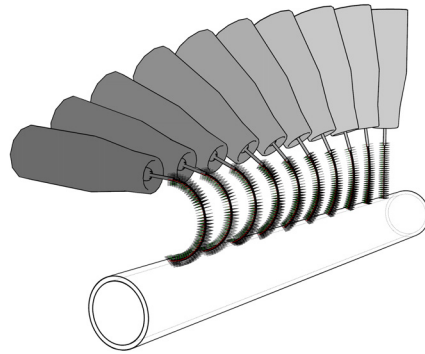
Figure 3.33: *Curvature experiment setup*

Figure 3.34: *Curvature experiment setup*

Results   There is a good agreement between target and resulting shapes (Figure 3.35). The target curvature is visibly maintained, results that can be confirmed with the small variations between target and resulting parameters `overall height` and `middle ordinate` (See figures 3.36a and 3.36b, and measured values in the Appendix A.5).

(a) **(b)**

Figure 3.35: *Curvature results: (a) Zero curvature, and (b) Maximum curvature*

(a) **(b)**
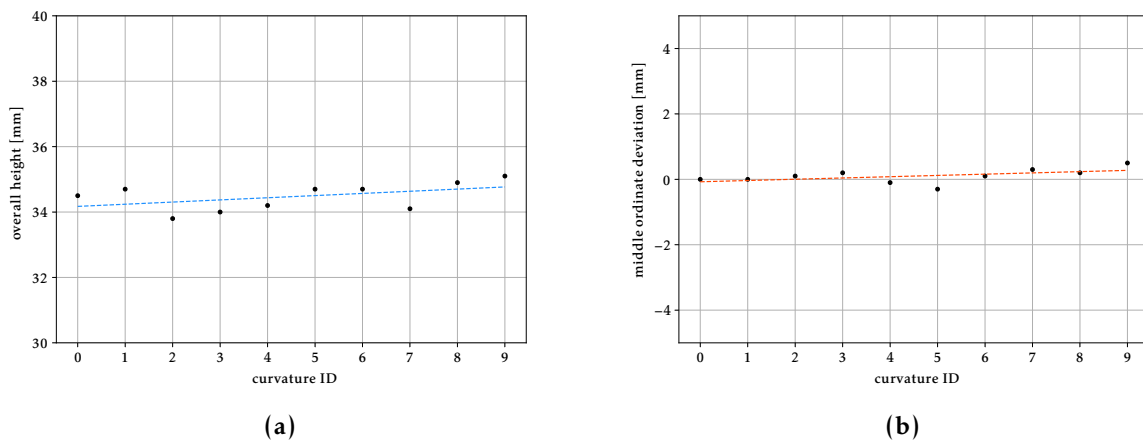
Figure 3.36: *Curvature results: (a) Effect of curvature on the overall height of the bar, and (b) Effect of curvature on middle ordinate deviation.*

3.6.4   Layer height

Objective   The goal of this experiment is to find a working value of the geometric variable `layer height` that will be controlled in the digital model during the slicing process. As explained in Martina and Williams (2015) and Ríos et al. (2018), it is not possible to predict the layer height output. In other words, there is no available equation for a set of parameters that will result in a known layer height. This is related to the interdependency of a large number of process variables (e.g. specific material characteristics, heat input, heat transfer during deposition, gas flow before, during and after deposition, contact tip to

workpiece distance, motion speed of the robot, wire feed speed, etc.) which is to this date under active investigation.

The ultimate purpose of this experiment is to find a working value for the layer height that, even if not fully predicting the physical output, will result in a sound and approximate result from our given input. To this end, with a target of a specific column height, the layer height is changed until the overall column layer height of the physical column matches the overall height of the digital counterpart.

Relevant parameters The `layer height` is increased while all other parameters are kept constant. The control variable is the `overall height` of the column and the `CTWD`, the distance between the end of the copper tip and workpiece (center of idealized sphere or seam). Additionally, the diameter of the column is measured to track the effect of the changing input on the geometry of the WAAM bar.

Description The experiment consists of 2 sets using the same set of process parameters presented in Table A.1:

Set 1) `C#304_01-05` 5 specimens in which the layer height of a WAAM bar is increased from 1.07 to 1.4. The control variable `overall height` is measured in the resulting WAAM bar. If the `physical overall height` is equal to the `target overall height`, then the layer height in the digital model is properly calibrated. The `seam length` is kept constant at 1 mm.

Set 2) `C#304_06-08` 3 specimens where the `CTWD at end` is measured and compared to the `CTWD at start` for a constant layer height and varying process parameters (Figure 3.37). If the `CTWD at start` and `CTWD at end` match, the layer height in the digital model is properly calibrated. The `seam length` is kept constant at 1 mm.
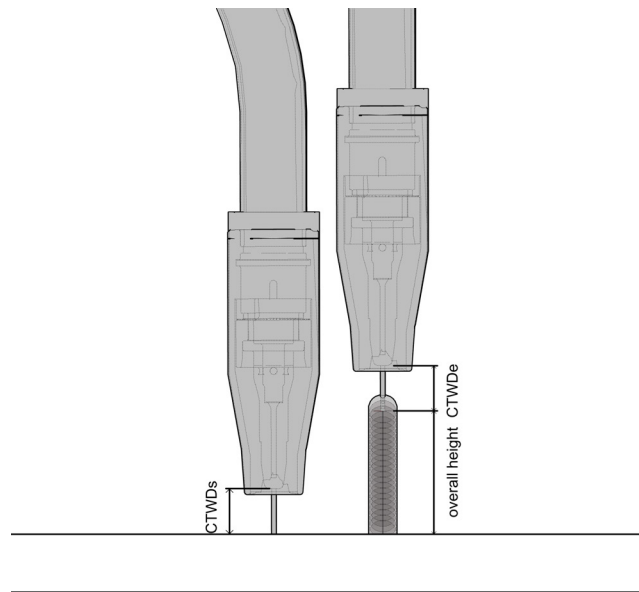
Figure 3.37: *Layer height description*

Results   Specimen `C#304_04` in Table A.1 and Figure 3.38d shows that
the best match of the layer height for the tested process parameters is
1.3 mm. `C#304_07-08` confirm this result (Table A.1). However, this
result is expected to be limited to the geometric parameters of build and
tool angle, and should not be generalized for other printing conditions,
materials, or process parameters.[15]

In addition, it was observed that the first few layers present different
surface and geometric characteristics than the rest of the bar (Figure
3.38). This agrees with observations in Martina and Williams (2015)
and Z. Yu, Pan, et al. (2021) and could be attributed to the fast heat
transfer that occurs when the column is in contact with a large substrate
surface acting as a heat sink (See related experiment in Section 3.6.6.5).

---

[15]While a systematic investigation of the layer height could be conducted to model
the discrete WAAM process more accurately, in this research this variable became
inconsequential as the build-up height uncertainty is handled with the touch-
sensing procedure.

ID	lh [mm]	sh [mm]	th [mm]	h [mm]	CTWDs [mm]	CTWDe [mm]
C#304_01	1.07	1	35.3	39.0	N/A	N/A
C#304_02	1.1	1	37.4	40.5	N/A	N/A
C#304_03	1.2	1	34.8	35.0	N/A	N/A
C#304_04	1.3	1	35.1	35.0	N/A	N/A
C#304_05	1.4	1	35	33.0	15.1	12
C#304_06	1.3	1	N/A	N/A	14.0	11
C#304_07	1.3	1	N/A	N/A	12.0	12.0
C#304_08	1.3	1	N/A	N/A	12.3	12.3

Table 3.4: *Layer height: ID (specimens), lh (layer height), sh (seam height), th (target overall height), h (overall height), CTWDs (contact tip to workpiece distance at start), CTWDe (contact tip to workpiece distance at end).*

(a)   (b)   (c)   (d)
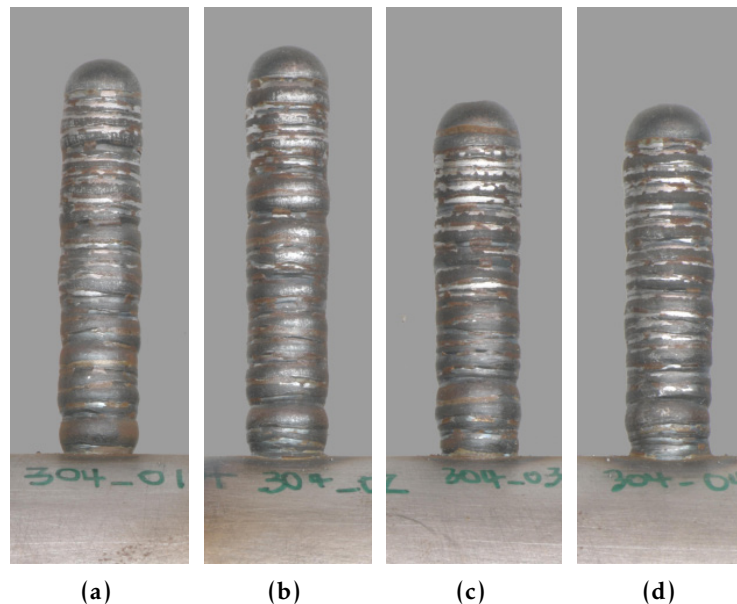
Figure 3.38: *Layer height experimental results: (a) C#304_01, (b) C#304_02, (c) C#304_03, and (d) C#304_04.*

3.6.5 Primitive connection

Objective This experiment presents a primitive connection with three relevant sections: the *entry*, or the discrete deposition of the start point of a column on the base element or base substrate; the *column*, the discrete layers that form a linear element or bar; and the *exit*, the continuous deposition of the final joint between the end of the column and the target element, or target substrate. The microstructure of the

sections is inspected under the microscope to have a first impression of the material structure and fusion qualities of the IPWAAM technique.[16]

Relevant parameters   In this experiment, all the process parameters are taken into account (Tables A.7-A.14).

Description   The specimens consist of four columns of 11 mm height with variable `tool orientations` for each target `Frame` in between base and target elements. The elements' substrate is mild steel (S235) with a circular cross-section of 30 mm diameter and 2 mm thickness. The height of the column was defined based on the maximum diameter of the hot-mounting[17] plate (40 mm with a free offset of 5 mm). The `tool angles` are the minimum feasible rotations to avoid collisions between the torch nozzle and the in place elements (Figure 3.39).
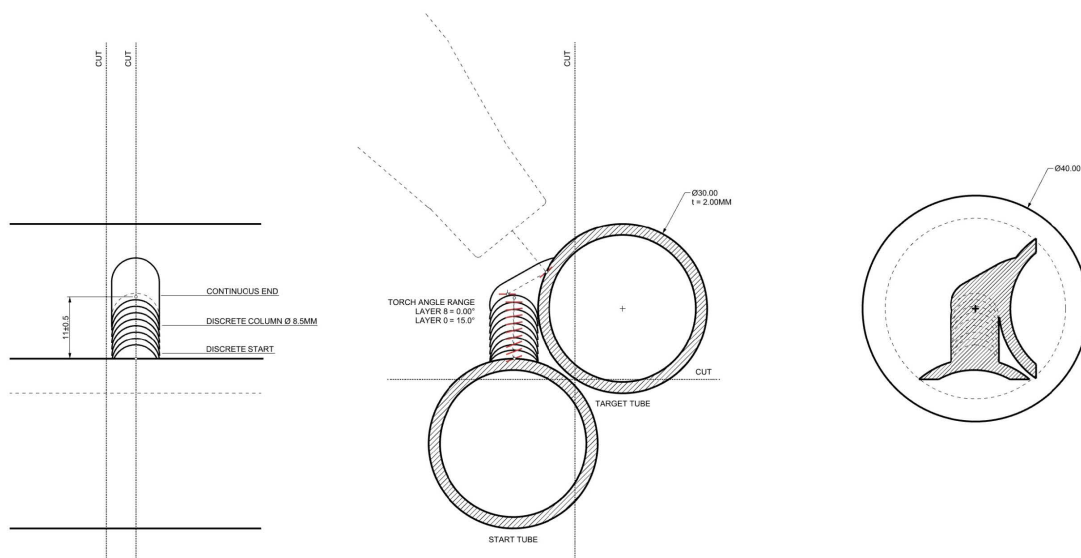
Figure 3.39: *Primitive connection: front view with sections (left), cross-section view with `tool_orientation` ranges (center), final specimen (right).*

---

[16]The study was carried out with the support of Ph.D. researcher Maicol Fabbri, from the Institute of Machine Tools and Manufacturing (IWF) at ETH Zurich.

[17]Hot-mounting is the procedure consisting of fixing a specimen sample into a pressed resin cylinder to ease its manipulation during all the stages of a metallographic study.

The manufacturing procedures include localization, printing of the discrete entry and column layers, touch-sensing of the end of the column, and printing of the continuous exit.

Localization of the base and target elements was done with a manual TCP measurement. The geometry of the base and target elements is then reconstructed in the CAD environment, and the start and end points of the entry, column and exit are adapted to fit the exact position between the elements.

Printing is divided into two procedures, with a touch-sensing measurement in between. The first printing procedure includes the entry point and the column layers. The geometric parameters of this procedure range over the height of the column between 15 degrees at the start and 0 degrees at the end. The contact tip to work distance, or CTWD, is 11 mm at the start. Once the column is printed, a measurement of the actual location of the final layer seam is done with a touch-sensing procedure. With this measurement, the start point of the exit (continuous printed path) is adapted. The `tool orientation` values of each point are recorded in Tables A.7-A.14.

The preparation of the specimen for optical inspection includes the typical steps of a metallographic study: **i)** cutting along specimens' axes (tolerance +/-0.5mm) (Figure 3.40a) **ii)** hot-mounting (Figure 3.40b) **iii)** grinding up to 4000 grit **iv)** polishing up to 1 micron **v)** inspection of pores and cracks with microscope and image capturing of relevant areas on column section **vi)** etching (Nital) **vii)** inspection of penetration area with digital microscope and image capturing of relevant sections of entry and exit sections.

(a)　　　　　　　　　　　　　　　　　　　(b)

Figure 3.40: *Primitive connections process: (a) Specimens before cutting, and (b) Specimens after hot-mounting.*

Results

Porosity   The specimens show varying porosity densities (Figure 3.41). Specimen C#308_04 is the only one of the batch that was cut precisely on the axis of the column. This specimen shows less porosity than the others. The hypothesis is that there could be more pores near the border than in the middle of the weld pool. A transversal section could confirm this.
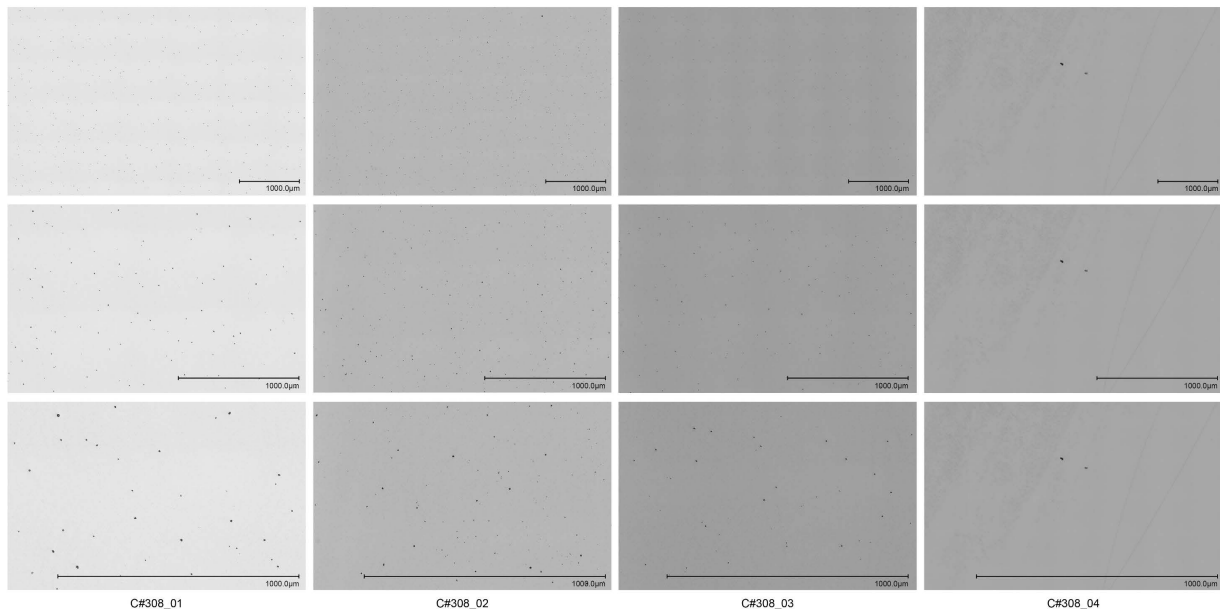
Figure 3.41: *Porosity on the column section of a primitive connection. Microscopy images: Maicol Fabbri, IWF, ETH Zurich.*

Fusion at entry section The fusion between the entry point and the base element shows good penetration for specimens 1, 2 and 4, and superficial penetration for specimen 3 (Figures 3.42 and 3.43). The varying penetration areas ranging from 2.4 mm² to 17 mm² inform that a variable is not consistent among specimens. The varying penetration can be caused by the varying `stick-out length`, i.e., the actual length of the wire at the start, for columns 3-4, as this variable was not verified during the experiment.

Fusion at exit section The fusion between the final layer of the column end with a continuous weld and the target tube show consistent shape and relatively similar penetration areas (Figures 3.44 and 3.45). In all cases, there is an excess of penetration going all through the tube cross-section.
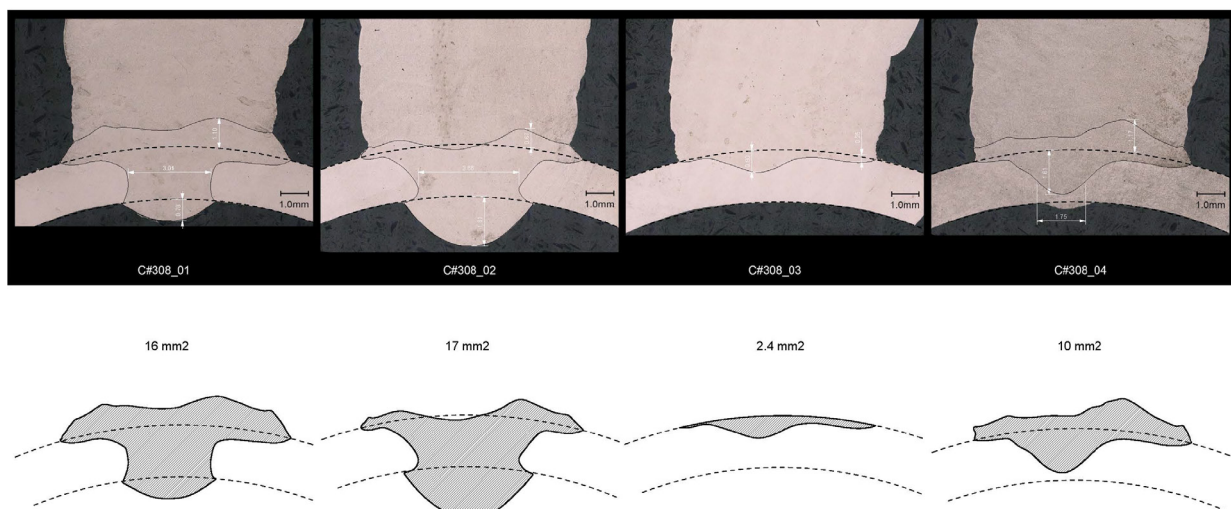
Figure 3.42: *Fusion at the entry point of the column. Microscopy images: Maicol Fabbri, IWF, ETH Zurich.*
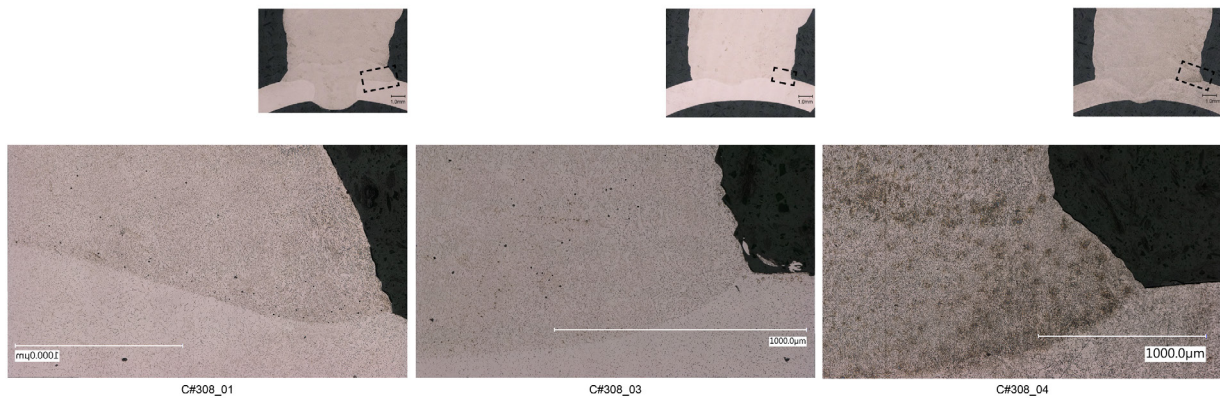
Figure 3.43: *Fusion at the entry point of the column. Microscopy images: Maicol Fabbri, IWF, ETH Zurich.*
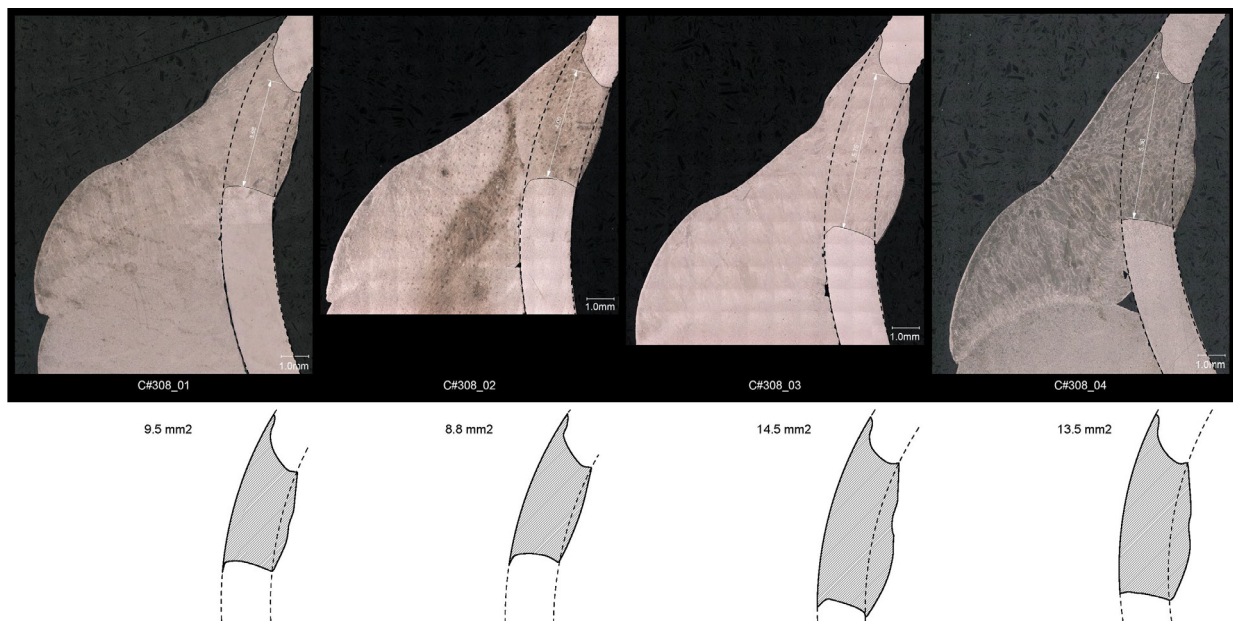
Figure 3.44: *Fusion at exit of column. Microscopy images: Maicol Fabbri, IWF, ETH Zurich.*
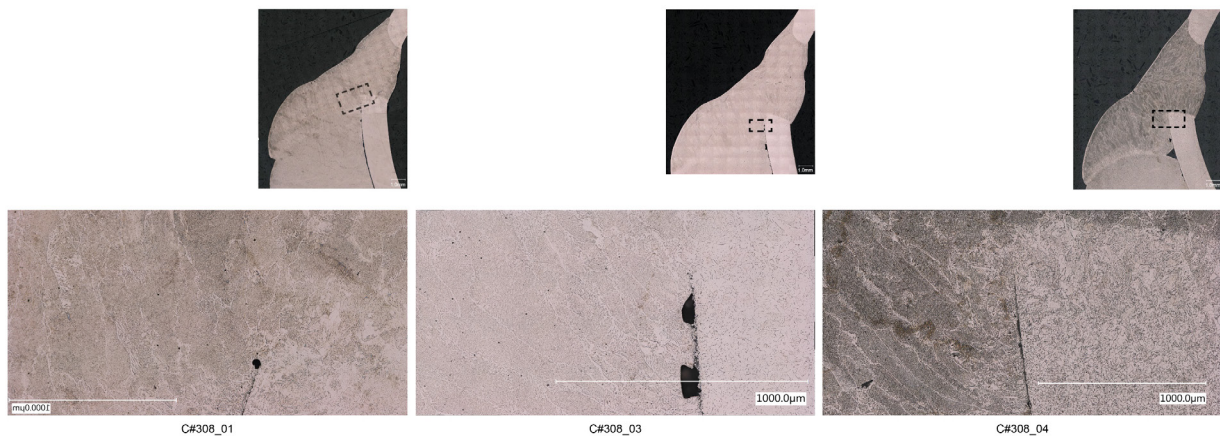
Figure 3.45: *Fusion at exit of column. Microscopy images: Maicol Fabbri, IWF, ETH Zurich.*

Geometry Figure 3.46 shows the longitudinal cross-section of the four specimens. Here, it is evident that the columns are easily deformed near the tube proximity. This premature overlap results from the flow of liquid metal during deposition towards the tube, a condition that is supported by the tool orientation at this stage of the path length (3.39). The microscopy also shows a clear gap between the column and the pipe, indicating a lack of fusion. This gap could potentially be a point of failure or water accumulation and should be avoided. A possible solution would be to orient the path's intrados instead of the path's axis tangent to the pipe.
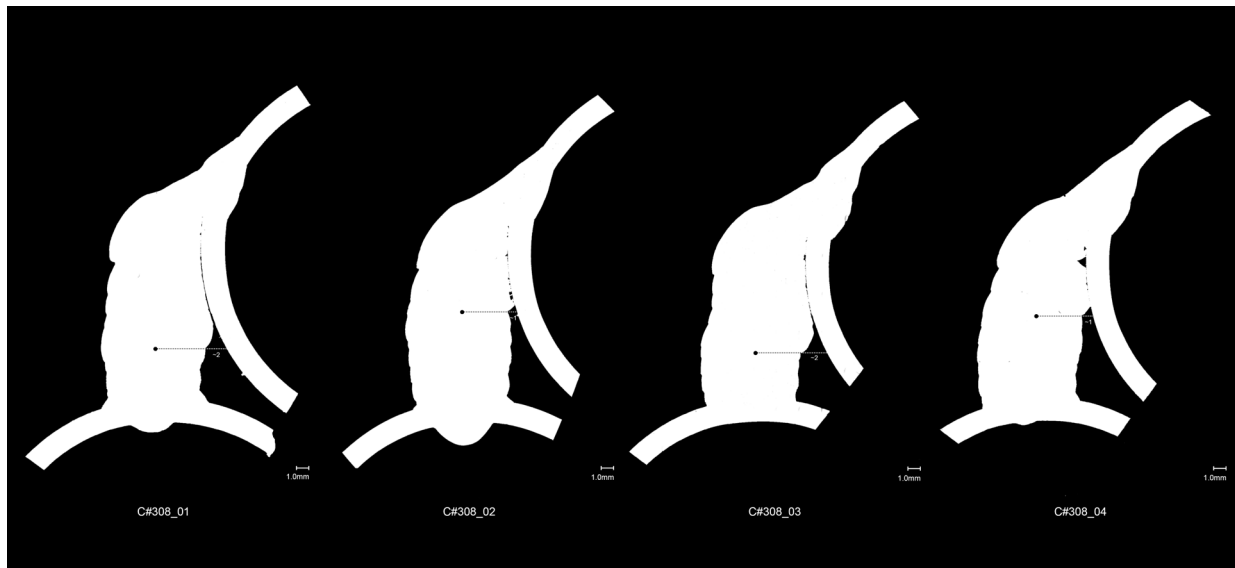
Figure 3.46: *Longitudinal cross-section before etching: overall view of specimens. Microscopy images: Maicol Fabbri, IWF, ETH Zurich.*

3.6.6   Collaborative investigations

During the development of the IPWAAM printing technique, it became increasingly evident that numerous aspects of IPWAAM were still unknown, and that the application of the technique for architectural applications will require further research in adjacent fields. This section presents interdisciplinary collaborative efforts to characterize the point-by-point WAAM printed material and to develop an understanding of the heat development during the printing process.

During the winter of 2020, two collaborations with engineers and scientists from the Institute of Structural Engineering, led by Prof. Andreas Taras and Dr. Vlad Silvestru, and the Institute for Building Materials at ETH Zurich led by Prof. Ueli Angst were established to investigate the material properties of the printed bars. These collaborations resulted in two publications that are summarized in the following subsections (Silvestru, Ariza, Vienne, et al., 2021; Michel et al., 2022). In the summer of 2020, a third collaboration with the Chair of Advanced Manufacturing at ETH led by Prof. Markus Bambach, supervised by Dr. Katharina Eissing, and developed by Ph.D. researcher Andrej Stoy was set to study the heat development during printing. This section presents the reasoning behind these investigations, summarizes the published and

unpublished findings, and points to the next steps in characterizing
the WAAM printed material and process for architectural applications.

3.6.6.1 Surface quality

Context   A visible characteristic of the material printed with WAAM
is the strong irregularity of its surface. These irregularities have been
reported to be dependent on the thermal cycles of the layer-by-layer
process, with a strong dependency on the energy input, and cumulative
heat on the printed part during the build-up process (Köhler, Hensel,
and Dilger, 2020). Supporting the results of these studies, one could
easily see in the experiments reported in this section that the geomet-
ric, execution and welding parameters have a strong influence on the
surface roughness.

This characteristic was expected to affect the mechanical properties
of the material, as the varying cross-sections and overall thickness in-
crease the number of potential failure points along the length of the
bars. Moreover, the valleys between layers seemed to be ideal loca-
tions to trap water droplets, potentially favoring corrosion initiation,
and ultimately suggesting a challenge for considering an architectural
application with WAAM.

To answer these questions, a characterization of the topography of the
surface was performed by a team from the Chair of Steel and Composite
Structures. Using an optical 3D scanner, the team evaluated 35 bar
specimens of the fictive diameter of 8 mm and 40 mm length printed
with varying nozzle and build angles (Figure 3.47). The topographies
were then reconstructed, compared and evaluated. The method and
results are described in Silvestru, Ariza, Vienne, et al. (2021).

Figure 3.47: *Surface quality of printed bars with different building and nozzle angles from Michel et al., 2022.*
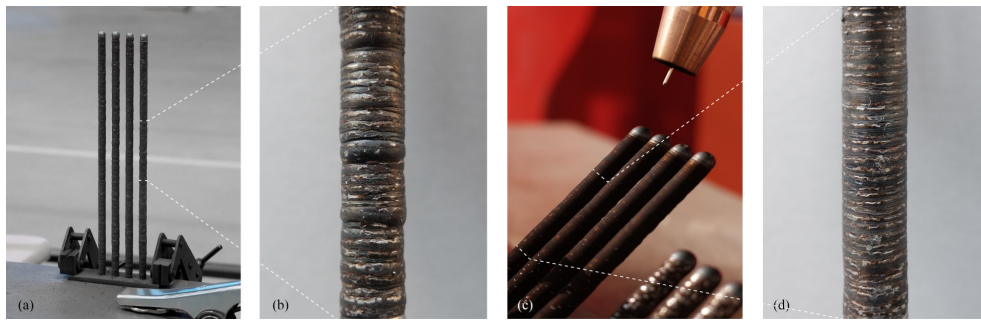
Figure 3.48: *Surface quality of printed bars with different building angles from Michel et al., 2022.*

Findings   From these investigations, one could quantify the extent to which the geometric parameters, nozzle angle and build angle, influence the geometry of the surface. The cross-section area varies ±18% depending on the geometric printing parameters. The rougher surfaces were found on the bars printed with a build angle and nozzle angle of 0 degrees, even when welding parameters changed. Moreover, the evaluation confirmed that the location of the nozzle has an important influence on the smoothness of the surface (Figures 3.48-3.49). For nozzle angles different from 0 degrees, the surface is always smoother on the nozzle side than on the opposite side. The static tests presented in 3.6.6.2, show that the material properties of the WAAM bars are not influenced by the surface roughness. However, the structural performance of WAAM printed components is affected by the bar geometry and surface roughness, as it was found that the bars are likely to fail where cross-section areas are smaller (Silvestru, Ariza, Vienne, et al., 2021). This is as well relevant for the corrosion behavior, as the presence of valleys where water can accumulate could be a detrimental aspect for the durability of the WAAM printed products (Michel et al., 2022, see Corrosion behavior).

Moreover, the development needed for the production of the specimens proved substantial for the author's understanding, development and control of the process parameters. In particular, the large number of specimens allowed to empirically determine the minimum cooling time parameter at 30 seconds (Figure 3.50).

Next steps   To better understand the effect of welding parameters on the surface topography a matrix of experiments correlating energy
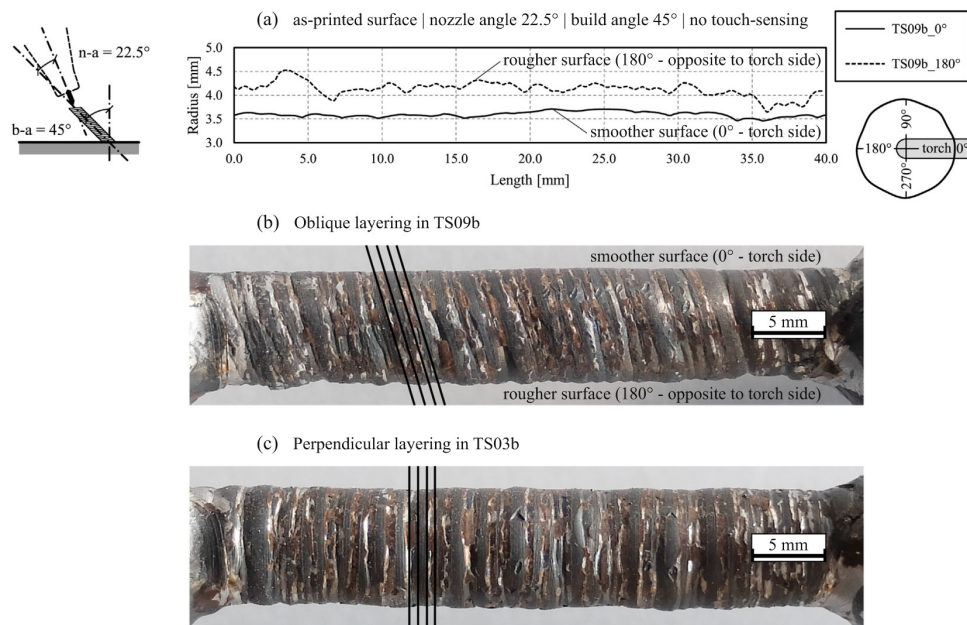
Figure 3.49: *Variation in smoothness on different sides of WAAM printed bars, from Silvestru, Ariza, Vienne, et al., 2021.*

input and surface quality should be performed.

3.6.6.2 Structural behavior under tensile loading

Context In order to assess the suitability of the IPWAAM technique for architectural applications, an understanding of the mechanical properties of the IPWAAM printed material is needed. Previous work had characterized WAAM-printed bars with different build angles as ductile and suitable for engineering applications (Müller et al., 2019, Joosten, 2015). To understand how the varying geometric conditions of the IPWAAM point-by-point process affect the mechanical behavior of WAAM-printed bars, two types of uniaxial tensile tests were performed[18]: (1) locally milled WAAM bars were loaded to determine the mechanical properties, i.e., yield and ultimate strength, of the printed material, and (2) as-built WAAM bars were loaded to determine the influence of the changing geometric parameters for the different nozzle and build angles (Figure 3.51). Additionally, specimens using the touch-sensing procedure were tested to understand the influence of

---

[18]The study was carried out by the Chair of Steel and Composite Structures (Dr. Vlad Silvestru, Prof. Andreas Taras) in collaboration with the Chair of Architecture and Digital Fabrication (Romana Rust, Julie Vienne and the author) and the Durability of Materials Group (Prof. Ueli Angst, Lucas Michel and Asel Maria Aguilar Sanchez) from ETH Zurich.
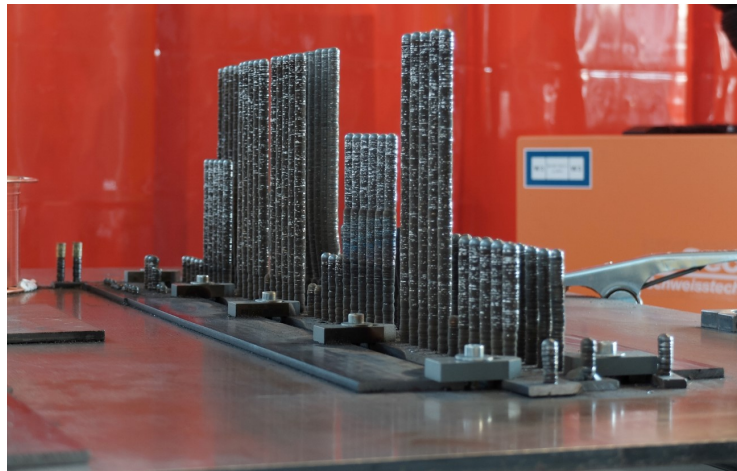
Figure 3.50: *Experimental tests to control the geometric accuracy and surface quality of the printed bars.*

the increased cooling time and the resumed print process. Finally, an elastic-plastic model built with the data found in (1) (Figure 3.52) was used to simulate different as-built surface conditions showing similar points of failure to the specimens tested in (2). The method and results are described in Silvestru, Ariza, Vienne, et al. (2021).
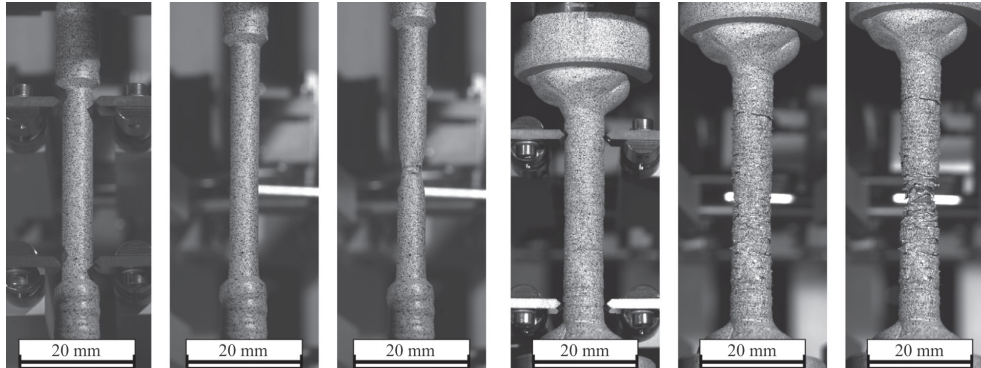
Figure 3.51: *Stages of the tensile tests (before loading, at maximum load and shortly before failure) of WAAM printed bars with milled surfaces and as-printed surfaces, from Silvestru, Ariza, Vienne, et al., 2021.*

Findings   The comprehensive study of 42 specimens with changing build and nozzle angles shows promising results. First, the milled specimens (1) showed a consistent behavior of the point-by-point WAAM-printed material.[19] The material properties found through these tests are similar to the strength values of steel S355 with a ductile behavior

---

[19]The study of the microstructure of material across printing conditions studied in Michel et al., 2022 confirmed this point.

under tensile loading. Second, the as-built bars (2) exhibit more diverse displacements at failure. This could be correlated to the smaller local cross-section area produced by the WAAM printing process and particularly by the touch-sensing procedure. The proposed model was able to closely predict the structural behavior of WAAM-printed bars with as-built surface roughness, including the failure position (Figure 3.53). These results support the suitability of point-by-point WAAM products for structural applications.
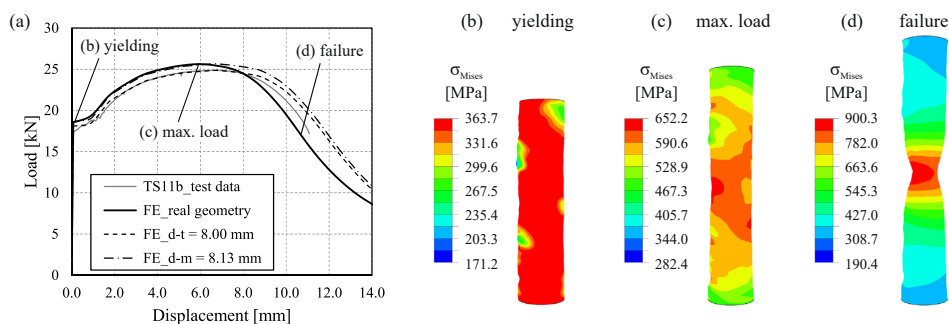
Figure 3.52: *Comparison between the load–displacement curves from the simulation and the tensile test (DIC displacement) on specimen TS11b with the as-printed surface (a) and approximate von Mises true stress distribution at yielding (b), at the maximum load (c) and at failure (d). Silvestru, Ariza, Vienne, et al., 2021.*
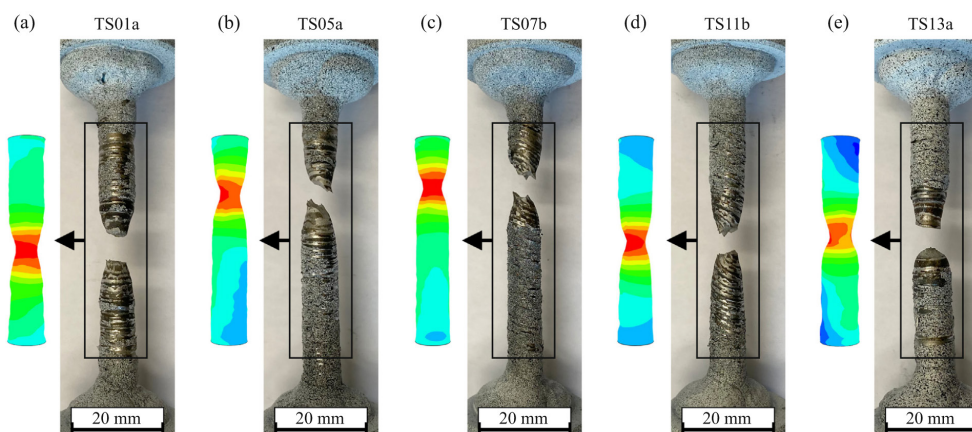
Figure 3.53: *Verification of the elastic-plastic model: comparison of the von Mises stress at the failure of simulated WAAM bars with typical surface roughness and the WAAM bars loaded to failure, from Silvestru, Ariza, Vienne, et al., 2021.*

Next steps The tensile experiments showed that precise control of printing process parameters and heat development is paramount to avoid smaller cross-section areas through the printed parts that can result in failure points. Moreover, in order to consider the WAAM bar

results for architectural applications, the connection points between the
bars and the substrate elements, as well as more complex geometries
should be studied next.

3.6.6.3 Structural behavior under compressive loading

Context   Given the possible slender characteristic of the products
manufactured with the point-by-point WAAM deposition, the buck-
ling behavior under compressive loading is another critical aspect to
consider. To characterize the structural behavior under compressive
loading of the WAAM bars previously studied under tensile loading
(Structural behavior under tensile loading), a subgroup of the printing
conditions was manufactured in different lengths to provide varying
slenderness.[20] The experiments consisted of uniaxial compression tests
of the WAAM bars with clamped and hinged supports (Figure 3.54). In
addition, the elastic-plastic model derived from the material properties
study under tensile loading (Structural behavior under tensile loading)
was tested here to predict the buckling behavior.
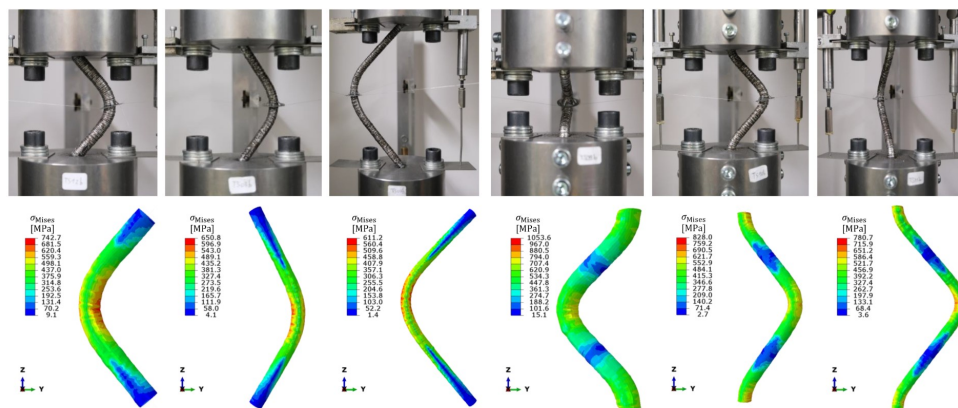
Figure 3.54: *Comparison of the von Misses stress for simulated WAAM bars with
typical surface roughness under compression loading and buckling of the WAAM
bars of different lengths, with hinged and clamped configurations, from Solcà, 2021.*

Findings   The study consisted of 39 specimens showing different
nozzle and build angles as well as different lengths/slenderness (see
Silvestru, Ariza, and Taras, 2022; Solcà, 2021). A buckling behavior

---

[20]The study, the first of its kind, was the topic of investigation of the master's thesis
of Andreà Solca, supervised by Dr. Vlad Silvestru, Prof. Andreas Taras and the
author.

following the standard Eurocode 3/SIA 263 *buckling curve c* was observed, i.e., longer bars present smaller buckling forces than shorter bars. The *buckling curve c* can then be used to determine reduction factors based on the average cross-section area of a WAAM bar. In terms of numerical simulations, the material model was able to predict the buckling behavior for WAAM bars of fictive varying cross-sections with clamped supports and presents good prospects for predicting other boundary conditions if the modeling of friction is taken into account (Solcà, 2021, Figure 3.54). In short, the buckling load of point-by-point WAAM bars could be predicted with standard buckling curves if an accurate average cross-section area and diameter of the WAAM bar is known (Figure 3.55).
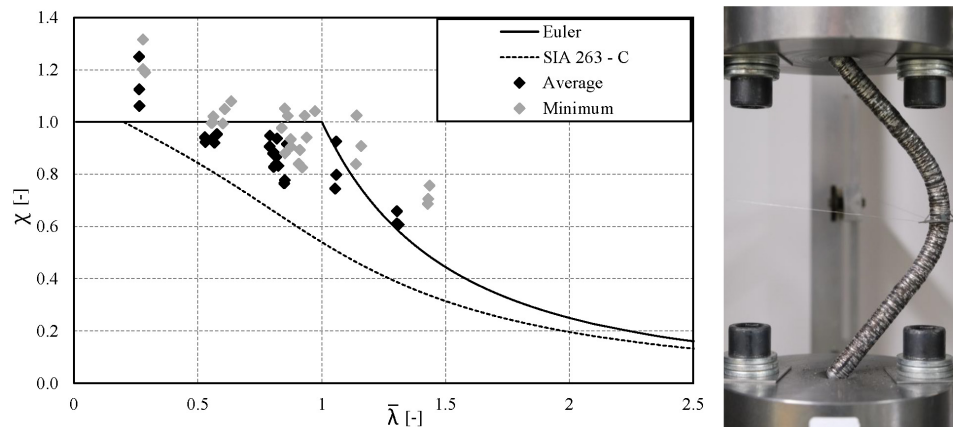
Figure 3.55: *Relative slenderness* (x axis) *and buckling reduction factors* (y axis) *for hinged configurations, from Solcà, 2021. Using the average cross-section and diameter values instead of the minimum values results in closer fitting to the standard curve.*

3.6.6.4 Corrosion behavior

Context The coarse surface roughness of the WAAM bars presents questions about the durability and corrosion behavior of the WAAM products, as valleys are typical zones prone to water accumulation. However, no study to date has tackled the corrosion behavior of discrete WAAM bars. To understand the susceptibility of corrosion initiation in the WAAM products, a study was carried out in parallel with the

aforementioned experiments on mechanical properties.[21] A subgroup
of 32 specimens with different printing conditions and post-processing
surface treatments were studied with metallographic and microscopic
analyses, tested for corrosion initiation under simulated atmospheric
exposure conditions and electrochemically characterized to understand
the corrosion susceptibility related to material heterogeneities and
geometric variations (Michel et al., 2022).
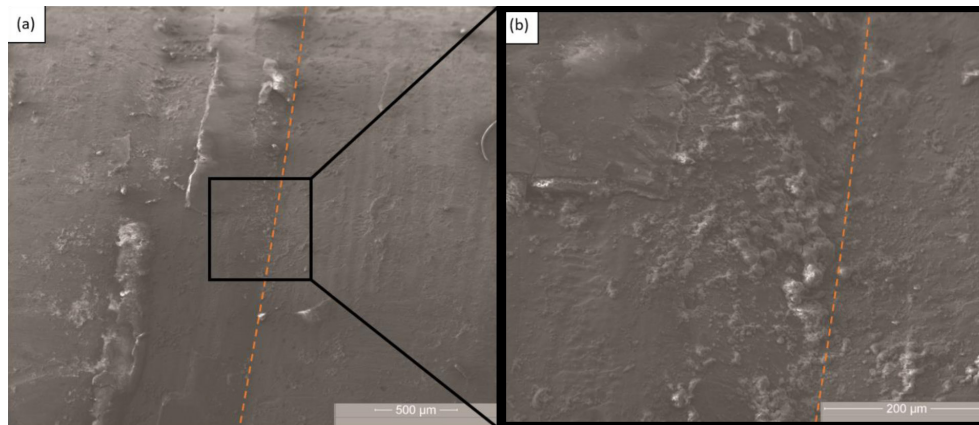
Figure 3.56: *Scanning electron microscopy (SEM) where corrosion products can
be observed in the valleys between two layers (in orange), from Michel et al., 2022.*

Findings   The results showed a homogeneous microstructure of the
WAAM bars along their length for all the different printing conditions,
even for interlayer zones. Simulated atmospherical conditions have
shown that corrosion initiation is present only at severe 100% relative
humidity or when water condensation is possible at the surface of the
WAAM bars. The corrosion initiation occurs on water layers present
in the valleys or interlayer areas which are prone to wetness for longer
periods, and to oxide scales, both of these conditions favoring corrosion
initiation (Figure 3.56). Post-processing surface treatments such as
brushing, and especially sandblasting, can improve the corrosion resis-
tance by removing oxide scales (Figure 3.57). These findings determine
that geometry and surface roughness are the main design variables to
consider for durable WAAM products.

---

[21]The study was carried out by the Durability of Materials Group (Prof. Ueli Angst,
Lucas Michel and Asel Maria Aguilar Sanchez) in collaboration with the Chair
of Architecture and Digital Fabrication (the author) and the Chair of Steel and
Composite Structures (Dr. Vlad Silvestru, Prof. Andreas Taras) at ETH.
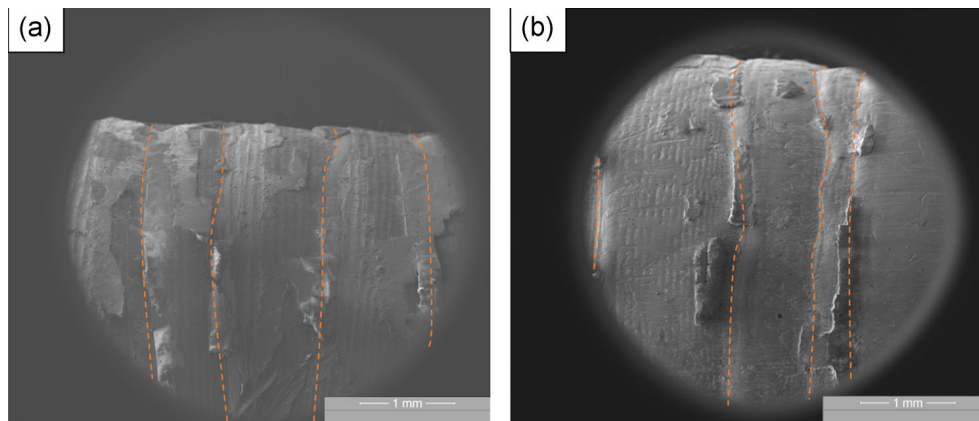
Figure 3.57: *Scanning electron microscopy (SEM) of non-brushed (left) and brushed (right) bars showing the partial removal of oxide scales after brushing, from Michel et al., 2022.*

3.6.6.5 Heat transfer

Context   During the production of the specimens for tensile testing where numerous WAAM columns were printed, it was observable that the change in the cooling time for a single drop affects the characteristics of the surface roughness of the printed product.[22] In order to find the required cooling time for each drop, a study was set to understand the heat transfer during the discrete WAAM deposition.[23] To this end, a simulation of the thermal development on a WAAM column was developed (Figure 3.60). A series of 90 mm height columns were recorded with a thermal camera to calibrate the simulation of the printing process (Figure 3.58).

Findings   The simulation of the cooldown of a single drop shows that the heat transfers through the air, i.e., convection, and through the column, i.e., conductive heat flow, at different rates (Figure 3.59). This confirms the experimental observation that the waiting time is a critical factor, as this time window allows the heat to be transferred through the air, which is faster compared to the heat being transferred through the column. It is also possible to see that, over time, the column will act as a heat sink, enabling a heat loss entirely through convection,

---

[22]This may influence the variability on the cross-section area of the specimens printed with different cooling times presented in Silvestru, Ariza, Vienne, et al., 2021.

[23]The study was carried out in collaboration with Andrej Stoy and Dr. Katharina Eissing from the Advanced Manufacturing Lab, ETH Zurich.
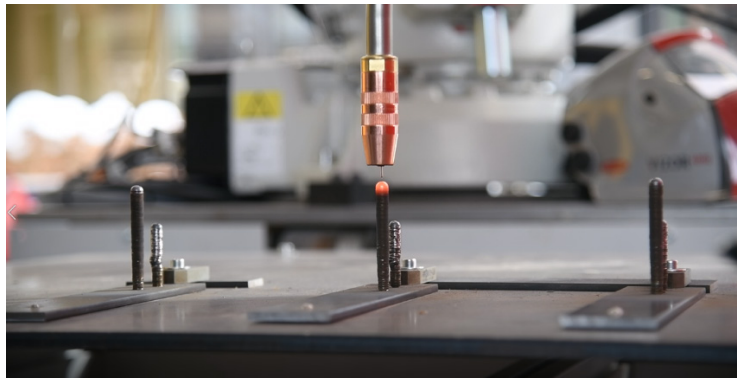
Figure 3.58: *Heat transfer study: recording of point-by-point WAAM deposition over time.*

allowing the wait times to stabilize. Once this point is reached, the wait time can be kept constant, as no increase in the length of the column will have an effect on the heat transfer rate.
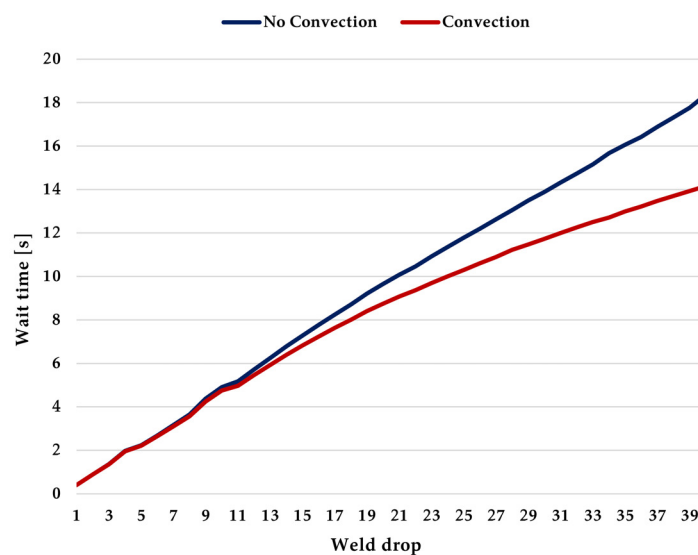
Figure 3.59: *Comparison of wait time required for the tip to cool down to 500°C with and without convection. Simulation: Andrej Stoy, ETH Zurich.*

Next steps These preliminary experiments showed the influence of the heat transfer through convection, and therefore how dependent the process is on the cooling time in between drops, especially at the start of the process. Additional simulations should be run to find the stabilization point of the cooling time. In addition, the interdependence of more complex geometries should be studied, which can lead to the development of a path planning and geometry generation strategy
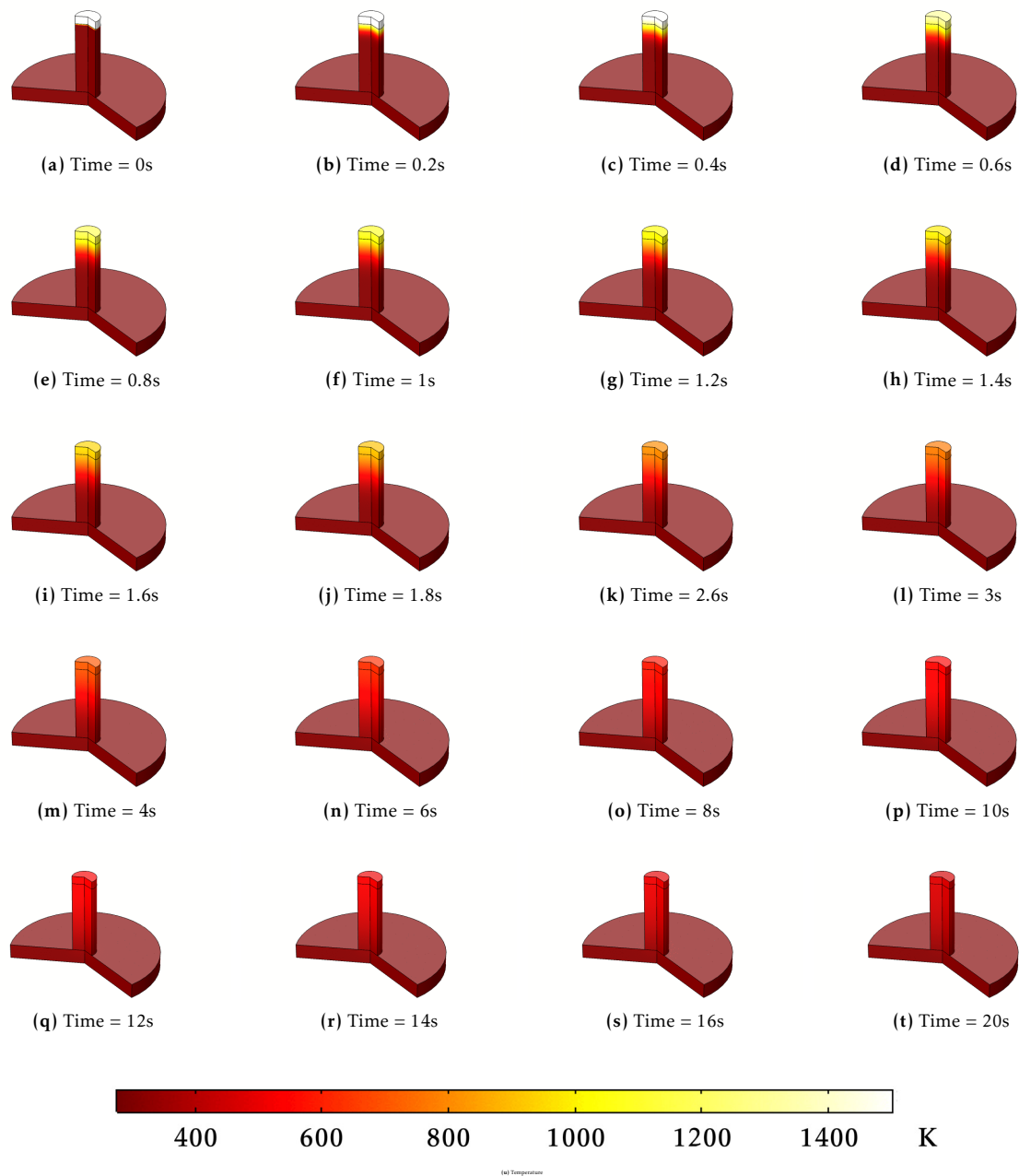
Figure 3.60: *Sequence of temperature fields (in K) during the cooling down of a single drop on a 25 mm WAAM column from t=0 to 20 s. Simulation: Andrej Stoy, ETH Zurich.*

that considers the optimal cooling time as a process time and distance between consecutive drops.

3.7   Summary

This chapter presented the IPWAAM technique, an additive joining approach tailored for the robotic assembly of spatial structures. The technical foundations have been described in terms of setup equipment, software, materials, and robotic procedures. In addition, the chapter described a first set of experiments that served to identify the process parameters and calibrate the most relevant variables.

The following points summarize the takeaways of the work presented in this chapter:

- Compared to conventional GMAW, the CMT technology provides very high deposition control and reliability, a particular benefit for IPWAAM geometries in terms of surface quality and related structural and corrosion performance.

- The material experiments have shown the interdependencies of the geometric, motion, and welding variables involved in the WAAM process. An in-depth study of process parameters is required to further understand and predict desired outcomes. In particular, the integration of thermal sensing would help to control the surface quality of the products and optimize the production time.

- Each deposition technique exhibits advantages and challenges. Point-by-point printing allows placing precise units of material suitable for detailed, material-optimized high-performance structures. The cooling time between depositions allows for heat management that can be explored further on to ensure a good material product at the microstructure level. Moreover, idle time could be explored as a design constraint to develop optimal path planning strategies. In contrast, continuous deposition can be used to quickly deposit material, however, heat control may introduce challenges on distortion and residual stresses on the elements.

The flexibility in the tool orientation provided by the continuous printing can be an advantage as the build gets spatially constrained. The hybrid approach of printing on top of existing paths presents promising applications such as reinforcement of the build at different stages of production or later life cycle of the parts.

- Until now, uncertainties in the process control have been dealt with sensing techniques. To this end, the two-way communication platform for sending and receiving fabrication data implemented through the `COMPAS FAB` and `compas_rrc` libraries have been critical steps. However, process modeling and simulation would be required for understanding and predicting the effects of the process adaptation.

- During its development, IPWAAM has been identified as a technique that could be used for joining reused components. The integration of more versatile scanning methods would be required for dealing with the uncertainty of the geometry and surface quality of reused stock.

- The aimed application of IPWAAM as a joining technology requires an understanding of the product behavior on many fronts: structural performance, mechanical and corrosion behavior, production optimization and design requirements. This complexity can only be tackled by combined expertise. The collaborative investigations have been key drivers of the process development.

4 Adaptive detailing

This chapter presents the components of a pipeline for the design and production of connection details using in place WAAM, referred to as `Adaptive Detailing with IPWAAM` or `AD` in short from now on. As discussed in the introduction, this thesis investigates an adaptive approach to detailing tailored for:

i.   a robotic assembly process performed with a multi-robotic setup

ii. a differentiated spatial structure where elements present geometric, dimensional, and orientation variations

iii. the IPWAAM additive joining technique carried out during the robotic assembly process

The chapter starts with the *Introduction* section giving an overview of the pipeline and its components (4.1). *Initialization* presents the entry points and data structures of the pipeline (4.2). The *Components* section describes each of the methods used in the pipeline (4.3). The summary and discussion briefly discuss common challenges, known limitations, and opportunities of the approach (4.4). Finally, the implementation and evaluation of the pipeline are explained in Chapter 5 in the form of demonstrators; therefore, links between both chapters are made available throughout this chapter.

4.1   Introduction

Adaptive detailing (AD) is a design-*and*-production strategy[1] where the design of interfaces between parts is explicitly informed by the production setup, materials, and processes *before* and *during* construction. Before construction starts, the pipeline maps and explicitly incorporates manufacturing constraints to design interfaces within the production

---

[1]In contrast to the known term design-*to*-production, a computational design approach to inform design with production *in advance* of production.

capabilities. During construction, the pipeline enables the adaption of the interface design based on as-found conditions.[2]

The AD pipeline targets one connection detail at a time, and it assumes a global design model consisting of an assembly of discrete elements as a starting point. The pipeline is structured in the following group tasks (Figure 4.1):
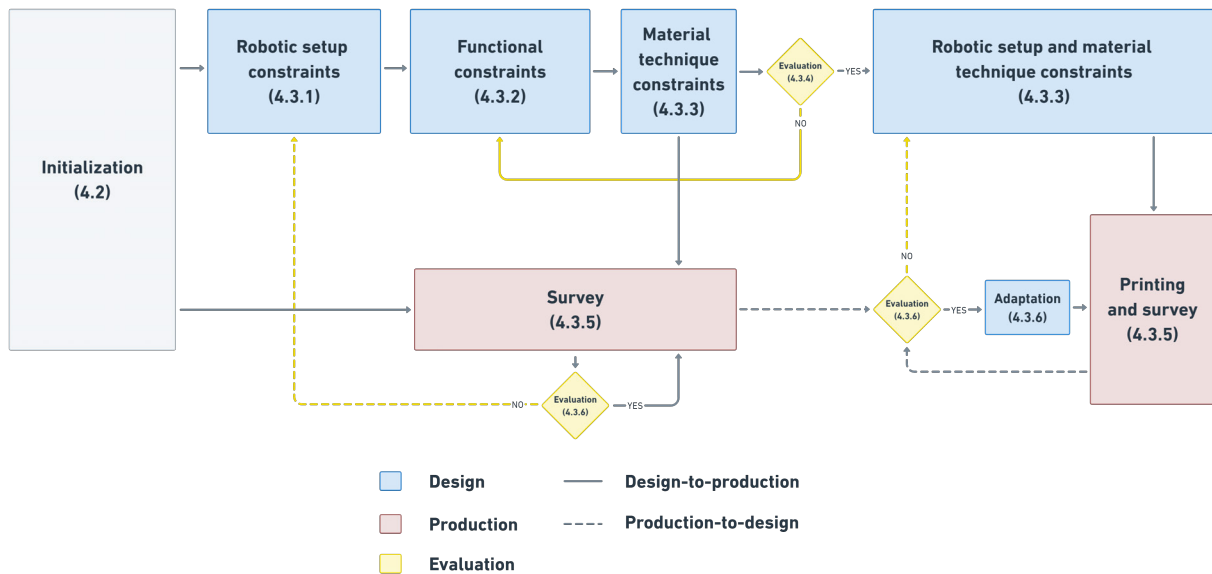
Figure 4.1: *Overview of the adaptive detailing pipeline*

Initialization (4.2) One overarching goal in detailing is to formalize the interactions between the different elements of an assembly. To this end, the entry point of the AD pipeline consists in structuring incoming global design data into relevant data structures, assigning identifiers, sorting topological relationships, sequencing, and naming the intervening elements.

Components (4.3)

Considering the robotic setup (4.3.1) A detail solution is heavily informed by the tools used to process and fix materials in place. When designing with robots in the loop, an explicit understanding of the robot's capabilities is needed and for printing spatial connections in place, there is a need to know where connections can be placed based on

---

[2]The term *connection detail* and *interface* are used interchangeably.

the geometric and kinematic constraints of the welding tool and robot. These constraints are taken into consideration by the `Tool accessibility` and `Robot reachability` components of the AD pipeline.

Considering the functional requirements (4.3.2) A connection detail's main function is to transfer the loads between the elements it connects. The spatial in place connection developed in the AD pipeline does not solve the load problem by looking at previous typologies of connections and applying a known type, but by first calculating a feasible space where connections can be built, and then computing a suitable material distribution inside this space. With this approach, the mass distribution responsible for transferring loads to the supports is a function of both the structural and fabrication constraints. The AD pipeline implementation includes two functional components for `Stability` and `Material distribution` based on a hypothetical material model as placeholders for further development of accurate structural analysis methods that are beyond the focus of this thesis.

Considering the material technique (4.3.3) Current approaches to detailing are primarily based on the assembly of prefabricated products with known material characteristics and assembly instructions. Computational design and adaptive fabrication with IPWAAM expand this detailing approach with the possibility of shaping material on demand and on the spot during assembly. For the design of spatial in place connections, this translates into programmable material deposition and connection techniques. The `Path generation`, `Path slicing`, and `Path sorting` components deal with these aspects providing a visualization environment and exposing process control parameters to the designer.

Integrative design considerations (4.3.4) At the core of detailing lies the task of negotiating between often conflicting constraints. In an explicit design process, this negotiation

needs to be handled explicitly as well. At this stage, before production starts, the design needs to be checked holistically to verify that all the design and production criteria are met. To this end, the `Evaluation of design of paths` is discussed.

Execution and survey (4.3.5) In conventional detailing, idealized detail drawings anticipate building operations as much as possible. In the AD pipeline, where execution is explicitly planned in the form of robot instructions, controlling the machine's output requires integrating surveying procedures. To this end, the `Printing` component is supported by the survey components for `Localization` of elements before printing, and the `Touch-sensing` component before and during printing. The procedures are presented in Chapter 3 and integrated here with the rest of the pipeline.

Survey evaluation and adaptation (4.3.6) The motivation of detail drawings is to ensure the correct implementation of the design throughout the phases of construction. However, it is rarely the case that, at the detail scale, things go according to plan. Conventional detailing handles possible deviations by planning anticipated solutions in advance of assembly. In the AD pipeline, the `Evaluation of position of elements` and `Evaluation of position of paths` components provide heuristics for assessing the severity of as-built deviations from the pre-computed design. In order to tackle possible deviations, the `Path adaption to as-built elements` and `Path adaption to as-built paths` components provide methods for fitting the pre-computed design to the as-built parts during production.

4.2 Initialization

How do we start? How does design data enter the pipeline?
How is design data managed and structured?

This section describes the preliminary tasks of the AD pipeline: formatting design data and assigning relevant characteristics.

Data structures   To enter the pipeline, incoming design data needs to be structured in a meaningful way. These data structures contain properties of the assembly and fabrication setup and are used to exchange data between the different components. Their implementation is heavily influenced by the data structures of the COMPAS framework.
[3]

The design is structured in four data structures, each one represented by a different class of objects:

Assembly
: A collection of architectural components or elements constituting a spatial structure.

Element
: An architectural component part of the Assembly.

Connection
: An architectural component between Elements. The class is introduced in Section 3.3.2 in relation to the fabrication data structure WAAMConnection. Connections can be single-step, connecting only two Elements, or multi-step, connecting more than two Elements.

Path
: A divisible part, a curve or a line, of a Connection. The class is explained in Section 3.3.2 in relation to the fabrication data structure WAAMPath.

An analogy can be drawn between the interaction between the Assembly and Element data structures and the Connection and Path. The Assembly object organizes Element objects, and likewise, the Connection object organizes Path objects (Figure 4.2):

---

[3]For example, |Assembly| and |Element| are data structures that have become useful in discrete assemblies projects and teaching activities, including brick walls and other discrete element structures (*Workshop TU Munich 2020* 2020; *COMPAS Assembly* 2022).

`Assembly ↔ Element ⇔ Connection ↔ Path`
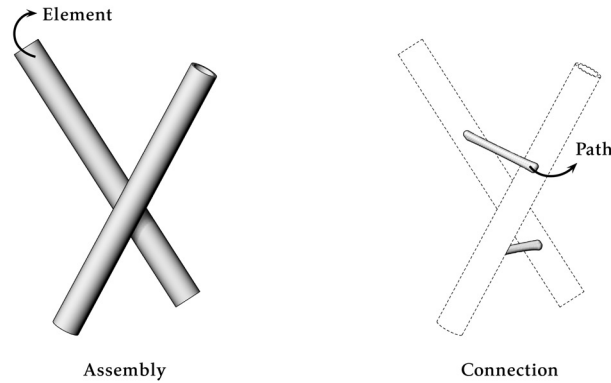
Figure 4.2: *Data structures: Assembly, Element, Connection, and Path.*

The fabrication setup is structured in:

`Tool`	The end-effector used to print `WAAMPaths`, e.g., welding tool or torch, or placing `Elements`, e.g., gripping tool.
`Robot`	The manipulator(s) of a `Tool`.
`Planning Scene`	The container description of `Robots`, `Tools`, and collision objects present in the physical or virtual assembly.

Besides structuring, several aspects of the design need to be organized at this stage:

Identifiers	Query, and if needed, assign human-readable IDs to the `Assembly` and its `Elements`.
Topology	Define or query the connectivity between `Elements` and `Connections`.
Sequence of assembly	Define or get the order of assembly of `Elements`.
Attributes	Based on the sequence of assembly, for each `Connection` define or derive base and target attributes for each `Element`, i.e., for each connection,

define the function of each intervening element as *load*
of *support*.

Setup scene   Specify other relevant setup characteristics in the
`Planning Scene`, e.g., other collision objects other than
the `Elements` themselves.

4.3 Components

As presented above, the AD pipeline combines design, evaluation,
and production tasks that, in conventional detailing, are divided by
stakeholders, software environments, and expertise. Therefore, the
structure of the AD pipeline aims to expose the expert needs and each
domain's dependencies in a shared workflow (Figure 4.3).

The implementation of the AD pipeline's components conforms to the
following premises:

i.   each component can run and be modified independently, without
causing breaking changes on other components

ii.   the inputs and outputs of each component work as interfaces
handled by the COMPAS framework

iii.   internally, each component is implemented in its environment
and programming language

Each component consists of an implementation environment, inputs
and outputs through the COMPAS framework interface, and a custom
combination of functions and settings or parameters (Figure 4.4).
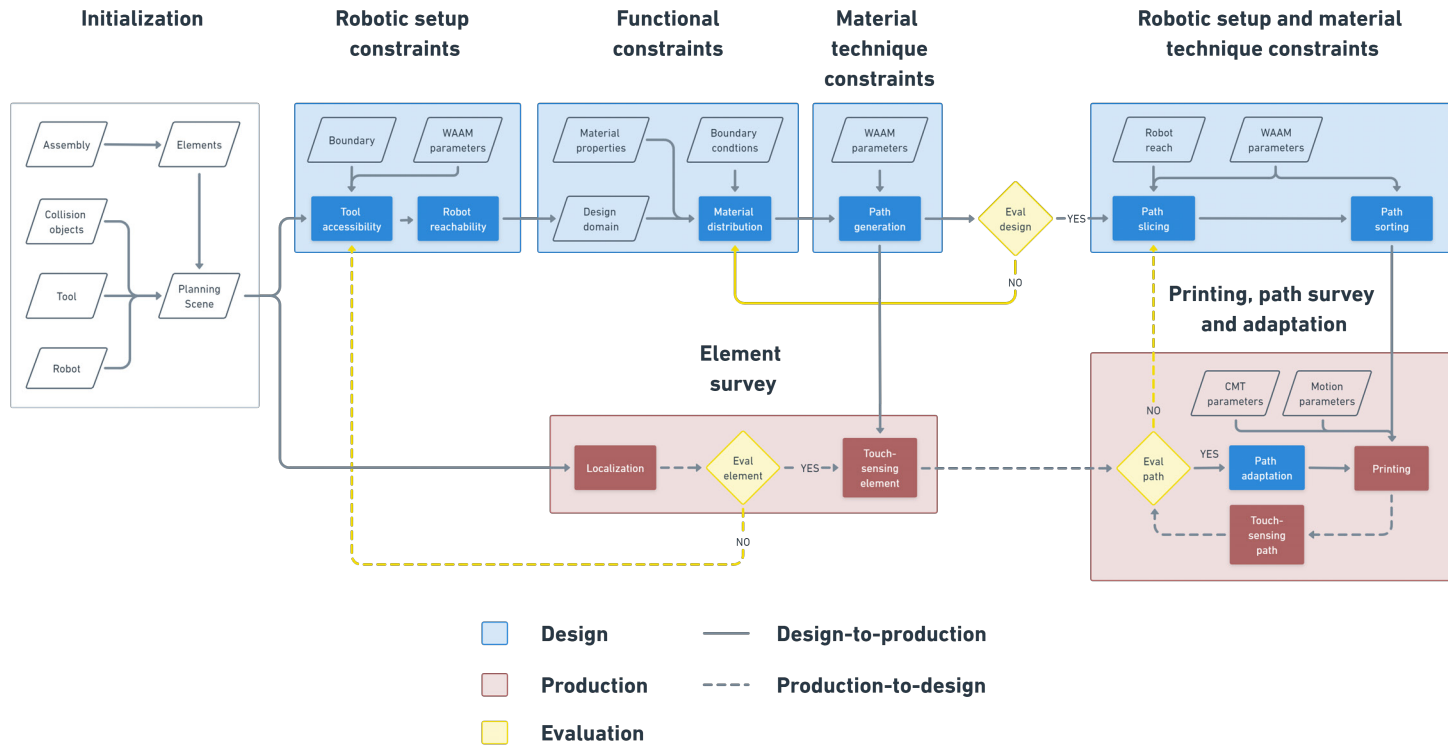
Figure 4.3: *Adaptive detailing pipeline with components*
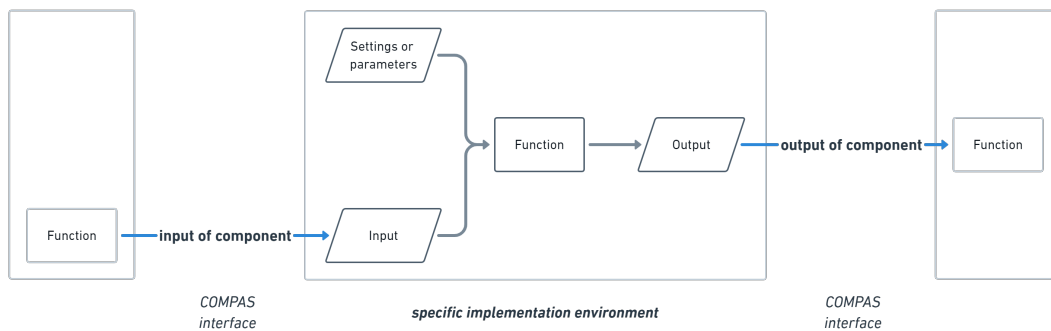
Figure 4.4: *Component's template*

The following sections present each component of the pipeline in roughly chronological order of operations applied to design an *in place spatial connection*.[4] Each section opens with the driving questions or aims of the component, presents relevant background, and describes the most relevant aspects of its implementation.

4.3.1 Considering the robotic setup

Understanding the capabilities and constraints of the tools is fundamental to design with robots in the loop.[5] To design feasible IP-WAAM connections, this challenge is handled with two components: `Tool accessibility` and `Robot reachability` (Figures 4.5, 4.6). `Tool accessibility` studies the space that is free of collisions around the elements for a certain tool geometry, in this case, the welding torch (Section 4.3.1.1), whereas `Robot reachability` maps the space around the elements that the robot can reach with valid joint configurations (4.3.1.2).

---

[4]See the key terminology introduced in Chapter 2 for definition (2.1)

[5]This does not mean that the setup needs to be fully specified in advance, as the role of the data structures is to provide consistency even in the case of future changes in the setup, i.e., the tool and robot descriptions can be updated at any time by replacing their geometric and description attributes. This is particularly useful when working with new materials and processes, as the tooling is usually developed over the lifetime of a project. For example, in this project, the tool was updated from Setup A (Experimental setup A) to Setup B and later on to Setup B with a localization sensor (Experimental setup B).

(a)   (b)
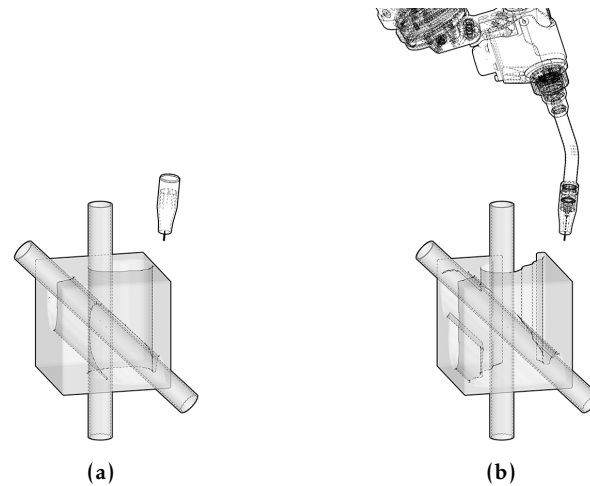
Figure 4.5: *Components considering the robotic setup: (a) Accessibility of the tool, and (b) Reachability of the robotic arm.*

4.3.1.1   Tool accessibility

What can the tools do? How accessible is the space around the elements? Which section of the space around the elements can be accessed by the tool?

Background   The concept of *inaccessible space* was conceived during the development of Ioanna Mitropoulou's MAS thesis *Numerical sculpting of in place wire arc additive manufacturing connections* in the summer of 2018 (Mitropoulou, 2018).[6] Here, a volumetric modeling approach is used to characterize the space around the elements. With this approach, the space is discretized and queried in the form of distances between the discrete units and the elements and stored as a Signed Distance Field (SDF). Within the SDF, multiple queries are possible, such as the level-set of the space that cannot be accessed by a predefined range of tool orientations (Figure 4.7) or the derivatives of the distances that describe the tendencies where objects are located. These queries have meaningful design implications, for example, finding the shortest paths between elements or collision-free tool orientations (Mitropoulou, Ariza, et al., 2019).

---

[6]The project was co-tutored by Mathias Bernhard from the Chair of Digital Building Technologies and the author.
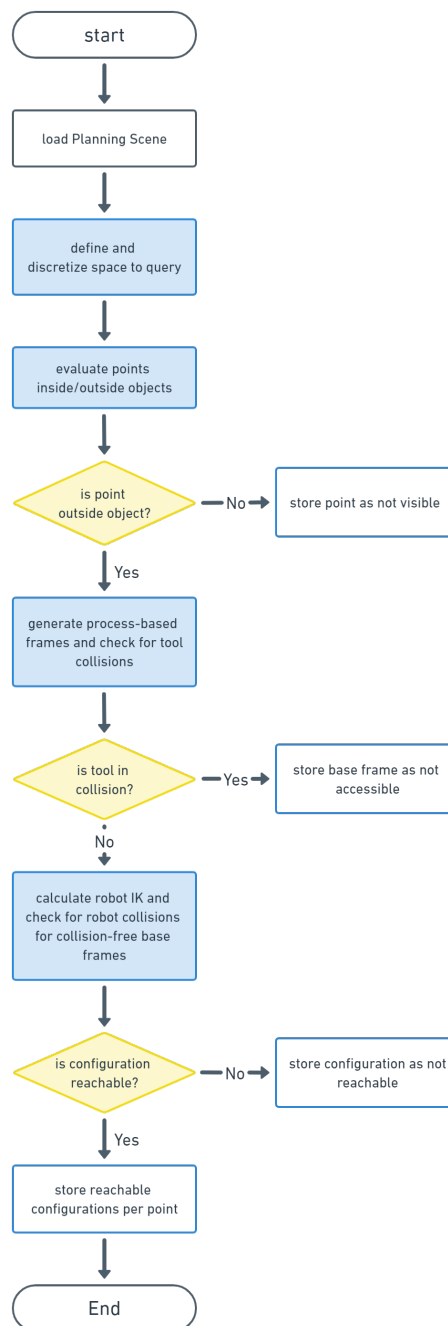
Figure 4.6: *Flowchart accessibility and reachability components.*
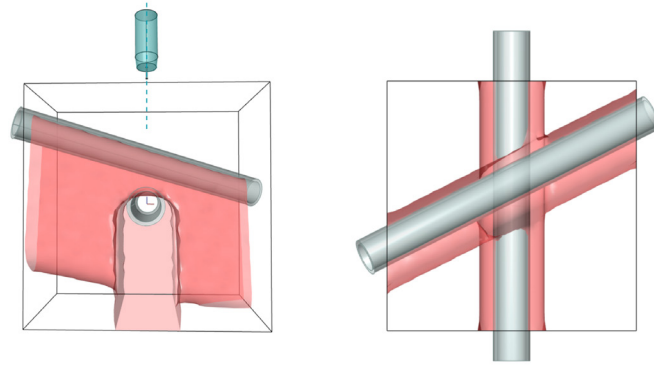
Figure 4.7: *Examples of inaccessible spaces for one tool orientation from Mitropoulou, 2018: side and plan views.*

The *accessible space*, or the space that can be accessed by the tool, is the inversion of the *inaccessible space*. The goal of the `Tool accessibility` component is to determine the accessible space, or the section of the spatial interface that is free of tool collisions, in order to use it as a design canvas of the spatial connections.
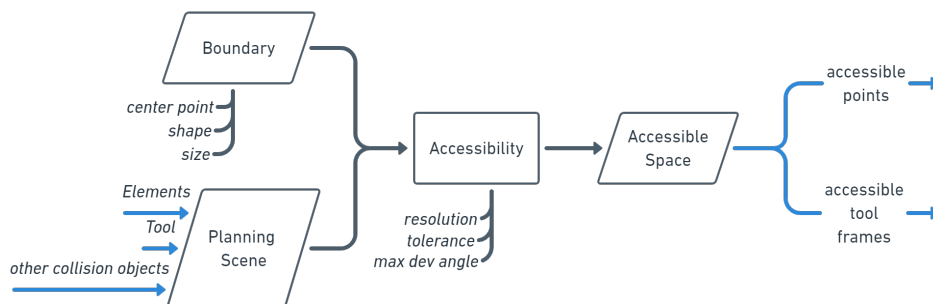
Figure 4.8: *Tool accessibility component*

Implementation

Inputs   With this component, the spatial interface starts taking shape by retrieving components of the `Planning scene`. The `Elements` of the connection, the `Tool`, and any other relevant obstacle, e.g., previously deposited paths in the case of multi-step connections, are virtually placed in the CAD environment by calling the `Planning scene` (Figure 4.8).

A `center point` of the space to query, i.e., the space where the spatial in place connection is expected to be placed, is automatically determined

and saved in the `Planning scene` (Figure 4.9a). The center point is typically the intersection of the axes of the elements or the midpoint of the shortest line between the two axes. This point can be as well conveniently dragged around in the CAD interface, in the case, for example, if a side (not-centered) connection is preferred.

The next point to consider is the shape of the space to query. The `Boundary` is a geometric object, such as a box or sphere. In this implementation, a `compas.Box` whose `compas.Frame` is located at the previously defined `center point` is used. The size of the box finally defines the volume of the space to be queried (Figure 4.9a).

(a)   (b)
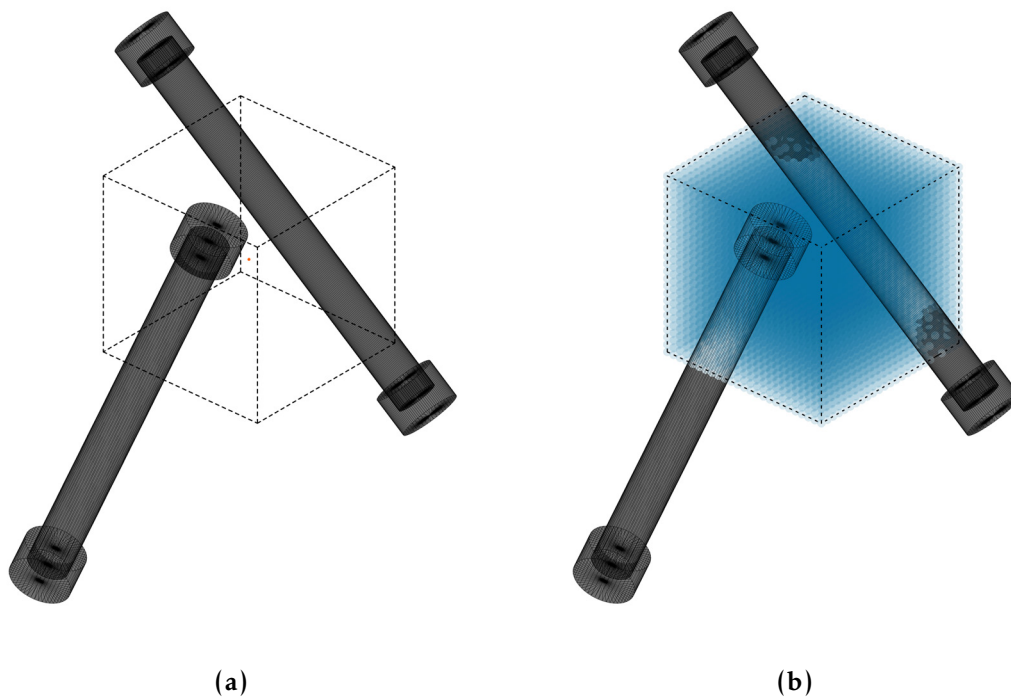
Figure 4.9: *Tool accessibility inputs: (a) Elements, boundary and center point, and (b)* Outside *points to be queried.*

Methods   The boundary space needs to be discretized to carry out the queries. The number of discrete units or grid points in each direction is determined by the `resolution` of the subdivision. In the pipeline implementation, the resolution can easily be changed according to the task at hand. For example, a rough subdivision can be computed first to have a faster result and then replaced by a finer resolution. As the computation time of the accessibility and reachability components

depend on the volume of data to process, a reasonable resolution should be determined based on the type of detail present on the surface and the scale of the collision objects (Figure 4.9b).

To determine which grid points of the space should be queried for accessibility, the grid points are first categorized as *inside* or *outside* the Elements or any other existing obstacles with a distance function. If the resulting distance is 0 or smaller than 0, the point is stored as *interior*. Only *exterior* points, or points outside the elements, are subject to further investigation.

(a)   (b)
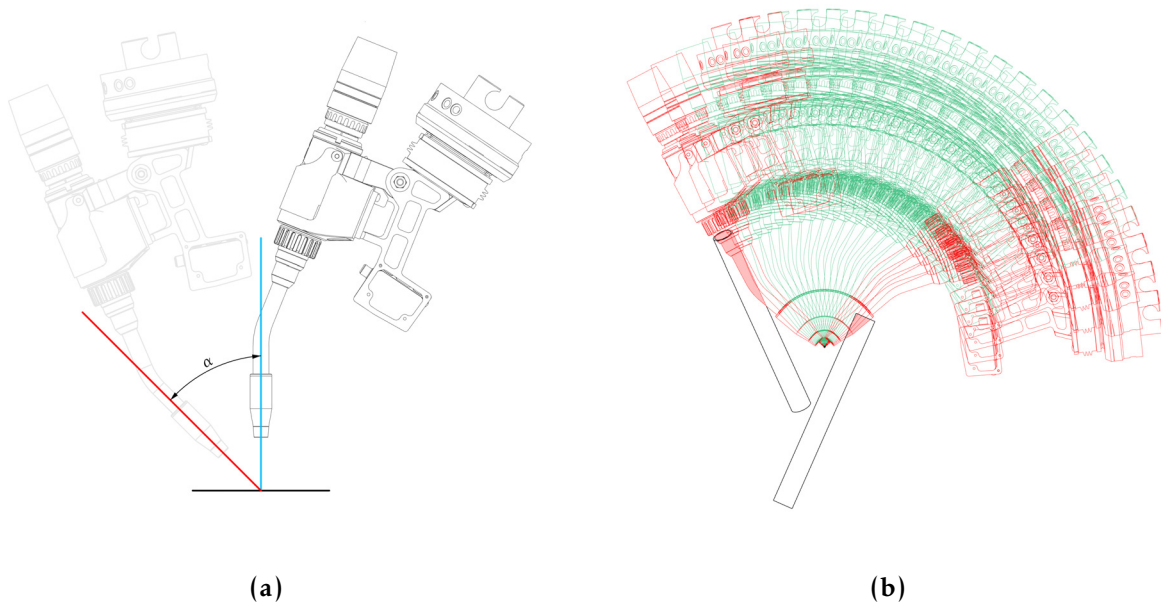
Figure 4.10: *Tool accessibility settings: (a) Tool, base tool axis (in blue), maximum deviation angle, alpha, and maximum deviation tool axis (in red), and (b) Simulated Tool orientations in an example point. Orientations in red are in collision with the elements; orientations in green are free of collisions.*

Calculating the accessibility of each grid point is finally carried out in two steps: creating a pool of possible tool orientations and then checking for collisions for each tool position at each grid point. In the first step, equally distributed vectors are generated with a maximum deviation angle from a base tool axis, in this case, the gravity vector, representing possible tool orientations around a base point. The maximum deviation angle is an important parameter to

consider, as it represents the maximum allowable deviation of the tool relative to the target during the printing process (Figure 4.10a). The second step is the collision check between the `Tool` and the collision objects -`Elements` and any other static collision objects-, which is carried out with the `PyBullet` library by simulating all the possible tool orientations in each grid exterior grid point (Figure 4.10b). `Accessible tool frames`, i.e., accessible tool orientations described with a `compas.Frame` are stored, and the total number of successful frames per point is computed. Finally, grid points are flagged as *accessible* or *not accessible* points (Figure 4.11).[7]

Outputs The `Accessible Space` is populated with the resulting `accessible points`, `accessible tool frames`, and finally stored as an attribute of the `Connection`.

(a)   (b)
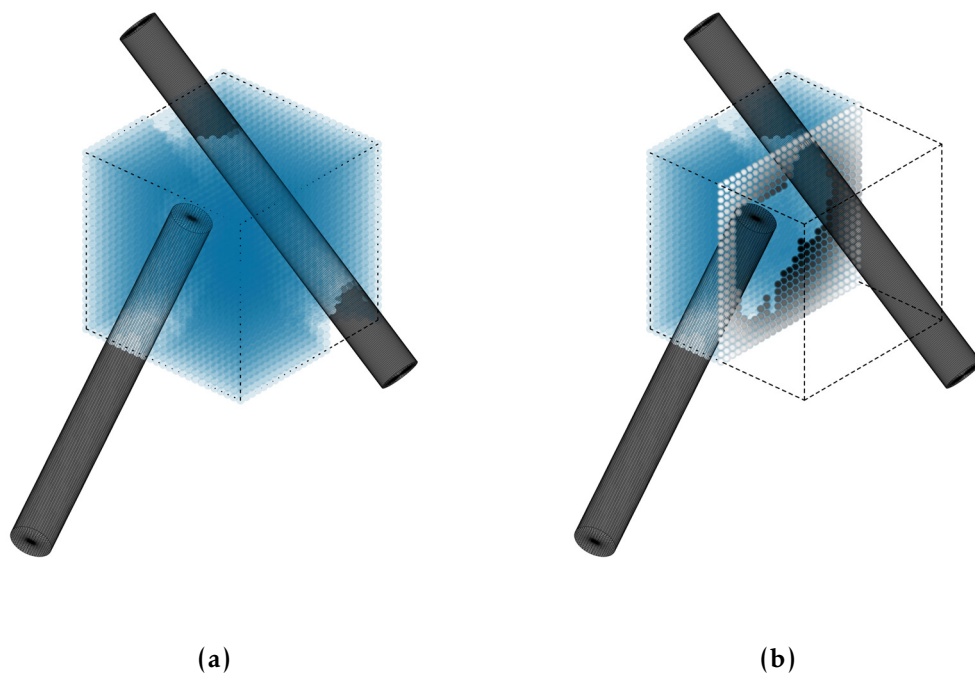
Figure 4.11: *Tool accessibility outputs: (a) Accessible points (in blue), and (b) Section cut of the accessible space showing internal, non-accessible voids.*

---

[7]The functions of this implementation consist in the first steps of the Reachability Map feature of the COMPAS FAB library developed by Romana Rust.

Visualization   Methods to corroborate the inputs and outputs (e.g., boundary, collision objects, accessible points, and accessible boundary mesh) are provided through the `Accessible Space Artist`.[8]

Discussion on accessibility

Validity   The grid points contain tool accessibility information based on the input range of possible approach orientations of the tool. For example, looking at the accessible space visualization (Figure 4.11) without information about these tool settings can be misleading, as space could have been computed with more or less constrained tool settings. Therefore, the results of this step are intentionally uncategorized and only used as an input in the next `Robot reachability` step.

Settings and performance   For the next component in the pipeline, the `Robot reachability` component, an open multi-dimensional `numpy.meshgrid`, or `numpy.ogrid`, was used to facilitate the implementation of the marching cubes algorithm.[9] However, it is known that different discretizations and matching algorithms could significantly improve the performance of this and subsequent components, for example, using an `Octree` data structure or a sparse grid.

The shape of the boundary space should be considered with care to additionally improve performance. The results have consistently shown that information in the corners of the cube is rarely useful; therefore, a sphere instead of a cube would significantly improve the computation time without diminishing the understanding of the spatial interface. Alternatively, the boundary shape could be generated or found based on the supplied inputs, for example, by offsetting the result of the convex hull of the elements' endpoints.

The results heavily depend on the selected inputs, as a small total number of tool orientations or a too-constrained deviation angle often results in a low degree of reachability. Therefore, a trade-off needs to be

---

[8]The components' Artists provide visualization functionality similar to COMPAS Artists (*COMPAS: Artists* 2022).

[9]The marching cubes algorithm will be introduced in the next section.

considered between the resolution, the number of possible tool orientations to check, and the angle deviation to obtain a meaningful space in a reasonable computation time (see 5.1.2.2 and 5.2.1 for benchmarks).

Alternative methods   An alternative workflow based on a volumetric modeling (VM) approach (see Bernhard, 2017) is described in Mitropoulou, Ariza, et al. (2019). The modeling approach provided several benefits such as the possibility of numerically *sculpting* designs. However, due to the time performance and incompatible data structures with successive components of the AD pipeline, this approach was not pursued further.

4.3.1.2   Robot reachability

> *What can the robot do? Which section of the accessible space*
> *around the elements can be reached by the robot? How reachable*
> *is the space around the elements?*

The first step provided information on the accessibility of the tool around the elements to be connected. However, the robot that manipulates the tool may not be able to *reach* all the valid, accessible, tool orientations. Therefore, the second step in understanding the collision-free space where connections can be placed is to check for the reachability of the robotic arm. This is performed by checking for valid robot configurations for each tool frame stored in the previously calculated accessible points.

Background   To visualize and quickly compute tasks inside the reachable workspace, a reachability indicator can be captured in the form of a reachability map (Min et al., 1996, Zacharias, Borst, and Hirzinger, 2007). The reachability map is also a measure of robotic dexterity, or the kinematic ability to change orientations within a given space (Porges et al., 2015, R. R. Ma and Dollar, 2011). For IPWAAM, this kinematic ability of the robotic system is a fundamental measure to consider, as the printing task is constantly constrained by collision objects. In this component, a reachability map is created to capture the

robot's workspace in order to define areas where connections can be
placed (Figure 4.12).[10]
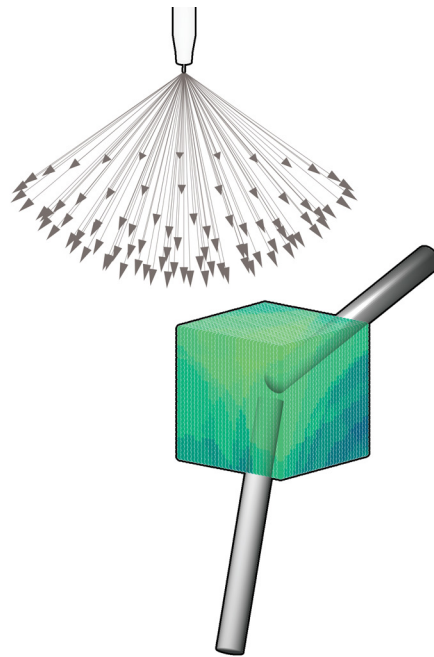
Figure 4.12: *Robot reachability space with the range of tested tool orientations.*
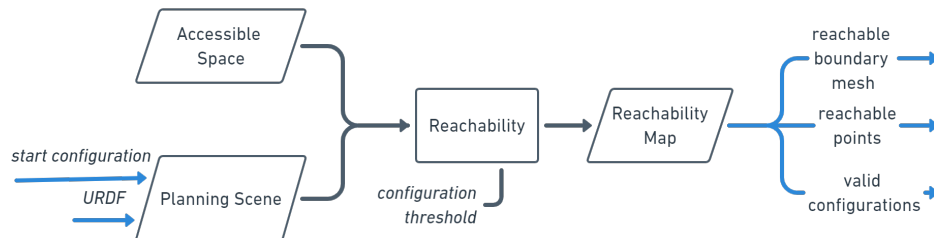
Figure 4.13: *Robot reachability component*

Implementation

Inputs   Two inputs are needed to compute the connection reachability:
first, the `Planning Scene`, containing the Unified Robot Description
Format or `URDF` of the robot, and a `robot start configuration`, i.e.,
pose of the assembly robot and position of the welding robot on the

---

[10]The reachability map used in this pipeline was developed by Dr. Romana Rust as a
    planning feature of the COMPAS FAB library (Rust, 2022a).

linear axis; and second, the previously computed `Accessible Space`, which contains the `accessible tool frames` and `accessible points` to be checked (Figure 4.13).

Methods To compute the `Reachability Map`, an analytical inverse kinematics (IK) function is calculated for each `accessible tool frame` in each `accessible point` (Rust, 2022b). The analytical IK function calculates, for a certain target frame, all the possible robot configurations with valid joint angles to reach the target frame (Rust, 2022c). If an IK solution is found, this means that the robot can reach the queried `accessible tool frame`. A second collision check is performed concurrently to verify that the robot arm is as well free of collisions. If a collision-free IK solution is found, the result is stored as a `valid configuration` using the respective `COMPAS FAB` data structure (Figure 4.14a).

(a)   (b)
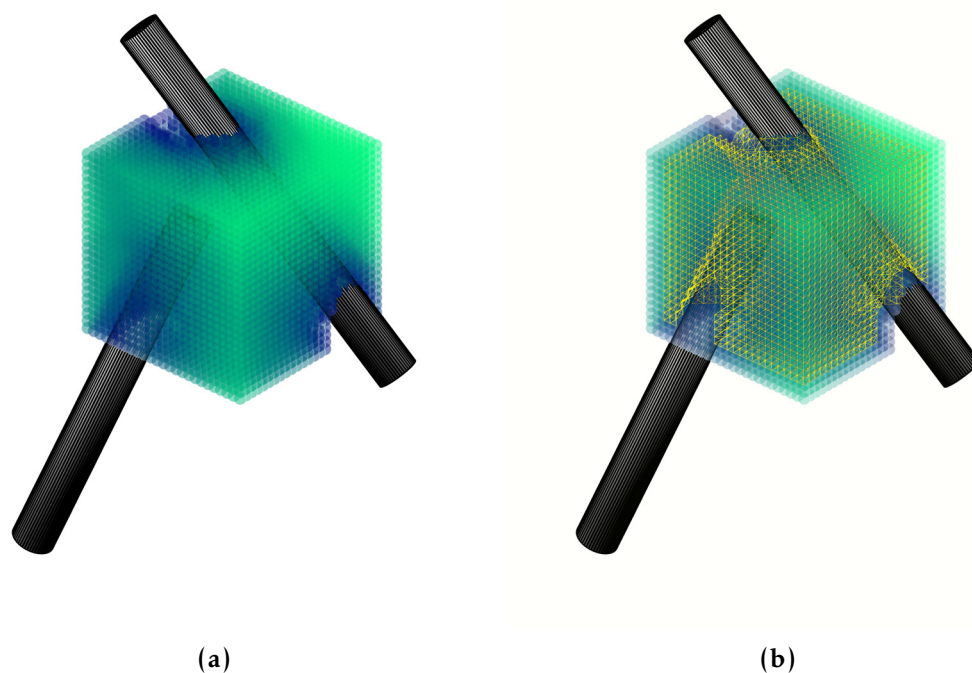
Figure 4.14: *Reachability map: (a) Reachable points with gradient of valid configurations. Points with a higher number of valid configurations in green and points with a lower number of valid configurations in blue, and (b) Reachability map and reachable boundary mesh (in yellow).*

Next is the calculation of the `Reachable Space` where connections can

be placed. This is the boundary, or `reachable boundary mesh`, containing the `reachable points` that have a minimum number, or `threshold`, of `valid configurations` (Figure 4.14b). The `threshold` determines how many `valid configurations` per point should be satisfied for the point to be included as a reachable point (Figure 4.15). A reasonable threshold number depends on the number of configurations to be checked in the first place. Finally, the `reachable boundary mesh` is computed using the marching cubes algorithm[11] from `scikit-image` with additional utilities from the `compas_vol` library (Walt et al., 2014; Bernhard and Clemente, 2022).

Outputs The total number of `valid configurations` per point, each `valid configuration`, and the `reachable boundary mesh` are stored in the `Reachability Map` as an attribute of the `Connection`.

(a)   (b)   (c)
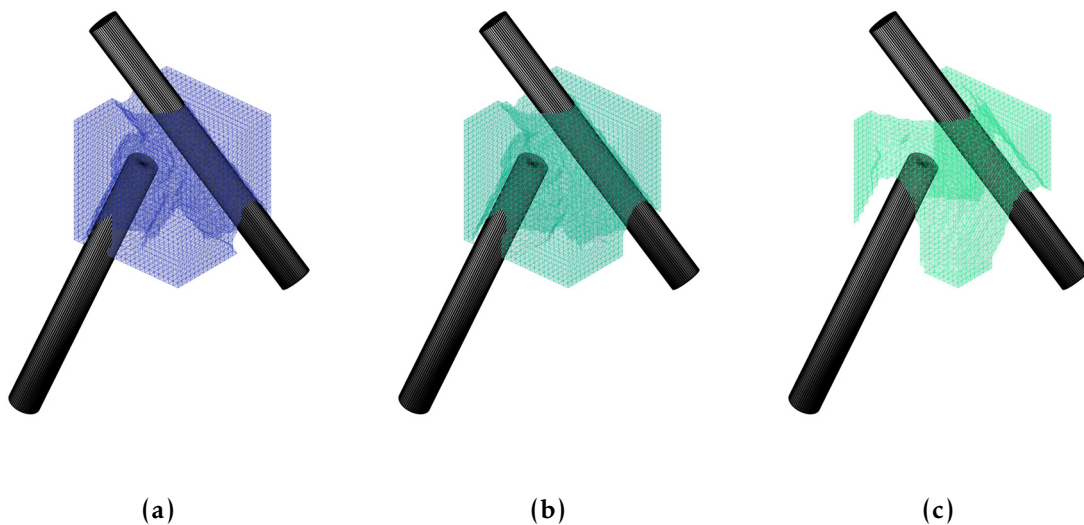
Figure 4.15: *Reachability boundary mesh with different threshold of valid configurations: (a) At least 1 valid configuration, (b) At least 10 valid configurations, and (c) At least 50 valid configurations.*

Visualization Methods to verify the inputs and outputs (e.g., reachable boundary mesh, reachable points, reachable tool frames, and the number of configurations per point as a gradient) are provided through the `Reachability Map Artist`.

---

[11] The marching cubes algorithm is used to render an approximation of a contour surface, or the isosurface, i.e., a surface containing the contour levels or isolevels, of a scalar field ("Marching Cubes" 2022)

Discussion on reachability

Validity   The results of the reachability map are based on the tool accessibility settings defined in the previous `Tool accessibility` component.   These settings, i.e., `maximum deviation angle` and `base tool axis` for the tool orientation should be considered carefully, as neither the accessibility nor reachability calculations per se select orientations that are preferable for discrete WAAM paths.[12]

Discretization and computation time   The implementation operates on discrete grid points presented in 4.3.1.1 providing a `resolution` setting to control the density of the discretization and queries. However, in practice, the computation time required to build a realistic map is too high to use very dense grids. Therefore, maps can leave potentially significant sections of the space without being queried. This could be further explored with a learning strategy to fill in between the existing data points.

Reachable boundary representation   The implementation uses a boundary mesh to determine which section of the space is considered "reachable." Because each point contains several valid configurations, but ultimately a boolean result is needed to determine which units are inside and which units are outside this "reachable" space, a threshold of a minimum number of configurations is used (Figure 4.15).   This boundary representation of the space is produced to facilitate the implementation of the next step in line, the 4.3.2.2 component using a boundary design space. However, a field representation instead of a boundary representation of reachability could be beneficial to maintaining previously calculated data available throughout the next steps.

Performance   The Functional connection demonstrator presented in Chapter 5 provides benchmarks for the components' runtime. The computation time is significantly higher (80%) than the rest of the AD

---

[12]For example, if printing from a wall at an angle of 90 degrees from the gravity vector, it is not beneficial to use a `base tool axis` aligned with the gravity vector as, in this scenario, half of the possible tool orientations will be filtered as in-collision with the wall. An illustration of these settings can be found in Figure 4.10a.

components, with implications for design-and-production planning. The time is particularly dependent on the following variables: number of frames to test, resolution, and boundary volume. The resolution could be handled dynamically with more efficient input data structures, such as `Octrees`. The overall boundary volume could be further improved as discussed in 4.3.1.1. Alternatively, learning strategies could be considered to skip and fill in intermediate points.

Input parameters   Several parameters are used as static inputs in the current implementation to reduce computation time. However, they could be considered dynamic variables to enlarge the degree of reachability of the map. First, the base of the welding robot is considered fixed; however, the degree of freedom of the linear axis could be used to extend the reachability of the map. Setups with even more DOF could exponentially increase the reachability of a connection, a scenario that should be studied closely along with the component's performance. Second, for connections calculated in a virtual cooperative assembly setup such as the ones in Structures with IPWAAM connections, the gripper's position of the placing robot is also considered fixed. Similar considerations by testing different gripping positions could potentially improve the degree of reachability. Lastly, the current approach considers the structure a static input attached to the ground. The structure location could be considered a variable, particularly in multipurpose robotic setups where manipulators collaborate to orient parts in space to benefit from gravity to obtain high-quality welding results.

Alternative implementation   The reachability map is now calculated based on the accessibility information; however, the robot's reach, the time-consuming task, could be as well calculated in advance as a full dense space, without the preliminary pruning of the tool's collision information. In that case, the map would be queried as needed when as-built positions of elements are received. This approach is currently used in robotics for online queries of real-time tasks and could be further explored to reduce the bottleneck of computation time during time-sensitive tasks (Porges et al., 2015).

4.3.2 Considering the functional requirements

As discussed in Chapter 2, the computational modeling and analysis of connection details is a challenging task, even in the scope of standard structural typologies and known materials of which there are uncountable built and virtual examples (Rugarli, 2018). It is therefore expected to find more challenges in answering these questions within the new context of **i.** spatial assemblies **ii.** with varying spatial interfaces **iii.** using a novel manufacturing technique **iv.** with an unknown material behavior **v.** implemented in a design-and-production pipeline.
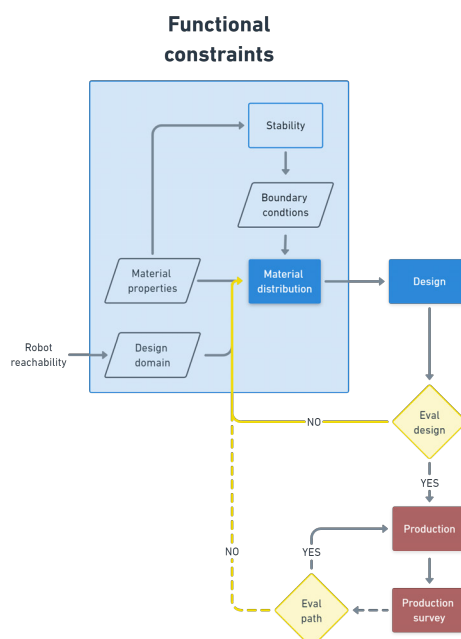
Figure 4.16: *Adaptive detailing pipeline concerning the functional requirements.*

Such an unprecedented combination of conditions (**i.-v.**) demands an expert evaluation of the suitability of existing modeling and analysis methods and the development of new approaches. Intending to pave the way for further developments in this direction, the AD pipeline intentionally positions unanswered functional considerations such as structural modeling and evaluation challenges[13] at the core of the

---

[13]This group of considerations positions function at the core of the AD pipeline. While the discussion here is focused on the main function of the case study's connection, which is transferring forces across elements, the group is intentionally named *functional* as a placeholder for other functions of connection details besides the structural such as thermal or acoustic control.

design workflow (See Figure 4.16). As discussed in Section Joining to support in Chapter 2, computationally designed structures provide an exciting context of inquiry to reset certain conventional approaches that lack integration between constructability and functional requirements such as structural behavior.

The existence of open challenges in the pipeline is here consolidated as open questions, and their inclusion at the core of the pipeline has several consequences. First, their inclusion sheds light on structural modeling and analysis problems, and optimal material distribution concerning spatial interfaces when using new materials (Questions 1-2 and 3-4). Second, they provide a more tangible understanding of the dependencies of the early integration of constructability and structural constraints in the design phase (Question 5). Third, they anticipate the effects of the lack or inclusion of integrative methods within a design-and-production pipeline (Question 6). The questions are linked to their respective components and are discussed in their respective sections:

Stability

1. *What is the type and magnitude of the forces involved in a spatial structure for a given load case?*

2. *What connection modeling techniques are pertinent if the structural elements are not in contact with each other?*

Material distribution

3. *Where should the connection material be placed to satisfy the transfer of forces given the load cases?*

4. *How can we model material placement without a known material model?*

Evaluation of position of elements

5. *How is the connection's force transfer satisfied across all the steps of the design pipeline?*

Evaluation of position of paths

6. *How is the connection's force transfer satisfied if the as-built geometry differs from the as-planned geometry during the construction phases?*

Questions 1 and 2 are discussed in section `Stability`. Questions 3 and 4 were prototyped within the `Material distribution` component. Questions 5 and 6 are respectively discussed in `Evaluation of position of elements` and `Evaluation of position of paths`. Questions concerning the application of the AD pipeline within an assembly are further discussed in Chapter 5 through the Structures with IPWAAM connections demonstrators.

4.3.2.1 Stability

What is the type and magnitude of the forces involved in a spatial structure for a given load case? What connection modeling techniques are pertinent if the structural elements are not in contact with each other?

This step concerns the global stability analysis of the whole structural system. This component is an essential part of the modeling and analysis of spatial structures and is included in the pipeline to explain the relationship between the connection and the rest of the elements of the structure. The required structural evaluation inside this component is out of the scope of this thesis, and therefore its implementation was not put forward. However, the component's relevant functions and outputs are explained below and commented on the discussion section of the `Material distribution` component (4.3.2.2).

Required methods   To find out the forces acting on each connection, a static analysis of the structural system under existing load cases should be performed first. In the context of robotic assembly without using scaffolding, each assembly state should be considered as a sub-assembly

and calculated individually. Then, an envelope of the forces acting
on a node in each assembly stage should be considered. To develop
this, a modeling strategy for connections for non-contact and/or non-
convergent structural elements should be studied.[14]

Required outputs   This component should result in the internal, or
cross-section forces of the structure (Holst et al., 2021).

4.3.2.2   Material distribution

> *How are the structural requirements satisfied? Where should
> the connection material be placed to satisfy the transfer of forces
> given the load cases? How can we model material placement
> without a known material model for steel printed with WAAM?*

Provided that information about the structure's external loads and
internal forces is available, the next step is to understand the location,
mass, and distribution of the connection material to transfer forces
between structural members. As presented in 2.3.3, structural opti-
mization methods such as topology, shape, and size optimization can
be used to find optimal layouts of material to fulfill certain perfor-
mance criteria. In the context of in place fabrication, the first step to
consider is that material can only be placed within regions accessible
by the welding torch and reachable by the robot arm. These regions
or boundaries, in turn, can be used as constraints during the material
placement optimization. With this, the conventional formulation of
the forward problem, e.g., "for a given structure, find the structural
responses," can be formulated as an inverse problem "for a desired
structural response given the accessibility and reachability constraints,
find the structure(s) that satisfy these constraints" using a topology
optimization (TO) approach.

Background   In the last few decades, many TO techniques have been
developed to incorporate diverse constraints in the optimization task
in order to improve manufacturability (e.g., Jikai Liu and Y. Ma, 2016;
Vatanabe et al., 2016; Thompson et al., 2016; Jikai Liu, Gaynor, et al.,

---

[14]An approach is provided by the *Element Felting* component of Karamba3D that
automatically generates connections between nearly touching neighboring elements
(Preisinger, 2010).

2018; J. Zhu et al., 2021). Concerning accessibility constraints, Chen, Lu and Wei (Y. Chen, Lu, and Wei, 2016) propose an application of the concept of visibility (Woo, 1994) in the TO task. Alternative projection-based approaches have been proposed for several machining processes (Guest and M. Zhu, 2013; Vatanabe et al., 2016). Florea et al. propose the addition of the accessibility constraint for multi-material and multi-joint topology optimization (Woischwill and Kim, 2018), differentiating between accessible and not accessible areas and types of joining operations that can be used in contact regions between components (Florea et al., 2019). Morris et al. (Morris, Butscher, and Iorio, 2020) propose and compare different algorithms to restrict non-accessible or machinable areas. In these cases, the topology optimization formulation includes restrictions to avoid the production of unfeasible geometries. While these approaches show a promising direction to generate valid solutions from the start, in practice, including the reachability constraints of the robotic arm as an additional check during the TO task would require a highly computationally expensive operation.

To avoid searching for a material distribution of areas that are un-reachable, a *pruning of the design space* is done before the optimization task is performed as described in Mirzendehdel et al. (Mirzendehdel, Behandish, and Nelaturi, 2019). This concept uses a *subspace* that is already valid before any optimization task is pursued.[15] With this approach, the TO task can be carried out in a "safe" space found within the previously obtained robot's reachability boundary.

Implementation

An implementation of this approach that could be easily integrated into the design-and-production workflow was favored. A 3D TO using `tOpos`, a plugin for Grasshopper developed by Sebastian Białkowski (Białkowski, 2016, Białkowski, 2017, Białkowski, 2018) was selected as it fulfills a smooth integration with the CAD environment, providing intuitively acceptable results. Alternative options with more elaborated setups and integrations were tested early on during the development of

---

[15]This approach is additionally supported by the "set constraint" nature of the reachability problem, which Mirzendehdel et al. identify as not straightforward to integrate into a TO task due to its "non-smoothness and computational intensity" (Mirzendehdel, Behandish, and Nelaturi, 2019).

this thesis and are described in the discussion section of this component. This section describes the input, methods, and outputs based on the `tOpos` plugin implementation on the AD pipeline. A discussion on the validity of the results is also included at the end of the section.
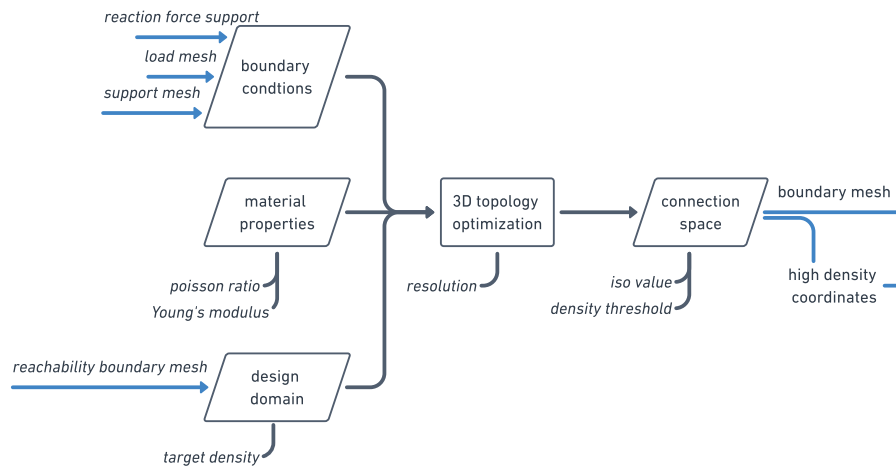
Figure 4.17: *Material distribution component*

Inputs   A typical setup in `tOpos` includes the following inputs (Figure 4.17): `boundary conditions`, `design domain`, `material properties`, and `element density`.

The `boundary conditions` include the `base elements` and `target elements` assigned as *support* and *load* elements, respectively (Figure 4.18). *Supports* include all the previously and virtually assembled or printed elements or paths. The *load* element is the element to be assembled next, always one at a time. Additionally, a `load vector` is required (Figure 4.18a). The magnitude of the load vector is an important factor, as it represents the load the connection should transfer from the load element to the support element. The interpretation of the load vector magnitude is discussed at the end of this section.

(a) **(b)**
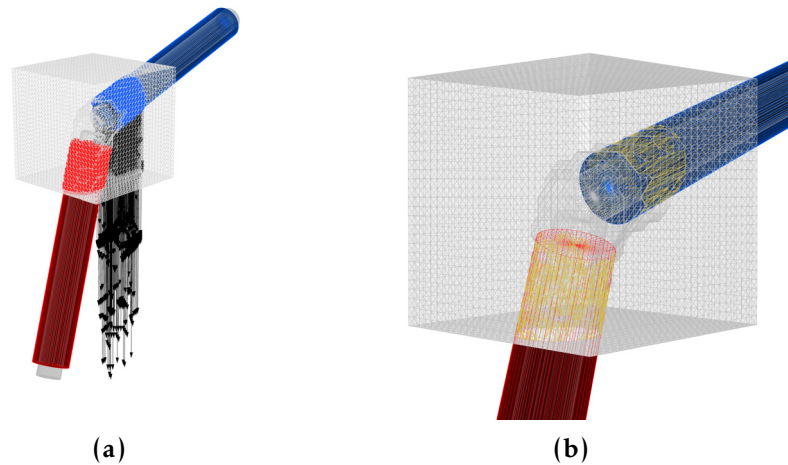
Figure 4.18: *Boundary conditions: (a) Base/support Elements (in red), target/load Element (in blue), load vectors (in black) and reachable design domain (in gray), and (b) Design domain with intersection areas with base and target elements (in yellow).*

The `design domain` is the `reachability boundary mesh` described as an output of the `Robot reachability` component (4.3.1.2). A minimum resolution of the boundary mesh and an overlap with the load and support meshes are required for the solver to start (Figure 4.18b). The solver also requires a clean non-manifold mesh with no open edges.

The `material properties` inputs, i.e., the Poisson ratio (0.3) and Young's modulus (195 GPa) are taken from the mechanical tests described in Chapter 3 (3.6.6.2).

Methods A TO problem inside `t0pos` consists in an *objective* (e.g., minimize the mass), inside a *design domain* (i.e., the reachable space), within certain *constraints* (e.g., desired stiffness and prescribed volume fraction) under certain *boundary conditions* (loads and supports). The problem is solved with two `t0pos` Grasshopper components that implement a Solid Isotropic Microstructure with Penalization (SIMP) algorithm using the optimality criteria method (Bendsøe, 2004), which is described in Białkowski (2016) and Bendsøe (2004) and roughly includes the following steps[16]:

---

[16]Steps are reproduced based on the original formulation by Bendsøe and Sigmund, as unclear discrepancies were found on the plugin documentation

  i. subdivide the design space into discrete elements with a certain resolution

 ii. fill the elements homogeneously with the prescribed element density

iii. run a Finite Element (FE) Analysis to find the strains and the displacements of the design under the prescribed loads and boundary conditions

iv. compute the compliance (a global measure of all displacements) and sensitivities (derivatives of the density of each unit) of the design

 v. check if the compliance has improved (i.e., decreased) from the previous iteration. If so, continue. Otherwise, stop

vi. update the density value of each cell [17]

vii. filter sensitivities [18]

viii. recompute.

The solver stops after a certain number of iterations or if the stopping conditions are met, in this case, if compliance has decreased less than a user-defined value. The running time varies greatly depending on the `resolution` setting, which defines the size or number of elements of the FE model (Figure 4.19).

(a)   (b)   (c)
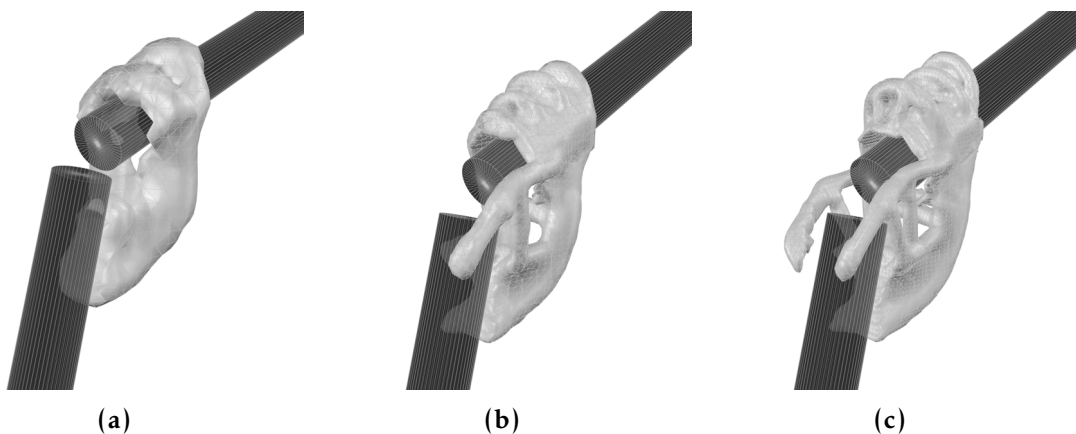
Figure 4.19: *Isomesh result from model computed with different resolutions: (a) Low, (b) Medium, and (c) High.*

---

[17] This step can be achieved with different methods. In this case, the algorithm applies a minimum compliance (maximum stiffness) problem with a SIMP interpolation within the specified volume constraint (see Sigmund and Petersson, 1998).

[18] In other words, numerically stabilize the density of a specific unit based on the weighted average of the neighborhood densities (see Sigmund and Petersson, 1998).

Outputs The result of the TO task is the `connection space`, which can be represented as a boundary mesh or `isomesh`, or as `high density coordinates`, point representations of the areas of higher material densities (see Figure 4.20).

(a) **(b)** **(c)**
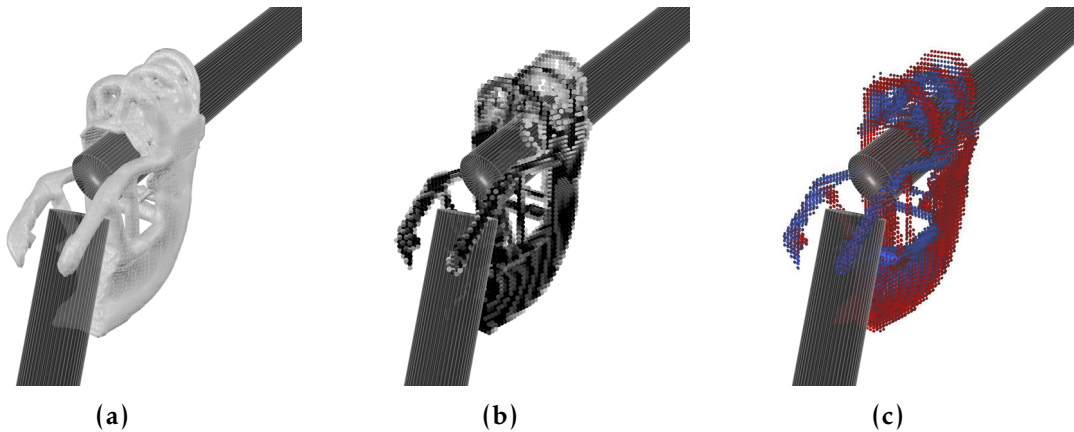
Figure 4.20: *Results of material distribution task: (a) Isomesh, (b) High density coordinates, and (c) Principal stresses: tension (blue) and compression (red).*

`tOpos` provides a volume representation of the density results as an isomesh computed with the marching cubes algorithm. The algorithm computes the isosurface, or the surface representing points of equal value of the scalar field of the resulting densities. The `isovalue`, the value for which the isosurface will be constructed, has a large effect on the mesh volume (Figure 4.21).[19] In addition, points of higher density can be filtered and visualized as discrete units, with a color indication of their density value. This output becomes useful as a visual overlay in combination with the `Path generation` component. Finally, the isomesh and high-density points are stored in the `Connection` for later access. A discussion on the different outputs in context is provided in Chapter 5 for the Simple connection demonstrator.

---

[19]However, in the plugin implementation, there is no setting to control the volume reduction to match the initially prescribed volume fraction (see discussion section).

(a)   **(b)**   **(c)**
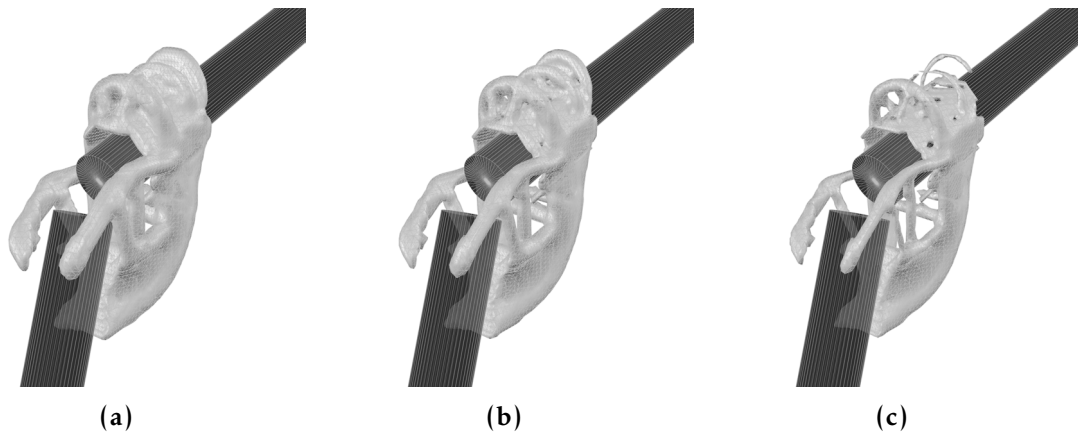
Figure 4.21: *Isomesh results from different isovalues for a high resolution model: (a) Isovalue 0.1, (b) Isovalue 0.25, and (c) Isovalue 0.5.*

Discussion on material distribution

Validity   The results from the proposed workflow can be used to indicate a tendency of how, under certain boundary conditions, a hypothetical homogeneous material with a prescribed stiffness would be distributed. The validation of this approach can be seen in the physical demonstrators presented in Chapter 5. The material tendency is understood to be verisimilar as much as the connections can hold the modeled physical loads.

Internal forces   As explained in 4.3.2.1, the internal forces of the members should be calculated based on a global static analysis. This becomes evident in the context of a structure with several elements. When elements that are not in contact with the connection under study exist, their influence should be included in the form of internal forces acting on the members under study. However, here, each connection is calculated in isolation, without the static analysis of the complete structure. As the choice of the plugin was decided early on, in part for its simplified version of the material distribution workflow, some limitations were imposed regarding the structural requirements. In particular, the selected plugin does not allow applying and differentiating the load vectors per input volume, and therefore even if calculated, the internal forces would not have been included due to the setup limitations. It is understood that with more control over the inputs

and settings, such as the ones available in other TO software packages, the calculation of the internal forces would be a requirement for the proper setup of the TO task. During the development of the structure demonstrators presented in Chapter 5 5.2, a compensatory measure of scaling the magnitude of the load vector based on the volume of the elements located upstream in the assembly sequence was taken to represent the additional loads brought by the elements not directly in contact.

Control of the volume ratio   The TO task results in a density scalar field but does not inform on the exact volume of the connection geometry required for the prescribed boundary conditions. This has a reason for allowing different solutions with different stiffness to still be valid solutions. Imposing smaller volume constraints (e.g., 1% of the design domain volume) would result in higher stresses on the members, while larger volume constraints (e.g., 5%) would make the connection stiffer. The decision on which exact stiffness should be selected for a node greatly depends on the desired overall structural behavior and is out of the scope of this study. An important next step would be to develop a system for tuning the required stiffness of the node based on the desired stresses and utilization of the elements.

Integration with material deposition steps   The main limitation of the approach lies in the lack of integration of the material deposition constraints, such as build angle relative to the gravity vector and the minimum and maximum member sizes of the connection's paths. To overcome this, ongoing research in the subfield of integrative topology optimization with additive manufacturing constraints show promising next steps in this direction (Garaigordobil et al., 2018; Mishra et al., 2021; J. Zhu et al., 2021). In the proposed pipeline, this is tackled by the `Path generation` component independently. A step forward in the integration of manufacturing constraints has been already tested successfully by including member sizes constraints in the Abaqus TO task setup[20].

---

[20]During the Spring semester of 2021, a study on the Topology Optimization of Structural Steel Nodes for Wire and Arc Additive Manufacturing was conducted at the Chair of Steel and Composite Structures led by Prof. Andreas Taras and Dr. Vlad Silvestru and developed by master students Hendrik Holst and Veton Beciri

Incomplete material model   While the material properties used in this component have been derived from the static tests presented in 3.6.6.2, these experiments also provided insights on the effect of the surface roughness of the point-by-point WAAM bars in the structural performance of the component, aspect that is not considered in the presented TO approach. Therefore, the cross-section variability should be considered as well, potentially as a safety factor on the minimum cross-section member diameter on the TO task.

Solver errors   Finally, the most common failure on the solver is due to input errors. To this end, a series of verification operations are performed on the input setup. These include performing a mesh intersection to verify overlaps between the design domain and the supports and loads and a validity check of the meshes. If the check is not passed, a mesh edit operation or/and a minimum offset of the design domain need to be performed. These steps are time-consuming and should be automated.

Alternative methods   As mentioned before, alternative TO setups were considered during the implementation of this component. The TOSCA topology optimization module integrated with Abaqus (*Tosca, Abaqus/CAE* 2000) presented a greater control of the TO task, such as the possibility of precisely imposing forces on custom areas of the model, specifying the objective function, and constraining the maximum size of the cross-section of the resulting parts. Although promising, a COMPAS interface for using the topology optimization module in Abaqus was not available at that time, and its development, evaluation, and validation would require structural engineering expertise.

A more recent alternative within Grasshopper developed by Huang and Xie, `Ameba`, uses a Bi-directional Evolutionary Structural Optimization (BESO) method (X. Huang and Xie, 2010) and provides more versatile input settings (Q. Zhou et al., 2018). However, this plugin did not provide a reliable workflow when using meshes, i.e., the reachable boundary mesh, as inputs of the design space compared to poly-surface inputs. The conversion from meshes to poly-surfaces proved inefficient and expensive; therefore, the plugin was only used for comparison of the workflow implementation. Alternative methods that do not use

topology optimization were also discussed, such as a "populate-and-filter" approach using, for example, the element stitching component available in the Karamba3D plugin (Preisinger, 2010).

4.3.3 Considering the material technique

The next series of components integrate the WAAM process constraints in the design of connections. As presented in Chapter 3, IPWAAM allows for different deposition techniques (3.5). Each of these techniques requires specific design strategies and imposes material processing constraints. The `Path generation` component shapes the material distribution result into printable paths, in this case, tailored to the discrete WAAM technique. The `Path slicing` component is used to segment the paths into discrete print points or layers, and finally, the `Path sorting` component organizes the layers in a feasible order.

4.3.3.1 Path generation

What is the shape of the connection path? How does the shape of the connection path follow the material process constraints?

This component provides two workflows, one manual and one automated, to create printing paths. The workflows can be used as separate alternatives, or as complementary if one fails. In both cases, the component provides visualization and post-processing features to create and *fit* the design to the elements to be connected.

Background The workflows were formulated as needed during the pipeline development. A manual workflow was first used to devise the first generation of connections by looking at the available reachability data. This manual workflow was useful to understand the constraints of WAAM connections in terms of robot reachability and was tested in the Preliminary studies and the Simple connection demonstrators. The intention to find a more robust generative system lead to the development of the second automated workflow used in the Functional connection and the Structures with IPWAAM connections demonstrators. The manual and automated workflows are named *path sketching* and *path finding*, respectively.

For path sketching, previously calculated design spaces such as the reachability space and/or material distribution result are loaded as a canvas where the designer can manually *sketch* connection paths. With this workflow, the path generation component functions as a visual interface for interacting with previously calculated data, providing filters and metrics to interpret it. The workflows rely on a CAD environment for visualization and user interaction.

For path finding, an output of the `Material distribution` component, the isomesh, is automatically skeletonized and post-processed to generate WAAM-like curvilinear paths. In this case, the CAD interface is only used to visualize the outputs.

While the implementations were developed consecutively, in practice the manual and automated workflows benefit from each other. The interactive features of the path sketching workflow can also be used in combination with path finding when the latter fails. The need for both approaches and their complementarity opens a discussion on the grade of automation the AD pipeline can and aims to provide. The discussion at the end of this section and the chapter's summary section 4.4) will return to this point. The flowcharts of both methods are illustrated in Figures 4.22 and 4.23.
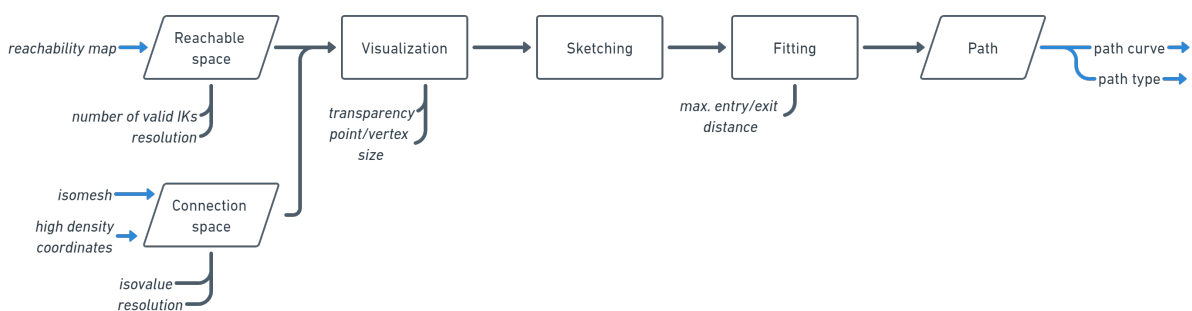
Figure 4.22: *Path generation component with path sketching workflow*
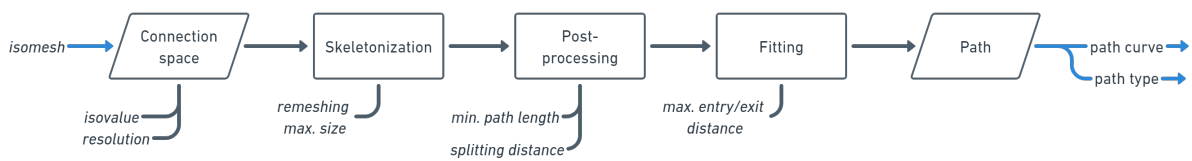
Figure 4.23: *Path generation component with path finding workflow*

Implementation of path sketching workflow

Inputs Previously calculated design spaces such as the reachability and/or the connection space, or `isomesh`, are loaded from the `Connection` with a custom `resolution` in the CAD environment (Figure 4.22).

Methods The workflow consists of: 1. visualization of relevant data, 2. informed sketching by the designer, and 3. manual fitting of the paths between the elements to be connected:

1. Visualization As discussed previously, each component is supported by a visualization method. However, visual representation of the pre-calculated data can be rendered in many ways according to the task at hand. The first step to support designers in their decision-making is to let them control and select what kind of input is useful at each stage of design. To this end, this component provides visualization controls in the form of filters.

With `Filter distances`, the user can select reachable or high-density coordinates within a distance from the base and target elements (Figure 4.24e). With `Filter thresholds` only valid configurations or density values within a threshold are selected (Figure 4.24f). For each filter, common visualization settings provided by the CAD environment, such as transparency and point size, are available (Figure 4.24).

2. Sketching On top of the visualization layers, the user can freely sketch path curves in the CAD environment, visually coordinating the available robot reachability or material tendency with the geometry of the curves (Figure 4.25). The sketched path curves can be selected at any point to retrieve information such as curvature, curve length,
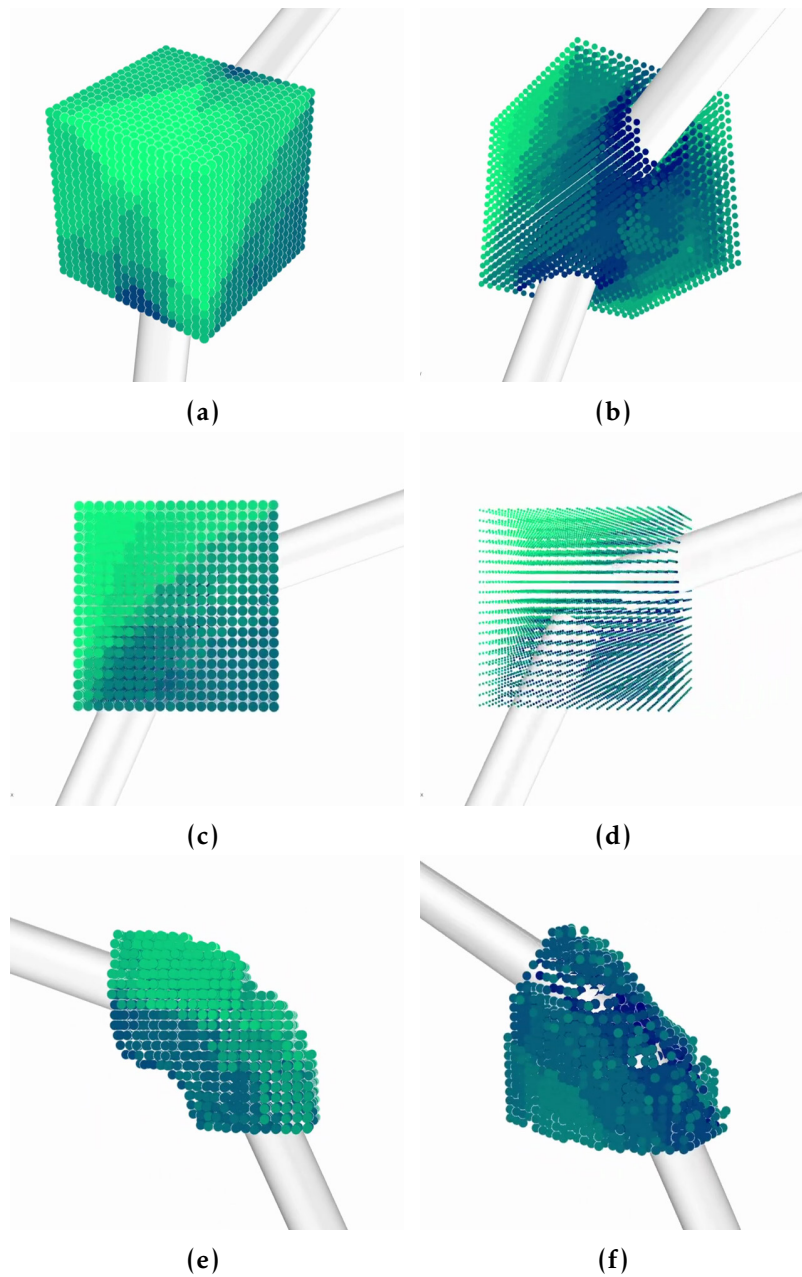
Figure 4.24: *Path sketching controls: (a-d) Reachability map visualization, (e) Filtering by distance to the base and target elements, and (f) Filtering by the number of valid configurations.*

and orientation to gravity using the standard CAD interface's functions. The designer is here free to decide which information to use to inform the aesthetics and function of the design.

3. Fitting   The sketched paths need to be finally fitted between the base and target elements. Each base and target element is, therefore, color-coded red or blue, respectively. The designer manually selects the

sketched curves and uses the `pull curve` Rhino command to fit entry and exit paths to the closest elements. As this is done manually, the designer directly picks towards which element each path should be pulled.
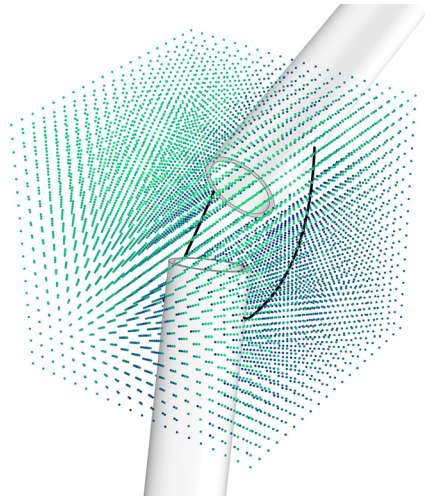
Figure 4.25: *Sketched path inside the reachable map.*

Outputs   Finally, the manually fitted path curves are stored as independent `Paths` and as attributes of the `Connection`.

Implementation of path finding workflow

Inputs   Path finding runs inside the material distribution result, which is loaded from the stored `isomesh`.

Methods   This workflow is achieved with three sequential operations: 1. skeletonization, 2. post-processing, and 3. fitting:

1. Skeletonization   The first step consists in turning the volume of the isomesh into interconnected curvilinear paths. The method employed extracts a 3D skeleton of a volume (Tagliasacchi et al., 2016) implemented using the Ameba component Skeleton3D that relies on the CGAL library's function *Triangulated Surface Mesh Skeletonization* (Q. Zhou et al., 2018; X. Gao, Loriot, and Tagliasacchi, 2021). The result of this operation greatly depends on the input mesh size and resolution (see the Simple connection demonstration for examples). Therefore

a remeshing operation is executed before the skeletonization step to allow for more control of the result (Figure 4.26).
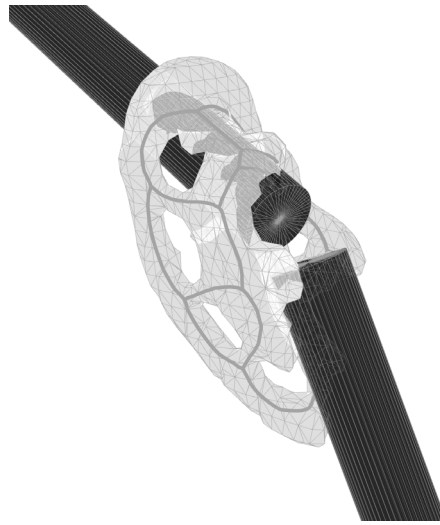
Figure 4.26: *Skeleton from isomesh*

2. Post-processing   The skeletonization operation does not result in clean paths. The output of the previous step consists of continuous curves with a high number of control points. Moreover, the paths show arbitrary continuities. A series of post-processing operations, including curves' rebuilding, splitting, and joining, are performed next to turn these rough skeletons into paths. In this step, WAAM process parameters such as minimum path length (20 mm), curve degree, and smoothness are enforced (Figure 4.27).

(a)   (b)   (c)
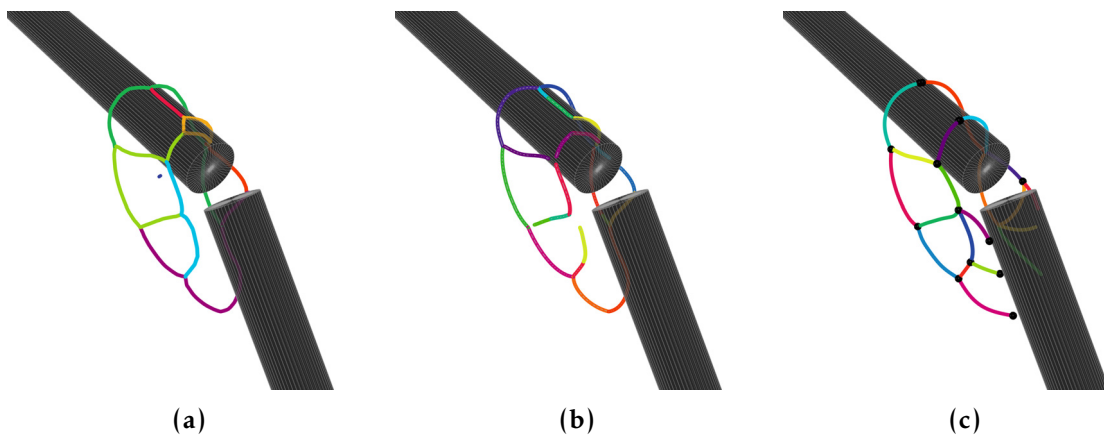
Figure 4.27: *Skeleton post-processing steps: (a) Skeleton unprocessed, (b) Splitting step, and (c) Final smooth skeleton curves.*

3. Fitting   Finally, the paths need to be fitted in between the elements. The fitting operation consists in first categorizing the paths in different types and then fitting, or *pulling*, the paths in between the elements. The paths types are `entry`, `internal`, `bridge` or `exit` (see color-coded Figure 4.28). The categorization is done by comparing the distances of the start and endpoints of each path to the base and target elements. If the sum of the distances of the endpoints to the base element is smaller than the sum of the distances of the endpoints to the target elements, the path is categorized as an `entry` path. Otherwise, as an `exit` path. If the distances are similar or too large, then it is an `internal` path. If both distances from start and endpoints to the base and target elements are very small, then the path is a `bridge`.
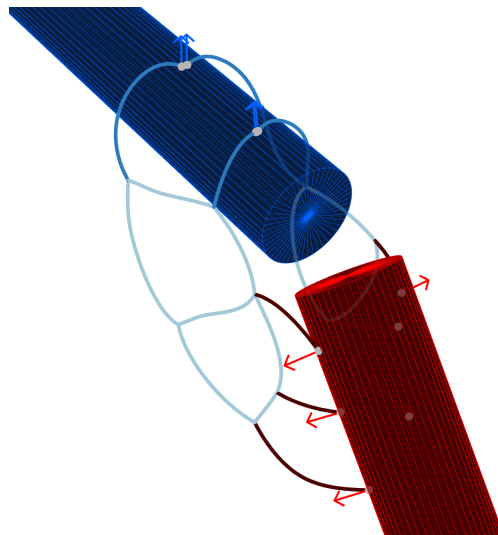
Figure 4.28: *Automatic fitting to base (red) and target (blue) Elements, entry (in bordeaux red), internal (in pale blue), and exit (in blue) paths.*

To implement this, for connections with more than one base element, it is needed to first iterate through the connection's base elements to find which one of these base elements is the closest one to the path and, therefore, towards which one the distances should be measured. For multi-step connections such as the one shown in 4.26, previously generated paths are also considered as possible base elements, i.e., new paths can be built on top of existing printed paths. Once the paths are categorized, start points of the `entry` paths and endpoints of the `exit` paths are pulled towards the closest base and target elements,

respectively. Finally, `bridge` paths are pulled in both directions and `internal` paths are left unmodified (Figure 4.28).

Outputs   Finally, the automated fitted path curves and path attributes are stored as independent `Paths` and as attributes of the `Connection`.

Discussion on path generation

Validity   Because there is no evaluation loop to constantly check the designer's sketched shapes or the results of the path finding, the resulting paths are not numerically validated in any form at this point but only in the subsequent components for `Path slicing` and `Path sorting`, and eventually the `Evaluation of design of paths` component.

For the current implementation of this workflow, the paths are valid if they 1) lie inside the reachable or connection space that has been already created inside a reachable space, 2) are correctly pulled between the base and target elements, i.e., entry and exit vectors are normal to the base and target elements' surface and 3) their slopes, the slope of a tangent measured at any point on the path curve, are always positive to comply with the future `Path sorting` step.

Known limitations   The main challenge of the interactive canvas in path sketching is to plot 3D data in a 2D interface. In particular, it is hard to visualize overlapping information, such as high-density points, simultaneously with reachability metrics. Many modeling techniques can be explored to overcome this. The visualization containers can be more diverse, making use of different geometric objects such as surfaces showing normal orientation vectors, for example, to indicate the curvature of the material tendency; colored meshes to indicate boundary thresholds inside the reachability map; vector fields to indicate directionality of tendency or reachability, etc. The designer could as well design filters according to the interests at hand. It is then acknowledged that this component would benefit from an XR immersive environment to enhance the user's understanding of 3D data. In this scenario, a more intuitive sketching experience, such as sculpting with

body gestures or a CAD interface that allows using a stylus, could be explored.
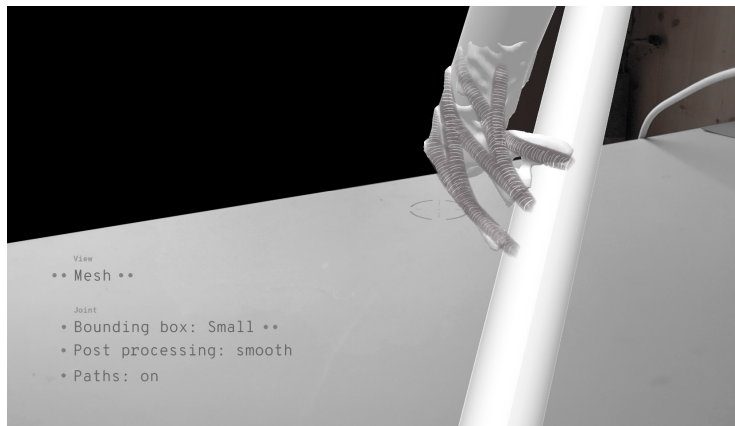
Figure 4.29: *Study for user interface: sketched paths on top of an isomesh in an XR environment (Fologram).*

The paths found through the path-finding workflow are a geometric simplification of the material tendency with no structural significance, as no mass or shape is maintained through the skeletonization approach.

The methods presented here are tailored to discrete WAAM depositions. However, alternative path finding methods could be implemented for continuous and hybrid printing techniques such as the ones described in Section 5.1.1. Eventually, the output of this component should be tightly integrated with the Evaluation of design of paths component to achieve printable and performative connection results.

The sketching workflow can also be used as a post-processing manual step of the previously automatically calculated paths. The possibility of an interactive step for the designer to tweak or modify the geometry of the automatic path generation opens the discussion on how much the pipeline should determine the results. While the intention of an alternative automated workflow was to systematize typical steps in the decision-making process, it is as well evident that the results can be insufficient when fully automated. These failures most often occur when the topology of the connection is too complex, or the volume of a branch is too massive. In these cases, a manual tweak to include additional curve skeletons is possible, as both workflows are

run through the same CAD interface. A second fail occurs on the fitting step, where the location of the control points of the path curves is key in the pulling operation. Tweaks of this step include modifying the control points so to favor smooth path transitions into the base and target elements.

Alternative methods As discussed in 4.3.2.2, an alternative approach integrating both `Material distribution` and this component should be considered, for example by performing a TO task with a maximum member cross-section area as a constraint (Holst et al., 2021).

4.3.3.2 Path slicing

How are path curves sliced and turned into print points? What is the feasible optimal orientation of the welding tool for each print point?

This component deals with the complexity of slicing a spatial path constrained by collision objects. To this end, material and fabrication constraints, such as the optimal tool angles and existing obstacles, need to be integrated to obtain a printable path. The goal of this component is to obtain two outputs: first, the location of the print points along the path, or layer height, and second, the orientation of the tool for each print point, or tool orientation.
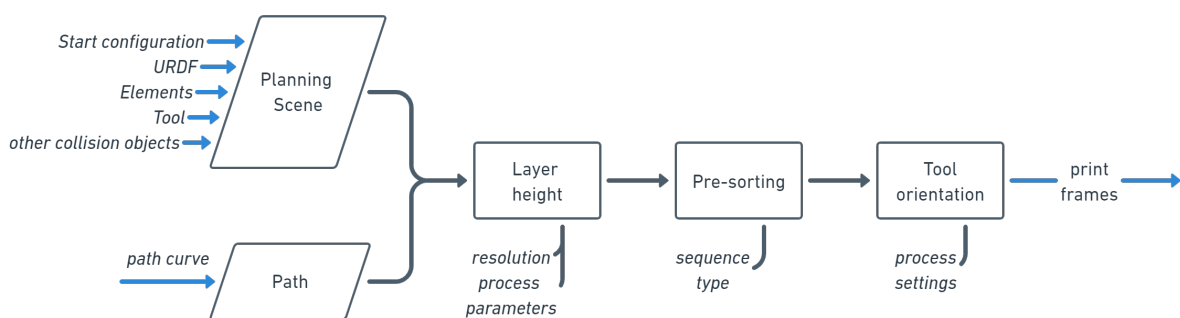
Figure 4.30: *Path slicing component*

Implementation

Inputs To start slicing, path curves are retrieved from each `Path` in the `Connection`, along with the robotic setup and collision objects stored in the `Planning Scene` (Figure 4.30).

Methods This component consists of three steps: 1. layer height, 2. layer sequencing, and 3. tool orientation:

1. Layer height Finding the location of the print points consists of subdividing the path curve with a suitable height for each path segment. Determining a *suitable* distance can be defined with different methods: it can be fixed for all layers, or it can be determined based on the build direction of each point on the path relative to the gravity vector. Both options were tested early on in the development of this component, as discussed in Section 3.6.4, the layer height in WAAM is a non-trivial problem determined by several process variables.

1.a Fixed layer height Path curves are subdivided using a "divide by length" operation. The length value is defined experimentally (see Layer height experiment) and preset for all layers (Figure 4.31a).

1.b Interpolated layer height Path curves are subdivided iteratively according to the angle between the curve tangent at the last subdivision point and the gravity vector. With this angle value, an interpolation between existing data of angles and layer heights retrieved from the Build orientation experiments can be done to return a value for the layer height that matches the expected deformation of the seam based on its angle relative to the gravity vector. This approach aims to counteract expected deformations produced by the gravity force on the seam shape and is supported by the observed linear behavior of the path elongation on the build direction experiment discussed in Section 3.6.1 (Figure 4.31b).

(a)   **(b)**
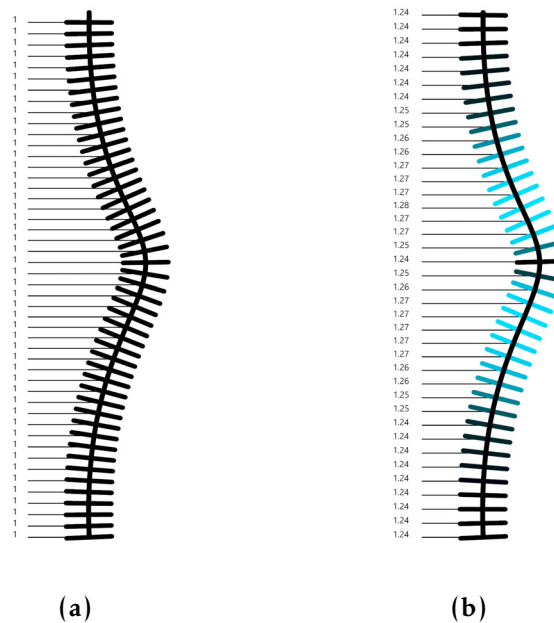
Figure 4.31: *Layer height methods: (a) Constant layer heights (in black), and (b) Interpolated layer height with variable heights.*

In principle, both approaches can be used to build solid WAAM paths, however, their application has different consequences. Fixing the layer height results in more consistent surface roughness, however, when used in spatial printing conditions, i.e., changing build and tool orientations, it has been observed that the overall height of the build is less accurate. The second method, determining the layer height based on the spatial printing conditions, yields more varying seam shapes and surface roughness but it presents more consistent overall heights on the build. Given that controlling the overall height using the touch-sensing method is a trivial problem for the adaptive pipeline, the benefits of a consistent surface roughness are preferred (See comments on 3.6.4 experiment's results).

2. Layer sequencing   Once the layers are created, their printing sequence needs to be determined for the following steps. Sequencing is first concerned with the type of paths and consequently with their data structure, and will be introduced in detail in the next component of the pipeline (see Section 4.3.3.3). At this stage, it is important to discern

between different types of paths relative to their sequencing methods. First, if the connection consists of independent, non-intersecting paths, layers are simply sequenced by their topological order (see Figure 4.37). If the connection consists of branching and divergent paths, layers can be sequenced by their topological order or by their origin's z-coordinates. Finally, if the connection combines path types, layers are sequenced by their origin's z-coordinates. Sequencing results in either a nested data structure where paths are preserved as entities when sorted by their topological order; or a flat data structure where paths are consolidated in one path when sorted by their z-coordinates. Illustrations of the types of paths and sequencing options are provided in the following section.

3. Tool orientation   The third slicing task is finding a collision-free tool orientation for each subdivision point along the path curve. Two methods have been used during the development of this component to obtain a collision-free frame: the first method *Tool orientation with mesh collisions* uses an iterative approach of testing tool orientations until an accessible tool orientation is found; the second method, *Tool orientation with path planning*, uses a search approach integrating the robot's reachability:

2.a Tool orientation with mesh collisions   With this method, the tool is iteratively re-oriented at custom angles and checked for collisions until an accessible *tool* position is found. At the start, the tool is oriented in its "ideal" position, tangentially aligned to the path. At each tool position, a mesh-mesh intersection between the tool geometry and the obstacle elements is computed. If the intersection is not empty, the tool is rotated with a custom angle around the frame origin, away from the elements (Figure 4.32)[21]. The challenge resides in finding the most relevant transformation or assigning which rotation axis should be used for the rotation to avoid the collision "faster"; in other words, to avoid rotating the tool more than the necessary minimum.

Implementations of this approach tested different strategies for assigning the rotation axis, such as prioritizing one meaningful axis until a maximum of iterations and then only rotating over a second axis.

---

[21] This method was first suggested in Cros (2017).

(a)   **(b)**   **(c)**
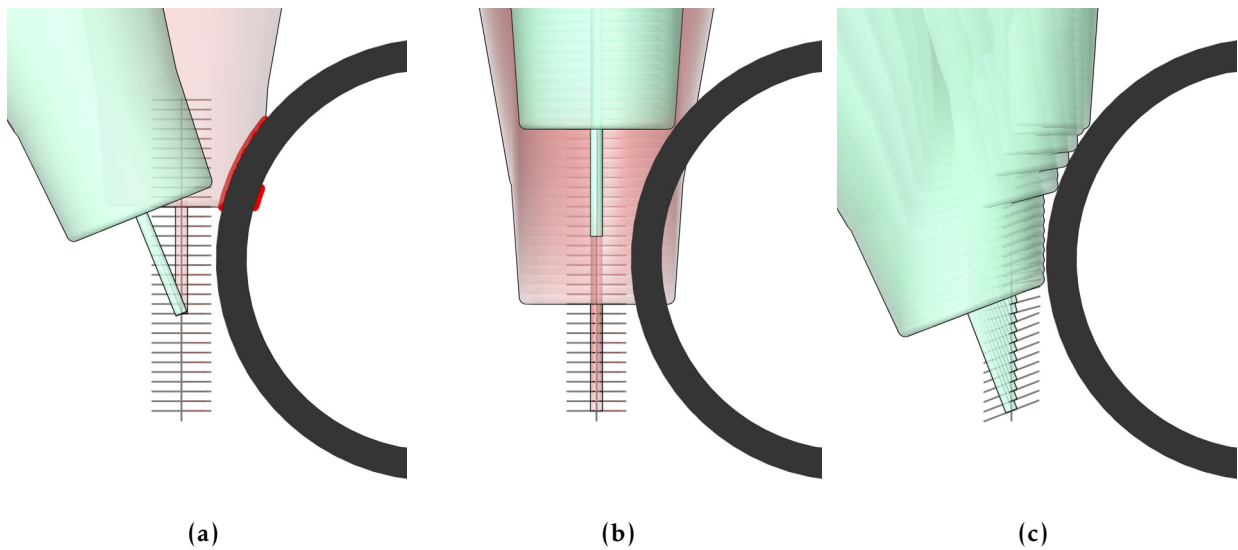
Figure 4.32: *Slicing with mesh collisions: (a) Example of a single frame before and after applying method, (b) Tool orientation results of an entire path before applying method -some orientations are valid (in green), some are invalid (in red)-, and (c) Tool orientation results of an entire path after applying method, all orientations are valid (in green).*

Depending on the configuration of the elements relative to the paths, finding a meaningful rotation axis could be a trivial or non-trivial task. Generally, given that the in place elements are linear bars, it is possible to use one of their axes as a primary rotation axis and its orthonormal axis as a secondary one. However, if the base and target elements differ in their orientation and print points are obstructed by both elements, an intermediate axis needs to be devised. In sum, this approach has not been proven to scale well, posing numerous -time-consuming- edge cases without a feasible generalization. An alternative solution for finding meaningful transformations using a Signed Distance Field approach is discussed in Mitropoulou, Ariza, et al. (2019) and at the end of this section.

2.b Tool orientation with path planning   This method evaluates the accessibility and/or reachability of the path to find an optimal tool orientation for each print point. The method is structured in several

steps[22]:

i. Base frames The print points are populated with *base frames* along the path. These base frames result from a spherical linear interpolation between two quaternions: the start and end frames' desired orientations (Figure 4.33a). Additional handles can be created at desired points along the path to better control the start and end conditions.

ii. Frame population Each print point is populated with *tool frames* representing possible tool orientations (Figure 4.33b). These tool frames are determined by the WAAM process parameters such as `max alpha angle`, the maximum angle deviation of the tool relative to the path. Additional parameters such as the `steps z axis` and the `angle step xy` enable a higher or lower number of tool orientations around the base frames (Rust et al., 2018).

iii. Tool accessibility check A simulation of each tool orientation at each tool frame is performed to check it for collisions with existing obstacles, including the seams downstream already deposited at each stage of the printing sequence (Figure 4.33c). Only the collision-free *accessible frames* are temporally stored.

iv. Robot reachability check For each stored accessible tool frame, an analytic inverse kinematic (IK) function is used to retrieve possible robot configurations. If a solution is found, the result is stored as a valid *reachable configuration* in the path's `Reachability map`. If zero IK solutions are found for all the checked accessible frames within a layer, the path curve or the tool accessibility settings need to be modified at this point.

---

[22]The path planning concept and first implementation of steps *i.-v.* was introduced and developed by Dr. Romana Rust. The final implementation of step *v.*, which uses a semi-constrained Cartesian planning approach, was developed by Yijiang Huang, PhD in the Digital Structures research group at the MIT Department of Architecture, building on existing literature (Yao and Gupta, 2007; Stilman, 2010; De Maeyer, Moyaers, and Demeester, 2017; *Descartes* 2014). The steps rely on infrastructure provided by the `COMPAS FAB` and `pyblullet_planning` libraries (Rust et al., 2018; C. Garrett, 2022)

(a) **(b)**

(c) **(d)**
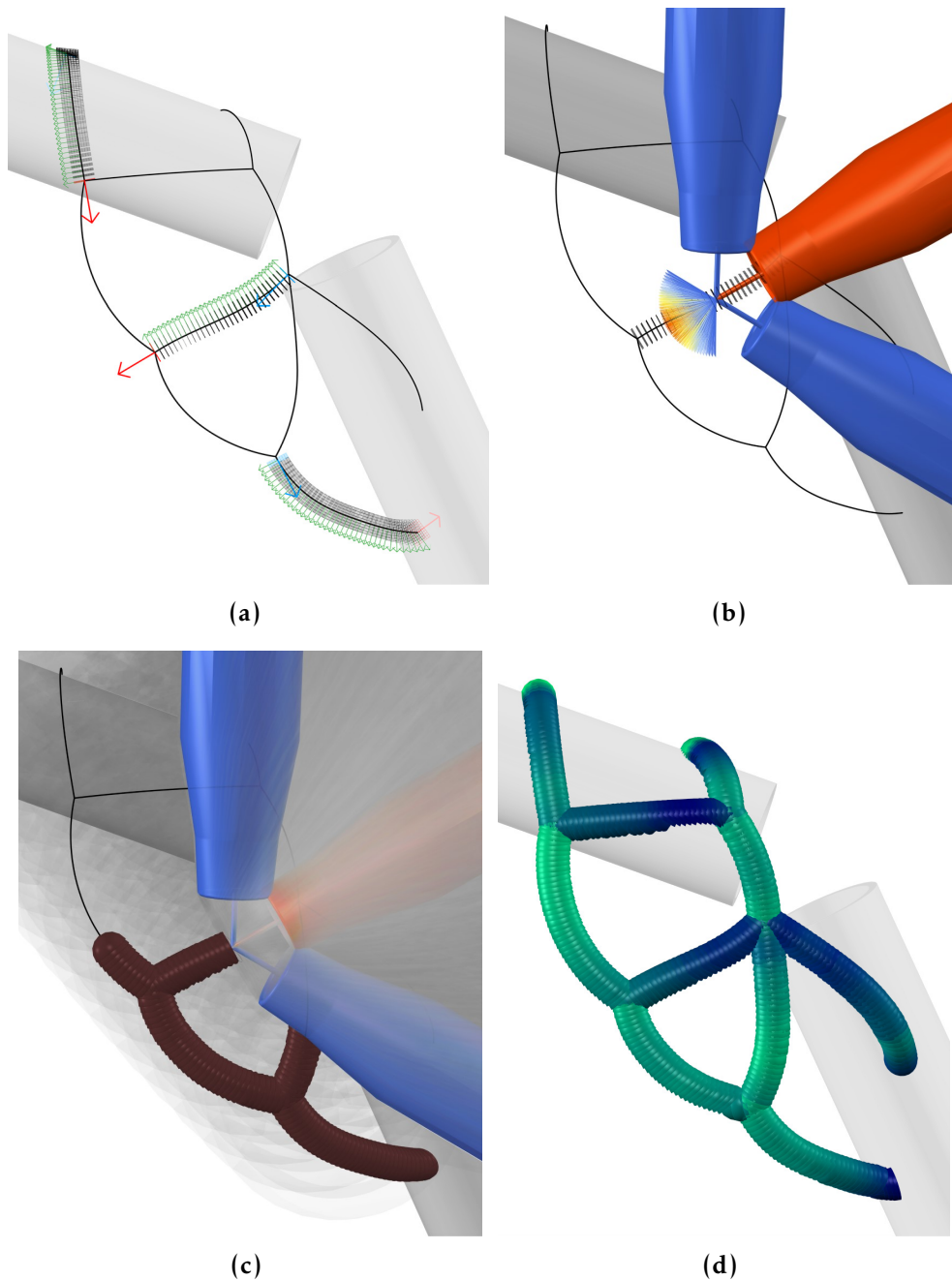
Figure 4.33: *Slicing with path planning, steps i. to iv.: (a) Base frames resulting from the interpolation between start and end frames for entry, internal, and exit paths, (b) Pool of tool deviation vectors from red to blue increasing max_alpha, i.e., deviation from the z axis of the base frame, and extreme tool orientations in blue, ideal tool orientation in red, (c) Simulated tool orientations in gray with already printed seams, i.e., collisions, in dark red, and (d) Path reachability results showing the range of reachable areas from green (more reachable) to blue (less reachable).*

v. Planning of robot targets To select optimal robot targets within the pool of valid configurations, two search algorithms are used.

In both cases, the goal is to find a reachable tool orientation that has the least possible *z* axis deviation from the ideal -tangent to the path- tool orientation while minimizing robot re-orientations between consecutive frames.

(a)   (b)

(c)   (d)
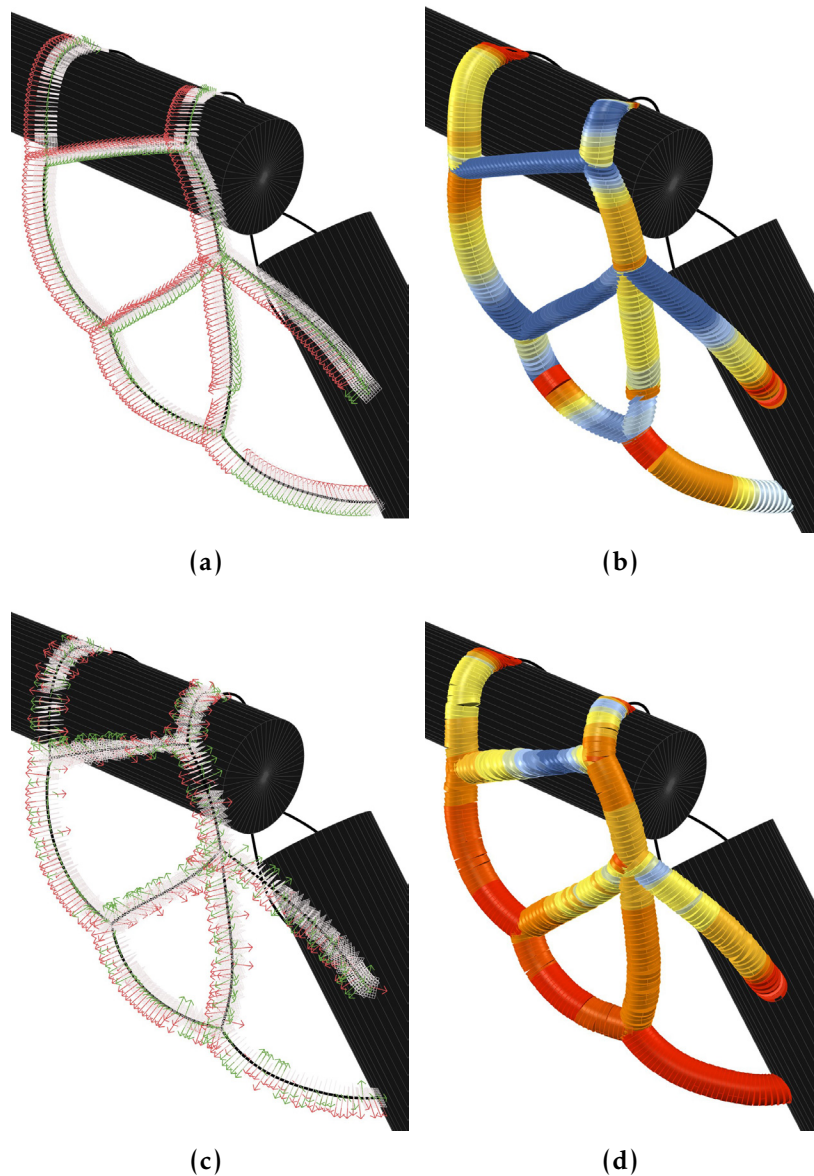
Figure 4.34: *Slicing with path planning, step v.: (a-b) Ladder graph algorithm results showing smooth selected frames with consistent x and y oriented axes and* z *axis deviations (from red to blue: increasing deviation from ideal), (c-d) Greedy algorithm results showing optimal* z *axis deviations (from red to blue: increasing deviation from ideal) and frames with unhandled x and y axes orientations.*

The first one, a *ladder graph search* algorithm, minimizes the angle differences between the robot's joints across the whole set of print

points while favoring configurations with smaller z axis deviation angles by adding weights in the search process (De Maeyer, Moyaers, and Demeester, 2017; *Descartes* 2014). The shortest-path search is performed within the pre-computed reachable frames stored in the reachability map from *step iv.* to reduce the computation time.

The second one, a *greedy* algorithm, is used to pick layer-by-layer a frame with minimal z axis deviation to the path tangent and minimal x axis deviation from a preferred one and search for a valid robot configuration similar to the last computed one (Stilman, 2010; Yao and Gupta, 2007). Using a randomized search to find a valid configuration, step *iv.* is skipped, considerably reducing the computation time. A comparison of the results of both algorithms is shown in Figure 4.34.

For both methods, steps can be run with low or high resolutions to get faster or complete solutions. A low resolution is the equivalent of a fictive layer height, i.e., five instead of one mm. The resolution is normally increased once a solution is found for all paths. However, if no reachable solution is found at a low resolution, it is necessary to go back to the previous `Path generation` step and modify the path curves.

Outputs   Finally, the `Reachability map` with final reachable frames is stored as an attribute of each `Path`.

Discussion on path slicing

Validity   Both approaches to defining a layer height present positive and negative effects related to the consistency in the column roughness and overall height of the build. This is expected due to the sensitivity of the weld characteristics to the energy inputs and conditions of the substrate, i.e., the CTWD -contact tip to workpiece distance- will have an effect on the strength of the electric arc and therefore on the shape and volume of the welded seam. The interpolated layer height approach aims to predict the height of the deposited seam based on the build orientation relative to gravity, however, because no correlation is done to the rest of the geometric, welding and motion process parameters

(see Section 3.5.1)), this anticipation effort is incomplete. In addition, the surface roughness with this approach is less consistent, which has potential detrimental performance effects. The fixed layer height method, on the contrary, does not aim to predict the shape of the seam, so it also produces greater tolerances in regard to the overall column height, i.e., the expected column height using this approach is less accurate than with the interpolated approach. However, given the availability of a corrective method with the adaptive printing technique and the more consistent surface roughness found with this method, the fixed layer height is the chosen method for the In place WAAM connections demonstrators.

The results of the two presented tool orientation methods show considerable differences in terms of their validity. First, the methods are not fully comparable in terms of results. Theoretically, the mesh intersection approach can only provide a valid *tool* position and orientation, which would require a second simulation step to verify that the *robot* can effectively reach the target frame in the provided sequence. However, in practice, this method has been proven enough to achieve simple and small geometries such as the Preliminary studies and Simple connection demonstrator presented in Chapter 5. The second method using path planning provides not only accessible collision-free positions and tool orientations but also reachable robot configurations, which are necessary for spatially constrained connection topologies such as the ones present in the Functional connection and Adaptive connection demonstrators.

Second, the methods present significant differences in computational performances. The mesh-mesh intersection method can greatly vary in performance depending on how fast the designer can find a suitable axis to re-orient the tool (usually between 2 and 15 minutes). However, this time is significantly faster compared to the methods using path planning (benchmarks are provided in Section 5.1.2.2, between 1 and 3 hours depending on the complexity of the inputs.).

It is arguable, then, when a computationally expensive method is required if a faster one can be used. The reason for introducing path planning is supported by a conceptual approach to generative methods.

The mesh-mesh intersection method classifies as a manual "guess-and-check" technique, yielding results that are not checked in terms of optimality criteria and that require knowledge and time from the designer to provide good results. In contrast, the methods using path planning provide automatic search methods with clearer metrics of their validity, i.e., for the ladder graph search, smooth transitions between reachable tool orientations are optimized, and for the greedy algorithm, the lowest z deviation axis is prioritized.

Known limitations   For the slicing with the path planning method and for connections with more than one path, the different sequencing methods present their own limitations:

If all the paths of a connection are organized as one consolidated WAAM path, and all layers are sequenced based on their Z-coordinates, then consecutive layers in the consolidated printing sequence do not necessarily belong to the same path curve, and are not necessarily directly next to each other. In these cases, both the ladder graph search and the greedy algorithm will try to consistently maintain the robot joint values of frames that are then not necessarily close to each other. This approach favors a smooth robot trajectory for the whole print job; however, it may not benefit the smoothness within consecutive frames within each individual path. Yet, this sequencing method facilitates the accessibility check step to include existing collision objects that had entered the scene at each step of the printing sequence.

If layers are sequenced based on their topological order keeping a nested data structure, i.e., keeping each independent path as an entity, tool orientations can be computed path-by-path individually, and smoother transitions between consecutive frames within each path can be achieved. This strategy, however, when applied to branching topologies requires more elaborate handling of collision objects in the

planning scene.[23]

Furthermore, none of the presented methods provide reachability checks for the entry and exit approach positions, in other words, for the transitions between frame targets. In practice, approach entries and exits are close enough to the checked frame targets that rarely pose problems. Nevertheless, a complete planning approach should consider path planning methods between frames to ensure that at the production stage, no singularities or maximum joint values are exceeded.

Alternative methods   An alternative volumetric modeling approach to find *accessible* tool orientations using the derivatives of the distance field of the in place geometry was described in Mitropoulou, Ariza, et al. (2019). In this approach, the tool is iteratively repositioned against the in place obstacles until a collision-free position is found. Further, vector smoothing was developed for the continuous WAAM deposition technique to obtain smooth transitions between frames. The approach was proven valid with the demonstrators presented in 5.4a and 5.4e for continuous printing and could be explored further for faster feedback to the user before any computationally-intensive reachability check is performed. This method is comparable with a guess-and-check approach as it does not provide assurance that a suitable solution within optimality criteria will be found, nor reachability checks.

4.3.3.3   Path sorting

What is the order of the production instructions? When should each print point be executed?

The results from the previous component, `Path slicing`, contain the fabrication information concerning the desired location of the printed

---

[23]This combination of path types and sequencing methods was implemented but discarded because it required a hard simplification of the existing collision objects in the planning scene. In short, if path planning is applied on a path-by-path data structure, it is not evident which other paths have been already printed and should be used as collision objects when planning each frame orientation. This could be potentially solved by introducing another data structure level, such as the print point (see Mitropoulou, Burger, et al., 2020), which could store a state of all collision objects per layer instead of per path. In any case, this approach seemed impractical as it will provide unrealistic path trajectories according to a path-by-path sequencing, that will have to be re-sorted in the next `Path sorting` step.

material and a feasible orientation of the tool to print it. However, the order and timing of the deposition of the seams is a matter of investigation in itself. First, seams need to be checked for possible material overlaps according to their pre-sorted printing sequence and their final frame orientations. Second, depending on which pre-sorting and slicing methods have been used and the type of material removal operations, a re-sorting operation might be required. Third, the deposition of molten metal, i.e., the phase transformation from solid to liquid and solid again, is a time-dependent process, as the energy used to melt the electrode produces heat that itself is dissipated through matter over time. Therefore, to successfully deposit molten metal additively, control of the time between successive points is needed, which is directly related to the geometry of the design and the sequencing of each point within the printing process (See section 3.6.6.5).

In sum, `Path sorting` aims to: **1.** control the excess material at node intersections, **2.** ensure a feasible self-supporting sequence for all the seams, and **3.** assign a cooling time, a time to allow the print point to cool down, to each target frame (Figure 4.35).
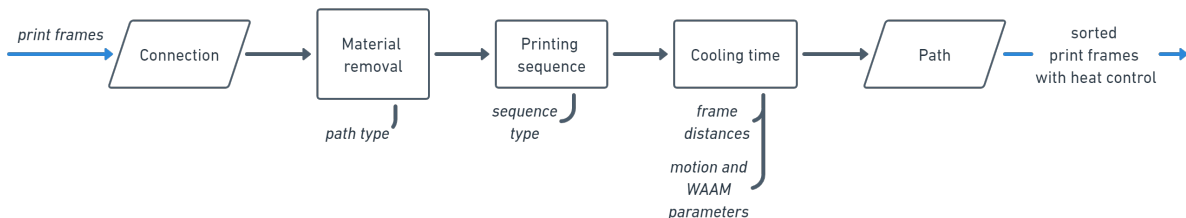
Figure 4.35: *Path sorting component*

Implementation

Inputs   All previously calculated reachable frames are needed for the sorting operation, as well as the motion and WAAM process parameters described in Section 3.5.1.

Methods   Goals 1-3 are respectively tackled with the three following steps: 1. material removal, 2. printing sequence, and 3. cooling time:

1. Material removal For both sequencing methods, branching topologies require specific handling of the path nodes or points where two paths meet (Z. Yu, Yuan, et al., 2019; Z. Yu, Ding, et al., 2021; Z. Yu, Pan, et al., 2021). At the nodes, an overlap of frames and therefore material, occurs. Generally, close to the nodes, removal of excess material is required. For divergent nodes, a number of frames should be skipped in both upstream paths. For convergent nodes, a number of frames should be skipped in the downstream paths. In all cases, how many frames should be skipped, if any, depends on the radius of the path volume once printed and the angle between the path curves (Figure 4.36).
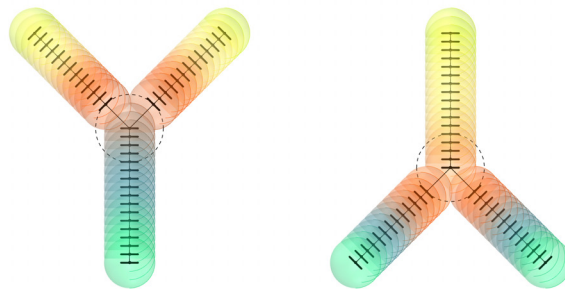
Figure 4.36: *Material removal: frames are removed at intersections at the start of divergent paths and at the end of convergent paths.*

2. Printing sequence In the previous slicing step, a pre-sorting of the print frames has already been done, i.e., keeping each path as an entity in a nested data structure or consolidating all intervening paths into a flat data structure as one single printing path. When the path data structure is preserved, a re-sorting of the frames needs to be done at this point to ensure a feasible printing sequence. To this end, two approaches have been used:

2.a Sequence by topological order The pre-sorting of the print frames following the path data structure is sufficient for self-supporting fabrication. In this case, the printing procedure iterated through the nested data structure, executing it point-by-point by the layer index (see 3.5),

automatically "sorting" the frames. This operation only works for independent or divergent path geometries, and convergent paths may fail if the number of layers differs across paths (Figure 4.37).

2.b Sequence by z-coordinates   With this approach, the origin of all intervening printing frames is sorted at once by their z-coordinates. This operation results in a flat data structure and can be produced with a respective printing procedure with a single list as an input. However, this operation only works for paths with a positive slope, as negative slopes would be incorrectly sorted (Figure 4.37).
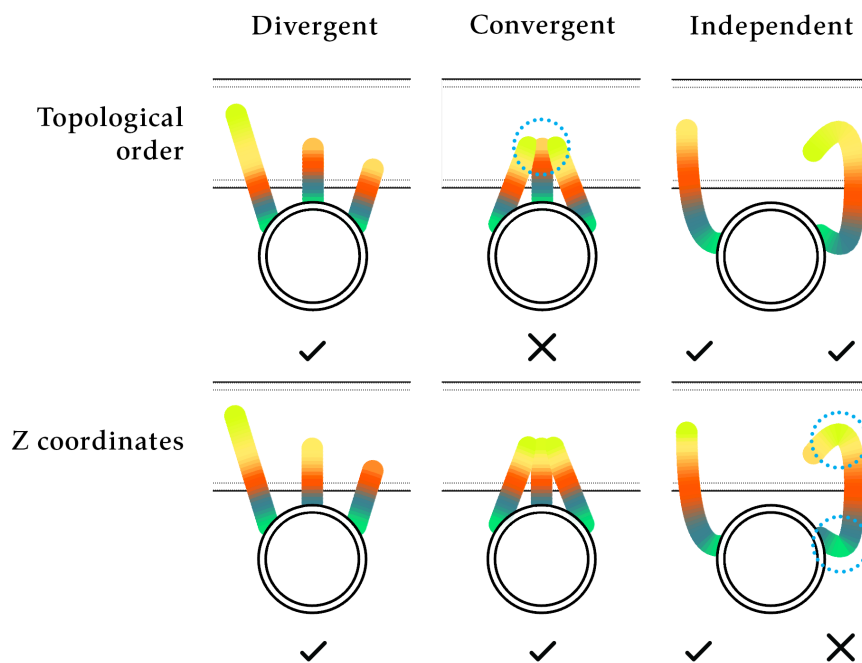
Figure 4.37: *Sequence by topological order vs. sequence by z-coordinates: Divergent paths can be sorted with no errors, convergent paths can only be sorted by z-coordinates, Independent paths with positive slopes can be sorted with no errors, independent paths with negative slopes can only be sorted by topological order.*

3. Cooling time   A minimum cooling time per print point should be allowed before the next print point immediately in contact is deposited to print self-supporting paths with as little deformation as possible. Otherwise, excessive deformation of the welded seam occurs (See Figure missing). The minimum cooling time value is set experimentally and discussed in Sections 3.6.6.1 and 3.6.6.5.

For connections with alternating sequences, i.e., print points being deposited in alternate paths instead of print points consecutively deposited path by path, it is possible to use the process time, the time for traveling, welding, and solidification between print points, as a cooling time. To verify if an extra cooling time is needed besides the mandatory process time, a comparison between the minimum cooling time and the process time for each print point is done.

The process time per print point is the sum of the motion travel times, the pre-and post-shielding gas times, and the welding times between overlapping print points (see Figure B.16f). If the process time is larger than the minimum cooling time, the assigned cooling time is 0. Otherwise, the difference between the process time and minimum cooling time is assigned as the cooling time value.

Outputs   Finally, the sorted frames are stored in the `Connection`.

Discussion on path sorting

Validity   The sorted sequence of frames is valid as long as two conditions are met: **1.** new frames (print points) are always placed on top of an already visited frame (print point) and **2.** the cooling time in between overlapping print points is equal or larger than the minimum cooling time.

Optimal cooling time   Although most of the heat transfer aspects of the discrete printing process are currently open for investigation, it can be confirmed that after the material has solidified and cooled down enough, another molten print point can be deposited on top of the previous one. However, based on the tensile strength tests 3.6.6.2 where a large number of print points were deposited and examined, it can also be confirmed that a delimited time window with minimum *and maximum* wait times for the deposition of the next print point benefits the surface qualities of the printed bars. This means that a *minimum* cooling time does not ensure an *optimal* cooling time or an optimal tensile strength. In other words, the minimum cooling is enough to print self-supporting paths but not enough to print the soundest printing path. Understanding the heat transfer process is

paramount to defining minimum *and maximum* cooling times so that
the sorting method can be targeted to increase the performance of the
printed product. As well, once the cooling time window is established
based on experimental tests, it would be possible to use it as a design
driver constraint that can enforce a minimum and maximum distance
between print points.

Integration of path planning to improve heat transfer   As mentioned
in 4.3.3.2, the integration of slicing and sorting of the printing paths
could be beneficial to achieve both performance and smooth results.
While slicing provides methods for smooth transitions between frames
of single paths, sorting provides a strategy to use the necessary cooling
time between print points as the production time of the next print
point. By integrating motion planning with these two aspects, complete
control of the operation time would allow to properly model the cooling
times between print points and consequently provide more control over
the product.

Negative slopes   The provided methods only work for paths with posi-
tive slopes. This limitation relates to the available sequencing methods.
For complex topologies including branching and convergent paths,
only sequencing by Z-coordinates is available. This limits the path type
to only positive slopes (see Figure 4.37 for a graphical explanation.)
Alternatives for curves with negative slopes should be investigated, for
example, with a combinatorial approach prioritizing the path types
(i.e., entries or bridge) and path locations over other aspects such as z
coordinates.

4.3.4   Integrative design considerations

The previous components are presented in successive cumulative order,
leading to a potential conflict as discussed in each respective discus-
sion section. This represents a uni-directional approach to constraint
modeling as presented in Kilian (2006). A bidirectional solution that
closes the design-analysis loop between components for each connec-
tion should be included at this stage.

While this thesis aims to understand the constraints and challenges of joining spatially and additively in its entirely design-and-production scope, it does not aim to provide a definite solution for all the intervening aspects, which are far too complex and beyond the scope of this work. For completeness of the AD pipeline's requirements and support for future work, this section includes a description of the design verification steps required before production is started.

4.3.4.1 Evaluation of design of paths

> *Does the design fulfill the functional and production requirements?*

At this stage of the pipeline, a verification of the structural performance of the connection to meet the allowable stresses on the paths should be included. Balanced stress distribution on the connection paths and the elements should also be verified to avoid peaks or a disagreement on the stiffness of the connection and the elements (Holst et al., 2021). A concurrent simulation of the heat transfer development during the production sequence should be considered. The heat development during production could create considerable distortions in the connection and the base and target elements, leading to potential structural failures. These checks should be supported by visualization tools to inform the design team of possible areas where a design revision is required. In this respect, in place WAAM offers unique design possibilities, for example, by using a hybrid deposition to reinforce previously printed paths that could be used where design checks are not passed. These critical, complex and multifaceted concerns will be further discussed in the final chapter 6.

4.3.5 Execution and survey

The next components are in charge of preparing and executing instructions to manipulate, print, and survey the elements and paths. Production components consider forward actions such as the `Printing` of WAAM paths, and feedback actions such as `Localization` of elements and `Touch-sensing` of elements or printed material. The specification of the printing and surveying procedures has already been presented

in Chapter 3; therefore, the following sections only discuss their integration in the AD pipeline skipping implementation details.

4.3.5.1 Localization

What has been already produced? Where are the elements to connect located?

As previously discussed (2.3.2), unplanned deviations are expected during the robotic assembly process (i.e., dimensional and/or geometric variation of the elements, accumulation of deformation of the built subassembly, thermal fluctuations, etc.). The `Localization` component picks up the production process after the robotic assembly of `Elements` is completed to update the state of the digital model based on the as-built results for the next operations in line. The information on the expected location of elements is retrieved from the `Planning Scene`, pre-processed and packed in a `SensePath` data structure. Execution consists in running the Localization procedure (Section 3.5.3) for each element of the `Connection` and results in the updated position of the `Elements`' axes (Figure 4.38).
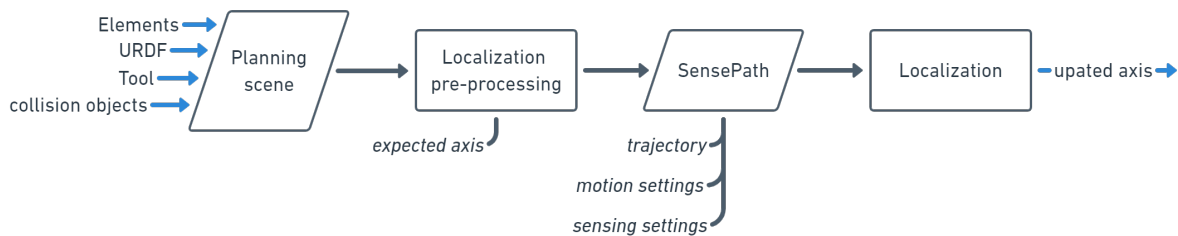
Figure 4.38: *Localization component*

4.3.5.2 Printing

How is the design executed?

In the context of the AD pipeline, printing consists of an IPWAAM discrete deposition. The component loads the printing `Path` with stored frames and cooling times and wraps it within the fabrication data structure `WAAMPath`, which contains additional production data such as motion (robot travel and welding speed), WAAM parameters (job number with the required voltage and current, gas valve times, etc.),

trajectory settings such as safe positions, approach and retract values, and additional metadata for documentation of the executed part. Finally, a printing procedure is selected, and the execution of the print path can start (Figure 4.39).
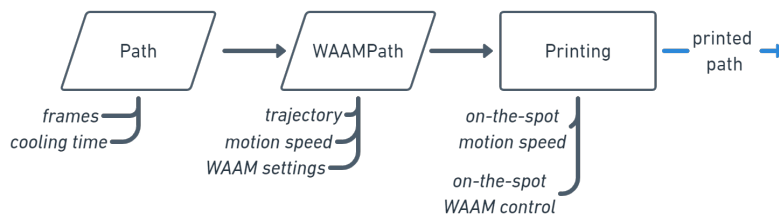
Figure 4.39: *Printing component*

4.3.5.3 Touch-sensing

What has been already produced? Where exactly should the print path start? Where exactly is the last layer located? Where exactly should the print path end?

As presented in 3.5.4, `Touch-sensing` consists in probing parts in known locations to verify their position before or during the printing process. The implementation of this component in the AD pipeline can be done at three different locations: before printing starts to measure and adapt the starting points of IPWAAM paths; during printing, to measure and adapt the printing paths on demand; and before the printed path is finalized, to accurately *fit* the connection to the target element. The component loads the `Planning Scene` and the connection's `Paths`, selects the desired layer to monitor (start, mid, or endpoints) as needed, and packs this into a `SensePath`. Finally, the touch-sensing procedure is executed, and the respective updated start, mid, or endpoints are stored (Figure 4.40).

Discussion on execution and survey tasks within the AD pipeline

Dependencies   The current implementation of this set of components relies on separate surveying, evaluation, and adapting processes. However, these dependent steps could also be implemented within a closed-loop system provided that the evaluation and adaptive measures can be encoded into rules.
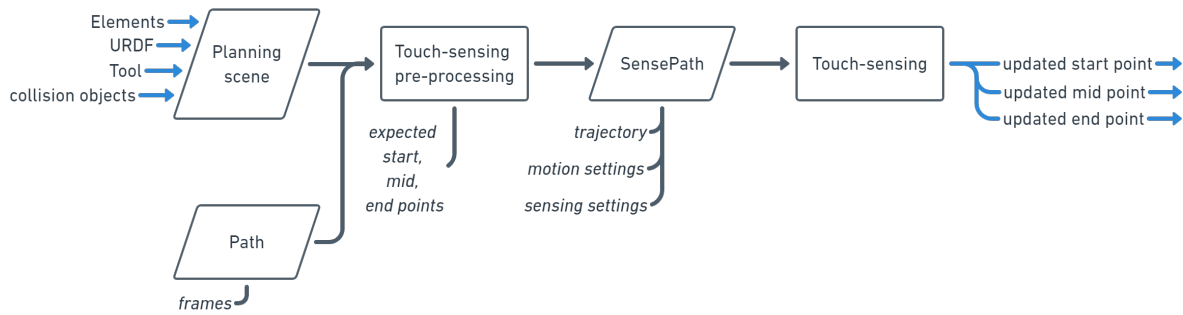
Figure 4.40: *Touch-sensing component*

When to execute the Localization procedure   An important aspect to consider is the order in which the `Localization` component is employed in the pipeline. The Simple connection and the Adaptive connection show differences in this respect, i.e., before the connection has been designed or once the design has been already computed, respectively. Scenarios where large deformations are expected would benefit from a real-time computation of the design during production; however, this option depends on the computational speed of the design tasks and the capacity to verify and validate the resulting design on-the-fly.

Monitoring   The function of this component can be generalized as the monitoring of material deposition, touch-sensing being the applicable technique for the discrete deposition approach. Therefore, other sensing techniques should be included at this stage for other printing procedures, such as seam tracking for continuous and/or hybrid deposition techniques. Regarding thermal development, the `Printing` component would benefit from thermal monitoring on the supporting elements and printed paths and further thermal adaptive measures. Moreover, welding, thermal, and geometric data could be stored as digital documentation, or twin, of the produced artifact enabling further assessment or more accurate compliance with performance requirements.

4.3.6 Survey evaluation and adaptation

While minimizing divergences between what was planned and approved during the design phase and what is ultimately built is paramount to avoid delays and to run above budget, architects often rely on an overlap of the design and construction phases to fine-tune and refine designs. In that sense, a design-*and*-construction pipeline is nothing new to the practice of architecture; however, its computational methods that require explicit control systems are.

Two types of components are outlined next to exemplify how a computational design-and-production pipeline incorporates explicit evaluation steps. `Evaluation of position of elements` and `Evaluation of position of paths` components assess if the position of already built elements and paths falls within acceptable tolerances. The `Path adaption to as-built elements` and `Path adaption to as-built paths` components interpret the updated as-built digital model and provide methods for the adaptation of the printed paths.

Background   Path adaption components formalize a critical need in digital fabrication, that is, the precise and explicit control of material deposition.[24] This is particularly relevant for welding and WAAM, as the high energy used in the melting process can result in serious damage to the parts or penetration defects that are difficult to assess visually. Typically, there are two conditions to avoid: **a.** the TCP, i.e., the electrode tip being too close to the part, and **b.** the TCP being too far from the part (Figure 4.41). If the rest of the welding parameters (e.g., wire feed speed) are not adapted, case **a.** can result in an undesired short arc and lower voltage which results in a deeper profile of the weld. This, in turn, can result in excessive penetration and melting through the part. Case **b.** can result in different outcomes: a larger arc and voltage and wider weld seam with an incorrect penetration profile, an unshielded arc resulting in a lack of fusion, or the complete miss of the target, which could be followed by an undesired wire feeding and deposit of molten metal at the wrong location (Figure 4.42).

---

[24]The manual production counterpart handles material placement by a constant and tacit reactive approach during the material formation process.
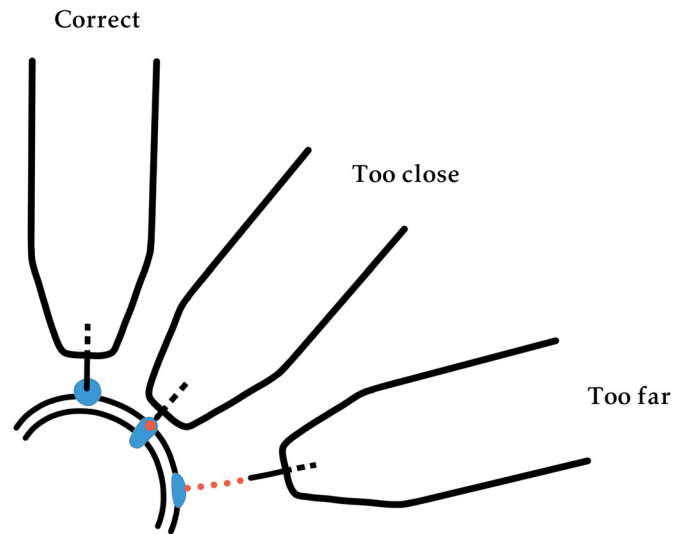
Figure 4.41: *Scenarios to avoid: (a) TCP in correct position, (b) TCP too close to element, and (c) TCP too far from element.*

(a)   (b)   (c)
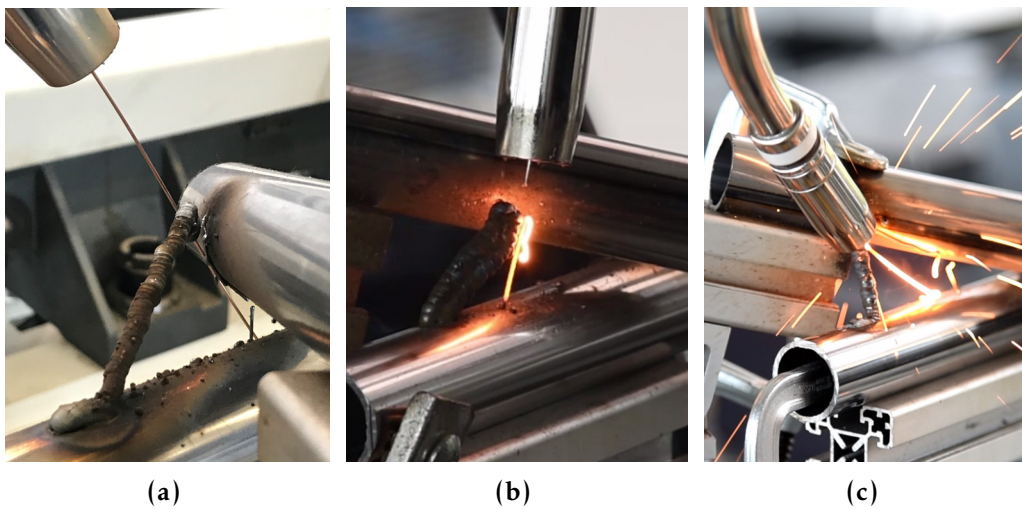
Figure 4.42: *Need of adaptation to as-built elements and paths found during the development of preliminary prototypes: (a) missed target element, (b-c) missed target path in discrete and continuous depositions.*

4.3.6.1 Evaluation of position of elements

Does the as-built design match the planned design? Does the position of the as-built elements fall within the admissible tolerance?

Different methods can be used to simulate the tolerance build-up of spatial assemblies *in advance* of production (Gandia, 2020). However, the evaluation of tolerance build-up *during* assembly is still an open research topic. The development of evaluation criteria for the structure's performance factors is out of the scope of this thesis. Yet, this section is intentionally included to provide an overview of possible control mechanisms compatible with the proposed AD pipeline.

This step aims to interpret the effect of the actual position of the as-built element within the rest of the planned assembly. This is of particular interest for spatial assemblies with spatial interfaces, as the correct position of parts is evident only after several elements are assembled and/or a "fitting" element enters the scene.

The `Evaluation of position of elements` component receives the updated elements' positions and deviations retrieved by the localization procedure (3.5.3 and 4.3.5.1) and outputs one of the following options:

Scenario 1 If deviations of the `base element(s)` and `target element` fall within an admissible range, the construction process can proceed as planned, and a local survey method 4.3.5.3 and path adaptation measures 4.3.6.2 can be employed.

Scenario 2 If deviations of the `target` element fall outside the admissible range, the production process should be halted, and the following options can be initiated:

> **Option A** Survey of the target element's dimensional and geometric tolerances[25] and replacement if necessary.
>
> **Option B** Repositioning of the target element.

Scenario 3 If deviations of the `base element(s)` fall outside the admissible range, the production process should be halted, and the following options can be initiated:

> **Option A** Reinforcement of the subassembly to match the base elements' expected position.
>
> **Option B** Re-calculation of the upstream design from the accessibility component onwards 4.3.1

---

[25]It is expected that a pre-production survey would have been conducted and that new, previously untracked divergences can be traced to thermal changes or affected by the placing procedure.

Scenario 1 continues production as planned. Scenarios 2A, 2B, and 3A halt production and force a revision of the previous production steps. Scenario 3B requires a forced re-design (Figure 4.43).
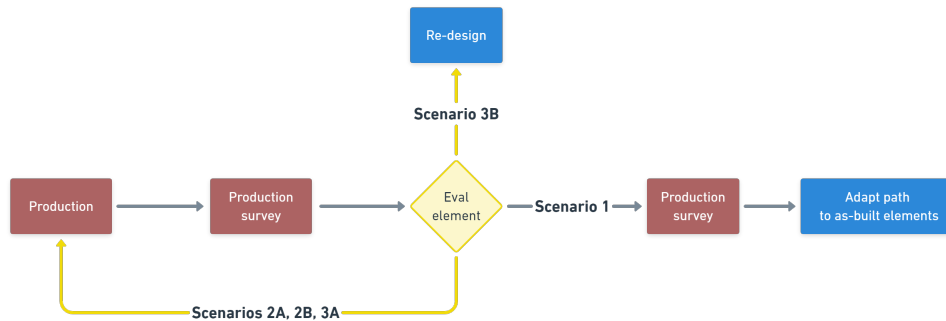
Figure 4.43: *Flowchart evaluation of the position of elements*

4.3.6.2   Path adaption to as-built elements

How is the design adapted during production? How are the paths adapted to the as-built elements?

This component is used in the case of Scenario 1 described in 4.3.6.1, in other words, only after the localization and touch-sensing procedures are executed, and the deviations of the position of the base and target elements fall within an admissible range. The component handles the fitting of the pre-computed paths to the actual location of the `base` and `target elements` (Figure 4.44).
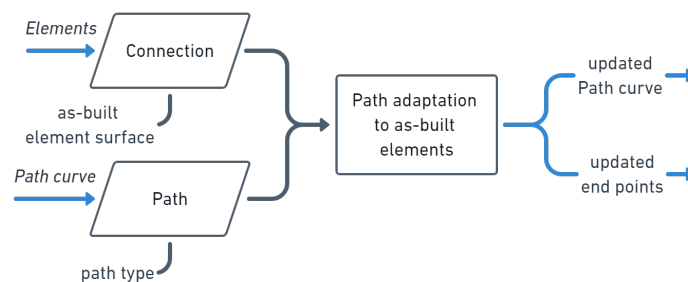
Figure 4.44: *Path adaptation to as-built elements*

Implementation

Inputs   The component loads the actual reconstructed surface of the base and target elements and the paths directly in contact with them, i.e., entry, exit, and bridge `Paths` stored in the `Connection`.

Methods   The following methods add or modify endpoints of the path curve to fit it within the actual position of the reconstructed elements. The best scenario consists in adapting the Path as little as possible. Hence, methods are presented in priority order:

1. Fit endpoints (priority 1)   The first method pulls entry and exit points to the base and target elements' surfaces. This operation is achieved in three steps. First, the endpoints need to be close (± 5 mm) to the surface of the elements. If this is not the case, the endpoints are moved by extending or shortening the path curve. Second, the closest point to the endpoint that lies on the element's surface is queried. Finally, the endpoint of the original path curve is replaced with the new endpoint lying on the surface, which results in a new path curve (Figure 4.45). For complex connection topologies, when more than one base element or several previously built paths exist, the identifiers of "base elements" for each WAAMPath are required so that the surface to pull the points onto is correctly assigned to the closest base element.

2. Add or remove control points (priority 2)   The previous operation may fail if the path curve has too many or too few control points; therefore, a rebuild curve operation may need to be done to reduce or increase the control points on the path curve. Once this operation is done, the *Fit endpoints* step needs to be executed again.

3. Modify control points (priority 3)   If the previous two steps are unsatisfactory, i.e., if the path curve shows torsion or an undesired curvature peak, a manual modification of the endpoints and the nearest control points must be done to match custom design criteria (See the discussion at the end of this section for an example regarding the Simple connection symmetry). Once this operation is done, the *Fit endpoints* step needs to be executed again.

(a)   (b)   (c)
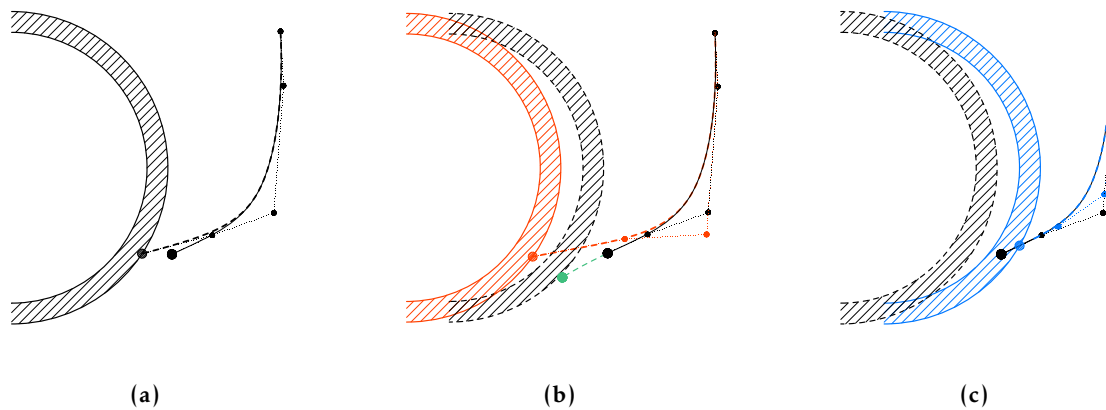
Figure 4.45: *Path adaptation to as-built elements, Fit endpoints method: (a) The element is in its expected position, the original path curve (continuous in black) is replaced with a fitted path curve (dashed in black) with its endpoint lying on the element's surface, (b) The element is farther to the path curve than expected, the original path curve (continuous in black) is extended (continuous in green) and replaced with a fitted path curve (in dashed red) with its endpoint lying on the element's surface; and (c) The element is closest to the path curve than expected, the original path curve (continuous in black) is trimmed at the intersection with the element and replaced with a shorter curve (in dashed blue) with its endpoint lying on the element's surface*

Outputs   Finally, the updated endpoints and new path curve are stored in the `Path`.

Discussion on path adaptation to as-built elements

Validity   The presented path adaption operations have been tested in flat and convex cylindrical surfaces for deviations below 10 mm. The Simple connection demonstrates the approach. Here, deviations of the pre-computed position of elements were found in the 3-5 mm range[26]. It is expected that concave or more complex surface conditions would require alternative approaches and a tighter integration of path planning to verify the feasibility of the new path geometry.

---

[26]As the elements were assembled by hand, these deviations were larger than the ones expected to be found if the assembly is realized robotically at the same scale

Known limitations

Manual handling   The implementation of this component was not automated in the pipeline for a good reason. Generally, given the range of complexity of spatial deviations, adaptation heuristics can be trivial or very complex. The example of the simple connection shows that the path adaptation operations, even when applied with minimal implementation differences, can greatly affect the connection expression (Figure 4.46). Although geometry visualization plays an important role in quickly informing the designer on the idealized path geometry, this representation lacks essential information on the outcome. A simulation of the material deposition and, in particular, of the profile of the bead geometry would benefit the understanding of the final surface roughness of the path, which plays an important role in the connection expression and performance (See discussions on Surface quality, Structural behavior under tensile loading, Corrosion behavior). Until these aspects can be simulated and integrated, a manual approach is of better use to the designer than an automated one.

Figure 4.46: *Expression on entries and exits*

Lack of verification loop   Slight modifications of the control points may end in unreachable path sections, and, therefore, immediate feedback on affected reachability would be required for a truly interactive design approach. In addition, although the premise of this component is that a global check has been passed (i.e., ensuring that only a minor

adaptation will be required), a verification of the adapted design should be pursued before production is restarted. This would entail a structural simulation check of the expected internal stresses on the paths and elements as prescribed by the global stability analysis performed in 4.3.2.1.

Adaptive regions   An important aspect to consider that has not been addressed in this component is what section of the path should be adapted. For example, in the Simple connection the path adaptation towards the `target element` is taken by the exit sections of the path. However, given the symmetric organization of the intended design, modifying the last discrete points of the main path would have resulted in an adaptive measure more faithful to the design.

Alternative methods   Exemplified by the different methods required by the entry and exit points, it is also plausible to encounter other types of geometric conditions that are not taken into account here. As the development of the design language of a connection evolves, the adaptive measures should also evolve to cover different conditions and design approaches. The experiments conducted during the development of the AD pipeline showed that entry and exit sections where the paths attach to the elements have a big impact on the expression of the connection as a whole; therefore, an exploration of this aspect would be a meaningful exercise.

4.3.6.3   Evaluation of position of paths

Does the position of the as-built paths fall within the admissible tolerance?

The goal of this step is to interpret the effect of the actual position of the last printed layer during the path printing process (Figure 4.47). The component receives the position and deviation of the last layer retrieved by the touch-sensing procedure (3.5.4 and 4.3.5.3) and outputs one of the following options:

Scenario 1 If deviations of the last printed layer fall within the admissible range, the printing process can proceed with a local adaptation of the layer height 4.3.6.4.

Scenario 2 If deviations of the last printed layer fall outside the admissible range, indicating a major deformation of the printed path, the printing process should be halted, and the following options can be initiated:

Option A Cutting and replacement of the deformed path with a new path printed with different process parameters.

Option B Complete the survey of the printed path, including more information than the last layer position.[27] Reconstruction of the printed path in the digital model. Recalculation of the material distribution step with consideration of the surveyed printed path as a collision object. Creation of new paths.
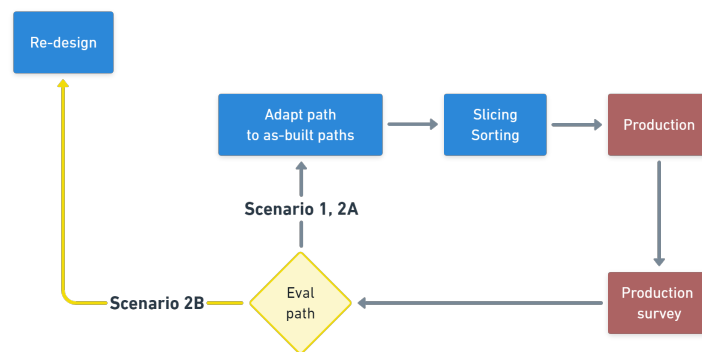
Figure 4.47: *Flowchart evaluation of the position of paths*

Scenario 1 continues production as planned. Scenario 2A halts production and forces a revision of the previous design and production steps. Scenario 2B requires a forced re-design (Figure 4.47)

Discussion   TBC: reply to *How is the connection's force transfer satisfied if the as-built geometry differs from the as-planned geometry during the construction phases?*

4.3.6.4   Path adaption to as-built paths

How is the print path geometry adapted during production?

---

[27]This action can be performed, for example, with a camera vision monitoring system.

At this stage, the touch-sensing survey procedure has retrieved and re-
constructed the position of the last printed layer, and the evaluation of
the path position has resulted in Scenario 1. This component then han-
dles how to continue printing a path that has already been started and
has accumulated a certain admissible deviation on its height (Figure
4.48).
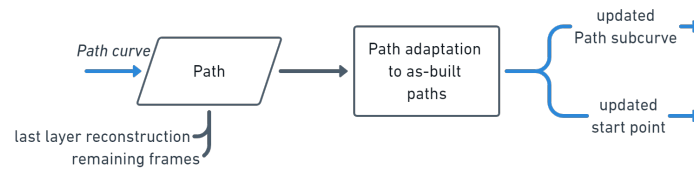
Figure 4.48: *Path adaptation to as-built paths*

This component can be used at any point in the printing procedure,
depending on the characteristics of the design. Generally, the following
conditions benefit from path adaptation: long paths of more than 35
mm, paths with high or changing curvatures, and branching topologies
(Figure 4.49).
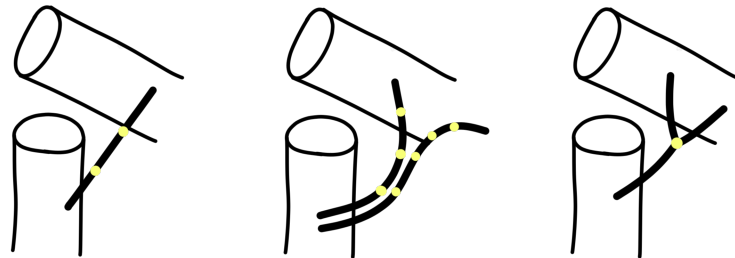
Figure 4.49: *Path adaptation conditions: (a) Long paths, (b) High or changing
curvatures, and (c) Branching topologies.*

Implementation

Inputs   This component requires the reconstruction of the profile of
the last printed layer, which was captured by `Touch-sensing` monitor-
ing and stored for each `Path` in the `Connection`.

Methods At this stage, the production survey provides the point coordinates of the head of the last printed layer in the build direction. This point is then first turned into a sphere to represent the last printed seam (Figure 4.50). Next, different operations can be used to adapt the remaining path to print. For the following operations, usually, two paths of action can be used. Either the operation is performed on the path curves to perform slicing and sorting operations on them subsequently, or the operation is performed on the path curve to provide start and end reference points in order to select or skip pre-computed slicing and sorted frames:

1. Trim path If the remaining path curve intersects the sphere, a simple trimming operation of the path curve can be performed. The intersection results in a new point, which needs to be offset in the direction of the path to create the next target frame at the center of the simulated last seam or select the next frame to print from the pool of pre-computed frames (Figure 4.50).

2. Extend path If there is no overlap between the sphere and the path, a new transition curve section between the original path and the existing path can be added by extending the path curve. The *Trim path* operation is carried out afterward. Alternatively, target frames between the expected and as-built path head can be skipped from the printing job.

3. Rebuild path If trimming or extending does not result in an intersection of the sphere and the remaining path curve, a replacement of the start point with the center point of the sphere is done. This operation forces the recomputation of the slicing and sorting steps.

4. Check continuity For path adaptation conditions except branching, and if the operation is carried out on curves to be sliced during production, a G1 continuity match is performed to ensure that no creases are found between the curve of the already printed path and the subcurve of the remaining path to be printed. In branching conditions, G0 continuity is enough.
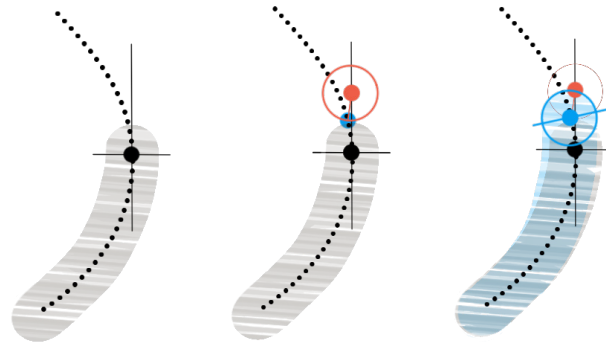
Figure 4.50: *Reconstruction of path head: (a) Expected location of target frame and search direction (in black), (b) Coordinates of the reconstructed point (in red), and position of the center of the path head sphere (in blue) by the intersection of the auxiliary sphere (in red), and (c) New path head sphere and target frame at its center (in blue).*

Outputs   An updated path subcurve with the new start point is stored in the `Path`.

Discussion on path adaptation to as-built paths

Validity   These methods were tested in long paths such as the Simple connection (80mm) and in experiments conducted for Structural behavior under tensile loading and Structural behavior under compressive loading tests with a straightforward application and consisting results. The method was found less consistent for branching topologies Adaptive connection with convergent and divergent paths. In these cases, larger discontinuities, cross-section variations, and deformation of the updated start layers were found (Figure 4.46).

Known limitations   Generally, a decrease in the cross-section area was found at the adapted layer, even when the WAAM parameters remained the same as in previous layers. This could be explained by a larger cooling time at that point, a result of the time spent on the touch-sensing procedure and consequent design adaptation measures.

Because, in some cases, the path slicing and sorting operations need to be re-executed for the adapted path, a new tool orientation may

be found. This new orientation can result in visible surface changes, which in turn can affect the path tensile or compressive performance and provide opportunities for corrosion initiation. A straightforward fix would be to ensure that the orientation of the tool at the adapted layer matches the last printed layer. However, this may not be possible in all conditions because new collisions on the adapted curve could be found. The observations discussed in 4.3.6.2 regarding the integration of the path slicing and simulation of thermal development and structural performance apply here as well: providing faster feedback on these aspects would allow the designer to interactively verify the path adaptation operations during production.

4.4 Summary

This chapter has introduced the aims, structure, and components of the adaptive detailing pipeline to design and produce additive spatial connections using IPWAAM. The key points and contributions of the pipeline are the following:

- The pipeline falls under two design and production strategies: a fabrication-aware design tool and an adaptive fabrication approach. These two aspects assist each other in fulfilling the design, documentation, and control tasks core to detailing. While the fabrication-aware tool supports designers in understanding the capabilities of the production setup to design feasible connections, adaptive fabrication keeps them informed of the production status allowing continuous control of the execution of the design. These two aspects contribute to the computational notion of detail and detailing, where knowledge is handled explicitly and dynamically during the design and production phases:

  · Components concerning production constraints, i.e., `Tool accessibility`, `Robot reachability`, `Path generation`, `Path slicing`, and `Path sorting`, spread throughout the pipeline enforcing constructability during the design and production phases.

  · Components enabling adaptive measures can be categorized into two subgroups: the feeding back of physical data

to the digital model, i.e., `Localization` , `Touch-sensing` , and the feeding forward of updated instructions to the actuation system, i.e., `Path adaption to as-built elements` and `Path adaption to as-built paths` . In between these two types, `Survey evaluation and adaptation` components ensure that the design status is on track and production can continue as planned.

To illustrate these two takes on design the cumulative In place WAAM connections in Chapter 5 discuss different scenarios with practical examples.

- The components presented here can be categorized in *must-have* and *nice-to-have* features of the pipeline. *Must-have* components are required for the pipeline to work, and *nice-to-have* components are additional features that could inform the process to achieve better results:[28]

Must-have	**Nice-to-have**
`Tool accessibility`	`Stability`
`Robot reachability`	`Material distribution`
`Path generation`	`Evaluation of design of paths`
`Path slicing`	
`Path sorting`	
`Localization`	
`Printing`	
`Touch-sensing`	
`Evaluation of position of elements`	
`Path adaption to as-built elements`	
`Evaluation of position of paths`	
`Path adaption to as-built paths`	

Table 4.1: *Types of components*

---

[28]To illustrate this point, a parallel can be made between these fictive categories and the composition of a team in architectural practice. A pipeline with only *must-have* components could be compared to a studio working with a small group of contractors (e.g., a construction company). A second scenario would be a team conformed of architects and a group of experts (e.g., a structural engineer, an environmental consultant, etc.). The experts would represent the *nice-to-have* components. Both scenarios are widespread practices in architecture, mostly differing on the scale of the project and budget, for example, the renovation of a kitchen versus the construction of a new building.

- While the ultimate aim of the pipeline is to support designers in the decision-making process, the type of information and the available tools to operate within the system can result in an unintentional over-constrained design. This can be illustrated by the results given by the `Material distribution` and `Path generation` components used for example in the Functional connection demonstrator.[29]

- Every computational design system raises the question of the designers' and the system's roles. In the proposed pipeline, the designer has few opportunities to interact with the model and propose alternative options. The pipeline should become more interactive at each process step in order to overcome this limitation. This entails different visualization and control strategies for tasks that benefit from automation or optimization and tasks that need unstructured input from the designer. In this respect, the work presented here represents a placeholder groundwork that should be developed further by the specific needs and design teams' characteristics.

- The componentization, or the process of breaking a system into identifiable parts, should as well be tailored to the team's needs. Some components, e.g., `Material distribution` and `Path generation` or `Path slicing` and `Path sorting` would benefit from tighter integration between each other (see respective discussion sections). However, the granularity greatly depends on the available expertise and the possibility of fully automating certain tasks. For example, if the material distribution and path finding were integrated into one component, the component's owner would need to be able to address any aspect of its features or rely on an automated system. Ultimately, these problems bring

---

[29]This aspect can as well be compared to conventional architectural practices. A big team of experts without the intention of enabling design iterations can over-constraint the design process. Ideally, however, working with experts, i.e., including more components in the pipeline, would be exactly the opposite: facilitating a more informed design process. The difference between good and bad practices can then be found in both conventional and digital design workflows and depends on the type and frequency of the communication, in one case, and the fluidity or iteration speed of the components in the digital pipeline counterpart.

back the question of the role of interfaces and what type of modeling approach is more suitable to share between stakeholders, which is one of the central questions of the COMPAS framework.

5 Demonstrators

This chapter presents and discusses in place WAAM (IPWAAM) and adaptive detailing (AD) demonstrators at two scales of focus: connections 5.1 and structures 5.2.

5.1   In place WAAM connections

The connection experiments range from exploratory to integrated solutions of the AD pipeline. The first section, the preliminary studies (5.1.1), present proto-IPWAAM connections together with first impressions on the use of WAAM as a joining technique collected during the early phase of the project. The second section, the pipeline studies (5.1.2), present a series of simple (5.1.2.1), functional (5.1.2.2) and adaptive (5.1.2.3) connections, and focuses on the development and integration of the adaptive detailing features. Finally, a discussion section summarizes the key findings of this set of demonstrators.

5.1.1   Preliminary studies

Before the presented work would find the current reasoned form, extensive experiments of the WAAM deposition techniques applicable to connecting parts were conducted. Here, a selection of these early studies is presented. These experiments share the overlapping goals of discovering and understanding process parameters, developing relevant computational descriptions, building and testing design-and-construction communication workflows, and structuring all the above in robotic procedures. These preliminary demonstrators are organized into three groups (Figure 5.1): by material deposition (5.1.1.1), by connection typology (5.1.1.2), and by path topology and geometry (5.1.1.3). To clarify their goal, each group is associated with a key driving question.
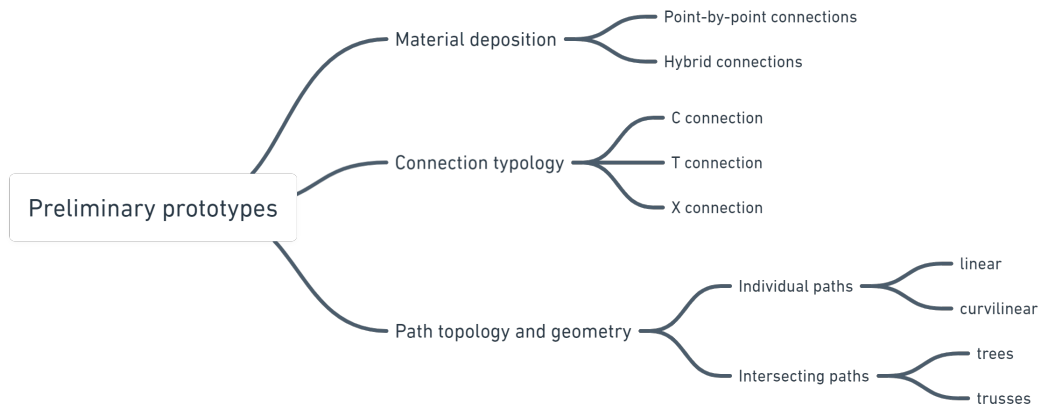
Figure 5.1: *Topics of the preliminary prototypes*

5.1.1.1   Material deposition

*What kind of material deposition techniques can be employed
when using IPWAAM as a connection technique?*

WAAM presents an outstanding versatility in terms of material depo-
sition, with some of these techniques applied as joining techniques
remaining unexplored to this date as shown in Figure 3.8. The follow-
ing sections present different materialities of the IPWAAM connections
using the point-by-point and hybrid deposition techniques that were
previously introduced in Chapter 3 (see Section 3.5):

Point-by-point connections   These connections present linear or
curvilinear paths bridging base and target elements. Figure 5.2 show
results with an incremental control over the IPWAAM process from
Experimental setup A to Experimental setup B. In terms of materi-
ality, these early experiments showed that connections using point-
by-point deposition can have a variety of material expressions based
on the shape, size, and number of paths. To avoid the tool touching
the elements during printing, the paths are sliced with non-parallel
collision-free robot target frames, which results in non-planar layers.
The uncertainty regarding the resulting layer height of each printed
point and consequent arc errors led to the development of the touch-
sensing procedure.
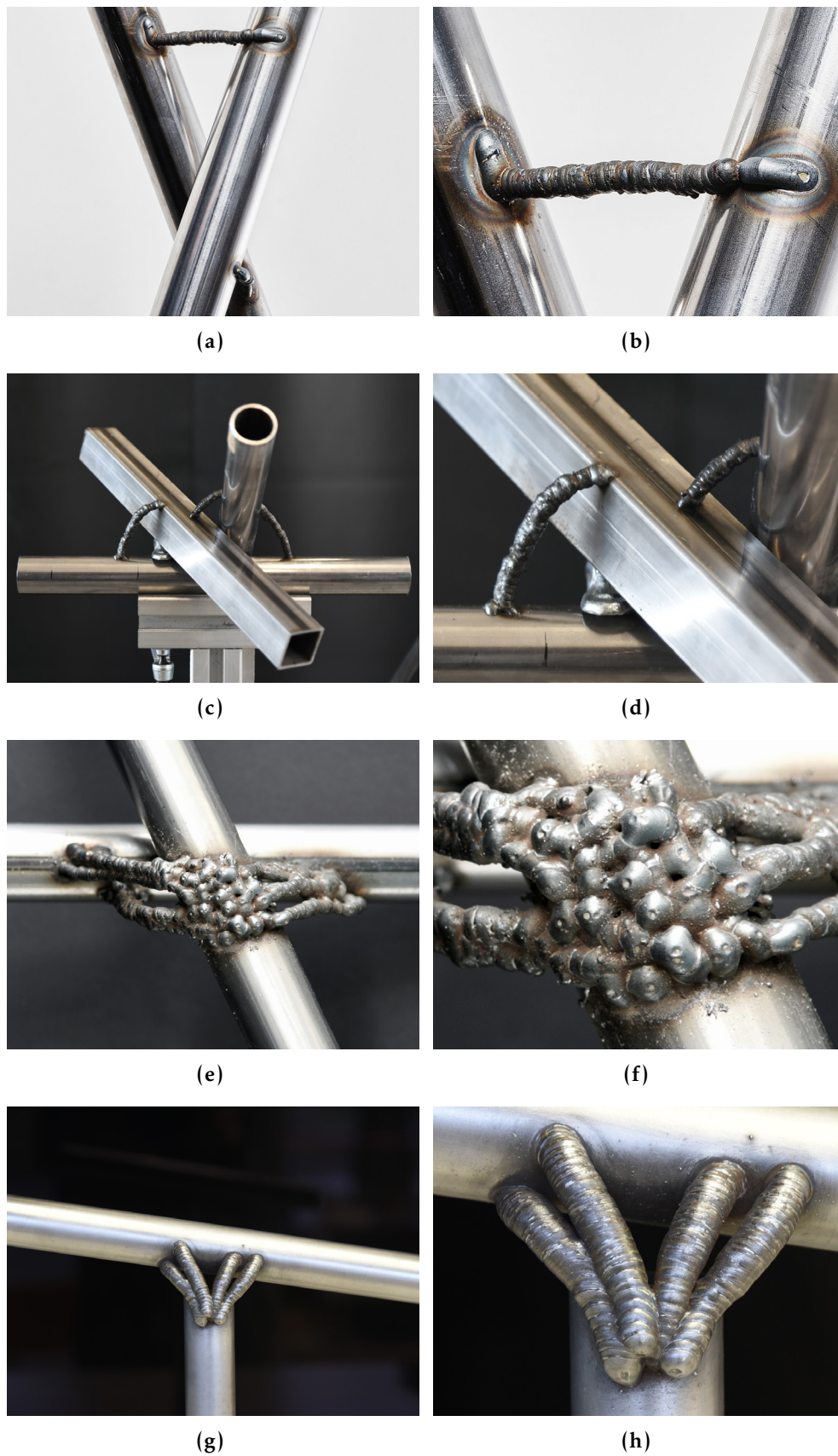
Figure 5.2: *Point-by-point connections: (a-b) from Setup A, Photo: Catherine Leutenegger, (c-f) from Setup A (Mitropoulou, 2018), Photos: Ioanna Mitropoulou, (e-f) from Setup B.*

Hybrid connections   The implied fragility and time-consuming aspect of the point-by-point connections led to considering continuous depositions approaches early on. The *hybrid* approach combines self-supporting point-by-point paths, to bridge the gap between elements, and continuous paths printed on top of the bridges as a reinforcement. Figures 5.3 and 5.4 show the increasing control of the printing approach.
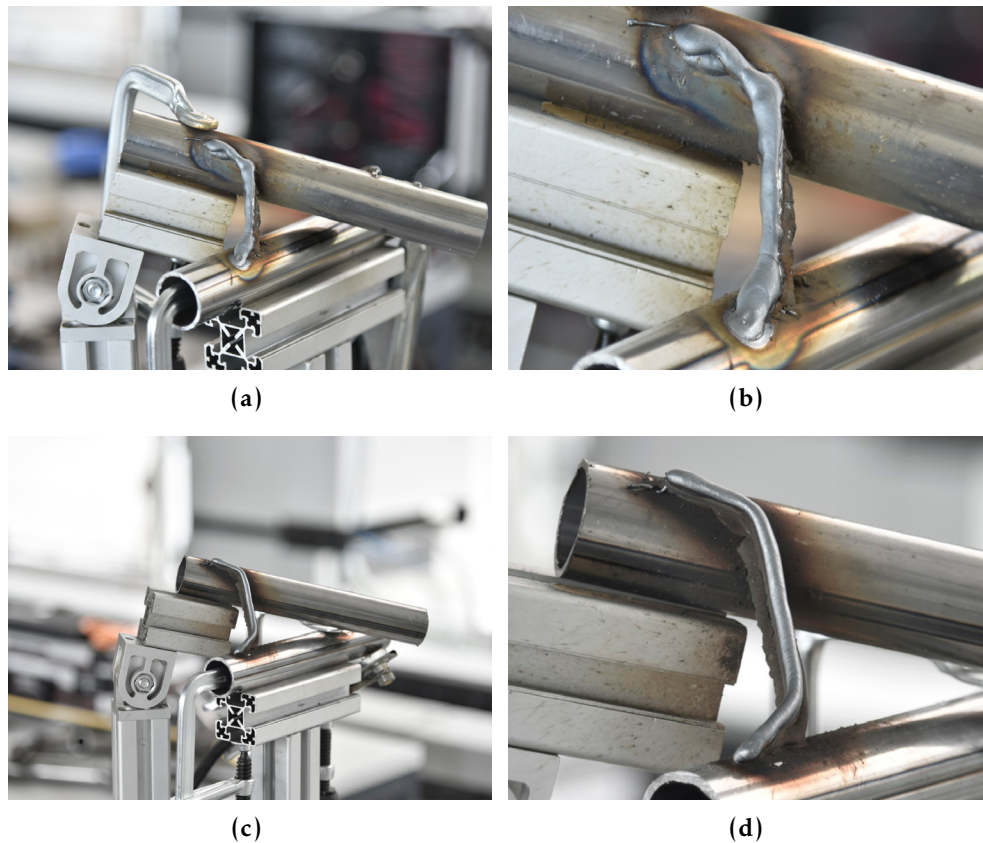
Figure 5.3: *Hybrid connections: (a-b) Uneven continuous deposition result on an early study on Setup A, and (c-d) Uniform result with a steady control over the process parameters of continuous deposition from a later study in Setup A.*

These studies proved as versatile as the point-by-point approach and suggested that the technique could be used to reinforce somewhat filigree bridges. The main task resided in consistently printing *on top* of the spatially complex and non-homogeneous surfaces of the point-by-point paths. This challenge led to testing *seam tracking*, a suitable sensing technique for continuous welding. The software and hardware development to implement the hybrid approach -scanning of the previously printed point-by-point bridge, sensing and adaptation

during continuous deposition- was, however, halted to prioritize the understanding and control over the point-by-point printing technique that is needed in the first place as a guide for the continuous deposition.

(a)   (b)

(c)   (d)

(e)   (f)
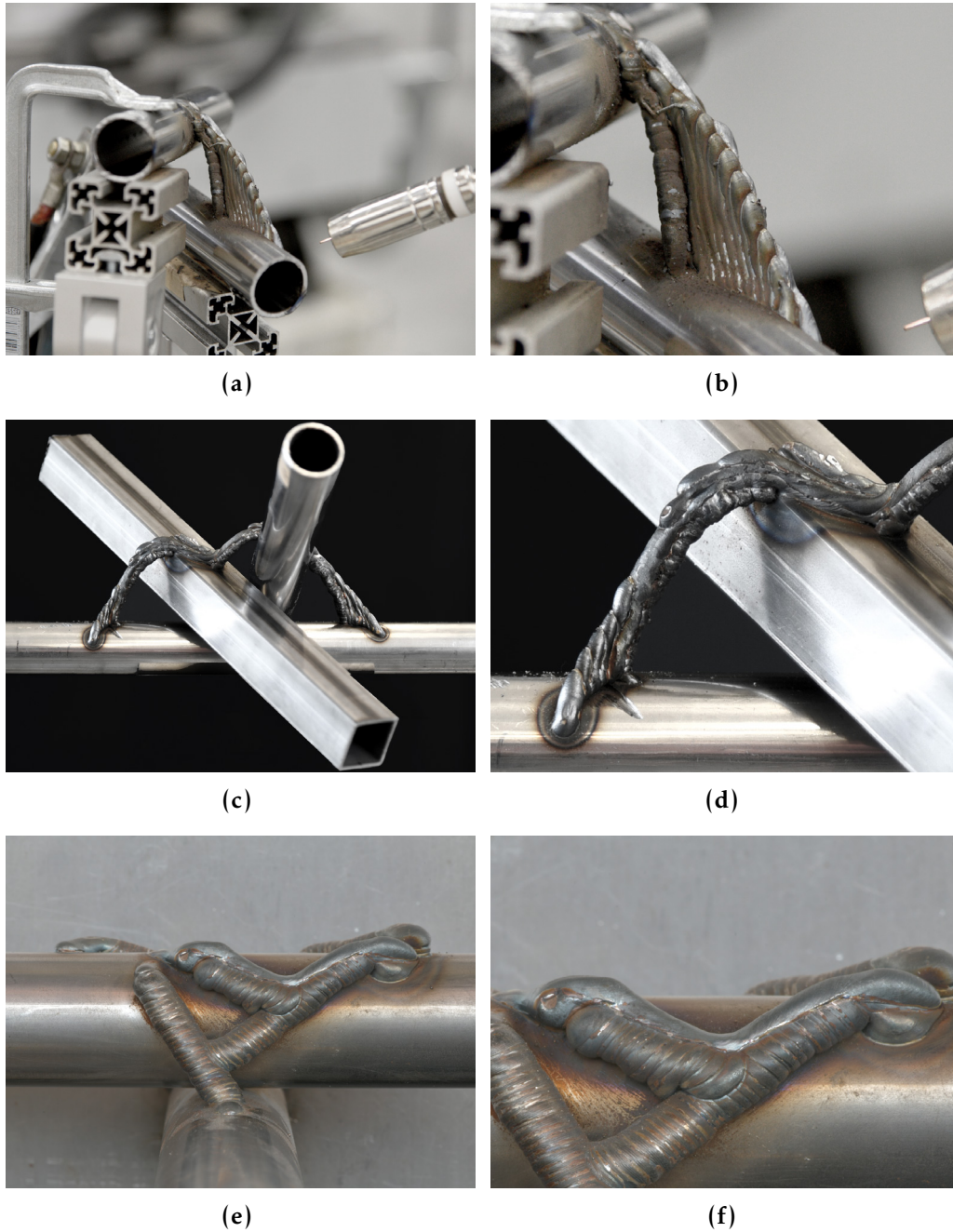
Figure 5.4: *Hybrid connections: (a-d) from Setup A (Mitropoulou, 2018), and (e-f) from Setup B.*

5.1.1.2   Connection typology

Which types of connections can be printed?

Generally, connections, joints, and nodes are categorized by the configuration of their intervening elements (see, for example, Roth, 1994b). In order to test the most common cases, a set of preliminary prototypes studied the corner -C-, tee -T-, or cross -X- connection types between two standard elements. All cases consist of non-machined, i.e., without pre-processed joining features such as miters or notches, and non-contact interfaces, i.e., without direct surface areas in contact with each other. Furthermore, the prototypes explore geometric characteristics that are rare in conventional nodes: they connect a pair of skew elements, i.e., elements that do not intersect, are not parallel nor coplanar, and are challenging to join with conventional techniques. This *skewed* condition was selected based on the aimed application of robotic assembly of spatial structures using only one robotic arm for assembly and no additional scaffolding as described in Section 1.4. In this scenario, the construction elements that are not supported by the assembly robot would likely deflect presenting medium to high tolerances at the interfaces between the elements to be joined.

C connection   The C, corner, or elbow consists of an end-to-end connection of elements (Figure 5.5). This type is often found as a convergent node, i.e., where the element's axes intersect. In this case, the elements are off-centered by 10 mm. The main challenge identified in this prototype was that the C typology results in relatively large connection layouts. This aspect is due to the fact that the printed material should not be placed too close to the edges of the elements to ensure that enough substrate around the entry and exit points is present. Because of this required offset from the elements' edges, the entry and exit locations of the printed paths are pushed far from each other resulting in larger, and likely, more intricate connection topologies than the ones found in the T and X types.[1]

---

[1]Similar results were found in the Pipeline studies and Structures with IPWAAM connections demonstrators.
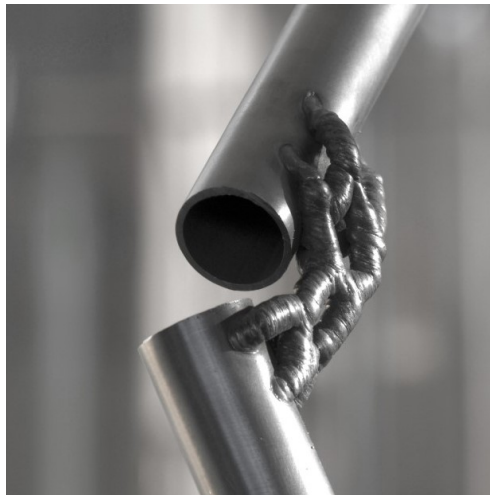
Figure 5.5: *C connection showing an entry section positioned very close to the edge of the bottom element, whereas the exit sections are positioned farther away from the edge of the top element.*

T connection   The T or tee consists of an end-to-side connection of elements. Here, the axes of elements can intersect or not, and the risk of applying material too close to the edge of the end-sided element applies as well as described in the previous C type. In comparison to the C connection, however, this type allows more compact layouts. Figure 5.6 shows a result of a T connection for two elements with an offset of their axes by 5mm.
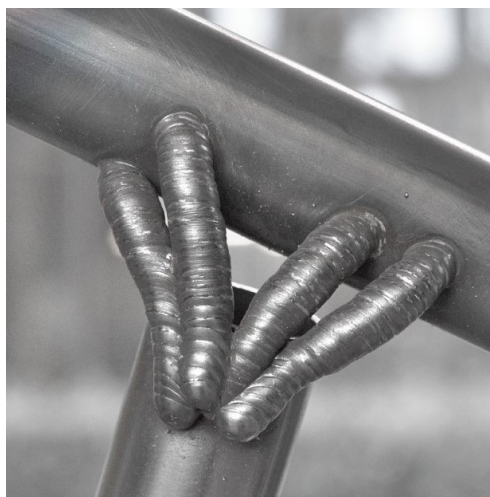
Figure 5.6: *T connection showing a relatively compact distribution of paths.*

X connection   The X or cross connection presents a side-to-side con-
nection of elements. Here, the axes of the elements are skewed and
cannot intersect.[2] This type presents a difficulty for prefabricated
nodes in terms of assembly —without proximity to the ends of the
elements, a node needs to be composed of several parts— whereas
IPWAAM connections benefit from side-to-side or X types as in this
case there is no need to restrict areas where material can be placed as in
the other two types (Figure 5.7). Conversely, this type is more spatially
constrained than the C and T types because the connection space gets
more obstructed by the elements than in the other two cases.
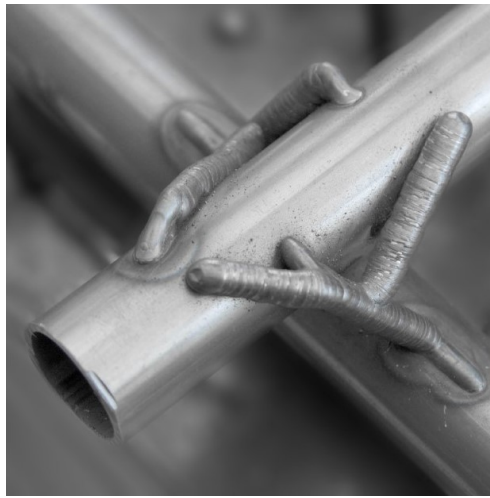
Figure 5.7: *X connection*

In hindsight, these connection typologies only present trivial differ-
ences between each other in terms of pipeline implementations. IP-
WAAM and AD seem to not require different approaches to tackle
the different geometric conditions of the elements to be joined. With
this in mind, it can be noted that typological differences may not im-
pose a strong design or fabrication constraint when using IPWAAM
connections.

---

[2]An example of an X type connection within a spatial assembly was used in Parascho,
2019.

5.1.1.3 Path topology and geometry

Which path topologies and geometries can be printed?

The structure and geometric properties of the printed paths are determining characteristics of IPWAAM connections. For example, understanding the topology of paths is critical for the success of the `Path sorting` component. In particular, it has important implications for the data manipulation and storing of geometric objects.

Individual paths Independent paths that bridge between base and target elements are the primitives of an IPWAAM connection. Individual paths can be further categorized as linear or curvilinear paths, a geometric property that has implications for the tool accessibility (see 3.32).

Linear paths One of the simplest geometric objects, IPWAAM linear paths are indeed not as simple to produce. In linear paths, the collision of the tool with the elements to be assembled results in non-planar layers (Figure 5.8a).

Curvilinear paths By following the boundaries of the accessible space between the elements, shorter, curvilinear paths can minimize the angle that the tool needs to rotate to avoid colliding with the elements (Figure 5.8b). Slicing curvilinear paths results as well in non-planar layers.

(a)

(b)
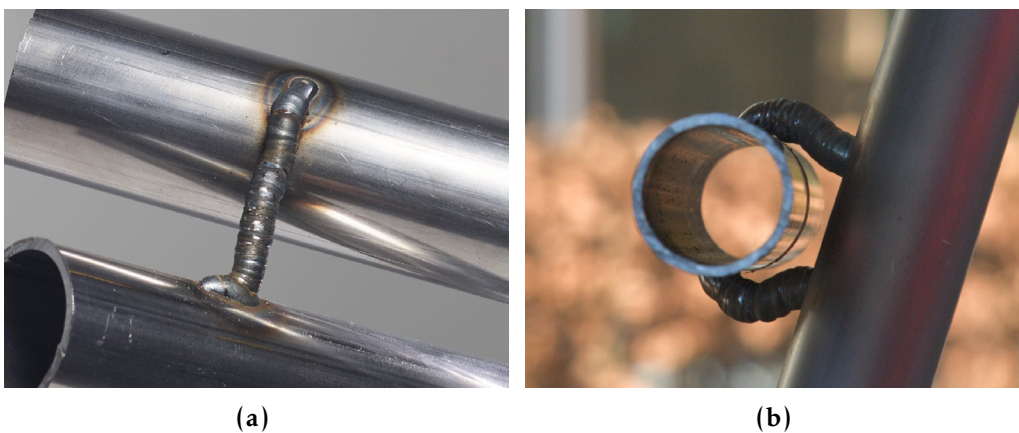
Figure 5.8: *Individual paths: (a) Linear, and (b) Curvilinear.*

Intersecting paths   Speculative early studies of material distribution approaches for IPWAAM connections showing more complex path topologies led to the investigation of intersecting paths (Figure 5.9). This group can be further categorized into branching topologies or truss-like topologies. In addition, and according to their printing sequence, paths need to be categorized into convergent and divergent for the `Path sorting` step.

| (a) | (b) | (c) |
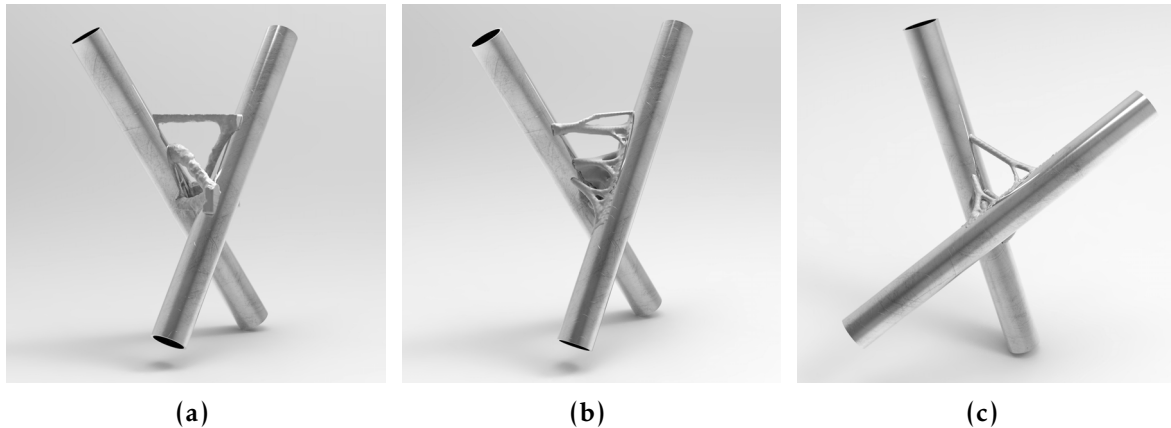
Figure 5.9: *Preliminary topology optimization results without consideration of fabrication constraints: (a) from Abaqus, and (b-c) from* `t0pos`.

Trees   Typically found in organic structures, tree topologies consist of trunks -*entry* paths-, branches -*internal* paths-, and leaves -*exit* paths-. Branching can be materialized as a fork (Figure 5.10a) or as a branch attachment (Figure 5.10b).[3] These experiments led to the development of the *material removal* step to avoid overlapping frames at intersection points in the `Path sorting` component.

The simultaneous convergence or divergence of different paths at seemingly the same locations, or *polytomy*, was also found often in the material distribution results. The crow's foot experiment (Figure 5.10c) showed the challenges of overcrowded areas and led to the development of the *sequence by Z coordinates* strategy in addition to the preliminary used *sequence by topological order* in the `Path sorting` component.

---

[3]In organic material or building systems such as piping, branch attachment usually means a reduction of the cross-section. In these experiments, the cross-section was maintained constant, however, column diameter changes with IPWAAM are possible and could be further studied.

Trusses Truss-like topologies are commonly found in human-made structures due to their high efficiency in transferring forces. Material distribution results showed similarities to trusses, however, not strictly straight or convergent/divergent nodes. A truss-like IPWAAM connection was tested early on, however, the overall size of the paths and the high heat present at the intersections resulted in high deformations of the path geometry (Figure 5.10d). This experiment led to the development of the *cooling time* step based on the distance between the points to print, i.e., the shorter the distance between consecutive points, the longer the cooling time that should be used, in the `Path sorting` component.

(a)

(b)

(c)

(d)
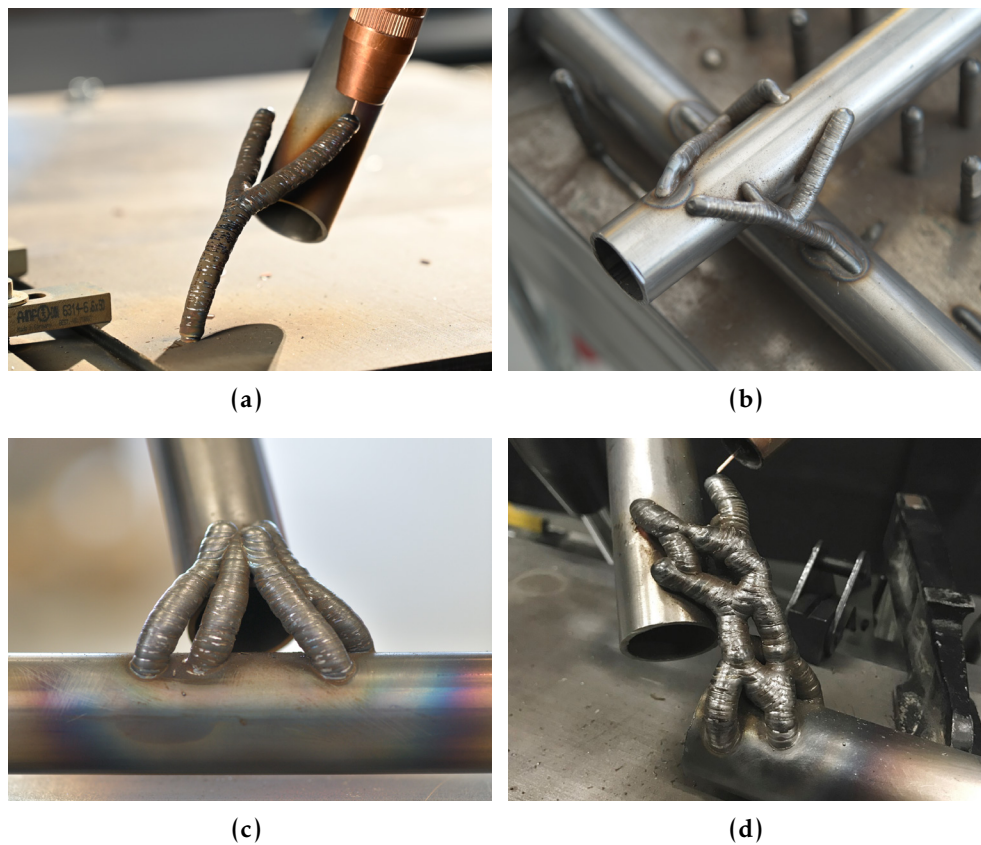
Figure 5.10: *Intersecting paths topologies: (a) Fork, (b) Tree, (c) Tree with polytomy (crow's foot), and (d) Truss-like.*

In sum, these preliminary prototypes looking at material depositions, connection types and path topology and geometry contributed to an understanding of the characteristics and constraints when using WAAM as a joining technique. In turn, this knowledge led to the development of the IPWAAM printing technique presented in Chapter 3 and the

rationale of the adaptive detailing pipeline for IPWAAM presented in Chapter 4 and tested in the following set of demonstrators.

5.1.2   Pipeline studies

This section presents implementation results of the adaptive detailing (AD) software pipeline for design and production of IPWAAM connections in three cumulative demonstrators: the simple (5.1.2.1), functional (5.1.2.2), and adaptive connections (5.1.2.3). The demonstrators present the aggregate features of the pipeline as they were developed based on an increasing need for control when facing more complex challenges. Table 5.1 shows which components of the AD pipeline have been tested in each demonstrator (denoted by the letter "x").

5.1.2.1   Simple connection

The simple connection tests a minimal pipeline for adaptive detailing with IPWAAM. The connection is *drawn* rather than *computed* using only must-have fabrication constraints as inputs. Ultimately, the simple connection aims to illustrate how conventional detailing approaches operate: certain aspects of the production process are known and can be explicitly described, while others are "filled in" implicitly during production.

Description

The simple connection is a C-type corner connection consisting of two non-touching, non-machined tubular standard elements of 30 mm diameter and 30 cm length. The concept consists of two symmetric paths placed in an intuitive position to support the cantilevering load (Figure 5.11). The paths are of type *bridge* and present point-by-point entries and exits.

Components and features	Simple connection	Functional connection	Adaptive connection
Tool accessibility	x	x	x
Robot reachability	x	x	x
Material distribution		x	x
Path generation with *path sketching*	x		
Path generation with *path finding*		x	x
Path slicing with *mesh collisions*	x		
Path slicing with *path planning*		x	x
Path sorting with *sequence by topological order*	x		
Path sorting with *sequence by Z coordinates*		x	x
Localization	x		x
Touch-sensing	x		x
Printing	x		x
Path adaptation to as-built elements	x		x
Path-adaptation to as-built paths	x		x

Table 5.1: *Development of AD components for the three connection demonstrators, e.g., the tool accessibility component has been tested in all three connections.*
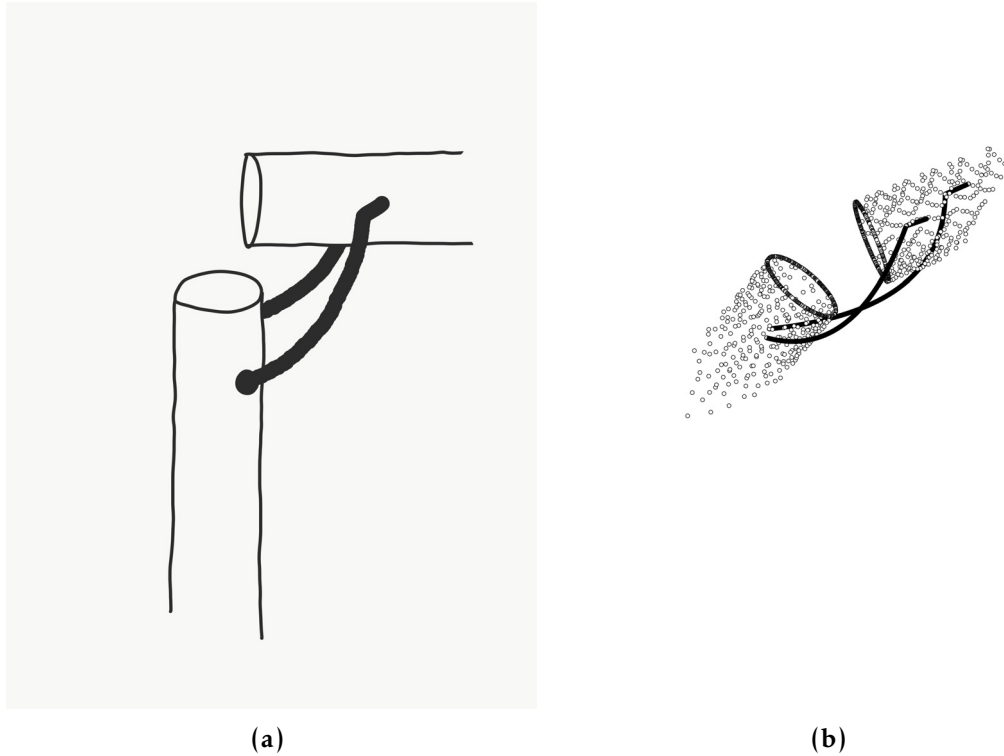
Figure 5.11: *Simple connection concept sketches*

Implementation and results

Figure 5.12 shows the simple connection pipeline including
the minimum required components for the design and fabrica-
tion of a simple connection. The experiment started by placing
the elements to connect in the physical space manually follow-
ing the design in the `Planning` scene. Then, the elements were
surveyed with the `Localization` procedure. The next steps
were then computed with relatively high certainty of the loca-
tion of each element. First, the `Tool accessibility` and the
`Robot reachability` were calculated to inform the designer about
reachable areas where the two bridging paths could be placed. Then,
using the `Path generation` component as a design canvas, paths
were sketched in reachable areas. Next, the `Path slicing` and

`Path sorting` components were used to produce the fabrication data. Finally, production was carried out with the `Touch-sensing`, `Printing`, `Path adaption to as-built elements` and `Path adaption to as-built paths` components. The following sections describe the implementation steps.
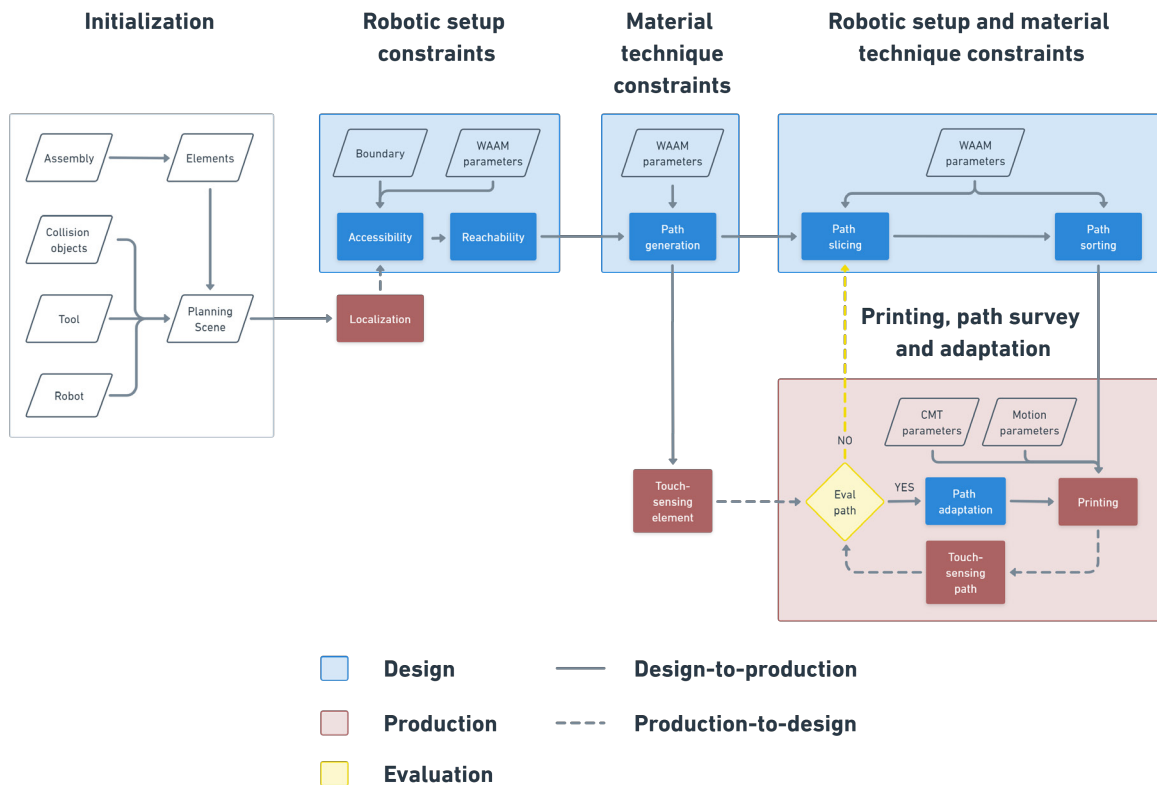
Figure 5.12: *Simple connection pipeline*

Initialization, positioning and localization To start, the elements to connect were placed manually in the robotic setup following design specifications. This was done by using the tool center point (TCP) as a reference coordinate at different locations to indicate where to place the elements. Because the positioning was done manually, it was expected that the elements would be placed within a certain tolerance. To verify their actual positions, the data in the Planning Scene was used to create localization frames for measuring the elements at specified locations. Finally, the localization procedure was run in two sections of each element (Figure 5.13a), and their axes were reconstructed in the

(a)

(b)

(c)

(d)

(e)

(f)

(g)

(h)

(i)

(j)

(k)

(l)

(m)

(n)

(o)
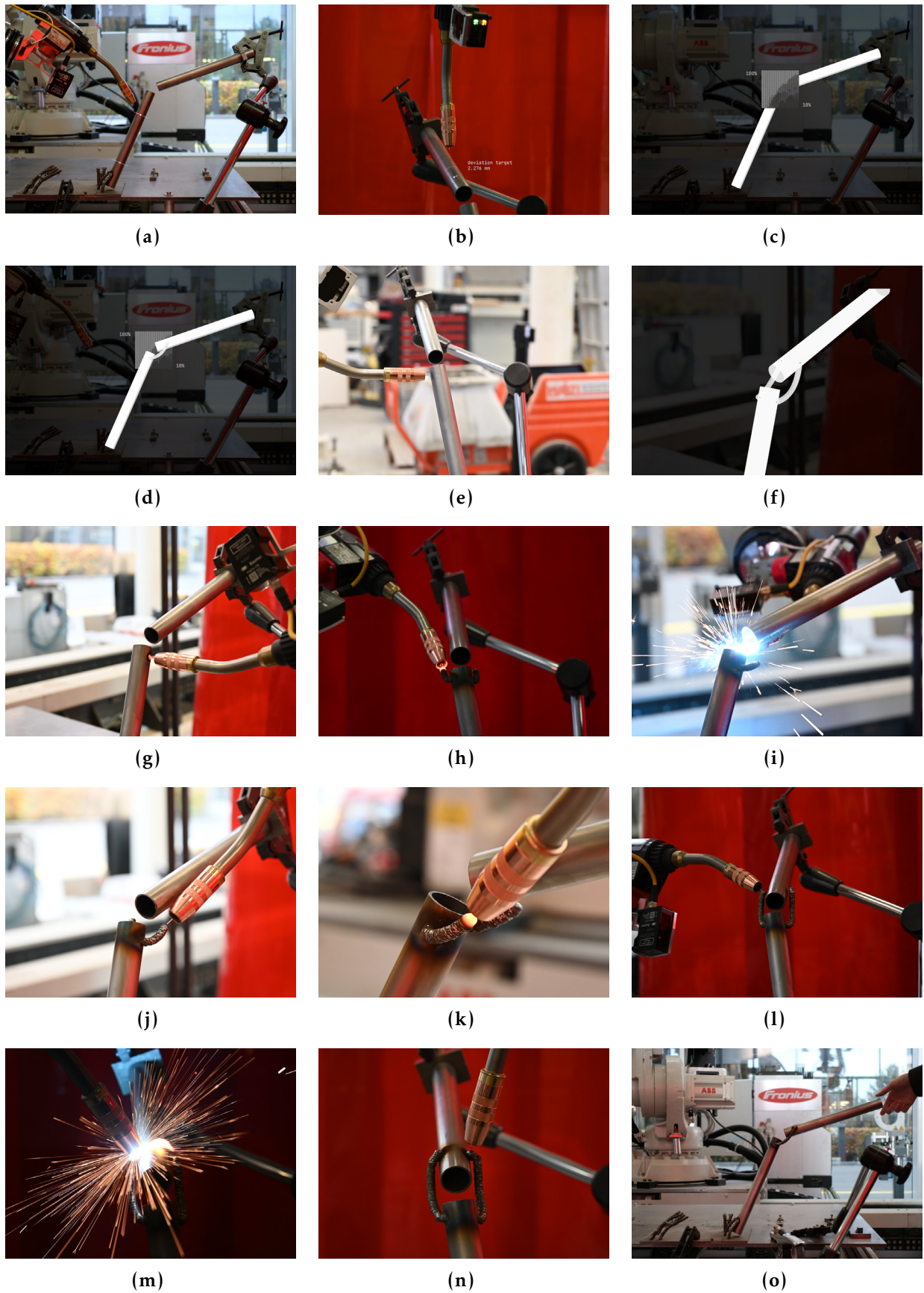
Figure 5.13: *Simple connection, stills from the production process. Video source: Gramazio Kohler Research, 2020.*

digital model. The recorded data shows a deviation of 3-5 mm for each section (Figure 5.13b).[4]

Tool accessibility, robot reachability and path generation With the updated positions of both elements, the tool accessibility and reachability map were then calculated (Figure 5.13c). Figure 5.14 shows results of high 5.14a and low 5.14b resolution maps (50 and 10 subdivisions). The high-resolution map gives a complete picture of the space while the low-resolution map allows for visualizing the points located in the interior of the map. Using the low dense map as a canvas, free-form paths were sketched on reachable areas (Figures 5.14b and 5.13c). Finally, the sketched curves were fitted between the cylinders' surfaces.

(a)   (b)
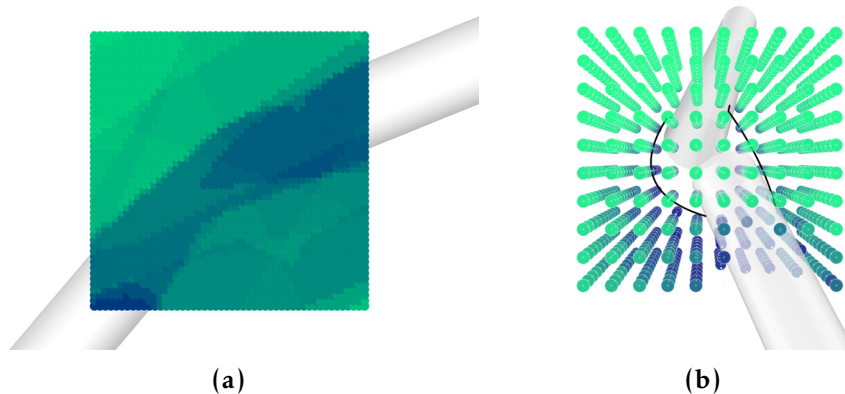
Figure 5.14: *Robot reachability and path generation (a) High-resolution visualization of reachability map, and (b) Path generation with path sketching in a low-resolution reachability map.*

Touch sensing and adaptation to as-built elements Once the final fitted path curves were obtained, the elements were probed at each expected entry and exit point with the touch-sensing procedure. Here, deviations within 2 mm were found.[5] Finally, the path's entry points were adapted with the pull points method to fit the as-built base element location (Figures 5.13d and 5.13e). At this point, the exit points remain stored for future adaptation of the exit section once the main

---

[4]It is expected that smaller deviations would be found when placing the elements robotically.

[5]These large deviations could be attributed to the calibration of the localization sensor (3.2.3).

path body is built. Figure 5.15 shows how the entry section, and therefore the fitting operation, has a big impact on the expression of the resulting connection.

| (a) | (b) |
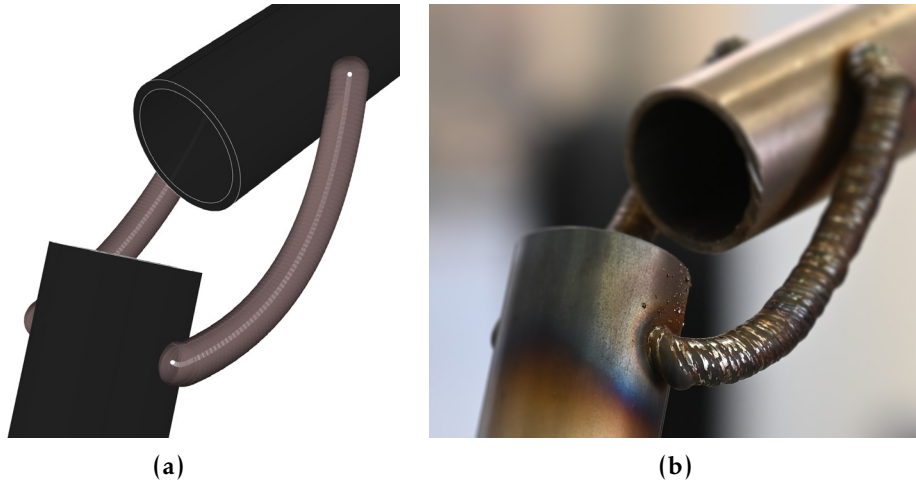
Figure 5.15: *Entry: (a) Adapted entry, and (b) Final result.*

Path slicing and sorting   The slicing component with the *Tool orientation with mesh collisions* method was used next. Figure 5.16 shows the visual feedback of the resulting tool orientations relative to the build direction and the gravity vector. Linear offsets of the printing frames were used as approach positions, and hard-coded robot joint targets were included during the traveling procedure to make sure that the robot approaches the printing targets in the right orientations (Figure 5.17). The sorting of the printing frames was achieved by the *Sequence by topological order* method, as the path topology with independent paths allows for it. Finally, the cooling time was calculated considering the traveling between drops. Given the symmetric geometry of the connection, the sorting results in an alternate sequence between the left and right sides and a travel time long enough to eliminate the need for an additional cooling time between consecutive print points.

Printing, touch-sensing, and path-adaptation to as-built paths   During the printing process (Figures 5.13f-5.13n), the touch-sensing procedure was used half-way through the path length to measure the layer height build-up (Figure 5.13j). The recorded path height was higher than the expected location, therefore the *Trim path* method (4.3.6.4) was used to adapt the remaining path curve to fit within the as-built
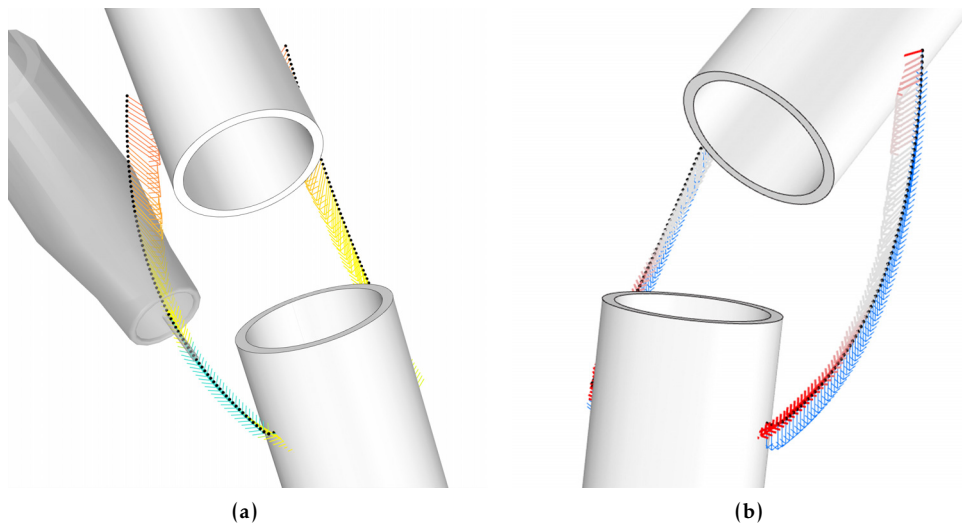
Figure 5.16: *Visualization of process constraints: (a) Tool relative to path from green (maximum alignment to path) to orange (maximum deviation from path), and (b) Tool relative to the gravity vector from red (maximum deviation from gravity) to white (maximum alignment to gravity). Gravity vector in blue.*
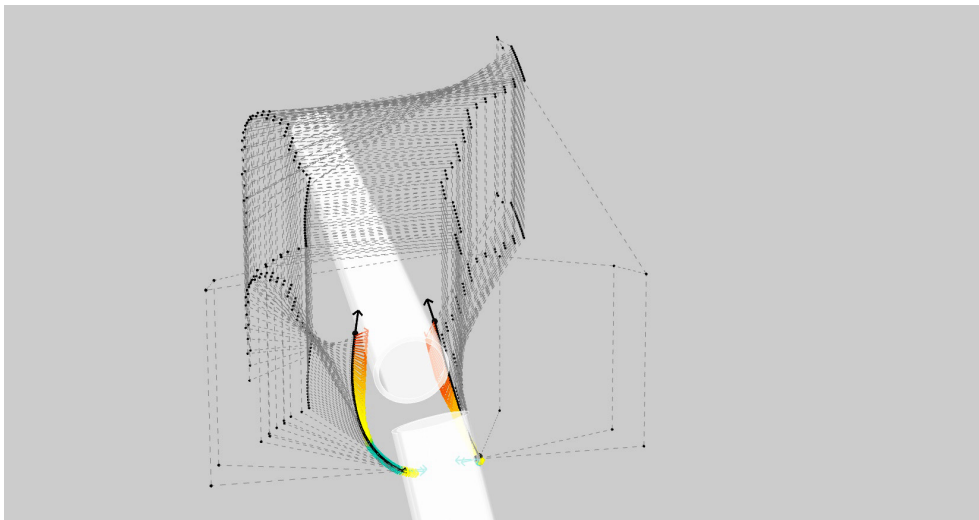
Figure 5.17: *Simple connection: linear trajectories between printing frames and approach positions.*

material. Once all the layers of the path were printed, the exit sections were calculated and printed. For this, the last layer of the printed path was measured (Figure 5.13l), reconstructed in the digital model, and the exit curves were fitted virtually between the path and the target element. Finally, a point-by-point deposition was used to print the exits (Figure 5.13n). Figures 5.13o and 5.18 show the result of the *simple connection*.

Figure 5.18: *Simple connection results*

5.1.2.2   Functional connection

The next demonstrator upgrades the intuitive design approach presented in Simple connection informing the design with functional constraints. The connection's geometry is *computed* based on a given load case and informed by the constraints of the fabrication and material technique with additional *higher-control* components.

Description

The functional connection setup consists of the base and target elements used in the Simple connection. There is, however, no specific concept behind how the connection should look beforehand.

Implementation and results

The design section of the simple connection pipeline (Figure 5.12) is extended here with structural considerations provided by the `Material distribution` component. With this step, the connections' topology and geometric complexity increase, which leads to stronger fabricability constraints. The need to resolve more spatially-constrained paths leads to the development of an alternative slicing method (*Tool orientation with path planning*). In addition, the more complex topology requires more control over the printing sequencing

handled by the `Path sorting` component. The complete pipeline is shown in Figure 5.19 and is developed and evaluated in a virtual environment.
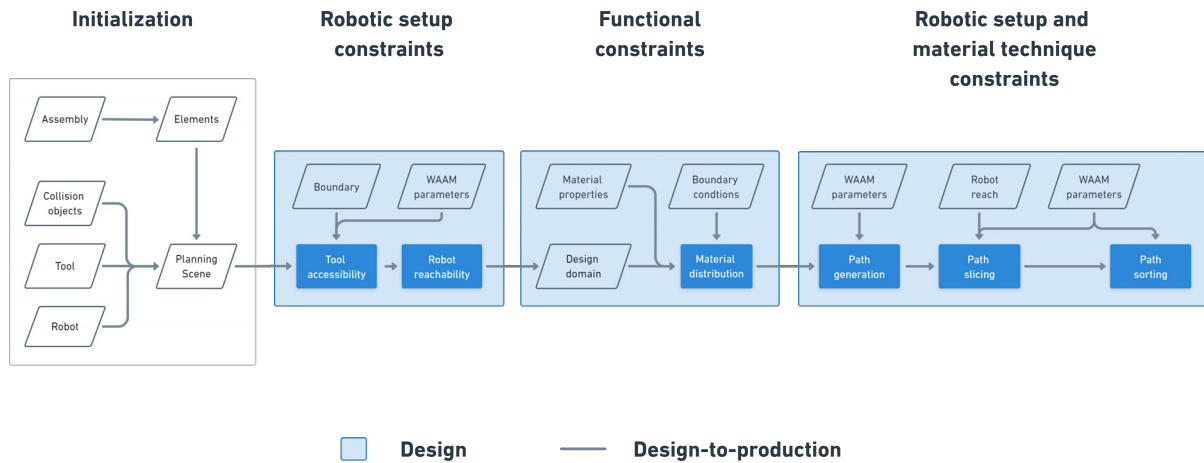
Figure 5.19: Functional connection pipeline

Accessibility and reachability   Here, the reachability map used in the simple connection is refined with an increased number of tool orientations. To reduce the calculation time[6], a medium resolution (25 units per side) and a larger number of tool orientations per point were used as inputs (108 frames per point, Figure 5.20a)[7]. Additionally, safe collision meshes were added to the element's endpoints to avoid the placement of material too close to the edges (Figure 5.20b). The boundary of the reachable space was then constructed based on a threshold of at least 10 tool orientations per point (Figure 5.20b).

Material distribution   This step looked for a tendency where material should be placed within the robotic setup constraints defined by the reachable boundary.

---

[6]The benchmark computation times are the following: Considering a computation time of 0.08 seconds per collision check of an IK solution, for a total of 108 frames for 8'000 points (= 864'500), with a reduction of the reachable frames by 47% a total of 9h 45 min.

[7]The settings used in the reachability step allowed for a `max alpha angle` of 45 degrees, `step z axis` of 2, and `angle step xy` of 40 degrees, see 4.3.1.2 for terminology.
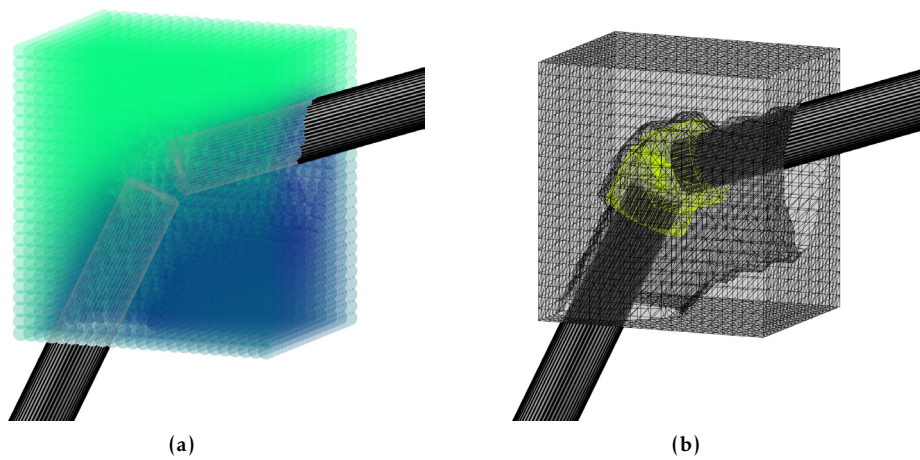
Figure 5.20: *Reachability of the functional connection: (a) Reachability map showing more reachable areas (in green) and less reachable areas (in blue), and (b) Reachable boundary with additional safe collisions (in yellow) to avoid future material placement on the elements' edges.*

Boundary conditions The base and target elements were used as support and load volumes respectively. The assumed load case was considered as the dead weight of the target element, therefore the load vector was set with the gravity vector (0,0,-1) and a magnitude based on the element's steel density (77 kN/m3)[8].

Design domain The reachable boundary space with a threshold of 10 tool orientations was used as design domain (Figures 5.20b and 5.21a). In addition, a larger reachability map and reachable boundary space were tested to compare load distribution tendencies (Figure 5.21b).

Settings The material properties used in the TO task were defined based on available data provided by the uniaxial tensile tests (3.6.6.2, Young's modulus $E = 195$ GPa, and the Poisson ratio $v = 0.30$, usually assumed for structural steels. The material density

---

[8]As discussed in Chapter 4, Section 4.3.2, these inputs are used as placeholders to be revised in a complete pipeline considering a static analysis that can be integrated into a more robust topology optimization setup.

for all elements was set to 0.3 and the rest of the `tOpos` solver parameters are set to default values[9].

Results   Figure 5.21 shows different results with varying reachable volumes, TO model resolutions and isovalues.[10] Here, it is visible that each of these inputs has a significant effect on the final volume and amount of detail of the members and therefore the overall topology. As `tOpos` does not provide a way to prescribe the desired stiffness of the node, the optimal volume ratio is unknown. This step should be overcome by providing more control over the TO task as previously noted. For the purpose of finding a distribution tendency, however, these results would be sufficient, as the material tends to be located in roughly the same areas.

Path generation with path finding   To find possible print paths that follow the material distribution tendencies, all stored `isomeshes` were skeletonized to compare results using the `Path generation` with the path finding method. The combination of TO model resolution, isovalue, volume of the available reachable space, and inclusion of collision obstacles, resulted in distinct boundary topologies, and consequently skeleton topologies (Figure 5.21).

The result with less volume overall (Figure 5.21a) was selected and the skeleton's curves were then post-processed and fitted (see Section 4.3.3.1) between the base and target elements, resulting in 17 path curves: 10 on the left side and 7 on the right side with two entry and exit paths each (Figure 5.22). Finally, the slopes of the final paths' curves were checked by testing the curve's subdivision tangents for negative values and negative slopes were manually modified.

Results   These results show a significant divergence between the volume of the `isomesh` and the expected printed volume of the resulting `skeleton` curve. In particular, these divergences are visible in

---

[9]Analyzer parameters: 5000 maximum iterations and 0.001 tolerance for termination of calculation. Optimus parameters: penalty factor between 2 and 3, difference between next compliance to terminate optimization: 0.005, radius for sensitivity filter: 1.5.

[10]Figures 4.19 and 4.21 in Chapter 4 have shown results for low, medium and high model resolutions with a constant and variable isovalues.

(a) Reachable space 0.15 x   **(b)** Reachable space 0.15 x
0.15 x 0.15 cm   0.15 x 0.20 cm

(c) Resolution 25   **(d)** Resolution 30   **(e)** Resolution 60

(f) Isovalue 0.05   **(g)** Isovalue 0.2
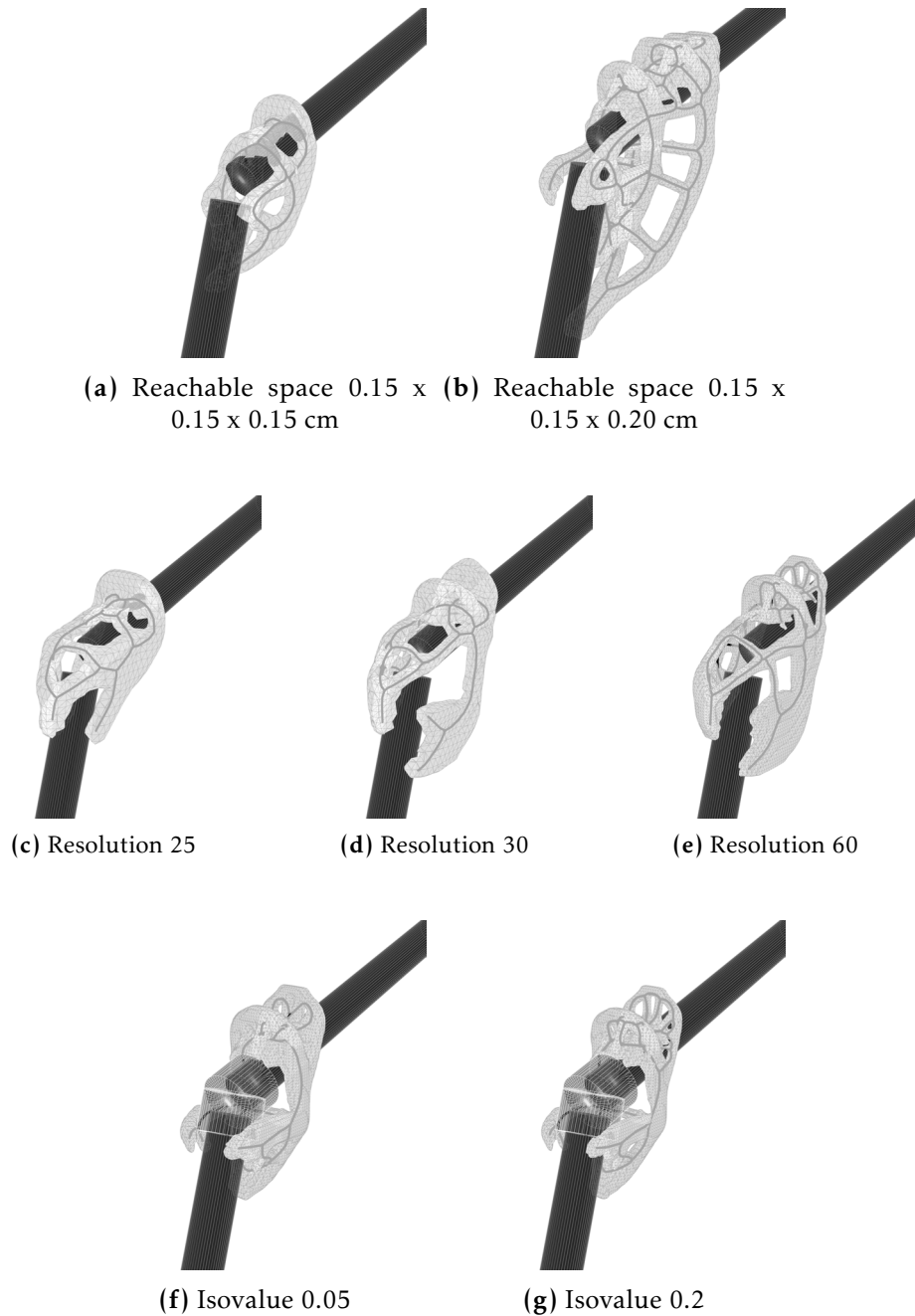
Figure 5.21: *Material distribution tendencies and skeleton results: varying reachable space volume (first row), varying TO model resolution (second row), varying isomesh isovalues with additional collision obstacles (third row).*

isomeshes presenting areas with massive volumes (see, for example, the right side of the connection in Figure 5.21e, and the discussion points at the end of this section).

(a)   (b)
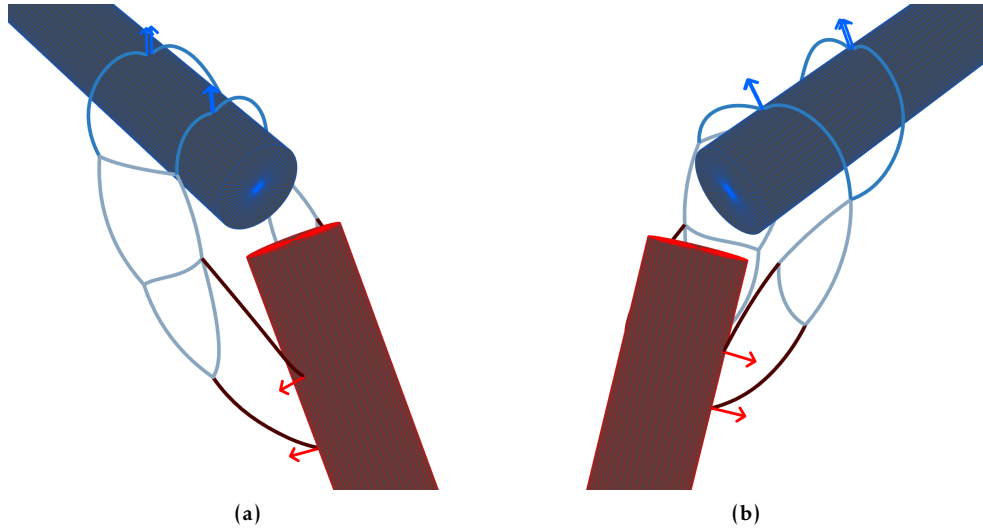
Figure 5.22: *Left and right views of the fitted skeleton between base (red) and target (blue) Elements; entry (in dark red), internal (in pale blue), exit (in blue) paths; and normal vectors at entries and exits.*

Path slicing with path planning   The resulting paths present several new challenges for slicing and data handling compared to the ones presented in the Simple connection. First, spatial and intersecting paths bring more variability in build directions conditions which results in an increased juxtaposition between ideal tool orientations and the paths themselves. Second, a higher density of paths in the same space presents extra collision objects during printing that further constrains the solution space of valid tool orientations. This scene's complexity led to the development of a path planning strategy for slicing. The next sections describe results following the *Tool orientation with path planning* method introduced in Section 4.3.3.2.

Layer height and base frames   First, the path curves were sub-divided with a fixed layer height of 1.2 mm (Figure 5.23a). To create the interpolated *base frames* at each subdivision position, additional handles were created at custom curve parameters, i.e., 0.2 for entry curves and 0.7 for exit curves, to further control the interpolation's boundaries (Figure 5.23b).
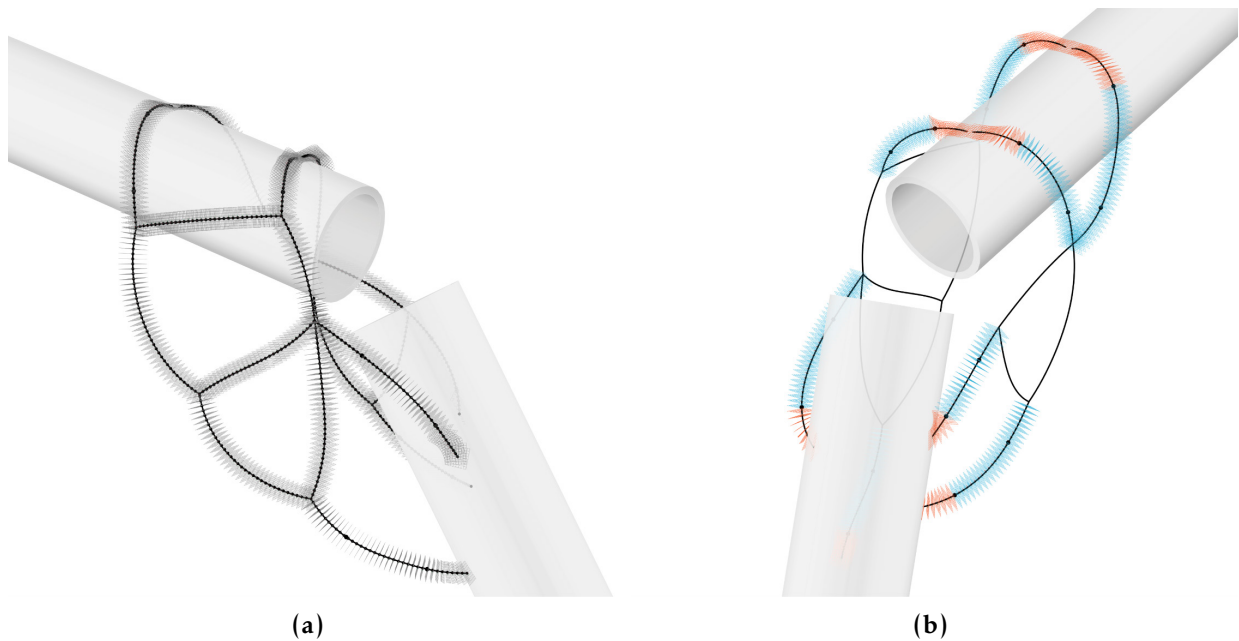
Figure 5.23: *Interpolation between start and end frames to generate base frames: (a) Interpolated base frames, and (b) Additional handles on entries and exits.*

Frame population   In this operation, the base frames are populated with a pool of possible tool positions at custom *deviation vectors* subject to WAAM constraints (see Figure 4.33b). The main WAAM constraint is the maximum allowed angle deviation, or `max alpha angle`, to the base frame. Based on the results in 3.6.2 and 3.6.6.2, a `max alpha angle` of 45 degrees would be ideal. However, this constraint did not satisfy path number 8, i.e., no valid tool orientation was found with these settings, therefore it was globally increased to 60 degrees[11].

Additional population settings define how large the possible pool of *deviation frames* is, which directly relates to the operation's computation time. The number of subdivisions, `steps z axis` between deviation extremes was set to 20 to minimize the angle deviation steps in the pool, i.e., the angle step between consecutive deviation vectors resulting in 3 degrees. Finally, for each deviation vector, additional tool orientation can be created as well with

---

[11]The global increase does have an impact when using the ladder graph search algorithm, as the algorithm prioritizes robot configurations first, and only second a minimization of the *z* deviation angle. However, when planning with the greedy algorithm, this global setting has no detrimental effect as the lower *z* deviation angle is always prioritized.

the `angle step xy`. However, limiting this variable considerably reduced the dispersion on the *x* and *y* axes' directions when using the greedy planning algorithm, therefore it was intentionally set to only 1, to get a fixed robot orientation in the *xy* plane per deviation vector[12].

Accessibility check The simulation of tool orientations at each *deviation frame* pruned 75 percent of the initial frame population.

| 10 | 650 |

(a)   (b)

Figure 5.24: *Reachability of paths calculated for the ladder graph search: greener sections of the paths are more reachable than blue sections. The lower bound is set to 10 reachable orientations; the upper bound is 650 reachable orientations, from an original pool of 1199 frames to test per point. On greener sections, more tool orientations are possible than on blue sections. Blue sections, the less reachable sections of the paths, influence the overall results of the ladder graph search.*

Reachability check The reachability check further pruned 7 percent of the remaining accessible frames. The result of this operation is shown in Figure 5.24: the reachability decreases when paths get closer to each other and to the base and target elements.

Planning of robot targets The selection of which robot pose should be used for each point was then analyzed for both path

---

[12]The effect of constraining this setting can be read in the comparison between the first and second halves of the left side of the Adaptive connection (5.32, see Figure 5.32a).
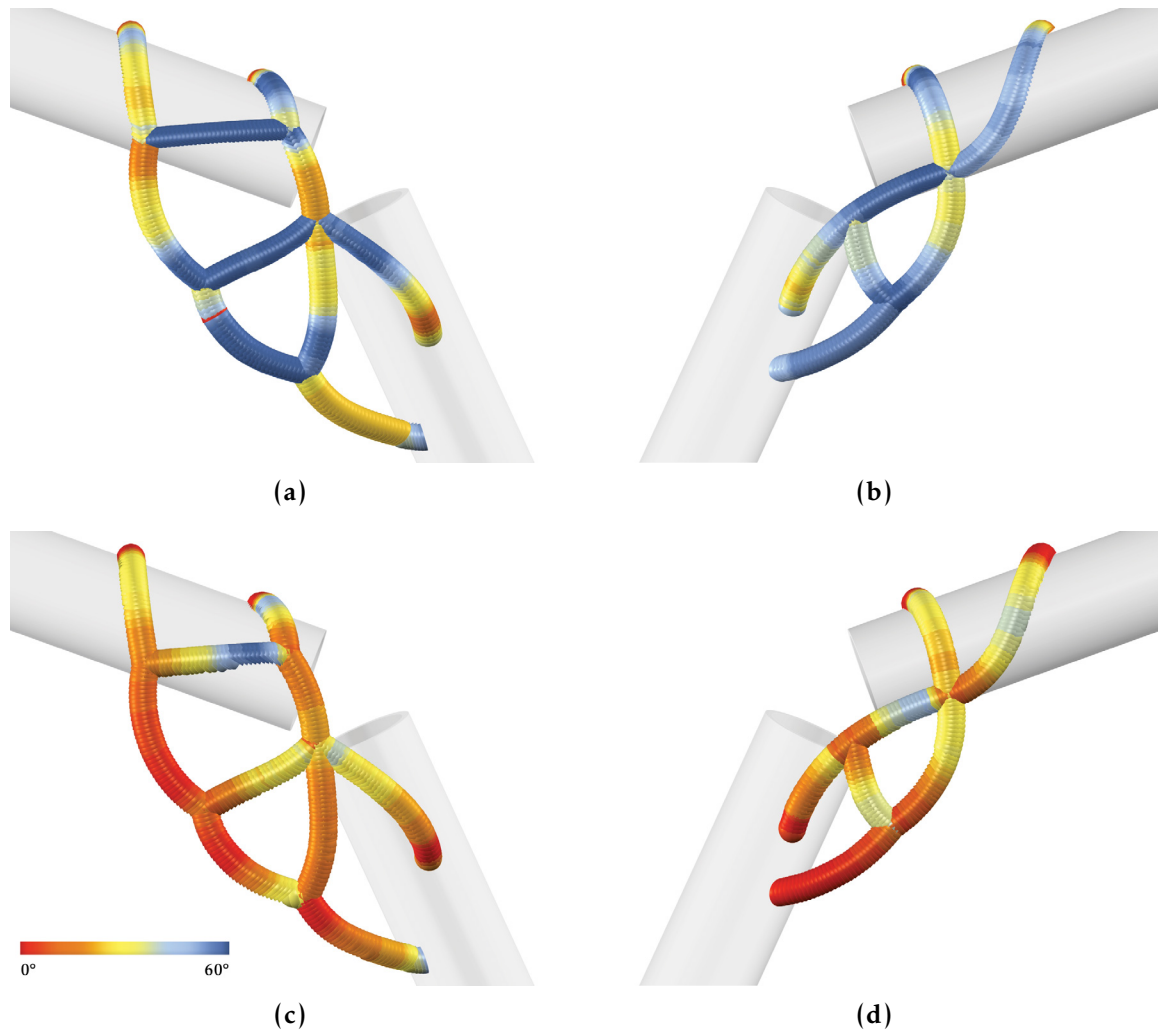
Figure 5.25: *Comparison of planning algorithms in final robot targets: target frames showing z axis deviation from red (lower deviations) to blue (higher deviations) for (a-b) Ladder graph search, and (c-d) Greedy search. The z axis deviations are much smaller overall for the greedy search.*

planning algorithms. A comparison of results is shown in Figures 5.25 and 5.27.

The results are compared with three metrics: deviation of the z axis of the final robot target relative to the z axis of the base frame in angle degrees; consistency of the x and y axis orientations in the resulting robot target; and computation time.

In terms of the deviation of the z axis relative to the base frame, the greedy algorithm favors 55 percent smaller deviations compared to the ladder graph algorithm (Figure 5.25). In terms of consistency of the robot target orientations, the ladder graph

search yields 10 percent more consistent results (Figure 5.25)[13]. Computation time depends greatly on the setup and the reachability of the connection - more pruning of the frame pool equals less computation time. Overall, the greedy algorithm is approximately 2.3 times faster[14]. In sum, the greedy algorithm provided faster results with the least *z* axis deviations, and not-critical re-orientations.

(a) (b)
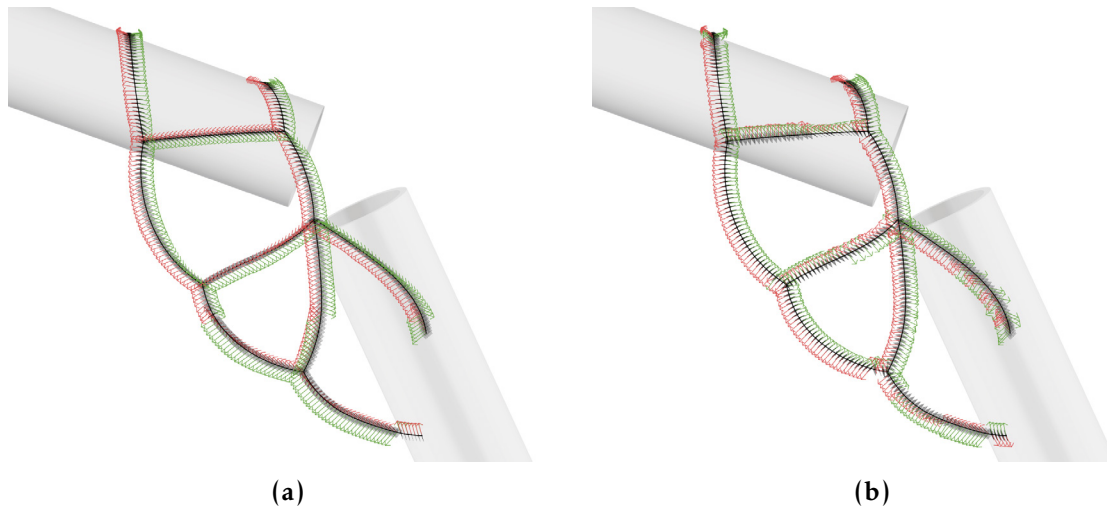
Figure 5.26: *Comparison of planning algorithms in final robot targets: target frames showing* x *axis (in red) and* y *axis (in green) for (a) ladder graph search, and (b) greedy search.*

Path sorting   The last component of this demonstrator outputs the final printing sequences considering the possible accumulation of material at nodes and cooling times.

Material removal   Figure 5.28a shows frames with an overlap at intersection nodes. The physical outcome of this overlap is an excess of material and increased heat and consequently requiring cooling time at the intersection nodes. The excess material at intersections was handled by removing frames on downstream and upstream branches. To this end, branching paths were split

---

[13]However, a considerably larger difference was found when using a more diverse frame population as the one shown in Figure 4.33.

[14]For the ladder graph search, the accessibility and reachability map calculation takes 40 percent of the total time, in this experiment roughly 2.5 hours of the total 6 hours. For the greedy search, the tool accessibility pruning takes 99.6 percent of the total time, around 2.5 hours, and the random search a marginal 40 seconds of that total

(a)   (b)
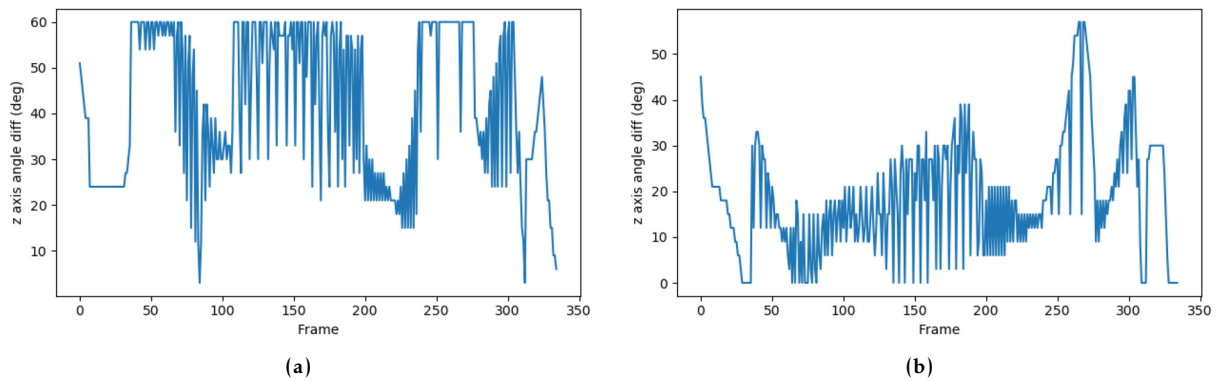
Figure 5.27: *Comparison of results of planning algorithms for the deviation of the z-axis: (a) Ladder graph, with a cumulative z angle deviation of 14,067 degrees, and (b) Greedy algorithm, with a cumulative z angle deviation of 6,321 degrees —less than half—.*

into halves and each half was categorized as convergent or divergent (Figure 5.28b). Then, a fixed amount of frames, equal to the radius of the expected printed paths (i.e., 4 mm) was culled at the start for divergent paths, and at the end for convergent paths, to avoid expected material accumulation. Non-branching halves remained unmodified (Figure 5.28c). Figure 5.28d shows the effect of this removal in a theoretical final result.

Printing sequence   The final sorting of the robot targets keeps the pre-sorted sequence and printing strategy, in this case, dividing the connection into left and right sides, and using the *Sequencing by z-coordinates* method (Section 4.3.3.3). The verification of the correct sequence is carried out visually with a color filter to illustrate the ordering, and computationally, by simulating the printing sequence orienting the robot at each frame in the CAD environment with the support of the `COMPAS FAB` library.

Cooling time   The cooling times for each frame can be now calculated by estimating the procedure's operation time. This includes calculating the travel time between approach offset positions and robot targets with the estimated motion speed, and the process parameters, e.g. gas valve and welding times. A comparison between the procedure's operation time between targets and the experimental minimum cooling time (30 sec) is computed and

(a)

(b)

(c)

(d)
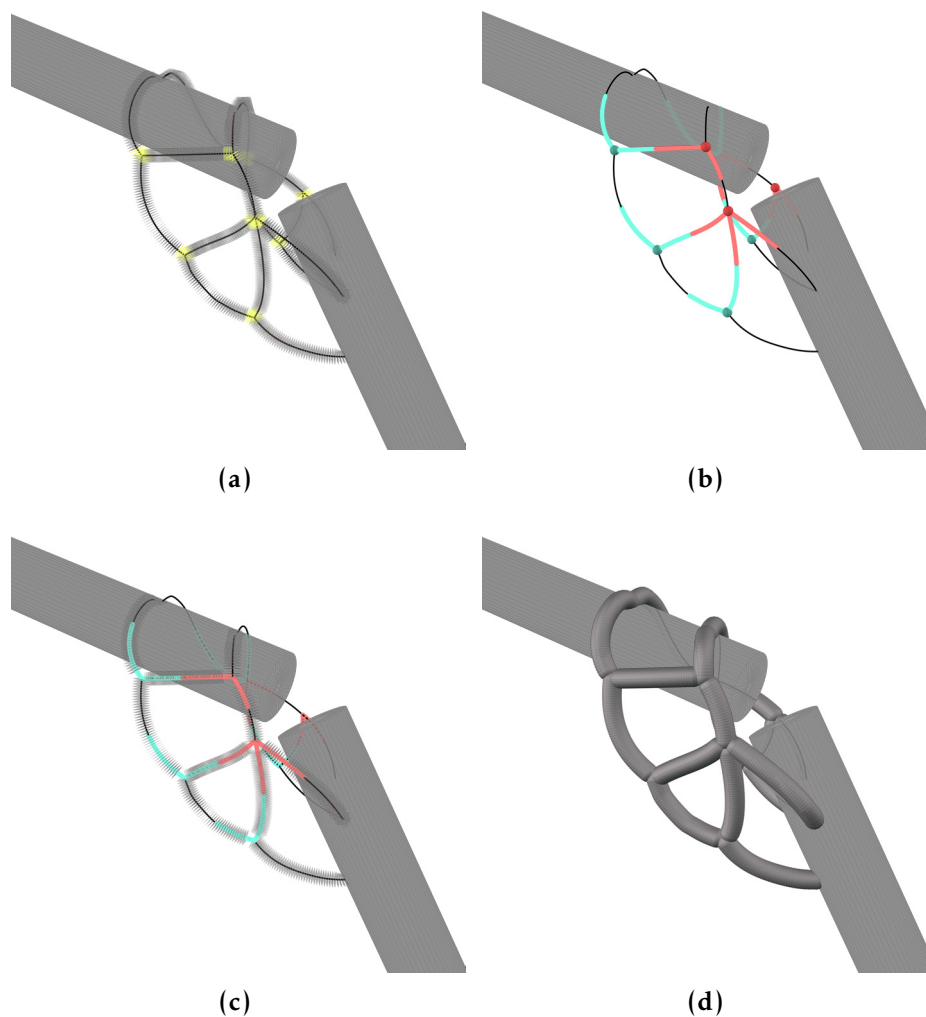
Figure 5.28: *Material removal in branching: (a) Final frames with overlapping areas at intersection nodes (in yellow), (b) Classification of half paths in convergent (in red) and divergent (in cyan) paths, (c) Removal of overlapping frames for each type of convergence type, and (d) Final expected outcome.*

the minimum value of the two is assigned to each frame. Finally, an increase of 0.10 sec is assigned to each frame in the printing sequence to counteract the heat buildup over time.

5.1.2.3 Adaptive connection

The adaptive connection demonstrates the complete adaptive detailing pipeline. The connection's geometry is pre-computed and *adapted* during production demonstrating the design-and-construction integration.

(a)   (b)
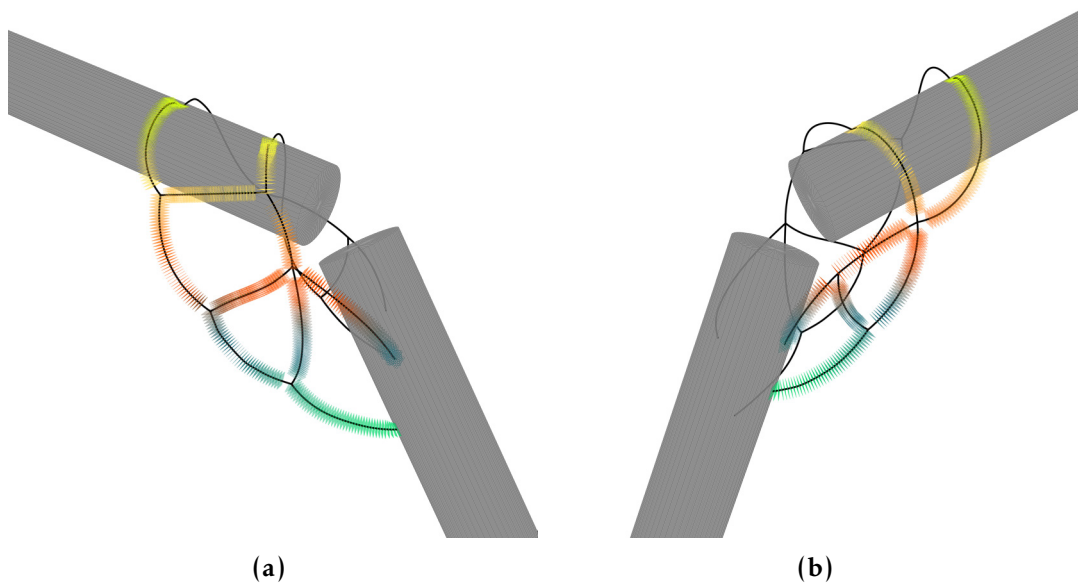
Figure 5.29: *Sequencing by z-coordinates from lower (in green) to upper (in yellow) frames: (a) Left side, and (b) Right side.*

Description

The adapted connection is based on the functional connection's geometry, slicing and sorting steps presented in Section 5.1.2.2 with `Path adaption to as-built elements` and `Path adaption to as-built paths` strategies employed during production.

Implementation and results

Here, the Simple connection and Functional connection pipelines are combined and tested together. However, an alteration concerning the sequencing of operations is introduced. Unlike the deployment in Simple connection, surveying components are executed *after* the geometry has been computed given that at this stage of development of the pipeline it is unrealistic to include the `Robot reachability`, `Material distribution`, and `Path slicing` steps during production due to the computation time they require. A scenario such as the one presented in the Simple connection, where all the design steps occur after the first survey construction step, would be in practice not likely and arguably not desirable. The adaptive connection pipeline (Figure 5.30), therefore, reflects and presents a feasible and desirable

workflow taking full advantage of the adaptive detailing approach. In addition, due to the complexity of the geometry of the connection, the responses given by the `Path adaption to as-built paths` component had to be diversified to handle the diverse material conditions measured during production.
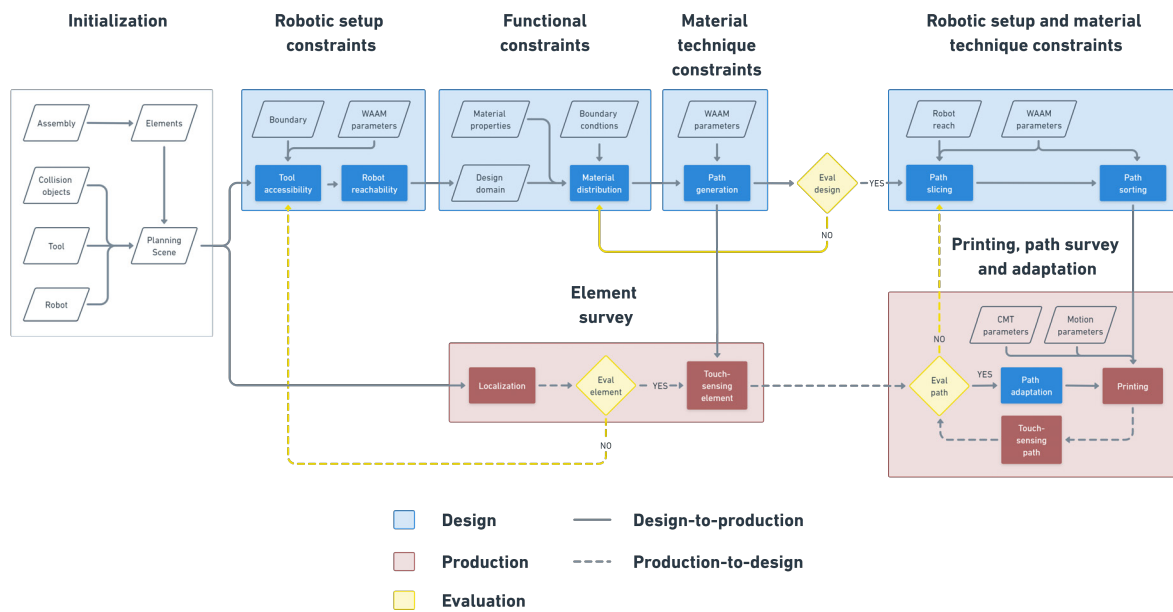
Figure 5.30: *Adaptive connection pipeline*

Survey, evaluation, and adaptation to as-built elements   The base and target elements were positioned manually. In order to record their actual positions, the survey components for localization and touch-sensing are used following the implementation discussed in Simple connection. Once the reconstruction of as-built elements was done, the new location of elements could be assessed. At this stage of the development of the pipeline, the deviation criteria only included a predefined and arbitrary maximum deviation value of 5 mm, which was met.[15] The deviation of the pre-computed entry points to the as-built base element was under 1 mm, and therefore no adaptations were made (Figure 5.31).

---

[15]As discussed in Chapter 4, this step should include performance criteria derived from static analysis and material behavior. As the reachability is computed to generate a material distribution tendency, the reachability map does not need to be recomputed below this value.

(a)   (b)
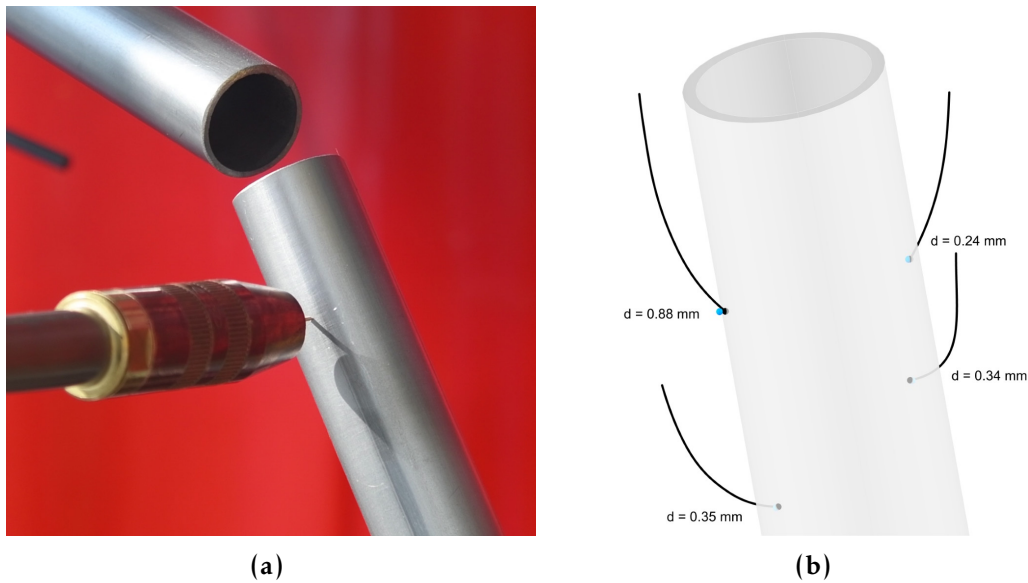
Figure 5.31: *Survey of entry paths: (a) Element's position survey with the touch-sensing procedure, and (b) Expected (in black) and measured (in cyan) entry points showing deviations under 1 mm.*

Printing, survey of paths and adaptation to as-built paths It was expected that deviations would be larger than in previous experiments given the truss topology and geometry of the connection presenting convergent and divergent paths, building directions close to 90 degrees relative to the gravity vector, and a high number of path intersections.

To assess and correct these deviations, the touch-sensing component was used at critical points during the printing process: before and after path intersections, halfway of the path length, and exit sections. These survey points organized the printing jobs into a total of 12 and 8 printing jobs for the left and right sides, respectively.

In addition, the left side was produced with a major modification halfway through the print to force a re-align of the x and y axis of the target frames. This change was introduced to react to the geometric variability of the surface roughness to this point of the print (Figure 5.32).[16]

---

[16]Settings before: `max alpha angle=60`, `steps z axis=8`, `angle step xy=6`; settings after: `max alpha angle=60`, `steps z axis=20`, `angle step xy=1`.

(a) (b)
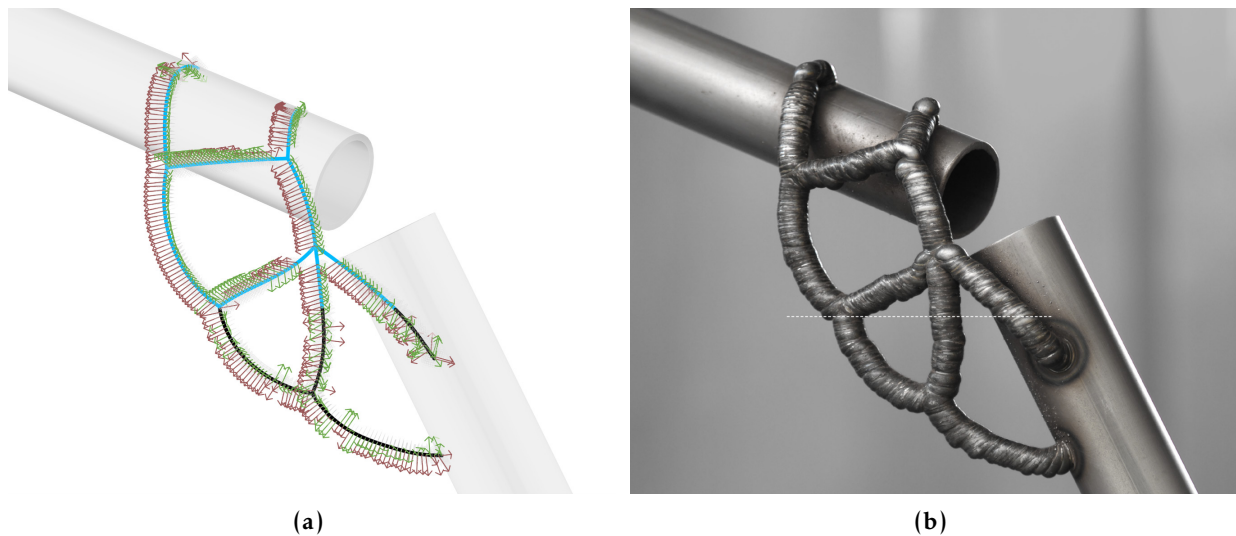
Figure 5.32: *Left side, orientations of target frames showing x and y axes (in green and red): (a) Jobs 1-5 (path curves in black) and of jobs 6-12 (path curves in cyan) showing re-aligned x and y axis, and (b) Printed result with an indication of slicing changes.*

(a) (b) (c)
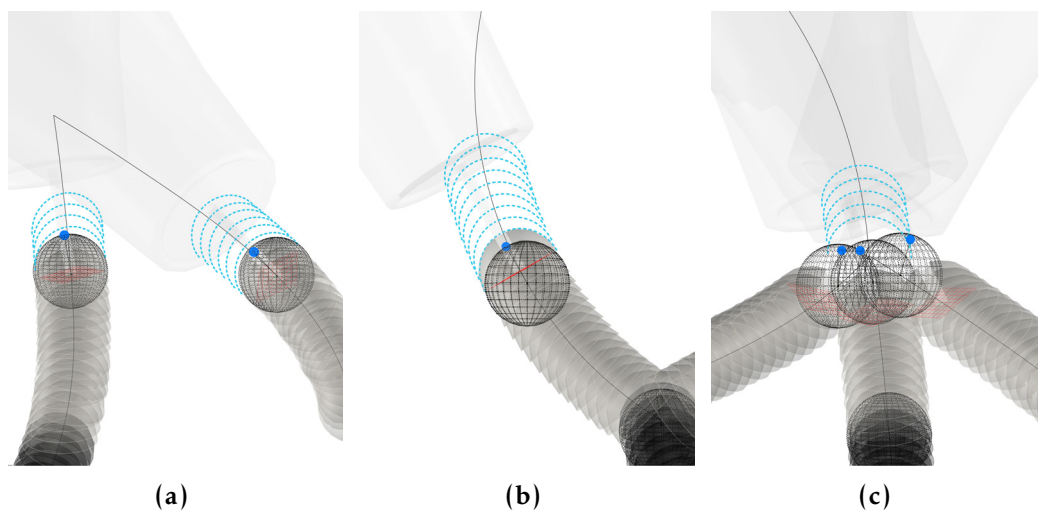
Figure 5.33: *Reconstruction of measured data for paths on-track showing search frames (in red), recorded coordinate point (in blue), reconstructed sphere (in black), expected printed seams (in gray), to-be-printed seams (in cyan): (a) Measurement is done half-way of the path. The recorded point lies inside the expected printed seam, the path is on track. The deviation is a negligible 0.2-0.3 mm, and the print can continue as planned, (b) Measurement is done halfway of the path. The recorded point lies inside the expected printed volume and is behind its expected location by 1.5 mm, the path is on track. The next print section needs to be adapted by adding an additional target frame using the extend path method, and (c) Measurement is done at the end of the path. The recorded point lies outside the expected printed volume and is ahead of its expected location by 2.3-3 mm, the path is on track. The next print section needs to be adapted by removing redundant frames with the trim path method.*

For the path's survey, printing frame targets were used as search targets on most occasions, except when additional orientations were needed and not available in the pre-computed data (Figure 5.33). The advantage of using existing pre-computed data for the search, i.e., printing frames computed in the slicing step using `Path planning`, is that these targets are already verified for reachability and free of collisions. Otherwise, a single pose IK and collision check could be performed using the `COMPAS FAB` pipeline. Recorded outcomes can be organized into the following groups:

(a)   (b)
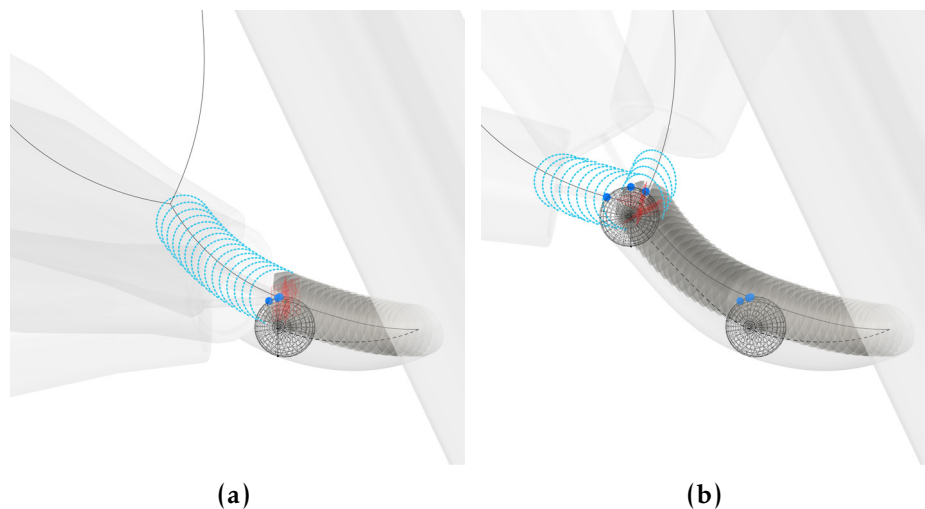
Figure 5.34: *Reconstruction of measured data for a path that is off-track showing search frames (in red), recorded coordinate point (in blue), reconstructed sphere (in black), to-be-printed seams (in cyan): (a) Measurement is done half-way of the path. The recorded points lie inside the path but with a relatively high offset (approx. 4mm) from the expected location, the path is off-track. Because the printed path presents a high overlap with the to-be-printed seams, production is continued with pre-computed data with no adaptation, and (b) Measurement is done at the end of the path. The recorded points lie inside or ahead of the path, the path is on track. The path direction was compensated by the direction of printing, resulting in a smaller deviation than the immediately previously recorded halfway measurement.*

1. **Path is on track on approximately expected location** Deviations below 1 mm were considered negligent and production was continued as planned without adaptation (Figure 5.33a).

2. **Path is on track behind of expected location** When the deviations are above 1 mm and the build is behind the expected location, an adaptation with the *extend path* method (Section 4.3.6.4), i.e.,

addition of printing targets by repeating previously executed frames, was made (Figure 5.33b).

3. Path is on track ahead of expected location When the deviations are above 1 mm and the build is ahead of the expected location, an adaptation with the *trim path* method, i.e., removal of printing targets by culling overlapping targets, was made (Figure 5.33c).

4. Path is off track In these cases, an evaluation was required. To decide if the next print job could be printed without an adaptation of the curve and subsequent re-slicing and sorting operations, the overlap between as-built and to-be-printed paths was studied. Given that the volume of the path to be printed overlapped by at least 50 percent with the cross-sectional area of the as-built path and that this overlap occurred on the top side of the printed volume, it was possible to continue printing with the current pre-computed data[17] (Figure 5.34).

These outcomes show an ideal scenario where paths are on track or off track without dependencies. In all resuming operations, the pre-computed target frames were used to continue printing. Off-track paths with dependencies were not found in the current experiment, however, the pipeline provides a solution for these cases allowing a re-computation of the slicing and sorting steps during production (Figure 5.30).

The limited deviations could be attributed to different aspects of the design and process parameters. First, all the paths consist in positive slopes, where *printed* and *to-be-printed* targets generally meet in a positively oriented interface relative to the gravity vector, therefore, reducing the deformation of the seam. Cases with less positive or parallel orientations to the gravity vector present higher deformations (Figure 5.35). Second, success is also attributed to the slicing with path planning strategy and the minimization of the z axis deviation. Cases with higher z axis deviations present higher deformations (Figure 5.36). Third, appropriate printing settings, in particular, the consideration

---

[17]If the overlap would have occurred in the underside of the as-built path, this operation might fail due to gravitational forces pulling the fluid metal down.

of longer cooling times were critical to stabilizing the overall temperature of the print during production, resulting in less deformation. Fourth, the high-frequency use of touch-sensing additionally reduces an accumulation of deviations.

(a)

(b)

(c)

(d)
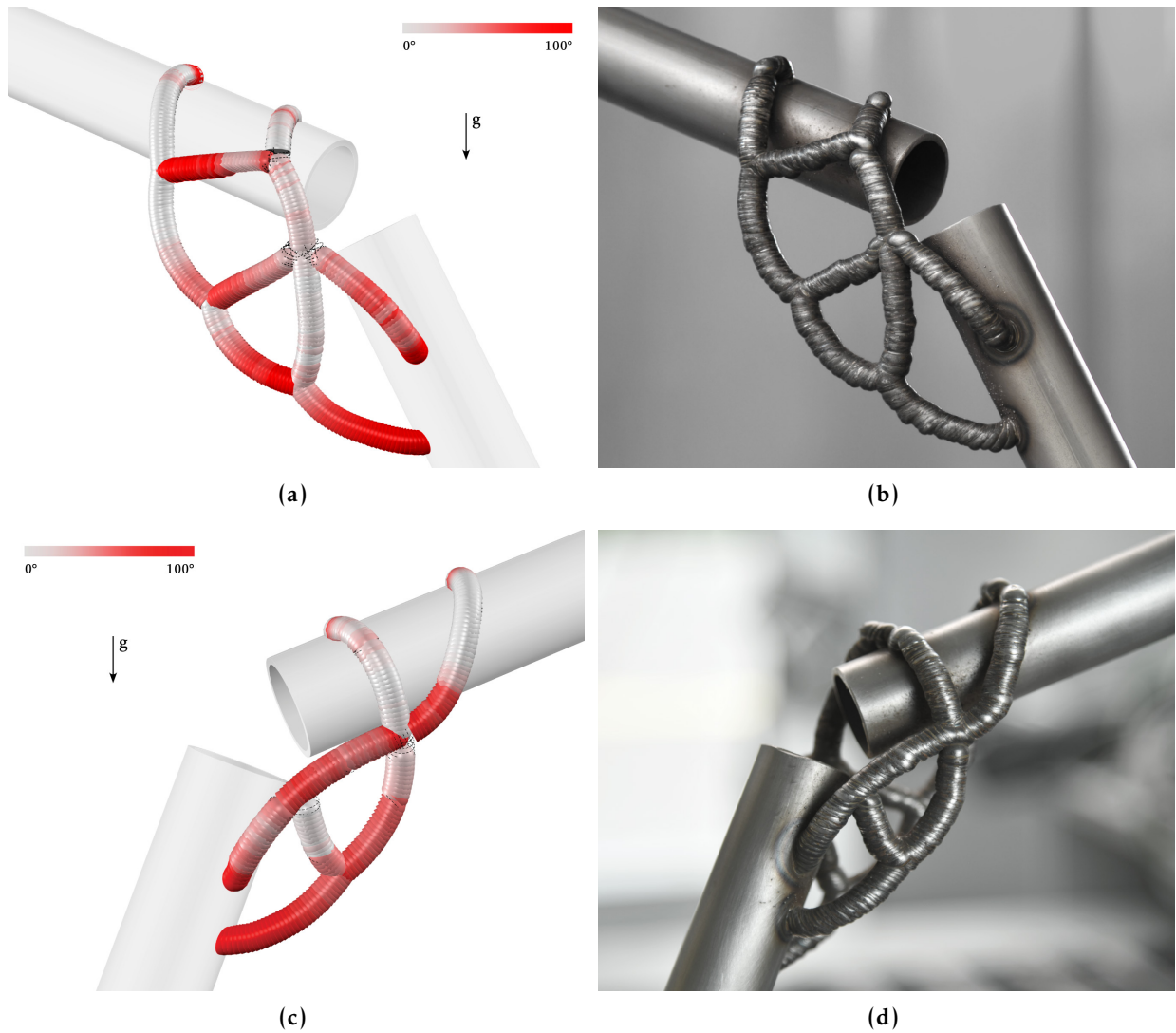
Figure 5.35: *Tool orientation relative to the gravity vector: seam interfaces aligned normal to the gravity vector in white and aligned parallel to the gravity vector in red, removed layers due to overlapping are shown in dashed lines.*

Following the adaptation strategies described in 4.3.6.4, cases 2 and 3 (Path is on track behind and ahead of expected location, respectively) were tackled with *extend* and *trim* path methods (Figure 5.33). In all cases, individual paths and branching conditions presented different challenges. For individual paths, continuity between frames proved to be a challenging aspect if trimming operations result in very different

(a)

(b)

(c)

(d)
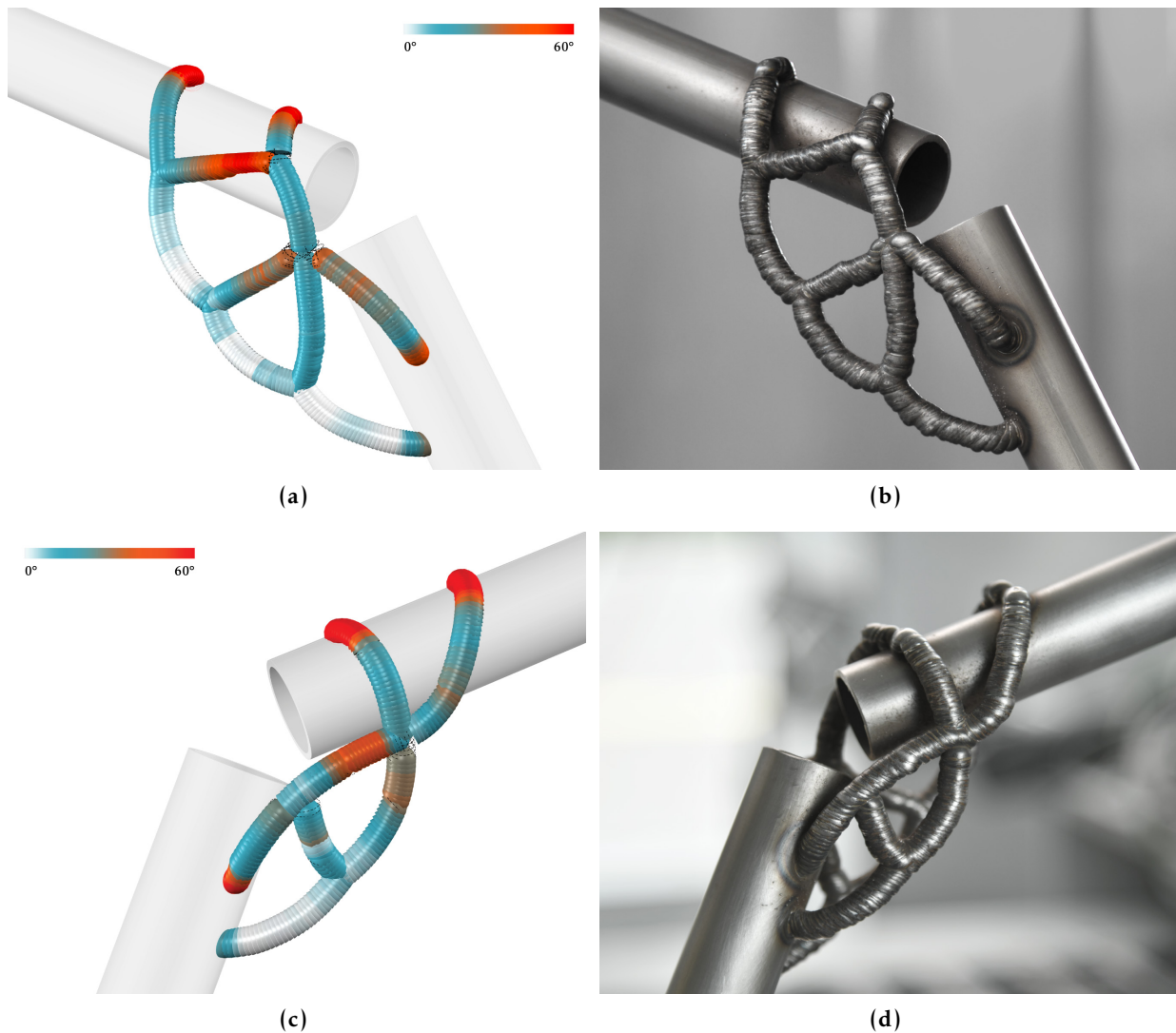
Figure 5.36: *Tool orientation relative to the build direction: seam interfaces aligned parallel to the curve tangent in white and deviated to the curve tangent in orange, skipped seams transparent.*

tool orientations. At branching nodes, continuity is also an issue, as it is hard to predict the exact shape that the next seam would take, therefore best-fit tool orientations are not guaranteed.

It is of interest that every adaptation of a path has a potential cost in terms of final performance and expression. The touch-sensing operation results in a different cooling time that the desired one, therefore a cross-sectional area variation is expected (Figure 5.37). As discussed in Chapter 3, these have a considerable effect on the material properties and the durability of the material 3.6.6.2 and 3.6.6.4. Potentially, these detrimental effects could be reduced by a close loop integration of the

touch-sensing operation, i.e., shorter operation time, and more control
over the seam formation.
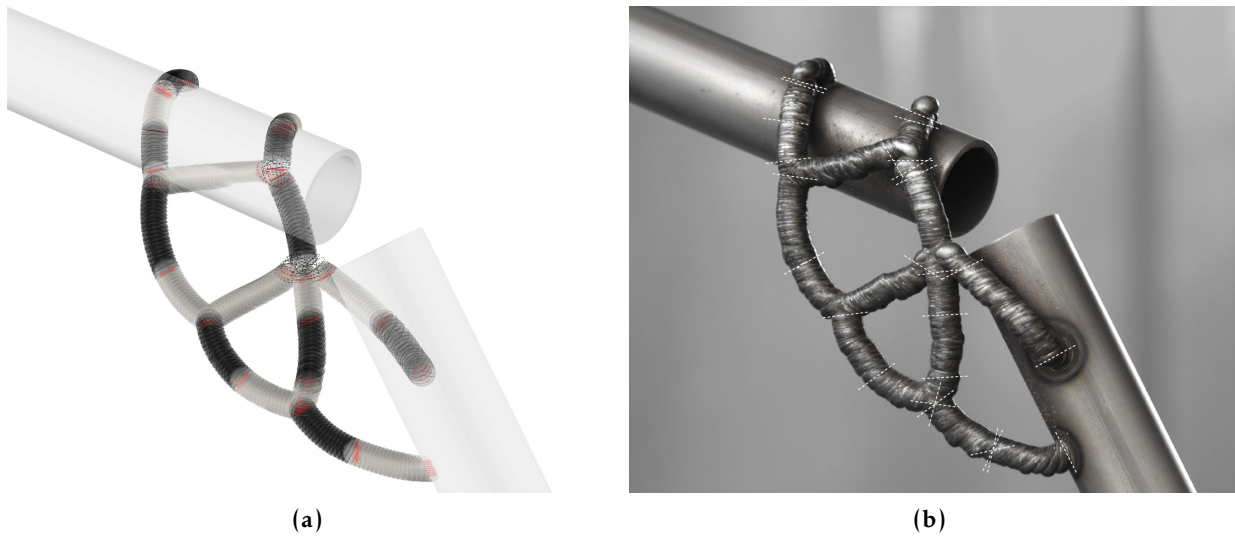
Figure 5.37: *Search procedures and adapted path results: (a) Search frames (in
red), and (b) Highlight on adapted layers.*

5.1.3   Discussion

Preliminary studies

The early adaptive connections explored the material depositions of
point-by-point and hybrid, IPWAAM connections; the X, T and C con-
nection types; and diverse connecting topologies and geometries. The
production of these demonstrators represents the most exploratory
phase of the project and led to the identification of key study topics of
IPWAAM connections:

First, it can be observed that the materiality of IPWAAM connections
strongly depends on the deposition type. Connections composed of
individual or intersecting paths present a filigree expression, which
contrasts with continuous deposition techniques such as the ones used,
for example, in the Takenaka connector (see Figure 2.10g)[18] or the
point-by-point *grape-like* deposition in Figure 5.2f. In addition, the
degree of control of the deposition technique, process settings selection
and admissible range of tool orientations, has a significant effect on the

---

[18]This could also be attributed to the amount of material present in both cases, a
comparison worth looking into.

expressive qualities (e.g. Figure 5.3b vs 5.3d). However, these examples only glance at the possible material qualities of IPWAAM.

Second, in the proposed pipeline, the typology of the connection becomes an irrelevant design constraint. Even without a sophisticated workflow, there was no adaptation of the pipeline made to handle different configurations of the objects to be assembled. In other words, the design and production procedures would not be modified based on the type of the intervening section of an element, i.e., a face or a butt, to be joined[19]. Typology, however, would be a highly relevant characteristic for structural assessments, as well as to validate the performance of the connections in comparison with other known joining techniques.

Third, the more dependent and probably more pressing aspect to investigate is the topology of the print paths. Different topologies, such as individual versus branching paths, have a large effect on workflow and data handling, adaptive measures, and heat control. By either limiting the types of involved printed objects or understanding better the edge cases, this topic should be made central in upcoming work.

Finally, although it was not here systematically investigated, the scale of the connection can be identified as an important aspect to study in itself. It is expected that larger design space volumes would result in more complex topologies (see, for example, a comparison between connection results in Figures 5.21a and 5.21b). The size of the design space volume depends on many aspects, including the distance between parts to connect, the typology of the connection —C connections tend to require larger spaces to avoid positioning material too close to the elements' edges—, the load to carry, and the skewness —the lack of alignment between parts extends the space needed to connect them—.

Pipeline studies

The simple, functional and adaptive connections presented a composable approach to the development and employment of a computational detailing pipeline for IPWAAM connections. The physical and virtual results have shown the integration and dependencies of components. Noteworthy topics concerning these experiments are discussed below:

---

[19]This point strongly disagrees with current connecting-types categorizations in use in various industries and literature (e.g., Roth, 2000).

Explicit approach to detailing   As claimed in the introductory chapters, detailing consists of coordinating knowledge dependencies related to the successful interfacing between the elements of construction. In contrast with conventional approaches to detailing where this coordination happens implicitly as the architect's capacity to coordinate a network of experts, the proposed computational pipeline aims to expose the communication between knowledge domains and turn it into a readable, scalable, and customizable software architecture (see, for an example, Figure 6.1).

The cumulative demonstrators for simple, functional, and adaptive connections aimed to validate this approach. As new needs and degrees of understanding of the specific detailing challenges with IPWAAM came in, new software components entered the pipeline to integrate incoming knowledge domains. This, in turn, requires more communication channels, interfaces and evaluation loops between the different components of the pipeline.

The Simple connection presents a basic scenario for a component-based IPWAAM detailing pipeline (Figure 5.12). Some features, for example, the connection's functionality, are handled intuitively without expert input. Other features, for example, fabricability before and during production, are explicitly integrated into the pipeline. The connection is *designed* based on implicit knowledge and visual feedback.

The Functional connection presents a scenario familiar to open-loop digital fabrication projects. Here, the mechanical properties of the material are known, which increases the available knowledge on its material behavior, propagating additional constraints in the form of functional requirements in the design of the connection. This in turn requires the involvement of additional structural and fabrication experts, or, in other words, material distribution and path slicing software components. The connection is *computed* based on available knowledge, and its performance can be measured according to specific metrics or expert domains. Improvement, however, can only be made at the design phase, as the knowledge pipeline is disconnected once a solution is found and the design is sent for fabrication. Any new further knowledge or valuable information for the design would be taken implicitly without corroboration of its dependencies.

The Adaptive connection presents an ideal digital fabrication scenario where design and production contribute to a shared feedback-based pipeline. Here, the design process can benefit, through the input provided by the production components, from new information at key instances of the production process. On its side, logistics benefits from an informed design, i.e., reducing the number of unknowns during the construction phases.

Single-task versus compounds The proposed approach has been implemented as a component-based software pipeline, due to its conceptual proximity and shared aimed properties -responsive, scalable, asynchronous, resilient through containment, composable- to reactive programming[20] A critical aspect of the component-based approach is to understand the required granularity of components. In the presented demonstrators, and with the aim of deconstructing and exposing the inner parts, only single-task components were used. However, components with strong dependencies would benefit by merging and creating new compounds.

As briefly mentioned, the `Material distribution` component should consider the integration of WAAM constraints such as the diameter, wall thickness of paths, maximum advisable tool orientations, and overhang constraints. With this, the `Path generation` component with path finding method could be entirely merged with the `Material distribution` or transformed into a fine-tuning step.

The increased geometric complexity of the functional and adaptive connections shows that the `Path slicing` and `Path sorting` components present strong dependencies. For the current status of the software implementation, the `Path slicing` with path planning remains a time-consuming step –depending on the choice of algorithms–.[21] Therefore, the isolation of the `Path sorting` step is practical in providing a rapid response through reusing pre-computed data during production when adaptation is needed. Provided that near real-time

---

[20]See *The Reactive Manifesto* for the reasoning behind this approach (Bonér et al., 2014).

[21]A similar time-performance challenge is faced by the `Robot reachability` and the `Material distribution` components, which could provide more flexibility if they would be able to be re-computed during production as needed.

planning could be done online, during production, these components would benefit from a tighter integration.

Composability   During the development of these experiments, components were added as needed and executed with a certain flexibility in the order of operations. Most notably, the simple and adaptive connections present two different approaches where the design is not yet fully computed once production starts (Simple connection) and where the design is pre-computed and only minimally modified during production (Adaptive connection). Both extremes are theoretically valid but expose drawbacks. On the one hand, and provided a scenario where the computation time is negligible, delaying the computation of the connection once the elements have been positioned would result in a fully adaptive approach, allowing large divergences from the original plan. However, this could only be functionally valid if an evaluation loop ensures the validity of the design during production, which could be time-consuming or practically impossible due to the nature of building procedures and regulations. On the other hand, the pre-computed version reduces uncertainty during the production phases but requires the elements to be placed within a certain tolerance (which is compatible with a robotic assembly system).

Alternative methods for automatic path generation   As discussed in chapter 4, the divergence between the volume of the isomesh and the skeletons could be addressed with an alternative path finding strategy that incorporates control over the volume ratio with a combination of point-by-point and continuous paths. Alternatively, the TO task could constrain the maximum cross-section of the resulting members to match a specific IPWAAM printing process characteristic. An evaluation component such as the one proposed in Section 4.3.4.1 should be integrated into the pipeline after the path generation step to address the validity of the final path curves in terms of their functional requirements.

Performance   Although the mechanical strength of the presented connections has not been tested yet, a series of characteristics of IPWAAM were identified as critical:

It can be claimed that exit sections are the least straightforward section of a connection, and a topic of investigation in itself. First, it is at the exits where the final accumulation of deviations is shown, and therefore these sections always require more touch-sensing operations and adaptations. Second, it is at this location where the actual load transfer is done, then their compliance with requirements is higher. Even small deviations from the expected result can be detrimental to the successful deposition of material (this can even be assessed visually, for example in Figure B.16f). For gaps between the printed paths and the substrate of max. 5mm, it is possible to use continuous depositions to connect them. However, larger gaps require discrete exits: building a point-by-point exit section. In sum, exits are critical parts of IPWAAM connections to validate in place printing.

The Heat Affected Zone or HAZ on the base and target elements needs to be taken with precaution (A HAZ is visible, for example, in Figure 5.38a). The whole design can fail if the wrong CTWD or WAAM settings are used in the entry or exit sections. Even if not failing, excess heat at these locations could potentially reduce the force transfer capacity as the base material would be reduced in strength. The use of touch-sensing and correct process parameters are then particularly vital at entry and exit points.

In sum, although in its early technological development, these experiments demonstrate that self-supporting connections between non-touching, non-machined steel elements can be designed and produced using the IPWAAM technique and adaptive detailing. This series of promising results leads to the study of the joining and detailing strategies in the context of larger assemblies.

(a)

(b)

Figure 5.38: *Comparison of simple and adaptive results: (a) Simple connection, and (b) Adaptive connection.*

5.2 Structures with IPWAAM connections

How do we design with IPWAAM and adaptive detailing?

The previous chapters and sections have discussed the IPWAAM joining technique and the adaptive detailing (AD) pipeline to design and produce connections between two elements. This section discusses the application of these techniques and pipeline in the context of robotic assembly of spatial structures. Ultimately, these exercises aim to hypothesize how to design with IPWAAM in the context of robotic-based construction scenarios.

Organization of this section The demonstrators consist of two virtual experiments that explore different aspects of designing with AD and IPWAAM[22]: the first demonstrator, the Base structure, proposes an experimental setup for including IPWAAM constraints to design a spatial structure (Figure 5.39a). The second demonstrator, the Structure with adapted sequence, is a set of sub-assemblies of the base structure with alternative sequences of assembly (Figure 5.39b-5.39d). These alterations require a reconfiguration of the planning scene and result in different reachability constraints and, in turn, alternative connection designs.

The results of the speculative experiments are then reviewed in Section 5.2.3 with focused discussions on their design implications at the global -structure- and local -connection- scales.

5.2.1 Base structure

This experiment speculates on a basic generative design workflow for structures with IPWAAM connections. This workflow is informed by a real-world robotic assembly setup and a fictive design brief:

---

[22]The structure demonstrator was originally planned to be a physical experiment but turned into a virtual demonstration during the 2020 COVID-19 pandemic. However, this resulted in a fruitful outcome as the possibility of exploring structures' variants instead of focusing on one single output allowed the work to gain critical knowledge in the capabilities and limitations of the computational detailing pipeline.
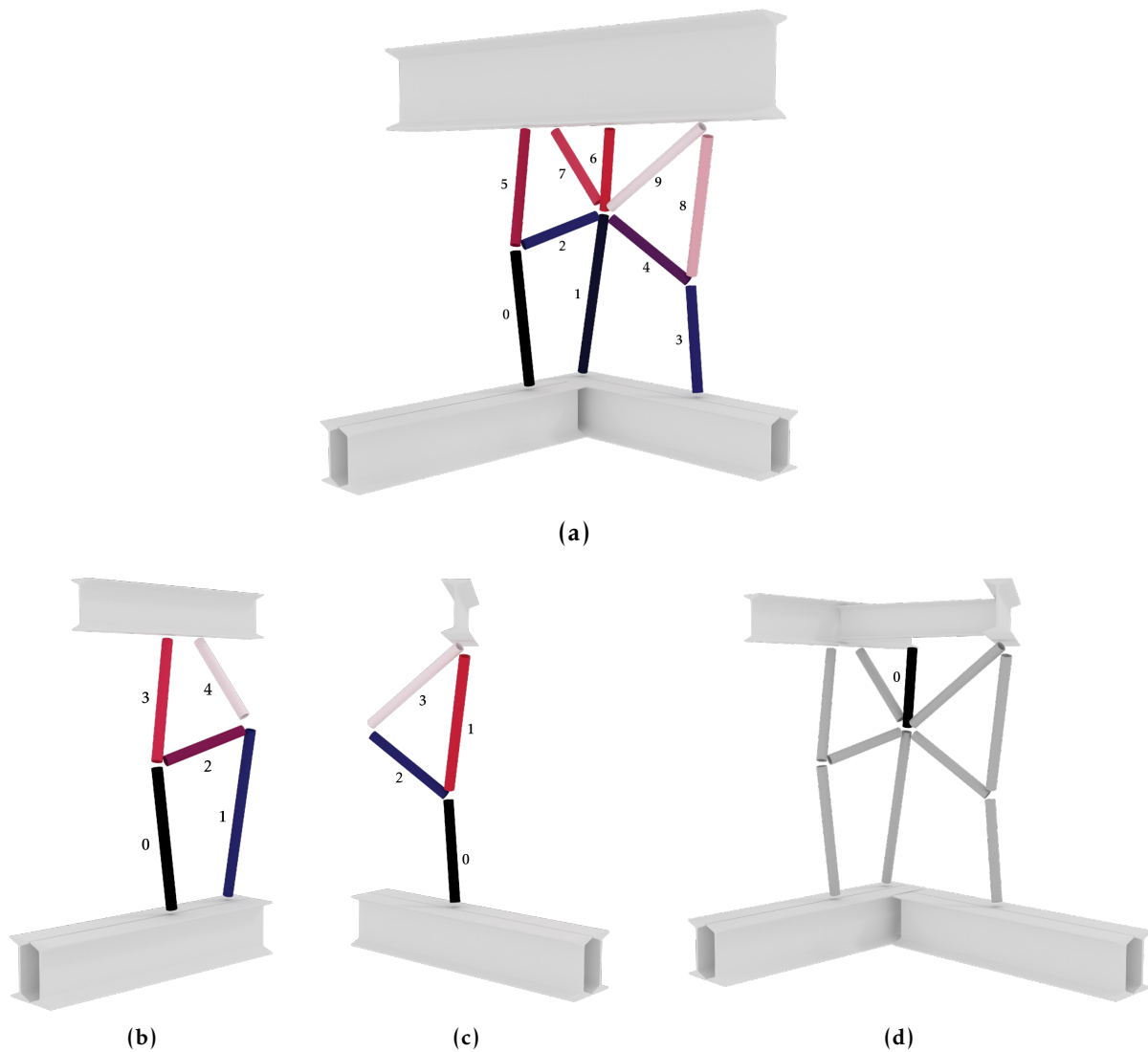
Figure 5.39: *Structures with IPWAAM connections: (a) Base structure, (b-d) Structure with adapted sequence: (b) Sub-assembly 101, (c) Sub-assembly 102, and (d) Sub-assembly 103.*

The robotic assembly setup   The structure is planned in the existing multi-robotic setup located at the Robotic Fabrication Laboratory at ETH Zurich comprised of two robots: one assembly robot and one welding robot (already introduced in Section 3.2).

The design brief   The structure aims to support the static load of an I-Beam with a small number of elements joined with IPWAAM connections.

The proposed generative workflow addresses the design brief using a multi-objective optimization (MOO) approach including design and

Figure 5.40: *Robotic assembly setup with welding robot on the left and assembly robot on the right (in gray) and unconnected elements of the base structure (in white).*

fabrication specifications as goals and constraints. The results consist of a pool of designs with associated fabrication and performance metrics. From this pool, and based on these metrics, one structure is finally selected as the *base structure* to be further studied.

The workflow is structured in the following parts:

1. Robotic assembly setup

2. Design and static analysis setup

3. Adaptive detailing setup

The first two setups are applied at the structure's scale. The adaptive detailing setup, i.e., the pipeline introduced in Chapter 4, is applied to each connection independently. The three setups have independent and chronologically consecutive software pipelines.

5.2.1.1 Robotic assembly setup

The first part of the workflow prepares the ground by *setting up the assembly scene*. The assembly setup consists of a 5-meter-long linear axis that supports an assembly and a joining robot. Both robots have identical technical specifications, except for their end-effectors. The assembly robot is equipped with a pneumatic gripper, and the joining robot is a CMT welding robot (previously introduced in Experimental setup).[23]

There is a large number of aspects to look at in a robotic assembly setup that can be used to inform the design of a structure and its connections. This workflow takes into account the following process characteristics:

Robotic procedures   The robotic assembly consists of a pick-and-place and an `IPWAAM` joining procedures. The assembly robot carries the elements from the picking position to their final position, and the joining robot connects the elements in place while the assembly robot holds them. The availability of two robots and the assignment of the assembly and joining procedures to each of them determines that elements are assembled one by one, and implies that the structure is stable on its own after each connection is completed and the gripper of the assembly robot is released.

Robot controller setup   The robot controllers used in this setup are independent of each other and perform assembly and joining tasks in separate procedures. This entails that the path planning programming is done for each robot independently, considering the second robot as a static collision object.

Robot workspace   The maximum reach of both robots from their calibration position is 2.55 m (*IRB 4600 Data* 2022). This reach is greatly extended by the 5-meter-long linear axis. The maximum reach is used to determine the size and location of the building volume.

---

[23]The `Planning Scene` was built by Dr. Romana Rust in a typical COMPAS FAB workflow using ROS as a backend and run inside Rhinoceros/Grasshopper (Casas, Rust, and Lytle, 2018). The gripper end-effector design was developed for the project *Robotic assembly of complex lightweight structures* (Parascho, 2019).

Robot payload The assembly robot's maximum payload is 40 kg; therefore, the mass of the elements needs to be within this number, ultimately constraining the length-to-cross-section ratio.

IPWAAM reachability A high degree of reachability on the interface between elements is of special interest for IPWAAM. The location of the connections, therefore, should be designated based on areas that are highly reachable by the welding robot[24].

While all of these aspects are relevant to designing a structure with IPWAAM connections, in the design of the Base Structure most of them were only implicitly taken into account, except the *IPWAAM reachability* that was explicitly used in the generative workflow as a design driver.

5.2.1.2 Design and static analysis setup

The second part of the workflow consists of a generative design setup to create, evaluate, and rank possible structures' solutions. This setup is built with the Grasshopper's plugins `Karamba3D` for structural analysis (Preisinger and Heimrath, 2014), and `Octopus` for multi-objective optimization (MOO, Vierlinger, 2012), based on their own prototypical examples for "Optimization of an Irregular Structure" and "Optimization of Column Positions" (Preisinger, 2014a; Preisinger, 2014b). In a nutshell, the MOO design and analysis setup searches for bar configurations within a design space, analyzes each solution in terms of its structural performance and outputs a range of optimized trade-off candidates based on the structural performance metrics. The MOO setup can be broken down into the following steps:

Step 1. Create design variables

Step 2. Structural analysis and optimization

Step 3. Design optimization

Step 4. Review and final selection

---

[24]This reasoning is built on the following assumptions: the higher the reachability of a location, the larger the design space for material distribution, and therefore, the higher the chances to create optimal, as short as possible, IPWAAM paths.

Step 5. Verification and tweaking

Step 1. Create design variables

The inputs formalize the characteristics of the robotic assembly setup described in the previous section (5.2.1.1):

Building volume   First, a building volume where the structure will be fabricated needs to be defined. In this case, it is a 1 m x 1 m x 2 m boundary located between the two robots. The x, y and z coordinates of the boundaries of the building volume are formalized as design variables in terms of boundary domains where the structure can be placed.

Node reachability   Second, because the connections are built in place, the positions of the nodes need to be within the robot's reach. To determine feasible locations for connections, a reachability map of the welding robot is calculated inside the building volume. This step follows the tool accessibility and robot reachability methods presented in Section 4.3.1, here applied to a *global* boundary space (Figure 5.41a).[25]

A threshold is set to filter the reachable points that have at least a minimum number of reachable configurations, as shown in Figure 5.41b. The goal of this step is to ensure that the end points of the bar elements of the structure, where the WAAM connections will be printed, are highly reachable. As the IPWAAM technique requires a high degree of flexibility in the tool orientation for printing in the collision-free space, a high degree of reachability around the nodes' location is needed. The x, y and z coordinates of the most reachable points are used later on as design variables.

Node types   The reachable nodes are filtered in *load*, *freestanding* and *support* points, based on their location in the z axis (Figure 5.42b). Furthermore, nodes are grouped in non-overlapping regions to avoid them being positioned in the same locations (Figure 5.42b).

---

[25]A reachability map of the assembly robot could also be applied at this stage, however, in this workflow assembly is only *checked* at the end of the generative workflow.
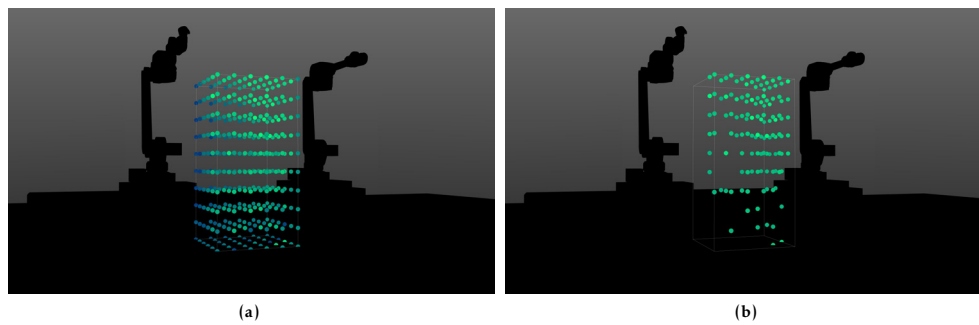
Figure 5.41: *Node reachability: (a) Robot reachability map of the building volume, and (b) Selection of most reachable nodes.*

Connectivity   A connectivity is forced between the support points and the freestanding points, and the freestanding points and the load points. These reachable points are assigned as the end points of the linear axes that represent the bar elements (Figure 5.42c). The goal of this step is to ensure that the endpoints of the elements of the structure are evenly distributed between load, freestanding and support regions.

Step 2. Structural analysis and optimization

The structure's purpose is to support the static load of a steel construction element, the I-Beam, with a series of steel tubes of circular cross-section elements.

Model   The design model is translated into a Karamba3D structural model (Figure 5.42d). All supports and nodes are considered fully fixed[26]. The I-Beam is considered as four point loads directly applied on the "load" nodes and a gravity load is additionally applied. Structural steel S355 is chosen for the cross-section selector.

Analysis and optimization   To reduce the complexity of the experiment, a minimal number of elements and connections is preferred. To formalize this requirement, a minimization of the number of elements together with a maximization of the cross-section utilization are included inside the analysis loop with the `Karamba3D`'s Bi-directional Evolutionary Structural Optimization (BESO) and cross-section optimization components.

---

[26]This aspect could be studied further, considering the ductility of the IPWAAM connections.

(a)

(b)

(c)

(d)
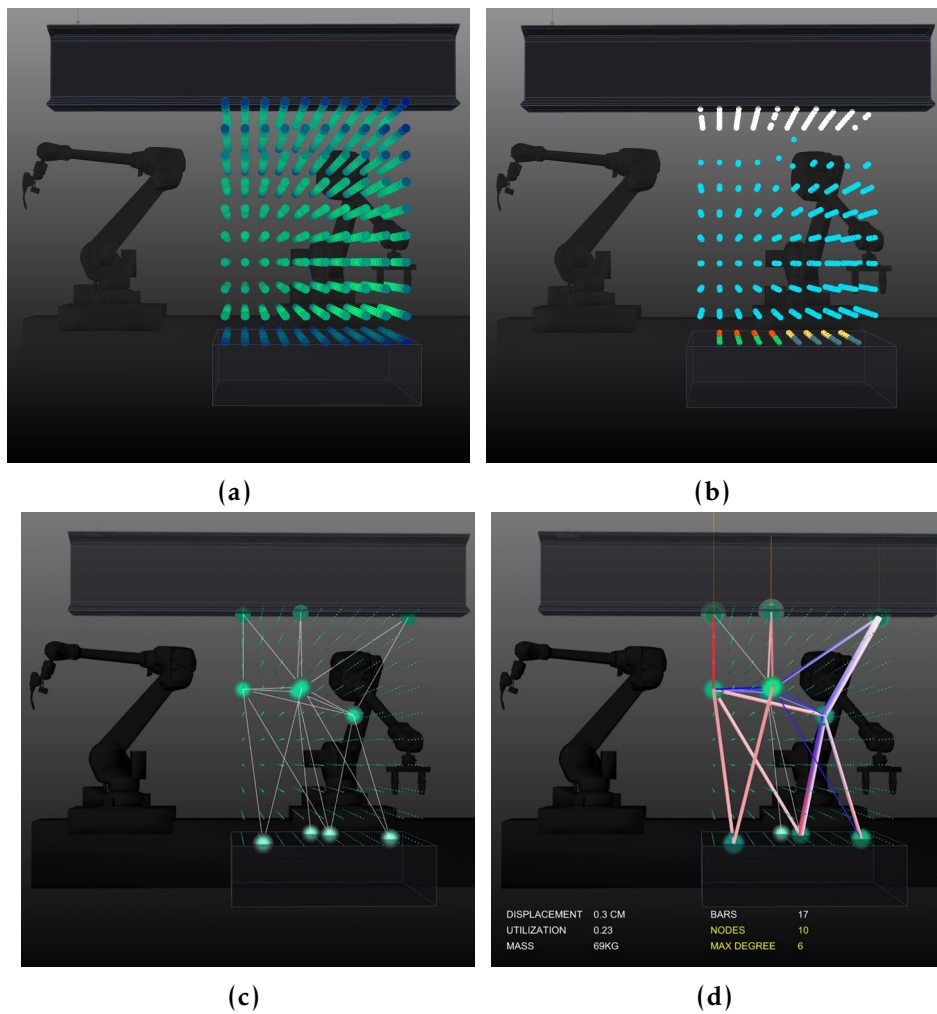
Figure 5.42: *Node types and connectivity: (a) Robot reachability map of the building volume, (b) Categorization of load (in white), freestanding (in cyan) and support (in many colors) points. Support points are further categorized in non-overlapping areas, (c) Random selection of highly-reachable points from the load, freestanding and support points with connectivity, and (d) Generated structure.*

Then, this step's goals are:

- minimize the number of elements
- select an optimal cross-section for each element

Step 3. Design optimization

This step assembles all the intervening numerical objectives and constraints:

Objectives The main design goal is to minimize the overall material use and maximize the overall structure's performance. One way to formalize these combined goals is to define an objective function with two fitness values to minimize: the total mass of the structure and the total displacements. Both mass and displacements are outputs of Step 2. Structural analysis and optimization, and are used as objectives in the main `Octopus` component to run the MOO algorithm:

- minimize the overall mass
- minimize the total sum of all displacements

Design variables Here, the x, y and z domain and coordinates of the building volume and reachable points created in Step 1. Create design variables are used as design variables or, in evolutionary terms, genomes, in the generative loop. All the genomes are assembled into the `Octopus` component and randomly tested during each MOO loop.

MOO loop During the MOO loop, x, y, and z coordinates inside the building volume are randomly changed, selecting at each iteration a set of —support, freestanding and load— reachable nodes that are treated as endpoints of the elements of a structure. For each structure, a static analysis is performed as described in Step 2. Structural analysis and optimization. Optimizing for minimum values of the overall mass and displacements the best genomes are selected over time to favor well-performing structures. At each iteration, structures are ranked and sorted according to their performance metrics.

Step 4. Review and final selection

Once the optimization converges, the `Octopus` viewer can be used to revisit the pool of structures with the best ranking. Perspective views of the structures with their associated values for each metric are finally plotted next to each other for comparison and interpretation (Figures 5.43-5.44).

The following design metrics are then used to review and inform the final selection:
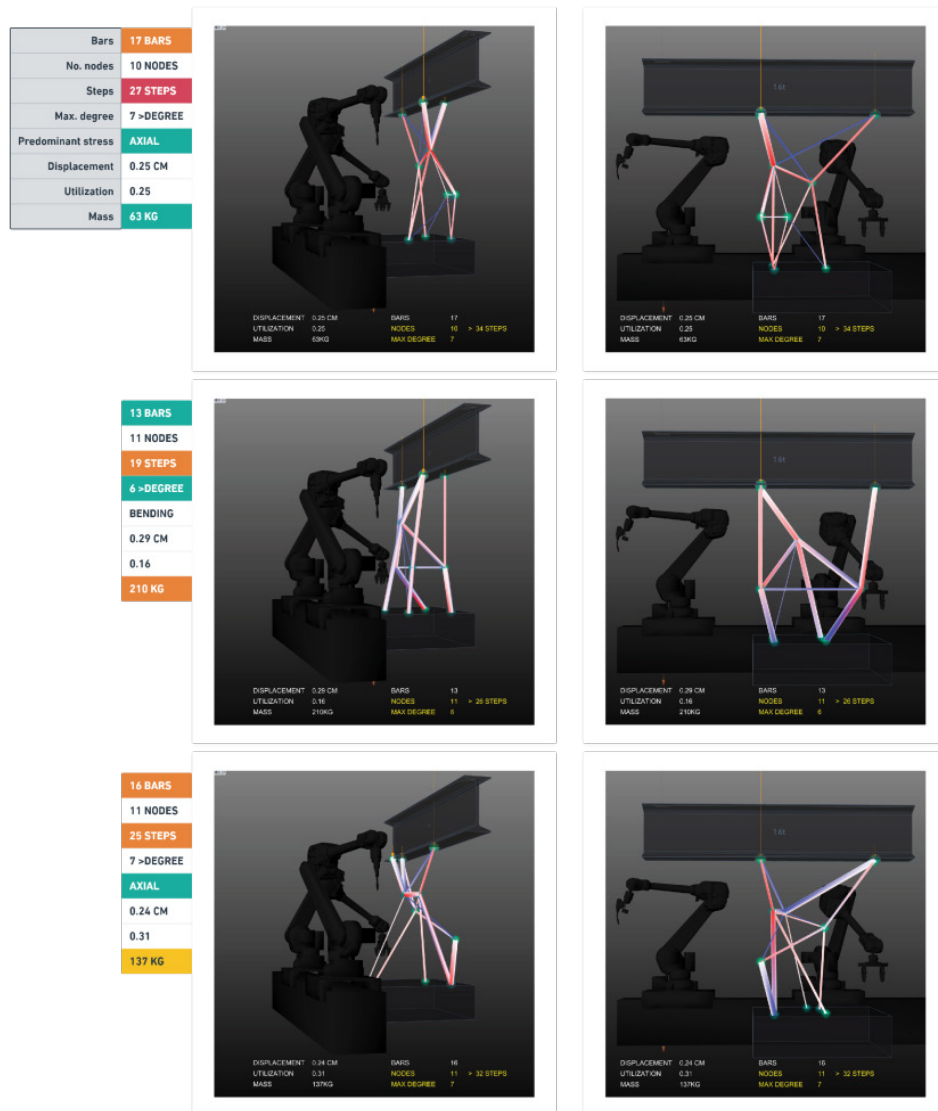
Figure 5.43: *Pool of best ranked and interesting structures. Highlighted metrics: number of bars, number of nodes, number of steps, maximum node degree, predominant stresses on bars, total displacement, total utilization, and overall mass.*
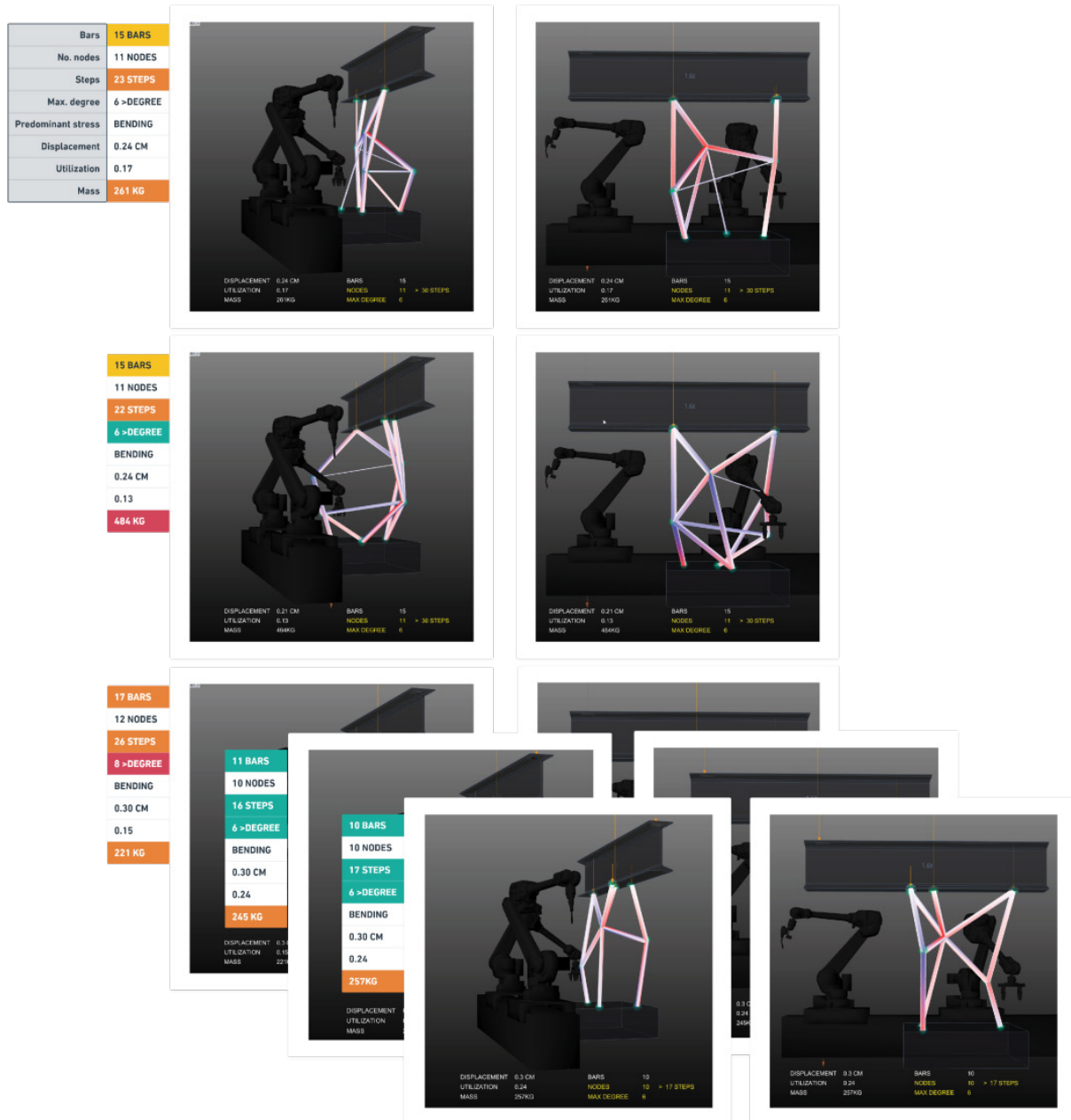
Figure 5.44: *Pool of best ranked and interesting structures including design iterations of the chosen one (on the bottom). Highlighted metrics: number of bars, number of nodes, number of steps, maximum node degree, predominant stresses on bars, total displacement, total utilization, and overall mass.*

Mass   The total mass of the structure in kilograms. The smaller the value, the least amount of material is required.

Displace-   The maximum displacement of the structure at the
ments   supports and/or mid-points of beams in centimeters. The smaller the value, the more statically feasible the structure results.

Utilization   The utilization is the ratio of the actual structural performance value to the maximum allowable structural performance value. Here, the utilization value is the maximum utilization of an element found in the structure as a percentage. The higher the number, the more efficient the use of the material is. The maximum allowed utilization is 1.

Predominant   Based on the axial forces and/or bending moments
stresses   contributions to the utilization of each element, an overall tendency of type of stresses in the structure can be determined.

Node degree   The minimization of the number of elements requested in Step 2. is in conflict with the complexity of the nodes. Reducing the total number of elements in the structure results in a consolidation of elements in less number of nodes. This consolidation can be measured in the *node degree*, which increases with the number of elements meeting in that node. The higher the node degree, the least reachable the node is, and therefore the more complex the connection results. This number should be kept as small as possible.

Number of   Connections with node degrees higher than two, i.e.,
connection   connections joining more than two elements, are called
steps   *multistep connections*, as they can only be fabricated in sequential "steps" after each additional element of the structure is assembled[27]. The sum of all node degrees

----

[27]In the assembly setup used here consisting of one assembly robot and one welding robot, elements are added one at the time.

in the structure is the total number of connection steps. The number of steps should be kept as small as possible to reduce the complexity of the experiment.

Number of   The total number of elements of the structure.
elements

The final selection prioritized a small number of bars, steps and node degrees and considered the elegance of the distribution of the bars –a combination of proportion and a sense of stability–.

Step 5. Verification and tweaking

Finally, once the base structure is selected, verification of its feasibility according to metrics not included in the generative workflow needs to be performed:

Sequence and assembly check   An assembly sequence needs to be determined and checked. To verify it, a robotic assembly simulation is performed in the Robotic assembly setup. If the assembly sequence does not pass the assembly check, an alternative sequence can be chosen. If none of the alternative sequences is feasible, then a different design needs to be picked.[28]

If the structure passes the assembly check, the Assembly is stored including all assembly process data, i.e., picking position, placing frames and configurations, and welding robot configuration.

Element overlap   In the translation from design to the structural model, a simplification was done considering the elements meeting at one singular point.[29]. At this stage, it is required to accommodate the element length, or its extension factor, so that the elements do not overlap with each other considering their sequence of assembly. At this stage, the maximum weight of each element is verified according to the robot payload.

---

[28]Note that this step could be used as well as a design driver instead of a check *a posteriori*.

[29]This simplification relates to the lack of a strategy for modeling the yet-to-be-calculated connections between non-touching elements.

The final base structure consists of a total of 10 bar elements, 1 I-Beam load, 2 sets of I-Beam supports, 10 nodes, and 17 connections or steps (Figure 5.40). Although the overall geometry of the structure results from an informed workflow, the result has not been tested in terms of structural performance.

5.2.1.3 Adaptive detailing setup

The base structure presents similar connection types as discussed in the Pipeline studies. There are connections in contact with I-Beams, and bar-bar connections, most relatable to corner-butt type connections. For the bar-bar connections, the complexity depends on the number of converging elements (nodes with degrees 2 to 6). Nodes with degrees greater than 2 are called *multistep connections*, as they need to be calculated in consecutive steps.

The adaptive detailing setup replicates the Functional connection pipeline with additional considerations in the context of a multi-bar `Assembly` (Figure 5.45).
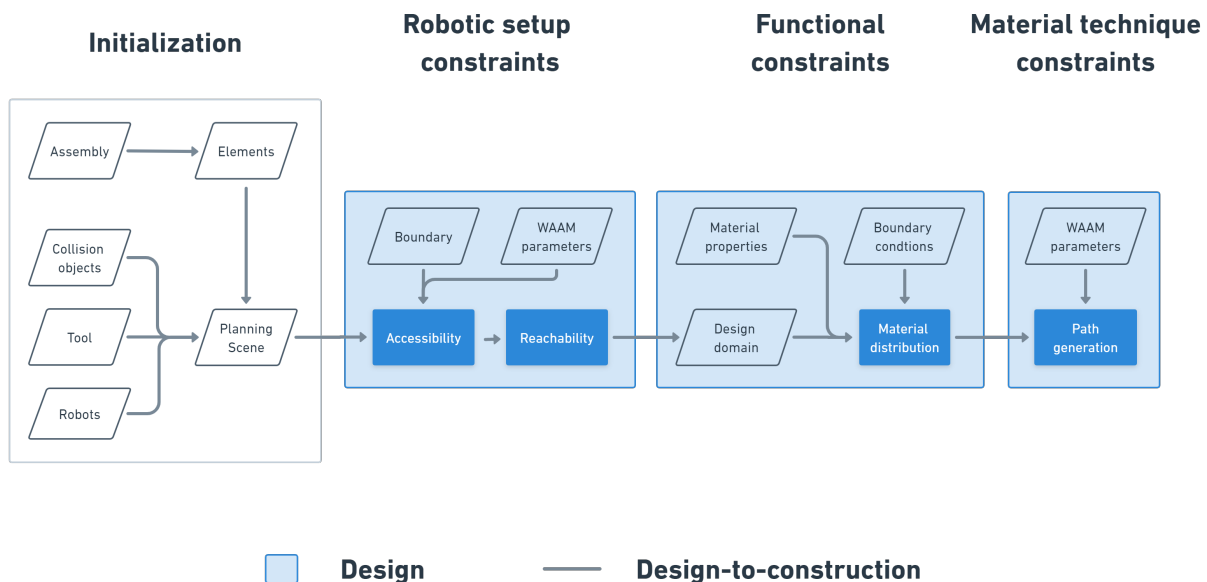
Figure 5.45: *Base structure pipeline*

The following additions take effect during initialization:

Topology   In order to later identify the elements and their connections, the topology of the structure needs to be known at this point and an

ID needs to be assigned to each connection. The topology of each connection is expressed in its ID, e.g., Connection 0-2 is the connection between elements 0 and 2, and connection [0,2]-5 is the connection between connection 0-2 and element 5. It is then possible to know if a connection is a single or multistep connection, and therefore its topology, by its ID.

Sub-assemblies and additional types of elements   For each assembly stage, an instance of the `Planning Scene` and a unique sub-assembly need to be created. For each sub-assembly, `Elements` are categorized into its respective types (Figure 5.46):

(a) Connection *[0,2]-5*   **(b)** Connection *[1,2]-4*   **(c)** Connection *[1,2,4]-6*
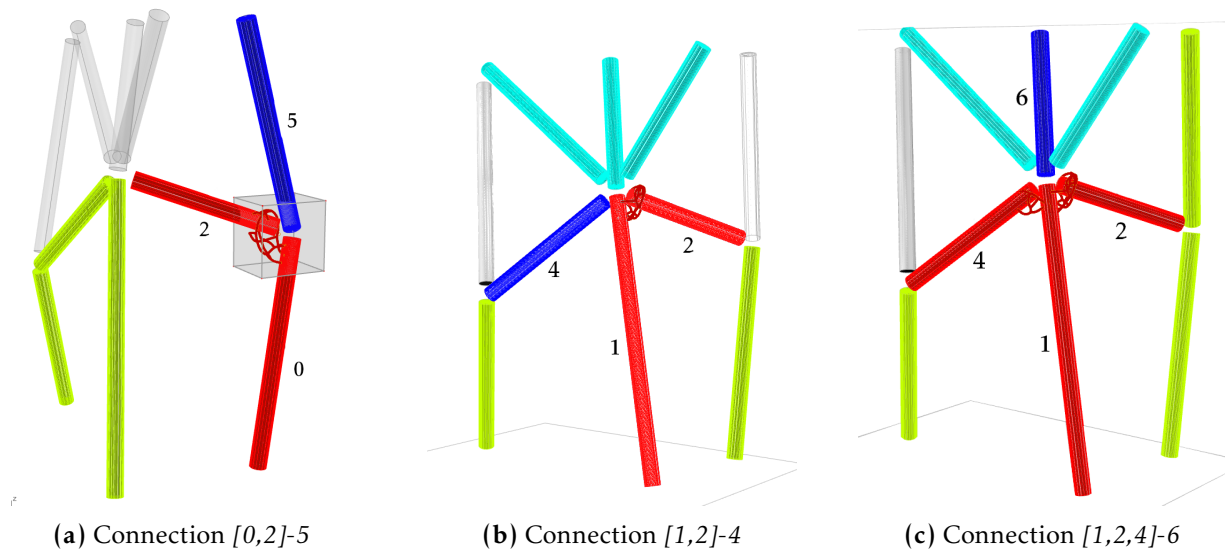
Figure 5.46: *Element types examples: base elements (in red), target elements (in blue), connection elements (in dark red), future elements (in cyan), collision elements (in yellow), elements that are not yet assembled nor participate in the current connection and are not present in the planning scene (in gray).*

> **Base elements**   `Elements` that have been already "placed" in the `Planning Scene` that are actively part of the connection and act as *support* elements.

> **Target element**   The single `Element` that will be "placed" at the current sub-assembly stage that is actively part of the connection as a *load* element.

Connection elements   Already "printed" `Paths` that are actively part of the connection and act as *support* elements.

Future elements   `Elements` that belong to subsequent assembly stages but need to be taken into account as placeholders to avoid a potential material distribution overlap on their expected location.

Collision elements   All other `Elements`, not actively participating in the connection that need to be taken into account as collision objects, i.e., all sub-assembly elements except the base, target, connection and future elements.

Robotic setup as additional static collisions   In addition, for each assembly stage, the placing configuration of the assembly robot needs to be included as an additional static collision object, as it serves as support of the yet unconnected element (Figure 5.47). As this is usually the greatest collision object close to the connection interface, the gripping position, which for circular cross-sections has a high degree of freedom, is a relevant variable to increase the reachability of the connection interface.
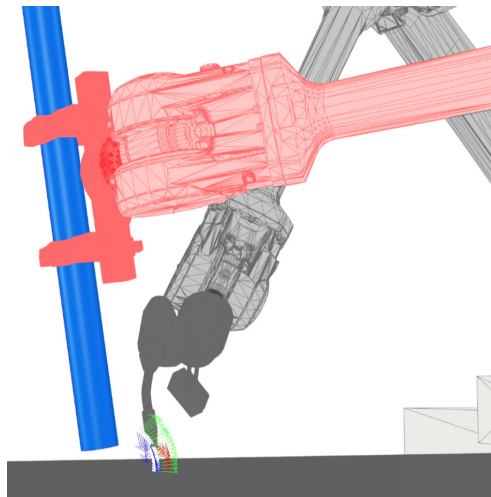
Figure 5.47: *Placing robot as collision object (in red)*

In sum, each connection requires a unique collection of collisions and reachable areas in the `Planning Scene`. This includes the assembly robot in its placing configuration (Figure 5.47), the elements of the

assembly that have been already or are being "placed" or "printed" at that assembly stage, and future elements that will be placed at later assembly stages (see element types in Figure 5.46). All these are loaded as obstacles, except the future elements that are considered as restricted areas where material cannot be placed.

Implementation and results

During the development of the base structure where the AD pipeline was systematically applied to 17 connection steps, several previously developed software components of the pipeline were modified to fit the needs of the assembly. The additions to the Functional connection pipeline components are summarized below:

Robot reachability   The multiplicity of obstacles -already placed elements, connections, and the constant presence of the assembly robot- significantly constrains the joining interfaces, particularly in multistep connections (Figure 5.48a) and/or advanced assembly stages (Figure 5.48b). As a consequence, the size, position, and orientation of the boundary object[30] become a harder guess. Because the location and specifications of the boundary object are important to collect relevant reachability data, additional control over the geometry and positioning of the boundary object were included (See, for example, Figure 5.48c).

---

[30]The boundary of the space that will be queried for Tool accessibility and Robot reachability to generate a reachable space to be later used as a design space for the connection

(a)   (b)   (c)
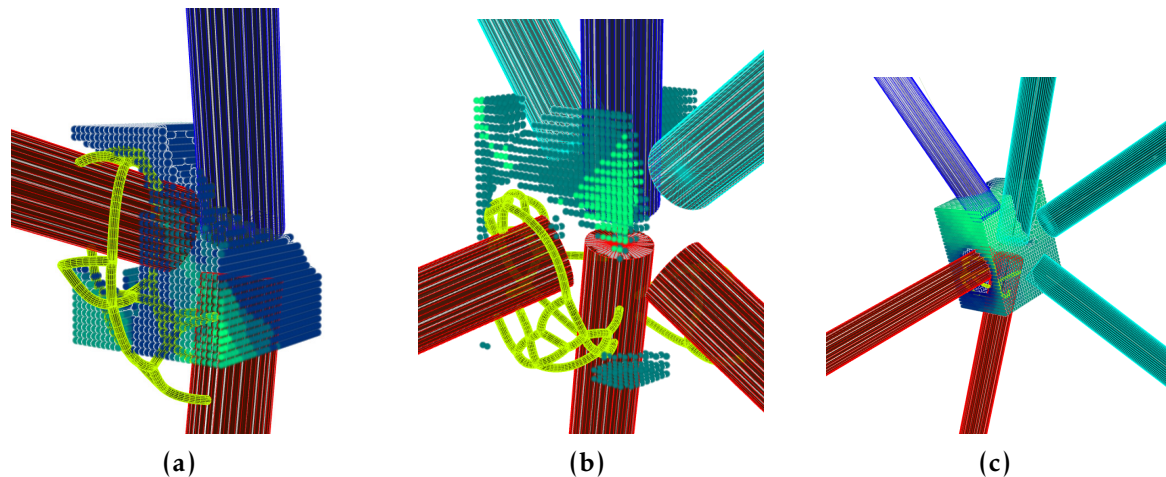
Figure 5.48: *Reachability in multistep connections: (a) Previous paths participate as collision and support objects (in yellow), (b) An over-constrained interface, only a few areas are reachable to place additional paths, and (c) A custom orientation of the boundary object and resulting reachable space.*

If the Material distribution accumulated on an extreme of the design space, the space was either wrongly positioned or too small. If the latter, additional reachable spaces were created and merged (see examples of compound reachability maps in Figures B.6a and Figures B.9a). In addition, smaller and medium-resolution reachable spaces were often calculated in order to run a low-resolution TO, to preview the material distribution tendency (Figure B.6a).[31] Based on the low-resolution feedback, a higher-resolution reachability map, that could include high-precision reachability data around the assembly elements, was calculated.

The accessibility settings were also modified for connections touching the I-Beam load. In these cases, the default base axis or base tool orientation from where the base frames are calculated was aligned *against* gravity.

Material distribution   To calculate each connection's material distribution, the sequence of assembly determines the loads that each

---

[31]With the current setup, it is not possible to run this step in a very low resolution. The marching cubes algorithm used to reconstruct the reachable boundary depends on the original data structure of the accessible space grid. It requires a certain resolution so that the resulting mesh is in full contact with the surrounding elements. This could be a good application of a non-homogeneous data structure, e.g., Octree.

connection receives. The implementation of this step is determined by the specificity of the current TO setup with the `t0pos` plugin, which only allows for a single load volume. As described in Chapter 4, other solvers allow for detailed and correct inputs such as reaction forces and moments. A simplification was therefore used to compute the cumulative "upstream load" as a single volume, i.e., adding the volumes of elements to be assembled, calculating the total weight that these elements contribute, and compensating that weight in kN/mass of the single target volume. As a result, each added element represents the cumulative load of the elements ahead in the sequence.[32]

Path generation   In multistep connections, the previously printed connection paths are now included as base elements and therefore considered as possible supports or *fitting* targets as in Figure 5.50h.
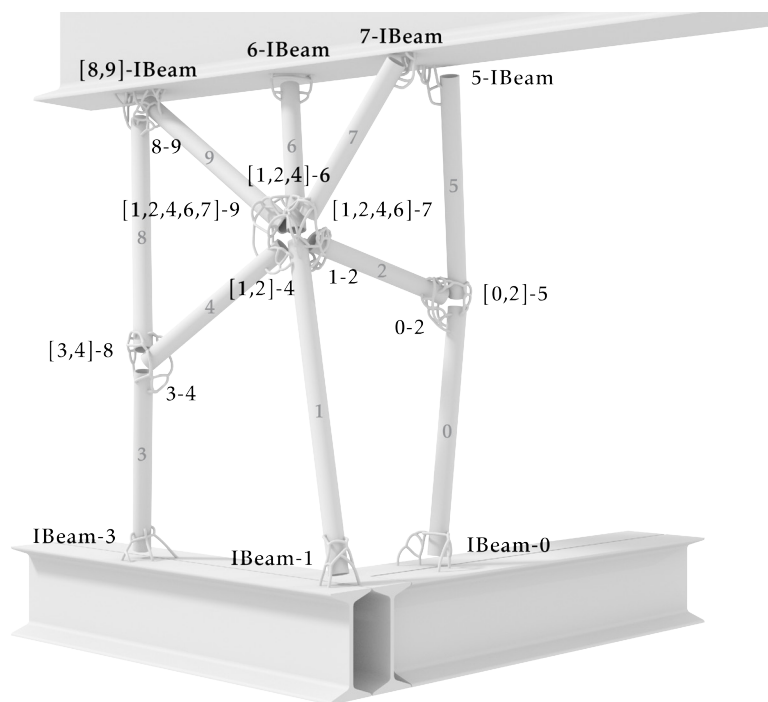
Figure 5.49: *Base structure: connections' IDs*

A selection of the results of the 10 connections calculated in 17 steps are shown in Figures 5.49-5.51, and the full set of results are shown in Appendix B. Figure 5.52 shows views of the final structure.

---

[32]A complete setup would not only consider the weight but the interactions of the whole `Assembly` at each assembly stage.

(a) *IBeam-1: Reachability map*

(b) *IBeam-1: TO and skeletons*

(c) *IBeam-1: Paths*

(d) *8-9: Reachability map*

(e) *8-9: TO and skeletons*

(f) *8-9: Paths*

(g) *[8,9]-IBeam: Reachability map* **(h)** *[8,9]-IBeam: TO and skeletons* **(i)** *[8,9]-IBeam: Paths*
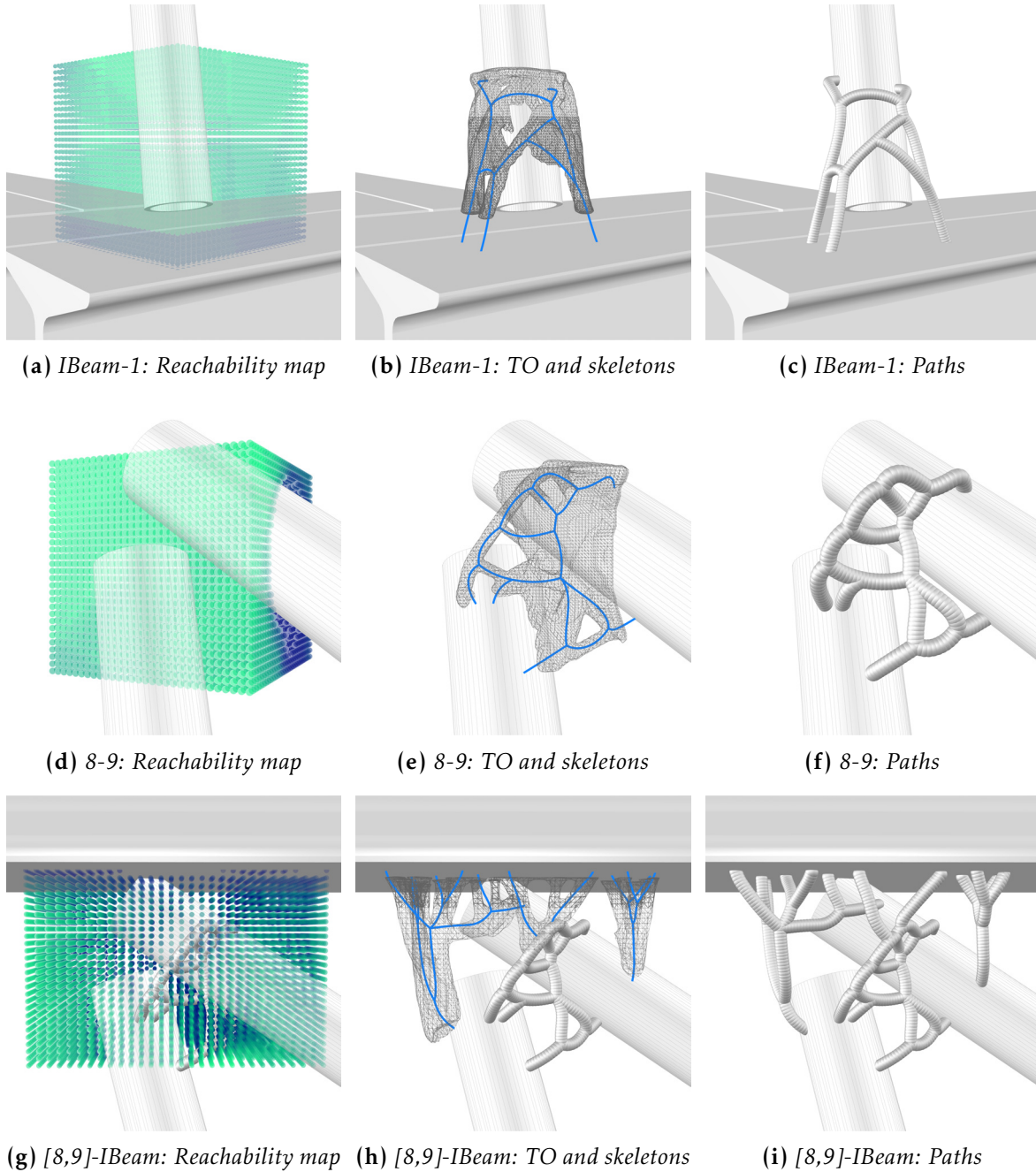
Figure 5.50: *Base structure: reachability maps, topology optimization (TO), skeletons, and paths.*

(a) *IBeam-6: Reachability map*

(b) *IBeam-6: TO and skeletons*

(c) *IBeam-6: Paths*

(d) *3,4: Reachability map*

(e) *3,4: TO and skeletons*

(f) *3,4: Paths*

(g) *[3,4]-8: Reachability map*

(h) *[3,4]-8: TO and skeletons*

(i) *[3,4]-8: Paths*
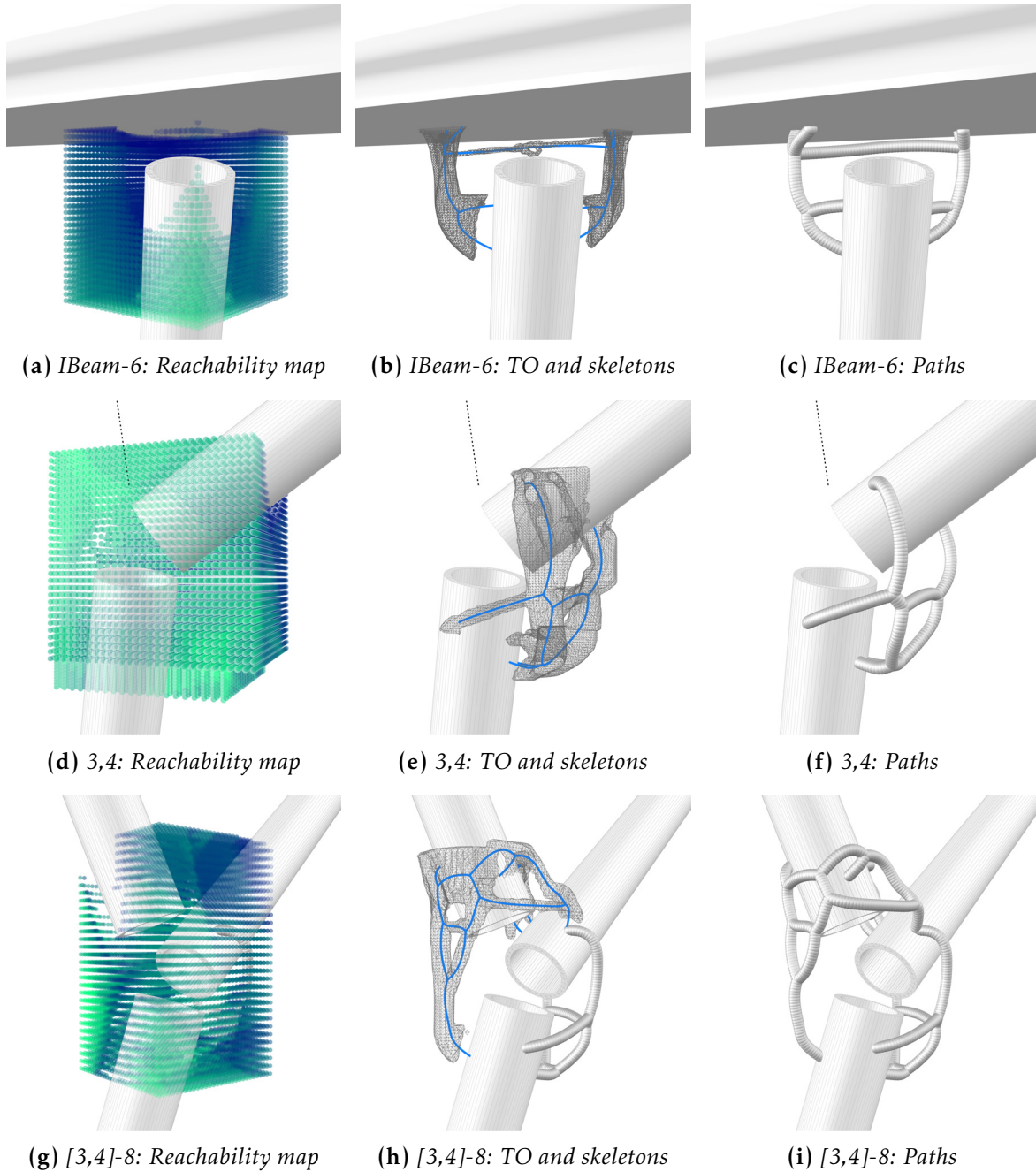
Figure 5.51: *Base structure: reachability maps, topology optimization (TO), skeletons, and paths.*

Performance   The total time spent on the design and computation of the base structure is an aspect to consider in further developments of the approach. Table 5.2 shows approximate times spent in each component per connection.

Task	Time	Contribution
Tool accessibility and robot reachability	3-6h	47%
Material distribution	10-20'	3%
Path generation	10-30'	3%
Path slicing with path planning (estimated)	2-4h	31%
Path sorting (estimated)	1-2h	16%

Table 5.2: *Performance of AD components per connection: estimated time including manual operations such as visual verification and data handling, e.g., selecting, importing, exporting. The given ranges reflect how much performance depends on the size of the connection boundary to test and how reachable this space is, i.e., more reachable connections take longer to calculate as there are more points to test. Here, the reachability map time estimate is based on medium-resolution settings. The Path slicing with path planning and path sorting components were not applied to these connections; only an estimate is given based on benchmarks collected in the Adaptive connection demonstrator.*

Roughly 50% of the design steps are taken by the calculation of the tool accessibility and robot reachability. This could be significantly improved as discussed in Sections 4.3.1.2 and 4.3.3.2.
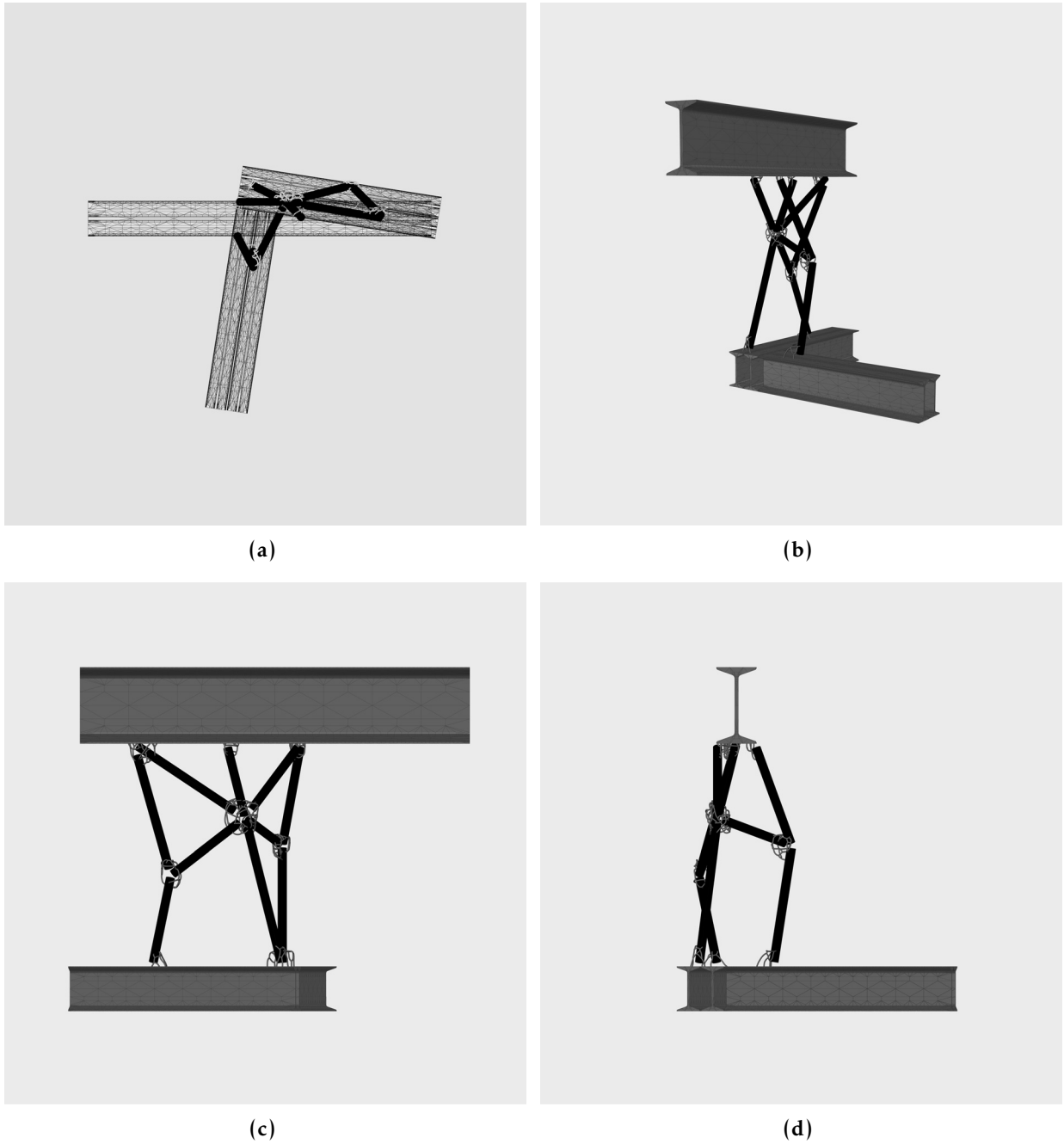
Figure 5.52: *Base structure: (a) Top, (b) Perspective, (c) Back, and (d) Side views.*

5.2.2   Structure with adapted sequence

This second demonstrator aims to further test the design-in-steps approach and compare how different reachability conditions yield different connection results. To do this, the base structure is split into three sub-assemblies –sub-assembly 101, 102, and 103 (Figure 5.53)– forcing a different sequence of assembly and, as a consequence, a different sequence of obstacles in the planning scene and reachability conditions.[33] A new set of connections is then recomputed for each sub-assembly in their updated planning scenes.

Implementation and results

As the geometry of the sub-assemblies pre-exists, the global scale workflow is modified to *evaluate* rather than *generate* the feasibility of the assembly:

Preparing the ground   As a starting point, each sub-assembly was placed in the robotic assembly setup (Section 5.2.1.1) in locations that benefit the reachability of their connections. This step relied on the previously calculated global robot reachability map as an "information canvas" (Figure 5.54). Once the sub-assemblies' positions were set, the assembly sequence was manually defined to differ as much as possible from the sequence used for the base structure.[34] Finally, a robotic assembly simulation was performed to verify the assembly feasibility and retrieve the configurations of the assembly robot for each assembly step, so each robot configuration can be used as an obstacle in the detailing pipeline.

---

[33]The original single I-Beam load is replaced by three independent smaller I-Beams. The change in the assembly sequence and the change in loading conditions are expected to affect as well the stability of the structure. However, this point was not included in this study. The aesthetic of a structure in a subtle equilibrium such as Subassembly 102 was first inspired by a small-scale prototype (Figure 5.53a).

[34]This step could be replaced by an algorithmic sequencing approach such as the one proposed in Y. Huang (2022).

(a)
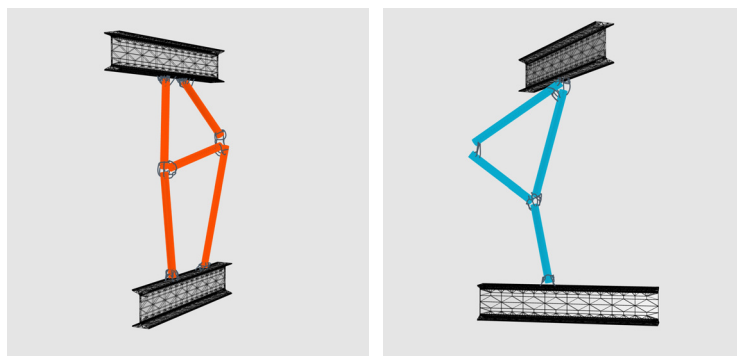
(b)   **(c)**
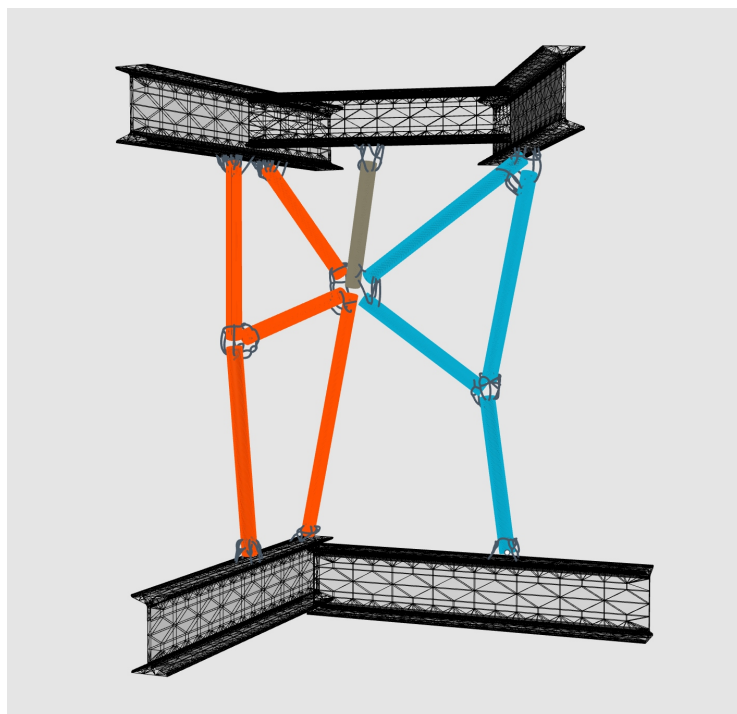
(d)

Figure 5.53: *Sub-assemblies with adapted sequences: (a) Concept: Small scale prototype of structure in a subtle equilibrium with spatial connections made with a 3D printed pen, Photo: Gerhard Bliedung, (b) Sub-assembly 101, (c) Sub-assembly 102, and (d) Sub-assembly 103: union of subassemblies 101 and 102 with an additional bar (in brown) and a bridging I-Beam element to lock the three assemblies together.*

(a)   (b)   (c)
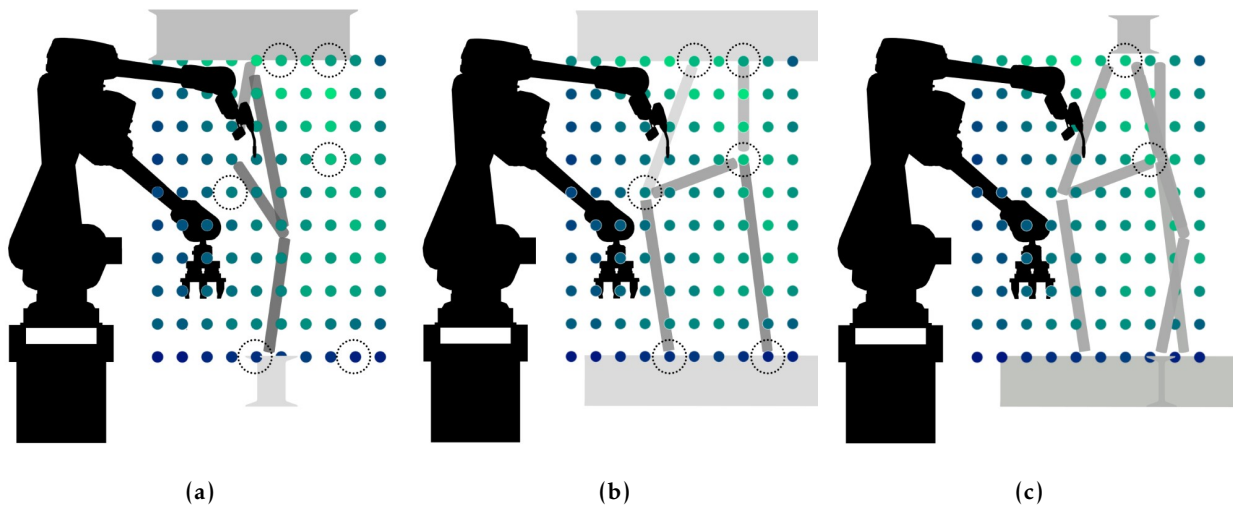
Figure 5.54: *Repositioning: (a) Sub-assembly 101, (b) Sub-assembly 102, and (c) Sub-assembly 103. The structure's connection areas are manually matched with greener nodes of the reachability map (from blue to green: increasing number of reachable configurations).*

The workflow for connection detailing remains the same as in the base structure's Adaptive detailing setup:

Detailing   In the same step-by-step fashion, connections were calculated one by one for each sub-assembly. Figures 5.55-5.59 show a selection of the recomputed connections. Generally, the character of the connections is similar to the ones generated for the Base structure; however, in comparison, the results are more compact (see Figures 5.60-5.61).[35]

---

[35]Only qualitative comparisons are used. A numerical evaluation would not be useful in this case because certain design variables, such as the positioning and sizing of the boundary object to be tested, are not the same in both demonstrators. The positioning of the boundary objects favors locations of maximum reachability for the connections that are different for each case. Therefore, the boundary objects' location and orientation differ. The size of the boundary was intentionally reduced in this second set of demonstrators as the results from the base structure were visually larger than needed.

(a)

(b)

(c)
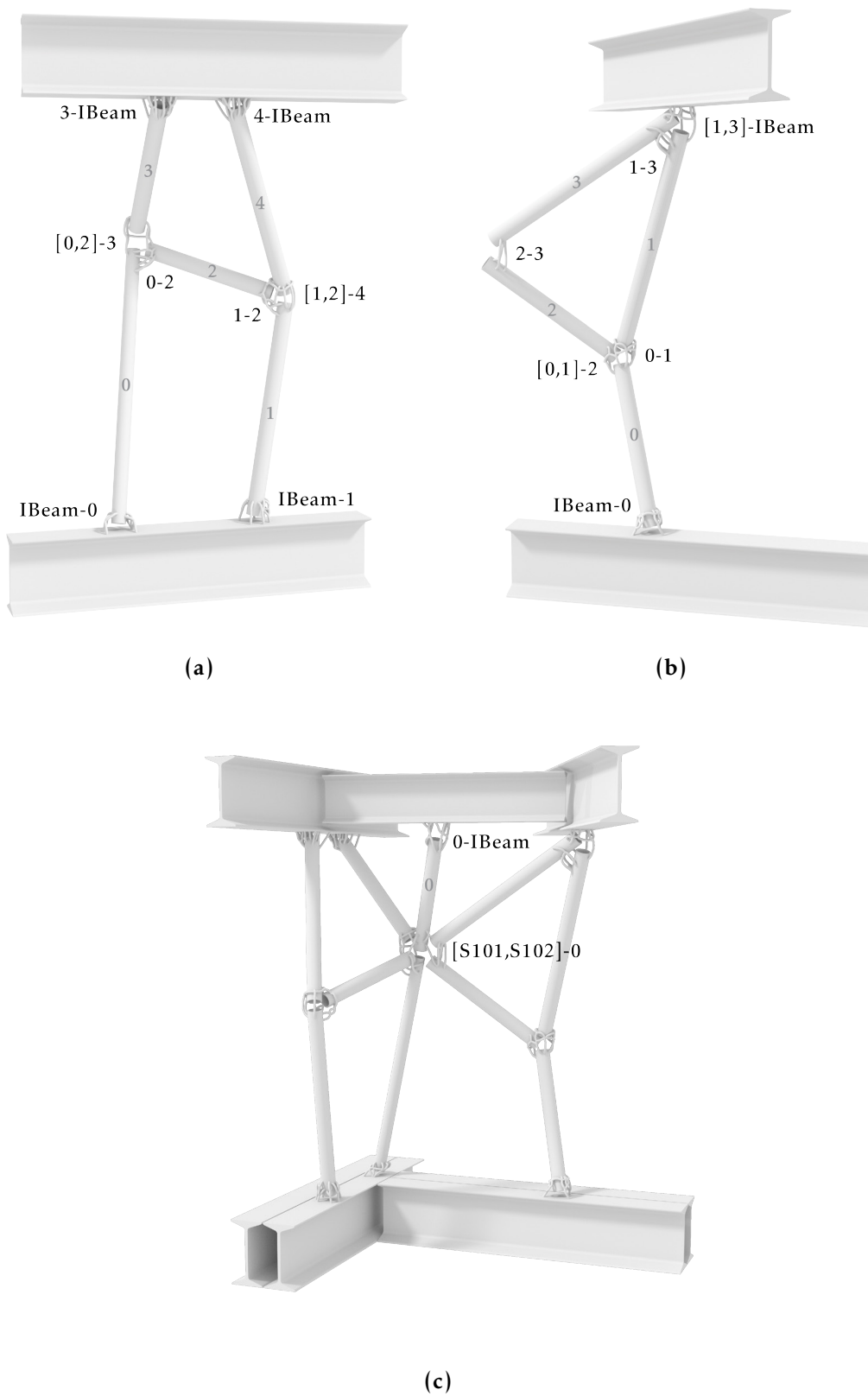
Figure 5.55: *Structures with adapted sequence, connections' IDs: (a) Sub-assembly 101, (b) Subassembly 102, and (c) Sub-assembly 103.*

(a) *IBeam-1: Reachability map* **(b)** *IBeam-1: TO and skeletons* **(c)** *IBeam-1: Paths*
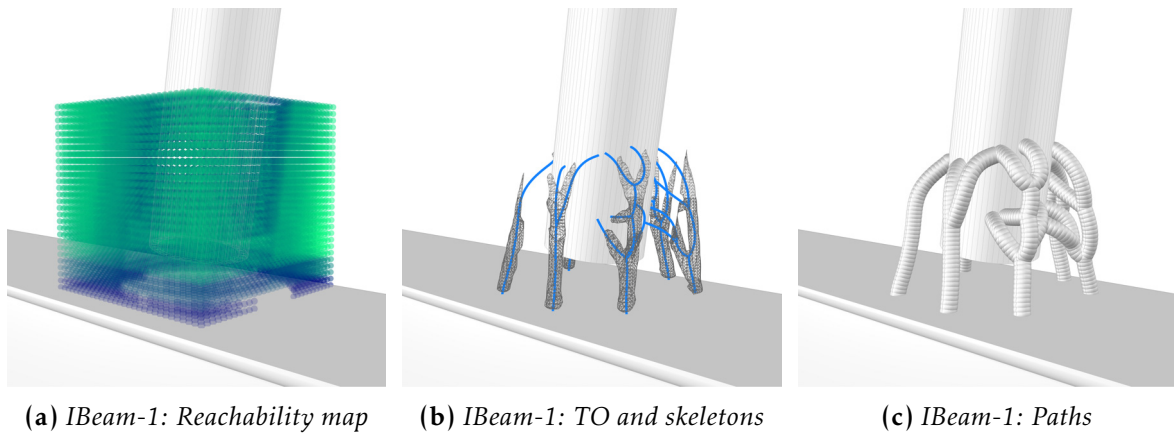
Figure 5.56: *Selection of connection results from sub-assembly 101: reachability maps, topology optimization (TO), skeletons, and paths.*

(a) *0-1: Reachability map* **(b)** *0-1: TO and skeletons* **(c)** *0-1: Paths*

(d) *[0,1]-2: Reachability map* **(e)** *[0,1]-2: TO and skeletons* **(f)** *[0,1]-2: Paths*
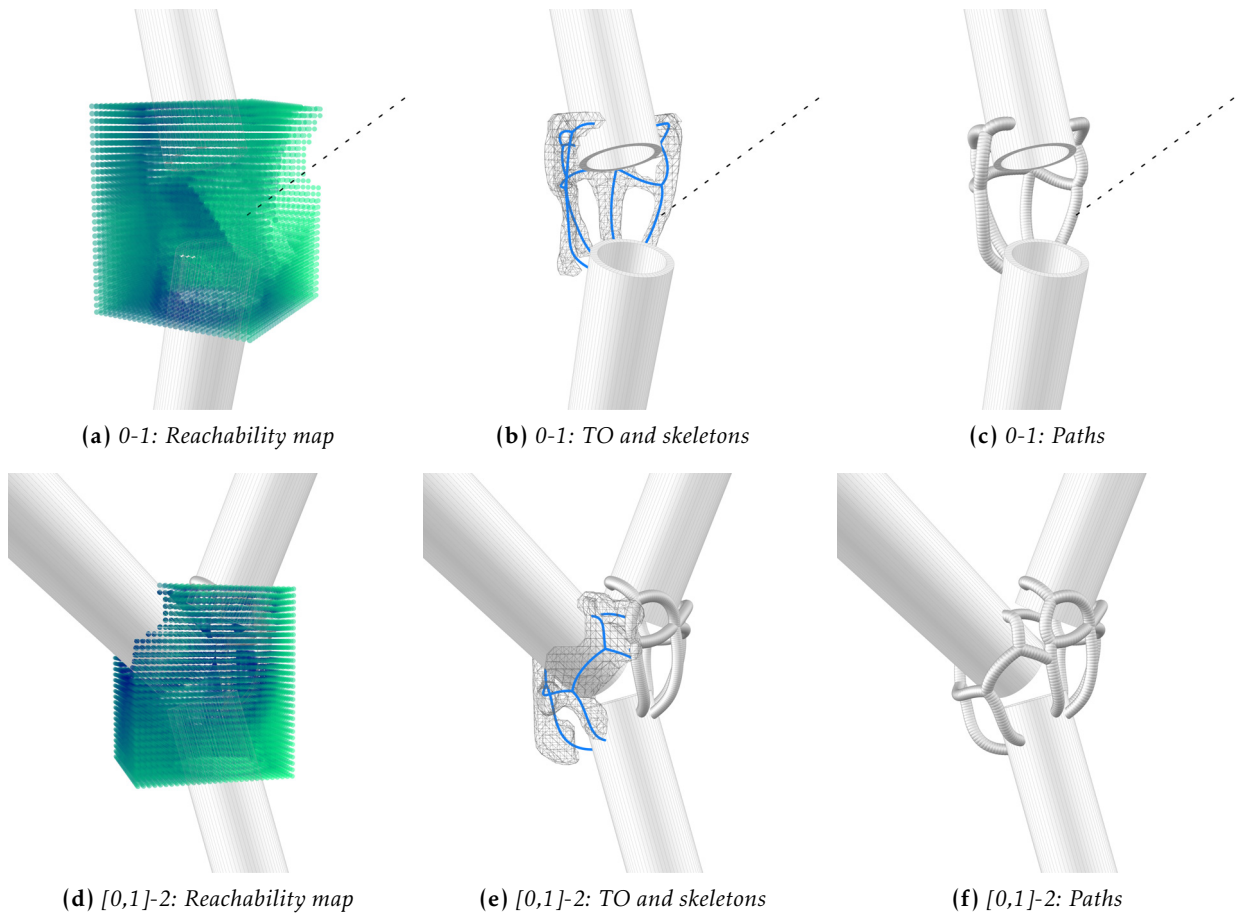
Figure 5.57: *Selection of connection results from sub-assembly 102: reachability maps, topology optimization (TO), skeletons, and paths.*

(a) *2-3: Reachability map*

(b) *2-3: TO and skeletons*

(c) *2-3: Paths*

(d) *[2,3]-IBeam: Reachability map*

(e) *[2,3]-IBeam: TO and skeletons*

(f) *[2,3]-IBeam: Paths*
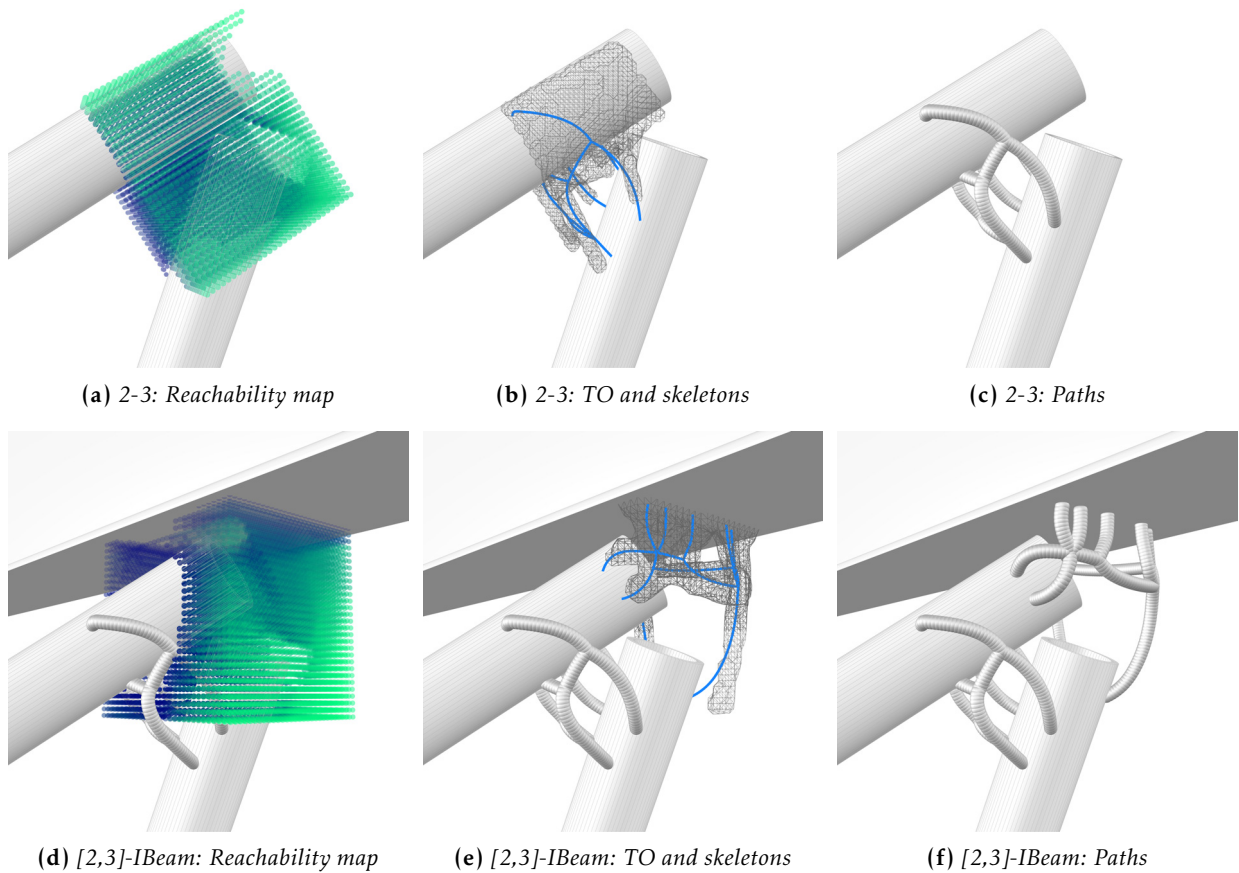
Figure 5.58: *Selection of connection results from sub-assembly 102: reachability maps, topology optimization (TO), skeletons, and paths.*

(a) *9-IBeam: Reachability map*

(b) *9-IBeam: TO and skeletons*

(c) *9-IBeam: Paths*
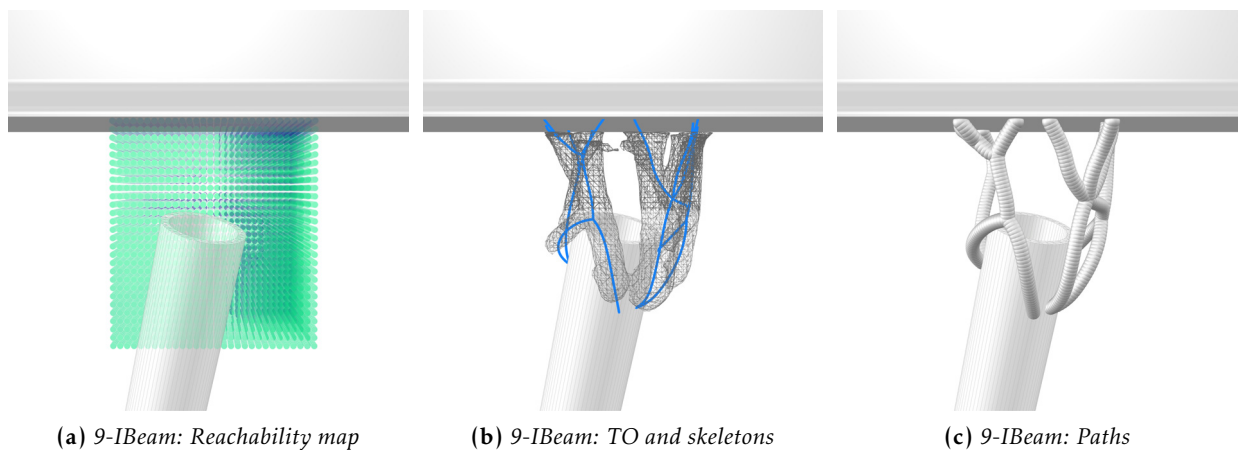
Figure 5.59: *Selection of connection results from sub-assembly 103: reachability maps, topology optimization (TO), skeletons, and paths.*

Table 5.3 shows the number of frames tested and the number of valid robot configurations of the base structure and sub-assemblies. Although a case-by-case comparison cannot be made for the reasons mentioned in footnote 35, the results show similar percentages of the degree of robot reachability for the base structure and the structure with adapted sequence. These results are in disagreement with the expected outcome in which fewer obstacles in the planning scene result in higher reachability, i.e., the structure with adapted sequence resulting in a higher reachability degree (for reference, a summary of all planning scenes is included in the Appendix section B.1). This disagreement can be attributed to the following aspects:

First, the base structure is calculated in a generative workflow, intentionally favoring the positions of the nodes in locations where high reachability is expected. The structure with adapted sequence was, on the contrary, manually placed in likely favorable locations. In this respect, the results suggest that the first method (generating a structure by its node locations) could have an advantage over the second (visually fitting a pre-generated structure in favorable locations). Second, different settings were used to calculate the reachability maps, i.e., a higher number of frames were tested for the structure with adapted sequence. This aspect, in principle, contradicts the expected outcome. However, it can be noted that the increase in the number of frames to be tested does not necessarily yield more reachable conditions, as the additional tested conditions were very similar to each other. Third, the sizes of the tested boundary objects are smaller in the structure with adapted sequence. This, in turn, results in frames located closer to each other and the elements/obstacles. This could mean that the tested points are too close to the obstacles and therefore, less reachable. Dedicated tests should be conducted to confirm each of these conditions.

Other aspects can be confirmed by the comparison of the results. In both cases, *multistep connections* remain less reachable than single-step connections. The least reachable connections are found in the base structure with a central node of degree 6 calculated in 5 steps. A similar lower number and constrained condition is the connection between Subassemblies 101, 102 and 103 ([S101,S102]-9 in Table 5.3 and Figure 5.62).

Structure	ID	Step	Tested frames	Valid configurations	Percentage
Base structure	Plate-0	1	1,488,000	259,789	17.5%
Base structure	Plate-1	2	648,000	131,643	20.3%
Base structure	0-2	3	648,000	56,554	8.7%
Base structure	1-2	4	648,000	80,854	12.5%
Base structure	Plate-3	5	1,296,000	182,411	14.1%
Base structure	3-4	6	840,000	86,768	10.3%
Base structure	4-[1,2]	7	648,000	76,083	11.7%
Base structure	[0,2]-5	8	648,000	99,864	15.4%
Base structure	5-IBeam	9	852,500	383,472	45.0%
Base structure	[1,2,4]-6	10	648,000	33,536	5.2%
Base structure	6-IBeam	11	540,000	169,965	31.5%
Base structure	[1,2,4,6]-7	12	648,000	21,258	3.3%
Base structure	7-IBeam	13	540,000	215,089	39.8%
Base structure	[1,2,4,6,7]-9	14	648,000	28,301	4.4%
Base structure	[3,4]-8	15	648,000	38,051	5.9%
Base structure	8-9	16	648,000	132,269	20.4%
Base structure	[8,9]-IBeam	17	540,000	113,246	21.0%
			12,576,500	**2,109,153**	**16.8%**

Structure	ID	Step	Tested frames	Valid configurations	Percentage
Subassembly 101	Plate-0	1	1,620,000	201,288	12.4%
Subassembly 101	Plate-1	2	1,620,000	284,491	17.6%
Subassembly 101	0-2	3	1,620,000	255,653	15.8%
Subassembly 101	1-2	4	1,620,000	222,068	13.7%
Subassembly 101	[0,2]-3	5	1,620,000	250,715	15.5%
Subassembly 101	3-IBeam	6	1,620,000	206,405	12.7%
Subassembly 101	[1,2]-4	7	1,620,000	161,288	10.0%
Subassembly 101	4-IBeam	8	1,620,000	255,757	15.8%
Subassembly 102	Plate-0	1	1,620,000	290,309	17.9%
Subassembly 102	0-1	2	1,620,000	297,921	18.4%
Subassembly 102	[0,1]-2	3	1,620,000	161,592	10.0%
Subassembly 102	2-3	4	1,620,000	258,072	15.9%
Subassembly 102	3-1	5	1,620,000	178,402	11.0%
Subassembly 102	[3-1]-IBeam	6	1,620,000	296,109	18.3%
Subassembly 103	[S101,S102]-9	1	1,620,000	107,822	6.7%
Subassembly 103	9-IBeam	2	1,620,000	362,689	22.4%
			25,920,000	**3,790,581**	**14.6%**

Table 5.3: *Robot reachability of the base structure (top) and structure with adapted sequence (bottom) showing: ID, name of the connection; Step, the location in the fabrication sequence; Tested frames, the total number of frames tested for accessibility and reachability; Valid configurations, the total number of valid configurations in the reachability map; Percentage, the reachability degree of the connection as a percentage (%). Low reachability degrees are highlighted in red.*

The compactness of the connections of the sub-assemblies is attributed to the 20% reduction of the volume of the accessible boundary used as input in all three sub-assemblies.[36] The reduced volume produces shorter paths, which are visibly more stable and could potentially be less prone to buckling.[37] However, the connections of the sub-assemblies are also denser than the ones of the base structure, a characteristic that could make the slicing, sorting, and printing tasks more challenging.[38].

(a)   (b)

(c)   (d)
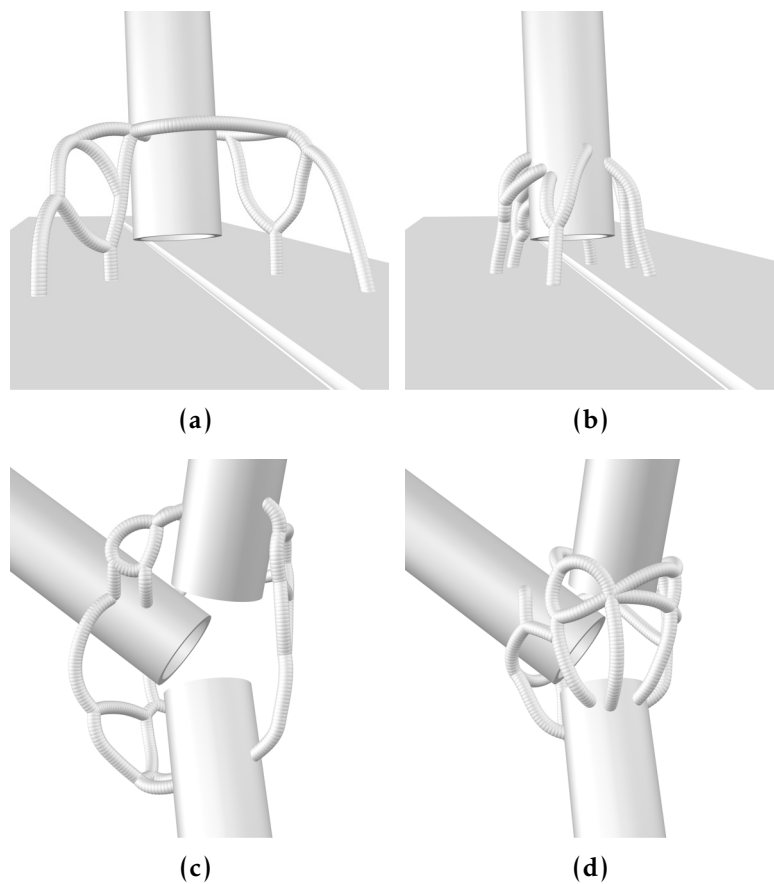
Figure 5.60: *Comparison of connections of the base structure and structure with adapted sequence: (a-b) A single step connection in contact with an I-Beam, and (c-d) A freestanding multistep connection. In all cases, the connections of the adapted structure show more compact results.*

---

[36]This reduction was performed based solely on the visual aspects, or expression, of the base structure's connections.

[37]An accurate TO task could equalize these differences.

[38]Even if reachable, the paths computed before the path slicing step are not here yet qualified in terms of *how* reachable they are. This only becomes visible when applying the path slicing with path planning method (see for example Figure 4.33d)

(a) **(b)**

(c) **(d)**
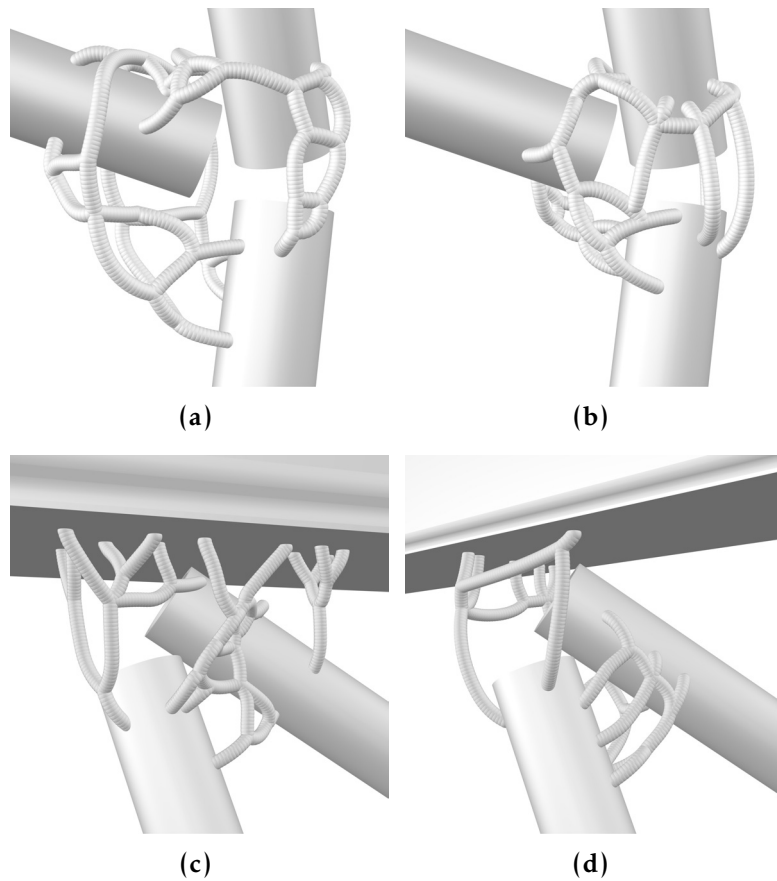
Figure 5.61: *Comparison of connections of the base structure and structure with adapted sequence: (a-b) A freestanding multistep connection, and (c-d) A multistep connection attached to an I-Beam. In all cases, the connections of the adapted structure show more compact results.*

(a) **(b)**
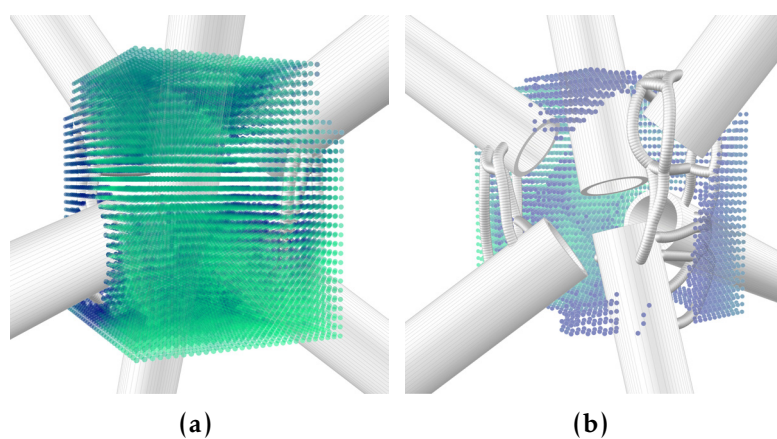
Figure 5.62: *Comparison of front and back sides of the reachability map of the central node in Sub-assembly 103.*

5.2.3   Discussion

Base structure

Designing in steps   The base structure was and had to be calculated step-by-step following the assembly sequence. This design approach in steps is tightly related to the robotic assembly strategy. In this assembly scenario, each assembly stage is considered a stand-alone and self-supporting structure or sub-assembly with its own modified planning scene and collision objects.

In Figure 5.63 it can be noticed that the *multistep connections* have a distinct, less synthetic character than single-step connections. Single-step connections are easier to "read", i.e., intuitively understand their shape and behavior, while the readability of a multistep connection is more challenging. This peculiarity can be attributed to the step-by-step design workflow in at least two ways. First, multistep connections are intrinsically more complex and constrained as bars and connections are added one by one, increasingly shrinking the available design space at the interface. Second, as the final connection is not visible until the last step of the connection is computed, a complete reading of the node is only possible once all the steps have been computed. This is emphasized by the fact that connections result from computed steps with minimal intervention from the designer.

In terms of processing time, the design-in-steps approach only allows parallelizing work on unrelated connection locations. For multistep connections, it is required to initiate the pipeline only when the previous step has been finalized, so the previously calculated step can be used as a collision and support object of the next step. This aspect can be inconvenient for a designer, particularly if the computation time per connection is as high as the one recorded during the current implementation. In addition, for multistep connections, it is unintuitive to "fix" or stop modifying a design, i.e., the design of the connection between the first 2 elements of a node with 3 elements, without knowing how the upcoming connecting paths will look like. Ideally, multistep connections would be designed interactively, allowing modifications to all their steps synchronously.

A related challenge is found on a global scale. It is unintuitive for a designer to not be able to foresee how the design of the total number of connections will look like. Compared to other connecting methods, the AD pipeline for IPWAAM connections yields significantly unexpected results. This limitation could be attributed to the pipeline speed and could be dramatically reduced by alternative software implementations.[39]

These points could be challenging aspects for a designer. Designing in steps could become counter-intuitive and over-structured. An overview of the final layout of multistep connections and the constellation of all connections would likely be preferred. This lack of control of the global output could be handled in the future by a second interactive design phase after connections have been roughly pre-computed (i.e., after `Path generation` and before `Path slicing`) for example supported by sketching features presented in `Path generation`. Drastically speeding up the computation routines and allowing more feedback instances would enable the workflow to influence rather than regulate the connection design.

Considering the structural behavior   Assembling structures without scaffolding has functional implications for the behavior of the connections: each connection has to function during all the stages of the assembly sequence and simultaneously contribute, together with the rest of the elements and connections, to support the different loading conditions once the assembly is in use. This functional behavior of the node in multiple scales was not included in the scope of this work.

---

[39]For reference, the sole computation of the 17 steps of the base structure from initialization to the path generation component took several days. Depending on the size and reachability degree of the connections' design space, the minimum and maximum computation times -minimum if all connections would be small and with a low reachability degree, maximum if large and highly reachable- were estimated between 6 and 13 hours. It follows that for 17 connections, the minimum and maximum estimated times to calculate the whole structure add up to 102 and 218 hours (see Table 5.2 for estimations). Furthermore, it should be taken into account the volume of data to process. Although this aspect strongly depends on the software implementation, the increase of data volume and consequent efficient handling workflow from a single connection, e.g. the adaptive connection with 20 paths and approximately 500 printed points, to a collection of connections, e.g. 300 paths with 6000 printed points, is worthy of study in itself.

(a) *[8,9]-IBeam*   **(b)** *5-IBeam and 7-IBeam*   **(c)** *6-IBeam*

(d) *[3,4]-8*   **(e)** *[1,2,4,6,7]-9*   **(f)** *[0,2]-5*

(g) *IBeam-0*   **(h)** *IBeam-1*   **(i)** *IBeam-3*
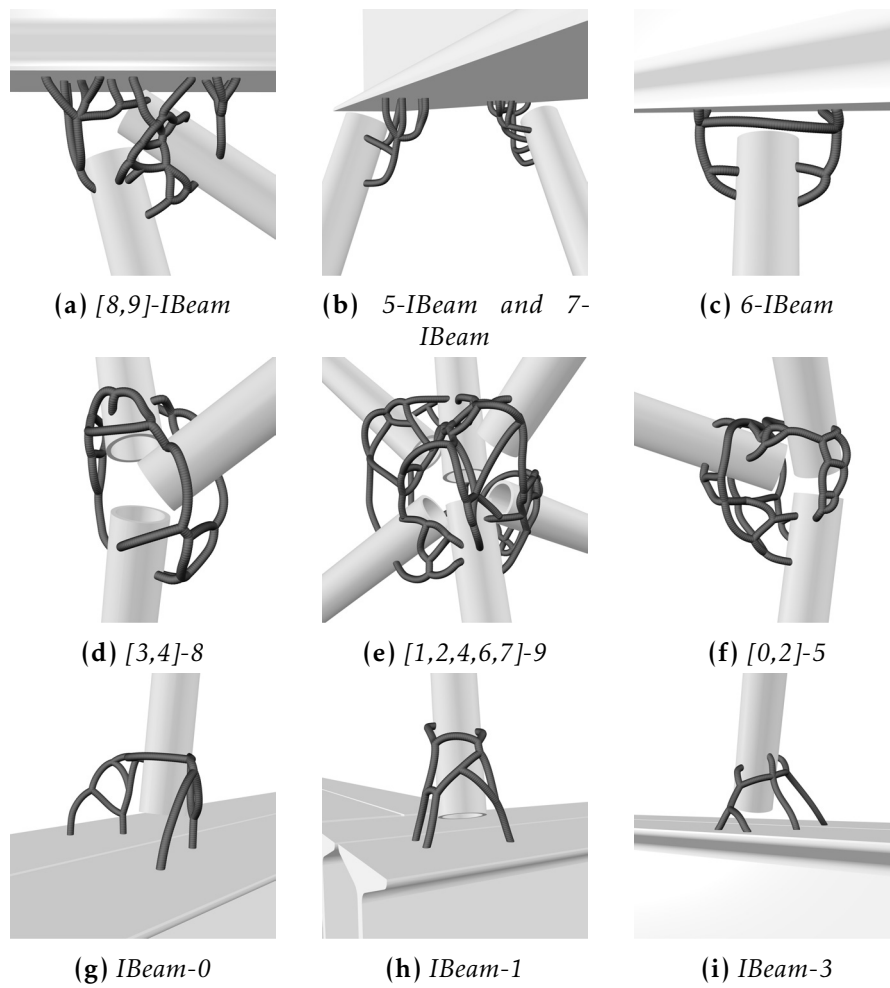
Figure 5.63: *Summary of connections of the base structure: of the 10 nodes and 17 connections, only 6 connections, are single-step connections (b, c, g, h, i). Single-step connections are all "leaf" cases: bars in contact with the IBeams, either acting as supports or loading points. All freestanding nodes are multistep connections, with node degree 3 (a, d, f), and 6 (e).*

Understanding this aspect would require a sub-assembly static analysis at each stage of assembly, an understanding of the WAAM bars' mechanical behavior, and a reliable strategy for structural modeling of connections between non-touching elements. So far, no structural assessment has been conducted on the scale of the entire nodes or the global structure. The structural evaluations conducted so far described in Section 3.6.6 were limited in scope to the level of the WAAM welded buildup for the simplified problem of straight bars.

Iterative refinement   The pipeline has several components that can be computed with high or low resolutions. This can be useful for time-consuming tasks such as the calculation of the reachability map or the material distribution; therefore, the possibility of computing low-resolution results is an asset for designing in steps. The concept of iterative refinement is critical to architectural practice and therefore, computational design must as well provide strategies to deal with it. Another way to refine results would be to use non-homogeneous data structures, such as Octrees, to refine and compute time-consuming operations only where needed.

Early understanding of production constraints   Another critical challenge in the application of the adaptive detailing pipeline is the very first premise of this thesis: the need for the designer to be explicitly knowledgeable of the production constraints. This thesis has investigated this premise on several scales, however, only in laboratory settings without real-world production logistics. Even for the author of this thesis, the need to be extremely explicit in the planning scenes for each structure and each design step has been intricate and unforgiving to even small errors. For example, if a collision object were not properly loaded in the scene, the calculation of a reachability map would have to be discarded.[40]   This aspect entails that the design process cannot be started until the production setup is well-documented. This is not typical in conventional production processes. An application of this pipeline, therefore, will require assembling a fabrication team

---

[40]The pipeline here could allow revisiting certain regions of the reachability map and re-compute only sections of it as needed.

and setup at a very early design stage, and very good communication between fabricators and designers, or a fusion between these two roles.

In addition, it is worth mentioning that the requirement of understanding, handling data, and operating within the robotic setup at each step of the design process adds considerable computational overhead for manipulating geometric objects. Compared to conventional scenarios where production considerations are implicitly understood by designers rather than explicitly described, this operative aspect requires a rather different set of design steps and, likely, working mindset. Conversely, the early integration of production in the design pipeline benefits the design and planning process, as designers understand *in detail* the construction challenges in advance of the production stage and, in addition, have the tools to incorporate changes even at advanced stages of the design-production process.

Production estimation   The results of the Base structure give enough information to calculate the theoretical printing time of its connections: a total of 60 hours, considering a conservative printing time of 40 seconds per print point without any sorting optimization nor adaptive measures –localization, touch-sensing, adaptation and resuming of the printing process-. This estimate includes the deposition of 298 paths containing 5.287 seams or WAAM print points.

Adaptive measures are calculated as follows: for each path, at least two search operations should be performed at the start and midway through the path and at the ends of exit paths. Each search procedure takes, on average, 45 seconds. Adaptive measures to elements and paths were not automated nor optimized for speed, but in the best case scenarios where paths are on track and considering an automated procedure, they can be estimated to take on average 3 minutes, including loading of search procedures, storing measured data, visual verification of adaptive measure, and resuming of printing operations. For 298 paths with two measured locations, considering that 20 percent of them are exit paths with three measured locations, adaptive operations add roughly 33 hours of production time. In addition, each element should be localized twice, before and after it is connected, adding 2 minutes for each localization procedure – or less than 1 hour in total.

In addition, the pick and place of the 10 elements should be considered, for example, with a conservative time of 10 minutes per element, including manually locating the element in the pick-up station, robotic gripping, and placement. This adds roughly 2 hours of production time.

With these estimates, the total production time for assembly and joining of the base structure would take around 100 hours or roughly 10 hours per element. Although this number does not reflect a time-optimized workflow, it could still be competitive compared with pre-fabrication of nodes in a separate additive manufacturing process (consider printing time per node, plus their labeling and transport, their positioning within the assembly, and additional joining or fixing with the elements in place). However, a conventional miter joint (typically machining of both ends of elements, positioning, and conventional seam welding) could still be faster if high-precision machining is done at the production location.

Structure with adapted sequence

Maximizing reachability of the connections   Placing sub-assemblies in positions that maximize the reachability of the connections poses a non-trivial problem, given mainly by the non-regular and spatially heterogeneous characteristics of the sub-assemblies. While in this demonstrator placing was done intuitively, i.e., trying to maximize the location based on visual feedback given by the reachability map (Figure 5.54), optimal positions could also be automatically searched within the reachability map nodes. It is of interest to highlight the complexity involved in this task compared to other non-spatial cases (see contrasting examples in 2.2.2) where visual feedback would be a good enough method to optimally solve the positioning problem.

Designing for reachability versus checking for reachability   This demonstrator presents the same configuration of elements subdivided into three sub-assembly sequences. It could be assumed that removing elements from the planning scene would result in higher reachability of the connections. However, results in Table 5.3 show the opposite: the overall reachability of the base structure is slightly higher (16.8%)

than the reachability of the structure with adapted sequence (14.6%). Although these results are not conclusive to determine whether designing for reachability (approach used in the Base structure) is better than checking for reachability (approach used in the Structure with adapted sequence) for the reasons mentioned in footnote 35, they suggest that considering the reachability of the connections during the structure's design process can only benefit the outcome.

(a) *[2,3]-IBeam*

(b) *[0,2]-4*

(c) *1-2*

(d) *IBeam-0*
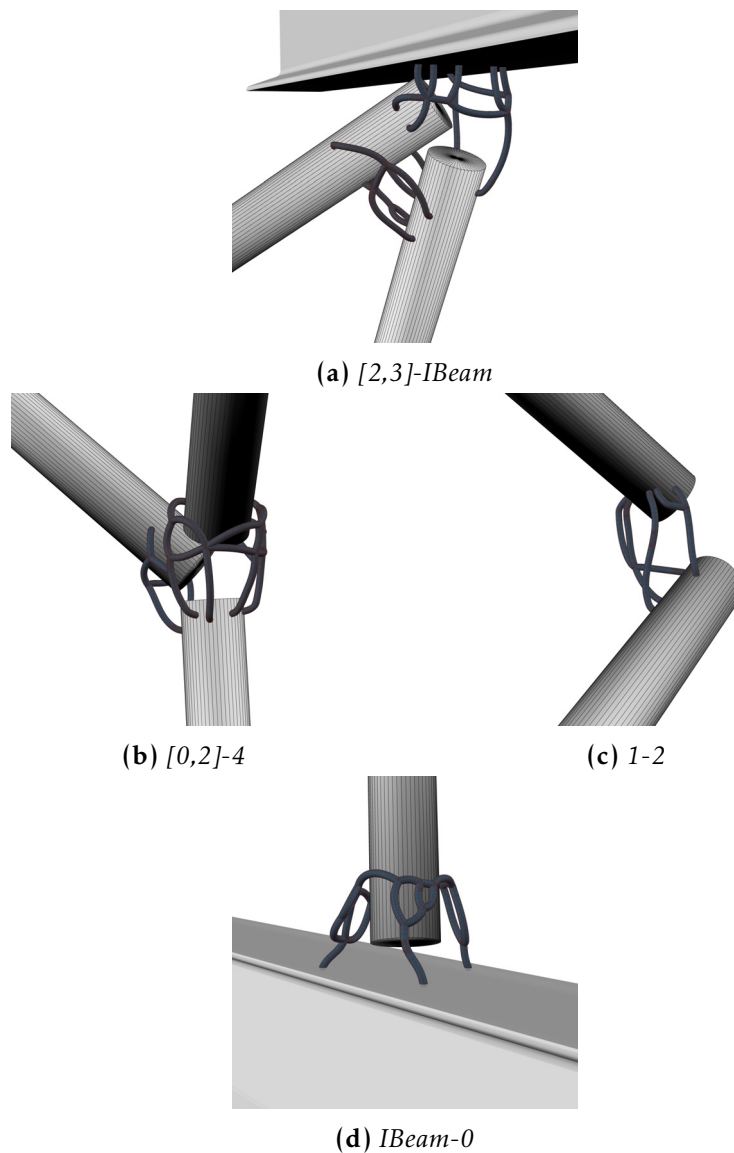
Figure 5.65: *Summary of connections of the sub-assembly 102.*

(a) *3-IBeam*

(b) *4-IBeam*

(c) *[1,2]-3*

(d) *[0,2]-4*

(e) *IBeam-0*

(f) *IBeam-1*
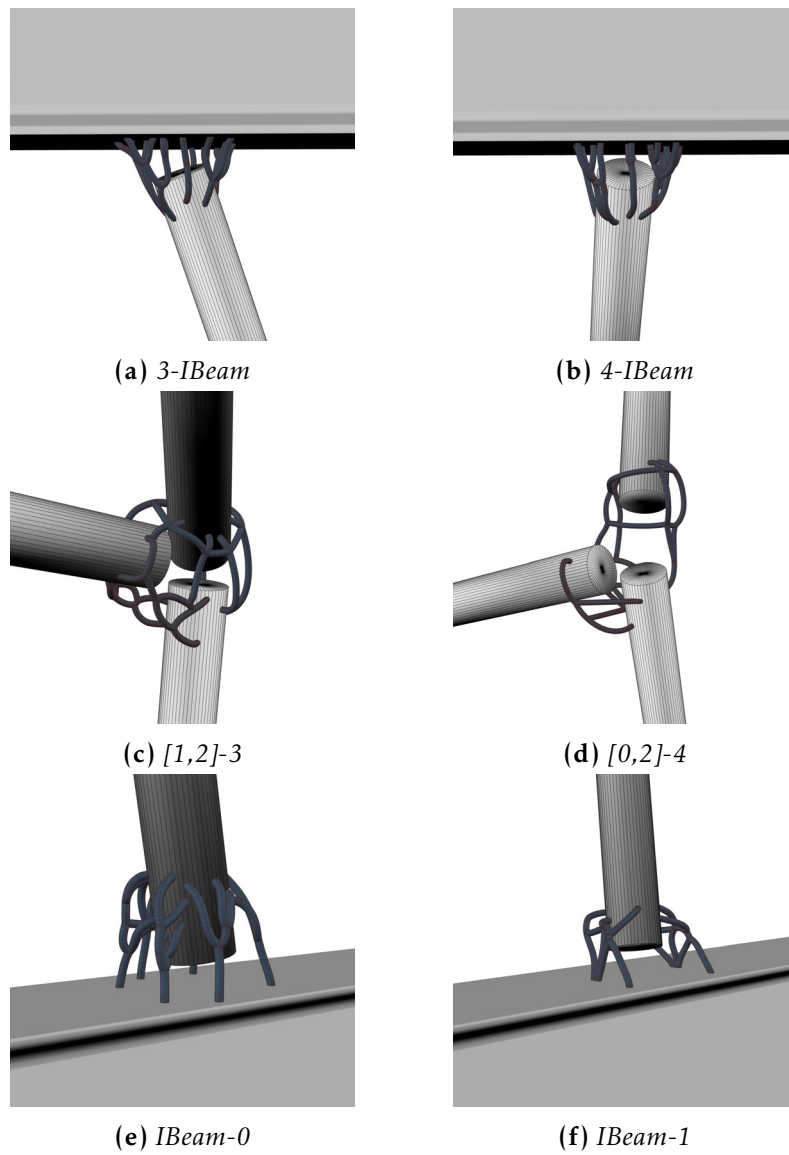
Figure 5.64: *Summary of connections of the sub-assembly 101.*

(a)

(b)
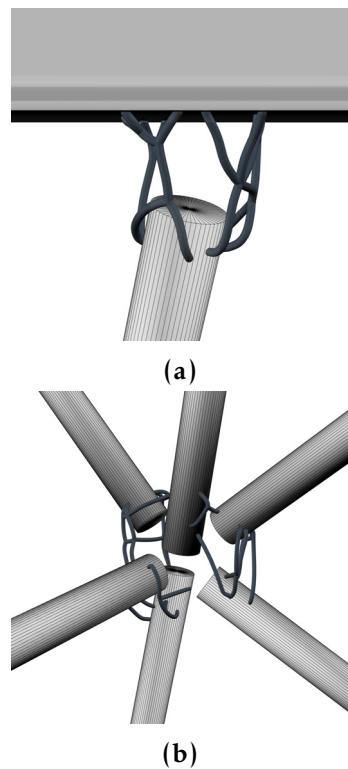
Figure 5.66: *Summary of connections of the sub-assembly 103.*

Production estimation   The Structure with adapted sequence contains 313 paths with 5.222 print points and results in a total of 102 hours of production using the same estimates as in the Base structure. In addition to the Base structure's time estimation, this structure requires additional time for setting up each sub-assembly.

5.3   Summary

This chapter has presented physical demonstrators and virtual, speculative exercises on a broad range of aspects concerning the application of the IPWAAM technique and the AD pipeline. A discussion of each set of experiments has been included in each section. This section presents a summary of results organized in the two scales studied in this chapter: connections and structures.

IPWAAM and AD have been physically tested for connections between two elements. These physical demonstrators have dealt, cumulatively, with all the stages of the design and production pipeline, and

the Adaptive connection has tested the integration of all components. The summary of findings based on this set of demonstrators are the following:

- The IPWAAM technique has been used to join two lightweight (under 0.5 kg) non-touching non-machined steel elements. All printed connections, including simple (5.1.2.1) and more complex topologies (5.1.2.3) were successful in transferring the loads between elements without the assistance of external supports during or after the joining process.

- A diversity of connection typologies and path topologies have been explored. Simpler topologies, such as the one of the Simple connection are easier to process in terms of computation time and data handling and as well prone to fewer errors during printing. Complex topologies such as the ones of the Adaptive connection require more data and material deposition control during planning and production. Truss or tree topologies present paths with changing directions with "crowded" node areas. In these areas, it has been observed that even if using the material removal strategies proposed in `Path sorting`, the flow and shape of the material rarely follow a standard expected result. These non-standard seams, in turn, require the use of adaptive measures while the simpler, non-branching topologies -i.e., short (less than 50 mm) and not overlapping paths- could be printed without these measures.

- Entries and exits sections of the paths are areas of special interest. Excessive heat, wrong printing parameters, and too small or too large CTWD (contact tip to workpiece distance) result in visible errors and potential failure points. To further control the depositions in these areas, localization and touch-sensing strategies have been used to measure and reconstruct the start and ends of the paths on the substrate. These two procedures are critical for a proper fusion between the paths and the elements and should not be skipped.

- The touch-sensing procedure is very suitable for the point-by-point deposition technique applied in linear or curvilinear paths.

Depending on the degree of deformation of the welded seam, an aspect that is related to the varying build and tool orientations, increasing the number of points to measure can give a complete reconstruction of the deposited seam. During the experiments, it was observed that measuring more than one point at a time does not consume significantly more time than measuring only 1 point at a time.

• When applied spatially, a connection built with the IPWAAM technique faces the main challenge of handling collisions with existing objects and, for complex intricate geometries, with itself. Two methods have been proposed for collision-free slicing: a geometry-based approach and a path-planning-based approach. The first one only yields robot targets without checking their robot configurations. The second one uses search algorithms to find valid robot configurations providing assurance of their success during production. It is possible to print IPWAAM connections with both methods; however, the first one is only suitable for simple and small connections whenever fast results are needed, and the second one, more time-consuming, when more re-orientations of the robot are expected, such as in the case of multiplicity of paths with varying build orientations.

• The presented demonstrators focused on point-by-point printing due to its versatility and availability of straightforward sensing techniques. The development of in place continuous depositions will require different slicing techniques, a better understanding of the heat accumulation during the buildup, and appropriate sensing strategies.

In addition, the AD pipeline for IPWAAM has been put to the test for the design of hypothetical structures. These virtual exercises have focused on anticipating the challenges concerning the application of the presented methods and techniques in the context of design for robotic assembly. The main outcomes of this set of experiments are the identification and/or qualification of fabrication constraints for the design of IPWAAM connections and the challenges concerning their integration into an adaptive detailing pipeline:

The AD pipeline has been applied from the Initialization to the `Path generation` sections of the pipeline to a total of 34 connections using 1 multi-robotic assembly setup equipped with 1 assembly robot and 1 welding robot. This section of the pipeline has been proven versatile to resolve different geometric conditions for connecting non-touching non-machined standard elements with circular and I-Beam cross-sections.

Based on these experiments, the following aspects are expected to provide maximum tool access and robot reach around the connection design space:

- **A high degree of freedom of the robotic assembly setup**

  The higher the degree, the more options for aiming at a location exist. In particular, an external axis to move the structure to be assembled, as conventionally used in state-of-the-art welding setups, would be highly beneficial to IPWAAM. Alternatively, the use of multi-robotic setups with more than one welding robot is as well expected to significantly increase the robotic reachability around the connection space.

- **Small and compact assembly and joining end-effectors**

  Grippers of the assembly robot and sensors mounted on the welding robot occupy significant space around the connection space. Therefore, the tooling should be as compact as possible to avoid reducing the connection space's accessibility.

- **A low degree of the structure's nodes, i.e., the number of elements to be joined at a single location**

  The number of elements meeting at one single connection point should be as minimum as possible. The experiments have shown that nodes with more than 3 elements result in low reachability spaces and therefore are highly challenging to resolve with short and uncomplicated IPWAAM paths.

- **Assembly sequences with accessibility/reachability priority**

  Although this thesis did not touch on assembly sequencing aspects, during the development of the structure demonstrators

it became evident that to find good results for in place joining, the connection reachability should be included as a design driver criterion during the determination of the assembly sequencing.

The demonstrators presented in this chapter also open a discussion regarding *adaptive design*. *Adaptivity* is a broad notion that has become useful in many stages of the experiments presented in this chapter. While the physical experiments have shown that adaptive detailing supports an *adaptation of the design during the production process* to handle small variations of the positioning of elements and printed paths, the virtual experiments suggest that algorithmic workflows that link design and production at the global -structure- and local -detail- scales are the backbone of a broader notion of *adaptive building*. Chapter (6) will return to this point to clarify the different uses given to the term *adaptive*.

6 Conclusion

This thesis has identified challenges and provided strategies for joining and detailing spatial metal structures assembled with robotic arms. This final chapter first summarizes the aims and the results of the work (6.1), then provides an overview of its contributions (6.2), discusses its relevance and directions for future work (6.3), and closes with final words (6.4).

6.1 Summary

This thesis has identified the following existing needs and new challenges concerning joining and detailing for complex assemblies built by robotic means:

- The need for a multipurpose robotic setup for assembly and joining

- The challenge of understanding the space between parts where tools and materials can be placed to join them

- The lack of existing joining techniques and materials that can be used to fix non-regular, non-orthogonal interfaces robotically

- The need for tolerance-handling strategies compatible with robotic fabrication and spatial joining techniques

- The need to explicitly integrate robotic fabrication constraints with functional requirements at an early design stage

- The lack of overarching methods to combine and address these problematics into an integrative design-and-production method

The work practically investigates these challenges through an exemplary case study in additive robotic joining for lightweight spatial metal structures. The work presents two complementing developments:

- To address the lack of suitable techniques and materials, a versatile robotic joining technique has been developed that can fix elements of variable dimensions, geometry, and configuration during robotic assembly processes (summarized in Section 6.1.1)

- To address the lack of conceptual and practical methods to conceive and robotically produce functional spatial connections, the work proposes a computational detailing pipeline that embodies concepts to support a transition from existing, implicit detailing approaches to explicit handling of design-and-production tasks (summarized in Section 6.1.2)

6.1.1   In place WAAM

The proposed fabrication technique, *in place wire and arc additive manufacturing*, or IPWAAM, is an application of the existing WAAM 3D printing process as a joining technique carried out between parts, in place, during the assembly process. The proposed technique is a good candidate for joining in the context of robotic assembly processes for several reasons. First and foremost, IPWAAM presents versatility for depositing material under different geometric conditions, presenting broad flexibility in the tool and path orientations required to avoid collisions while printing between obstacles. In addition, IPWAAM can be categorized as highly performative as it provides an ample choice of metals that can perform under various loading conditions. In sum, IPWAAM combines the flexible deposition methods of WAAM with the versatile high-strength performance of metal fusion.

The work presents the principal components required to deploy IPWAAM in a robotic assembly scenario. Two robotic setups have been described, where the setup using the Fronius CMT process has shown superior suitability for the task at hand. The main communication environments and code libraries needed to create, send, process, and retrieve production data have been explained, and the fundamental printing and surveying procedures have been outlined. After a review of the different possible deposition techniques, the work has focused on the point-by-point deposition type as a first step for joining non-touching, non-machined parts. The set of experiments conducted to

calibrate and control the point-by-point deposition has shown consistency and versatility, supporting the use of IPWAAM as an additive, spatial joining technique. The investigations conducted in collaboration with researchers in the fields of structural engineering, durability of materials, and mechanical and process engineering have opened relevant directions of research. Most notably, the results of the structural and corrosion performance evaluation of IPWAAM parts have shown promising results that support the suitability of the process for architectural purposes.

6.1.2   Adaptive detailing

The proposed adaptive detailing pipeline, or AD pipeline, provides a design-and-production step-by-step process to conceive and build connections of spatial structures assembled robotically. Due to the unprecedented challenges regarding joining spatially and additively and the lack of established methods to overcome them, the main robotic and material fabrication constraints of the IPWAAM joining technology are interpreted and integrated as drivers of the design process.

The pipeline is structured in 15 software components that integrate one-by-one robotic, material, and functional constraints. In addition, the tasks within each component can be categorized into design or production tasks. Production tasks can be further categorized as surveying or printing tasks. Most design tasks are handled before production, as they require computationally-expensive operations. However, alternative and faster software implementations could parallelize the design-and-production phases, such as re-computing path-planning tasks when necessary.

In a nutshell, the pipeline's final implementation consists of the following steps: the first set of components handles the robotic setup's constraints by calculating the tool accessibility and robot reachability to identify areas where the tool and robot can access and reach the interfaces between the structure's elements. The next set of components handles the functional requirements by allowing the designer to sketch connection solutions within the robotic setup's constraints or automatically calculate a material distribution tendency and generate

a connection within this material tendency.[1] Once the paths have been generated manually or automatically, they are sliced with collision-free robot orientations and finally sorted for production. Production is then started by surveying the elements to be connected and adapting the printing paths to fit within them. Printing can then start. At each path start, middle, and end, a touch-sensing operation measures the last printed layer to compensate for any differences that may have occurred during depositions. After each measuring operation, divergences are evaluated, and paths are adapted, re-sliced, and re-sorted if needed.

Adaptive detailing has been physically demonstrated in connections between two standardized elements and virtually tested in connections within spatial structures composed of 10 elements. These experiments have opened many exciting directions for future work, particularly the potential to apply adaptive detailing to reuse reclaimed, imperfect building stock.

6.2   Contributions

The summary of contributions of this thesis is organized here in response to the open challenges presented in Chapters 1 and 2:

6.2.1   On preparing the ground

This contribution supports the early and explicit understanding of the constraints of the manufacturing setup for joining and detailing for robotic assembly:

1. **Developed the concept of *spatial interface* between construction elements assembled robotically and identified methods to describe, design, and build within it. Specifically:**

   - Identified and contextualized the difference between *planar* and *spatial* interface in the context of structures assembled robotically (Chapter 2, Section 2.2.2)

---

[1]Aspects concerning the structural function of the connections, such as calculating the intervening forces between elements and the overall structural performance, have been addressed in a simplified form as they lie outside the scope of this thesis. Their integration requires a dedicated investigation.

- Introduced the concepts of *tool accessibility* and *robot reachability* to describe the tool's and robot's constraints in accessing and reaching the space between construction elements where connections can be placed (Chapter 4, Sections 4.3.1.1 and 4.3.1.2)

- Introduced the concept and a pertinent representation of a reachability map as a *reachable boundary* where the connections' material can be safely placed by the robot (Chapter 4, Section 4.3.1.2)

While *design for manufacturing* (DfM) is a well-known practice in engineering fields, these are still foreign concepts for designers and architects. The demonstrators described in Chapter 5 have explored the DfM concepts of *tool accessibility* and *robot reachability* and validated them as suitable methods to understand and plan the connections between elements of spatial structures that are assembled robotically.

6.2.2 On joining

The unprecedented challenge of joining spatial, non-standard assemblies with robots required the research and development of a suitable joining technique. This contribution can be summarized in the following:

2. **Characterized and developed IPWAAM as an additive robotic joining technique suitable for spatial interfaces for non-touching non-machined metal parts. In particular:**

   - Characterized, developed, and reported on soft- and hardware setups, process parameters, deposition strategies, and printing procedures of point-by-point WAAM performed *in place* (Chapter 3; Ariza et al., 2018)

   - Characterized, implemented, and reported on suitable sensing techniques for localization and probing of as-built elements and IPWAAM paths that can be employed before and during the production process (Chapter 4; Ariza et al., 2018)

- Developed and validated slicing and sorting techniques for point-by-point IPWAAM (Chapter 4 and 5, Sections 4.3.3.2 and 4.3.3.3; 5.1.2.3)

- Investigated and illustrated the design versatility of point-by-point and continuous IPWAAM (Chapter 5, Section 5.1; Mitropoulou, Ariza, et al., 2019)

- Conducted foundational interdisciplinary investigations and reported on key characteristics of IPWAAM products: surface quality, mechanical and corrosion behavior suitability of point-by-point WAAM for structural applications (Chapter 3, Section 3.6.6; Silvestru, Ariza, Vienne, et al., 2021; Silvestru, Ariza, and Taras, 2022; Michel et al., 2022)

These steps contribute to the current state of technology on joining in the context of robotic assembly of spatial structures. In particular, these contributions bridge the fields of additive manufacturing and robotic assembly proposing an additive robotic joining technique. While the setup, parameters, printing and touch-sensing procedures are only relevant to further research on WAAM, the concept of in place printing together with the localization procedure and path slicing methods are transferable to other materials and robotic processes.

6.2.3   On detailing

The following contribution relates to the integration of design and production domains:

3. **Introduction of an integrative pipeline for adaptive design-and-production of in place WAAM connections tailored for robotic assembly of spatial structures. Particularly:**

   - Proposed an adaptive approach to detailing that spans design-*and-production* including design, production execution, and surveying tasks

   - Proposed an integrative approach to detailing for robotic processes that combines the robotic setup and material processing constraints with functional needs (Chapter 4, Sections 4.3.1, 4.3.3, 4.3.2)

- Introduced the concept of *componentization* of detailing tasks that can be interpreted and further implemented as expert domains (Chapter 4, Section 4.3)

- Reported on the specific dependencies present between the pipeline's tasks, in particular between the path generation, slicing, and sorting components (Chapter 4, Sections 4.3.3.1, 4.3.3.2, and 4.3.3.3, and 4.4)

- Introduced the reachable boundary resulting from the robot reachability map as a design space to perform a material distribution calculation and demonstrated through a virtual and physical demonstrator that the result can be safely used to transfer the load between elements (Chapters 4 and 5, Section 4.3.2.2, 5.1.2.2 and 5.1.2.3)

- Provided an example of a generative workflow for the design of structures, taking into account the connections' reachability as a design driver (Chapter 5, Section 5.2.1)

These steps contribute to a software-based culture of detailing with a particular focus on robotic-based processes.

6.3 Discussion and directions for future work

The following sections discuss the contributions of the work, outlining its limitations and providing directions for future development:

6.3.1 Joining with digitally-manufactured materials

This work has explored a novel robotic joining technique that shapes the joining material on demand. The target application, the robotic assembly of spatial structures, benefits from a spatial, additive deposition that can fit and fix elements in varying configurations, cross-sections, and orientations against gravity. The investigated technique and material -in place WAAM with mild steel- present strength and ductility suitable for architectural applications.

While the programmable deposition of the material results convenient to accommodate different conditions, the technique relies on precise

sensing technologies to identify the geometric and surface qualities of the parts to be joined. This work has tested localization approaches for standardized components; however, the investigation of other survey-ing methods would enable using IPWAAM to join parts that present variability in their geometric or surface conditions, such as reclaimed metal elements suitable for adaptive reuse.

In addition, it is critical to control the adaptive printing further. In some of the presented experiments, it has been observed that the adapted points reduced the cross-section of the printed paths influenc-ing its structural performance. Therefore, the process parameters of the adapted points should be studied further, looking at the possibility of increasing instead of reducing the paths' cross-sections and their performance.

Based on the complexity and interdependencies of the control of the IPWAAM process parameters, it follows that a critical stream of further research should focus on modeling the process parameters and the effect of heat during the deposition of the printed parts and substrates. These developments would also contribute to understanding the inter-actions between the mechanical properties of the printed products and the substrates.

These next steps are expected to bring many questions about the struc-tural behavior of the IPWAAM connections. Although barely addressed, these questions have impregnated the work, directing efforts to estab-lish collaborations and studies focused on the behavior of these new materials. The challenges ahead in introducing new processes and materials are manifold, not only technically but also in terms of their acceptance by architects and engineers.[2]

6.3.2   Working with machines in the loop

This thesis started with the premise that designs fabricated entirely by machines require specifying, in a very explicit manner, the charac-teristics of the construction process to be feasible. This condition is

---

[2]On this note, see "The First Steps of Construction in Iron: Problems Posed by the Introduction of a New Construction Material" for a review on the struggles of the architects of the 18th and 19th century when introducing iron challenged the prevalent Vitruvian notions of solidity (Picon, 2010).

particularly critical in complex assemblies, where the spatial reconstruction of the interface between parts is less intuitive. The work has corroborated this premise by illustrating what kind of knowledge the designer needs to acquire when: counting with a robot reachability map, the designer is informed on the actual design space of the machine and therefore anticipates where material can be placed by the robot. The pipeline proposed here makes this information available before the design starts taking shape. However, this level of specification, i.e., the machine's specifications or the location of objects during production, is difficult to imagine in today's Architecture, Engineering, and Construction (AEC) context, where architects and fabricators are disciplinary and contractually separate entities. To make this scenario possible, designers and fabricators would require tight communication workflows and sharing design-and-construction pipelines like the one outlined in this work.

In the current pipeline implementation, the design is only minimally adapted on the printed paths once production starts, as the calculation of the robotic constraints is computationally too expensive to run during production. However, based on current research developments, it is foreseeable that a learned map, a map that is not explicitly computed but inferred from available data points, could be built to give faster feedback during production. In that scenario, the need for a high level of specification in advance of production would be reduced, allowing designers to work with good guesses that would be fined-tuned based on the machine's characteristics once this information is known.

An open question for fabrication-aware design is if fabrication constraints should inform the design or the designer. In the presented pipeline, this question is materialized by the parallel development of the path generation component using the path finding *or* the path sketching methods. These developments were implemented in parallel either by having the material distribution step run automatically inside the reachable boundary or by plotting constraints to let the designer decide how to operate within them. A unifying approach could be to use both in a complementary way. For example, the designer could sketch computationally generated alternatives or modify the results within the production constraints if the automatic approach fails.

6.3.3 Detailing computationally

Detailing is a complex task that designers undertake in numerous ways. The current professional landscape already presents a diversity of computational strategies, and the advancements in digital fabrication in the construction industry are expected to disrupt detailing tasks even more. The presented pipeline acknowledges the inherent complexities of detailing when using robots to build architectural components and presents conceptual tools to organize the robotic, material, and functional challenges of a robotically-manufactured connection detail.

The pipeline proposes a componentization approach to handle each task individually. This approach aims to be compatible with the expert knowledge required to solve each aspect of a detailing problem (Figure 6.1c). Compared to conventional and manual approaches (Figure 6.1a), the pipeline makes each function or task explicit and their dependencies visible to all parts of the design team. A forward-looking approach could enable designers to be supported by available databases to automate recurring problems (Figure 6.1b). A more realistic and hybrid scenario could combine each of these approaches whenever they become pertinent.
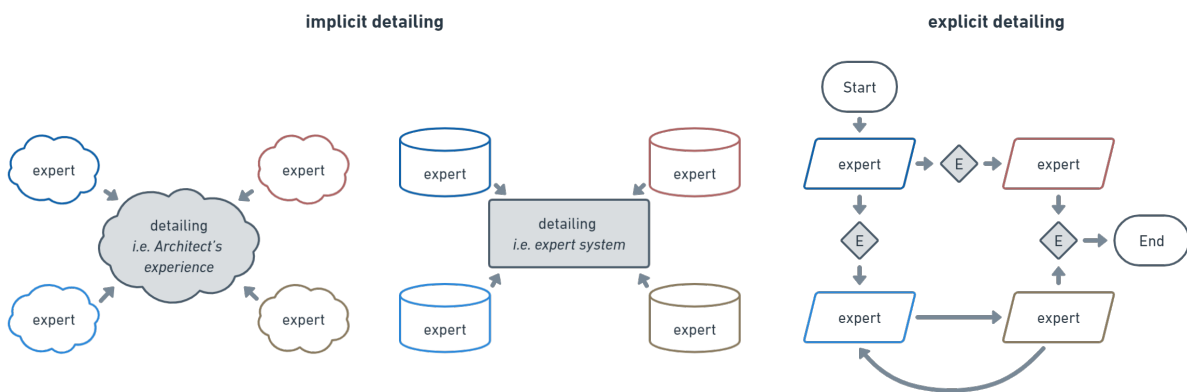
Figure 6.1: *Detailing mindsets: (a) implicit based on experience, (b) implicit based on learned material, (c) explicit based on software components.*

In the proposed pipeline, the integrative nature of detailing as bridging knowledge domains becomes more tangible. The work presented here aims to contribute to an understanding of detailing as shared,

compoundable and accessible knowledge described in a transferrable method. Therefore, the specific implementation of each component can be fully replaced, while the conceptual framework of exposing the inner dependencies should be kept. These concepts align with current efforts in open-source computational frameworks for the AEC industry, such as COMPAS. It is expected that as these software-based practices become more accessible, computational detailing evolves into the task of assembling software pieces together, while experts can focus on the development of each component individually. Good detailing has relied on and will rely on solid team collaboration, and software can only support this with more explicit and faster communication.

6.3.4   Designing adaptive systems

In this work, the term *adaptive* has been used in different contexts with slightly distinct but overlapping meanings:

First, the IPWAAM paths are *adaptive* because they can be *changed* if needed during production to fit and support the as-built positions of elements of a structure. In the same sense, the collection of adaptive paths can be called *adaptive connection detail*, and the assemblies built with them, *adaptive structures*.

Second, the pipeline is called *adaptive detailing* because it provides the means to create adaptive paths, connection details and, in turn, structures. The detailing pipeline receives incoming inputs and outputs a solution based on the actual building conditions. In this sense *adaptive* detailing shares the meaning with *algorithmic* detailing: its components are *programmable*, i.e., different inputs result in different outputs. The novel aspect of the pipeline is that the algorithm does not stop at the design stage but continues throughout production, enabling a truly design-and-production system.

Finally, the possibility of algorithmically shaping, virtually and physically, adaptive connections, unlocks an immense *versatility* for the design-and-production of structures. Although this work has not explored the extent to which adaptive connections can be used in the

design of structures, in its concept it provides a new type of universal, "infinitely shapable" connector that could potentially unlock the materialization of high-performance designs.[3]

Besides the promising directions, all these usages of *adaptive* present challenges related to the control measures to verify that incoming changes result in valid, feasible, and performative solutions. Therefore, there is a path of research for adaptive building on how to implement design checks for algorithmic workflows, validate changeable conditions, and handle the propagation of changes across the different parts of the design-and-production system.

6.4   Final words

Detailing addresses one of the essential tasks of the designer: understanding what tools and materials can do to respond to function and use. Computational detailing has the potential to make that understanding even more explicit. In turn, explicit detailing could enable designers to better understand construction problems to find novel, pertinent, and performative detail solutions. The possibility of shaping the connection detail on demand and refining it with adaptive strategies during or even after its production opens many exciting new directions for building architecture that accurately responds to needs and can be revisited during its lifetime. With these possibilities in mind, this work aims to support an architectural practice that inspires the production of building knowledge in accessible and tangible formats.

---

[3]The term "infinitely shapable" is used by Mario Rinke in "The Infinitely Shapable Structure: Structural Iron and the Decontextualization of Construction" to explain the abundance of spatial, material and structural possibilities introduced by structural iron in the 18th century (Rinke, 2010).

List of Figures

List of Tables

List of Acronyms

AD   Adaptive Detailing

AM   Additive Manufacturing

CMT   Cold Metal Transfer

DFAB   Digital Fabrication

DfAM   Design for Additive Manufacturing

DfM   Design for Manufacturing

GMAW Gas Metal Arc Welding

IK   Inverse Kinematics

IPWAAM In place Wire and Arc Additive Manufacturing

TO   Topology Optimization

VM   Volumetric Modeling

WAAM Wire and Arc Additive Manufacturing

Bibliography

Abdelwahab, Moustafa and Konstantinos Daniel Tsavdaridis (Jan. 2019). "Optimised 3D-Printed Metallic Node-Connections for Reticulated Structures". In: *Proceedings of the 9th International Conference on Steel and Aluminium Structures (ICSAS19)*. Ed. by D. Lam, X. Dai, T. Yang, and K. Zhou. Bradford, UK: Independent Publishing Network, pp. 423–434. ISBN: 978-1-78972-197-3. DOI: 10.31224/osf.io/jkexd.

Abe, Takeyuki and Hiroyuki Sasahara (Aug. 2019). "Layer Geometry Control for the Fabrication of Lattice Structures by Wire and Arc Additive Manufacturing". In: *Additive Manufacturing* 28, pp. 639–648. ISSN: 2214-8604. DOI: 10.1016/j.addma.2019.06.010.

Adel, Arash, Andreas Thoma, Matthias Helmreich, Fabio Gramazio, and Matthias Kohler (Oct. 2018). "Design of Robotically Fabricated Timber Frame Structures". In: *ACADIA 2018: Recalibration. On Imprecision and Infidelity. Proceedings of the 38th Annual Conference of the Association for Computer Aided Design in Architecture (ACADIA)*. Mexico City, Mexico, pp. 394–403. ISBN: 978-0-692-17729-7. DOI: 10.52842/conf.acadia.2018.394.

Agapakis, John E. (1984). "Vision-Aided Remote Robotic Welding". PhD thesis. Massachusetts Institute of Technology.

Allen, Edward and Patrick Rand (2007). *Architectural Detailing : Function, Constructibility, Aesthetics*. Hoboken, N.J. : John Wiley & Sons, c2007. ISBN: 978-0-471-48817-0.

Allen, Edward and Waclaw Zalewski (2012). *Form and Forces: Designing Efficient, Expressive Structures.* Hoboken: John Wiley & Sons. ISBN: 978-0-470-64035-7.

Alvarez, Martin E., Erik E. Martínez-Parachini, Ehsan Baharlou, Oliver David Krieg, Tobias Schwinn, Lauren Vasey, Chai Hua, Achim Menges, and Philip F. Yuan (2019). "Tailored Structures, Robotic Sewing of Wooden Shells". In: *Robotic Fabrication in Architecture, Art and Design 2018*. Ed. by Jan Willmann, Philippe Block, Marco Hutter, Kendra Byrne, and Tim Schork. Cham: Springer International Publishing, pp. 405–420. ISBN: 978-3-319-92294-2. DOI: 10.1007/978-3-319-92294-2_31.

Apolinarska, Aleksandra Anna (2018). "Complex Timber Structures from Simple Elements: Computational Design of Novel Bar Structures for Robotic Fabrication and Assembly". PhD thesis. ETH Zurich, 164 p. DOI: 10.3929/ETHZ-B-000266723.

Apolinarska, Aleksandra Anna, Ralph Bärtschi, Reto Furrer, Fabio Gramazio, and Matthias Kohler (2016). "Mastering the Sequential Roof: Computational Methods for Integrating Design, Structural Analysis, and Robotic Fabrication". In: *Advances in Architectural Geometry 2016*. Ed. by Sigrid Adriaenssens, Fabio Gramazio, Matthias Kohler, Achim Menges, and Mark Pauly. CH: vdf Hochschulverlag AG an der ETH Zürich, pp. 240–258. DOI: 10.3218/3778-4.

Ariza, Inés (2016). "Decoding Details: Integrating Physics of Assembly in Discrete Element Structures". MA thesis. Cambridge, Massachusetts: Massachusetts Institute of Technology.

Ariza, Inés, Ammar Mirjan, Augusto Gandia, Gonzalo Casas, Samuel Cros, Fabio Gramazio, and Matthias Kohler (Oct. 2018). "In Place Detailing: Combining 3D Printing and Robotic Assembly". In: *ACADIA 2018 Recalibration: On Imprecision and Infidelity. Proceedings of the 38th Annual Conference of the Association for Computer Aided Design in Architecture*. Mexico City, pp. 312–321. ISBN: 978-0-692-17729-7. DOI: 10.52842/conf.acadia.2018.312.

AWS D1.1: Structural Welding Code–Steel (1999).

Baker, Ralph (Apr. 1925). "Method of Making Decorative Articles". US1533300A.

Ballast, David Kent (2007). *Handbook of Construction Tolerances*. Hoboken, N.J.: John Wiley & Sons. ISBN: 978-0-471-93151-5.

Bañón, Carlos and Félix Raspall (2021). "Optimized Structures: AirMesh". In: *3D Printing Architecture: Workflows, Applications, and Trends*. Ed. by Carlos Bañón and Félix Raspall. SpringerBriefs in Architectural Design and Technology. Singapore: Springer, pp. 21–37. ISBN: 978-9-8115-8388-9. DOI: 10.1007/978-981-15-8388-9_3.

Bechthold, Martin (2010). "The Return of the Future: A Second Go at Robotic Construction". In: *Architectural Design* 80.4, pp. 116–121. ISSN: 1554-2769. DOI: 10.1002/ad.1115.

Bendsøe, Martin P. (2004). *Topology Optimization: Theory, Methods and Applications*. Second edition, corrected printing. Berlin: Springer. ISBN: 978-3-642-07698-5.

– (2009). "Topology Optimization". In: *Encyclopedia of Optimization*. Ed. by Christodoulos A. Floudas and Panos M. Pardalos. Boston, MA: Springer US,

pp. 3928–3929. ISBN: 978-0-387-74759-0. DOI: 10.1007/978-0-387-74759-0_685.

Bergmann, Jean Pierre, Jörg Lange, Jörg Hildebrand, Mathias Eiber, Maren Erven, Christof Gaßmann, Chen-Hao Chiang, Claus Lenz, Thorsten Röder, and Wais Bashariar (2020). "Herstellung von 3D-gedruckten Stahlknoten". In: *Stahlbau* 89.12, pp. 956–969. ISSN: 1437-1049. DOI: 10.1002/stab.202000080.

Bermano, Amit H., Thomas Funkhouser, and Szymon Rusinkiewicz (May 2017). "State of the Art in Methods and Representations for Fabrication-Aware Design". In: *Computer Graphics Forum* 36.2, pp. 509–535. ISSN: 0167-7055. DOI: 10.1111/cgf.13146.

Bernhard, Mathias (2017). *Volumetric Modelling*. Digital Building Technologies, ETH Zürich, https://dbt.arch.ethz.ch/research-stream/volumetric-modelling/.

Bernhard, Mathias and Remy Clemente (Jan. 2022). *Compas_vol*. Digital Building Technologies, https://github.com/dbt-ethz/compas_vol.

Bi, Zhu Ming (2011). "Multi-Process Tools for Fabrication, Assembly and Inspection". In: *Advanced Materials Research* 338, pp. 670–676. ISSN: 1662-8985. DOI: 10.4028/www.scientific.net/AMR.338.670.

Białkowski, Sebastian (Aug. 2016). "Structural Optimisation Methods as a New Toolset for Architects". In: *Proceedings of the 34th eCAADe Conference: Complexity & Simplicity*. Oulu, pp. 255–264. DOI: 10.52842/conf.ecaade.2016.2.255.

– (2017). "tOpos - GPGPU Accelerated Structural Optimisation Utility for Architects". In: *Proceedings of the 35th eCAADe Conference: ShoCK! - Sharing Computational Knowledge!* Rome, pp. 679–688. DOI: 10.52842/conf.ecaade.2017.1.679.

– (Sept. 2018). "Topology Optimisation Influence on Architectural Design Process - Enhancing Form Finding Routine by tOpos Toolset Utilisation". In: *Proceedings of the 36th eCAADe Conference: Computing for a Better Tomorrow*. Lodz, pp. 139–148. DOI: 10.52842/conf.ecaade.2018.1.139.

Boake, Terri Meyer (2013). *Understanding Steel Design: An Architectural Design Manual*. Birkhäuser. ISBN: 978-3-0346-1048-3. DOI: 10.1515/9783034610483.

– (2014). *Diagrid Structures: Systems, Connections, Details*. Birkhäuser. ISBN: 978-3-03821-482-3. DOI: 10.1515/9783038214823.

– (2015). *Architecturally Exposed Structural Steel*. Birkhäuser. ISBN: 978-3-03821-483-0. DOI: 10.1515/9783038214830.

Bock, Thomas (Oct. 2008). "Construction Automation and Robotics". In: ISBN: 978-953-7619-13-8. DOI: 10.5772/5861.

Bock, Thomas and Willi Viktor Lauer (June 2010). "Location Orientation Manipulator by Konrad Wachsmann, John Bollinger and Xavier Mendoza". In: *2010 Proceedings of the 27th ISARC (International Symposium on Automation and Robotics in Construction)*. Bratislava, Slovakia: IAARC, pp. 704–712. ISBN: 978-80-7399-974-2. DOI: 10.22260/ISARC2010/0075.

Bock, Thomas and Thomas Linner (2015). *Robot-Oriented Design: Design and Management Tools for the Deployment of Automation and Robotics in Construction*. Cambridge: Cambridge University Press. ISBN: 978-1-107-07638-9. DOI: 10.1017/CBO9781139924146.

Bonér, Jonas, Dave Farley, Roland Kuhn, and Martin Thompson (2014). *The Reactive Manifesto*. https://www.reactivemanifesto.org/.

Bonwetsch, Tobias (Oct. 2012). "Robotic Assembly Processes as a Driver in Architectural Design". In: *Nexus Network Journal* 14.3, pp. 483–494. ISSN: 1522-4600. DOI: 10.1007/s00004-012-0119-3.

– (2015). "Robotically Assembled Brickwork: Manipulating Assembly Processes of Discrete Elements". PhD thesis. Zurich, Switzerland: ETH Zurich. DOI: 10.3929/ETHZ-A-010602028.

Bruun, Edvard P. G., Rafael Pastrana, Vittorio Paris, Alessandro Beghini, Attilio Pizzigoni, Stefana Parascho, and Sigrid Adriaenssens (Sept. 2021). "Three Cooperative Robotic Fabrication Methods for the Scaffold-Free Construction of a Masonry Arch". In: *Automation in Construction* 129, p. 103803. ISSN: 0926-5805. DOI: 10.1016/j.autcon.2021.103803.

Buchli, Jonas, Markus Giftthaler, Nitish Kumar, Manuel Lussi, Timothy Sandy, Kathrin Dörfler, and Norman Hack (Oct. 2018). "Digital in Situ Fabrication - Challenges and Opportunities for Robotic in Situ Fabrication in Architecture, Construction, and Beyond". In: *Cement and Concrete Research* 112, pp. 66–75. ISSN: 00088846. DOI: 10.1016/j.cemconres.2018.05.013.

BullsEye (2022). ABB, https://perma.cc/FRP7-GFX6.

Casas, Gonzalo, Beverly Lytle, Augusto Gandia, and Inés Ariza (2021). *COMPAS_FAB: compas_fab.Sensors*. Gramazio Kohler Research, ETH Zürich, https://perma.cc/T3VM-CS47.

Casas, Gonzalo, Beverly Lytle, Mathias Lüdtke, Alexis Jeandeau, Hiroyuki Obinata, Pedro Pereira, and Domenic Rodriguez (2018). *Roslibpy: ROS Bridge Library*. Gramazio Kohler Research, ETH Zürich, https://github.com/gramaziokohler/roslibpy.

Casas, Gonzalo, Romana Rust, and Beverly Lytle (2018). *Compas_fab: Backends: ROS*. Gramazio Kohler Research, ETH Zürich, https://perma.cc/AVL5-J63H.

Chan, Paul W (Nov. 2020). "Briefing: Industry 4.0 in Construction: Radical Transformation or Restricted Agenda?" In: *Proceedings of the Institution of Civil Engineers - Management, Procurement and Law* 173.4, pp. 141–144. ISSN: 1751-4304. DOI: 10.1680/jmapl.20.00036.

Chen, Yonghua, Jianan Lu, and Ying Wei (Jan. 2016). "Topology Optimization for Manufacturability Based on the Visibility Map". In: *Computer-Aided Design and Applications* 13.1, pp. 86–94. ISSN: 1686-4360. DOI: 10.1080/16864360.2015.1059199.

Chilton, John (Dec. 1999). *Space Grid Structures*. London: Routledge. ISBN: 978-0-08-049818-8. DOI: 10.4324/9780080498188.

Chong, Oscar Wong, Christopher Baker, Kereshmeh Afsari, Jiansong Zhang, and Michael Roach (Nov. 2020). "Integration of BIM Processes in Architectural Design, Structural Analysis, and Detailing: Current Status and Limitations". In: *Construction Research Congress 2020*. Tempe, Arizona: American Society of Civil Engineers, pp. 1203–1212. DOI: 10.1061/9780784482865.127.

Classen, Martin, Jan Ungermann, and Rahul Sharma (May 2020). "Additive Manufacturing of Reinforced Concrete—Development of a 3D Printing Technology for Cementitious Composites with Metallic Reinforcement". In: *Applied Sciences* 10.11, p. 3791. ISSN: 2076-3417. DOI: 10.3390/app10113791.

COMPAS Assembly (2022). Block Research Group, ETH Zürich, https://github.com/BlockResearchGroup/compas_assembly.

COMPAS: Artists (2022). https://perma.cc/QWR7-4QVF.

Connection Design Static Loading: Simple Connections for Buildings. (2000). https://perma.cc/R8K7-RMEK.

Connector for Takenaka (2019). MX3D and Tanekana Corporation, https://mx3d.com/industries/construction/connector-for-takenaka/.

Cook, George E. (Aug. 1983). "Robotic Arc Welding: Research in Sensory Feedback Control". In: *IEEE Transactions on Industrial Electronics* IE-30.3, pp. 252–268. ISSN: 1557-9948. DOI: 10.1109/TIE.1983.356736.

Crolla, Kristof, Nicholas Williams, Manuel Muehlbauer, and Jane Burry (Apr. 2017). "SmartNodes Pavilion - Towards Custom-optimized Nodes Applications in Construction". In: *Proceedings of the 22nd CAADRIA Conference*. Xi'an Jiaotong-Liverpool University, Suzhou, China, pp. 467–476. DOI: 10.52842/conf.caadria.2017.467.

Cros, Samuel (2017). "Spatial Robotic Welding". MA thesis. Zurich, Switzerland: ETH Zurich.

Dackweiler, Marius, Tobias Mayer, Sven Coutandin, and Jürgen Fleischer (Oct. 2019). "Modeling and Optimization of Winding Paths to Join Lightweight Profiles with Continuous Carbon Fibers". In: *Production Engineering* 13.5, pp. 519–528. ISSN: 1863-7353. DOI: 10.1007/s11740-019-00914-2.

Danhaive, Renaud and Caitlin T. Mueller (July 2021). "Design Subspace Learning: Structural Design Space Exploration Using Performance-Conditioned Generative Modeling". In: *Automation in Construction* 127, p. 103664. ISSN: 0926-5805. DOI: 10.1016/j.autcon.2021.103664.

De Maeyer, Jeroen, Bart Moyaers, and Eric Demeester (Sept. 2017). "Cartesian Path Planning for Arc Welding Robots: Evaluation of the Descartes Algorithm". In: *2017 22nd IEEE International Conference on Emerging Technologies and Factory Automation (ETFA)*, pp. 1–8. DOI: 10.1109/ETFA.2017.8247616.

Deplazes, Andrea, ed. (2005). *Constructing Architecture: Materials, Processes, Structures, a Handbook*. Basel; Boston: Birkhäuser-Publishers for Architecture. ISBN: 978-3-0356-1670-5.

Descartes (2014). ROS-Industrial Consortium, http://wiki.ros.org/descartes.

"Detail" (2022). In: *Online Etymology Dictionary*. URL: https://www.etymonline.com/word/detail.

Doerfler, Kathrin (2018). "Strategies for Robotic In Situ Fabrication". PhD thesis. ETH Zurich. DOI: 10.3929/ethz-b-000328683.

Eames Office (1972). *DESIGN Q&A*. URL: https://www.youtube.com/watch?v=bmgxDCujTUw.

"Edge jointing" (2022). In: *Wikipedia*. URL: https://en.wikipedia.org/wiki/Edge_jointing.

Emmitt, Stephen (2003). "Learning to Think and Detail From First (Leaner) Principles". In: *11th Annual Conference of the International Group for Lean Construction*. Virginia, USA.

Erven, Maren, Jörg Lange, and Thilo Feucht (2021). "3D-Printing with Steel of a Bolted Connection". In: *ce/papers* 4.2-4, pp. 825–832. ISSN: 2509-7075. DOI: 10.1002/cepa.1367.

Feucht, Thilo, Jörg Lange, and Maren Erven (Sept. 2019). "3-D-Printing with Steel: Additive Manufacturing of Connection Elements and Beam Reinforcements". In: *ce/papers* 3.3-4, pp. 343–348. ISSN: 2509-7075, 2509-7075. DOI: 10.1002/cepa.1064.

Feucht, Thilo, Jörg Lange, Maren Erven, Christopher Borg Costanzi, Ulrich Knaack, and Benedikt Waldschmitt (June 2020). "Additive Manufacturing

by Means of Parametric Robot Programming". In: *Construction Robotics* 4.1-2, pp. 31–48. ISSN: 2509-811X, 2509-8780. DOI: 10.1007/s41693-020-00033-w.

Fleischmann, Philippe, Gonzalo Casas, and Michael Lyrenmann (July 2020). *COMPAS RRC: Online Control for ABB Robots over a Simple-to-Use Python Interface.* DOI: 10.5281/zenodo.4639418.

Florea, Vlad, Manish Pamwar, Balbir Sangha, and Il Yong Kim (Dec. 2019). "3D Multi-Material and Multi-Joint Topology Optimization with Tooling Accessibility Constraints". In: *Structural and Multidisciplinary Optimization* 60.6, pp. 2531–2558. ISSN: 1615-1488. DOI: 10.1007/s00158-019-02344-1.

Ford, Edward R. (2011). *The Architectural Detail*. 1st ed. New York: Princeton Architectural Press. ISBN: 978-1-56898-978-5.

Frampton, Kenneth (1995). *Studies in Tectonic Culture: The Poetics of Construction in Nineteenth and Twentieth Century Architecture*. Ed. by John Cava. Cambridge, Mass.: MIT Press. ISBN: 978-0-262-56149-5.

Fronius (2004). *Cold Metal Transfer*. https://perma.cc/P22F-QH68.

– ed. (2022a). *60i Robacta Drive*. https://perma.cc/K2B2-3AEW.

– ed. (2022b). *TPS500i Operating Manual*. https://perma.cc/K2B2-3AEW.

Galjaard, Salomé, Sander Hofman, and Shibo Ren (2015). "New Opportunities to Optimize Structural Designs in Metal by Using Additive Manufacturing". In: *Advances in Architectural Geometry 2014*. Springer, Cham, pp. 79–93. ISBN: 978-3-319-11417-0. DOI: 10.1007/978-3-319-11418-7_6.

Gandia, Augusto (2020). "Robotic Fabrication Simulation: A Computational Method for the Design of Fabrication-aware Spatial Structures". PhD thesis. ETH Zurich. DOI: 10.3929/ethz-b-000478068.

Gao, Xiang, Sébastien Loriot, and Andrea Tagliasacchi (2021). "Triangulated Surface Mesh Skeletonization". In: *CGAL User and Reference Manual*. 5.2.1. CGAL Editorial Board.

Garaigordobil, Alain, Rubén Ansola, Javier Santamaría, and Igor Fernández de Bustos (Nov. 2018). "A New Overhang Constraint for Topology Optimization of Self-Supporting Structures in Additive Manufacturing". In: *Structural and Multidisciplinary Optimization* 58.5, pp. 2003–2017. ISSN: 1615-1488. DOI: 10.1007/s00158-018-2010-7.

Gardner, Leroy, Pinelopi Kyvelou, Gordon Herbert, and Craig Buchanan (Sept. 2020). "Testing and Initial Verification of the World's First Metal 3D Printed Bridge". In: *Journal of Constructional Steel Research* 172, p. 106233. ISSN: 0143-974X. DOI: 10.1016/j.jcsr.2020.106233.

Garrett, Caelan (2022). *Pybullet-Planning: A Suite of Utility Functions to Facilitate Robotic Planning Related Research on the Pybullet Physics Simulation Engine*. https://github.com/caelan/pybullet-planning.

Ghaffar, Seyed Hamidreza, Jorge Corker, and Paul Mullett (2020). "The Potential for Additive Manufacturing to Transform the Construction Industry". In: *Construction 4.0*. Routledge. ISBN: 978-0-429-39810-0.

Gramazio, Fabio, Matthias Kohler, and Jan Willmann (2014). *The Robotic Touch: How Robots Change Architecture*. Zurich: Park Books. ISBN: 978-3-906027-37-1.

Gramazio Kohler Research (2009). *Voxels 2*. https://gramaziokohler.arch.ethz.ch/web/e/projekte/172.html.

– (2020). *Adaptive Detailing with WAAM*. https://vimeo.com/manage/videos/544532543/d934bdd991.

– (2021). *Data-Driven Acoustic Design*. https://gramaziokohler.arch.ethz.ch/web/e/forschung/363.html.

– (2022). *Semiramis*. https://gramaziokohler.arch.ethz.ch/web/e/projekte/409.html.

Graser, Konrad, Arash Adel, Marco Baur, Daniel Sanz Pont, and Andreas Thoma (Jan. 2021). "Parallel Paths of Inquiry: Detailing for DFAB HOUSE". In: *Technology|Architecture + Design* 5.1, pp. 38–43. ISSN: 2475-1448. DOI: 10.1080/24751448.2021.1863668.

Guest, James K. and Mu Zhu (Sept. 2013). "Casting and Milling Restrictions in Topology Optimization via Projection-Based Algorithms". In: *ASME 2012 International Design Engineering Technical Conferences and Computers and Information in Engineering Conference*. American Society of Mechanical Engineers Digital Collection, pp. 913–920. DOI: 10.1115/DETC2012-71507.

Hack, Norman, Willi Viktor Lauer, Fabio Gramazio, Matthias Kohler, and Silke Langenberg (2017). "Mesh-Mould: Robotically Fabricated Spatial Meshes as Concrete Formwork and Reinforcement". In: *Fabricate 2014*. DGO - Digital original. Negotiating Design & Making. UCL Press, pp. 224–232. DOI: 10.2307/j.ctt1tp3c5w.31.

Heerdegen, James (Sept. 2021). "Non-Linear Fabrication: A Dialogue between Architecture and Robotic Wire-Arc Additive Manufacture". MA thesis. University of Wellington. DOI: 10.26686/wgtn.16644829.v1.

Holst, Hendrik, Veton Beciri, Vlad-Alexandru Silvestru, and Andreas Taras (2021). *Topology Optimization of Structural Steel Nodes for Wire and Arc Additive Manufacturing*. Tech. rep. ETH Zurich.

Hong, T.S., Morteza Ghobakhloo, and Weria Khaksar (May 2014). "Robotic Welding Technology". In: *Comprehensive Materials Processing* 6, pp. 77–99. ISSN: 978-0-0809-6533-8. DOI: 10.1016/B978-0-08-096532-1.00604-X.

Horn, Abbigayle (2015). "Integrating Constructability into Conceptual Structural Design and Optimization". MA thesis. Cambridge, Massachussetts: Massachusetts Institute of Technology.

Hoyt, Robert, Jesse Cushing, Greg Jimmerson, Jeffrey Slostad, Robert Dyer, and Steve Alvarado (2016). *SpiderFab™: Process for On-Orbit Construction of Kilometer-Scale Apertures*. Tech. rep. Tethers Unlimited, Inc.

Huang, Xiaodong and Yi Min Xie (2010). *Evolutionary Topology Optimization of Continuum Structures: Methods and Applications*. Chichester, West Sussex: Wiley. ISBN: 978-0-470-68948-6.

Huang, Yijiang (2022). "Algorithmic Planning for Robotic Assembly of Building Structures". PhD thesis. Massachusetts Institute of Technology.

Huang, Yijiang, Josephine V Carstensen, and Caitlin T Mueller (July 2018). "3D Truss Topology Optimization for Automated Robotic Spatial Extrusion". In: *Proceedings of the IASS Symposium 2018 Creativity in Structural Design*. Vol. 2018. Boston, MA: International Association for Shell and Spatial Structures (IASS), pp. 1–8.

Huang, Yijiang, Caelan R. Garrett, Ian Ting, Stefana Parascho, and Caitlin T. Mueller (June 2021a). "Robotic Additive Construction of Bar Structures: Unified Sequence and Motion Planning". In: *Construction Robotics* 5.2, pp. 115–130. ISSN: 2509-8780. DOI: 10.1007/s41693-021-00062-z.

– (June 2021b). "Robotic Additive Construction of Bar Structures: Unified Sequence and Motion Planning". In: *Construction Robotics* 5.2, pp. 115–130. ISSN: 2509-8780. DOI: 10.1007/s41693-021-00062-z.

Huang, Yijiang, Pok Yin Victor Leung, Caelan Garrett, Fabio Gramazio, Matthias Kohler, and Caitlin Mueller (Oct. 2021). "The New Analog: A Protocol for Linking Design and Construction Intent with Algorithmic Planning for Robotic Assembly of Complex Structures". In: *SCF '21: Symposium on Computational Fabrication*. Virtual Event USA: Association for Computing Machinery, pp. 1–17. ISBN: 978-1-4503-9090-3. DOI: 10.1145/3485114.3485122.

IRB 4600 Data (2022). ABB, https://perma.cc/9B75-JNR4.

Jaspart, Jean-Pierre (2016). *Design of Joints in Steel and Composite Structures*. ECCS Eurocode Design Manuals. Berlin, [Germany: Ernst & Sohn. ISBN: 978-1-5231-1514-3.

Jiang, Tao and Mehran Chirehdast (Mar. 1997). "A Systems Approach to Structural Topology Optimization: Designing Optimal Connections". In: *Mechanical Design* 119.1, pp. 40–47. DOI: 10.1115/1.2828787.

Johns, Ryan Luke and Jeffrey Anderson (Oct. 2018). "Interfaces for Adaptive Assembly". In: *ACADIA // 2018: Recalibration. On Imprecisionand Infidelity. [Proceedings of the 38th Annual Conference of the Association for Computer Aided Design in Architecture (ACADIA)*. Mexico City, pp. 126–135. DOI: 10.52842/conf.acadia.2018.126.

Johns, Ryan Luke, Martin Wermelinger, Ruben Mascaro, Dominic Jud, Fabio Gramazio, Matthias Kohler, Margarita Chli, and Marco Hutter (Dec. 2020). "Autonomous Dry Stone". In: *Construction Robotics* 4.3, pp. 127–140. ISSN: 2509-8780. DOI: 10.1007/s41693-020-00037-6.

"Jointing (sharpening)" (2022). In: *Wikipedia*. URL: https://en.wikipedia.org/w/index.php?title=Jointing_(sharpening)&oldid=982346057.

Joni, Nicolae and Andreea Dobra (2010). "Specialized Positioners and Manipulators for Robotic Welding". In: *Solid State Phenomena* 166–167, pp. 235–240. ISSN: 1662-9779. DOI: 10.4028/www.scientific.net/SSP.166-167.235.

Joosten, S. K. (2015). "Printing a Stainless Steel Bridge: An Exploration of Structural Properties of Stainless Steel Additive Manufactures for Civil Engineering Purposes". MA thesis. Delft: TU Delft.

Kah, P., R. Suoranta, and J. Martikainen (July 2013). "Advanced Gas Metal Arc Welding Processes". In: *The International Journal of Advanced Manufacturing Technology* 67.1-4, pp. 655–674. ISSN: 0268-3768, 1433-3015. DOI: 10.1007/s00170-012-4513-5.

Keating, Steven and Neri Oxman (Dec. 2013). "Compound Fabrication: A Multi-Functional Robotic Platform for Digital Design and Fabrication". In: *Robotics and Computer-Integrated Manufacturing* 29.6, pp. 439–448. ISSN: 0736-5845. DOI: 10.1016/j.rcim.2013.05.001.

Kilian, Axel (2006). "Design Exploration through Bidirectional Modeling of Constraints". PhD thesis. Massachusetts Institute of Technology.

Köhler, Markus, Jonas Hensel, and Klaus Dilger (July 2020). "Effects of Thermal Cycling on Wire and Arc Additive Manufacturing of Al-5356 Components". In: *Metals* 10.7, p. 952. DOI: 10.3390/met10070952.

Kohlhammer, Thomas, Aleksandra Anna Apolinarska, Fabio Gramazio, and Matthias Kohler (June 2017). "Design and Structural Analysis of Complex Timber Structures with Glued T-joint Connections for Robotic Assembly". In: *International Journal of Space Structures* 32.3-4, pp. 199–215. ISSN: 0956-0599, 2059-8033. DOI: 10.1177/0266351117746268.

Kumar, Nitish, Norman Hack, Kathrin Doerfler, Alexander Nikolas Walzer, Gonzalo Javier Rey, Fabio Gramazio, Matthias Daniel Kohler, and Jonas Buchli (May 2017). "Design, Development and Experimental Assessment of a Robotic End-Effector for Non-Standard Concrete Applications". In: *2017 IEEE International Conference on Robotics and Automation (ICRA)*. Singapore, Singapore: IEEE, pp. 1707–1713. ISBN: 978-1-5090-4633-1. DOI: 10.1109/ICRA.2017.7989201.

Kumpusch, Christoph a (2016). *Detail Kultur: If Buildings Had DNA : Case Studies of Mutations : The Complex Behavior of Collective Detail*, *10 Lenses*, *12+1 Projects*. Beijing: AADCU Program. ISBN: 978-0-692-67389-8.

Labonnote, Nathalie, Anders Rønnquist, Bendik Manum, and Petra Rüther (Dec. 2016). "Additive Construction: State-of-the-art, Challenges and Opportunities". In: *Automation in Construction* 72, pp. 347–366. ISSN: 0926-5805. DOI: 10.1016/j.autcon.2016.08.026.

Laghi, Vittoria, Michele Palermo, Giada Gasparini, and Tomaso Trombetti (Dec. 2020). "Computational Design and Manufacturing of a Half-Scaled 3D-printed Stainless Steel Diagrid Column". In: *Additive Manufacturing* 36, p. 101505. ISSN: 22148604. DOI: 10.1016/j.addma.2020.101505.

Lange, Jörg, Thilo Feucht, and Maren Erven (Aug. 2020). "3D Printing with Steel: Additive Manufacturing for Connections and Structures". In: *Steel Construction* 13.3, pp. 144–153. ISSN: 1867-0520, 1867-0539. DOI: 10.1002/stco.202000031.

Leary, Martin (Jan. 2020a). "6 - Topology Optimization for AM". In: *Design for Additive Manufacturing*. Ed. by Martin Leary. Additive Manufacturing Materials and Technologies. Elsevier, pp. 165–202. ISBN: 978-0-12-816721-2. DOI: 10.1016/B978-0-12-816721-2.00006-3.

– (Jan. 2020b). "Chapter 1 - Introduction to AM". In: *Design for Additive Manufacturing*. Ed. by Martin Leary. Additive Manufacturing Materials and Technologies. Elsevier, pp. 1–6. ISBN: 978-0-12-816721-2. DOI: 10.1016/B978-0-12-816721-2.00001-4.

Leder, Samuel, Ramon Weber, Dylan Wood, Oliver Bucklin, and Achim Menges (Oct. 2019). "Distributed Robotic Timber Construction". In: *ACADIA 19:UBIQUITY AND AUTONOMY [Proceedings of the 39th Annual Conference of the Association for Computer Aided Design in Architecture (ACADIA)*. Austin, Texas, pp. 510–519. DOI: 10.52842/conf.acadia.2019.510.

Lee, Juney, Tom Van Mele, and Philippe Block (June 2018). "Disjointed Force Polyhedra". In: *Computer-Aided Design* 99, pp. 11–28. ISSN: 0010-4485. DOI: 10.1016/j.cad.2018.02.004.

Leung, Pok Yin Victor (2023). "Spatial Timber Assembly with Distributed Architectural Robotics". PhD thesis. Zurich, Switzerland: ETH Zurich.

Leung, Pok Yin Victor, Aleksandra Anna Apolinarska, Davide Tanadini, Fabio Gramazio, and Matthias Kohler (Mar. 2021). "Automatic Assembly of Jointed Timber Structure Using Distributed Robotic Clamps". In: *PROJECTIONS - Proceedings of the 26th CAADRIA Conference*. Hong Kong, pp. 583–592. DOI: 10.52842/conf.acadia.2019.510.

Li, Yongzhe, Qinglin Han, Imre Horváth, and Guangjun Zhang (Dec. 2019). "Repairing Surface Defects of Metal Parts by Groove Machining and Wire + Arc Based Filling". In: *Journal of Materials Processing Technology* 274, p. 116268. ISSN: 0924-0136. DOI: 10.1016/j.jmatprotec.2019.116268.

Li, Zhengyao, Konstantinos Daniel Tsavdaridis, and Leroy Gardner (2021). "A Review of Optimised Additively Manufactured Steel Connections for Modular Building Systems". In: *Industrializing Additive Manufacturing*. Ed. by Mirko Meboldt and Christoph Klahn. Cham: Springer International Publishing, pp. 357–373. ISBN: 978-3-030-54334-1. DOI: 10.1007/978-3-030-54334-1_25.

Liu, Jienan, Yanling Xu, Yu Ge, Zhen Hou, and Shanben Chen (Nov. 2020). "Wire and Arc Additive Manufacturing of Metal Components: A Review of Recent Research Developments". In: *The International Journal of Advanced Manufacturing Technology* 111.1, pp. 149–198. ISSN: 1433-3015. DOI: 10.1007/s00170-020-05966-8.

Liu, Jikai, Andrew T. Gaynor, Shikui Chen, Zhan Kang, Krishnan Suresh, Akihiro Takezawa, Lei Li, Junji Kato, Jinyuan Tang, Charlie C. L. Wang, Lin Cheng, Xuan Liang, and Albert. C To (June 2018). "Current and Future Trends in Topology Optimization for Additive Manufacturing". In: *Structural and Multidisciplinary Optimization* 57.6, pp. 2457–2483. ISSN: 1615-1488. DOI: 10.1007/s00158-018-1994-3.

Liu, Jikai and Yongsheng Ma (Oct. 2016). "A Survey of Manufacturing Oriented Topology Optimization Methods". In: *Advances in Engineering Software* 100, pp. 161–175. ISSN: 0965-9978. DOI: 10.1016/j.advengsoft.2016.07.017.

Liu, Yan, Lijuan Ren, and Xincheng Tian (Nov. 2019). "A Robot Welding Approach for the Sphere-Pipe Joints with Swing and Multi-Layer Planning". In: *The International Journal of Advanced Manufacturing Technology* 105.1, pp. 265–278. ISSN: 1433-3015. DOI: 10.1007/s00170-019-04216-w.

Lógó, János and Hussein Ismail (Sept. 2020). "Milestones in the 150-Year History of Topology Optimization: A Review". In: *Computer Assisted Methods*

in Engineering and Science 27.2–3, pp. 97–132. ɪssɴ: 2299-3649. ᴅoɪ: `10.24423/cames.296`.

Lussi, Manuel, Timothy Sandy, Kathrin Dorfler, Norman Hack, Fabio Gramazio, Matthias Kohler, and Jonas Buchli (May 2018). "Accurate and Adaptive in Situ Fabrication of an Undulated Wall Using an On-Board Visual Sensing System". In: *2018 IEEE International Conference on Robotics and Automation (ICRA)*. Brisbane, QLD: IEEE, pp. 3532–3539. ɪsʙɴ: 978-1-5386-3081-5. ᴅoɪ: `10.1109/ICRA.2018.8460480`.

Ma, Raymond R. and Aaron M. Dollar (June 2011). "On Dexterity and Dexterous Manipulation". In: *2011 15th International Conference on Advanced Robotics (ICAR)*, pp. 1–7. ᴅoɪ: `10.1109/ICAR.2011.6088576`.

Mandil, Guillaume, Alain Desrochers, and Alain Rivière (Oct. 2009). "Framework for the Monitoring of Functional Requirements Along the Product Life Cycle". In: *6ème Conférence "Conception et Production Intégrées"*. Fes, Morocco.

"Marching Cubes" (2022). In: *Wikipedia*. ᴜʀʟ: `https://en.wikipedia.org/wiki/Marching_cubes`.

Martina, Filomeno (2014). "Investigation of Methods to Manipulate Geometry, Microstructure and Mechanical Properties in Titanium Large Scale Wire+Arc Additive Manufacturing". PhD thesis. Cranfield University.

Martina, Filomeno and Stewart Williams (Apr. 2015). *Wire+arc Additive Manufacturing vs. Traditional Machining from Solid: A Cost Comparison*. Tech. rep.

Matheson, Eloise, Riccardo Minto, Emanuele G. G. Zampieri, Maurizio Faccio, and Giulio Rosati (Dec. 2019). "Human–Robot Collaboration in Manufacturing Applications: A Review". In: *Robotics* 8.4, p. 100. ᴅoɪ: `10.3390/robotics8040100`.

McNeel, Robert (2010). *Rhinoceros 3D*. McNeel & Associates, `https://www.rhino3d.com/`.

Mechtcherine, Viktor, Jasmin Grafe, Venkatesh N. Nerella, Erik Spaniol, Martin Hertel, and Uwe Füssel (Aug. 2018). "3D-printed Steel Reinforcement for Digital Concrete Construction – Manufacture, Mechanical Properties and Bond Behaviour". In: *Construction and Building Materials* 179, pp. 125–137. ɪssɴ: 09500618. ᴅoɪ: `10.1016/j.conbuildmat.2018.05.202`.

Menges, Achim and Jan Knippers (Dec. 2020). *Architecture Research Building: ICD/ITKE 2010-2020*. Birkhäuser. ɪsʙɴ: 978-3-0356-2040-5. ᴅoɪ: `10.1515/9783035620405`.

Menges, Achim, Hans Jakob Wagner, Dylan Marx Wood, Tiffany Cheng, Luis Orozco, Chai Hua, and Yasaman Tahouni (2020). *DualAdditive Manufacturing*. URL: https://perma.cc/QJ85-ZQGN.

Messler, Robert W. (1993). *Joining of Advanced Materials*. Stoneham, Massachusetts: Butterworth-Heinemann. ISBN: 978-1-4832-9214-4.

– (1999). *Principles of Welding: Processes, Physics, Chemistry, and Metallurgy*. First. Wiley. ISBN: 978-0-471-25376-1. DOI: 10.1002/9783527617487.

– (2004). *Joining of Materials and Structures: From Pragmatic Process to Enabling Technology*. Burlington, Mass. ; Elsevier Butterworth-Heinemann. ISBN: 978-1-4175-4436-3.

– (2006). *Integral Mechanical Attachment: A Resurgence of the Oldest Method of Joining*. Amsterdam ; Butterworth-Heinemann. ISBN: 978-1-280-64267-8.

Meyer Boake, Terri (2020). *Complex Steel Structures: Non-Orthogonal Geometries in Building with Steel*. Basel: Birkhäuser, ISBN: 978-3-03821-430-4. DOI: 10.1515/9783038214304.

Michel, Lucas, Asel Sanchez, Vlad-Alexandru Silvestru, Inés Ariza, Andreas Taras, and Ueli Angst (Feb. 2022). "Corrosion Behaviour of Point-by-point Wire and Arc Additively Manufactured Steel Bars". In: *Materials and Corrosion*. DOI: 10.1002/maco.202112994.

MIG MAG Inverter CITOMIG 200MP Brochure (2013). https://perma.cc/ZH4V-4PT7.

MIG/MAG 180 EASY (2022). Séchy, https://perma.cc/HL2V-HTVN.

Min, Byung-Kwon, Dong Woo Cho, Sang-Jo Lee, and Young-Pil Park (Mar. 1996). "Exploration of a Mobile Robot Based on Sonar Probability Mapping". In: *Journal of Dynamic Systems, Measurement, and Control* 118.1, pp. 150–157. ISSN: 0022-0434, 1528-9028. DOI: 10.1115/1.2801136.

Mirzendehdel, Amir M., Morad Behandish, and Saigopal Nelaturi (Oct. 2019). "Exploring Feasible Design Spaces for Heterogeneous Constraints". In: *Computer-Aided Design* 115, pp. 323–347. ISSN: 0010-4485. DOI: 10.1016/j.cad.2019.06.005.

Mishra, V., C. Ayas, M. Langelaar, and F. van Keulen (June 2021). "Simultaneous Topology and Deposition Direction Optimization for Wire and Arc Additive Manufacturing". In: *Manufacturing Letters*. ISSN: 2213-8463. DOI: 10.1016/j.mfglet.2021.05.011.

Mitchell, William J. (2005). "Constructing Complexity". In: *Computer Aided Architectural Design Futures 2005*. Ed. by Bob Martens and Andre Brown. Dordrecht: Springer Netherlands, pp. 41–50. ISBN: 978-1-4020-3698-9. DOI: 10.1007/1-4020-3698-1_3.

Mitropoulou, Ioanna (2018). "Numerical Sculpting of In Place Wire Arc Additive Manufacturing Connections". MA thesis. ETH Zurich.

Mitropoulou, Ioanna, Inés Ariza, Mathias Bernhard, Benjamin Dillenburger, Fabio Gramazio, and Matthias Kohler (2019). "Numerical Sculpting: Volumetric Modelling Tools for In Place Spatial Additive Manufacturing". In: *Impact: Design With All Senses*. Ed. by Christoph Gengnagel, Olivier Baverel, Jane Burry, Mette Ramsgaard Thomsen, and Stefan Weinzierl. Cham: Springer International Publishing, pp. 132–145. ISBN: 978-3-030-29828-9 978-3-030-29829-6. DOI: 10.1007/978-3-030-29829-6_11.

Mitropoulou, Ioanna, Mathias Bernhard, and Benjamin Dillenburger (Nov. 2020). "Print Paths Key-framing: Design for Non-Planar Layered Robotic FDM Printing". In: *Symposium on Computational Fabrication*. SCF '20. New York, NY, USA: Association for Computing Machinery, pp. 1–10. ISBN: 978-1-4503-8170-3. DOI: 10.1145/3424630.3425408.

Mitropoulou, Ioanna, Joris Burger, Gonzalo Casas, Andrei Jipa, and Mathias Bernhard (2020). *Compas-Dev/Compas_slicer: Slicing Functionality for COMPAS*. DOI: 10.5281/zenodo.7362195.

Mitterberger, Daniela, Kathrin Dörfler, Timothy Sandy, Foteini Salveridou, Marco Hutter, Fabio Gramazio, and Matthias Kohler (Dec. 2020). "Augmented Bricklaying: Human-machine Interaction for in Situ Assembly of Complex Brickwork Using Object-Aware Augmented Reality". In: *Construction Robotics* 4. DOI: 10.1007/s41693-020-00035-8.

Morris, Nigel, Adrian Butscher, and Francesco Iorio (Apr. 2020). "A Subtractive Manufacturing Constraint for Level Set Topology Optimization". In: *Structural and Multidisciplinary Optimization* 61. DOI: 10.1007/s00158-019-02436-y.

Mueller, Caitlin T. (2014). "Computational Exploration of the Structural Design Space". PhD thesis. Massachusetts Institute of Technology.

Müller, Johanna, Marcel Grabowski, Christoph Müller, Jonas Hensel, Julian Unglaub, Klaus Thiele, Harald Kloft, and Klaus Dilger (June 2019). "Design and Parameter Identification of Wire and Arc Additively Manufactured (WAAM) Steel Bars for Use in Construction". In: *Metals* 9.7, p. 725. ISSN: 2075-4701. DOI: 10.3390/met9070725.

Naidu, D. S., Selahattin Ozcelik, and Kevin L. Moore (2003). *Modeling, Sensing and Control of Gas Metal Arc Welding*. Amsterdam ; New York: Elsevier. ISBN: 978-0-08-044066-8.

Network, Autodesk Revit Knowledge (2020). *Place a Structural Connection*. Autodesk, https://perma.cc/VT78-4CJT.

Nisja, Georg Aarnes, Anni Cao, and Chao Gao (2021). "Short Review of Nonplanar Fused Deposition Modeling Printing". In: *Material Design & Processing Communications* 3.4, e221. ISSN: 2577-6576. DOI: 10.1002/mdp2.221.

Novillo, Andrew (2019). "Experimentation of a Topology-Optimized Metal Structural Connection under Casting Constraints". MA thesis. Massachusetts Institute of Technology.

Pan, Zengxi, Donghong Ding, Bintao Wu, Dominic Cuiuri, Huijun Li, and John Norrish (2018). "Arc Welding Processes for Additive Manufacturing: A Review". In: *Transactions on Intelligent Welding Manufacturing*. Ed. by Shanben Chen, Yuming Zhang, and Zhili Feng. Singapore: Springer, pp. 3–24. ISBN: 978-981-10-5355-9. DOI: 10.1007/978-981-10-5355-9_1.

Papert, Seymour (1980). *Mindstorms: Children, Computers, and Powerful Ideas*. New York: Basic Books. ISBN: 978-0-465-04627-0.

Parascho, Stefana (2019). "Cooperative Robotic Assembly: Computational Design and Robotic Fabrication of Spatial Metal Structures". PhD thesis. ETH Zurich. DOI: 10.3929/ethz-b-000364322.

Parascho, Stefana, A. Gandia, Ammar Mirjan, Fabio Gramazio, and Matthias Kohler (2017). "Cooperative Fabrication of Spatial Metal Structures". In: DOI: 10.3929/ETHZ-B-000219566.

Pashkevich, Anatol, Alexandre Dolgui, and Konstantin Semkin (June 2003). "Kinematic Aspects of a Robot-Positioner System in an Arc Welding Application". In: *Control Engineering Practice* 11, pp. 633–647. DOI: 10.1016/S0967-0661(02)00177-6.

Paulson, Boyd C. (Dec. 1976). "Designing to Reduce Construction Costs". In: *Journal of the Construction Division* 102.4, pp. 587–592. DOI: 10.1061/JCCEAZ.0000639.

Petersen, Kirstin H., Nils Napp, Robert Stuart-Smith, Daniela Rus, and Mirko Kovac (Mar. 2019). "A Review of Collective Robotic Construction". In: *Science Robotics* 4.28. DOI: 10.1126/scirobotics.aau8479.

Picon, Antoine (2010). "The First Steps of Construction in Iron: Problems Posed by the Introduction of a New Construction Material". In: *Before Steel: The Introduction of Structural Iron and Its Consequences*. Zurich, Switzerland: Niggli.

Pires, J. Norberto, Altino Loureiro, and Gunnar Bolmsjö (2006). *Welding Robots: Technology, System Issues and Applications*. 1st ed. London: Springer. ISBN: 978-1-85233-953-1.

"Robotic Welding" (2006a). "Robotic Welding: System Issues". In: *Welding Robots: Technology, System Issues and Applications*. Ed. by J. Norberto Pires,

Altino Loureiro, and Gunnar Bölmsjo. London: Springer, pp. 105–145. ISBN: 978-1-84628-191-4. DOI: 10.1007/1-84628-191-1_4.

"Sensors for Welding Robots" (2006b). In: *Welding Robots: Technology, System Issues and Applications*. Ed. by J. Norberto Pires, Altino Loureiro, and Gunnar Bölmsjo. London: Springer, pp. 73–103. ISBN: 978-1-84628-191-4. DOI: 10.1007/1-84628-191-1_3.

"Welding Technology" (2006c). In: *Welding Robots: Technology, System Issues and Applications*. Ed. by J. Norberto Pires, Altino Loureiro, and Gunnar Bölmsjo. London: Springer, pp. 27–71. ISBN: 978-1-84628-191-4. DOI: 10.1007/1-84628-191-1_2.

Polini, Wilma (2011). "Geometric Tolerance Analysis". In: *Geometric Tolerances: Impact on Product Design, Quality Inspection and Statistical Process Monitoring*. Ed. by Bianca M. Colosimo and Nicola Senin. London: Springer, pp. 39–68. ISBN: 978-1-84996-311-4. DOI: 10.1007/978-1-84996-311-4_2.

Porges, Oliver, Roberto Lampariello, Jordi Artigas, Armin Wedler, Christoph Borst, and Maximo A Roa (May 2015). "Reachability and Dexterity: Analysis and Applications for Space Robotics". In: *Workshop on Advanced Space Technologies for Robotics and Automation (ASTRA)*. Noordwijk, Netherlands.

PosCon CM (2017). *PosCon CM for Measurement of Round Objects without Reflector*. Baumer, https://perma.cc/TF93-W3MN.

Prayudhi, Bayu (2016). "3F3D: Form Follows Force with 3D Printing Topology Optimization for Free-form Building Envelope Design with Additive Manufacturing". MA thesis. Delft: TU Delft.

Preisinger, Clemens (2010). *Karamba3D*.

– (2014a). *Optimization of an Irregular Structure*. Karamba3D, https://perma.cc/E79X-VV6U.

– (2014b). *Optimization of Column Positions*. Karamba3D, https://perma.cc/H3CF-UFD2.

Preisinger, Clemens and Moritz Heimrath (May 2014). "Karamba—A Toolkit for Parametric Structural Design". In: *Structural Engineering International* 24.2, pp. 217–221. ISSN: 1016-8664. DOI: 10.2749/101686614X13830790993483.

Prouvé, Jean (1990). *Prouvé : Cours Du CNAM : 1957-1970 : Essai de Reconstitution Du Cours à Partir Des Archives Jean Prouvé*. ISBN: 2-87009-434-5.

Puppe, Frank (1993). "Characterization and History of Expert Systems". In: *Systematic Introduction to Expert Systems: Knowledge Representations and Problem-Solving Methods*. Ed. by Frank Puppe. Berlin, Heidelberg: Springer, pp. 3–8. ISBN: 978-3-642-77971-8. DOI: 10.1007/978-3-642-77971-8_1.

Radel, S., A. Diourte, F. Soulié, O. Company, and C. Bordreuil (Mar. 2019). "Skeleton Arc Additive Manufacturing with Closed Loop Control". In: *Additive Manufacturing* 26, pp. 106–116. ISSN: 2214-8604. DOI: 10.1016/j.addma.2019.01.003.

Radford, A.D. and J.S. Gero (Nov. 1985). "Towards Generative Expert Systems for Architectural Detailing". In: *Computer-Aided Design* 17.9, pp. 428–435. ISSN: 0010-4485. DOI: 10.1016/0010-4485(85)90290-8.

Radford, Anthony D. (Dec. 1985). "Approaches to Knowledge-Based Architectural Detailing". In: *Architectural Science Review* 28.4, pp. 88–94. ISSN: 0003-8628. DOI: 10.1080/00038628.1985.9697258.

Raspall, Felix (2015). "Design with Material Uncertainty: Responsive Design and Fabrication in Architecture". In: *Modelling Behaviour*. Ed. by Mette Ramsgaard Thomsen, Martin Tamke, Christoph Gengnagel, Billie Faircloth, and Fabian Scheurer. Cham: Springer International Publishing, pp. 315–327. ISBN: 978-3-319-24206-4. DOI: 10.1007/978-3-319-24208-8_27.

Reimann, Jan, Philipp Henckell, Yarop Ali, Stefan Hammer, Alexander Rauch, Jörg Hildebrand, and Jean Bergmann (Apr. 2021). "Production of Topology-optimised Structural Nodes Using Arc-based, Additive Manufacturing with GMAW Welding Process". In: *Journal of Civil Engineering and Construction Technology* 10, pp. 101–107. DOI: 10.32732/jcec.2021.10.2.101.

Reimann, Jan, Jörg Hildebrand, and Jean Pierre Bergmann (2020). *3D-Weld - 3D gedruckte Knotenpunkte aus Stahllegierungen für bionische Tragstrukturen*. Forschungsinitiative Zukunft Bau F 3208. Stuttgart: Fraunhofer IRB Verlag. ISBN: 978-3-7388-0472-0.

Ribeiro, Tiago P., Luís F. A. Bernardo, and Jorge M. A. Andrade (Jan. 2021). "Topology Optimisation in Structural Steel Design for Additive Manufacturing". In: *Applied Sciences* 11.5, p. 2112. ISSN: 2076-3417. DOI: 10.3390/app11052112.

Rinke, Mario (2010). "The Infinitely Shapable Structure: Structural Iron and the Decontextualization of Construction". In: *Before Steel. The Introduction of Structural Iron and Its Consequences*. Zurich, Switzerland: Niggli.

Ríos, Sergio, Paul A. Colegrove, Filomeno Martina, and Stewart W. Williams (May 2018). "Analytical Process Model for Wire + Arc Additive Manufacturing". In: *Additive Manufacturing* 21, pp. 651–657. ISSN: 2214-8604. DOI: 10.1016/j.addma.2018.04.003.

Robeller, Christopher, Paul Mayencourt, and Yves Weinand (Oct. 2014). "Snap-Fit Joints - CNC Fabricated, Integrated Mechanical Attachment for Structural Wood Panels". In: *ACADIA 2014 Design Agency: Proceedings of the 34th*

Annual Conference of the Association for Computer Aided Design in Architecture. Los Angeles, CA: Riverside Architectural Press, pp. 189–198. ɪsʙɴ: 978-1-926724-47-8. ᴅoɪ: `10.52842/conf.acadia.2014.189`.

Robeller, Christopher, Yves Weinand, Volker Helm, Andreas Thoma, Fabio Gramazio, and Matthias Kohler (2017). "Robotic Integral Attachment". In: *Fabricate 2017*. Ed. by Achim Menges, Bob Sheil, Ruairi Glynn, and Marilena Skavara. UCL Press, pp. 92–97. ɪsʙɴ: 978-1-78735-000-7. ᴅoɪ: `10.2307/j.ctt1n7qkg7.16`.

Robotstudio (2010). ABB, `https://perma.cc/W9V6-T9K5`.

Rodrigues, Tiago A., V. Duarte, R.M. Miranda, Telmo G. Santos, and J.P. Oliveira (Apr. 2019). "Current Status and Perspectives on Wire and Arc Additive Manufacturing (WAAM)". In: *Materials* 12.7, p. 1121. ɪssɴ: 1996-1944. ᴅoɪ: `10.3390/ma12071121`.

Rolvink, Anke, Caitlin Mueller, and Jeroen Coenders (Sept. 2014). "State on the Art of Computational Tools for Conceptual Structural Design". In: *Proceedings of IASS Annual Symposia*, *IASS 2014 Brasilia Symposium: Shells*, *Membranes and Spatial Structures: Footprints – Structural Morphology 1: Design and Engineering Computing*. Brasilia, Brazil: International Association for Shell and Spatial Structures (IASS), pp. 1–8.

Roth, Karlheinz (1994a). *Konstruieren mit Konstruktionskatalogen*. [Various editions]. Berlin: Springer. ɪsʙɴ: 978-3-540-57324-1.

– (1994b). *Konstruieren mit Konstruktionskatalogen: Band 2: Kataloge*. 2nd ed. 1994. Berlin, Heidelberg: Springer Berlin Heidelberg. ɪsʙɴ: 978-3-662-08150-1. ᴅoɪ: `10.1007/978-3-662-08150-1`.

– (2000). *Konstruieren mit Konstruktionskatalogen: Band 1: Konstruktionslehre*. 3rd ed. 2000. Konstruieren mit Konstruktionskatalogen ; Bd. 1. Berlin, Heidelberg: Springer Berlin Heidelberg. ɪsʙɴ: 978-3-642-17466-7. ᴅoɪ: `10.1007/978-3-642-17466-7`.

Rozvany, G. I. N., M. P. Bendsoe, and U. Kirsch (Feb. 1995). "Layout Optimization of Structures". In: *Applied Mechanics Reviews* 48.2, pp. 41–119. ɪssɴ: 0003-6900. ᴅoɪ: `10.1115/1.3005097`.

Rugarli, Paolo (2018). *Steel Connection Analysis*. Hoboken, New Jersey: Wiley Blackwell. ɪsʙɴ: 978-1-5231-2379-7.

Rust, Romana (2022a). *Compas_fab - Planning: Reachability Map*. Gramazio Kohler Research, ETH Zürich, `https://perma.cc/A49Z-9BEZ`.

– (2022b). *Compas_fab: Analytical Inverse Kinematics*. Gramazio Kohler Research, ETH Zürich, `https://perma.cc/DY2N-7B79`.

– (2022c). *Compas_fab: Forward and Inverse Kinematics*. Gramazio Kohler Research, ETH Zürich, `https://perma.cc/6AY8-52XF`.

Rust, Romana, Gonzalo Casas, Stefana Parascho, David Jenny, Kathrin Dörfler, Matthias Helmreich, Augusto Gandia, Zhao Ma, Inés Ariza, Matteo Pacher, B. Beverly, and Yijiang Huang (2018). *COMPAS FAB: Robotic Fabrication Package for the COMPAS Framework*. Gramazio Kohler Research, ETH Zürich, https://gramaziokohler.github.io/compas_fab/latest/.

Rutten, David (2007). *Grasshopper: Algorithmic Modeling for Rhino*. McNeel & Associates, https://www.grasshopper3d.com/.

Sawik, Tadeusz (1999). "Flexible Assembly Systems — Hardware Components and Features". In: *Production Planning and Scheduling in Flexible Assembly Systems*. Ed. by Tadeusz Sawik. Berlin, Heidelberg: Springer, pp. 1–15. ISBN: 978-3-642-58614-9. DOI: 10.1007/978-3-642-58614-9_1.

Schittich, Christian (2000). "Detail(s)". In: *DETAIL* 8/2000, pp. 1426–1438.

Schor, Naomi (2007). *Reading in Detail: Aesthetics and the Feminine*. ISBN: 978-1-135-86347-0 978-0-203-94421-9.

Seifi, H. (2019). "Topology Optimisation and Additive Manufacturing of Structural Nodes of Gridshell Structures". PhD thesis. RMIT University.

Seifi, Hamed, Anooshe Rezaee Javan, Shanqing Xu, Yang Zhao, and Yi Min Xie (Apr. 2018). "Design Optimization and Additive Manufacturing of Nodes in Gridshell Structures". In: *Engineering Structures* 160, pp. 161–170. ISSN: 0141-0296. DOI: 10.1016/j.engstruct.2018.01.036.

Selvi, S., A. Vishvaksenan, and E. Rajasekar (2018). "Cold Metal Transfer (CMT) Technology - An Overview | Elsevier Enhanced Reader". In: *Defense Technology* 14.1, pp. 28–44. DOI: 10.1016/j.dt.2017.08.002.

Semper, Gottfried, Harry Francis Mallgrave, and Michael Robinson (2004). *Style : Style in the Technical and Tectonic Arts, or, Practical Aesthetics*. Texts & Documents. Los Angeles : Getty Research Institute, c2004. ISBN: 0-89236-597-8.

Sennett, Richard (2008). *The Craftsman*. New Haven: Yale University Press. ISBN: 978-0-300-11909-1.

Sequeira Almeida, Pedro M. and Stewart Williams (2010). "Innovative Process Model of TI-6AL-4V Additive Layer Manufacturing Using Cold Metal Transfer (CMT)". In: p. 12.

Shelden, Dennis R (July 2014). "Information, Complexity and the Detail". In: *Architectural Design* 84.4, pp. 92–97. ISSN: 1554-2769. DOI: 10.1002/ad.1786.

Sheng, Yu-Ting, Shih-Yuan Wang, Mofei Li, Yu-Hung Chiu, Yi-Heng Lu, Chun-Man Tu, and Yi-Chu Shih (Dec. 2019). "Spatial Glass Bonds Computation and Fabrication System of Complex Glass Structure". In: *Blucher Design*

Proceedings. Porto, Portugal: Editora Blucher, pp. 251–260. DOI: `10.5151/proceedings-ecaadesigradi2019_368`.

Sigmund, Ole and Kurt Maute (Dec. 2013). "Topology Optimization Approaches". In: *Structural and Multidisciplinary Optimization* 48.6, pp. 1031–1055. ISSN: 1615-1488. DOI: `10.1007/s00158-013-0978-6`.

Sigmund, Ole and J. Petersson (1998). "Numerical Instabilities in Topology Optimization: A Survey on Procedures Dealing with Checkerboards, Mesh-Dependencies and Local Minima". In: *Structural Optimization* 16, pp. 68–75.

Silvestru, Vlad-Alexandru, Inés Ariza, and Andreas Taras (2022). "Ductility and Buckling Behaviour of Point-by-Point Wire Arc Additively Manufactured Steel Bars". In: *ce/papers* 5.4, pp. 226–234. ISSN: 2509-7075. DOI: `10.1002/cepa.1750`.

Silvestru, Vlad-Alexandru, Inés Ariza, Julie Vienne, Lucas Michel, Asel Maria Aguilar Sanchez, Ueli Angst, Romana Rust, Fabio Gramazio, Matthias Kohler, and Andreas Taras (July 2021). "Performance under Tensile Loading of Point-by-Point Wire and Arc Additively Manufactured Steel Bars for Structural Components". In: *Materials & Design* 205, p. 109740. ISSN: 0264-1275. DOI: `10.1016/j.matdes.2021.109740`.

SmarTac, *Application Manual* (2021). ABB, `https://perma.cc/YR27-9MJ7`.

Welding Smoke Extractor (2022). *SmartMaster Welding Smoke Extraction System*. Kemper, `https://perma.cc/B4YM-W94E`.

Solcà, Andrea (2021). "Experimental and Numerical Investigations on the Behaviour of Point-by-Point WAAM Steel Bars under Compressive Loading". MA thesis. Zurich, Switzerland: ETH Zurich.

Standard Guide for Directed Energy Deposition of Metals (n.d.). https://www.astm.org/f3187-16.html.

Stilman, Mike (June 2010). "Global Manipulation Planning in Robot Joint Space With Task Constraints". In: *IEEE Transactions on Robotics* 26.3, pp. 576–584. ISSN: 1941-0468. DOI: `10.1109/TRO.2010.2044949`.

Swift, K. G. and J. D. Booker (Jan. 2003). "7 - Joining Processes". In: *Process Selection (Second Edition)*. Ed. by K. G. Swift and J. D. Booker. Oxford: Butterworth-Heinemann, pp. 189–248. ISBN: 978-0-7506-5437-1. DOI: `10.1016/B978-075065437-1/50011-1`.

Tagliasacchi, Andrea, Thomas Delame, Michela Spagnuolo, Nina Amenta, and Alexandru Telea (2016). "3D Skeletons: A State-of-the-Art Report". In: *Computer Graphics Forum* 35.2, pp. 573–597. ISSN: 1467-8659. DOI: `10.1111/cgf.12865`.

Tam, Kam-Ming Mark, Daniel J. Marshall, Mitchell Gu, Jasmine Kim, Yijiang Huang, Justin Lavallee, and Caitlin T. Mueller (Jan. 2018). "Fabrication-Aware Structural Optimisation of Lattice Additive-Manufactured with Robot-Arm". In: *International Journal of Rapid Manufacturing* 7.2-3, pp. 120–168. ISSN: 1757-8817. DOI: 10.1504/IJRAPIDM.2018.092908.

Tamboli, Akbar R (2017). *Handbook of Structural Steel Connection Design and Details*, *Third Edition*. ISBN: 978-1-259-58552-4.

Tarn, Tzyh-Jong, S.-B. Chen, and Changjiu Zhou, eds. (2007). *Robotic Welding, Intelligence and Automation*. Lecture Notes in Control and Information Sciences 362. Berlin: Springer. ISBN: 978-3-540-73373-7.

The Fronius Welding Dictionary (2021). http://www.fronius.com/en/welding-technology/welding-wiki-en.

Thoma, Andreas, Arash Adel, Matthias Helmreich, Thomas Wehrle, Fabio Gramazio, and Matthias Kohler (2019). "Robotic Fabrication of Bespoke Timber Frame Modules". In: *Robotic Fabrication in Architecture*, *Art and Design 2018*. Ed. by Jan Willmann, Philippe Block, Marco Hutter, Kendra Byrne, and Tim Schork. Cham: Springer International Publishing, pp. 447–458. ISBN: 978-3-319-92294-2. DOI: 10.1007/978-3-319-92294-2_34.

Thoma, Andreas, David Jenny, Matthias Helmreich, Augusto Gandia, Fabio Gramazio, and Matthias Kohler (Dec. 2019). "Cooperative Robotic Fabrication of Timber Dowel Assemblies". In: *Research Culture in Architecture*. Birkhäuser, pp. 77–88. ISBN: 978-3-0356-2023-8. DOI: 10.1515/9783035620238-008.

Thompson, Mary Kathryn, Giovanni Moroni, Tom Vaneker, Georges Fadel, R. Ian Campbell, Ian Gibson, Alain Bernard, Joachim Schulz, Patricia Graf, Bhrigu Ahuja, and Filomeno Martina (2016). "Design for Additive Manufacturing: Trends, Opportunities, Considerations, and Constraints". In: *CIRP Annals* 65.2, pp. 737–760. ISSN: 00078506. DOI: 10.1016/j.cirp.2016.05.004.

Tofail, Syed A. M., Elias P. Koumoulos, Amit Bandyopadhyay, Susmita Bose, Lisa O'Donoghue, and Costas Charitidis (Jan. 2018). "Additive Manufacturing: Scientific and Technological Challenges, Market Uptake and Opportunities". In: *Materials Today* 21.1, pp. 22–37. ISSN: 1369-7021. DOI: 10.1016/j.mattod.2017.07.001.

Tosca, *Abaqus/CAE* (2000). Dessault Systèmes Simulia, https://perma.cc/L8ZX-226K.

Treutler, Kai and Volker Wesling (Jan. 2021). "The Current State of Research of Wire Arc Additive Manufacturing (WAAM): A Review". In: *Applied Sciences* 11.18, p. 8619. DOI: 10.3390/app11188619.

Tyagi, Vinay Kumar (2002). "Understanding the Influence of Alloy Aditions on Microstructure and Mechanical Properties of Weld Metal from Gas-Shielded Processes". PhD thesis. University of Adelaide.

Ushio, Masao (Dec. 1991). "Sensors in Arc Welding". In: *Transactions of JWRI* 20.2, pp. 303–309. ISSN: 0387-4508. DOI: 10.18910/9559.

van der Linden, Lennert (Apr. 2015). "Innovative Joints for Gridshells: Joints Designed by Topology Optimization and to Be Produced by Additive Manufacturing". MA thesis. Delft: TU Delft.

van Mele, Tom and many others (2017). "COMPAS: A Framework for Computational Research in Architecture and Structures." In: DOI: 10.5281/zenodo.2594510.

Vasey, Lauren, Iain Maxwell, and Dave Pigram (2014). "Adaptive Part Variation". In: *Robotic Fabrication in Architecture*, *Art and Design 2014*. Ed. by Wes McGee and Monica Ponce de Leon. Springer, Cham, pp. 291–304. ISBN: 978-3-319-04662-4. DOI: 10.1007/978-3-319-04663-1_20.

Vatanabe, Sandro L., Tiago N. Lippi, Cícero R. de Lima, Glaucio H. Paulino, and Emílio C. N. Silva (Oct. 2016). "Topology Optimization with Manufacturing Constraints: A Unified Projection-Based Approach". In: *Advances in Engineering Software* 100, pp. 97–112. ISSN: 0965-9978. DOI: 10.1016/j.advengsoft.2016.07.002.

Vierlinger, Robert (2012). *Octopus*. University of Applied Arts Vienna and Bollinger+Grohmann Engineers, https://perma.cc/DQ8D-6YAU.

Wagner, Hans, Dominga Garufi, Tobias Schwinn, Dylan Wood, and Achim Menges (Aug. 2021). *Three-Dimensional Fibre Placement in Wood for Connections and Reinforcements in Timber Structures.*

Walt, Stéfan van der, Johannes L. Schönberger, Juan Nunez-Iglesias, François Boulogne, Joshua D. Warner, Neil Yager, Emmanuelle Gouillart, Tony Yu, and the scikit-image contributors (June 2014). "scikit-image: image processing in Python". In: *PeerJ* 2, e453. ISSN: 2167-8359. DOI: 10.7717/peerj.453. URL: https://doi.org/10.7717/peerj.453.

Wan, Weiwei, Kensuke Harada, and Kazuyuki Nagata (Sept. 2016). "Assembly Sequence Planning for Motion Planning". In: *Assembly Automation* 38.2, pp. 195–206. ISSN: 0144-5154. DOI: 10.1108/AA-01-2017-009.

Wang, Baicun, S. Jack Hu, Lei Sun, and Theodor Freiheit (July 2020). "Intelligent Welding System Technologies: State-of-the-art Review and Perspectives". In: *Journal of Manufacturing Systems* 56, pp. 373–391. ISSN: 0278-6125. DOI: 10.1016/j.jmsy.2020.06.020.

Williams, Stewart, F. Martina, A. C. Addison, J. Ding, G. Pardal, and P. Colegrove (May 2016). "Wire + Arc Additive Manufacturing". In: *Materials*

Science and Technology 32.7, pp. 641–647. ISSN: 0267-0836. DOI: [10.1179/1743284715Y.0000000073](10.1179/1743284715Y.0000000073).

Willmann, Jan, Michael Knauss, Tobias Bonwetsch, Anna Aleksandra Apolinarska, Fabio Gramazio, and Matthias Kohler (Jan. 2016). "Robotic Timber Construction — Expanding Additive Fabrication to New Dimensions". In: *Automation in Construction* 61, pp. 16–23. ISSN: 0926-5805. DOI: 10.1016/j.autcon.2015.09.011.

Wire and Arc Additive Manufacturing (WAAM) of Complex Individualized Steel Components (2022). Tech. rep. Technische Universität Braunschweig.

Woischwill, Christopher and Il Yong Kim (2018). "Multimaterial Multijoint Topology Optimization". In: *International Journal for Numerical Methods in Engineering* 115.13, pp. 1552–1579. ISSN: 1097-0207. DOI: [10.1002/nme.5908](10.1002/nme.5908).

Woo, Tony C. (Jan. 1994). "Visibility Maps and Spherical Algorithms". In: *Computer-Aided Design* 26.1, pp. 6–16. ISSN: 0010-4485. DOI: [10.1016/0010-4485(94)90003-5](10.1016/0010-4485(94)90003-5).

Robotic Assembly with COMPAS (2019). *Workshop Robotic Assembly with the COMPAS Framework*. Gramazio Kohler Research, ETH Zürich, https://github.com/gramaziokohler/robotic_assembly_workshop. Zurich, Switzerland.

Workshop TU Munich 2020 (2020). Gramazio Kohler Research, ETH Zürich, https://github.com/gramaziokohler/workshop_munich_2020.

Wu, Bintao, Zengxi Pan, Donghong Ding, Dominic Cuiuri, Huijun Li, Jing Xu, and John Norrish (Oct. 2018). "A Review of the Wire Arc Additive Manufacturing of Metals: Properties, Defects and Quality Improvement". In: *Journal of Manufacturing Processes* 35, pp. 127–139. ISSN: 1526-6125. DOI: 10.1016/j.jmapro.2018.08.001.

Wu, Kaicong (2019). "Robotic Assembly: A Generative Architectural Design Strategy Through Component Arrangements In Highly-Constrained Design Spaces". PhD thesis. Princeton, NJ : Princeton University.

Wu, Kaicong and Axel Kilian (2016). "Developing Architectural Geometry Through Robotic Assembly and Material Sensing". In: *Robotic Fabrication in Architecture, Art and Design 2016*. Ed. by Dagmar Reinhardt, Rob Saunders, and Jane Burry. Cham: Springer International Publishing, pp. 240–249. ISBN: 978-3-319-26378-6. DOI: [10.1007/978-3-319-26378-6_18](10.1007/978-3-319-26378-6_18).

– (2019). "Designing Natural Wood Log Structures with Stochastic Assembly and Deep Learning". In: *Robotic Fabrication in Architecture, Art and Design 2018*. Ed. by Jan Willmann, Philippe Block, Marco Hutter, Kendra Byrne,

and Tim Schork. Cham: Springer International Publishing, pp. 16–30. ISBN: 978-3-319-92294-2. DOI: 10.1007/978-3-319-92294-2_2.

Xia, Chunyang, Zengxi Pan, Joseph Polden, Huijun Li, Yanling Xu, Shanben Chen, and Yuming Zhang (Oct. 2020). "A Review on Wire Arc Additive Manufacturing: Monitoring, Control and a Framework of Automated System". In: *Journal of Manufacturing Systems* 57, pp. 31–45. ISSN: 0278-6125. DOI: 10.1016/j.jmsy.2020.08.008.

Xizhang Chen, Chuanchu Su, Yangfan Wang, Arshad Noor Siddiquee, Konovalov Sergey, S. Jayalakshmi, and R. Arvind Singh (Nov. 2018). "Cold Metal Transfer (CMT) Based Wire and Arc Additive Manufacture (WAAM) System". In: *Journal of Surface Investigation: X-ray, Synchrotron and Neutron Techniques* 12.6, pp. 1278–1284. ISSN: 1819-7094. DOI: 10.1134/S102745101901004X.

Yablonina, Maria and Achim Menges (Sept. 2018). "Towards the Development of Fabrication Machine Species for Filament Materials". In: *Robotic Fabrication in Architecture, Art and Design 2018*. Ed. by Jan Willmann, Philippe Block, Marco Hutter, Kendra Byrne, and Tim Schork, pp. 152–166. ISBN: 978-3-319-92293-5. DOI: 10.1007/978-3-319-92294-2_12.

Yao, Zhenwang and Kamal Gupta (Apr. 2007). "Path Planning with General End-Effector Constraints". In: *Robotics and Autonomous Systems* 55.4, pp. 316–327. ISSN: 0921-8890. DOI: 10.1016/j.robot.2006.11.004.

Yu, Lei, Yijiang Huang, Zhongyuan Liu, Sai Xiao, Ligang Liu, Guoxian Song, and Yanxin Wang (Oct. 2016). "Highly Informed Robotic 3D Printed Polygon Mesh: A Nobel Strategy of 3D Spatial Printing". In: *ACADIA 2016: POSTHUMAN FRONTIERS: Data, Designers, and Cognitive Machines [Proceedings of the 36th Annual Conference of the Association for Computer Aided Design in Architecture (ACADIA)*. Ann Arbor, MI, pp. 298–307. ISBN: 978-0-692-77095-5. DOI: 10.52842/conf.acadia.2014.189.

Yu, Ziping, Donghong Ding, Zengxi Pan, Huijun Li, Qinghua Lu, and Xuewei Fang (May 2021). "A Strut-Based Process Planning Method for Wire Arc Additive Manufacturing of Lattice Structures". In: *Journal of Manufacturing Processes* 65, pp. 283–298. ISSN: 1526-6125. DOI: 10.1016/j.jmapro.2021.03.038.

Yu, Ziping, Zengxi Pan, Donghong Ding, Joseph Polden, Fengyang He, Lei Yuan, and Huijun Li (June 2021). "A Practical Fabrication Strategy for Wire Arc Additive Manufacturing of Metallic Parts with Wire Structures". In: *The International Journal of Advanced Manufacturing Technology*. ISSN: 1433-3015. DOI: 10.1007/s00170-021-07375-x.

Yu, Ziping, Lei Yuan, Fengyang He, Donghong Ding, Joseph Polden, and Zengxi Pan (July 2019). "The Strategy for Fabricating Wire-Structure Parts Using Robotic Skeleton Arc Additive Manufacturing". In: *2019 IEEE 9th Annual International Conference on CYBER Technology in Automation*, *Control*, *and Intelligent Systems (CYBER)*. Suzhou, China: IEEE, pp. 119–124. ISBN: 978-1-72810-770-7. DOI: 10.1109/CYBER46603.2019.9066636.

Yuan, Lei, Zengxi Pan, Donghong Ding, Ziping Yu, Stephen van Duin, Huijun Li, Weihua Li, and John Norrish (Mar. 2021). "Fabrication of Metallic Parts with Overhanging Structures Using the Robotic Wire Arc Additive Manufacturing". In: *Journal of Manufacturing Processes*. Trends in Intelligentizing Robotic Welding Processes 63, pp. 24–34. ISSN: 1526-6125. DOI: 10.1016/j.jmapro.2020.03.018.

Zacharias, Franziska, Christoph Borst, and Gerd Hirzinger (Oct. 2007). "Capturing Robot Workspace Structure: Representing Robot Capabilities". In: *Proceedings of the IEEE International Conference on Intelligent Robots and Systems (IROS)*. San Diego, CA: IEEE, pp. 3229–3236. ISBN: 978-1-4244-0911-2. DOI: 10.1109/IROS.2007.4399105.

Zargham, Sajjad, Thomas Arthur Ward, Rahizar Ramli, and Irfan Anjum Badruddin (June 2016). "Topology Optimization: A Review for Structural Designs under Vibration Problems". In: *Structural and Multidisciplinary Optimization* 53.6, pp. 1157–1177. ISSN: 1615-147X, 1615-1488. DOI: 10.1007/s00158-015-1370-5.

Zhang, Yu Ming, Yu-Ping Yang, Wei Zhang, and Suck-Joo Na (Nov. 2020). "Advanced Welding Manufacturing: A Brief Analysis and Review of Challenges and Solutions". In: *Journal of Manufacturing Science and Engineering* 142.11, p. 110816. ISSN: 1087-1357, 1528-8935. DOI: 10.1115/1.4047947.

Zheng, Hao, Vahid Moosavi, and Masoud Akbarzadeh (Nov. 2020). "Machine Learning Assisted Evaluations in Structural Design and Construction". In: *Automation in Construction* 119, p. 103346. ISSN: 0926-5805. DOI: 10.1016/j.autcon.2020.103346.

Zhou, Qiang, Wei Shen, Jin Wang, Yi Yi Zhaou, and Yi Min Xie (July 2018). "Ameba: A New Topology Optimization Tool for Architectural Design". In: *Proceedings of IASS Symposium 2018: Creativity in Structural Design*. Bostom, MA: International Association for Shell and Spatial Structures (IASS).

Zhu, Jihong, Han Zhou, Chuang Wang, Lu Zhou, Shangqin Yuan, and Weihong Zhang (Jan. 2021). "A Review of Topology Optimization for Additive Manufacturing: Status and Challenges". In: *Chinese Journal of Aeronautics* 34.1, pp. 91–110. ISSN: 1000-9361. DOI: 10.1016/j.cja.2020.09.020.

Appendix

A Experimental data

A.1 Process parameters

A.1.1 Discrete printing

Parameter	Value	Parameter	Value
Welding mode	MIG CMT	SFI	off
Trigger mode	2-step	SFI Hot start	off
Material	Steel	Wire retract	0.0
Diameter	1.2 mm	Synchropulse enable	off
Gas	M21 Ar21-20%CO2	Delta wire feed	2.0 m/min
Property	universal	Frequency	3.0 Hz
Characteristic-ID	3542	Duty cycle	50
Wire Feed Speed	3.5 m/min	Arc length corr. high	0.0
Current	129 A	Arc length corr. low	0.0
Voltage	13.9 V	High power time corr.	0.0
Material Thickness	1.0 mm	Low power time corr.	0.0
Arclength corr.	-4.0	Low power corr.	0.0
Pulse/dynamic corr.	0.0	Power corr. high	0 %
Penetration stabilizer	0.0 m/min	Power corr. low	0 %
Arc length stabilizer	0.0	Arc length corr. high	0.0
Gas preflow	0.5 s	Arc length corr. low	0.0
Inching value	3.0 m/min	Command value gas	15.0 l/min
Starting current	135 %	Gas factor	auto
Start Arclength corr.	0.0	Job slope	0.0 s
Start current time	0.2 s	Sampling rate	off
Slope 1	1.0 s	Spot welding time	1.0 s
Slope 2	1.0 s	CMT Cycle Step	off
End current	50 %	Cycles (Spot size)	1
End Arclength corr.	1.0	Interval break time	0.01 s
End current time	off	Interval cycles	1

Table A.1: *Example of discrete printing job settings (Setup B).*

A.1.2 Continuous printing

Parameter	Value	Parameter	Value
Welding mode	MIG CMT	SFI	off
Trigger mode	2-step	SFI Hot start	off
Material	Steel	Wire retract	0.0
Diameter	1.2 mm	Synchropulse enable	off
Gas	M21 Ar21-20%CO2	Delta wire feed	2.0 m/min
Property	universal	Frequency	3.0 Hz
Characteristic-ID	3542	Duty cycle	50
Wire Feed Speed	2.1 m/min	Arc length corr. high	0.0
Current	82 A	Arc length corr. low	0.0
Voltage	12.2 V	High power time corr.	0.0
Material Thickness	0.9 mm	Low power time corr.	0.0
Arclength corr.	-5.0	Low power corr.	0.0
Pulse/dynamic corr.	0.0	Power corr. high	0 %
Penetration stabilizer	0.0 m/min	Power corr. low	0 %
Arc length stabilizer	0.0	Arc length corr. high	0.0
Gas preflow	0.5 s	Arc length corr. low	0.0
Inching value	3.0 m/min	Command value gas	15.0 l/min
Starting current	125 %	Gas factor	auto
Start Arclength corr.	0.0	Job slope	0.0 s
Start current time	0.2 s	Sampling rate	off
Slope 1	1.0 s	Spot welding time	1.0 s
Slope 2	1.0 s	CMT Cycle Step	off
End current	50 %	Cycles (Spot size)	1
End Arclength corr.	1.0	Interval break time	0.01 s
End current time	off	Interval cycles	1

Table A.2: *Example of continuous printing job settings (Setup B).*

A.2 Material tests

A.2.1 Build orientation

ID	a	h	d0	d1	d2	d3	d4	d5	d6	d7	davr
	[deg]	[mm]	[mm]	[mm]	[mm]	[mm]	[mm]	[mm]	[mm]	[mm]	[mm]
C#305_01	0	**33.60**	8.44	8.66	8.70	9.06	8.60	8.65	8.85	8.70	**8.68**
C#305_02	10	**34.60**	8.90	8.50	8.65	8.90	8.70	8.80	8.40	8.90	**8.75**
C#305_03	20	**34.10**	8.90	8.80	9.01	8.65	8.95	9.30	8.60	8.90	**8.89**
C#305_04	30	**34.50**	9.15	9.02	8.90	8.70	8.95	9.04	8.93	8.87	**8.93**
C#305_05	40	**34.50**	8.44	8.98	8.90	9.03	8.77	8.80	8.70	8.60	**8.75**
C#305_06	50	**36.00**	7.13	7.67	7.80	7.50	7.47	7.40	7.50	8.33	**7.56**
C#305_07	60	**35.80**	7.29	7.59	7.60	7.65	7.47	7.63	7.72	7.83	**7.55**
C#305_08	70	**37.00**	7.66	7.52	7.55	7.40	7.23	7.36	7.57	7.49	**7.44**
C#305_09	80	**37.90**	7.40	7.35	7.30	7.18	7.36	7.06	7.13	7.15	**7.20**
C#305_10	90	**38.90**	7.72	6.99	7.08	6.95	7.02	7.19	7.04	7.15	**7.10**

Table A.3: *Results of build orientation variation for each ID (specimen): a (build angle), h (overall height of bar), d0-d7 (measured diameters along the height), and davr (diameter average along the bar).*
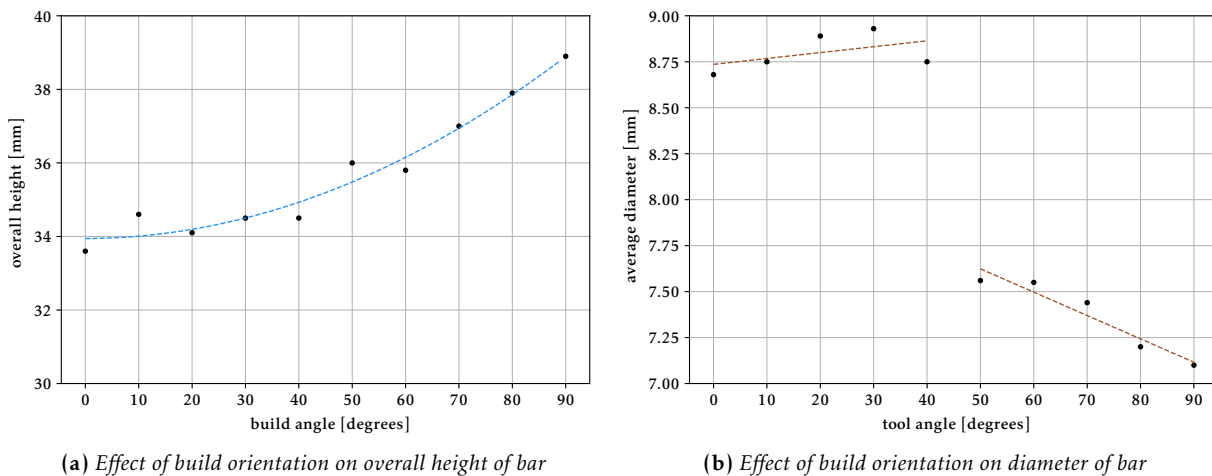
(a) *Effect of build orientation on overall height of bar*

(b) *Effect of build orientation on diameter of bar*

Figure A.1: *Build orientation results*

A.2.2 Tool orientation

ID	t [deg]	h [mm]	d0 [mm]	d1 [mm]	d2 [mm]	d3 [mm]	d4 [mm]	d5 [mm]	d6 [mm]	d7 [mm]	davr [mm]
C#306_01	0	**33.9**	7.9	7.4	7.7	7.6	8.3	8.1	8.4	7.3	**7.8**
C#306_02	10	**34.97**	7.5	7.8	7.6	7.7	8.4	8.2	8.3	8.0	**7.9**
C#306_03	20	**35.1**	7.5	7.9	7.3	8.0	7.8	7.7	8.4	7.7	**7.8**
C#306_04	30	**33.85**	7.3	7.9	8.5	7.7	7.6	8.1	8.0	8.1	**8.0**
C#306_05	40	**33.82**	7.2	7.7	8.0	7.7	8.0	7.7	7.8	7.6	**7.8**
C#306_06	50	**33.62**	7.8	8.0	7.8	8.0	8.2	7.9	8.1	7.4	**8.0**
C#306_07	60	**33.3**	8.1	7.6	8.4	8.2	8.3	8.6	8.7	8.3	**8.3**
C#306_08	70	**33.58**	8.4	8.5	8.6	8.7	8.4	8.7	8.6	8.6	**8.6**
C#306_09	80	**33.95**	8.3	8.3	8.5	8.7	8.6	9.0	9.1	8.9	**8.7**
C#306_10	90	**35.75**	8.5	8.5	8.6	8.4	8.2	8.7	8.4	8.5	**8.5**

Table A.4: *Results of tool orientation variation for each ID (specimen): t (tool angle), h (overall height of bar), d0-d7 (measured diameters along the height), and davr (diameter average along the bar).*
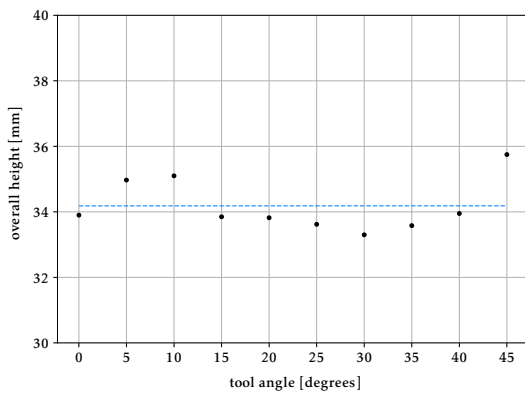
(a) *Effect of tool orientation on overall height of bar*
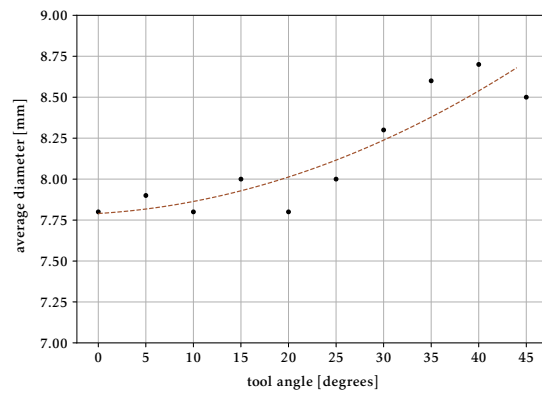
(b) *Effect of tool orientation on diameter of bar*

Figure A.2: *Tool orientation results*

A.2.3 Curvature

ID	r [deg]	a [def]	b [deg]	h [mm]	emd [mm]	rmd [mm]	d [mm]	d [%]
C#307_01	infinite	0	0	**34.5**	0	0	0	**0.00**
C#307_02	100.8	20	0.7	**34.7**	1.5	1.5	0	**0.00**
C#307_03	51.2	40	1.5	**33.8**	3.1	3	0.1	**-3.23**
C#307_04	35	60	2.1	**34**	4.7	4.5	0.2	**-4.26**
C#307_05	27.2	80	2.7	**34.2**	6.4	6.5	-0.1	**1.56**
C#307_06	22.8	100	3.3	**34.7**	8.2	8.5	-0.3	**3.66**
C#307_07	20.2	120	3.7	**34.7**	10.1	10	0.1	**-0.99**
C#307_08	18.6	140	4	**34.1**	12.3	12	0.3	**-2.44**
C#307_09	17.8	160	4.2	**34.9**	14.7	14.5	0.2	**-1.36**
C#307_10	17.5	180	4.3	**35.1**	17.5	17	0.5	**-2.86**

Table A.5: *Curvature:* r *(arc radius),* a *(arc sweep angle),* b *(relative angle change),* h *(overall height),* emd *(expected middle ordinate),* rmd *(resulting middle ordinate),* d *(deviation), and* d *(percent deviation) [%].*
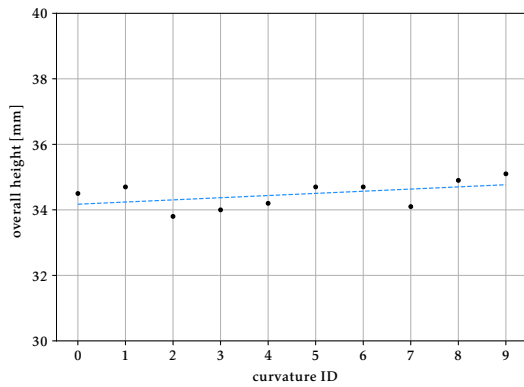
(a) *Effect of curvature on overall height of bar*
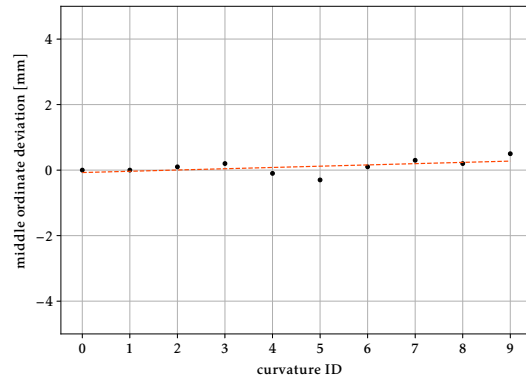
(b) *Effect of curvature on middle ordinate deviation*

Figure A.3: *Curvature results*

A.2.4 Layer height

ID	lh [mm]	sh [mm]	d0 [mm]	d-1 [mm]	davr [mm]	th [mm]	h [mm]	CTWDs [mm]	CTWDe [mm]
C#304_01	1.07	1	7.81	8.17	7.9	35.3	39.0	N/A	N/A
C#304_02	1.1	1	7.41	8.14	7.8	37.4	40.5	N/A	N/A
C#304_03	1.2	1	7.64	8.64	8.3	34.8	35.0	N/A	N/A
C#304_04	1.3	1	8.07	8.42	8.4	35.1	35.0	N/A	N/A
C#304_05	1.4	1	8.4	8.65	8.6	35	33.0	15.1	12
C#304_06	1.3	1	7.14	8.32	8.05	N/A	N/A	14.0	11
C#304_07	1.3	1	8.18	8.48	8.43	N/A	N/A	12.0	12.0
C#304_08	1.3	1	7.56	8.63	8.3	N/A	N/A	12.3	12.3

Table A.6: *Layer height: ID (specimens), lh (layer height), sh (seam height), d0 (diameter at base), d-1 (diameter at top), davr (average diameter), h (overall height), CTWDs (contact tip to workpiece distance at start), and CTWDe (contact tip to workpiece distance at end).*

A.2.5 Primitive connection

ID	layer	lh [mm]	sh [mm]	sa [deg]	pl [mm]	tags [deg]	tage [deg]	taps [deg]	tape [deg]	ba [deg]
C#308_01	0	1.26	1.3	0	-	15	-	15	-	90
C#308_01	1	1.26	1.3	0	-	15	-	15	-	90
C#308_01	2	1.24	1.3	0	-	10	-	10	-	90
C#308_01	3	1.24	1.3	0	-	10	-	10	-	90
C#308_01	4	1.24	1.3	0	-	6	-	6	-	90
C#308_01	5	1.24	1.3	0	-	6	-	6	-	90
C#308_01	6	1.24	1.3	0	-	3	-	3	-	90
C#308_01	7	1.24	1.3	0	-	0	-	0	-	90
C#308_01	8	1.24	1.3	0	-	0	-	0	-	90
C#308_01	9	-	-	-	9.6	0	39.3	60	100	60

Table A.7: *Primitive connection, geometric parameters for specimen C#308_01: ID (specimens), layer (layer number), lh (layer height), sh (seam height), sa (seam angle relative to path), pl (path length), tags (tool angle relative to gravity at start), tage (tool angle relative to gravity at end), taps (tool angle relative to path at start), tape (tool angle relative to path at end), and ba (build angle relative to gravity).*

ID	layer	wdt	wtime [s]	I [A]	U [V]	wfs [m/min]	pow [W]	E [kJ]	ws [mm/s]	ct [s]
C#308_01	0-8	Input	-	129	13.9	3.5	-	-	-	-
C#308_01	0	Output	1.4	109	12	1.7	1797.4	2.6	1	32
C#308_01	1	Output	1.5	97	12.6	2	1498.8	2.3	1	37
C#308_01	2	Output	1.5	102	13.3	2.3	1687.7	2.6	1	49
C#308_01	3	Output	1.5	98	13.1	2.2	1579.5	2.4	1	58
C#308_01	4	Output	1.5	104	13.5	2.2	1686.4	2.6	1	59
C#308_01	5	Output	1.5	109	13.5	2.3	1778.9	2.8	1	57
C#308_01	6	Output	1.5	105	13	1.9	1704	2.6	1	58
C#308_01	7	Output	1.5	104	13.6	2.5	1722.3	2.7	1	58
C#308_01	8	Output	1.5	90	12.4	1.9	1356.5	2.1	1	648
C#308_01	9	Input	-	82	12.2	2.1	-	-	-	-
C#308_01	9	Output	7.9	71	11	0.7	1058.8	8.4	1.25	-

Table A.8: *Primitive connection, welding parameters for specimen C#308_01: ID (specimens), layer (layer number), wdt (welding data type), wtime (welding time), I (current), U (voltage), wfs (wire feed speed), pow (power), E (energy), ws (wedling speed), and ct (cooling time).*

ID	layer	lh [mm]	sh [mm]	sa [deg]	pl [mm]	tags [deg]	tage [deg]	taps [deg]	tape [deg]	ba [deg]
C#308_02	0	1.26	1.3	0	-	15	-	15	-	90
C#308_02	1	1.26	1.3	0	-	15	-	15	-	90
C#308_02	2	1.26	1.3	0	-	15	-	15	-	90
C#308_02	3	1.24	1.3	0	-	10	-	10	-	90
C#308_02	4	1.24	1.3	0	-	10	-	10	-	90
C#308_02	5	1.24	1.3	0	-	6	-	6	-	90
C#308_02	6	1.24	1.3	0	-	3	-	3	-	90
C#308_02	7	1.24	1.3	0	-	0	-	0	-	90
C#308_02	8	1.24	1.3	0	-	0	-	0	-	90
-	-	-	-	-	-	-	-	-	-	-
C#308_02	9	-	-	-	9.6	0	39.3	60	100	60

Table A.9: *Primitive connection, geometric parameters for specimen C#308_02: ID (specimens), layer (layer number), lh (layer height), sh (seam height), sa (seam angle relative to path), pl (path length), tags (tool angle relative to gravity at start), tage (tool angle relative to gravity at end), taps (tool angle relative to path at start), tape (tool angle relative to path at end), and ba (build angle relative to gravity).*

ID	layer	wdt	wtime [s]	I [A]	U [V]	wfs [m/min]	pow [W]	E [kJ]	ws [mm/s]	ct [s]
C#308_02	0-8	Input	-	129	13.9	3.5	-	-	-	-
C#308_02	0	Output	1.5	92	12.8	2	1448	2.2	1	34
C#308_02	1	Output	1.5	101	13.2	2.2	1635.4	2.5	1	38
C#308_02	2	Output	1.5	102	13.1	2.3	1640.1	2.6	1	58
C#308_02	3	Output	1.5	96	12.7	2.2	1549.4	2.4	1	59
C#308_02	4	Output	1.5	103	13.2	2.2	1676.9	2.6	1	58
C#308_02	5	Output	1.5	111	13.9	2.5	1902.3	2.9	1	58
C#308_02	6	Output	1.5	96	12.2	1.7	1494.1	2.3	1	58
C#308_02	7	Output	1.5	92	12.8	2.1	1414.7	2.2	1	59
C#308_02	8	Output	1.5	91	12.2	2	1327.9	2.1	1	431
C#308_02	9	Input	-	82	12.2	2.1	-	-	-	-
C#308_02	9	Output	7.9	75	10.9	0.7	1134.3	9	1	-

Table A.10: *Primitive connection, welding parameters for specimen C#308_02: ID (specimens), layer (layer number), wdt (welding data type), wtime (welding time), I (current), U (voltage), wfs (wire feed speed), pow (power), E (energy), ws (wedling speed), and ct (cooling time).*

ID	layer	lh [mm]	sh [mm]	sa [deg]	pl [mm]	tags [deg]	tage [deg]	taps [deg]	tape [deg]	ba [deg]
C#308_03	0	1.26	1.3	0	-	15	-	15	-	90
C#308_03	1	1.26	1.3	0	-	15	-	15	-	90
C#308_03	2	1.26	1.3	0	-	15	-	15	-	90
C#308_03	3	1.26	1.3	0	-	15	-	15	-	90
C#308_03	4	1.24	1.3	0	-	10	-	10	-	90
C#308_03	5	1.24	1.3	0	-	6	-	6	-	90
C#308_03	6	1.24	1.3	0	-	6	-	6	-	90
C#308_03	7	1.24	1.3	0	-	1	-	1	-	90
C#308_03	8	1.24	1.3	0	-	0	-	0	-	90
C#308_03	9	-	-	-	9.6	0	39.3	60	100	60

Table A.11: *Primitive connection, geometric parameters for specimen C#308_03: ID (specimens), layer (layer number), lh (layer height), sh (seam height), sa (seam angle relative to path), pl (path length), tags (tool angle relative to gravity at start), tage (tool angle relative to gravity at end), taps (tool angle relative to path at start), tape (tool angle relative to path at end), and ba (build angle relative to gravity).*

ID	layer	wdt	wtime [s]	I [A]	U [V]	wfs [m/min]	pow [W]	E [kJ]	ws [mm/s]	ct [s]
C#308_03	0-1	Input	-	129	13.9	3.5	-	-	-	
C#308_03	0	Output	1.4	113	12.1	1.6	1888.7	2.7	1	510
C#308_03	1	Output	1.4	109	11.9	1.5	1775.2	2.5	1	60
C#308_03	2	Output	1.5	105	13.3	2.4	1771.3	2.8	1	62
C#308_03	3	Output	1.5	104	13.3	1.9	1696.4	2.6	1	63
C#308_03	4	Output	1.5	106	13.2	2	1723.5	2.6	1	65
C#308_03	5	Output	1.5	107	13.3	2.1	1726.6	2.6	1	66
C#308_03	6	Output	1.5	105	13.3	2.4	1738	2.6	1	68
C#308_03	7	Output	1.6	103	14.3	2.6	1682.4	2.8	1	70
C#308_03	8	Output	1.5	97	12.9	2.2	1503	2.4	1	1791
C#308_03	9	Input	-	82	12.2	2.1	-	-	-	-
C#308_03	9	Output	7.6	70	10.9	0.7	1051.8	8	1	-

Table A.12: *Primitive connection, welding parameters for specimen C#308_03: ID (specimens), layer (layer number), wdt (welding data type), wtime (welding time), I (current), U (voltage), wfs (wire feed speed), pow (power), E (energy), ws (wedling speed), and ct (cooling time).*

ID	layer	lh [mm]	sh [mm]	sa [deg]	pl [mm]	tags [deg]	tage [deg]	taps [deg]	tape [deg]	ba [deg]
C#308_04	0	1.27	1.3	0	-	21	-	21	-	90
C#308_04	1	1.26	1.3	0	-	15	-	15	-	90
C#308_04	2	1.26	1.3	0	-	15	-	15	-	90
C#308_04	3	1.26	1.3	0	-	15	-	15	-	90
C#308_04	4	1.24	1.3	0	-	10	-	10	-	90
C#308_04	5	1.24	1.3	0	-	10	-	10	-	90
C#308_04	6	1.24	1.3	0	-	6	-	6	-	90
C#308_04	7	1.24	1.3	0	-	3	-	3	-	90
C#308_04	8	1.24	1.3	0	-	0	-	0	-	90
C#308_04	9	-	-	-	9.6	0	39.3	60	100	60

Table A.13: *Primitive connection, geometric parameters for specimen C#308_04: ID (specimens), layer (layer number), lh (layer height), sh (seam height), sa (seam angle relative to path), pl (path length), tags (tool angle relative to gravity at start), tage (tool angle relative to gravity at end), taps (tool angle relative to path at start), tape (tool angle relative to path at end), and ba (build angle relative to gravity).*

ID	layer	wdt	wtime [s]	I [A]	U [V]	wfs [m/min]	pow [W]	E [kJ]	ws [mm/s]	ct [s]
C#308_04	0-1	Input	-	129	13.9	3.5	-	-	-	
C#308_04	0	Output	1.5	103	13.5	2.2	1739.4	2.7	1	491
C#308_04	1	Output	1.5	96	12.9	2.1	1504.3	2.4	1	60
C#308_04	2	Output	1.5	101	13.1	2	1628.8	2.5	1	62
C#308_04	3	Output	1.5	95	12.7	2.1	1524.3	2.3	1	63
C#308_04	4	Output	1.5	103	13.3	2.4	1691.2	2.6	1	66
C#308_04	5	Output	1.5	116	14.1	2.5	2036.8	3.1	1	67
C#308_04	6	Output	1.5	103	13	2	1650.3	2.6	1	68
C#308_04	7	Output	1.5	105	13.1	2.1	1702.8	2.6	1	70
C#308_04	8	Output	1.5	105	13.1	2.2	1658.7	2.5	1	2.074
C#308_04	9	Input	-	82	12.2	2.1	-	-	-	-
C#308_04	9	Output	7.2	74	10.8	0.6	1119	8.1	1	-

Table A.14: *Primitive connection, welding parameters for specimen C#308_04: ID (specimens), layer (layer number), wdt (welding data type), wtime (welding time), I (current), U (voltage), wfs (wire feed speed), pow (power), E (energy), ws (wedling speed), and ct (cooling time).*

B   Virtual experiments

B.1   Reachability maps of the structures with IPWAAM connections

(a)
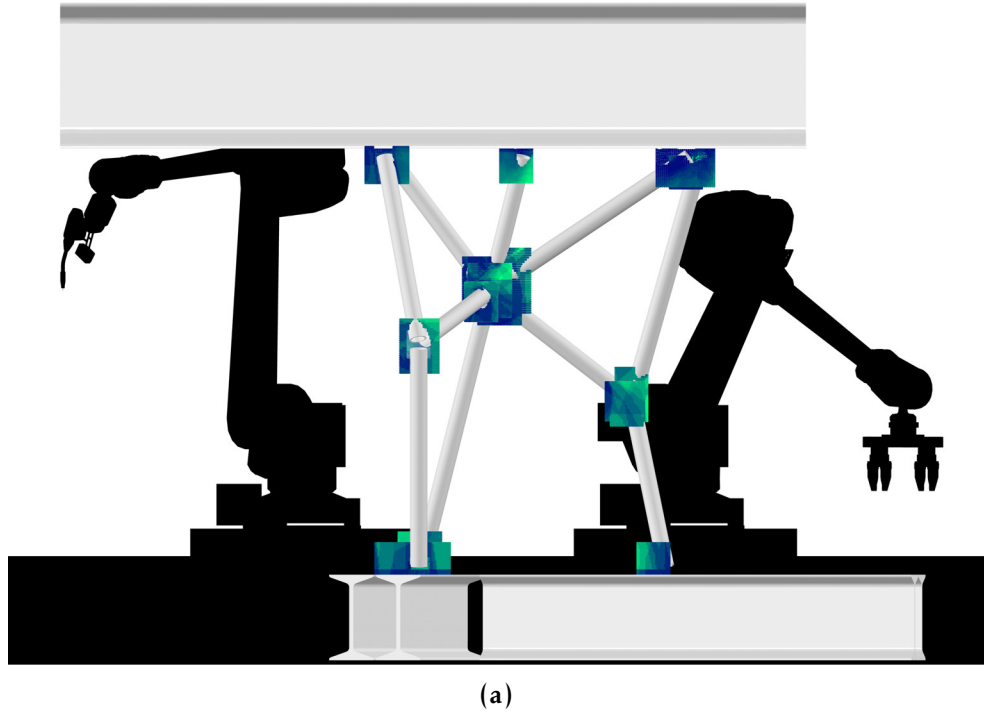
Figure B.1: *Front view of the planning scenes and reachability maps of the base structure.*

(a)
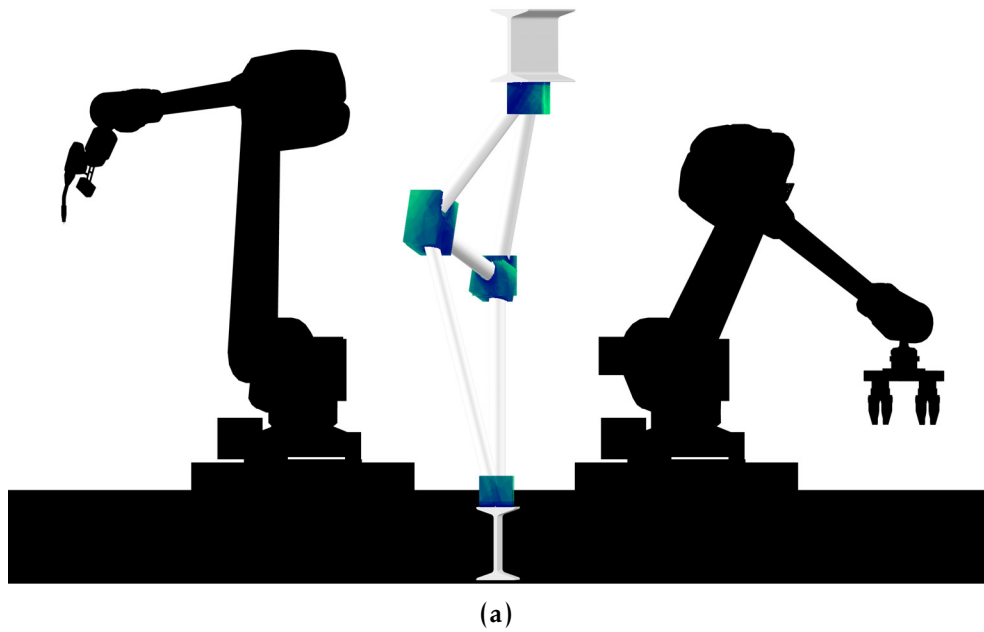
Figure B.2: *Front view of the planning scenes and reachability maps of sub-assembly 101.*

(a)
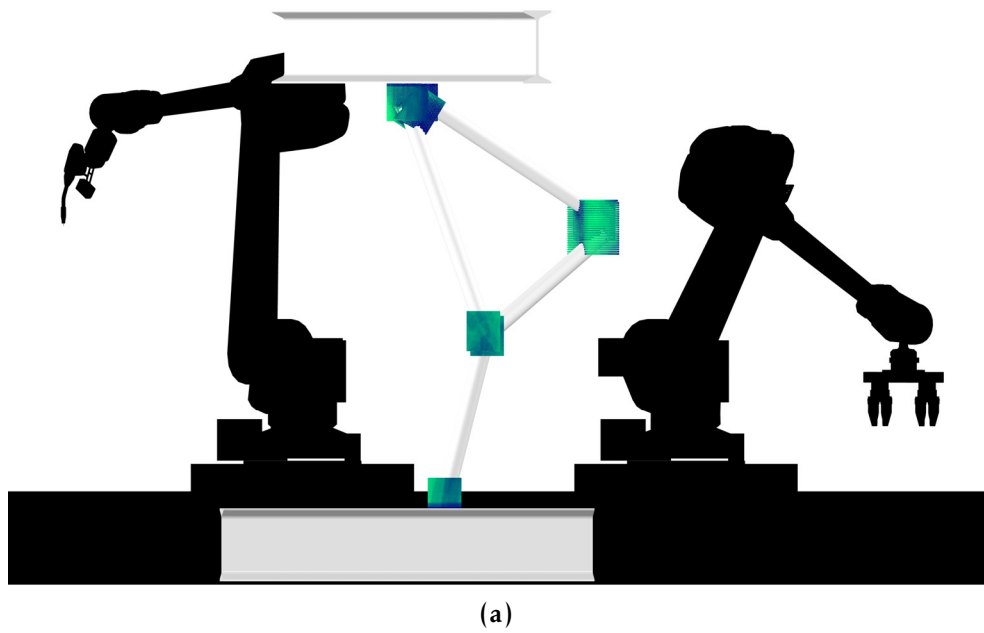
Figure B.3: *Front view of the planning scene and reachability map of sub-assembly 102.*

(a)
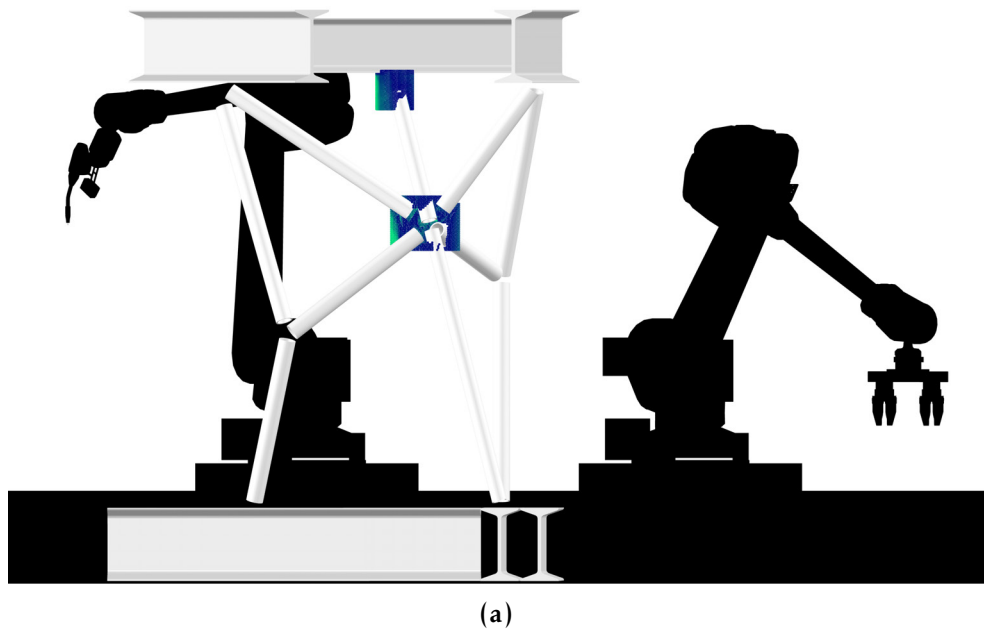
Figure B.4: *Front view of the planning scenes and reachability maps of sub-assembly 103.*

B.2 Connections of the base structure
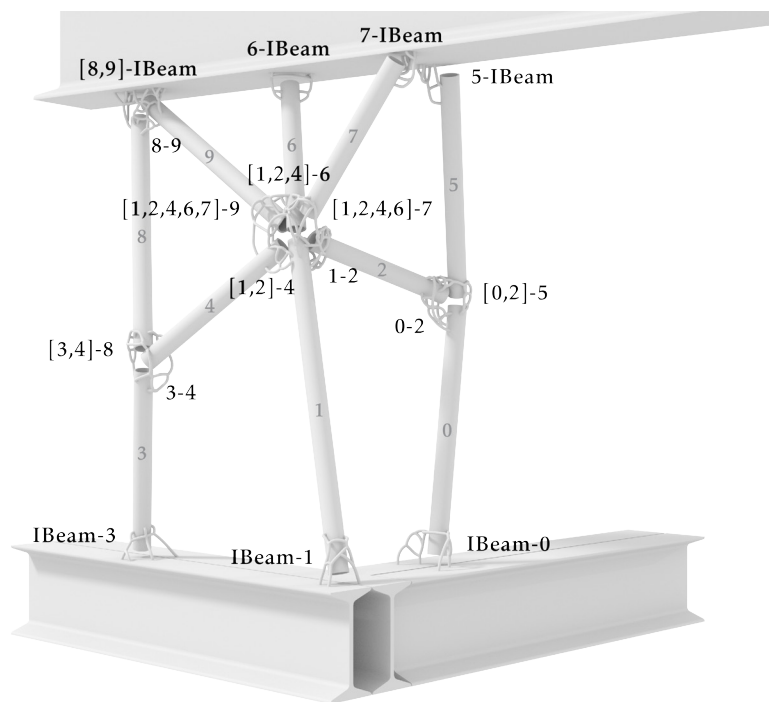
Figure B.5: *Base structure: connections' IDs*

(a) *IBeam-0: Reachability map*

(b) *IBeam-0: TO and skeletons*

(c) *IBeam-0: Paths*

(d) *IBeam-1: Reachability map*

(e) *IBeam-1: TO and skeletons*

(f) *IBeam-1: Paths*

(g) *IBeam-3: Reachability map*

(h) *IBeam-3: TO and skeletons*

(i) *IBeam-3: Paths*

(j) *1-2: Reachability map*

(k) *1-2: TO and skeletons*

(l) *1-2: Paths*
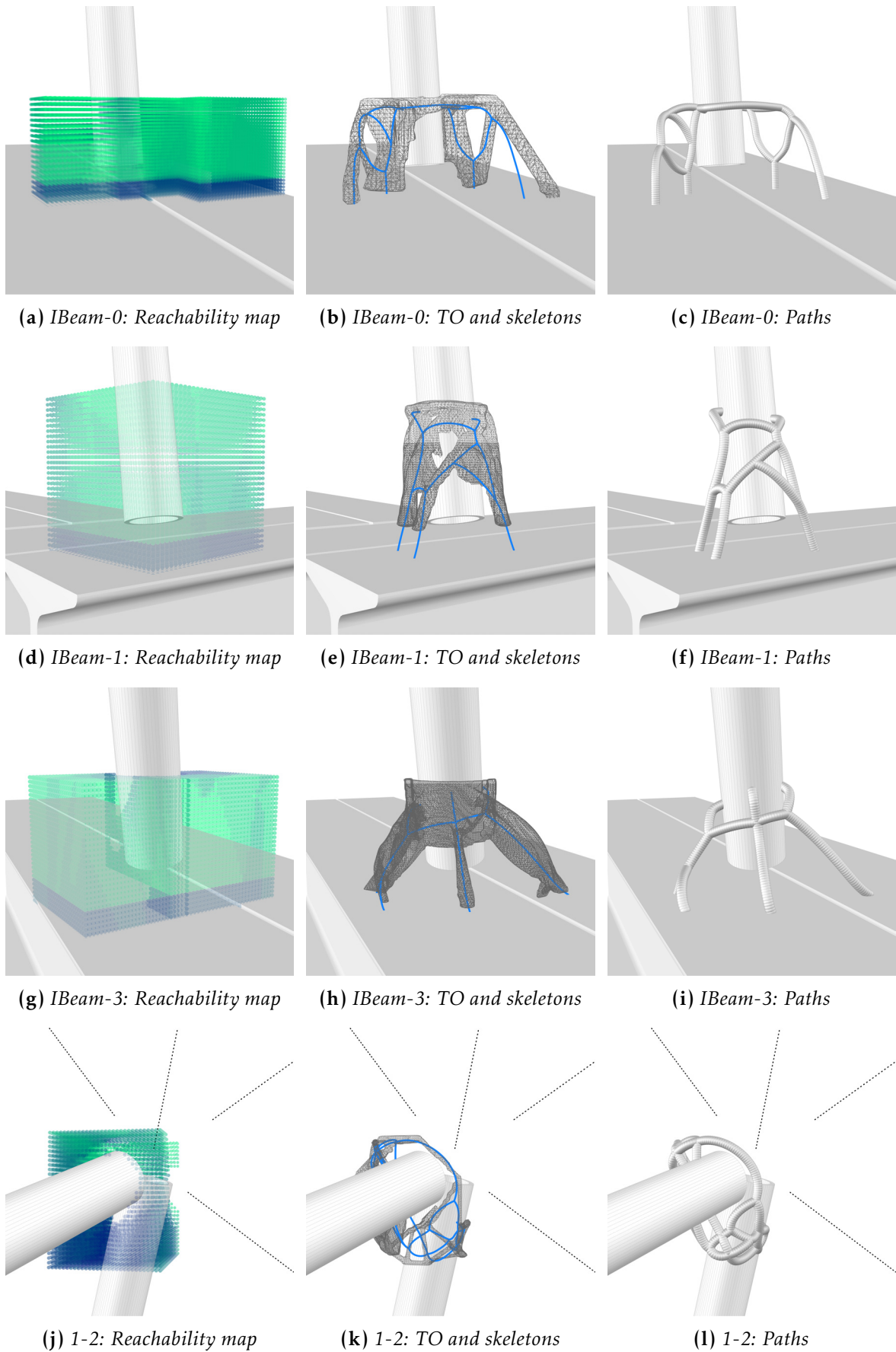
Figure B.6: *Base structure: reachability maps, topology optimization (TO), skeletons, and paths.*

(a) *[1,2]-4: Reachability map* (b) *[1,2]-4: TO and skeletons* (c) *[1,2]-4: Paths*

(d) *[1,2,4]-6: Reachability map* (e) *[1,2,4]-6: TO and skeletons* (f) *[1,2,4]-6: Paths*

(g) *[1,2,4,6]-7: Reachability map* (h) *[1,2,4,6]-7: TO and skeletons* (i) *[1,2,4,6]-7: Paths*

(j) *[1,2,4,6,7]-9: Reachability map* (k) *[1,2,4,6,7]-9: TO and skeletons* (l) *[1,2,4,6,7]-9: Paths*
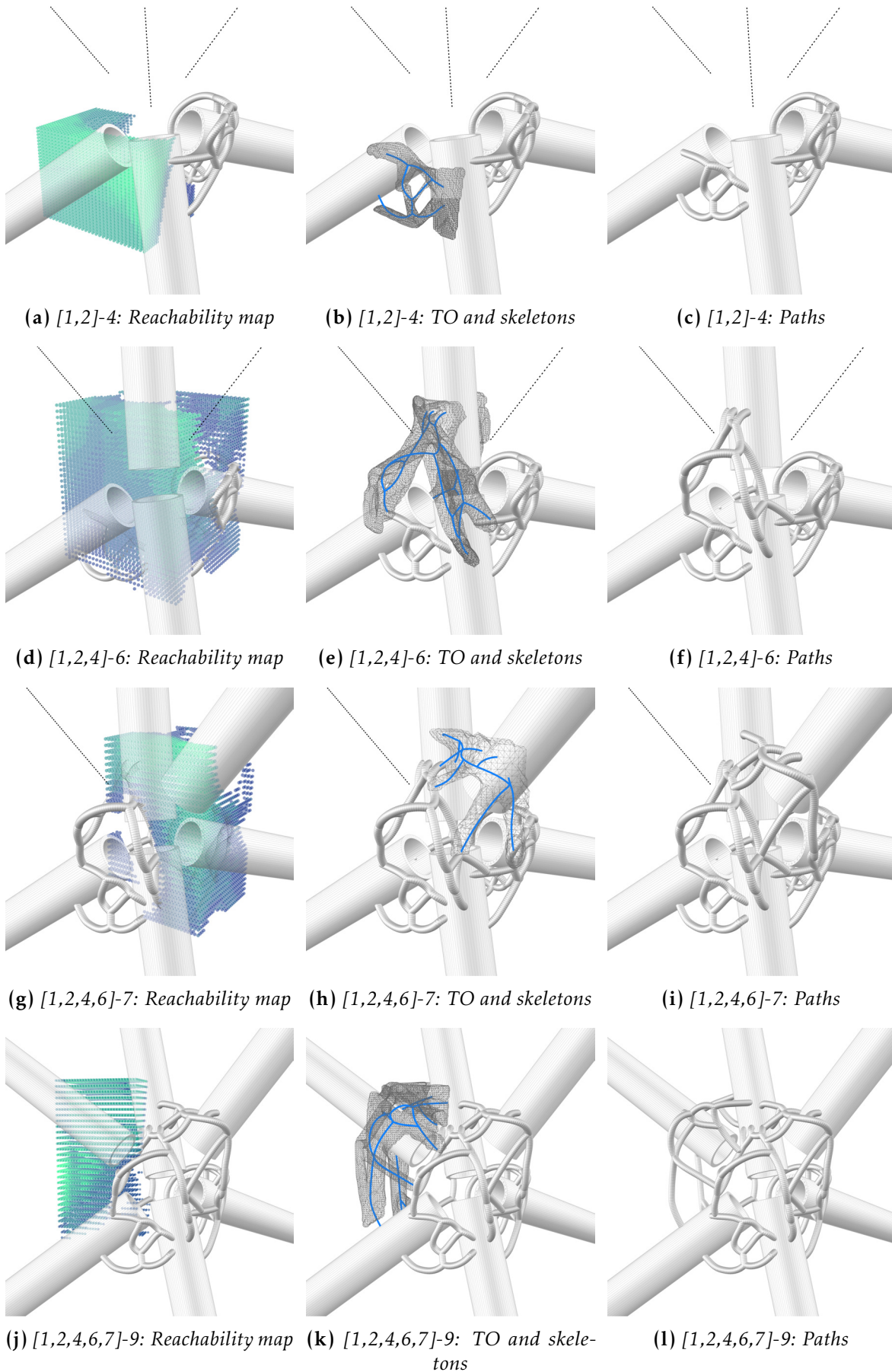
Figure B.7: *Base structure: reachability maps, topology optimization (TO), skeletons, and paths.*

(a) *0-2: Reachability map*

(b) *0-2: TO and skeletons*

(c) *0-2: Paths*

(d) *[0,2]-5: Reachability map*

(e) *[0,2]-5: TO and skeletons*

(f) *[0,2]-5: Paths*

(g) *3,4: Reachability map*

(h) *3,4: TO and skeletons*

(i) *3,4: Paths*

(j) *[3,4]-8: Reachability map*

(k) *[3,4]-8: TO and skeletons*

(l) *[3,4]-8: Paths*
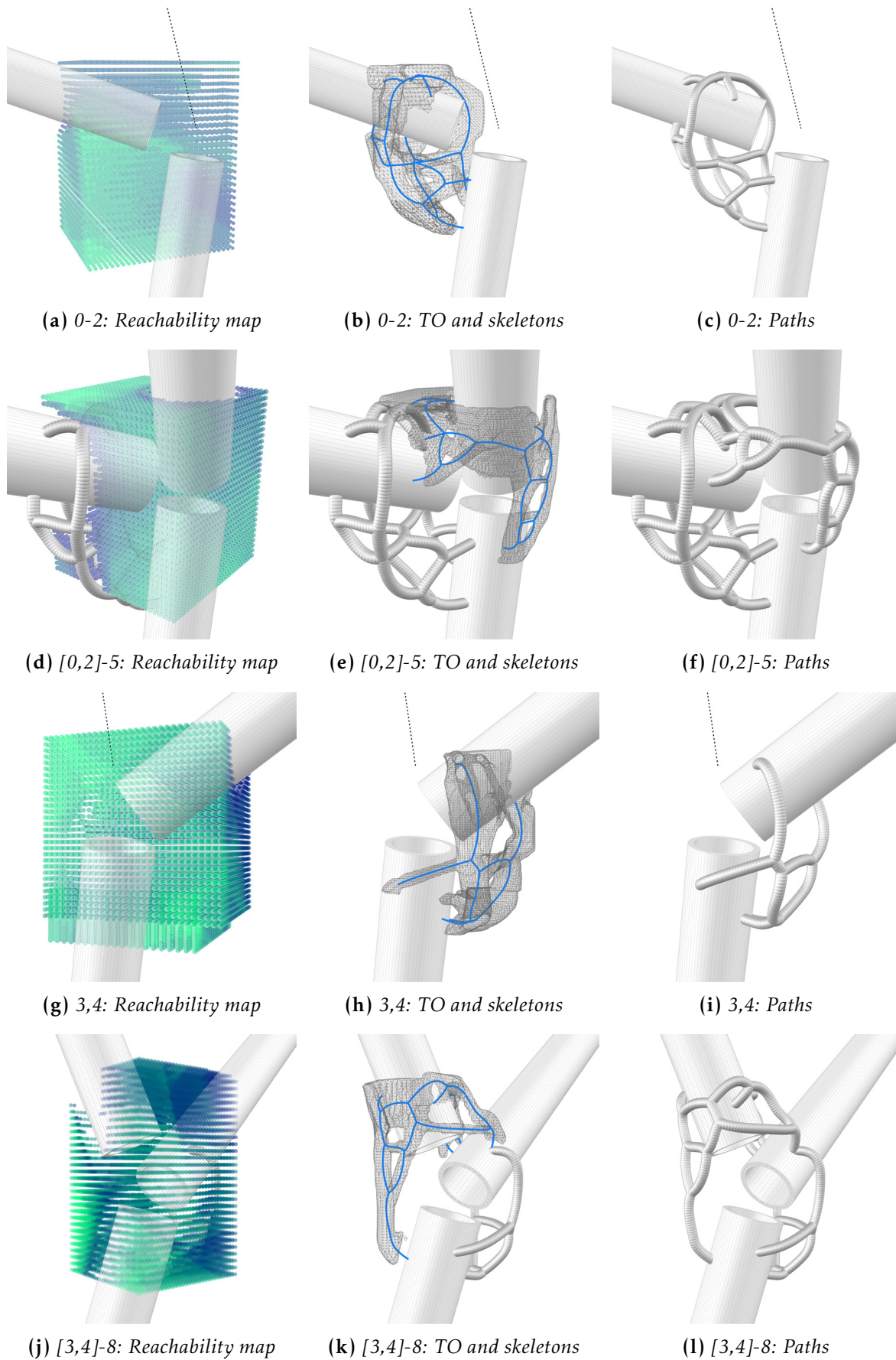
Figure B.8: *Base structure: reachability maps, topology optimization (TO), skeletons, and paths.*

(a) *IBeam-5: Reachability map*

(b) *IBeam-5: TO and skeletons*

(c) *IBeam-5: Paths*

(d) *IBeam-6: Reachability map*

(e) *IBeam-6: TO and skeletons*

(f) *IBeam-6: Paths*

(g) *IBeam-7: Reachability map*

(h) *IBeam-7: TO and skeletons*

(i) *IBeam-7: Paths*
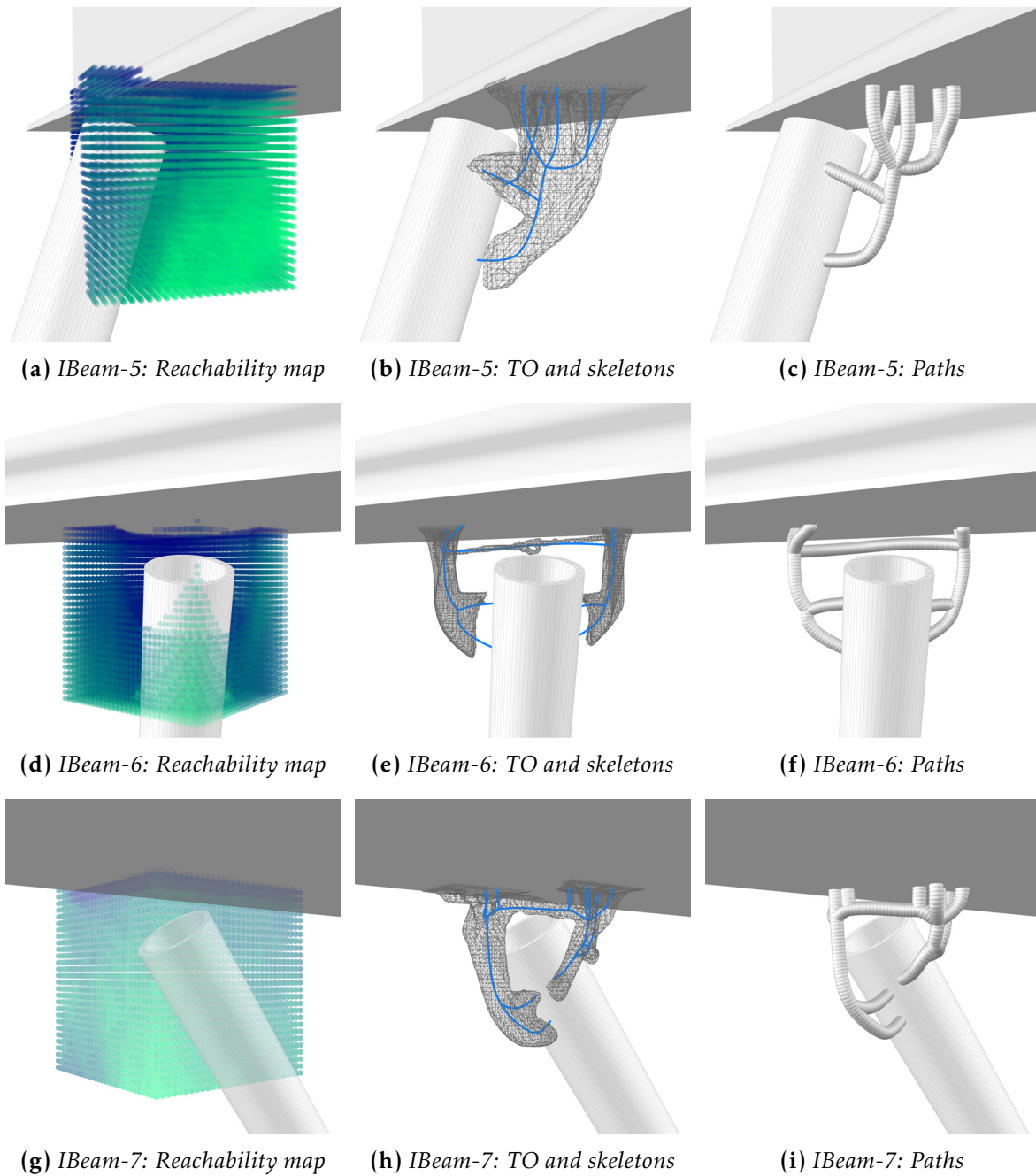
Figure B.9: Base structure: reachability maps, topology optimization (TO), skeletons, and paths.

(a) *8-9: Reachability map*

(b) *8-9: TO and skeletons*

(c) *8-9: Paths*

(d) *[8,9]-IBeam: Reachability map*

(e) *[8,9]-IBeam: TO and skeletons*

(f) *[8,9]-IBeam: Paths*
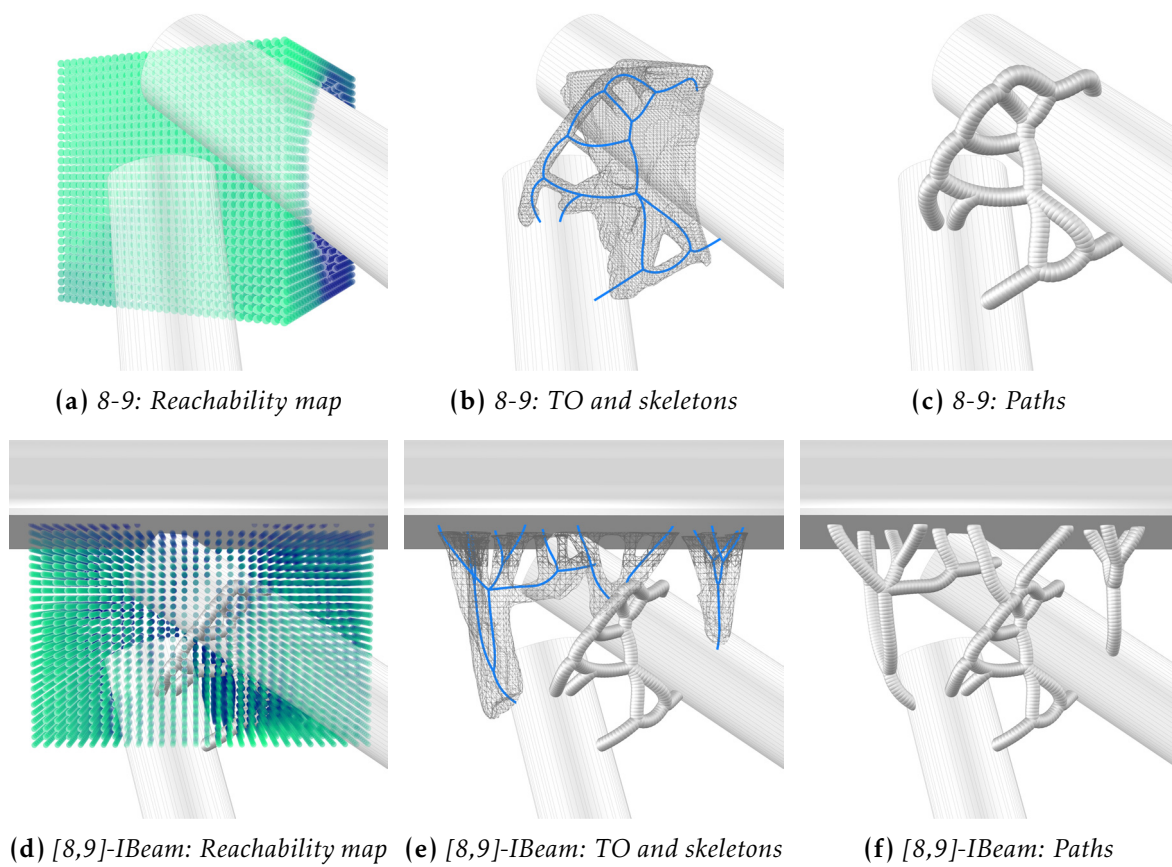
Figure B.10: *Base structure: reachability maps, topology optimization (TO), skeletons, and paths.*

B.3   Connections of the structure with adapted sequence

(a)

(b)

(c)
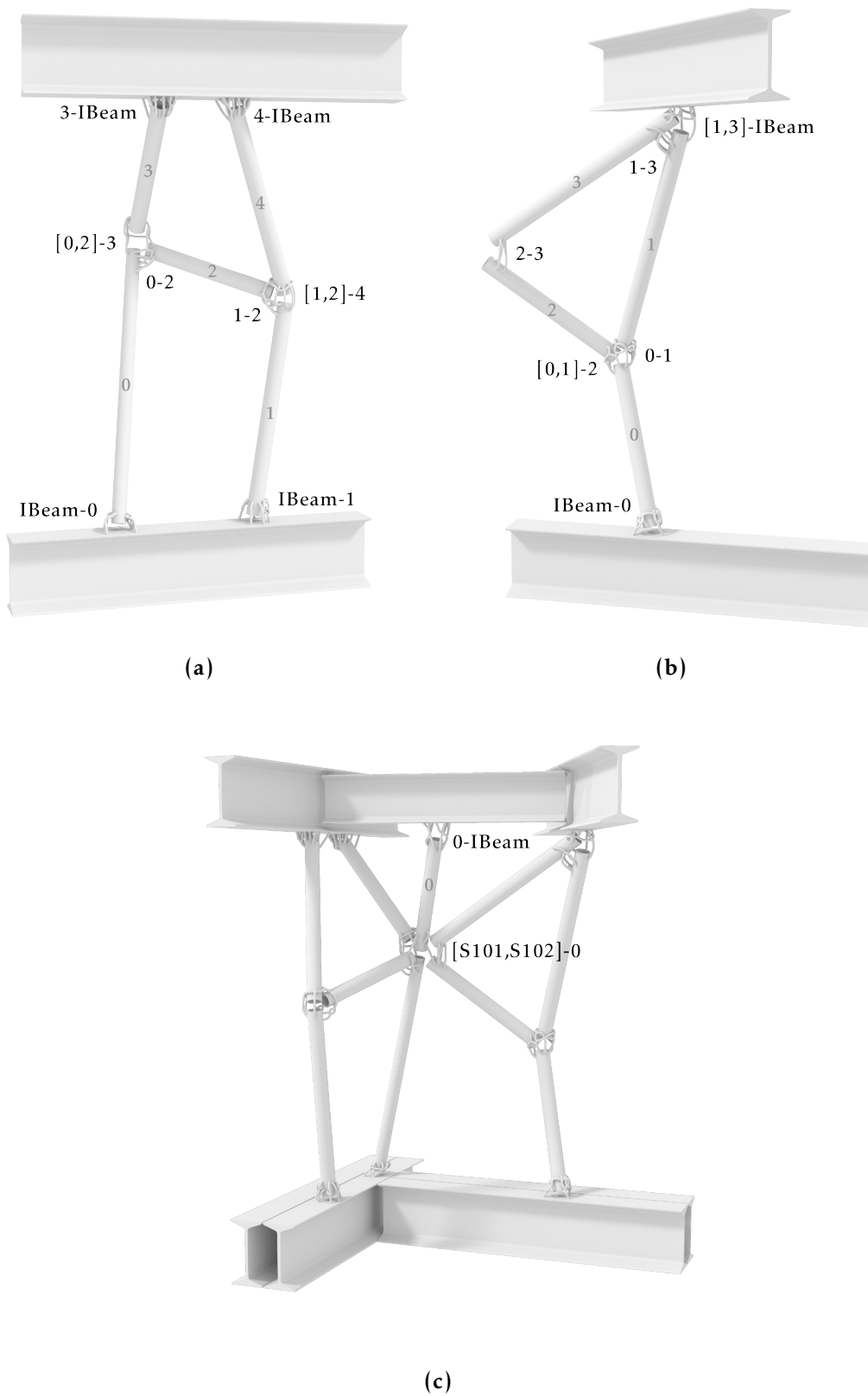
Figure B.11: *Structures with adapted sequence, connections' IDs: (a) Sub-assembly 101, (b) subassembly 102, and (c) sub-assembly 103.*

(a) 0-2: Reachability map   (b) 0-2: TO and skeletons   (c) 0-2: Paths

(d) [0,2]-3: Reachability map   (e) [0,2]-3: TO and skeletons   (f) [0,2]-3: Paths

(g) 3-IBeam: Reachability map   (h) 3-IBeam: TO and skeletons   (i) 3-IBeam: Paths

(j) 4-IBeam: Reachability map   (k) 4-IBeam: TO and skeletons   (l) 4-IBeam: Paths
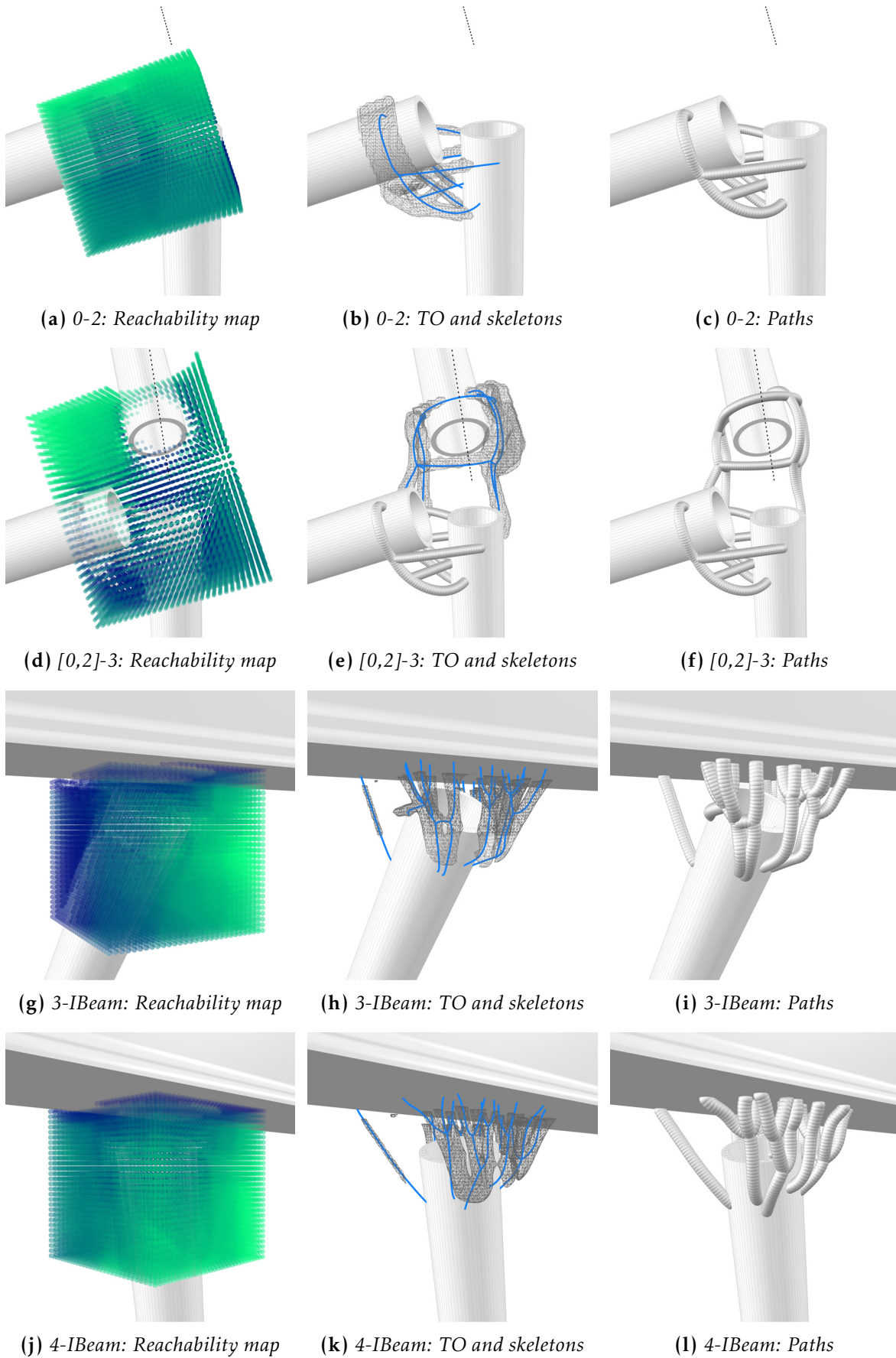
Figure B.13: *Sub-assembly 101: reachability maps, topology optimization (TO), skeletons, and paths.*

(a) *IBeam-0: Reachability map*

(b) *IBeam-0: TO and skeletons*

(c) *IBeam-0: Paths*

(d) *IBeam-1: Reachability map*

(e) *IBeam-1: TO and skeletons*

(f) *IBeam-1: Paths*

(g) *1-2: Reachability map*

(h) *1-2: TO and skeletons*

(i) *1-2: Paths*

(j) *[1,2]-4: Reachability map*

(k) *[1,2]-4: TO and skeletons*

(l) *[1,2]-4: Paths*
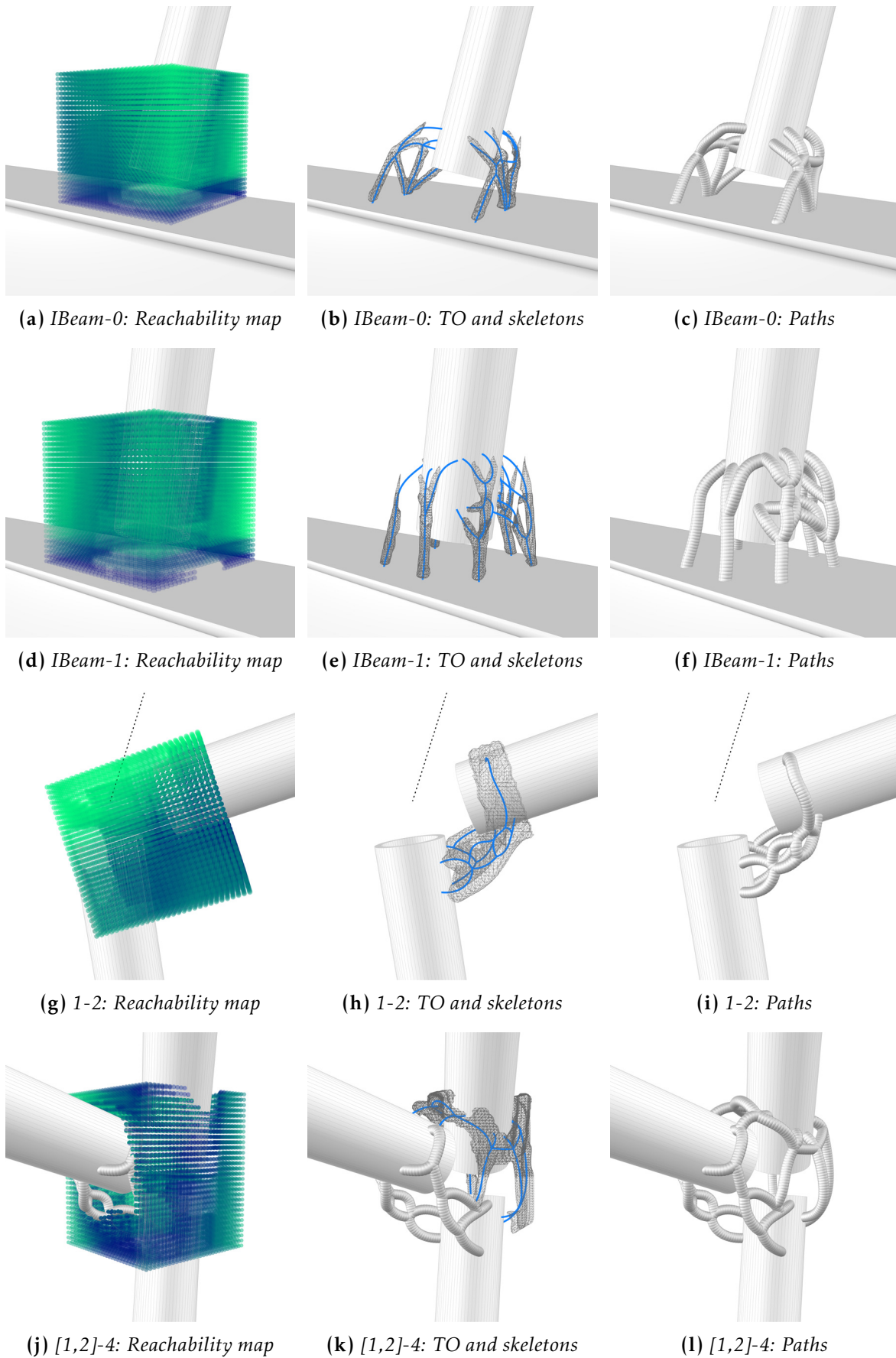
Figure B.12: *Sub-assembly 101: reachability maps, topology optimization (TO), skeletons, and paths.*

(a) *IBeam-0: Reachability map*

(b) *IBeam-0: TO and skeletons*

(c) *IBeam-0: Paths*

(d) *0-1: Reachability map*

(e) *0-1: TO and skeletons*

(f) *0-1: Paths*

(g) *[0,1]-2: Reachability map*

(h) *[0,1]-2: TO and skeletons*

(i) *[0,1]-2: Paths*
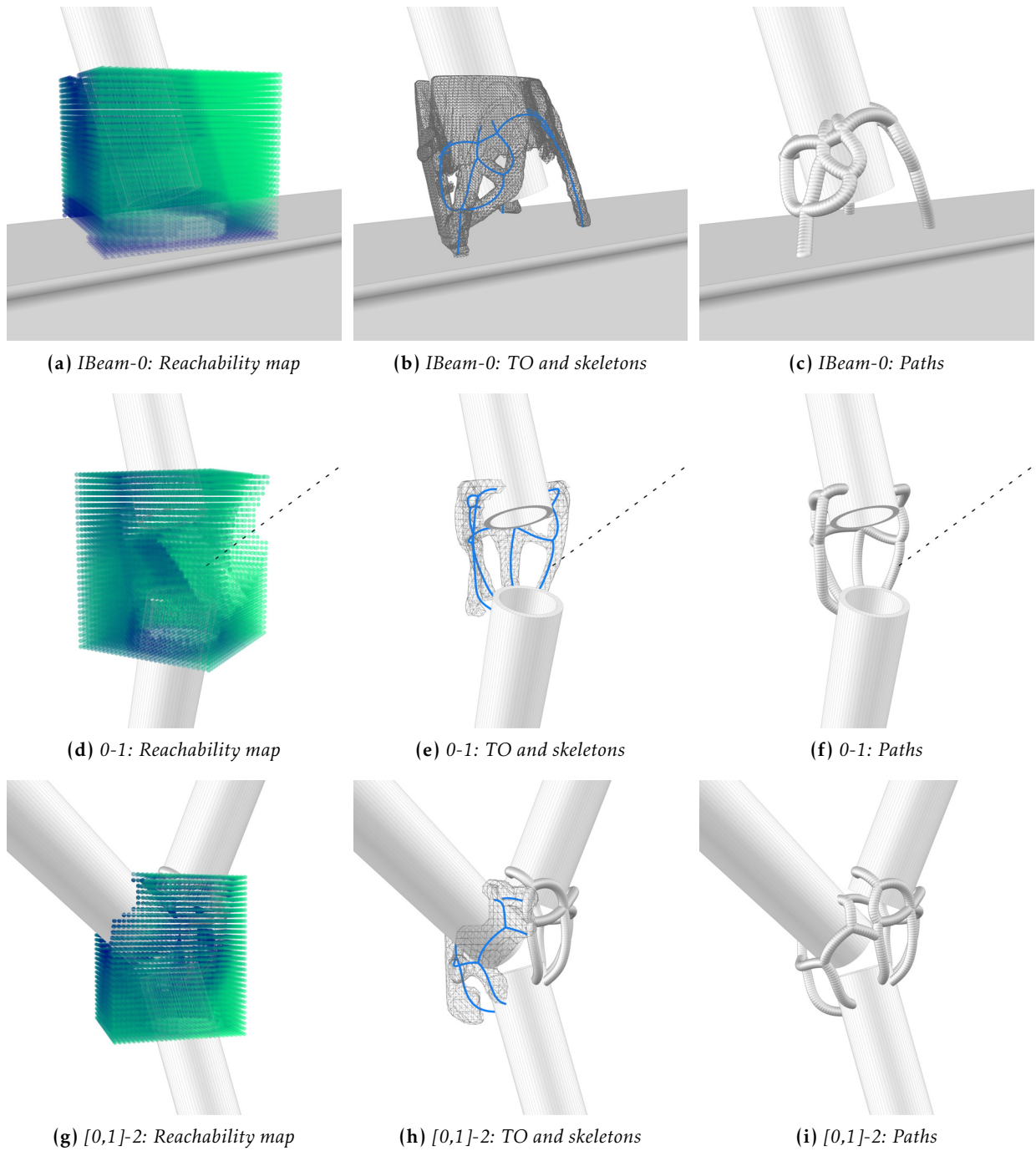
Figure B.14: *Sub-assembly 102: reachability maps, topology optimization (TO), skeletons, and paths.*

(a) *1-3: Reachability map*

(b) *1-3: TO and skeletons*

(c) *1-3: Paths*

(d) *2-3: Reachability map*

(e) *2-3: TO and skeletons*

(f) *2-3: Paths*

(g) *[2,3]-IBeam: Reachability map*

(h) *[2,3]-IBeam: TO and skeletons*

(i) *[2,3]-IBeam: Paths*
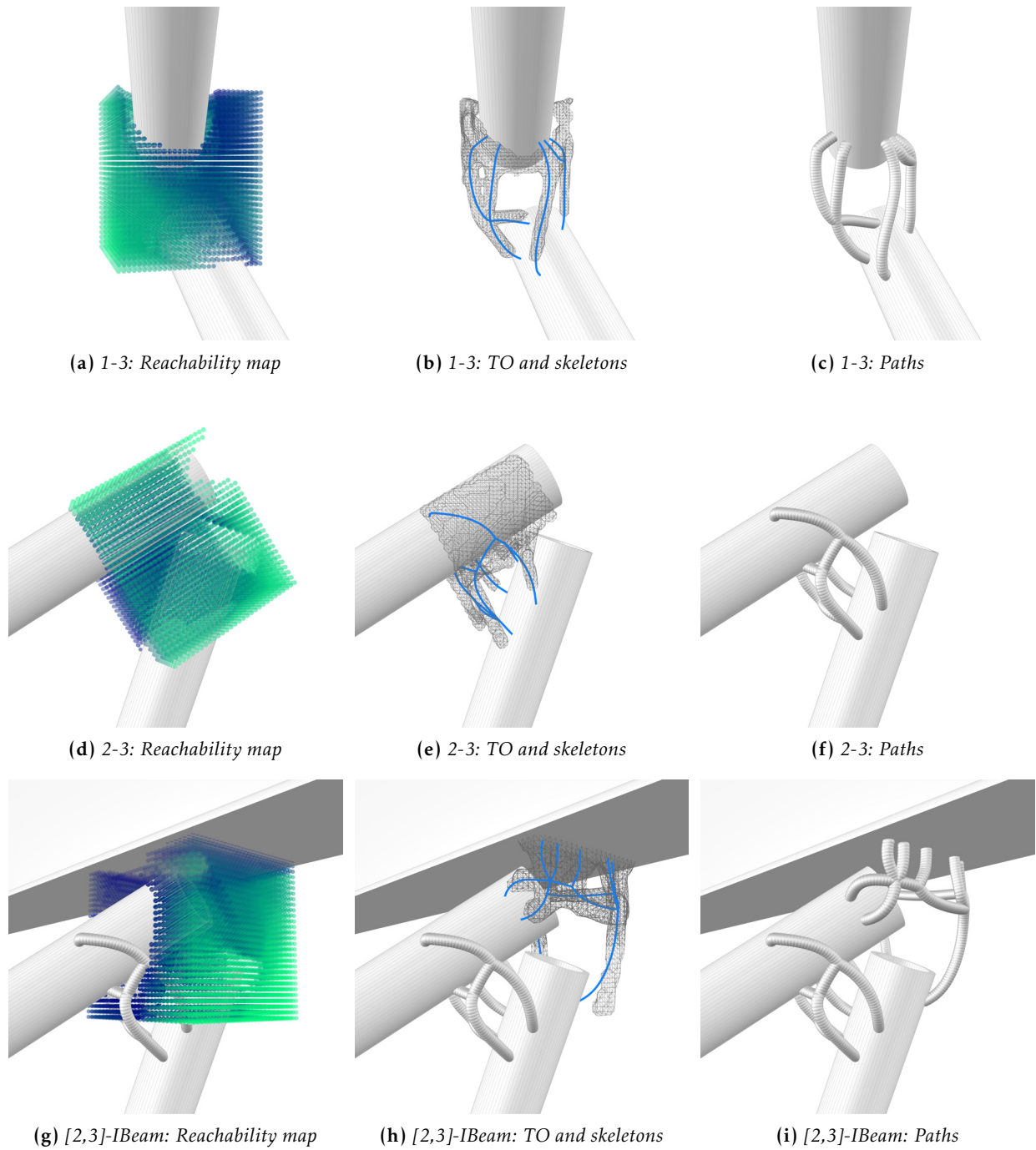
Figure B.15: *Sub-assembly 102: reachability maps, topology optimization (TO), skeletons, and paths.*

(a) *[S101,S102]-9: Reachability map*

(b) *[S101,S102]-9: TO and skeletons*

(c) *[S101,S102]-9: Paths*

(d) *9-IBeam: Reachability map*

(e) *9-IBeam: TO and skeletons*

(f) *9-IBeam: Paths*

Figure B.16: *Sub-assembly 103: reachability maps, topology optimization (TO), skeletons, and paths.*

C Project credits

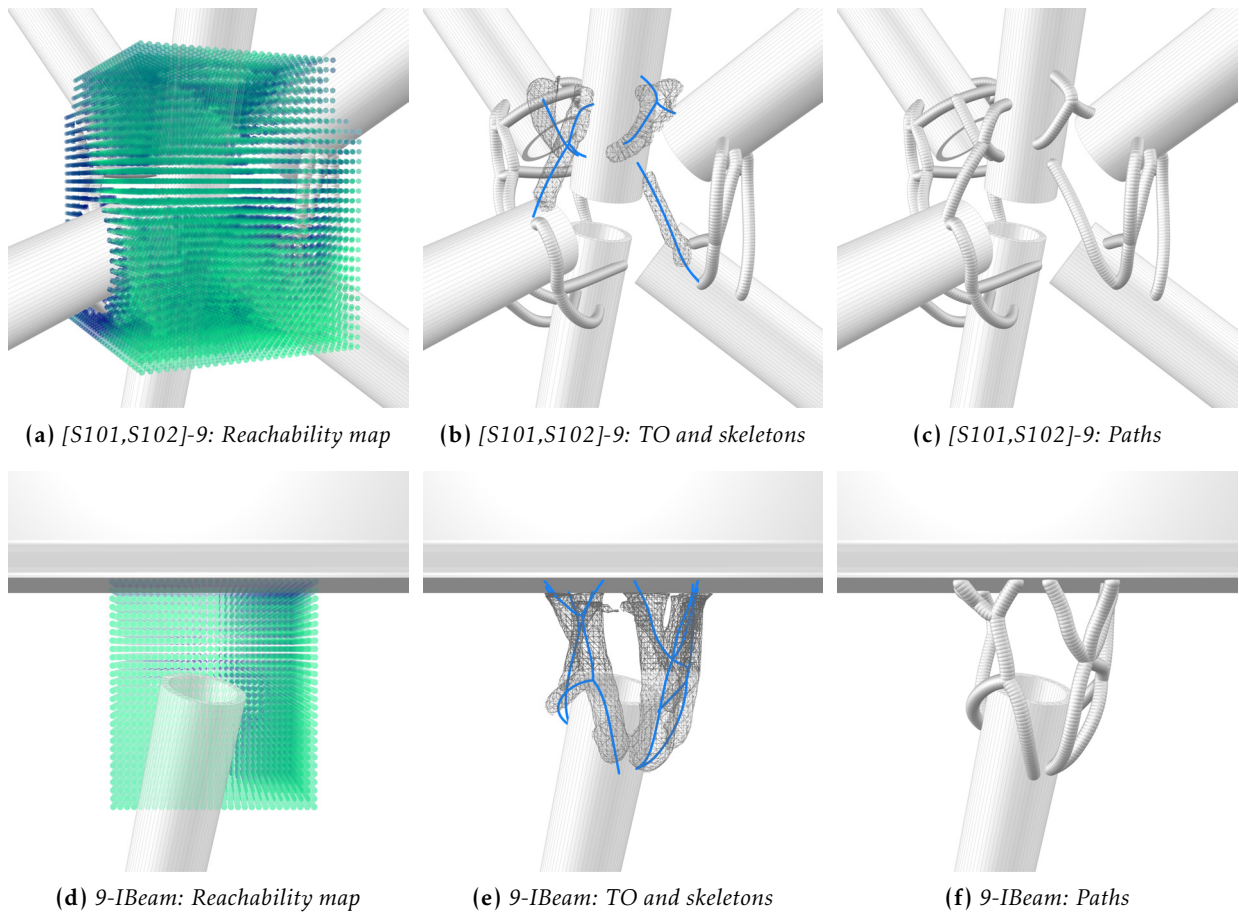This research project is funded through the Architecture & Technology Doctoral Fellowship from the Institute of Technology in Architecture (ITA) of ETH Zurich. The project is associated with the NCCR Digital Fabrication, which supported finding industry sponsors, and additional project funding, including the Young Women Interns Support Grant. The project would not have been possible without the generous sponsorship of the welding setup provided by Fronius Schweiz AG.

Through its development, the project built internal and external collaborations, whose participants and credits are listed below.[1]

Software and hardware

- **Dr. Romana Rust**, Senior Researcher at Gramazio Kohler Research, ETH Zurich, fundamentally contributed to the development of the research project on numerous topics in her role of second advisor. In particular, Romana Rust contributed to the integration of robotic constraints in the adaptive detailing pipeline by developing the concept and most of the scripts used to calculate the tool accessibility and robot reachability methods using the COMPAS FAB package. In addition, Dr. Rust developed the first version of the path slicing with path planning method and provided a path planning setup for robotic assembly for the virtual structures presented in section 5.2.

- **Philippe Fleischmann**, Robotics Technician at Robotic Fabrication Laboratory, ETHZ, fundamentally contributed to the development of the IPWAAM technique by securing, installing, testing, integrating and developing hardware and software interfaces for the robotic welding and WAAM setups in the Robotic Fabrication Laboratory. In addition, Philippe Fleischmann contributed substantially to the project by developing the compas_rrc package that provides smooth communication between the design and production components of the adaptive detailing pipeline.

- **Gonzalo Casas**, Software Engineer at Gramazio Kohler Research, ETHZ, fundamentally contributed, both intellectually and practically, to solving the diverse software challenges found during the development of the project. In particular, Gonzalo Casas contributed by developing a

---

[1]Roles and institutions refer to the time of the respective contributions. Everything else not mentioned here has been contributed by the author.

ROS communication setup to send and receive information from the profile sensor used for localization. In addition, Gonzalo Casas intensively contributed and/or developed libraries that the project relies on, such as `COMPAS`, `COMPAS FAB`, `roslibpy` and `compas_rrc_ros`.

- **Yijiang Huang**, PhD researcher at Digital Structures, MIT, fundamentally contributed to the project developing the final version of the semi-constrained Cartesian planning ladder graph and greedy algorithms (Section 4.3.3.2) that are essential to the success of the printing process when using the Path slicing with path planning method.

- **Mathias Bernhard**, Senior Researcher at Digital Building Technologies, ETHZ, fundamentally contributed to the development of the IPWAAM technique and adaptive detailing pipeline with the first concept of the tool accessibility component (Section 4.3.1.1) using a volumetric modeling approach. Mathias Bernhard directly contributed to the project by providing a working example of the tool accessibility method using the `compas_vol` library he developed. In addition, Mathias Bernhard co-supervised the masters' thesis where these concepts were first tested (Mitropoulou, 2018) and contributed to its publication Mitropoulou, Ariza, et al., 2019.

- **Ioanna Mitropoulou**, master's student of the Master of Advanced Studies in Digital Fabrication, ETHZ, fundamentally contributed to the project by demonstrating a variety of IPWAAM deposition strategies and volumetric modeling approaches in the thesis (Mitropoulou, 2018) and subsequent publication (Mitropoulou, Ariza, et al., 2019).

- **Dr. Ammar Mirjan**, Senior Researcher at Gramazio Kohler Research, ETHZ, fundamentally contributed to the work with the concept of spatial welding for connection details. Ammar Mirjan proposed and supervised the proof-of-concept work and the first year of this research.

- **Samuel Cros**, master's student of the Master of Advanced Studies in Digital Fabrication, ETHZ, conducted the proof-of-concept work of the IPWAAM technique in the master's thesis Cros, 2017. This work contributed to a great extent to the first iteration of path slicing with mesh collision method.

- **Augusto Gandia**, PhD researcher at Gramazio Kohler Research, ETHZ, contributed to the software development with the first iteration of the communication framework for the profile sensor used for localization.

- **Michael Lyrenmann**, Head of the Robotic Fabrication Laboratory, ETHZ, fundamentally contributed to the work with hardware development at all stages of the project and contributed, in particular, to the development of the profile sensor hardware.

Material development

- **Dr. Vlad Silvestru**, Postdoctoral researcher at the Chair of Steel and Composite Structures, ETHZ, fundamentally contributed to the understanding and demonstration of the IPWAAM material behavior presented in Section 3.6.6. Vlad Silvestru led investigations on the tensile and compressive performance and surface characterization of the point-by-point WAAM bars and the publication of the results. These contributions are critical to support the next steps towards the development of the IPWAAM process, and their potential application in the Architecture, Engineering, and Construction industry.

- **Lucas Michel**, PhD at Durability of Engineering Materials, ETHZ, contributed to the demonstration of the IPWAAM material durability presented in Section 3.6.6.4. Lucas Michel led investigations on the corrosion behavior of point-by-point WAAM bars and the publication of the results. These contributions are as well critical to support the next steps for the development of the IPWAAM process and their potential application in the Architecture, Engineering and Construction industry.

- **Prof. Andreas Taras**, Professor of Steel Construction and Composite Structures, ETHZ, supported the development of the collaborative investigations presented in Section 3.6.6 regarding the material performance and surface characteristics of the WAAM products and contributed to the dissemination of the results.

- **Prof. Ueli Angst**, Professor of Durability of Engineering Materials, ETHZ, supported the development of the collaborative investigations presented in Section 3.6.6 regarding the corrosion behavior of the WAAM products and contributed to the dissemination of the results presented in Section 3.6.6.4.

- **Julie Vienne**, NCCR DFAB Intern, ETHZ, contributed to the investigation of the tensile performance of the point-by-point WAAM bars and their surface characterization presented in Section 3.6.6.2.

- **Andrea Solcà**, masters' student at the Dept. of Civil, Environmental and Geomatic Engineering, ETHZ, contributed to the investigation of

the compression performance of the point-by-point WAAM bars and their surface characterization presented in Section 3.6.6.3.

- **Andrej Stoy**, PhD in the Department of Mechanical and Process Engineering, ETHZ, contributed to the understanding of the point-by-point WAAM deposition process by developing physical experiments and simulations of the heat transfer phenomenon presented in Section 3.6.6.5.

- **Maicol Fabbri**, PhD at the Institute of Machine Tools and Manufacturing, ETHZ and Inspire AG, contributed to the understanding of the point-by-point deposition process by providing access and support in the metallographic studies presented in Section 3.6.5.

- **Asel Maria Aguilar Sanchez**, Technician at Chair of Physical Chemistry of Building Materials, ETHZ, contributed with microscopy imaging of the WAAM bars presented in Section 3.6.6.4.